VOLUME 68 JUNE, 1964 NUMBER 6

THE JOURNAL OF PHYSICAL CHEMISTRY

PUBLISHED MONTHLY BY THE AMERICAN CHEMICAL SOCIETY

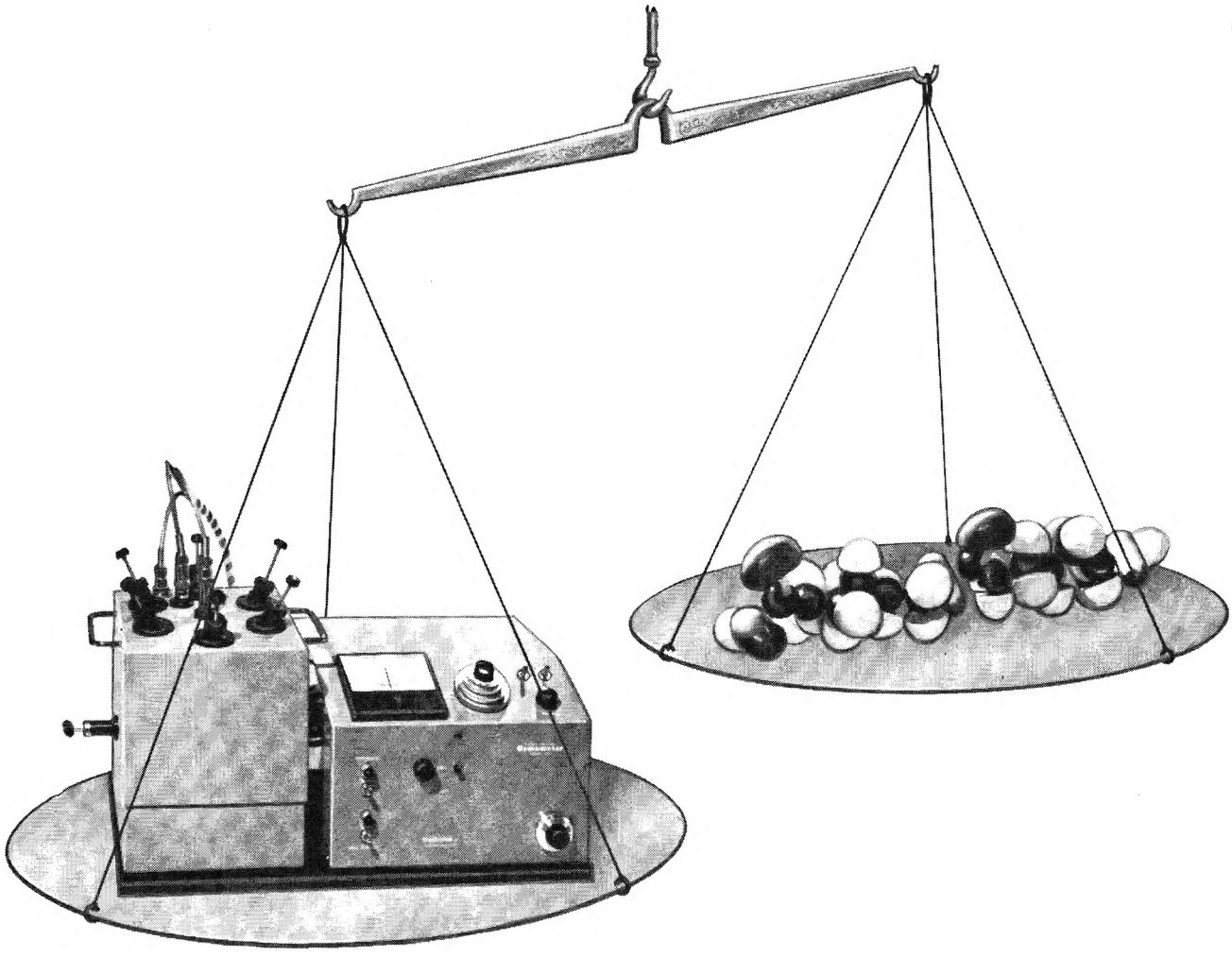

The Only Way to Weigh a Molecule

For osmolalities and molecular weight determinations from 100 to 25,000 (number average), Mechrolab's Vapor Pressure Osmometer has proved to be the most satisfactory —if not the only—way of doing the job.

Operating on the principle of vapor pressure lowering, more than 700 VPOs are now in use, replacing other techniques such as ebulliometry and cryoscopy. Why? Because the VPO is: *rapid* (you can make 60 to 80 individual measurements each 8-hour day); *precise* (1% accuracy for low molecular weight polymers, useful data for molecular weights to 25,000); *convenient* (it's compact and is designed for routine operation); *versatile* (wide choice of solvents [aqueous or organic], operating temperatures, broad range of molecular weights and samples, with sample size requirements as low as 10 microliters).

Mechrolab's standard Model 301A VPO, maximum operating temperature 65°C, costs $2,390. High temperature Model 302 operates to 130°C, price $2,900. Direct sales and service by Mechrolab technical field personnel.

Call or write for further details on 300 series VPO's and/or a demonstration by a factory representative. Also, be sure to ask for your free subscription to our news letter, "The Molecule." Write to 1062 Linda Vista, Mountain View 24, California.

Typical Applications

Bio-Medical Osmolalities · Osmotic Coefficients Proteins · Sugars.

Chemical Monomers · Hydrocarbons · Prepolymers Polyolefins · Polyamides · Cellulosics · Elastomers Petrochemicals · Silicones.

Mechrolab, INC.

"Advanced Instrumentation for Increasing Laboratory Productivity"
High Speed Membrane Osmometers, Light-Scattering Photometers, Automanometers

THE JOURNAL OF

PHYSICAL CHEMISTRY

Volume 68, Number 6 June, 1964

NOTES

AUTHOR INDEX

THE JOURNAL OF
PHYSICAL CHEMISTRY

VOLUME 68, NUMBER 6 JUNE 15, 1964

Rate Constants of Hydrated Electron Reactions with Organic Compounds[1]

by Edwin J. Hart, Sheffield Gordon, and J. K. Thomas

Argonne National Laboratory, Argonne, Illinois *(Received February 1, 1964)*

The second-order rate constants of reaction of some aliphatic, aromatic, and heterocyclic compounds with the hydrated electron are reported. These constants were measured in unbuffered and in alkaline solutions by following the decay of the hydrated electron absorption band produced by a single 0.2- or 0.4-μsec. pulse of 15 Mev. electrons. Unreactive compounds with second-order rate constants less than 10^8 M^{-1} sec.$^{-1}$ include saturated organic compounds containing carbon, hydrogen, and oxygen. Representative compounds are hydrocarbons, alcohols, fatty acids, esters, and amino acids. Unreactive also are unsaturated compounds including aromatic derivatives such as ethylene, benzene, aniline, and hydroquinone. Reactive compounds with rate constants in the range of 10^9 to 3×10^{10} M^{-1} sec.$^{-1}$ are: unhydrated aldehydes, ketones, compounds containing C=C or C≡N, disulfides, peroxides, and purine and pyrimidine heterocyclic derivatives.

Introduction

Previous work has shown that the hydrated electron, e_{aq}^-, demonstrates high selectivity in its reactions with organic compounds.[2,3] Second-order rate constants, in general, vary from the diffusion controlled rates of 10^{10} M^{-1} sec.$^{-1}$ for very reactive compounds to 10^6 M^{-1} sec.$^{-1}$ for unreactive compounds. In the present paper we report absolute rate constants for reaction of some aliphatic, aromatic, and heterocyclic compounds with the hydrated electron.

Experimental

The technique of pulsed radiolysis has been described elsewhere.[4-8] Hydrated electrons are generated in aqueous solution by a single 0.2- or 0.4-μ sec. pulse of 15 Mev. electrons at a concentration of the order of 10^{-6} M. Decay of the hydrated electron spectrum is followed at 5780 Å. at an appropriate concentration of solute where pseudo-first-order kinetics prevail.

Great care must be paid to the removal of oxygen and carbon dioxide from the irradiated solutions because of their high reactivity with the hydrated electron.[2] Therefore, special consideration was given to the preparation of the solutions. The method of evacuation and filling of the syringes with the solutions to be

(1) Based on work performed under the auspices of the U. S. Atomic Energy Commission.

(2) S. Gordon, E. J. Hart, M. S. Matheson, J. Rabani, and J. K. Thomas, *Discussions Faraday Soc.*, **36**, 193 (1963).

(3) E. J. Hart, S. Gordon, and J. K. Thomas, *Radiation Res. Suppl.*, **4**, 74 (1964).

(4) S. Gordon, E. J. Hart, M. S. Matheson, J. Rabani, and J. K. Thomas, *J. Am. Chem. Soc.*, **85**, 1375 (1963).

(5) E. J. Hart and J. W. Boag, *ibid.*, **84**, 4090 (1962).

(6) M. S. Matheson and L. M. Dorfman, *J. Chem. Phys.*, **32**, 1870 (1960).

(7) L. M. Dorfman, I. A. Taub, and R. E. Bühler, *ibid.*, **36**, 3051 (1962).

(8) S. Gordon, E. J. Hart, and J. K. Thomas, *J. Phys. Chem.*, **68**, 1262 (1964).

irradiated consists of a preliminary pumping of 600 ml. of solution in a 1000-ml. evacuation chamber. This solution is then saturated with helium (or argon) and re-evacuated. By this procedure, the oxygen and carbon dioxide concentrations are reduced to less than 10^{-7} M and 10^{-6} M, respectively. Before the syringes are filled with the deaerated solution, they are purged with helium several times in order to remove air.[5,9,10] Since a small amount of helium remains in the syringe, the initial 10 ml. of solution introduced into the syringes is expelled with the remaining bubble of helium. In this way, completely filled syringes of the stock solution, usually triply distilled water or 0.01 N sodium hydroxide, are prepared. Solutions at the desired concentration are obtained by adding helium-purged concentrated solutions to the oxygen-free stock solutions described above. For added volumes in the range from 0.05 to 1.0 ml., the helium-purged solution is injected through the capillary tip of the syringe shown in Fig. 1a by means of a microsyringe

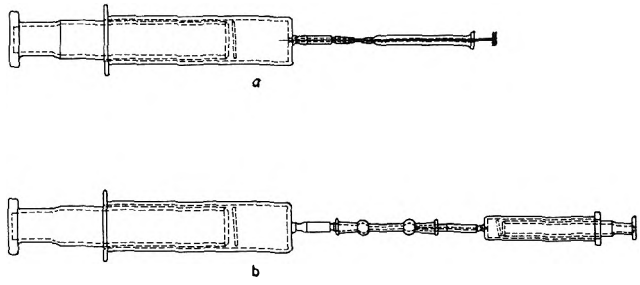

Figure 1. Syringes for sample preparation and dilution.

provided with a very fine Teflon capillary tube. The technique used for larger volumes, particularly for volatile solutes, is shown in Fig. 1b. The solution in the smaller syringe is purged by adding helium to the solution in the syringe, then shaking and expelling the gases. This procedure, repeated four times, reduces the oxygen concentration in the solution to less than 10^{-6} M. The solution was then transferred through a capillary tube (see Fig. 1b) into the larger syringe. Flat glass plates of about 1-ml. volume were present in the large syringes and permitted thorough mixing of the solution by repeated inversions of the syringe. Dilutions, too, were carried out by transferring the degassed solution into the appropriate volume of the concentrated solution in 50- or 100-ml. syringes used to supply solution to the irradiation cell. The technique of introducing and removing these solutions from the irradiation cell is identical with the method described elsewhere.[5]

In general, reagent-quality chemicals were used without further purification. The gases were condensed in a liquid nitrogen or carbon dioxide trap, evacuated further, and then the solution was prepared by saturation of the solution at a pressure of 1 atm. or less. For compounds with rate constants of the order of 10^{10} M^{-1} sec.$^{-1}$, purity is of lesser importance than for compounds with rate constants in the range below 10^{9} M^{-1} sec.$^{-1}$. Consequently, the rate constants given in Table I are more reliable for the group above 10^{9} M^{-1} sec.$^{-1}$. Methanol was used as a solvent in many experiments in order to prepare stock solutions, particularly of the more volatile and water-insoluble chemicals. Solutions of volatile chemicals such as chloroform, carbon tetrachloride, carbon disulfide, benzene, styrene, and nitrobenzene were prepared in the following way: helium-purged solutions of these pure chemicals were injected directly into 10-ml. syringes of deaerated methanol. The final solution was then made by the injection of the required amount of this solution into a syringe of previously deaerated water. For the more insoluble and less reactive compounds, this procedure frequently gave a solution high in methanol concentration; and for this reason methanol solutions above 0.01 M were occasionally used. However, methanol at this concentration and even in concentrations up to 1 M has little or no effect on rate-constant measurements. This low reactivity of methanol is further supported by the results of Taub, Sauer, and Dorfman, who showed that the electron solvates in pure methanol.[11]

Discussion of Results

Our hydrated electron rate constants were measured either in neutral solution containing methanol or in alkaline solutions at pH 12 or greater. The results are presented in Table I. In both cases methanol was usually added in order to eliminate the reactions of the hydrated electron with the hydroxyl radical and hydrogen atoms. These free radicals are very reactive with e_{aq}^- while the resulting CH_2OH radical is relatively unreactive.[2] Alkaline solutions were used in order to neutralize hydrogen ions formed in the "spur" and thereby eliminate the reaction

$$e_{aq}^- + H^+ \longrightarrow H$$

The effect of added methanol and alkali can be deduced from the slope of the hydrated electron decay curves

(9) C. Senvar and E. J. Hart, *Proc. 2nd Intern. Conf. Peaceful Uses At. Energy, Geneva*, **29**, 19 (1959).

(10) A. R. Anderson and E. J. Hart, *J. Phys. Chem.*, **66**, 70 (1962).

(11) I. A. Taub, M. C. Sauer, Jr., and L. M. Dorfman, *Discussions Faraday Soc.*, **36**, 1 (1963).

Table I: Hydrated Electron Rate Constants of Organic Compounds

Compound	Concn., mM	CH_3OH, mM	pH	Slope[a] × 10^{-5}	k,[a] M^{-1} sec.$^{-1}$
Aliphatic					
Acetaldehyde	0.10	...	6.55	1.5	3.5×10^{9}[b]
Acetone	0.20	...	7[c]	4.95	5.9×10^{9}
	0.06	...	7[c]	1.60	
Acrylamide	0.10	...	7.0	7.84	1.8×10^{10}
Butadiene	0.144	1.0	7[c]	5.0	8×10^{9}
Carbon disulfide	0.20	6.0	7.7	25.0	3.1×10^{10}
	0.05	2.25	...	7.1	
Carbon tetrachloride	0.060	16.2	7[c]	8.2	3.0×10^{10}
	0.066	1.0	7[c]	8.0	
Chloroform	0.033	1.0	7[c]	4.38	3.0×10^{10}
L-Cystine	0.10	1.0	12.0	1.48	3.4×10^{9}
Fumarate ion	0.133	1.0	13	4.65	7.5×10^{9}
Maleate ion	0.455	1.0	8.45	3.35	1.7×10^{9}
	0.020	1.0	12.7	1.9	2.2×10^{9}
Maleic acid	0.021	...	6.5	1.0	1.2×10^{10}
Methacrylate ion	0.2	1.0	10.1	7.4	8.4×10^{9}
	0.1	1.0	10.1	3.2	7.2×10^{9}
Pyruvate ion	0.2	1.0	12.7	5.95	6.8×10^{9}
Tetracyanoethylene	0.10	...	7[c]	4.8	1.5×10^{10}
Thiourea	0.10	...	6.41	1.25	2.9×10^{9}
Trichloroacetate	0.111	...	10.7	2.27	6.2×10^{9}
	0.037	...	~10	1.26	
Aromatic					
Aniline	10	1.0	11.94	0.80	$<2 \times 10^{7}$
Benzene	20	...	7[c]	0.6	$<7 \times 10^{6}$
Benzoquinone	0.50	1.0	6.6	2.73	1.25×10^{9}
Hydroquinone	2.0	1.0	13	0.08	$<10^{7}$
Naphthalene	0.5	...	7[c]	6.8	3.1×10^{8}
β-Naphthol	1.0	1.0	11	7.2	
	1.0	1.0	11	7.8	1.8×10^{9}
	1.0	1.0	11	8.1	
Nitrobenzene	0.02	...	7[c]	2.35	3.0×10^{10}
	0.01	...	7[c]	1.3	
Phenylalanine	1.0	...	11	0.29	$<10^{7}$
Phthalate ion	0.50	1.0	12.8	4.3	2.0×10^{9}
Picric acid	0.10	1.0	13	12.6	3.5×10^{10}
	0.333	1.0	13	4.65	
	0.01	...	5.36	1.6	3.9×10^{10}
Styrene	0.13	1.0	12.7	5.96	1.1×10^{10}
	0.089	...	7[c]	5.75	1.5×10^{10}
Heterocyclic					
Adenosine	0.02	1.0	12.0	0.9	1.0×10^{10}
Cytidine	0.02	1.0	12.0	1.0	1.2×10^{10}
Hypoxanthine	0.02	...	6.6	1.46	1.7×10^{10}
5-Methylcytosine	0.02	...	7.72	0.89	1.0×10^{10}
Orotic acid	0.02	...	6.56	1.3	1.5×10^{10}
Purine	0.33	...	7.2	2.1	1.7×10^{10}
Pyridine	1.0	...	7.3	0.38	1.0×10^{9}
	0.33	...	6.9	0.17	
Thymine	0.020	...	6.0	7.4	1.7×10^{10}
	0.200	1.0	12.0	2.35	2.7×10^{9}
Uracil	0.100	...	12.2	0.97	2.3×10^{9}
	0.033	...	6.4	1.1	7.7×10^{9}

[a] Slope, $\Delta \log D/\Delta t$, of the first-order plot of log of the optical density (D) *vs.* time, $k = 2.3\Delta \log D/\Delta t \times 1/C_0$ where C_0 = concentration of solute. [b] Unhydrated acetaldehyde = 0.64[CH_3CHO], $k = 5.4 \times 10^{9}$ M^{-1} sec.$^{-1}$. [c] Unbuffered, pH not measured.

in pure water, in 1 mM methanol, and in 0.01 N sodium hydroxide with methanol added. The decay curves of these solutions follow first-order kinetics indicating that the principal mode of hydrated electron disappearance is by reaction with the water. First-order kinetics prevail at hydrated electron concentrations of the order of 10^{-6} M when the solute is present at concentrations above about 2.0×10^{-5}. The second-order rate constants are then determined by dividing the first-order rate constant by the concentration of solute. The slopes of the log D_0/D curves vary from $3–5 \times 10^{4}$ sec.$^{-1}$ for 1 mM methanol to $1.4–1.8 \times 10^{4}$ sec.$^{-1}$ in the 0.01 N sodium hydroxide solution. Consequently, solutes with decay curves with slopes in these ranges demonstrate low reactivity, and reliable rate constants cannot be obtained.

Unreactive Compounds

As a general rule saturated organic compounds containing carbon, hydrogen, and oxygen are either unreactive toward e_{aq}^- or show low reactivity. For example, methane, methanol, and diethyl ether are unreactive. This low reactivity is also found in the ions of the saturated acids such as formic, acetic, and succinic acids. Ethyl acetate also is unreactive. The acids however do possess low reactivity, probably because of the reaction

$$RCOOH + e_{aq}^- \longrightarrow RCOO^- + H$$

Saturated amino acids, too, are unreactive having rate constants of less than 10^{7} M^{-1} sec.$^{-1}$ in the series: glycine, alanine, phenylalanine, glycylglycine, L-histidine, serine, DL-tyrosine, and threonine. Unreactive, too, are unsaturated compounds including aromatic derivatives such as ethylene, benzene, aniline, and hydroquinone. However, since the solubility of the compound is limited as in the case of benzene and ethylene, only relatively reactive compounds can be measured with any certainty.

Reactive Compounds

Aldehydes and Ketones. Ketones, halogenated hydrocarbons, and halogenated acids are well-known e_{aq}^- scavengers.[12–15] The reaction of e_{aq}^- with acetone has been studied by Riesz,[13] who finds relatively high yields of 2-propanol in acetone–1-propanol solutions. Here 1-propanol, inert to e_{aq}^-, and reactive with hydrogen atoms and hydroxyl radicals eliminates the H and OH reactions with acetone. 2-Propanol is a hydrogen-atom donor to the isopropoxy free

(12) J. T. Allan and G. Scholes, *Nature*, **187**, 218 (1960).

(13) P. Riesz, *Radiation Res. Suppl.*, **4**, 152 (1964).

(14) E. Hayon and J. Weiss, *Proc. 2nd Intern. Conf. Peaceful Uses At. Energy, Geneva*, **29**, 80 (1958).

(15) E. Hayon and A. O. Allen, *J. Phys. Chem.*, **65**, 2181 (1961).

radical formed by e_{aq}^-. The mechanism of isopropoxy radical formation is

$$CH_3COCH_3 + e_{aq}^- \longrightarrow CH_3\dot{C}(O^-)CH_3$$

and

$$CH_3\dot{C}(O^-)CH_3 + H^+ \longrightarrow CH_3\dot{C}(OH)CH_3$$

The rate constant for the reaction with acetone is $5.9 \times 10^9\ M^{-1}$ sec.$^{-1}$ (see Table I).

Acetaldehyde in its unhydrated form is as effective as acetone in reactions with e_{aq}^-. Correcting for the hydrated form from the data of Bell and Cluine[16] the rate constant, $k_{(e_{aq}^- + CH_3CHO)}$, is $5.4 \times 10^9\ M^{-1}$ sec.$^{-1}$ compared with the acetone value of $5.9 \times 10^9\ M^{-1}$ sec.$^{-1}$. Hydration of the carbonyl group in formaldehyde is complete and this compound suppresses the hydrated electron reaction completely. The above reactions show one general type of hydrated electron reaction, namely, its addition to an unsaturated group forming a negative radical ion. The general reaction is

$$RCOR + e_{aq}^- \longrightarrow R\dot{C}(O^-)R$$

Halogen Compounds.—The second general reaction is one where detachment of a negative ion occurs. This is illustrated by the work of Hayon and Weiss[14] and Hayon and Allen[15] on monochloroacetic acids.

$$ClCH_2COOH + e_{aq}^- \longrightarrow Cl^- + CH_2COOH$$

In general, chlorine compounds such as chloroform and carbon tetrachloride and chloroacetic acid have rate constants of the order of $3 \times 10^{10}\ M^{-1}$ sec.$^{-1}$ (see Table I).

Conjugated Compounds. Conjugation involving carbon–carbon double bonds with C=C, C=O, or CN are reactive. Butadiene with a rate constant of $8 \times 10^9\ M^{-1}$ sec.$^{-1}$ is much more reactive than ethylene, but styrene with a rate constant of $1.5 \times 10^{10}\ M^{-1}$ sec.$^{-1}$ shows much greater reactivity than benzene. Acrylamide, too, has a high rate constant as expected from its excellent scavenging action.[17]

The unconjugated carboxyl group in formic and acetic acids[2] does not react. Unsaturated acids such as maleic and fumaric, by comparison with succinic, are also reactive. A similar high reactivity is found in phthalic acid and benzoquinone. In general, negative groups such as COOH, halogens, and NO_2 on the aromatic nucleus are very reactive. Miscellaneous groups such as C=S, —S—S—, and —O—O— in molecules are also highly reactive. For example, high rate constants are found for carbon disulfide, cystine, hydrogen peroxide, and perdisulfuric acid.

Heterocyclic Compounds. While the aromatic nucleus is of low reactivity as in benzene, hydroquinone, and phenylalanine (see Table I), the heterocyclic pyrimidine and purine bases show high reactivity. A few compounds representative of the units in nucleic acid with rate constants varying from 2.4×10^9 to $1.7 \times 10^{10}\ M^{-1}$ sec.$^{-1}$ are given in Table I. In general, rate constants are lower for the ionized forms of these molecules in alkaline solution than they are in neutral solution. Because of the low reactivity of the hydrated electron with amino acids, it is very likely that the primary mode of attack of e_{aq}^- is on the nucleic acid rather than on the proteins. However, because the disulfide linkage is also reactive it is possible that this group, too, is affected in proteins.

The rate constants given in Table I are measured by the decay of the hydrated electron spectrum and provides a direct measure of the reactivity of the compound being studied. In some compounds, new transient spectra appear that may be derived from the formation of the negative ion of the organic compound or by a free radical. Much remains to be done in order to determine the products resulting from the direct interaction of the hydrated electron with organic compounds. We propose to study these reactions by irradiating the organic compounds in alkaline solution at high hydrogen pressures. Under these conditions hydroxyl radicals as well as hydrogen atoms are converted into hydrated electrons by the reactions

$$OH + H_2 \longrightarrow H + H_2O$$

$$H + OH^- \longrightarrow e_{aq}^- + H_2O$$

Even the molecular hydrogen peroxide can be converted into hydrated electrons after first forming a hydroxyl radical by the reaction

$$e_{aq}^- + H_2O_2 \longrightarrow OH + OH^-$$

By working at suitably low concentrations of the organic molecules the hydrogen atoms, hydroxyl radicals, and hydrogen peroxide eventually form hydrated electrons. With this system it is hoped that the complex array of irradiation products normally found in radiation chemistry can be avoided.

Acknowledgment. We wish to acknowledge the technical assistance of Miss P. Walsh and the helpful cooperation of the entire accelerator crew, particularly Messrs. B. E. Clifft and E. R. Backstrom, for operating the Linac.

(16) R. P. Bell and J. C. Cluine, *Trans. Faraday Soc.*, **48**, 439 (1952).

(17) E. Collinson, F. S. Dainton, and G. S. McNaughton, *ibid.*, **53**, 357 (1957).

Carbon Isotope Effects in the Pyrolytic Decomposition of Zinc Oxalate

by Peter E. Yankwich and Petros D. Zavitsanos

Noyes Laboratory of Chemistry, University of Illinois, Urbana, Illinois *(Received February 5, 1964)*

The C^{13} isotope fractionation in the pyrolytic decomposition of anhydrous zinc oxalate (prepared from the dihydrate precipitating upon admixture of solutions of zinc nitrate and sodium oxalate) has been studied as a function of temperature. Between 282 and 500°, the intramolecular isotope effect observed at complete reaction falls from 0.79 to 0.36%, thus exhibiting normal magnitude and temperature dependence (the lead and manganous oxalate systems serving for comparison). *Ab initio* calculations of the intramolecular isotope effect *via* the Wilson–Johnston method, and employing a three-particle model C–O–Zn, replicate the experimental results well. In one experiment at 300°, the intramolecular and both the intermolecular isotope effects were measured for 0–2% and 2–4% decomposition. The intramolecular isotope effects at complete and partial decomposition are the same, as expected for this type of zinc oxalate. The pattern of intermolecular isotope effects is the same as observed in the manganous oxalate pyrolysis (dependent upon degree of decomposition) and may afford a useful probe for elucidation of mechanisms operating in early stages of such crystal decompositions.

Introduction

This paper is a report on experiments designed to establish the magnitude and temperature dependence of the C^{13} isotope effects in the pyrolysis of anhydrous zinc oxalate. The kinetics and stoichiometry of the decomposition were subjects of an earlier report from this laboratory.[1] The current study is the third in a series on isotope effects in thermal decompositions of metal oxalates, the previous investigations having dealt with the anhydrous salts of lead[2] and manganese.[3]

Experimental

Preparation of Zinc Oxalate Dihydrate. Aqueous solutions of equal volume of 0.10 *M* zinc nitrate and of 0.11 *M* sodium oxalate[4] (reagent grade chemicals in deionized water) were brought to their boiling points and the former added rapidly to the latter; the mixture was stirred occasionally as it cooled to room temperature. The precipitate is rather fine (particle size 20–25 μ), and uniform in dimension. The crystals were washed several times with distilled water, air-dried for 2–3 hr. at 110°, and stored over magnesium perchlorate in a desiccator.

Apparatus and Procedure. The thermal decomposition apparatus and the procedures employed in both the kinetics and the isotope fractionation studies have been described in detail in an earlier publication from this laboratory.[1] It is important to recall here the fact that each sample of anhydrous zinc oxalate was prepared from the dihydrate just before being brought to the decomposition temperature and in the decomposition apparatus. The sample size in the complete pyrolysis runs was approximately 0.25 mmole; in the single experiment where it was only partially decomposed, the sample consisted of 3.0 mmoles of zinc oxalate.

Isotope Analyses. Carbon isotope analyses were carried out with a Consolidate-Nier isotope-ratio mass spectrometer; the analytical procedures and methods for correcting the raw output data have been described in earlier publications from this laboratory.[2,5]

(1) P. E. Yankwich and P. D. Zavitsanos, *J. Phys. Chem.*, **68**, 457 (1964).

(2) P. E. Yankwich and J. L. Copeland, *J. Am. Chem. Soc.*, **79**, 2081 (1957).

(3) P. E. Yankwich and P. D. Zavitsanos, *Pure Appl. Chem.*, in press.

(4) Preparations of zinc oxalate are designated A when precipitated by oxalic acid, C when precipitated by sodium oxalate. The two types of solids may exhibit different kinetic and isotope effect behavior.[3]

(5) P. E. Yankwich and R. L. Belford, *J. Am. Chem. Soc.*, **75**, 4178 (1953); *ibid.*, **76**, 3067 (1954).

Notation and Calculations. Isotope effects in oxalate decompositions are reported conveniently in the notation of Lindsay, McElcheran, and Thode[6]

$$\left.\begin{matrix} C^{12}OO^- \\ | \\ C^{12}OO^- \end{matrix}\right\} \xrightarrow{k_1} C^{12}O_2 + C^{12}O$$

$$C^{13}OO^- \xrightarrow{k_2} C^{13}O_2 + C^{12}O$$

$$\left.\begin{matrix} C^{12}OO^- \\ | \\ C^{12}OO^- \end{matrix}\right\} \xrightarrow{k_3} C^{12}O_2 + C^{13}O$$

Let α_0 be the mole fraction of C^{13} in carbon dioxide obtained from the combustion of the original zinc oxalate, $(X_d)_t$ be that in the carbon dioxide collected up to time t, and $(X_m)_t$ be that of carbon dioxide obtained by combustion of carbon monoxide produced up to time t. It can be shown that

$$\frac{k_2}{k_3} = \frac{(X_d)_t}{(X_m)_t} \qquad (1)$$

that is, this ratio of isotopic rate constants results from the indicated quotient of mole fractions for any time t, any degree of decomposition, and, therefore, any increment of decomposition. Further

$$\frac{k_1}{2k_2} = \frac{\alpha_0}{(X_d)_0} \qquad (2)$$

and

$$\frac{k_1}{2k_3} = \frac{\alpha_0}{(X_m)_0} \qquad (3)$$

where the subscript zero denotes, rigorously, the limit of zero time or infinitesimal degree of pyrolysis; practically, these equations yield results valid within limits imposed by the mass spectrometry if the products are collected up to about 5% reaction.[7,8] In later tabulations, use will be made of two additional quantities: α' is the calculated mean of X_m and X_d for the increment 0–2% decomposition; and α'' is that calculated mean for the increment 2–4% decomposition. One would expect $\alpha' = \alpha''$.

Results

Complete decomposition isotope effect measurements were obtained at eight temperatures between 282 and 500°; values of $(k_2/k_3)_{obsd}$ for each run are listed in Table I. The computed average values of this rate constant ratio is shown in the last column of the table, the appended errors being average deviations from the mean; the mean precision of individual $(k_2/k_3)_{obsd}$ values is estimated to be ±0.0003. Values of $L(k_2/k_3) = 100 \ln (k_2/k_3)$ calculated from the last column of Table I are plotted *vs.* $\theta = (1000/T)$ in Fig. 1; the open

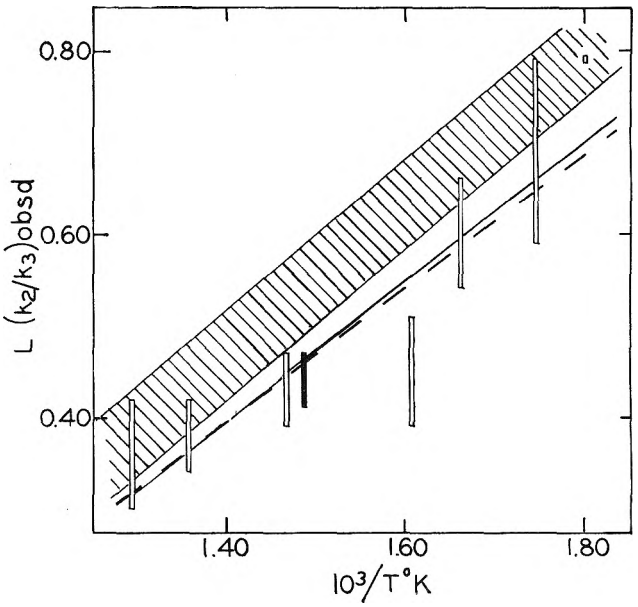

Figure 1. Influence of temperature on intramolecular carbon isotope effect. – – – –, eq. 4, ZnC_2O_4; ———, eq. 5, ZnC_2O_4; shaded band, MnC_2O_4.[3]

rectangles encompass the average deviations, while the solid rectangle for the single run at 400° has a length equal to the estimated mean precision of a single datum. The dashed and solid lines, respectively, are obtained from least-squares fitting of the data to equations of the form

$$L(k_2/k_3)_{obsd} = M_1\theta + B_1 \qquad (4)$$

and

$$L(k_2/k_3)_{obsd} = M_2\theta^2 + B_2 \qquad (5)$$

A single partial decomposition experiment was carried out at 300°; product gases were collected for the first 2% and the second 2% reaction. In Table II are collected the various C^{13} mole fractions observed and isotopic rate constant ratios calculated for the two parts of this experiment. The results are compared with those obtained with manganous oxalate, as are the values of the M's and B's for eq. 4 and 5, and several other quantities. The mean deviations of the experimental points from the least squares fitted (4) and (5) are ±0.06 in L, or approximately 12% of the average isotope effect observed.

The average value of the ratio CO_2/CO for the product gases from the pyrolysis of anhydrous zinc oxalate

(6) J. G. Lindsay, D. E. McElcheran, and H. G. Thode, *J. Chem. Phys.*, **17**, 589 (1949).

(7) J. Bigeleisen, *Science*, **110**, 14 (1949).

(8) J. Y.-P. Tong and P. E. Yankwich, *J. Phys. Chem.*, **61**, 540 (1957).

Table I: Observed Intramolecular Isotope Effects in the Pyrolysis of Zinc Oxalate: $(\alpha_0)_C \times 10^6 = 10692 \pm 4$

Temp., °C.	$(X_d) \times 10^6$	$(X_m) \times 10^6$	$(k_2/k_3)_{obsd}$	Av. $(k_2/k_3)_{obsd}$
282	10725	10641	1.0079	
	10723	10639	1.0079	1.0079 ± 0.0000
300	10717	10659	1.0054	
	10728	10658	1.0065	
	10728	10639	1.0084	
	10716	10638	1.0073	1.0069 ± 0.0010
330	10731	10660	1.0067	
	10714	10654	1.0056	
	10737	10684	1.0050	
	10729	10666	1.0059	
	10730	10656	1.0069	1.0060 ± 0.0006
350	10707	10654	1.0050	
	10707	10669	1.0036	
	10711	10666	1.0042	
	10709	10660	1.0046	
	10707	10667	1.0037	
	10711	10656	1.0052	
	10709	10651	1.0054	1.0045 ± 0.0006
400	10722	10675	1.0044	...
410	10709	10666	1.0040	
	10705	10665	1.0038	
	10718	10663	1.0052	
	10707	10664	1.0040	
	10711	10665	1.0043	1.0043 ± 0.0004
465	10704	10665	1.0037	
	10700	10657	1.0040	
	10698	10659	1.0037	
	10709	10675	1.0032	
	10715	10666	1.0046	1.0038 ± 0.0004
500	10707	10669	1.0036	
	10696	10660	1.0034	
	10701	10675	1.0024	
	10705	10659	1.0043	
	10707	10661	1.0043	1.0036 ± 0.0006

was found to be 1.10 ± 0.02 in earlier experiments[1] over approximately the range of temperatures encompassed by the results in Table I; there was no sensible temperature dependence of this ratio. The astoichiometry of the pyrolysis evidently is small, and no correction for its possible effect was made because the mechanism for the effect is unknown.

Discussion

The kinetics of the zinc[1] and manganous[3] oxalate pyrolyses exhibit an acceleratory phase, lasting only for the first 5–10% decomposition, followed by a decay period in which the rate is approximately first order. A- and C-type samples[4] of manganous oxalate displayed the same gross kinetic characteristics, but very

Table II: Comparison of Isotope Effects Observed in Pyrolyses of Manganous[3] and Zinc Oxalates

	MnC_2O_4	ZnC_2O_4
$(\alpha_0)_C \times 10^6$	10691 ± 3	10692 ± 4
A. Partial Decomposition at 300°		
First 2% reaction		
$(X_d) \times 10^6$	10648 ± 55	10671
$(X_m) \times 10^6$	10567 ± 55	10591
$(\alpha') \times 10^6$	10608 ± 55	10631
$(k_2/k_3)_{obsd}$	1.0076 ± 0.0010	1.0076
$(k_1/2k_3)_{obsd}$	1.0117 ± 0.0052	1.0095
$(k_1/2k_2)_{obsd}$	1.0041 ± 0.0052	1.0020
Second 2% reaction		
$(X_d) \times 10^6$	10737 ± 7	10717
$(X_m) \times 10^6$	10658 ± 3	10639
$(\alpha'') \times 10^6$	10697 ± 5	10678
$(k_2/k_3)_{obsd}$	1.0074 ± 0.0005	1.0073
$(k_1/2k_3)_{obsd}$	1.0031 ± 0.0003	1.0050
$(k_1/2k_2)_{obsd}$	0.9957 ± 0.0007	0.9977
B. Complete Decomposition Experiments		
M_1	0.844 ± 0.076	0.722 ± 0.091
B_1	−0.717 ± 0.117	−0.612 ± 0.141
M_2	0.263 ± 0.026	0.240 ± 0.029
B_2	−0.061 ± 0.062	−0.076 ± 0.070
$(X_d + X_m)/2$(no. of experiments)	10685 ± 4 (6)	10687 ± 5 (34)

different isotope fractionation effects; $(k_2/k_3)_{obsd}$ was normal in magnitude and temperature dependence in the pyrolysis of C-type samples, but enormous in both respects when A-type samples were decomposed. No simple explanation for these observations is available.

The results shown in Table I indicate a carbon isotope effect of small magnitude and normal temperature dependence for the thermal decomposition of C-type samples of zinc oxalate. The comparison figures in part B of Table II indicate that the manganous and zinc oxalate complete decomposition isotope effects are very similar, those for zinc oxalate being somewhat the smaller.

The data shown in part A of Table II illustrate the detailed similarity of the partial decomposition isotope effects for the two salt pyrolyses. Note that the intermolecular isotopic rate constant ratios $(k_1/2k_3)_{obsd}$ and $(k_1/2k_2)_{obsd}$ not only are both significantly different from $(k_2/k_3)_{obsd}$ but also exhibit dependence upon the degree of reaction. (Significant dependence upon degree of pyrolysis is not expected below 5–6% decomposition.[7,8]) In this regard it is important to compare α_0, α', and α''; α'' and α_0 are very similar, while α' is definitely smaller. This may be an indication that isotopically *lighter* microcrystals of oxalate

yield a large fraction of the initial gaseous products collected. In such a situation, the intramolecular *isotopic rate constant ratio* $(k_2/k_3)_{obsd}$ *is consistently* defined by eq. 1, but α_0 in eq. 2 and 3 should perhaps be replaced by some other quantity; it is not obvious that the appropriate replacement is α' or α'', depending upon the segment of decomposition observed.

These considerations lead us to the conclusion that only $(k_2/k_3)_{obsd}$ from the present experiments can be treated even approximately by current isotope effect theory.

Ab initio calculation of the intramolecular isotope effect. In general, we can write

$$(k_2/k_3) = (\text{TDF})(\text{TIF}) \qquad (6)$$

TIF is the ratio (ν_{2L}/ν_{3L}) of the imaginary vibration frequencies associated with the reaction coordinate; TDF, the temperature-dependent factor, arises in the mass dependence of the genuine vibrations of the normal and transition-state species. The small size of the intramolecular isotope effect and its moderate temperature dependence indicate that TIF is nearly unity, *i.e.*, that the contribution of the reaction coordinate to the observed isotope fractionation is small.

Equations 4 and 5 are of the form $L(k_2/k_3) = L(\text{TDF}) + L(\text{TIF})$. The dependence of $L(k_2/k_3)$, or L(TDF), on temperature is expected to be as $1/T$ at "low" temperatures and as $1/T^2$ at "high" temperatures. These being extremal situations, it seems likely that B_1 represents a minimum value for L(TIF), and B_2 a maximum. Since temperatures a hundred degrees on either side of 400° are relatively high (at least for stretching vibrations of systems like Zn–O–C, O–C–C, etc.) in the case of a metal oxalate, it seems likely that B_2 should be a good approximation to L(TIF). As inferred in the paragraph above, B_2 is close to zero.

Examination of the intramolecular isotope effect using the "γ-bar" method of Bigeleisen and Wolfsberg[9] suggests that a good approximation to the reaction coordinate is an asymmetric stretching vibration involving at least three centers, such as O–C–O or C–O–Zn.

The three-particle system C–O–Zn was investigated, vibration frequencies being obtained by matrix methods.[10] The asymmetric stretching vibration was taken as the reaction coordinate, and the frequency associated with this motion was driven to zero in the activated complexes by setting the bond-stretching force constants equal to each other and to an interaction force constant, f_i, as suggested by Johnston, Bonner, and Wilson.[11] The input parameters for this calculation and the results are shown in Table III.

Table III: C–O–Zn, Isotope Effect Calculated by Wilson–Johnston Method ($m_1 = 12$, $m_2 = 16$, $m_3 = 65.4$, $m'_1 = 13$, $m'_2 = 16$, $m'_3 = 65.4$

Normal Molecules

$r_{12} = 1.38$ Å.; $r_{23} = 1.87$ Å.; $\phi = 180°$
$f_{12} = 6.0$ mdynes/Å.; $f_{23} = 3.0$ mdynes/Å.;
$f_\varphi/r_{12}r_{23} = 1.0$ mdyne/Å.

Activated Complexes

$r_{12} = 1.47$ Å.; $r_{23} = 1.87$ Å.; $\phi = 180°$
$f_{12} = f_{23} = f_i = 4.0$ mdynes/Å.; $f_\varphi/r_{12}r_{23} = 0.25$ mdyne/Å.
Reaction coordinate: $Q = (q_{12}/\sqrt{2}) - (q_{23}/\sqrt{2})$

Results

	Calculated	Observed: eq. 5
L(TIF)	0.105	-0.076 ± 0.070
L(TDF) at 282°	0.800	0.779 ± 0.094
at 500°	0.448	0.401 ± 0.049

The agreement for TDF is satisfactory, but the calculated TIF is high. For this model, which is more successful than any other three-particle system studied, a better TIF is secured at the cost of any correspondence between the observed and calculated temperature dependence, a result hardly to be desired. Especially since this model requires $(k_1/2k_2) = 1$, a more complicated system apparently would have to be devised were better agreement between calculation and experiment desired. Even so, it is striking that an approach which assumes essentially an ideal gas system yields such good results when applied to the decompositions of crystals.

It appears that the intermolecular isotope effects in the zinc oxalate pyrolysis may provide a useful probe for details of the mechanism of the early stages of the decomposition. Even when anomalous observations on the intramolecular isotope effect are absent, the intermolecular isotope effects appear to depend in a complicated manner on the degree of decomposition.

Additional experimentation on this and similar systems is in progress in this laboratory.

Acknowledgments. We are indebted to Dr. Geneva Belford for generous assistance in programming certain of the theoretical calculations, and to Mrs. Eula Ihnen for all mass spectrometric analyses.

This research was supported by the United States Atomic Energy Commission.

(9) J. Bigeleisen and M. Wolfsberg, *Advan. Chem. Phys.*, **1**, 15 (1958).

(10) E. B. Wilson, Jr., J. C. Decius, and P. C. Cross, "Molecular Vibrations," McGraw-Hill Book Co., Inc., New York, N. Y., 1955.

(11) H. S. Johnston, W. A. Bonner, and D. J. Wilson, *J. Chem. Phys.*, **26**, 1002 (1957).

Lifetime of Activated Platinum Surface

by William G. French and Theodore Kuwana

Department of Chemistry, University of California, Riverside, California (*Received January 25, 1964*)

The electrochemical reduction of preoxidized platinum electrodes produced a surface state that exhibited decreased "activity" toward the prewave of adsorbed hydrogen with time. The half-life of this activated surface state was of the order of 46 min. The ratio of coulombs for platinum oxidation compared to the hydrogen prewave gave for m in $Pt^*\cdots(H_2)_m$ (adsorbed) a value of 0.3, where Pt* designates the activated platinum.

Introduction

Various pretreatment methods have been employed to "activate" a platinum surface where the activation supposedly produced an enhancement in the reversibility of the electrode reaction. Attempts have been made to explain this phenomenon of activation in terms of the chemical and physical nature of the platinum surface. Lingane[1] and Sawyer and Interrante[2] for example have observed the necessity of preoxidizing the electrode prior to the reduction of oxygen and have proposed a mechanism which involved platinum oxide. Others, notably Anson,[3,4] Anson and King,[5] and Davis[6] have studied the effect of oxide on the reversibility of electrode reactions at platinum. An oxide bridge-type mechanism has been invoked[6-8] to explain the increased activity associated with a preoxidized platinum electrode, but Anson and King's results do not support this contention.

The activity of platinum electrodes in relation to surface structural changes has been studied by Shibata.[9-11] On the basis of visible "coarsening" of the surface by alternating current electrolysis[9,10] and of decreased rates of activity in terms of hydrogen overpotential associated with varying pretreatment times,[11] Shibata had concluded that when an electrode was oxidized and then reduced, a thin layer of unstable atoms was formed. The high activity was due to the presence of these unstable surface platinum atoms whose rate of crystallization was apparently slow.[11,12] Anson[4,8] and Anson and King[5] on the basis of the similarity in behavior between a preoxidized and reduced electrode and a chemically platinized electrode concluded that the electrochemical reduction of oxide formed a thin platinized surface which accounted for the enhanced activity. The platinized surface would be the same surface as described by Shibata[11] and Bonnemay,[12] and henceforth will be designated as Pt*.

The overpotential for the reduction of proton or water to form hydrogen[13] or the oxidation of hydrogen[11,14] decreased when a preoxidized and subsequently either electrochemically or chemically reduced electrode was used. On the reduction a small prewave occurred immediately before the hydrogen evolution. This prewave has been interpreted as being due to adsorbed hydrogen on the platinized surface.[4,14,15] The possibility of more than one form of adsorbed hydrogen to produce fine structure on the prewave has been investigated by Franklin and Cooke.[16]

There has been presented evidence that oxygen at

(1) J. J. Lingane, *J. Electroanal. Chem.*, 2, 296 (1961).

(2) D. T. Sawyer and L. V. Interrante, *ibid.*, 2, 310 (1961).

(3) F. C. Anson and J. J. Lingane, *J. Am. Chem. Soc.*, 79, 4901 (1957).

(4) F. C. Anson, *Anal. Chem.*, 33, 934 (1961).

(5) F. C. Anson and D. M. King, *ibid.*, 34, 362 (1962).

(6) D. G. Davis, Jr., *Talanta*, 3, 335 (1960).

(7) I. M. Kolthoff and E. R. Nightingale, *Anal. Chim. Acta*, 17, 329 (1957).

(8) F. C. Anson, *J. Am. Chem. Soc.*, 81, 1554 (1959).

(9) S. Shibata, *J. Chem. Soc. Japan, Pure Chem. Sect.*, 79, 239 (1958).

(10) S. Shibata, *ibid.*, 80, 453 (1959).

(11) S. Shibata, *Bull. Chem. Soc. Japan*, 36, 525 (1963).

(12) M. Bonnemay, *Z. Elektrochem.*, 59, 798 (1955).

(13) L. P. Hammett, *J. Am. Chem. Soc.*, 46, 7 (1924).

(14) D. T. Sawyer and E. T. Seo, *J. Electroanal. Chem.*, 5, 23 (1963) (and pertinent references therein).

(15) R. P. Buck and L. R. Griffith, *J. Electrochem. Soc.*, 109, 1005 (1962).

(16) T. C. Franklin and S. L. Cooke, Jr., *ibid.*, 107, 556 (1960).

platinum exists as a oxide film, while at the same time, the evidence does not preclude the possibility that oxygen is an absorbed film.[17] Feldberg, Enke, and Bricker[18] have studied the anodic and cathodic polarization of a platinum electrode and concluded that the active electrode was the "half-reduced" state.

In this paper the dependence of the number of coulombs consumed in the cathodic and anodic hydrogen prewave will be investigated with respect to the number of coulombs involved in the oxidation and reduction of the platinum oxide, and the variation with the time following activation. The data are consistent with reduction of oxide surface producing Pt*.

Experimental

The experimental arrangement for the chronopotentiometric measurements were conventional in all respects. The triangular wave generator and potentiostat used for cyclic voltammetry were built following the circuit design of Alden, Chambers, and Adams.[19] A Leeds and Northrup Model H Azar strip chart recorder or Electro-Instruments Model 100TB X-Y recorder were used for the current–voltage (CV) traces.

The following additions or changes were made to a previously described[20] special quartz cell: A Leeds and Northrup No. 117136 bridge containing the same solution as in the cell made connection to a commercial Leeds and Northrup calomel electrode which served as the reference electrode; and either platinum wire or planar foil sealed in soft glass tubing were used for the working electrodes. Platinum was obtained from two different sources: Wildberg Bros. Smelting Co., San Francisco, Calif., 99.98% Pt; and Engelhard Industries, Inc., Newark, N. J., 99.989% Pt, (main impurities: Fe 34 p.p.m. and Pd 25 p.p.m.). The bridge and electrodes were sealed to an O-ring top which fitted the cell tightly. All seals were air tight against leakage. The degassing procedure and equipment was previously described.[21]

The areas of the electrodes were evaluated through ferrocyanide oxidation using the diffusion coefficient value[22] of 0.67×10^{-5} cm. sec.$^{-1}$. They compared favorably to the measured geometric areas. The electrodes were stored in 1 F H_2SO_4.

Reagent grade sulfuric acid and sodium or potassium carbonate were used without further purification. Water was redistilled from alkaline permanganate.

Results and Discussion

A platinum foil or wire electrode stored for several hours in a 1 F H_2SO_4 solution exhibits the cyclic CV patterns shown in Fig. 1 and 2 for polarization in

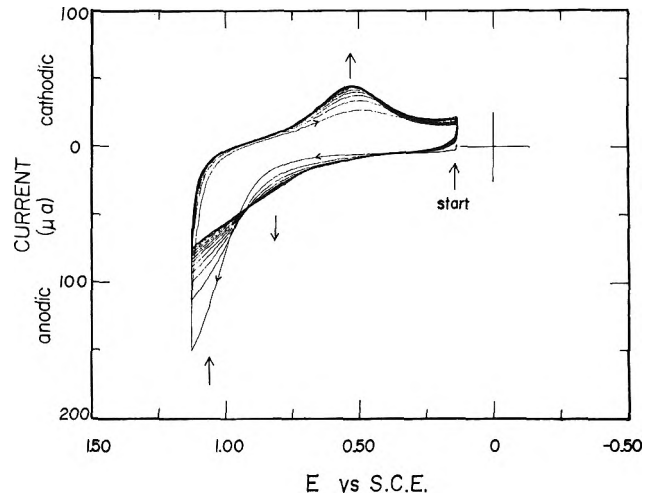

Figure 1. Cyclic scan of platinum electrode in 1 F H_2SO_4. Electrode stored for 24 hr. in 1 F H_2SO_4 prior to scan. Steady-state CV reached after about 10 cycles. (Arrows indicate direction of current change with each scan.) Scan rate is 0.13 v. sec.$^{-1}$.

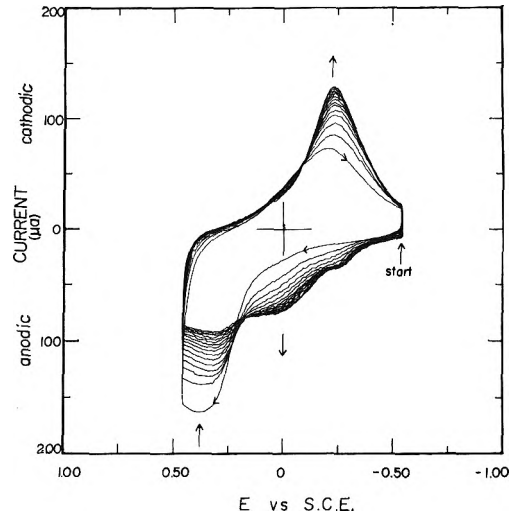

Figure 2. Cyclic scan of platinum electrode in 1 F Na_2CO_3. Electrode stored for 12 hr. in 1 F H_2SO_4 prior to scan. Steady state reached after about 15 cycles. (Arrows indicate direction of current change with each scan.) Scan rate is 0.13 v. sec.$^{-1}$.

(17) M. W. Breiter and J. L. Weininger, *J. Electrochem. Soc.*, **109**, 1135 (1962).

(18) S. W. Feldberg, C. G. Enke, and C. E. Bricker, *ibid.*, **110**, 826 (1963).

(19) J. R. Alden, J. Q. Chambers, and R. N. Adams, *J. Electroanal. Chem.*, **5**, 152 (1963).

(20) J. N. Pitts, Jr., H. W. Johnson, and T. Kuwana, *J. Phys. Chem.*, **66**, 2456 (1962).

(21) T. Kuwana, *Anal. Chem.*, **35**, 1398 (1963).

(22) M. von Stackelberg, M. Pilgram, and V. Toome, *Z. Elektrochem.*, **57**, 342 (1953).

Table I: Coulombs for Oxidation and Reduction at Platinum[a]

Electrode area, cm.²	Solution, 1 *F*	Q_a	Q_c	Q'_c	Q'_a	$T_{0.5}$, min.	$\frac{Q'_a}{Q_a}$	$\frac{Q_c}{Q_a}$	$\frac{Q'_a}{Q'_c}$	$\frac{Q_c + Q'_c}{Q_a + Q'_a}$
5.44	Na_2CO_3	860	718	184	136	52.0	0.158[b]	0.835	0.740	0.906
5.44	H_2SO_4	410	398	147	133	41.5	0.325	0.970	0.905	1.00
5.44	Na_2CO_3	925	758	310	271		0.293	0.820	0.875	0.892
0.81	Na_2CO_3	612	503	205	179		0.342	0.820	0.873	0.894
0.60	Na_2CO_3	1105	987	386	326		0.295	0.895	0.845	0.960
0.60	H_2SO_4	765	666	422	227		0.297	0.870	0.538[b]	1.09
0.10	Na_2CO_3	330	310	925	90	40.0	0.272	0.940	0.973	0.961
0.10	H_2SO_4	570	570	390	338	51.3	0.593[b]	1.00	0.867	1.06
					Av.:	46.2 ± 5.4	0.304 ± 0.20	0.894 ± 0.051	0.868 ± 0.037	0.970 ± 0.050

[a] Scan rate: 0.13 v. sec.$^{-1}$; all values of Q in μcoulombs/cm.². [b] Scan limits: 1 *F* H_2SO_4: Q_a and Q_c, 1.125 to 0.125 v. *vs.* s.c.e.; Q'_a and Q'_c, 0.125 to −0.190. 1 *F* Na_2CO_3: Q_a and Q_c, 0.50 to −0.50 v. *vs.* s.c.e.; Q'_a and Q'_c, −0.50 to −0.85. Omit these values in average.

degassed solutions of 1 *F* H_2SO_4 and 1 *F* Na_2CO_3, respectively. The shape of the polarization curves changes with each cycle until a steady-state pattern is attained. In the basic carbonate solution the steady-state CV patterns are more reproducible from day to day than the sulfuric acid solution. In both cases, however, the number of coulombs consumed in the anodic wave, Q_a, is *ca.* 10% greater than the coulombs, Q_c, consumed in the cathodic portion (see Table I, columns 3 and 4). The values of Q_a and Q_c for a given scan limit of potential appears to be independent of the scan rate between 0.13 and 0.0195 v.-sec.$^{-1}$. Data for basic carbonate solution are summarized in Table II.

If a platinum electrode is cycled as above and then allowed to polarize cathodically, a wave is observed to precede the larger current for the hydrogen evolution. The prewave only appears if the electrode is preoxidized and then reduced and undoubtedly corresponds to the chronopotentiometric prewave previously observed by Anson.[4] The cyclic CV curves for activated electrode in 1 *F* Na_2CO_3 and 1 *F* H_2SO_4 are shown in Fig. 3A and 3B, respectively. The CV curve in acid is closely similar to one shown previously by Buck and Griffith.[15] In carbonate, the potential of the cyclic pattern shifts by *ca.* 0.06 v./pH from the acid and appears similar with the exception of some loss in the fine structure of the prewave. If the direction of the polarization is reversed at the foot of the current for the evolution of hydrogen into solution, an anodic wave, which is essentially a mirror image of the cathodic prewave, is obtained. The number of coulombs for the cathodic prewave, Q'_c, and the anodic wave, Q'_a, are summarized in columns 5 and 6 of Table I. The values of Q'_c and Q'_a appear to be independent of the scan rate (see Table II). The average ratio of $Q'_a:Q'_c$ is 0.868 ± 0.037 for the data in Table I. The inequality between the values of Q_a and Q_c, and Q'_c and Q'_a indicates that all of the oxide is not reduced

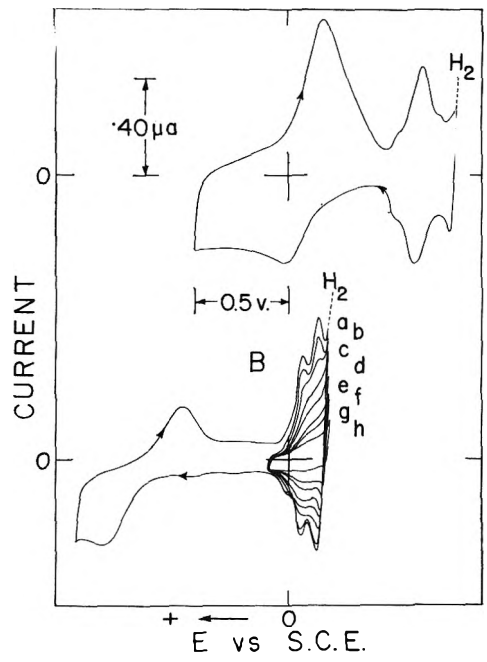

Figure 3. Trace A: Cyclic scan of activated platinum electrode in 1 *F* Na_2CO_3 between the potential limits of +1.125 to −0.190 v. *vs.* s.c.e. Trace B: Cyclic scan of activated platinum electrode in 1 *F* H_2SO_4 between the potential limits of +1.125 to −0.190 v. *vs.* s.c.e. Traces a–g between the potential limits of 0.125 and −0.190 v. *vs.* s.c.e. were taken after intervals of time: 0, 10, 25, 40, 70, 100 and 130 min., respectively. Scan rate: 0.13 v. sec.$^{-1}$.

Table II: Effect of Scan Rate

Scan rate, v. sec.$^{-1}$	Q_a[a]	Q_c	Q'_c	Q'_a	Q'_c, recycle[b]	Q'_a, recycle	$\frac{Q_c + Q'_c}{Q_a + Q'_a}$
0.13	1060	920	386	317	342	334	0.950
0.0625	1140	1000	343	334	342	317	0.912
0.0325	1110	990	402	308	350	325	0.985
0.0195	1130	1050	410	342	360	334	0.990
Av.	1110 ± 30	990 ± 35	385 ± 21	325 ± 13	349 ± 6	328 ± 6	0.960 ± 0.030

[a] Scan of Pt electrode in 1 F Na_2CO_3. All values of Q in μcoulombs/cm.^{2}. [b] Q'_a and Q'_c recycle is coulombs consumed when electrode is cycled once around (scan limits: −0.50 to −0.87 v. *vs.* s.c.e.) the hydrogen prewave after a complete cycle was made around both the oxide and hydrogen prewave (scan limits: +0.50 to −0.87 v. *vs.* s.c.e.).

in the potential region of the main oxide reduction wave but continues into the potential region of the hydrogen prewave. If this is the case, the value of $(Q_c + Q'_c)/(Q_a + Q'_a)$ should approach unity. Experimentally, the average values are 0.97 ± 0.05 and 0.96 ± 0.03 for the data presented in Tables I and II, respectively. If the above reasoning is correct, the value of $Q'_a:Q'_c$ should also approach unity upon each successive cycle if the electrode is cycled only in the potential region of the prewave. Columns 6 and 7 of Table II shows the values of Q'_c and Q'_a for the recycle in the prewave region. The average ratio of $Q'_a:Q'_c$ is 0.94 as compared to 0.85 for the ratio of the first cycle (data: column 4 and 5 of Table II). If the potential is allowed to continued cycling around the prewave region, the values of Q'_a and Q'_c become equal.

Both the oxide and prewave CV curves are independent of solution stirring. When both the oxide and hydrogen prewave CV's are affected by stirring, the solution contains some dissolved oxygen. If only the values of Q'_a to Q'_c are changed by stirring, the potential range being scanned is sufficiently cathodic to evolve hydrogen into the solution. When the value of Q'_a remains constant irrespective of whether or not the solution is stirred and whether hydrogen is evolved in the cathodic portion during stirring, it is an indication that the Pt* is saturated or at a maximum coverage with adsorbed hydrogen. Thus, the reactions involved at the platinum surface consistent with the above results and the conclusions of other workers[4,5,11,14] are

$$PtO + 2H^+ + 2e^- = Pt^* + H_2O \quad (1)$$

$$Pt^* + 2mH^+ + 2me^- = Pt^* \ldots (H_2)_m \text{ adsorbed} \quad (2)$$

or, if an oxidized electrode is immersed in dissolved hydrogen

$$PtO + H_2 = Pt^* + H_2O \quad (3)$$

and

$$Pt^* + mH_2 = Pt^* \ldots (H_2)_m \text{ adsorbed} \quad (4)$$

where PtO represents platinum oxide (not distinguished from possibility of $Pt(OH)_2$ in basic solutions, but differentiated from molecular oxygen held on platinum surface through weak electrostatic forces) and m may be any positive integer or noninteger value. If the Pt* is a real physical state, the formation and subsequent reduction of oxide seems to necessitate the formation and rupture of bonds between platinum and oxygen atoms.

The values of Q_a and Q_c depend on the anodic and cathodic potential limits as well as somewhat on the prior history of the electrode. In particular, care must be taken to prevent oxygen evolution on the anodic limit. (There is indication from previous work that the potential for oxygen evolution can be differentiated during oxide formation at least in basic solutions.[23]) It is interesting to note that the value of Q'_c or Q'_a is directly related to the amount of oxide formed. In Table I the average ratio of $Q'_a:Q_a$ is 0.304 ± 0.020. A similar result is found in Table II. If one assumes that platinum oxide formation and reduction is a two electron per atom process and that adsorbed hydrogen is molecular, the value of m is 0.3.

The values of Q'_a and Q'_c are time dependent. That is, if the activated electrode is allowed to stand for periods of time (no electrical connections) in a thoroughly degassed solution and then cycled around the hydrogen prewave, both Q'_a and Q'_c decrease (see Fig. 3B, traces a–h). In Fig. 4, curve B, a typical plot of the logarithm of the values of Q'_a as a function of time for carbonate solution is shown. The curve is

(23) T. Kuwana, *J. Electroanal. Chem.*, **6**, 164 (1963).

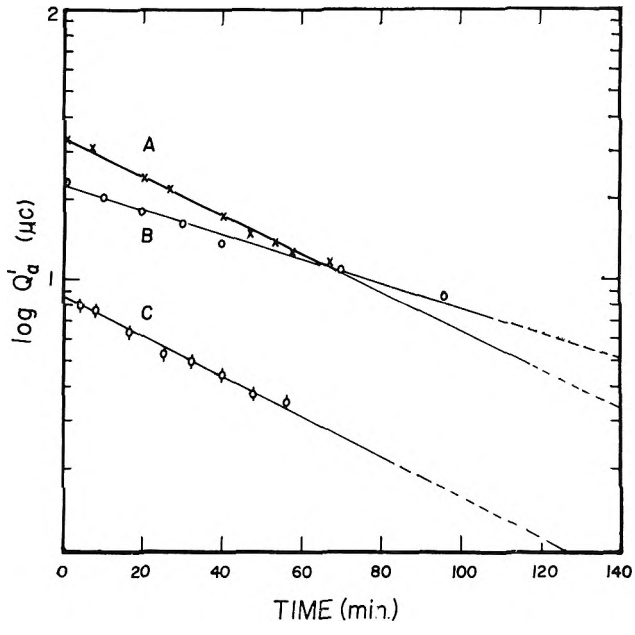

Figure 4. Logarithm of Q'_a plotted as a function of time. Curves A and C evaluated from continuously cycling the electrode in 1 F Na_2CO_3 and 1 F H_2SO_4, respectively. Potential limits of scan: -0.50 to -0.85 and $+0.125$ to -0.190 v. *vs.* s.c.e.; 1 F Na_2CO_3 and 1 F H_2SO_4, respectively. Curve B: Q'_a evaluated from intermittently cycling a platinum electrode in 1 F Na_2CO_3.

linear. The slope of the curve is similar to those found in 1 F H_2SO_4. Several values of the decay of Q'_a in terms of half-life, $T_{0.5}$, are given in Table I.

If Pt* is truly a dislocated, either atomic or small crystalline platinum, the more stable thermodynamic state should be the larger, crystalline platinum, Pt_c. The rate of the conversion of the reaction

$$Pt^* \xrightarrow{k_1} Pt_c \qquad (5)$$

where k_1 is the rate constant and is expected to depend only on the rate of surface migration and reorientation of Pt* as it "fits" into the larger crystalline lattice structure. If the hydrogen prewave is Pt*. . . (H_2) (adsorbed), then the decrease of Q'_a and Q'_c with time is perhaps a measure of k_1.

If Pt* conversion is purely random and statistical, the rate will be first order with respect to the surface concentration of Pt*. Furthermore, the validity of measuring the apparent rate of Pt* conversion by the hydrogen prewave will depend on the constancy of m and on the following reactions

$$Pt^*\ldots(H_2)_m \text{ (adsorbed)} \xrightarrow{k_2} Pt^* + mH_2 \text{ (soln.)} \qquad (6)$$

$$Pt^*\ldots(H_2)_m \text{ (adsorbed)} \xrightarrow{k_3} Pt_c + mH_2 \text{ (soln.)} \qquad (7)$$

$$Pt^*\ldots(H_2)_m \text{ (adsorbed)} \xrightarrow{k_4} Pt_c\ldots(H_2)_m \text{ (adsorbed)} \qquad (8)$$

$$Pt + 2H^+ + 2e^- \longrightarrow Pt\ldots(H_2) \text{ (adsorbed)} \qquad (9)$$

The constancy of the values of Q'_a to Q'_c with scan rate (see Table II) in the basic solution indicates, at least, that the rate of reaction 6 is slow if it occurs at all to any extent. A completely deactivated electrode (allowed to stand in degassed solution 12 hr. or more) shows no prewave and only the normal, large current due to hydrogen formation into solution. On cycling, the anodic prewave is also absent for a deactivated electrode and there is no evidence for contributions from reaction 9 in the potential region of the prewave. If reaction 8 occurs, it is only an additional path by which Pt* is removed from the system. Just by studying the prewave, reaction 8 cannot be distinguished from reaction 7. Conversion of Pt* by these two reactions should have a different rate than by reaction 5.

Rather than allowing the electrode to stand for various periods and then evaluating the prewave, the electrode was continuously cycled around the prewave at a scan rate of 0.13 v. sec.$^{-1}$. The values of Q'_a evaluated in this manner are plotted as a function of time for 1 F Na_2CO_3 and 1 F H_2SO_4 in Fig. 4, curves A and C, respectively. The curves are both linear with similar slopes. If both the values of Q'_a and Q'_c for the same run are plotted as a function of time as above, two linear curves, which intersect due to a slight difference of slopes, are obtained. The reason for this is believed to be attributable to the slow absorption of hydrogen into the platinum metal which makes the value of Q'_c slightly larger than Q'_a during the early part of the run. At longer times, however, the amount of absorbed hydrogen becomes appreciable and contributes to Q'_a. During these latter stages, if the potential is allowed to scan in the region between the oxide and hydrogen prewave, an anodic wave attributed to absorbed hydrogen[16] is observed.

The first-order decay in quantity of reaction 2 is an indirect measure of the rate of reaction 5. The value of Q'_a can, thus, be expressed at any time, t, as follows

$$(Q'_a)_t = (Q'_a)_{t=0}e^{-k_1 t} \qquad (10)$$

where

$$(Q'_a)_{t=0} = mQ_a \qquad (11)$$

and the value of k_1 calculated is 0.015 min.$^{-1}$.

A relationship of similar form as (10) has been set forth by Bonnemay[24,25] for poisoning of "active" sites on platinized platinum by bromine. Poisoning by other halogens was also investigated. It cannot be disputed that "active" sites of Pt* may be deactivated by adsorption of certain anions or organic molecules or through chemical reaction to form a platinum compound on the surface. Presence of oxygen in alkaline solution to form oxide would be an example of the latter. It seems unlikely, however, that any of the above reasons accounts satisfactorily for the present experimentally observed results, particularly to explain the similarity of the half-lives irrespective of whether the solution was 1 *F* H_2SO_4 or 1 *F* Na_2CO_3 or whether the electrode was continuously or intermittently cycled to obtain the decay data.[26]

An interesting question arises with regard to the mechanism of hydrogen evolution or hydrogen oxidation. Does electron transfer occur through the adsorbed hydrogen without any appreciable exchange of the adsorbed with the solution hydrogen? Recent tracer experiments by Osteryoung and Anson[27] has indicated that adsorbed iodide on platinum does not exchange and is inactive electrochemically as far as the oxidation of solution iodide or iodine is concerned. A similar situation, perhaps to a lesser extent, may exist with the hydrogen system.

Acknowledgment. Financial support for this work by the Air Force Cambridge Research Laboratories, Office of Aerospace Research, under contract AF 19 (604) 8069, and by the University of California, Riverside, Calif., under Intramural Grant No. 4003, is gratefully acknowledged. Fruitful discussion during the early part of the work with Dr. C. N. Reilley and Dr. J. Aikens is greatly appreciated.

(24) M. Bonnemay, *J. Chim. Phys.*, **50**, 142 (1952).

(25) M. Bonnemay, *Compt. rend.*, **239**, 642 (1954).

(26) NOTE ADDED IN PROOF.—Polarization characteristics of absorbed hydrogen have been recently examined in the presence of chloride, cyanide, and perchlorate ions. The half-life of decay was essentially independent of these ions. Closer examination of decays at short times revealed a fast decay with half-life the order of 3–5 min. It has been brought to our attention that Breiter and Kennel (*Z. Elektrochem.*, **64**, 1180 (1960)) had examined similar short decays over a period of 20 min. Our short decay data are in fair agreement with theirs.

(27) R. Osteryoung and F. C. Anson, private communication.

Self-Interaction Coefficients and Henry's Law Constants for Benzyl Chloride in a Variety of Solvents. Extrathermodynamic Prediction of Self-Interaction Coefficients[1a]

by Warren J. Miller[1b] and Ernest Grunwald

Chemistry Department, Florida State University, Tallahassee, Florida *(Received March 29, 1963)*

The variation of the partial vapor pressure of benzyl chloride with concentration was measured in dioxane, ethanol, methylcyclohexane, propionitrile, and several dioxane–water mixtures. Henry's law constants and solute self-interaction coefficients (k_{33}) were calculated for benzyl chloride in each of the solvents. Two extrathermodynamic relationships are derived for the prediction of k_{33}. In one, k_{33} is related to the Henry's law constant. In the other, k_{33} for a mixed binary solvent is related to k_{33} in the separate one-component solvents. The two relationships have been tested successfully by means of the data for benzyl chloride. Results are also given of a preliminary study of the thermodynamic properties of naphthalene in the system dioxane–water.

Introduction

In this paper we consider solutions consisting of a single nonelectrolyte solute in a series of one-component or binary solvents. We use the subscript 3 to designate the solute in both binary and ternary solutions. In any given solvent, the logarithm of the molal activity coefficient, γ_3, can be expressed as a power series function of the molal concentration m_3, as in

$$\ln \gamma_3 = k_{33}m_3 + l_{33}m_3^2 + \ldots \qquad (1)$$

where the coefficients k_{33}, l_{33}, . . ., are characteristic of the solvent as well as the solute. Experience shows that for m_3 less than about 0.5 m, the terms $l_{33}m_3^2 + \ldots$ are negligible compared to $k_{33}m_3$, so that eq. 1 reduces to

$$\ln \gamma_3 = k_{33}m_3 \ (m_3 < \backsim 0.5) \qquad (2)$$

The coefficient k_{33} is often called the *self-interaction coefficient* of the solute.[2]

Although the self-interaction term $k_{33}m_3$ may be substantial, experimental data concerning k_{33} are surprisingly few. We now report measurements of k_{33} for the solute benzyl chloride ($C_6H_5CH_2Cl$) in a series of organic solvents and dioxane–water mixtures. As far as we know, our study is the first to provide values of k_{33} for a single solute in a wide range of solvents.

To determine γ_3, we have investigated the gas phase in equilibrium with a series of solutions of benzyl chloride by the dynamic method of vapor pressure measurement. Treating the *gas phase* as an ideal solution, we first calculated the partial pressure p_3 of benzyl chloride for each solution and then γ_3 from

$$\gamma_3 = p_3/H_3^0 m_3 \qquad (3a)$$

$$H_3^0 = \lim_{m_3 \to 0} (p_3/m_3) \qquad (3b)$$

Consequently, we are able to report also values of the Henry's law constant, H_3^0, for benzyl chloride in a wide range of solvents.

Because of the scarcity of data concerning k_{33} (which is due in part to the difficulty of measuring this quantity), we devote the final part of this paper to the extrathermodynamic prediction of k_{33}. In one method,

(1) (a) Work supported by the National Science Foundation; (b) Research Laboratories, Eastman Kodak Company, Rochester 4, N. Y.

(2) F. A. Long and W. F. McDevit, *Chem. Rev.*, 51, 119 (1952). "Self-interaction" is used here in a phenomenological rather than a mechanistic sense since the magnitude of k_{33} depends not only on solute–solute, but also on solvent–solute pairwise interactions.

we try to relate k_{33} to the more readily measured H_3^0. In another method, we try to predict k_{33} for a binary solvent mixture from the values of k_{33} in the pure solvent components.

Experimental

Materials. Distilled water was redistilled from alkaline potassium permanganate solution in an all-glass system. Practical grade 1,4-dioxane was further purified by a method similar to that used by Marshall and Grunwald.[3] After being stored at least 48 hr. over ferrous sulfate, dioxane was refluxed over a mixture of sodium hydroxide and silver oxide for at least 48 hr. and fractionated through a 20-plate Bruun column. Approximately the first one-fifth of the distillate was discarded. The product of this distillation was refluxed with sodium and distilled as needed through a 1.2-m. long column packed with Berl porcelain saddles, about the first one-tenth being discarded as predistillate.

Absolute ethanol was fractionated through a 20-plate Bruun column to remove aromatic impurities. The ethanol was then dried of water by the method of Smith and Manske.[4]

Phillips Petroleum Corp. pure grade methylcyclohexane was purified by the method of Potts.[5] The hydrocarbon was stirred vigorously with reagent grade sulfuric acid for 4 hr., washed twice with distilled water, and dried over anhydrous calcium sulfate. The methylcyclohexane was then passed through a silica gel column 76 cm. long and 2.5 cm. in diameter, employing Fisher 20–200 mesh silica gel. The silica gel was activated in the column before use by evacuating the column while heating it to 350° for 12 hr. and then cooling it in a moisture-free atmosphere.

Propionitrile, free of isonitrile, from Distillation Products Industries was fractionated through a 76-cm. column of 15-mm. i.d., packed with 0.050 × 0.100 × 0.100-in. Type 316 stainless steel Heli-Pak packing, at a reflux ratio of 50:1.

Matheson Coleman and Bell practical grade benzyl chloride was stored over anhydrous potassium carbonate and further purified by distillation and fractional crystallization just before use. Benzyl chloride of comparable purity was also prepared by distilling Baker A.R. grade benzyl chloride, which had previously been stored over anhydrous potassium carbonate, through a 30-cm. Vigreux column and collecting the middle third of the distillate (b.p. 60–61° (10 mm.), $n^{25}D$ 1.5366). In most of the work the solute was prepared by the latter method.

The dioxane, ethanol, and propionitrile prepared by he preceding methods were free of all impurities that could be detected by vapor-phase chromatography. The methylcyclohexane and benzyl chloride prepared by either method were better than 99.95 mole % pure by vapor-phase chromatography.

Method of Measurement. As mentioned earlier, we determined the partial pressure of a volatile solute, benzyl chloride, in a one-component or binary solvent by the dynamic method of vapor pressure measurement.[6] Vapor in equilibrium with a liquid phase at a total pressure of 1 atm. was carried to a tared cold trap in a stream of nitrogen. This same stream of nitrogen was then passed over a second solution differing only in solute concentration, and that vapor was carried to a second tared cold trap. The two samples of condensed vapor were then weighed and analyzed. Knowing the vapor pressure of the solvent and the composition of the vapor, the partial pressure of the solute was calculated.

The apparatus is similar to that described previously,[6] but has been modified for handling organic solvents in such a way that the vapor is never in contact with grease.[7] In the modified apparatus, each "train" of saturators is fixed in one structural unit that includes gas entrance and exit tubes, the latter extending several inches above the water level of the thermostat. Each of the saturators has been provided with a vertical tube, about 6.4 cm. long and topped with an inner 10/30 standard tappered ground joint, through which the solution can be admitted. These joints are fitted with machined Teflon plugs that provide a grease-free vapor seal. The inner joint with plug in place is then capped with a greased outer 10/30 ground joint to provide a tight seal against the water of the thermostat.

A separate study[7] had shown that the solvolysis of benzyl chloride in the hydroxylic solvents is sufficiently slow to be neglected under our experimental conditions.

Spectrophotometric Measurements. After roughly 4 g. of vapor had been collected and the traps brought to room temperature at atmospheric pressure and weighed, a transfer funnel with an 18/6 socket joint on its large end was attached to the inlet arm of the trap and the solution was poured either directly into a glass-

(3) H. P. Marshall and E. Grunwald, *J. Am. Chem. Soc.*, **76**, 2000 (1954).

(4) E. L. Smith, *J. Chem. Soc.*, 1288 (1927); R. H. Manske, *J. Am. Chem. Soc.*, **53**, 1106 (1931).

(5) W. J. Potts, Jr., *J. Chem. Phys.*, **20**, 809 (1952).

(6) (a) A. L. Bacarella, A. Finch, and E. Grunwald, *J. Phys. Chem.*, **60**, 573 (1956); (b) E. Grunwald and A. L. Bacarella, *J. Am. Chem. Soc.*, **80**, 3840 (1958).

(7) For complete details see W. J. Miller, Ph.D. Dissertation, Florida State University, Tallahassee, Fla., 1962.

stoppered 1-cm. Beckman cell or, when the sample required dilution before analysis, into a 25-ml. glass-stoppered erlenmeyer flask. The optical densities of the samples and of at least two reference solutions were measured at 2640, 2620, 2600, 2580, and 2560 Å. using a Beckman DU spectrophotometer. A Cary Model 14 recording spectrophotometer was also used occasionally after it was determined that the two instruments yielded results of comparable precision.

In order to improve the analytical accuracy to less than 1% error, special techniques were developed. All dilutions were made by volume using calibrated automatic pipets with Teflon stopcocks. Even the smallest of these pipets, 1.014 ml., could easily be used with a standard error of less than 0.1%. Solvents used for dilutions, which were also used as reference solvents in the analyses, were prepared by weight to the composition of the vapor that would be in equilibrium with the mixed solvent used in the experiment. Great care was taken in cleaning all glassware, especially the spectrophotometer cells, and the blank reading of each cell with solvent was checked before each analysis.

It was discovered early in this work that special precautions must be taken in the method of analysis. Solutions of dioxane containing dissolved oxygen absorb in the ultraviolet at wave lengths shorter than about 3200 Å., while oxygen-free pure dioxane is transparent to wave lengths longer than about 2400 Å. The "extra" absorption is ascribed by Tsubomura and Mulliken[8] to a charge-transfer interaction complex of oxygen and dioxane. Further investigation demonstrated that the absorption could be eliminated by bubbling nitrogen through the dioxane for several minutes. It was also found that the ultraviolet absorption of samples of dioxane that were thus swept with nitrogen and subsequently kept in glass-stoppered 1-cm. Beckman cells slowly increased linearly with time. Within 5 hr. the ultraviolet spectrum of such a dioxane sample was identical with that of a reference sample that was initially in equilibrium with the atmosphere. Identical results were observed regardless of which of our cells was used.

Since in our experiments the samples were essentially oxygen-free and the reference solvent was not, the samples were set aside for several hours before analysis, and the analysis was repeated after a minimum time lapse of 1 hr. to be sure that no further change was taking place. No measurable change in benzyl chloride could be detected in samples that were let stand up to 12 hr.

Calculations

In binary solutions values of p_3 were calculated by standard methods from the composition of the condensed vapor and the vapor pressure of the solvent. The values of solvent vapor pressures that were used are given in Table I.

In ternary solutions p_3 was calculated from the mole fraction of benzyl chloride in the condensed vapor and the partial pressures of dioxane and water. The latter were calculated from the experimentally determined mass ratio, ρ, and previously reported values of the partial pressures over the mixed solvents in the absence of solute.[6] The calculation of the partial pressures of dioxane and water over the benzyl chloride solutions followed methods described previously, and our symbols will conform to those used in the previous paper.[9] The calculation requires values of the osmotic coefficient of the solute, $g = 1 - (k_{33}m_3/2)$, which in turn depends on k_{33}. It was necessary, therefore, to calculate k_{33} by successive approximations, with the first approximation being $g = 1$ for all solute concentrations. The calculation also requires a knowledge of n_g/n_g^*, the ratio of the total number of moles of gas over the solution to the total number of moles of gas over the solvent. Experimentally, the same amount of

$$\frac{n_g}{n_g^*} = \frac{(n_1)_g + (n_2)_g + (n_3)_g + (n_4)_g}{(n_1^*)_g + (n_2^*)_g + (n_4^*)_g} \qquad (4)$$

nitrogen was passed over the solvent and the solution: $(n_4)_g = (n_4^*)_g$. Using this fact, it can be shown that for dilute solutions

$$\frac{n_g}{n_g^*} \approx 1 + [(x_1^*)_g Z_2 - (x_2^*)_g Z_1] \ln (\alpha_1/\alpha_2) \qquad (5)$$

where Z_1 is the mole fraction of component 1 in the liquid solvent, $(x_1^*)_g$ is the mole fraction of component 1 in the vapor phase over the solvent, and α_1 is the ratio of the activity of component 1 in the ternary solution to that in the binary solvent of equal Z_1. The subscript 2 designates the second solvent component. For example, for a 50 weight % dioxane–water solvent eq. 5 reduces to eq. 5′.

$$\frac{n_g}{n_g^*} = 1 - 0.0202 \ln (\alpha_1/\alpha_2) \qquad (5')$$

By using eq. 6, the detailed derivation of which is given in ref. 6b, we were also able to calculate the quantity $d\bar{F}_{3m}^0/dZ_1$. In eq. 6, $\bar{F}_{3m}^0$ is the *standard*

(8) H. Tsubomura and R. S. Mulliken, *J. Am. Chem. Soc.*, **82**, 5966 (1960).

(9) E. Grunwald, G. Baughman, and G. Kohnstam, *ibid.*, **82**, 5801 (1960).

Table I: Results[a] for the Solute, Benzyl Chloride, at 25.00°

Solvent: Composition (wt. %)	Vapor pressure (mm.)	Series	m_3	p_3/m_3	$d\bar{F}_{3m}^0/dZ_1$, kcal.	k_{33}, kg./mole	H_3^0
Dioxane	36.18[b]	1	0.0281	0.0971_0		$0.13_5 \pm 0.07$	0.0964 ± 0.0004
			.2002	$.0996_5$			
		2	.0390	$.0962_5$			
			.2089	$.1011_0$			
		3	.0469	$.0967_2$			
			.3112	$.0984_3$			
Dioxane (70.50)–water	(1) 18.90[c,d]	1	.0083	.6618	4.4 ± 0.2[e]	$-0.65_4 \pm 0.12$	$.660 \pm 0.006$
	(2) 26.90		.0954	.6115	4.8 ± 0.5[f]		
		2	.0658	.6314			
			.2159	.5795			
Dioxane (60.72)–water	(1) 19.67[c,d]	1	.0051	1.573_7	7.2 ± 0.1[e]	$-1.19_0 \pm 0.01$	1.584 ± 0.001
	(2) 24.57		.1015	1.405_5	7.2 ± 0.7[f]		
		2	.0168	1.554_0			
			.1715	1.290_6			
Dioxane (50.00)–water	(1) 20.46[c,d]	1	.0127	4.379_1	8.2 ± 0.4[e]	$-1.75_2 \pm 0.04$	4.488 ± 0.016
	(2) 21.21		.0429	4.157_6	10.2 ± 1.0[f]		
		2	.0055	4.457_7			
			.0364	4.222_8			
Water	23.752[b]						(1.6×10^3)[g]
Benzyl chloride				0.153			
Methylcyclohexane	46.33[h]	1	.0046	$.406_6$		$+0.67 \pm 0.06$	0.414 ± 0.007
			.0512	$.441_6$			
		2	.0258	$.427_7$			
			.1059	$.435_8$			
Ethanol	57.66[h]	1	.0084	.4365		$-0.26_5 \pm 0.07$	0.442 ± 0.004
			.0855	.4379			
		2	.0436	.4403			
			.3935	.3957			
Propionitrile	46.67[h]	1	.0116	.1004		$+0.089 \pm 0.04$	0.1005 ± 0.0003
			.0419	.1006			
		2	.0314	.1011			
			.1065	.1016			
Dioxane (60.72)–water, 5.00°	(1) 5.349[i]	1	.0043	.4074	7.6 ± 0.2[e]	$-1.21_5 \pm 0.19$	0.415 ± 0.005
	(2) 8.172		.0963	$.377_1$			
		2	.0130	.4119			
			.1907	.3243			

[a] p_3 in mm., m_3 in moles of solute per kg. of solvent, H_3^0 in units of p_3/m_3. [b] See ref. 6. [c] (1) is water, (2) is dioxane. [d] Calculated using the activity data of ref. 6a and assuming ideal behavior in the vapor phase. [e] Calculated from the mass ratios. [f] By graphical differentiation on a large-scale plot of $RT \ln H_3^0$ *vs.* Z_1. [g] Calculated from the orthobaric vapor pressure and the water solubility of pure benzyl chloride at 25.00°. The vapor pressure is 1.21 mm.: J. O. Halford and E. B. Reid, *J. Am. Chem. Soc.*, **63**, 1873 (1941). The solubility in water was estimated using the equations of N. C. Deno and H. E. Berkheimer, *J. Chem. Eng. Data*, **5**, 1 (1960). The result is believed to be reliable within a factor of two. [h] Calculated from the data given by A. Weissberger, "Technique of Organic Chemistry," Vol. 7, 2nd Ed., Interscience Publishers, Inc., New York, N. Y., 1955. [i] Determined by interferometric analysis of condensed solvent vapor.

$$\frac{1}{RT}\frac{d\bar{F}_{3m}^0}{dZ_1} = \frac{1}{m_3'}\left[\frac{1000}{M_{12}}\ln\frac{\alpha_1}{\alpha_2} + \frac{(M_1 - M_2)k_{33}(m_3')^2}{2M_{12}}\right] + \frac{(M_1 - M_2)}{M_{12}} \quad (6)$$

partial molal free energy (on the m-scale) of the solute; $m_3 = g_2(m_3)_2 - g_1(m_3)_1$, the difference in the "effective" concentrations of the solute in the two solutions used in a single experiment; g_1 and g_2 are osmotic coefficients;

and $M_{12} = Z_1M_1 + Z_2M_2$, the molar weight of the binary solvent.

k_{33} and H_3^0 are the slope and intercept, respectively, of the plot ln (p_3/m_3) *vs.* m_3. The reported results are averages of two methods of calculation. (1) All results for a given solvent were subjected to a single linear least-squares calculation. (2) Each individual experiment involved a pair of solutions in the same solvent and yielded a separate set of values for k_{33} and H_3^0. The separate results obtained in individual experiments were then averaged. Method 2 has the advantage that each value of k_{33} and H_3^0 is obtained from two solutions that were studied simultaneously and, therefore, subjected to identical experimental conditions. The two methods of calculation yielded closely similar results.

Results

The results for benzyl chloride are given in Table I. The solvents cover a wide range of polarity and molecular structure. The solvent effects on k_{33} within this range are relatively very large, the values of k_{33} ranging from positive to negative. Moreover, with the apparent exception of the result for methylcyclohexane, the *sign of* k_{33} *is opposite to that of the deviation from Raoult's law*, the latter being obtained from the difference between H_3^0 and p_3/m_3 for pure benzyl chloride. In 60.72% dioxane–water we have data at both 25 and 5° which indicate that k_{33} is rather insensitive to changing temperature.

It can be seen from Table I that the values of H_3^0 are much more accurate than those of k_{33}. This is understandable because the change in p_3/m_3 with m_3 is relatively small. The standard error in H_3^0 is of the same order as that in p_3/m_3, and is usually within 1%. On the other hand, the standard error in k_{33} exceeds 10% in a majority of cases. It should be pointed out, however, that an error of as much as 0.10 in k_{33} results in an error of only 1% in γ_3 at 0.1 *m* concentration.

Table II shows the results of a preliminary investigation of the solute, naphthalene, in dioxane–water mixtures, carried out with the collaboration of Mr. George Baughman. Unfortunately this work had to be interrupted prematurely, and we take this opportunity to publish the results. Although less complete and less accurate than the data for benzyl chloride, the data for naphthalene show the same trend for k_{33} to decrease and H_3^0 to increase with increasing water content of the solvent.

Table II: Preliminary Results for Naphthalene in the System Dioxane–Water at 25.00°[a]

Dioxane, wt. %	$d\bar{F}_{3m}^0/dZ_1$, kcal.	k_{33}, kg./mole	H_3^0, p_3(mm.)/m_3(molal)
100		-0.105 ± 0.02	0.027 ± 0.003
70.50	5.1 ± 0.1	-0.567 ± 0.16	0.205 ± 0.001
50.00	11.9 ± 0.2	-2.10 ± 0.20	1.63 ± 0.03

[a] Obtained by the authors with the collaboration of G. Baughman.

Extrathermodynamic Prediction of k_{33}

For nonelectrolytes at moderate concentrations, γ_3 differs enough from unity to make a knowledge of its precise value desirable, yet not usually by enough to justify the lengthy experiments required to measure it. For this reason, it is particularly appropriate to develop extrathermodynamic methods for predicting k_{33}. In the extrathermodynamic approach, one predicts the values for one thermodynamic quantity from other, more readily available, thermodynamic quantities. The approach is extrathermodynamic because the relationship is not derivable from the laws of thermodynamics alone. However, this does not imply a random search for correlations with other physical properties. An extrathermodynamic relationship is most likely to be of wide usefulness if the assumed functional dependence is suggested by theory.

First, we would like to explore a possible correlation between k_{33} and H_3^0 for a given nonelectrolyte solute in a series of solvents. The qualitative justification for expecting such a correlation can be given by reference to Fig. 1. In that figure, curve A represents a positive deviation from Raoult's law, curve I represents an ideal mixture, and curve B represents a negative deviation from Raoult's law. Since curves A and B must approach curve I as the mole fraction, x_3, approaches unity, we expect that at low x_3 the sign of the curva-

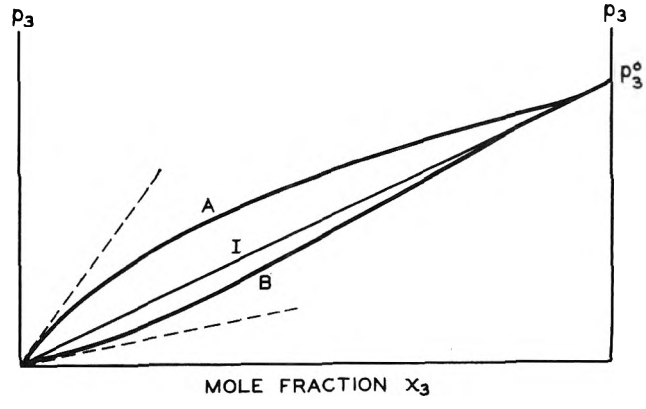

Figure 1. This figure may suggest the existence of a relationship between H_3^0 and k_{33}.

ture is opposite to that of the deviation from Raoult's law. Hence k_{33} should be negative when H_3^0 is greater than the ideal value, and positive when H_3^0 is less than the ideal value.

These qualitative ideas are readily made quantitative by means of the Scatchard and Prentiss[10] expansion of the free energy of a mixture in power series, shown in eq. 7. Here, n_i = number of moles of the

$$\frac{F}{RT} = \Sigma_i n_i(B_i + \ln x_i) + \frac{1}{V}\Sigma_{ij}\beta_{ij}n_in_j + \frac{1}{V^2}\Sigma_{ijk}\Delta_{ijk}n_in_jn_k + \ldots \quad (7)$$

ith component, V is the volume of the solution, and B_i, β_{ij}, and Δ_{ijk} are coefficients.[11]

From eq. 7 we obtain a power series expression for $\ln \gamma_3$ as a function of m_3 by straightforward manipulation. The first term in this series is proportional to m_3, and the coefficient of m_3 can be identified with k_{33}. For a solute in a binary solvent mixture, we thus obtain eq. 8. In this equation, $V_3 = \partial V/\partial n_3$, the partial

$$\frac{1000k_{33}}{M_{12}} = -1 + \frac{2}{V_{12}}\left[\beta_{33} - \frac{V_3}{V_{12}}(2\beta_{13}Z_1 + 2\beta_{23}Z_2) + \left(\frac{V_3}{V_{12}}\right)^2(\beta_{11}Z_1^2 + \beta_{22}Z_2^2 + 2\beta_{12}Z_1Z_2)\right] \quad (8)$$

molal volume of the solute; similarly $V_{12} = Z_1V_1 + Z_2V_2$, where V_1 and V_2 are the partial molal volumes of the solvent components; the β_{ij} are the respective pairwise interaction coefficients.

To derive an approximate relationship between k_{33} and H_3^0, we express H_3^0 also in terms of the β_{ij} and then eliminate these parameters between eq. 8 and the resulting expression. It is convenient to express H_3^0 in terms of standard free energy quantities, as in eq. 9. Upon solving eq. 7 for $\bar{F}_{3m}^0$ and *neglecting interactions of higher order than pairwise,* we obtain eq. 10. The parameters β_{ij} are readily eliminated between

$$-RT \ln H_3^0 = F_3^0(g) - \bar{F}_{3m}^0 \quad (9)$$

$$\frac{\bar{F}_{3m}^0}{RT} = B_3 + \ln\frac{M_{12}}{1000} + \frac{1}{V_{12}}(2\beta_{13}Z_1 + 2\beta_{23}Z_2) - \frac{V_3}{V_{12}^2}(\beta_{11}Z_1^2 + \beta_{22}Z_2^2 + 2\beta_{12}Z_1Z_2) \quad (10)$$

eq. 8 and 10, and $\bar{F}_{3m}^0$ is eliminated by means of eq. 9. The resulting relationship between k_{33} and H_3^0 is eq. 11. Since the quantities β_{33}, B_3, and $F_3^0(g)$ are

$$V_{12}\left(\frac{1000k_{33}}{M_{12}} + 1\right) = 2\beta_{33} - 2V_3\left[\frac{F_3^0(g)}{RT} - B_3\right] - 2V_3 \ln\left(\frac{1000H_3^0}{M_{12}}\right) \quad (11)$$

rigorously independent of the solvent, and since V_3 is nearly so, eq. 11 may be rewritten simply as eq. 12.

$$V_{12}\left(\frac{1000k_{33}}{M_{12}} + 1\right) = a\ constant - 2V_3 \ln\left(\frac{1000H_3^0}{M_{12}}\right) \quad (12)$$

However, the simple relationship expressed by eq. 12 is only approximate because higher-order terms have been neglected in eq. 10.[12]

A graph of the data for benzyl chloride according to eq. 12 is shown in Fig. 2. There is a strong linear trend, and most of the data can be fitted within their standard error. The slope of the best straight line is -0.364 l./mole, as compared to a theoretical value, $-2V_3$, of -0.232 l./mole. When the line is extrapolated to $\ln(1000H_3^0/M_{12})$ for pure water, a value of -3.8 is obtained for k_{33}.

Encouraged by the ease with which this approach will generate useful extrathermodynamic relationships, we have extended it to a somewhat simpler problem, the variation of k_{33} with the composition of a binary solvent system. In the following, we shall express k_{33} in a mixed solvent as a function of the values of k_{33} in the pure one-component solvents, and of properties of the components and the mixture. Expressions for $k_{33}^{(1)}$ and $k_{33}^{(2)}$ in each of the solvent components are obtained by solving eq. 8 for $Z_1 = 1$ or $Z_1 = 0$. Equations 8, 8′, and 8″ may be combined in such a way that the β_{i3} parameters, which are characteristic of the solute, cancel out. The result is eq. 13, where d_1, d_2, and d_{12} are the densities of the respective liquids.

$$\frac{1000k_{33}^{(1)}}{M_1} = -1 + \frac{2}{V_1}\left[\beta_{33} - \frac{2V_3\beta_{13}}{V_1} + \frac{V_3^2\beta_{11}}{V_1^2}\right] \quad (8')$$

$$\frac{1000k_{33}^{(2)}}{M_2} = -1 + \frac{2}{V_2}\left[\beta_{33} - \frac{2V_3\beta_{23}}{V_2} + \frac{V_3^2\beta_{22}}{V_2^2}\right] \quad (8'')$$

(10) G. Scatchard and S. S. Prentiss, *J. Am. Chem. Soc.*, 56, 1486 (1934).

(11) We use the symbols Δ_{ijk} rather than γ_{ijk} for the coefficients of the cubic terms to avoid confusion with the molal activity coefficient γ.

(12) These equations can also be derived using the volume fraction notation of J. H. Hildebrand and R. L. Scott, "The Solubility of Nonelectrolytes," 3rd Ed., Reinhold Publishing Corp., New York, N. Y., 1950, p. 124.

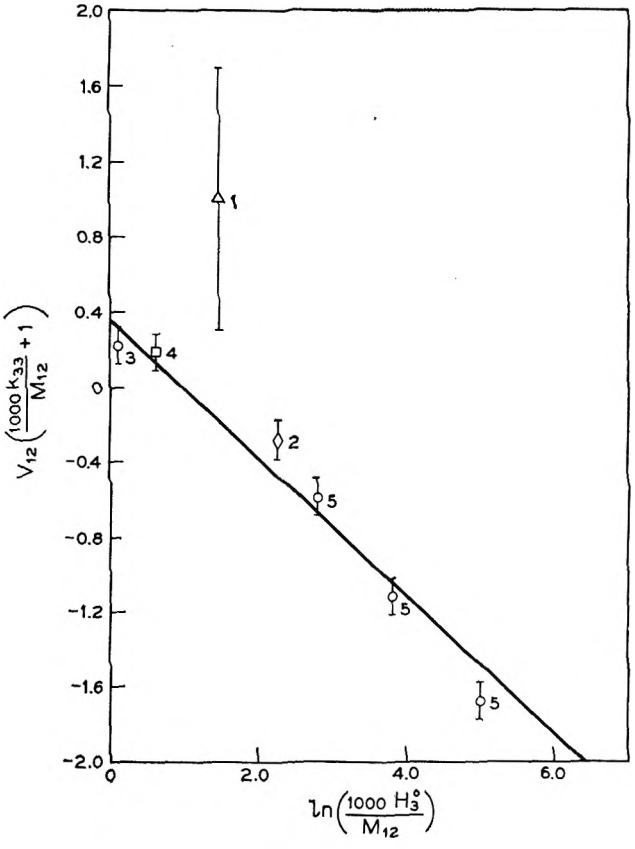

Figure 2. Correlation of k_{33} with H_3^0 for benzyl chloride in a variety of solvents at 25°, according to eq. 12. Numbers in figure refer to: 1, methylcyclohexane; 2, ethanol; 3, dioxane; 4, propionitrile; 5, dioxane–water mixtures. The straight line is drawn with slope = −0.364.

$$\frac{k_{33}V_{12}}{d_{12}} - \frac{Z_1V_1k_{33}^{(1)}}{d_1} - \frac{Z_2V_2k_{33}^{(2)}}{d_2} = Z_1Z_2(V_1 - V_2)^2 + \frac{2Z_1Z_2V_3^2}{V_{12}}\left[\frac{2\beta_{12}V_1V_2 - \beta_{11}V_2^2 - \beta_{22}V_1^2}{V_1V_2}\right] \quad (13)$$

The only parameters remaining in eq. 13 are β_{11}, β_{12}, and β_{22}, which appear in the last term. To eliminate these parameters we must look for an appropriate free energy quantity that is characteristic solely of the binary solvent system. In other words, we must apply eq. 7 to the special case that $n_3 = 0$. To derive the desired relationship, we first express $\bar{F}_1$ and $\bar{F}_2$ as functions of Z_1 and the β_{ij} parameters, using eq. 7 and neglecting higher-order terms. We let $\bar{F}_1^0$ and $\bar{F}_2^0$ denote the values of $\bar{F}$ for the pure solvent components ($Z_1 = 1$ or $Z_1 = 0$, respectively) and define activity coefficients as in eq. 14. We then find that eq. 15

$$\bar{F}_1 = \bar{F}_1^0 + RT \ln Z_1 + RT \ln \gamma_1 \quad (14a)$$

$$\bar{F}_2 = \bar{F}_2^0 + RT \ln Z_2 + RT \ln \gamma_2 \quad (14b)$$

is suitable for converting the last term of eq. 13 to a form consisting only of experimentally accessible quantities. The result is eq. 16. Since the only

$$Z_1 \ln \gamma_1 + Z_2 \ln \gamma_2 = -\frac{Z_1Z_2}{V_1V_2V_{12}} \times (\beta_{11}V_2^2 + \beta_{22}V_1^2 - 2\beta_{12}V_1V_2) \quad (15)$$

$$\frac{k_{33}V_{12}}{d_{12}} = \frac{Z_1V_1k_{33}^{(1)}}{d_1} + \frac{Z_2V_2k_{33}^{(2)}}{d_2} + Z_1Z_2(V_1 - V_2)^2 + 2V_3^2(Z_1 \ln \gamma_1 + Z_2 \ln \gamma_2) \quad (16)$$

approximation is the neglect of higher-order terms in the expression for the relatively small quantity ($Z_1 \ln \gamma_1 + Z_2 \ln \gamma_2$), we expect the fit of eq. 16 to be quite good.

Equation 16 has been tested by means of the data for benzyl chloride in the dioxane–water solvents, as shown in Table III. For each dioxane–water mixture, data have been combined with data for pure dioxane to calculate a value for $k_{33}^{(1)}$, the self-interaction coefficient of benzyl chloride in water. The values obtained in this way are listed in the last column of Table III and are constant within their precision measures, the average being −3.7. Unfortunately, we cannot measure $k_{33}^{(1)}$ directly because of the low solubility and hydrolysis of benzyl chloride in water. But the value is in good agreement with the previous extrathermodynamic estimate, $k_{33}^{(1)} = -3.8$, based on eq. 12. It is satisfying that our extrathermodynamic methods seem to work so well in such a nonideal system.

Table III: Test of Eq. 16 for Benzyl Chloride in Dioxane–Water Mixtures at 25.00°

Z_1	V_{12}, l./mole	d_{12}	γ_1	γ_2	k_{33}, obsd.	$k_{33}^{(1)}$, calcd.
0.0000	0.08569[a]	1.0280[a]	....	1.0000[b]	0.135	...
0.6717	.03954[c]	1.0372	1.1849[b]	2.2647	−0.654	−3.4 ± 0.4
0.7598	.03364	1.0349	1.0895	2.8310	−1.190	−3.8 ± 0.1
0.8302	.02900	1.0332	1.0376	3.4523	−1.752	−3.9 ± 0.1
1.0000	.01805	0.9971	1.0000	.....	.....	(av.) −3.7

[a] Data in this column were obtained by interpolation from F. Hovorka, R. A. Schaefer, and D. Dreisbach, *J. Am. Chem. Soc.*, **58**, 2264 (1936); **59**, 2753 (1937). [b] Data in this column were obtained by interpolation from J. R. Goates and R. J. Sullivan, *J. Phys. Chem.*, **62**, 188 (1958). [c] Data for V_1, V_2, Z_1: 0.01744, 0.08477, 0.6717; 0.01766, 0.08417, 0.7598; 0.01782, 0.08364, 0.8302.

Acknowledgment. It is a pleasure to thank Dr. Bruno Linder for helpful discussions.

Nonbonded Interactions and the Internal Rotation Barrier

by Maurizio Cignitti[1] and Thomas L. Allen

Department of Chemistry, University of California, Davis, California *(Received August 5, 1963)*

The role of nonbonded interactions in internal rotation is examined from several different points of view. Semi-empirical formulas indicate fairly large contributions (*ca.* 50%) of nonbonded H···H repulsions to the ethane barrier. Valence-bond calculations consistent with the valence-bond method and potential functions derived from data on intermolecular interactions show relatively small contributions (*ca.* 15% or less) from nonbonded interactions. It is proposed that hybridization by 2s and 2p hydrogen orbitals enhances the nonbonded repulsions, and that this may be an important factor in internal rotation.

Introduction

A number of theories have been proposed to explain the energy barrier to internal rotation in ethane and similar molecules, but none has gained very wide acceptance.[2] It is known that in the usual simple quantum mechanical treatments of ethane (either valence-bond or molecular orbital, with s and p orbitals), only hydrogen–hydrogen interactions contribute to the barrier.[2,3] A calculation of these interactions in the ethane molecule by Eyring in 1932 led to a predicted barrier of 0.36 kcal./mole, with the staggered configuration having the lower potential energy.[4] It is now known that the equilibrium configuration was correctly predicted, but the magnitude of the barrier in ethane is 2.7–3.0 kcal./mole.[2] (Because of uncertainty as to the shape of the potential function, the barrier might be as low as 1.55 kcal./mole.[5]) Perhaps partly as a consequence of the failure of nonbonded interactions to account for the size of the barrier, attention has shifted to more complex wave functions utilizing d and f hybridization,[6,7] excited valence-bond structures,[6,8-13] and electronic correlation.[14] However, recent calculations of the contributions of nonbonded interactions to internal rotation barriers have given the values 1.77 kcal./mole[15,16] and 2.63 kcal./mole[17] for ethane, and correspondingly good results for a number of other molecules. With the introduction of a suitable angular dependency of the nonbonded interaction, the former result increases to the experimental value.[16] Recent applications of the virial theorem to molecules with only hydrogens bonded to the axial atoms have shown that internal rotation barriers are closely related to differences in proton–proton repulsion energy between the eclipsed and staggered configurations.[18,19] In a treatment of the 42 singlet resonance bond structures of an H_3CCH fragment, Eyring, Grant, and Hecht found that the H···H interaction alone gave a barrier of 2.88 kcal./mole in ethane, and they conclude that this interaction may be the best explanation of the barrier.[12]

(1) On leave of absence from Istituto Superiore di Sanità, Rome, Italy, 1962–1963.

(2) E. B. Wilson, Jr., in "Advances in Chemical Physics," Vol. II, ed. by I. Prigogine, Interscience Publishers, Inc., New York, N. Y., 1959, p. 367.

(3) W. G. Penney, *Proc. Roy. Soc.* (London), **A144**, 166 (1934).

(4) H. Eyring, *J. Am. Chem. Soc.*, **54**, 3191 (1932).

(5) E. Blade and G. E. Kimball, *J. Chem. Phys.*, **18**, 630 (1950).

(6) E. Gorin, J. Walter, and H. Eyring, *J. Am. Chem. Soc.*, **61**, 1876 (1939).

(7) L. Pauling, *Proc. Natl. Acad. Sci. U. S.*, **44**, 211 (1958).

(8) H. Eyring, G. H. Stewart, and R. P. Smith, *ibid.*, **44**, 259 (1958).

(9) G. M. Harris and F. E. Harris, *J. Chem. Phys.*, **31**, 1450 (1959).

(10) M. Karplus, *ibid.*, **33**, 316 (1960).

(11) H. G. Hecht, D. M. Grant, and H. Eyring, *Mol. Phys.*, **3**, 577 (1960).

(12) H. Eyring, D. M. Grant, and H. Hecht, *J. Chem. Educ.*, **39**, 466 (1962).

(13) H. G. Hecht, *Theor. Chim. Acta*, **1**, 133 (1963).

(14) E. A. Magnusson and H. Shull, "Proceedings of the International Symposium on Molecular Structure and Spectroscopy," Science Council of Japan, Tokyo, 1962, p. C405.

(15) E. A. Mason and M. M. Kreevoy, *J. Am. Chem. Soc.*, **77**, 5808 (1955).

(16) K. E. Howlett, *J. Chem. Soc.*, 4353 (1957); 1055 (1960).

(17) V. Magnasco, *Nuovo Cimento*, **24**, 425 (1962).

(18) W. L. Clinton, *J. Chem. Phys.*, **33**, 632 (1960).

(19) M. Karplus and R. G. Parr, *ibid.*, **38**, 1547 (1963).

It is clear at this point that there is a wide divergence of opinion on the role of nonbonded interactions in internal rotation. We present here the results of a reinvestigation of this problem from several different points of view.

Magic Formula

Nonbonded interaction energies may be calculated from overlap integrals, exchange integrals, and atomic ionization potentials by means of Mulliken's "magic formula."[20] Pedley has recently used this formula to calculate the properties of a number of hydrocarbon molecules and radicals.[21]

For ethane in the eclipsed configuration, the magic formula gives 0.5604 e.v. for the total energy of repulsion between hydrogen atoms attached to different carbon atoms. In the staggered configuration, the same quantity is 0.5025 e.v., so that the contribution of hydrogen–hydrogen repulsions to the internal rotation barrier is 0.0579 e.v., or 1.34 kcal./mole. Details of the calculations are shown in Table I. Coefficients in the magic formula were taken from the $\nu = 0.70$ column of Table IV of ref. 20. Interatomic distances were computed for a structure with tetrahedral bond angles, a C–C distance of 1.54 Å., and a C–H distance of 1.10 Å.[22] The parameters for this simple structure are close to the averages of recent experimental determinations.[23,24]

Table I: Nonbonded H···H Interactions from Magic Formula

Dihedral angle, deg.	Distance, a.u.	Overlap integral[a]	$Y/2$,[b] e.v.	Coefficient
0	4.295	0.1560	0.1342	3 (eclipsed)
60	4.720	0.1171	0.0756	6 (staggered)
120	5.474	0.0690	0.0263	6 (eclipsed)
180	5.815	0.0543	0.0163	3 (staggered)

[a] For 1s atomic orbitals. [b] This is the nonbonded repulsion energy of a pair of hydrogen atoms at the distance tabulated. The factor of $^1/_2$ is sometimes incorporated into Y (see ref. 20 and 21).

Because of symmetry properties the contributions to the barrier of other nonbonded interactions must vanish identically.[2,3] We have verified this for the C···H and C···C interactions using the magic formula. All of the nonbonded C···C interaction terms are the same in the eclipsed and staggered configurations. The only nonbonded C···H interaction term dependent on the dihedral angle is $K'_{\pi h}/2$, which contributes 0.2600 e.v. to the atomization energies of both the staggered and eclipsed configurations. Details of the calculation are shown in Table II. The carbon atom SCF atomic orbitals of Shull,[25] as slightly modified by Higuchi,[26] were used in these calculations.[27] Integrals were evaluated on the IBM 7090 computer at the Computer Center of the University of California, Berkeley, with the Diatomic Molecular Integral Program.[28]

Table II: Nonbonded C···H Interactions from Magic Formula

Dihedral angle, deg.	$K'_{\pi h}/2$, e.v.	Coefficient
0	0.01733	6 (eclipsed)
60	0.01769	12 (staggered)
120	0.01300	12 (eclipsed)
180	0.00795	6 (staggered)

Thus the magic formula result for the internal rotation barrier in ethane is 1.34 kcal./mole, about half the experimental value. Application of the same method to methylsilane and methylgermane gives 0.49 and 0.41 kcal./mole, respectively; the corresponding experimental values are 1.715 and 1.27 kcal./mole.[29]

Another semi-empirical formula, $^1/_2AS^2I/(1 - S^2)$, with $A = 0.65$ and $I = 13.60$ e.v., has been used by Mulliken to calculate nonbonded H···H repulsions.[30] Application of this formula gives 1.15 kcal./mole for the contribution of nonbonded H···H repulsions to the ethane barrier.

(20) R. S. Mulliken, *J. Phys. Chem.*, **56**, 295 (1952).

(21) J. B. Pedley, *Trans. Faraday Soc.*, **57**, 1492 (1961); **58**, 23 (1962).

(22) K. S. Pitzer and E. Catalano, *J. Am. Chem. Soc.*, **78**, 4844 (1956).

(23) "Tables of Interatomic Distances and Configurations in Molecules and Ions," ed. by L. E. Sutton, Special Publication No. 11, Chemical Society, London, 1958, p. M135.

(24) W. J. Lafferty and E. K. Plyler, *J. Chem. Phys.*, **37**, 2688 (1962).

(25) H. Shull, *ibid.*, **20**, 1095 (1952).

(26) J. Higuchi, *ibid.*, **28**, 527 (1958).

(27) Some of the integrals are quite different when Slater AO's are used. It was found by Mulliken (ref. 20) that use of the more accurate SCF AO's in the magic formula is essential.

(28) A. C. Switendick and F. J. Corbató, "MI DIAT, Diatomic Molecular Integral Program, for 704, Fortran Coded," Massachusetts Institute of Technology Computation Center, Cambridge, Mass., Feb. 1, 1960, adapted to the 7090 by E. B. Moore, Jr., Boeing Scientific Research Laboratories, Seattle, Wash., and G. Wiederhold, University of California Computer Center, Berkeley, Calif.

(29) J. E. Griffiths, *J. Chem. Phys.*, **38**, 2879 (1963).

(30) R. S. Mulliken, *J. Am. Chem. Soc.*, **72**, 4493 (1950); **77**, 887 (1955).

Valence-Bond Method

For the conventional valence-bond structure of ethane ("perfect-pairing approximation"), nonbonded hydrogen–hydrogen repulsion energies may be calculated as

$$E_{hh} = Q_{hh} - {}^1/_2 J_{hh} \qquad (1)$$

where Q_{hh} is the Coulomb or direct integral and J_{hh} is the exchange integral.[4,31] The two integrals may be evaluated from the potential energy of a hydrogen molecule in its lowest $^1\Sigma$ and $^3\Sigma$ states. Neglecting S^2 with respect to unity, valence-bond theory gives these as

$$E(^1\Sigma) = Q_{hh} + J_{hh} \qquad (2)$$

$$E(^3\Sigma) = Q_{hh} - J_{hh} \qquad (3)$$

By combining these equations, the nonbonded repulsion energy may be expressed directly in terms of the potential energy functions[32]

$$E_{hh} = {}^1/_4 E(^1\Sigma) + {}^3/_4 E(^3\Sigma) \qquad (4)$$

The different methods for evaluating the integrals at the appropriate distances have led to a wide variety of results. Eyring originally used the Sugiura integrals plus an additional term for London forces.[4] More recent investigations have used potential energy functions for the $^1\Sigma$ state (experimental Morse curve[12,13,17]) or $^3\Sigma$ state[15,16]; the exchange energy has been taken as 85%[12,13] or 100%[15–17] of the total energy. In some calculations the factor of $^1/_2$ in eq. 1 has been dropped on empirical grounds.[15–17]

The most accurate $^1\Sigma$ and $^3\Sigma$ potential energy functions for the H_2 molecule have been obtained in recent theoretical investigations,[33–36] and in an analysis of spectroscopic data by the Rydberg–Klein–Rees method.[37] Figure 1 shows the $^1\Sigma$ functions and the experimental Morse curve for the range of internuclear distance appropriate to the internal rotation problem. The Morse function was calculated from data listed by Herzberg.[38]

The functions of Hirschfelder and Linnett[33] and Harris and Taylor[36] are almost identical in this range and are shown as a single curve. (These are the $W + I + P$ values from Table II of Hirschfelder and Linnett; they also list a most likely value of 10.0 kcal./mole at 4.0 a.u.) The results of Tobias and Vanderslice[37] and the function of Dalgarno and Lynn[34] agree very closely and are shown as one curve. Although there is some difference between the various theoretical functions, Fig. 1 shows that the Morse curve is in error throughout this range by a factor of about two.

By combining eq. 2 and 3, the following expression

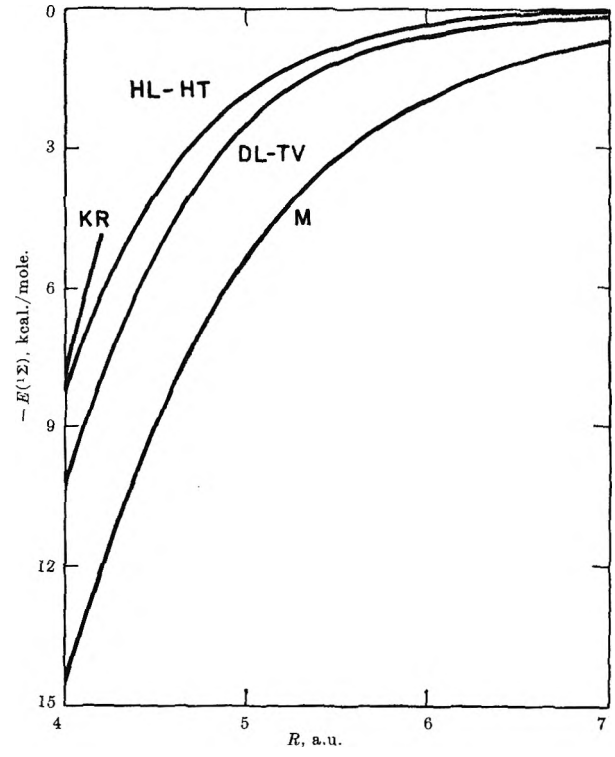

Figure 1. Potential energy functions for the $^1\Sigma$ state of the H_2 molecule. M is the Morse curve, DL-TV is from ref. 34 and 37, HL-HT is from ref. 33, Table II ($W + I + P$), and ref. 36, and KR is from ref. 35.

is obtained for the fraction of exchange energy in the binding energy of the $^1\Sigma$ state

$$\frac{J_{hh}}{E(^1\Sigma)} = \frac{E(^1\Sigma) - E(^3\Sigma)}{2E(^1\Sigma)} \qquad (5)$$

This quantity has been calculated from the potential energy functions of Hirschfelder and Linnett[33] and Dalgarno and Lynn.[34] The results, shown in Table III, are in striking contrast to calculations based on the Sugiura integrals, where the Coulomb energy is about 14% at 4.0 a.u., becoming even smaller as the internuclear distance increases.[39]

(31) F. J. Adrian, *J. Chem. Phys.*, **28**, 608 (1958).

(32) C. A. Coulson and D. Stocker, *Mol. Phys.*, **2**, 397 (1959).

(33) J. O. Hirschfelder and J. W. Linnett, *J. Chem. Phys.*, **18**, 130 (1950).

(34) A. Dalgarno and N. Lynn, *Proc. Phys. Soc.* (London), **A69**, 821 (1956).

(35) W. Kolos and C. C. J. Roothaan, *Rev. Mod. Phys.*, **32**, 219 (1960).

(36) F. E. Harris and H. S. Taylor, *J. Chem. Phys.*, **38**, 2591 (1963).

(37) I. Tobias and J. T. Vanderslice, *ibid.*, **35**, 1852 (1961).

(38) G. Herzberg, "Molecular Spectra and Molecular Structure. I. Spectra of Diatomic Molecules," 2nd Ed., D. Van Nostrand Co., Inc., New York, N. Y., 1950.

(39) J. O. Hirschfelder, *J. Chem. Phys.*, **9**, 645 (1941).

Table III: Contributions of Energy Terms to the H_2 Binding Energy

Distance, a.u.	Exchange energy, %: Hirschfelder and Linnett[a]	Exchange energy, %: Dalgarno and Lynn	London energy,[b] %
4.0	75.8	61.5	...
4.5	75.2	...	...
5.0	74.4	55.9	...
6.0	69.5	49.1	(25.7)[c]
7.0	57.6	38.4	37.0
8.0	38.3	24.8	54.1
10.0	6.6	4.1	84.9
12.0	0.6	0.0	94.1

[a] Data from Table II ($W + I + P$) and Table V ($W + P$) of ref. 33. [b] London energy from equation of Pauling and Beach (ref. 40); total energy from Dalgarno and Lynn (ref. 34). [c] For values of R much less than 7 a.u., this calculation of the London energy is not significant (ref. 40).

The principal source of the discrepancy is the London energy, which has been known for some time to be greater than the exchange energy at large internuclear distances.[40] Data for the contribution of this term are listed in the last column of Table III. The London energy depends on electronic correlation, which is not adequately represented by the Heitler–London wave function.

The proportion of the total binding energy attributed to the exchange term is critical in calculations of nonbonded repulsions. From the preceding equations

$$E_{hh} = (2 - 3x)E(^1\Sigma)/2 \qquad (6)$$

where x denotes the fraction of exchange energy. It is usual to assume that x is independent of distance in the relevant range, and the data in Table III show that this is approximately true. If E_ϕ designates $E(^1\Sigma)$ at the internuclear distance corresponding to the dihedral angle ϕ, as shown in Table I, then the contribution of nonbonded repulsions to the ethane barrier is

$$(2 - 3x)(3E_0 - 6E_{60} + 6E_{120} - 3E_{180})/2 \qquad (7)$$

This is a sensitive function of x. Calculations in which x is assumed to be 0.85 will give values 45% less than those with $x = 1.00$; if x is taken as 0.75, the calculated barrier is only one-fourth as large. Below $x = {}^2/_3$ the eclipsed configuration becomes the more stable.

The valence-bond method most compatible with the fundamental eq. 1–3 is the application of eq. 4, along with some set of mutually consistent potential functions. When these functions are based on the integrals which result from the Heitler–London wave function, and a London energy term is also included, the method is that which led to the earliest estimate of the barrier, 0.36 kcal./mole.[4] Alternatively, one may use the potential functions due to Hirschfelder and Linnett or Dalgarno and Lynn, which are found to give barrier heights of 0.42 and 0.07 kcal./mole, respectively. (In the latter case the eclipsed configuration is the more stable.)

The H···H potential function of Bartell[41] is based on the results of valence-bond calculations at longer distances, and one of the semi-empirical formulas of Mulliken[30] at shorter distances; it also includes a London energy term. The barrier height calculated from this function is 0.41 kcal./mole.

Intermolecular H···H Interactions

Studies of intermolecular phenomena (such as molecular scattering, second virial coefficients, and gas viscosity) provide data on nonbonded interactions. Vanderslice and Mason found that the following function was consistent with data on the H–H_2 and H_2–H_2 systems[42]

$$V(H\cdots H) = 30.21e^{-3.013R} \text{ e.v.};\ 0.8 \text{ Å.} \leq R \leq 2.1 \text{ Å.}$$

(This function is ${}^1/_2E(^3\Sigma)$, where $E(^3\Sigma)$ was obtained by fitting an exponential function[43] to the results of theoretical calculations.) If the above function is assumed to be valid at the longer distances involved in internal rotation, the resulting barrier is 0.45 kcal./mole.

A much different function was obtained by Amdur, Longmire, and Mason from studies of the CH_4–CH_4 interaction[44]

$$V(H\cdots H) = 1.44/R^{6.18} \text{ e.v.};\ 2.09 \text{ Å.} \leq R \leq 2.77 \text{ Å.}$$

The two functions are compared in Fig. 2. This latter function gives a barrier height of only 0.11 kcal./mole. (A short extrapolation beyond the recommended range was required for the longest H···H distances.)

Similar results have been obtained by Hill.[45] He derived different potential energy curves for the nonbonded interactions of hydrogen bonded to hydrogen and hydrogen bonded to carbon. The barrier heights calculated from these functions were 0.744 and 0.066 kcal./mole, respectively.

The various theoretical and semi-empirical methods used thus far to derive nonbonded H···H potential functions do not distinguish between H bonded to H

(40) L. Pauling and J. Y. Beach, *Phys. Rev.*, **47**, 686 (1935).

(41) L. S. Bartell, *J. Chem. Phys.*, **32**, 827 (1960).

(42) J. T. Vanderslice and E. A. Mason, *ibid.*, **33**, 492 (1960).

(43) R. J. Fallon, E. A. Mason, and J. T. Vanderslice, *Astrophys. J.*, **131**, 12 (1960).

(44) I. Amdur, M. S. Longmire, and E. A. Mason, *J. Chem. Phys.*, **35**, 895 (1961).

(45) T. L. Hill, *ibid.*, **16**, 399 (1948).

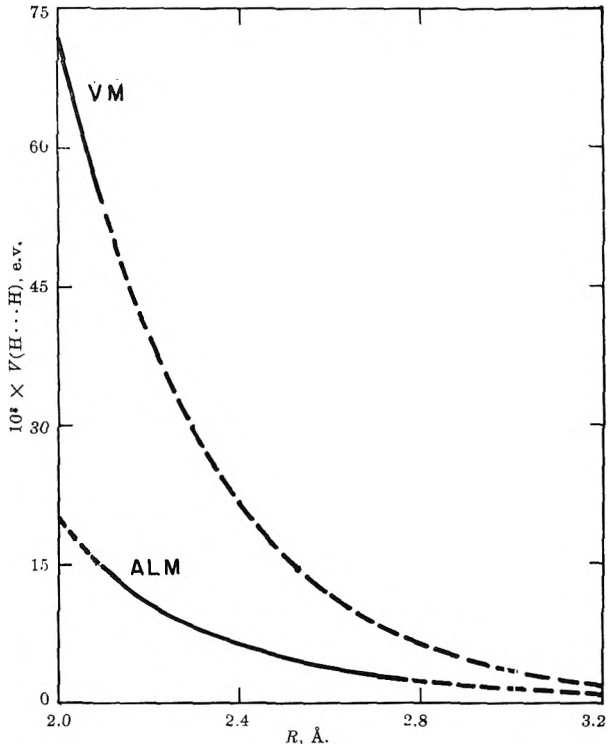

Figure 2. Potential energy functions for nonbonded H · · · H repulsions. VM is from ref. 42, and ALM is from ref. 44.

and H bonded to C. Therefore, a fundamental deficiency in these methods is indicated by the marked difference between the experimental potential functions.

Intermolecular repulsions are often represented by an inverse power law of the type λr^{-n}, where n is between 9 and 12.[46] Wilson assumes an inverse-tenth-power potential for intramolecular H · · · H repulsions, and shows on this basis that nonbonded interactions cannot be the sole source of the barrier in both ethane and methylsilane.[47] However, this function appears to decrease too rapidly with increasing distance to represent intramolecular interactions between nonbonded hydrogen atoms. The Amdur, Longmire, and Mason function for nonbonded H · · · H interactions is inversely proportional to the 6.18 power of the distance,[44] an empirical function of Aston, Isserow, Szasz, and Kennedy has an inverse fifth-power potential,[48] and the proton–proton repulsions, which must be included in any complete treatment of these molecules,[18,19] are of course inverse first-power.

H · · · H Interactions in Molecular Vibrations

Conventional Urey–Bradley analyses of vibrational spectra indicate anomalously low intramolecular repulsions between nonbonded hydrogen atoms. Bartell and Kuchitsu have recently used a modified Urey–Bradley analysis in studying the vibrational spectra of simple hydrides.[49] They find that nonbonded H · · · H repulsive forces in these molecules are compatible with the nonbonded potential functions of Bartell,[41] Hill,[45] and Vanderslice and Mason.[42] (These functions, and the corresponding contributions of nonbonded repulsions to the ethane barrier, have been considered above.)

Another modified Urey–Bradley analysis, the hybrid-orbital force field, gives a similar value for the nonbonded repulsive force constant in ammonia.[50] On the other hand, a modification which considers the lone pair of electrons leads to small values for nonbonded interactions in the group V hydrides.[51]

The vibrational amplitude of deuterium is smaller than that of hydrogen, and it has been suggested that the lack of sensitivity of the ethane barrier to deuterium substitution is therefore evidence that steric repulsion between hydrogen atoms is not the principal cause of the barrier.[52] Using Bartell's model of steric isotope effects,[53] the difference between the rotational barriers in ethane and deuterioethane is calculated to be about 0.031 kcal./mole. As mentioned above, the ethane barrier calculated from Bartell's H · · · H potential function is 0.41 kcal./mole. Thus, the steric effect of deuterium substitution is estimated to be only about 8% of the steric contribution to the barrier height.

Conclusions

Quantitative agreement among various methods of calculation is lacking, but this is not surprising considering the present state of quantum chemistry with regard to molecules as complex as ethane. The semi-empirical formulas of Mulliken indicate fairly large contributions (*ca.* 50%) of nonbonded H · · · H repulsions to the internal rotation barrier in ethane. Valence-bond calculations consistent with the valence-bond method, and potential functions derived from data on intermolecular interactions, show relatively small contributions (*ca.* 15% or less) from nonbonded interactions. A number of valence-bond calculations giving much larger contributions (*ca.* 60–100%) have been reported, but they all involve one or more of the following: (a) use of the Morse function; (b) assumption of an unrealistically high proportion (85–100%) of exchange energy; (c)

(46) J. E. Lennard-Jones, *Physica*, **4**, 941 (1937).

(47) E. B. Wilson, Jr., *Proc. Natl. Acad. Sci. U. S.*, **43**, 816 (1957).

(48) J. G. Aston, S. Isserow, G. J. Szasz, and R. M. Kennedy, *J. Chem. Phys.*, **12**, 336 (1944).

(49) L. S. Bartell and K. Kuchitsu, *ibid.*, **37**, 691 (1962).

(50) W. T. King, *ibid.*, **36**, 165 (1962).

(51) M. Pariseau, E. Wu, and J. Overend, *ibid.*, **39**, 217 (1963).

(52) W. F. Libby, *ibid.*, **35**, 1527 (1961).

(53) L. S. Bartell, *J. Am. Chem. Soc.*, **83**, 3567 (1961); *Iowa State J. Sci.*, **36**, 137 (1961); *J. Chem. Phys.*, **36**, 3495 (1962).

omission of the coefficient $^1/_2$ in eq. 1. Proton–proton repulsion energies consistently give very large contributions (*ca.* 170%) to the barrier in ethane and similar molecules.[19]

It should be emphasized that there exist several nonbonded potential functions which give good barrier heights for ethane and a number of other molecules.[15-19,48] Although the theoretical significance of these functions is not completely clear at present, their existence suggests that further work on the role of nonbonded interactions in internal rotation may be fruitful. One factor not previously considered in this connection is the role of hybridization by the excited 2s and 2p orbitals in expanding and polarizing the hydrogen atoms, which has proved to be so important in recent studies of the hydrogen bond.[54-57] The effect of these excited orbitals will be to increase the overlap between nonbonded hydrogens in the same molecule, and hence to increase the nonbonded repulsion energy above that calculated using 1s orbitals only for the hydrogen atoms.

Polarization will increase intramolecular repulsions, where the hydrogens form bonds in the same general direction, and decrease intermolecular repulsions where the bonds are in the opposite direction. Thus the appropriate potential function for intramolecular H · · · H interactions will be larger in magnitude for a given internuclear distance than the potential function for intermolecular H · · · H interactions. It will also have an angular dependence somewhat similar to that introduced empirically by Howlett.[16] Different potential functions for H bonded to H and H bonded to C should result from differences in the extent to which the hydrogen 2s and 2p orbitals participate in different molecules.

In the hydrogen molecule, the coefficient of the $2p\sigma$ orbital is about 0.10 (where the coefficient of the 1s orbital is taken as unity).[58] The corresponding value in H_2^+ is 0.1605 (or 0.145 if different effective nuclear charges are used for the 1s and 2p orbitals).[59] The coefficients of the hydrogen $2p\sigma$ and $2p\pi$ orbitals on the same basis are, respectively, 0.088 and 0.031 in H_2O and 0.107 and 0.002 in HF.[56] These rather large coefficients indicate that excited hydrogen orbitals may be of considerable importance in the theory of nonbonded H · · · H interactions.

Acknowledgments. The authors are indebted to Gio Wiederhold and Emmett B. Moore, Jr., for adaptation of the computer program. The financial assistance of a research grant from the National Science Foundation is gratefully acknowledged.

(54) I. Fischer-Hjalmars and R. Grahn, *Acta Chem. Scand.*, **12**, 584 (1958).

(55) L. Paoloni, *J. Chem. Phys.*, **30**, 1045 (1959).

(56) R. Grahn, *Arkiv Fysik*, **15**, 257 (1959).

(57) E. Clementi and A. D. McLean, *J. Chem. Phys.*, **36**, 745 (1962).

(58) N. Rosen, *Phys. Rev.*, **38**, 2099 (1931).

(59) B. N. Dickinson, *J. Chem. Phys.*, **1**, 317 (1933).

Nonresonant Dispersion and Absorption of Certain Polar Gases as Compressed Gas Mixtures in Helium[1a]

by Prasad K. Kadaba and Surendra K. Garg[1b]

Department of Electrical Engineering, University of Kentucky, Lexington, Kentucky
(Received August 7, 1963)

The dispersion and absorption of microwave radiation of 1650 ± 1 Mc. by $CClF_3$, CHF_3, $CHClF_2$, and COS has been studied in concentrations in helium ranging from 5 to 30% at a temperature of 28 ± 0.2°. The measurements were carried up to a pressure of 50 atm. unless limited by the vapor pressure of the polar constituent. The data of $CClF_3$ up to the concentrations studied and the 10 and 20% mixtures of CHF_3 in helium closely fit the Debye equation. Only in the case of 30% CHF_3–He mixture was there evidence of a distribution of line widths. The absorption of the slightly asymmetric top molecule $CHClF_2$ in helium was found to be of typical nonresonant type observed for symmetric top molecules and the absorption in COS–He mixture was not more than 3×10^{-7} atm.$^{-1}$ up to the highest pressure used. The results have been used to calculate the effective collision diameters both for mixed collisions and collisions between similar polar molecules, and the mixed-collision diameters in the various cases were found to be much less than the kinetic-collision diameters. The Clausius–Mosotti function in the various mixtures up to the pressure ranges covered was not constant but exhibited more or less linear behavior.

Introduction

The study of molecular spectra has provided a great deal of information about the magnitude and nature of interatomic forces. Less is understood, however, about the nature of intermolecular forces although a number of experimental methods are being used to examine them. The major interactions usually considered to operate between a molecule and its neighbors are dipole–dipole, dipole–induced dipole, dispersion (induced dipole), and repulsive (orbital overlap) interactions. A closer insight into the nature of dipolar and other intermolecular interactions can be obtained in simple cases from measurements on the pressure broadening of spectral lines. As coherent sources of radiation are readily available in the microwave region, it is possible to make accurate determinations of the width and shape of microwave spectral lines. At all but the lowest pressures, the width of the spectral lines in the microwave region is determined by collision broadening due to the effects of intermolecular collisions in the gas. Information about molecular force fields out to distances considerably greater than can be studied by kinetic theory methods can be obtained by such studies. Also this type of investigation provides a very good source of information concerning the angular distribution of angular momenta of the molecules. In particular the inversion transitions in nonplanar gaseous molecules have engaged the attention of many workers in recent years. The effect is studied either by measuring the nonresonant absorption in the microwave region[2a] or by examining the frequency variation of the permitivity of the gas.[2b] The existing theoretical treatments of nonresonant dispersion and absorption have proved to be of limited validity in the interpretation of the experimental results. In particular mention should be made of the line-shape equation of Van Vleck and Weisskopf[3] and the impact theory of Anderson.[4] For symmetric

(1) (a) This work was assisted by a contract with the U. S. Atomic Energy Commission; (b) Postdoctoral Research Fellow.

(2) (a) See, for example, G. Birnbaum and A. A. Maryott, *Phys. Rev.*, **92**, 270 (1953); (b) J. E. Boggs and A. P. Deam, *J. Phys. Chem.*, **64**, 248 (1960).

(3) J. H. Van Vleck and V. F. Weisskopf, *Rev. Mod. Phys.*, **17**, 227 (1945).

top molecules it has been found possible to calculate the observed intensity and frequency variation of the nonresonant microwave absorption from the Van Vleck–Weisskopf equation using the dipole moment matrix element for inversion and assuming the resonant frequency of inversion to be essentially zero.[5] Anderson's quantum mechanical treatment has been successful in predicting the line width of some resonance absorption lines, in particular those comprising the inversion spectrum of NH_3. His theory, however, has not been successful in the prediction of the magnitude of the line width parameter for nonresonant spectra.[6] Generalizations of Anderson's theory have been attempted by several workers[7-9]; but these theories although proven successful in particular cases nevertheless have not been successful in explaining the behavior of nonresonant spectra in general.

It has been found worthwhile to study the nonresonant absorption in gaseous mixtures with simple gases as solvents.[10] Such solvents present some advantages, namely, gaseous mixtures can be studied over a wide range of pressures, and as the relative broadening efficiencies of different solvents differ more markedly it is possible to study different types of intermolecular interactions from the effective collision diameters calculated from the results. It is in this direction that the present investigation is directed and the nonresonant spectra of simple molecules such as $CClF_3$, CHF_3, $CHClF_2$, and COS have been measured both through absorption and dispersion in concentrations in helium from 5 to 30%. The measurements have been carried up to 50 atm. unless limited by the vapor pressures of the polar constituent.

Experimental

Figure 1 shows a block diagram of the experimental setup. The general features of the design are similar to the method used by Heineken and Battaglia[11] at a frequency of 25 Gc. A 5837 Raytheon reflex klystron is frequency modulated at a frequency of 60 c.p.s. by a triangular voltage on its reflector. The triangular voltage was obtained by a function generator synchronized by a 60 cycle sine wave. Part of the frequency modulated output of the oscillator is transmitted through a directional coupler to a reference transmission cavity C_1 tuned to a frequency of 1650 ± 1 Mc. The rest of the output is transmitted to the test cavity C_2, also tuned to the same frequency as the reference cavity. The cavities are operated in the TE_{011} mode with a loaded Q of 40,000 for the evacuated cavities.[12] The outputs of the cavities after being detected by two 1N21E crystal detectors are amplified to 300 v. by linear amplifiers. The signals then pass through

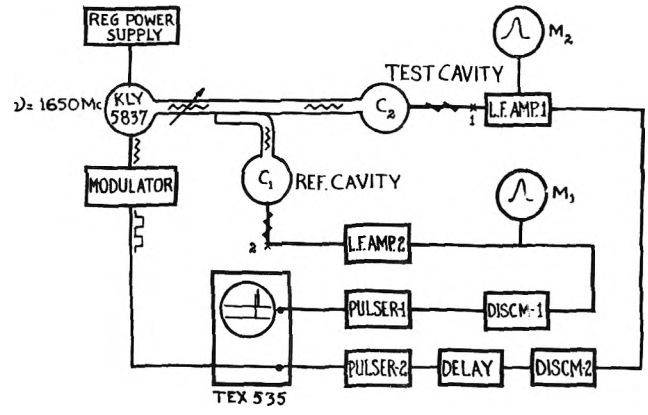

Figure 1. Schematic diagram of the set-up.

a set of discriminators and pulsers where pulses of channel 1 trigger the time base B of a Type 535 Tektronix scope and those of channel 2, after being sufficiently delayed, are put on the y-axis of the oscilloscope. Two pulses are seen on the screen, one for each half period of the triangular modulation voltage. The distance between the two pulses on the screen is proportional to the difference in the dielectric constants of gases in the cavities C_1 and C_2. The shift in the barycenter is a measure of the absorption coefficient of the gas. However, for the range of absorption encountered and the cavity "Q" available, it was more convenient and accurate to determine tan δ by the amplitude method[6] using the equation

$$\tan \delta = \frac{1}{Q_0}\left[\sqrt{\frac{P_0}{P}} - 1\right] \qquad (1)$$

This required measuring (1) the initial band width from which the quality factor Q_0 is obtained, (2) the initial resonance curve amplitude P_0, and (3) the amplitude P as a function of pressure of the experimental gas. In order to measure Q_0 a method similar to the one employed in an earlier investigation[13] was

(4) P. W. Anderson, *Phys. Rev.*, **76**, 647 (1949).

(5) G. Birnbaum, *J. Chem. Phys.*, **27**, 360 (1957).

(6) G. Birnbaum, Ph.D. Dissertation, George Washington University, 1956.

(7) M. Barnger, *Phys. Rev.*, 111, 481, 494 (1958); 112, 855 (1958).

(8) A. C. Kolb and H. Greim, *ibid.*, 111, 514 (1958).

(9) M. Mizushima, International Conference on Spectral Line Shape and Molecular Interactions, Weizmann Institute of Science, Rehovoth, Israel, August 28–31, 1961.

(10) G. Birnbaum and A. A. Maryott, Research Report No. 228, Hughes Research Laboratories, December, 1961.

(11) F. W. Heineken and A. Battaglia, *Physica*, **24**, 589 (1958).

(12) In order to split the interfering TM_{111} mode a concave end plate was used following a design by H. E. Bussey and G. Birnbaum, *Rev. Sci. Instr.*, **30**, 800 (1959).

used. It has been found possible to measure the dielectric constant to a relative uncertainty of 1×10^{-7} and the uncertainty in the measurement of tan δ is about 2×10^{-7}. Both the cavities were enclosed in an air thermostat and the temperatures were maintained at 28 ± 0.2°. The pressures up to 2 atm. were measured by a mercury barometer and higher pressures were measured by a set of calibrated Bourdon gages.

All of the gases used were of the purest commercially available grade and were obtained in mixture form from the Matheson Co.

Theoretical Relations

Under the assumptions of single line width parameter and the absence of significant resonance absorption the Van Vleck–Weisskopf expression[3] for the shape of the collision broadened lines can be put in the convenient form

$$\epsilon'' = \frac{4\pi N_0 p \mu^2}{3KT} \sum_{J,K} f_{JK} K^2/(J^2 + J) \frac{\nu \Delta\nu}{\nu^2 + \Delta\nu^2} \quad (2)$$

where ϵ'' is the imaginary part of the complex dielectric constant resulting from nonresonant absorption, N_0 is the ideal gas density at 1 atm., p is the pressure in atmospheres, μ is the total dipole moment, f_{JK} is the fractional number of molecules in the rotational state designated by the quantum numbers J and K, ν is the applied frequency, and $\Delta\nu$ is the half-width. It is well to point out that eq. 2 is similar to the familiar Debye equation except that only part of the dipole moment contributes to the intensity. Under the further assumption that $\Delta\nu$ is proportional to the pressure p, eq. 2 may be transformed to a linear form

$$p^2/\epsilon'' = a + bp^2 \quad (3)$$

useful for analyzing the data and particularly for demonstrating small departures from the Debye equation. The two quantities characterizing the Debye equation, namely, $\Delta\nu/p$ the line width parameter and the maximum value of tan δ/p, are related to the parameters of the preceding equation by

$$\Delta\nu/p = \nu\sqrt{b/a}$$

and

$$(\tan \delta/p)_{max} = (4ab)^{-1/2} = \frac{1.114 \times 10^{38}\mu^2}{T^2} \sum_{JK} f_{JK} K^2/(J^2 + J) \quad (4)$$

where $\tan \delta = \epsilon''/\epsilon'$, ϵ' being the real part of the complex dielectric constant.

When the data extend well above atmospheric pressure eq. 3 might need some modification for departures from the ideal gas density and for changes in the local, or polarizing, field when the dielectric constant can no longer be considered as unity. Equation 3 can then be modified to

$$(p/z)^2 F/\epsilon'' = a + b(p/z)^2 \quad (5)$$

where z is the compressibility factor and F is the local field factor which can be taken as $(\epsilon' + 2)^2/9$.[14] It should be emphasized that the factors F and z in eq. 5 both go to unity at low pressures.

Data that are not adequately represented by a single line width parameter (eq. 5) can be represented by plots of $\tan \delta/(p/z)$ as a function of $\log p/z$ provided the vapor pressure is sufficient to allow the complete curve to be delineated. The bell-shaped curve will be somewhat broader than the Debye curve for a single line width parameter and the value of $(\tan \delta/p)_{max}$ will be less than that computed from the right-hand side of eq. 4.

Experimental Results

The data for CHF_3–He mixtures at concentrations of 10, 20, and 30% of the polar constituent are plotted in Fig. 2 in the form $\tan \delta/(p/z)$ *vs.* $\log p/z$ to look for the possibility of a distribution of line widths. Figure 3 is a plot of the function $[(p/z)^2F]/\epsilon''$ *vs.* $(p/z)^2$ for the

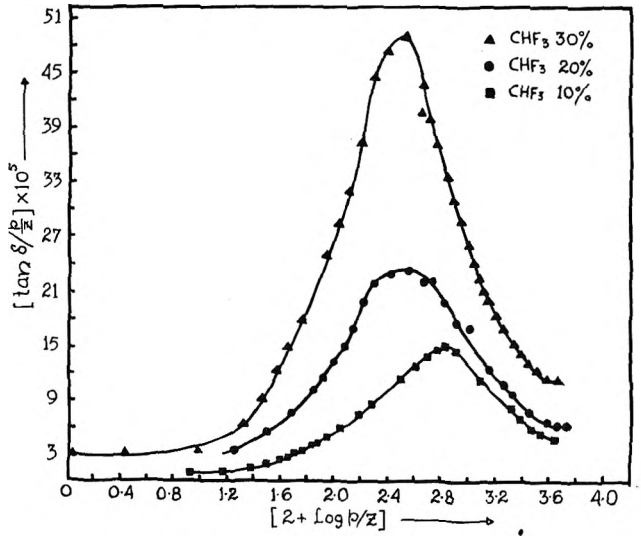

Figure 2. Variation of tan $\delta/(p/z)$ with $2 + \log p/z$ for CHF_3–He mixtures for 10, 20, and 30% concentrations of CHF_3 at 28° and 1650 Mc.

(13) D. Ilias and G. Boudouris, *IRE Trans. Microwave Theory Tech.*, 9, 144 (1961).

(14) A. A. Maryott and G. Birnbaum, *J. Phys. Chem.*, 64, 1778 (1960).

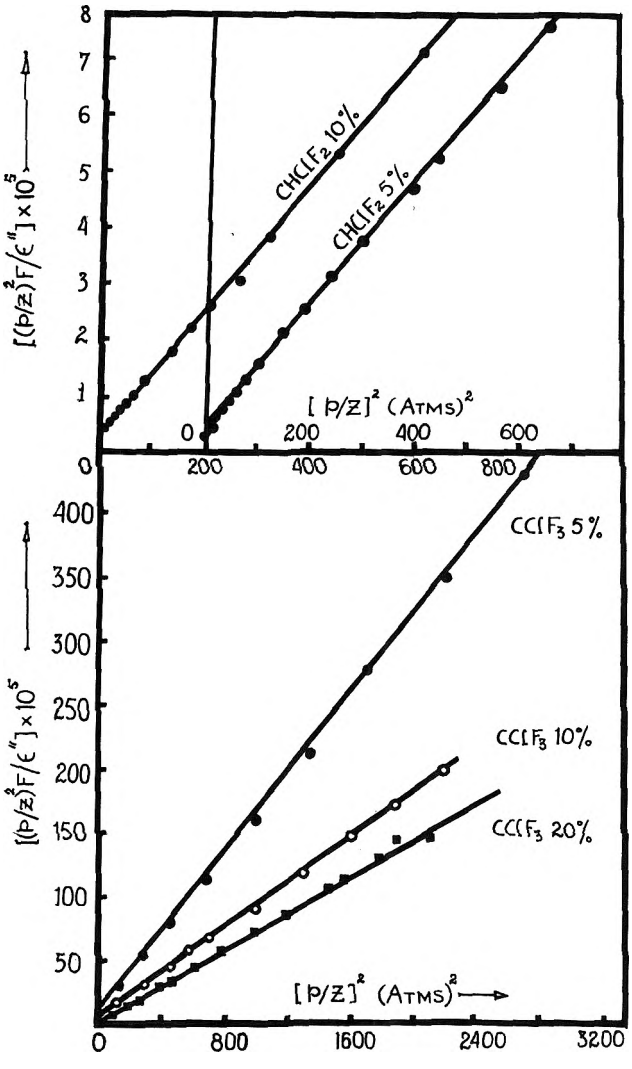

Figure. 3. Variation of $[(p/z)^2F]/\epsilon''$ with $(p/z)^2$ for mixtures of $CClF_3$ and $CHClF_2$ in helium at 28° and 1650 Mc.

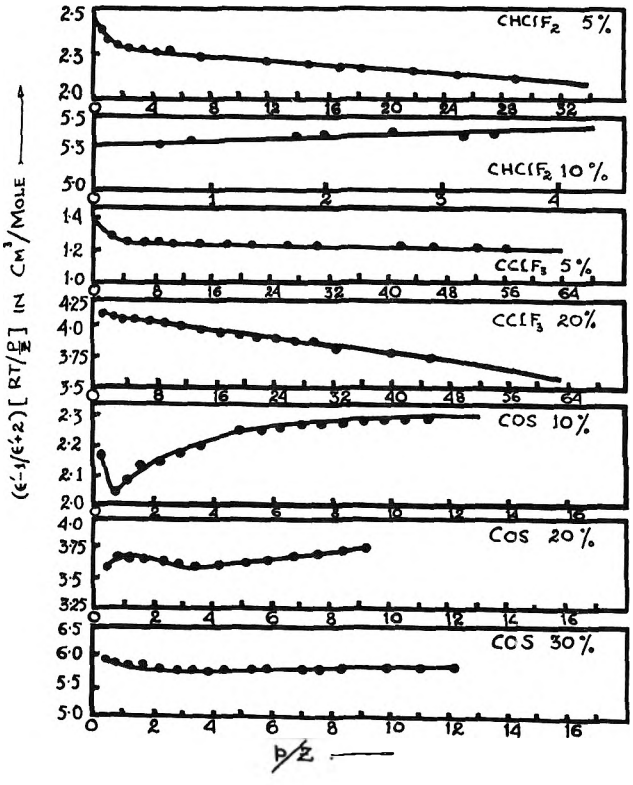

Figure 4. Variation of the Clausius–Mosotti function $[(\epsilon' - 1)/(\epsilon' + 2)][RT/(p/z)]$ with p/z for mixtures of $CHClF_2$, $CClF_3$, and COS in helium at 28° and 1650 Mc.

mixture of $CClF_3$ in helium at the various concentrations cited. Also included in the same figure are the plots for the mixture of the slightly asymmetric top molecule $CHClF_2$ in helium at concentrations of 5 and 10% of the polar component.

The loss tangent tan δ of COS–He mixtures at concentrations of 10, 20, and 30% of COS have been measured up to a pressure of 12 atm. The data indicate an anomalous dependence on pressure with the value of tan δ less than 3×10^{-7} atm.$^{-1}$ at the highest pressure. Very low loss has been observed even in pure COS at frequencies of 23.34 Gc. and 9.106 Gc.[15]

Figure 4 is a plot of the Clausius–Mosotti function $[(\epsilon' - 1)/(\epsilon' + 2)][RT/(p/z)]$ in cm.^{3}/mole, calculated from the dielectric constant–pressure data *vs.* p/z for the various gases at the concentrations in helium indicated in the figure.

The compressibility factor z was calculated with the help of the literature.[16,17] The calculations involved essentially the evaluation of the second virial coefficient from which z was derived. All data were obtained at 28 ± 0.2°.

Discussion

The 10 and 20% data in Fig. 2 for CHF_3–He mixtures follow closely eq. 5, which is the Debye equation. The closeness of the experimental data to the Debye shape for these two concentrations indicates that the results can be represented accurately by a single line width parameter. But in the case of 30% mixture the experimental curve is somewhat broader than the Debye curve indicating the possibility of a distribution of line widths. Such distribution of line widths has been ob-

(15) Private communication with Dr. A. A. Maryott, National Bureau of Standards, Washington, D. C.

(16) J. O. Hirschfelder, C. F. Curtiss, and R. B. Bird, "Molecular Theory of Gases and Liquids," John Wiley and Sons, Inc., New York, N. Y., 1954, Chapter 3, Section 10.

(17) L. F. Albright and J. J. Martin, *Ind. Eng. Chem.*, **44**, 188 (1952).

served for pure CHF_3 in an earlier investigation[18] of its relaxation absorption spectrum at a frequency of 1193 Mc. up to a pressure of a little over an atmosphere.

The linearity of the plots in Fig. 3 for $CClF_3$–He mixtures up to the range of pressures studied indicates that the data follow closely the Debye equation. Also the $(\tan \delta/p)_{max}$ values computed from the right-hand side of eq. 4 correspond closely with the experimental value. These results indicate clearly the absence of a distribution of line widths and also the absence of any significant resonance absorption in the various $CClF_3$–He mixtures up to a pressure of 49 atm., the highest pressure used in this investigation. Loss measurements on pure $CClF_3$ at a frequency of 1190 Mc. have been reported in an earlier investigation[14] up to a pressure of about 31 atm. at 30°. The results indicate that the loss arising from the rotational transitions is insignificant below 10 atm. and comprises about 25% of the total loss at the highest pressure used in their investigation.

The data presented in Fig. 3 for $CHClF_2$ in helium in a plot of $[(p/z)^2F]/\epsilon''$ against $(p/z)^2$ is linear at the higher pressures with a slight departure from linearity, if any, at the lower pressures in the case of the 5% mixture. The data on pure $CHClF_2$ at 9400 Mc. in an earlier work[19] showed a similar behavior, the curvature at low pressures being attributed to the effect of nearby rotational lines. $CHClF_2$ should have a component of dipole moment along the a-axis (least moment) which would allow transitions between the asymmetry doublet levels. Many of these levels will be nearly degenerate; and therefore, nearly zero inversion frequencies can occur.[20] Absorption which is of the nonresonant type has been reported for $CHCl_2F$ and also for certain other asymmetric rotors.[21,22]

Our data on COS–He mixtures are quite consistent with the data obtained on the pure gas.[15] In COS the diagonal element of the dipole interaction vanishes because the dipole is pictured as rotating about an axis perpendicular to its electric moment. Any contribution to the loss from a possible l-type doubling would be much too small to account for the observed loss.

The Clausius–Mosotti function represented in Fig. 4 indicates a more or less linear variation of C–M function with pressure over the ranges covered whereas according to the classical Lorentz theory, the C–M function should be independent of density.

The effective collision diameters which represent the relative effectiveness of collisions in changing the orientation of the molecules may be computed, both for mixed collisions and collisions between similar polar molecules, from the formula[23]

$$2\Delta\nu = n_a V_a (b_{PB})_{aa}^2 + n_b V_{ab} (b_{PB})_{ab}^2 \quad (6)$$

where $\Delta\nu$ is the line width, n_a and n_b are the number of molecules of the two species present, V_a is the velocity of the polar molecule, $V_{ab} = (V_a^2 + V_b^2)/2$ is the mean relative velocity, and $(b_{PB})_{aa}$ and $(b_{PB})_{ab}$ are the pressure-broadening collision diameters of collisions between similar polar molecules and mixed collisions, respectively. In the case of collisions between similar polar molecules, the collision diameters calculated from eq. 6 above agree very well with the values found in the literature.

Table I gives the numerical values of the collision diameters, b, of collisions between similar polar molecules obtained in this way from our measurements along with the values in the literature of collision diameters derived from nonresonant absorption of pure gases, viscosity data, and rotational absorption. Also included in Table I are the velocities V of the polar molecule. Table II gives the nonresonant line width parameters ν_{12}, in cm.$^{-1}$ atm.$^{-1}$, the mixed collision diameters b_{12}, and $(\tan \delta/p)_{max}$ values obtained from our measurements. Also included in this part of the table are the nonresonant collision diameters and kinetic theory collision diameters for mixed collisions available in the literature.

Table I: Nonresonant, Rotational, and Kinetic Collision Diameters of Halomethanes (from Gaseous Mixtures)

Gas	V,[a] cm./sec. × 10^{-4}	b, Å., our data, nonresonant	b, Å.,[b] viscosity data	b, Å.[c] nonresonant, pure, 26°	b, Å.,[d] rotation
$CClF_3$	3.49	5.16	4.96	5.2	21[d]
CHF_3	4.25	5.10	4.33	5.3	16[e]
$CHClF_2$	3.83	6.73	4.68		

[a] Relative velocity of impact which is equal to $\sqrt{2}$ times the mean velocity. [b] G. A. Miller and R. B. Bernstein, *J. Phys. Chem.*, **63**, 710 (1959). [c] G. Birnbaum, Ph.D. Dissertation, George Washington University, Washington, D. C., 1956. [d] For the $J = 2 \rightarrow 3$ transition. [e] For the $J = 1 \rightarrow 2$, $K = 1$ and $K = 0$ transitions.

The nonresonant collision diameters for collisions between similar polar molecules are substantially

(18) G. Birnbaum, *J. Chem. Phys.*, **27**, 360 (1957).
(19) J. E. Boggs and H. C. Agnew, *J. Phys. Chem.*, **63**, 1127 (1959).
(20) E. B. Wilson, Jr., *ibid.*, **63**, 1339 (1959).
(21) J. E. Boggs and A. P. Deam, *J. Chem. Phys.*, **32**, 315 (1960).
(22) Krishnaji and G. P. Srivastava, *Phys. Rev.*, **106**, 1186 (1957).
(23) J. O. Hirschfelder, *et al.*, ref. 16, Chapter 13, Section 7.

Table II: Nonresonant Line Width Parameters, ν_{12}, and Collision Diameters, b_{12}, at 28°. for Mixed Collisions at Different Concentrations

Gas	Percentage composition of polar constituent, %	ν_{12}, cm.$^{-1}$ atm.$^{-1}$ × 10^2	b_{12}, Å., nonresonant	b_{12}, Å.,[a] nonresonant	b_{12}, Å., kinetic	$(\tan \delta/p)_{max}$ × 10^5
$CClF_3$–He	4.96	0.706	1.22		3.76	0.427
$CClF_3$–He	9.75	0.923				0.721
$CClF_3$–He	22.2	1.332				1.637
CHF_3–He	10.2	0.784	0.95	0.92(30°)	3.30	1.430
CHF_3–He	21.5	1.252				2.335
CHF_3–He	30.7					4.740
$CHClF_2$–He	5.7	0.913	1.21		3.60	3.624
$CHClF_2$–He	12.3	1.342				7.640

[a] G. Birnbaum and A. A. Maryott, Research Report No. 228, Hughes Research Laboratories, December, 1961.

larger than those derived from Lennard-Jones potential and smaller than those derived from rotational spectral lines, which indicates that the pertinent forces are evidently of the long range dipole–dipole type and are predominant if not the principal interaction. In essence, this may be taken to indicate as Birnbaum has suggested[24] that it is more difficult to orient the molecule than to change the rotational energy, and even more difficult to transfer kinetic momentum.[25] In the case of collisions with helium it is reasonable to expect that the average kinetic collision causes only a small angular reorientation of the polar molecule so that a number of such collisions would be required for random reorientation. The nonresonant b_{12} values in Table II are much less than the kinetic collision diameters. A detailed explanation of this result could probably be based on repulsive forces in the same way as the high frequency shifts in the infrared spectra of liquids under pressure have been explained.[26] A quite different kind of evidence which may well be relevant comes from spectroscopic studies of frequency shifts on adding foreign gases of simple molecules. Studies of this kind on the 21-cm. line of atomic hydrogen and rotational lines in the first overtone band of HCl show shifts which are increasingly to longer wave lengths for more polarizable foreign gases. However, for helium the shifts are to shorter wave lengths, which have been attributed to relatively more important repulsive effects.[27] The qualitative behavior does not seem inconsistent with the observed dielectric interaction effects.

Acknowledgments. The authors wish to express their thanks to Dr. A. A. Maryott for a very helpful discussion and to Prof. P. J. Graham for helpful suggestions in the construction of the experimental apparatus.

(24) See ref. 6, p. 86.

(25) It is perhaps appropriate to mention that although the idea of collision diameters is useful, for instance in the determination of the force law, force law in many cases is so complicated that the collision diameters are hardly meaningful without detailed discussion.

(26) A. M. Benson, Jr., and H. G. Drickamer, *J. Chem. Phys.*, **27**, 1164 (1957).

(27) M. A. Hirshfeld, J. H. Jaffe, and S. Kimel, *ibid.*, **32**, 297 (1960).

Electron Spin Resonance of Some Free Radicals and Related Negative Ions[1a]

by Hisashi Ueda[1b]

Department of Chemistry, The University of British Columbia, Vancouver, B. C., Canada
(Received August 19, 1963)

Electron spin resonance (e.s.r.) spectra from diphenylpicrylhydrazine negative ion, Lophine-x negative ion, and from solutions of Lophine-x illuminated with light have been recorded and analyzed. The unpaired electron spin densities estimated from these spectra, using −22.5 as aromatic proton coupling constant together with the result from biphenylaminium ion, BPA, already reported, have been compared with computed spin densities. In these species with nitrogen atoms in their network of atomic nuclei, the shape of the wave function for the unpaired electron depends greatly upon the amount of electric charge on the species, since the value of the coulomb integral on the nitrogen atom is altered by its electric charge because the electronegativity of nitrogen is different from that of carbon. The computed results for BPA (+) agreed well except for the positions where negative spin densities should be placed. The computed values for BPA (−) showed smaller spin density for nitrogen. The computed result for Lophine-x illuminated with light agreed fairly well with the observed result for after a correction for negative spin densities had been made. However, the computed result for Lophine-x (−) did not agree well with the observed results. The computed spin densities for BPA (+), after being corrected for negative spin densities, gave the following relation for the nitrogen splitting constants: $Q_1 = 18.7 + 0.275Q_2$.

Introduction

Many studies of spin density distributions in aromatic free radicals and ions have been carried out. In most cases, the experimental result for a network of atomic nuclei is obtained either from a positive or negative ion alone or from a free radical alone. In some cases,[2a,b] both positive and negative ions were observed from the same network. In the present study, two paramagnetic species derived from the same network were observed, one of a free radical nature and the other of an ionic nature. Brown and his co-workers[3] have estimated the spin densities in the biphenylaminium ion, which is a fragment of a free radical, *i.e.*, DPPH, by the valence bond method, assuming the value 1.2 as the ratio of the C–N to C–C exchange integrals. The result of this calculation did not agree well with the experimental values obtained subsequently by the present author and his co-workers.[4]

In a molecular orbital calculation, the values for the coulomb and exchange integrals of a heteroatom can be varied more easily than in a valence bond calculation. Also, only the lowest eigenvalue of the energy level system gives an accurate eigenfunction in the case of valence bond calculations, while in the molecular orbital approach, the energy levels are filled with electrons according to the Auf-Bau principle. Therefore, a molecular orbital calculation is more convenient in a case where the same network of atomic nuclei can hold a different number of electrons.

One of such cases is that of the biphenylaminium ion, abbreviated BPA (+), and diphenylpicrylhydrazine ($DPPH_2$) negative ion (essentially BPA (−)). Another example is Lophine-x[5] and its negative ion, (−) or (2−). This had previously been found to give only a single e.s.r. absorption line.[5] However, the development of the 100-kc. high resolution-type spec-

(1) (a) Presented at the Annual Northwestern Regional Meeting of the American Chemical Society, Bellingham, Wash., June, 1963; (b) Department of Chemistry, The University of Texas, Austin, Texas.

(2) (a) A. Carrington, F. Dravniek, and M. C. R. Symons, *J. Chem. Soc.*, 947 (1959); (b) C. A. McDowell and J. R. Rowlands, *Can. J. Chem.*, **38**, 503 (1960).

(3) T. H. Brown, D. H. Anderson, and H. S. Gutowsky, *J. Chem. Phys.*, **33**, 720 (1960).

(4) H. Ueda, Z. Kuri, and S. Shida, *ibid.*, **36**, 1676 (1962).

(5) T. Hayashi, K. Maeda, S. Shida, and K. Nakada, *ibid.*, **32**, 1568 (1960).

trometer and an optical condenser system made it possible to observe the hyperfine splitting easily. Paramagnetic ion was also prepared by reducing Lophine-x with potassium.

Experimental

The negative ions were prepared by reducing the neutral compounds with potassium in pure dimethoxyethane. The e.s.r. signal from Lophine-x irradiated with light was observed from its benzene or dimethoxyethane solution. Both highly purified and crude undegassed solvents gave the same result. The solution was illuminated with 60-w. desk lamp, operated at 125 v. a.c. and at 60 c.p.s. The light was focused onto the sample tube through the slits of the microwave cavity.

E.s.r. spectra were taken with a high resolution-type spectrometer employing a modulation frequency of 100 kc.p.s. All the spectra were recorded as the first derivative of the absorption curve using a magnetic field modulation width less than 10% of the hyperfine line width. The errors in the measurements are less than ±70 mgauss. Therefore, if the error of the splitting constant (−22.5) is neglected, all the observed spin densities for =C—H carbons have an error of ±0.003

Results

1. Procedure for Analysis of the Spectra. If there are n groups of protons interacting with the unpaired electron with splitting factors $\rho_i Q'$ ($i = 1$ to n), where ρ_i denotes the spin density on the carbon atom to which one of the ith group of protons is attached, the resonance positions of the lines, H_r, numbered by r and measured from the center of the spectrum in gauss is shown to be

$$H_r(M_iM_jM_k) = (M_i\rho_i + M_j\rho_j + M_k\rho_k)Q' \quad (1)$$

where M_i is the total nuclear spin quantum number of the protons belonging to the ith group and is $-N_i/2 \leq M_i \leq N_i/2$. N_i is the number of protons in the ith group. If another combination of the nuclear spin quantum numbers $M_i'M_j'M_k'$ and spin densities $\rho_i'\rho_j'\rho_k'$ give H_s which is equal to H_r, then

$$H_r = H_s(M_i'M_j'M_k') = (M_i'\rho_i + M_j'\rho_j + M_k'\rho_k)Q'$$

The total intensity for this line, y, is

$$y = y_r + y_s = \mathrm{f}(N_i,M_i)\,\mathrm{f}(N_j,M_j)\,\mathrm{f}(N_k,M_k) + \mathrm{f}(N_i,M_i')\,\mathrm{f}(N_j,M_j')\,\mathrm{f}(N_k,M_k')$$

where $\mathrm{f}(N_i,M_i) = {}_{N_i}C_{N_i-2|M_i|}$.

2. The E.s.r. Spectrum of Diphenylpicrylhydrazine Negative Ion, $DPPH_2(-)$. Figure 1 shows the e.s.r. spectrum of $DPPH_2$ negative ion. The spectrum was analyzed in the manner described in section 1. The

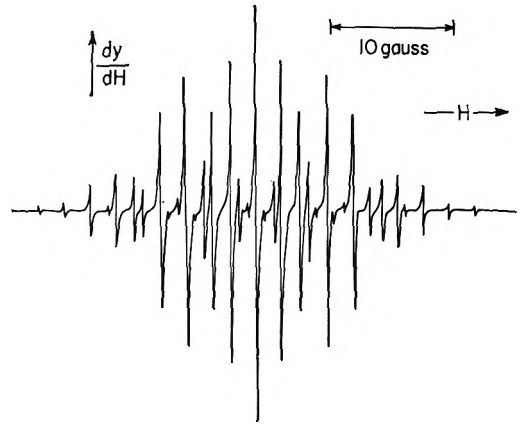

Figure 1. E.s.r. spectrum from diphenylpicrylhydrazine negative ion produced by potassium in dimethoxyethane.

observed H_r values for $DPPH_2$ (−) are $H_r = 5.70M_1 + 2.10M_2$, where $N_1 = 4$, $N_2 = 6$, $y_r = {}_4C_{4-2|M_1|} \times {}_6C_{6-2|M_2|}$. The calculated and observed e.s.r. intensities are listed in Table I. In the case of BPA (+) ion,[4] it was found that the *o*- and *p*-positions, Fig. 5A, had the same spin density. However, in the case of $DPPH_2$ (−), the six equivalent protons can be either 2*p*- + 4*o*- or 2*p*- + 4*m*-. The computed results (Table V), favor the latter possibility.

No splitting factor for the two nitrogens is observed. This indicates that the electron spin is localized on the two phenyl rings. Thus, the two protons attached to the picryl ring, *m'*-positions, can be excluded from the six equivalent positions. Therefore, M_1 is for the *o*- and M_2 for the *m*- and *p*-positions, respectively. The spin densities calculated, using $Q' = 22.5$, are listed in Table V. The sum of the absolute values of the spin densities for the *o*-, *m*-, and *p*-positions is 1.574. Therefore negative spin densities should be placed on some positions.

3. E.s.r. Spectra of Lophine-x, When Illiminated with Light. (A) Hyperfine Structure of the Spectrum from Solution. The spectrum as shown in Fig. 2 was observed. In this case either

$$H_r = 2.93M_1 + 1.75M_2;\ |M_1| \leq 1,\ |M_2| \leq 7 \quad \text{(A)}$$

or

$$H_r = 2.93M_1 + 1.75M_2 + 3.50M_3;\ |M_1| \leq 1,\ |M_2| \leq 2,\ |M_3| \leq 3 \quad \text{(B)}$$

interprets the positions of the lines. However, the intensity ratios from relation A deviate too much from the observed value. In this case, M_2 can be assigned to the two nitrogens. The intensity ratios at the center

Table I: Observed and Calculated E.s.r. Intensities for $DPPH_2$ (−) Ion

	r[a]																	
	1	2	3	5	7	9	12	4	6	8	11	14	16	17	10	13	15	18
Exptl.	1	4	14	21	13	4	1	3	18	56	76	56	18	4	6	28	85	120
Calcd.	1	6	15	20	15	6	1	4	24	60	80	60	24	4	6	36	90	120

[a] r is defined such that $H_r < H_{r+1}$; $r = 3$ means the third line from the lower field side of the spectrum.

Table II: Observed and Calculated E.s.r. Intensities for Lophine-x

	r[a]																								
	1	3	7	2	5	10	4	8	13	6	11	16	9	14	19	12	17	22	15	20	25	18	23	28	21	26
Obsd.	0	3	6	0	6	11	19	23	17	17	35	29	40	80	52	80	150	95	121	207	132	156	270	156	172	300
4-H	1	2	1	4	8	4	12	24	12	28	56	28	52	104	52	84	168	84	116	232	116	140	280	140	150	300
2-N	1	2	1	3	6	3	15	30	15	23	46	23	58	115	58	70	140	70	118	237	118	117	235	117	150	300

[a] In this column, r is from relations A and B, obsd. means the observed intensity ratios, and 4-H denotes the calculated spin densities assuming four protons for M_2, and 2-N denotes the same value for two nitrogens. r is defined such that $H_r \leq H_{r+1}$. r for the central line is 26.

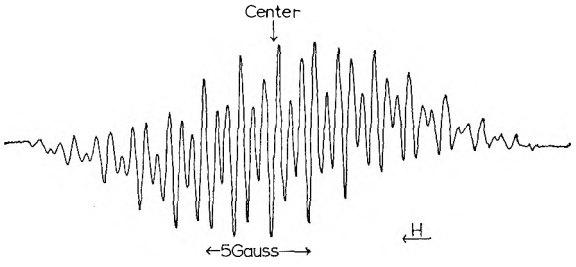

Figure 2. E.s.r. spectrum from benzene solution of Lophine-x observed when the solution was illuminated with a desk lamp.

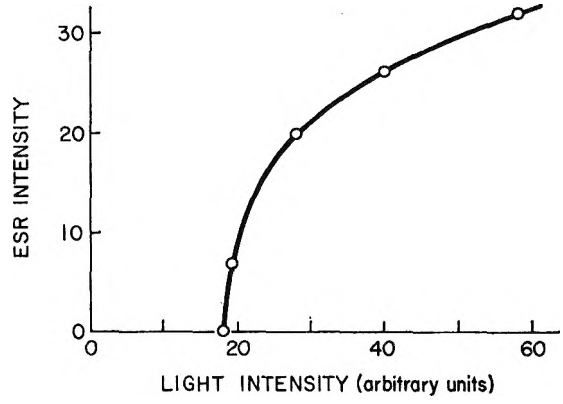

Figure 3. E.s.r. intensity of Lophine-x solution illuminated with light *vs.* light intensity.

of the spectrum are better explained by four protons than two nitrogens, Table II.

(*B*) *Decay and Formation of the E.s.r. Signal.* The decay of the e.s.r. signal after switching off the light was recorded while the magnetic field was being swept repeatedly in the range $H_1 \pm H_1'$, where H_1 is the center of the strongest line of the spectrum and H_1' is about 3 gauss. The intensity of this line, y, and the time measured from the instant when the light was switched off satisfy the relation $\log y/y_0 = -kt$ as was reported by former researchers.[5] The value k observed is 0.0820/min. at 20°. When the light is switched on again, the e.s.r. signal reappears. The intensity is expressed as a function of time, t, $y = A(1 - e^{-kt})$, where A is determined by the intensity. A is decided as $\lim (t \to \infty)y$. The relation between A and light intensity is shown in Fig. 3. The value of A does not increase linearly with respect to the light intensity. This is interpreted by the sparing solubility of this compound in the solvent.

4. The E.s.r. Spectrum of Lophine-x when Reduced with Potassium. The e.s.r. spectrum of this compound when reduced with potassium in dimethoxyethane is shown in Fig. 4. The position of resonance, H, is written as

$$H = \sum_i 1.173 i M_i$$

The spectrum shows that there are four exactly equivalent protons and another four approximately equivalent protons. If $|M_1| \leq 2$, $|M_4| \leq 1$, $|M_5| \leq 1$ are assumed, the intensity ratio calculated is as shown in Table III. The two nitrogens give intensity ratios similar to that of four protons, since $|M_1| \leq 2$; however, the four protons fit better (Table III). These four equivalent positions are the four *m*- or four *o*-positions,

Fig. 5B, and the two equivalent positions are two *p*-, two *m'*-, or two *o'*-positions.

Table III: Observed and Calculated E.s.r. Intensities for Lophine-x (−)

	1	2	3	4	5	6	7	8	9	10	11	12
Obsd.	1	4	7	4	3	11	21	21	11	11	24	32
4H for M_1	1	4	6	4	3	10	20	20	11	10	23	32
2N for M_1	2	4	6	3	6	12	20	20	14	16	24	32

5. Computing of the Spin Densities by the HMO Method.[6] *(A) Biphenylaminium Ion* (+). Spin densities in the biphenylaminium (+) ion have already been estimated by means of the valence bond theory.[3] In the present study the HMO method using a parameter $h_N = 0.5$ for the coulomb integral of nitrogen[7] was used. The parameters h_X are said to be equal to $\chi_x - \chi_c$ where χ_x denotes the electronegativity of the atom x and χ_c that of carbon.[7] From this respect it seems most reasonable to use the value 0.5 (3.0 − 2.5, the difference of the electronegativities of nitrogen and carbon) as the h_N value for a nitrogen atom in a molecule which does not have any extra charge on it. The coulomb and exchange integrals for nitrogen are $\alpha_N = \alpha_o + h_N\beta_o$, and $\beta_{N-C} = k_{N-C}\beta_o$,[7] where α_o and β_o are the integrals for carbon atomic orbitals. The secular equation thus obtained was solved by an electronic computer employing Householder-type programming. The seventh lowest energy eigenvalue was taken, and the spin densities from the corresponding eigenfunction are listed in Table IV.[8-12] It seems that except for the negative spin densities, the HMO method gives a good estimate.

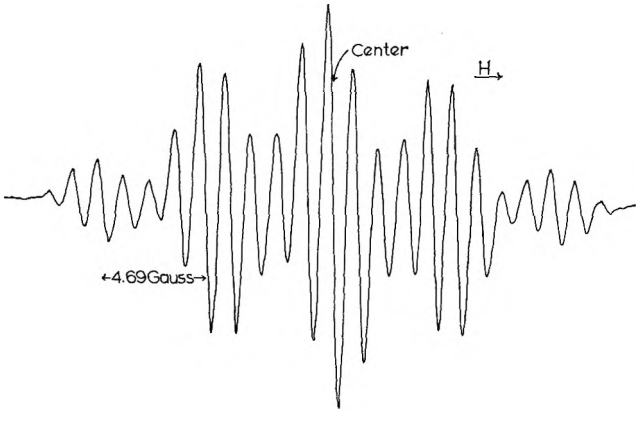

Figure 4. E.s.r. spectrum from Lophine-x negative ion produced by potassium in dimethoxyethane.

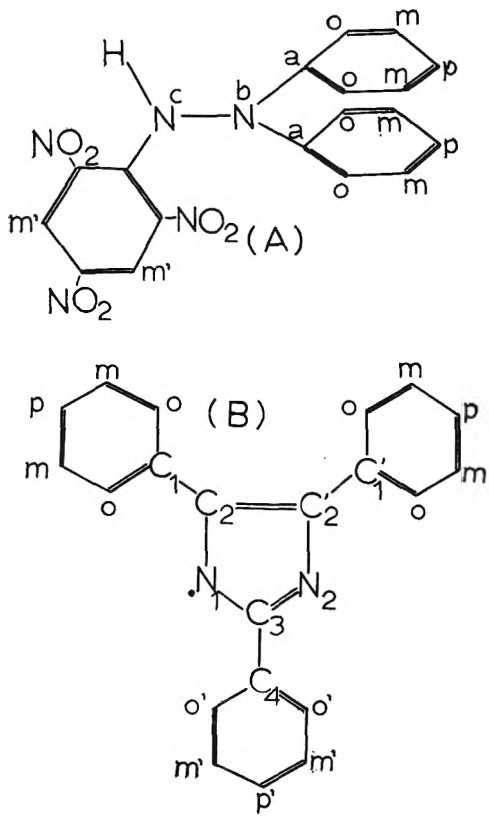

Figure 5. The networks of atomic nuclei for both BPA ions, A, and Lophine-x, B.

Table IV: Observed and Calculated Spin Densities for BPA (+)

	Positions					Parameter
	C(a)	*o*-	*m*-	*p*-	N(b)	
Obsd.-1[a]	0.046	0.084	−0.042	0.084	0.572	
Obsd.-2	0.084	0.084	−0.042	0.084	0.469	
Obsd.-3	0.102	0.084	−0.042	0.084	0.460	
Obsd.-4	0.148	0.084	−0.042	0.084	0.368	
Calcd. HMO	0.024	0.077	0.002	0.084	0.494	$h_N = 0.5$
Calcd. VB[1]	−0.258	0.262	−0.120	0.244	0.532	$k_{C-N} = 1.2$

[a] The row obsd.-1 was obtained using $Q_N = 24$ gauss and $Q_c = 49$[4] while obsd.-2 was obtained using $Q_1 = 21$ gauss and $Q_2 = 7.0$ gauss.[8-10] Obsd.-3 was obtained using 23.1 and 6.8 for Q_1 and Q_2, respectively.[11] If only Q_1 is considered (25 gauss) the result is as obsd.-4.[12]

(6) E. Hückel, *Z. Physik*, **70**, 204 (1931).

(7) A. Streitwieser, Jr., "Molecular Orbital Theory for Organic Chemists," John Wiley & Sons, Inc., New York, N. Y., 1961, p. 117.

(8) J. C. R. Henning and C. deWaard, *Phys. Letters*, **3**, 139 (1962).

(9) R. L. Ward, *J. Am. Chem. Soc.*, **83**, 3623 (1961); **84**, 332 (1962).

(10) H. Lemaire, A. Rassar, P. Servoz-Gavin, and G. Berthier, *J. chim. phys.*, **59**, 1247 (1962).

(11) P. H. Rieger and G. K. Fraenkel, *J. Chem. Phys.*, **39**, 609 (1963).

(12) A. Carrington and J. dos Santos-Veiga, *Mol. Phys.*, **5**, 21 (1962).

Table V: Observed and Calculated Spin Densities for BPA (−)

	Position					
	C(a)	*o*-	*m*-	*p*-	N(b)	Parameter
Obsd.[a]	−0.215	0.254	0.093	0.093	−0.144	
	0.550	−0.254	0.093	0.093	0.358	
	0.064	0.254	−0.093	0.093	0.074	
	−0.076	0.254	0.093	−0.093	−0.070	
Obsd.[b]	−0.287	0.254	0.093	0.093	0.000	
	0.729	−0.254	0.093	0.093	0.000	
	0.101	0.254	−0.093	0.093	0.000	
	−0.111	0.254	0.093	−0.093	0.000	
Calcd.-1	0.081	0.076	0.012	0.119	0.244	$h_N = 1.5, n = 13$
Calcd.-2	0.109	0.071	0.018	0.134	0.153	2.0 13
Calcd.-3	0.012	0.118	0.118	0.012	0.000	2.0 15

[a] These values were obtained by the relation $A_N = Q_1\rho_N - 2Q_2\rho_c$, where ρ_c is the spin density on the C(a) position in Fig. 5A. Q_1 and Q_2 used are 21 and 7 gauss, respectively. The pair of values 23.1 and 6.8 gauss gives a slightly different result. [b] These values were obtained using $Q_1 = 25$ gauss and $Q_2 = 0$ in the A_N formula. As the sign of the splitting factors cannot be decided by the e.s.r. method, two possible signs for the spin densities should be considered for *o*-, *m*-, and *p*-positions. In the table, therefore, each of these positions was assumed to be negative in the second to fourth rows.

(*B*) *Biphenylaminium Ion* (−). The unpaired electron of the $DPPH_2$ negative ion is localized on the two phenyl rings and on the nitrogen atom, b in Fig. 5A. There are 13 π-electrons in the network shown in Fig. 5A if the lone-pair electrons of nitrogen are not conjugating with the unpaired electron. If the lone-pair electrons are conjugating with the unpaired electron, there are 15 π-electrons. The eighth lowest eigenvalues obtained in the previous section are degenerate, and any linear combinations of the corresponding eigenfunctions are not good for this purpose.

McDowell and his co-workers[13] obtained the best agreement between the experimental and calculated spin densities when they used 0.6 and 0.7 as h_N values for negative ions of pyrazine and pyridazine, respectively. However, the values do not give reasonable calculated spin densities on the nitrogen atoms in the present system. This will be interpreted in the following manner. When the molecule has a positive or negative charge, the electronegativities of the nitrogen and carbon atoms in the molecule will deviate from the values in a neutral molecule. If there is an extra negative charge on the species, the electronegativity difference between nitrogen and carbon atoms will be larger because the electronic repulsion will be less on the nitrogen atom. Therefore, a larger h_N value than that used for BPA (+) will be more appropriate for this BPA (−) case. According to several authors,[7] the h_N values 1.5 and 2.0 were used and the result thus obtained is listed in Table V.

(*C*) *Lophine-x, L·, Formed by Illumination with Visible Light.* In the same manner as in section A, the computation for Lophine-x (assuming the network (Fig. 5B) which was proposed by Hayashi, *et al.*,[5] and has 23 atoms and 23 electrons) was made. As this species is more likely to be a free radical than an ion (which possibility is discussed in the Discussion section), a small h_N value for the nitrogen coulomb integral, 0.5, may seem to be reasonable here. However, this value gives small but appreciable spin densities on the nitrogen atoms. Considering that no spin densities were observed on these nitrogen atoms and that when h_N is increased up to 1.0 the calculated spin densities become almost negligible on the nitrogen atoms, the calculated spin densities using $h_N = 1.0$ are listed in Table VI. The twelfth lowest eigenvalue is $\alpha_0 + 0.380\beta_0$, and the corresponding eigenfunction yields the spin densities as shown in Table VI. The sum of the absolute values of the observed spin densities, which do not include the contribution from the carbon atoms C_1–C_4 in Fig. 5, is 1.810. Therefore, unless most of the carbon atoms C_1–C_4 have negative spin densities, the total of which would be −0.810, some of the positions *o*-, *p*-, *o'*-, and *m*- in Table VI should have negative spin densities. If the ratio ρ_{obsd}/ρ_{calcd} is assumed to be approximately 3.0 for the positive spin positions and 30 for the negative spin positions, that is, the ratio of the calculated spin densities is assumed to be correct so far as the positions have the same sign, an empirically corrected spin density ρ_{emp} is obtained from it. The positions *o*-, *p*-, *o'*-, C_2, and C_3 were considered to be positive while the positions *m*-, C_1, C_1', and C_4 were considered to be negative since the calculated values were very

(13) C. A. McDowell, K. F. Paulus, and J. R. Rowlands, *Proc. Chem. Soc.*, 60 (1962).

Table VI: Observed and Calculated Spin Densities for Lophine-x, L·

	Positions								
	o-	*p*-	*o'*-	*m*-	C_1	C_2	C_3	C_4	Total
Obsd.	0.156	0.156	0.130	−0.078					1.050
HMO method	0.053	0.062	0.036	0.002	0.018	0.170	0.114	0.012	0.972
ρ_0/ρ_{HMO}	2.9	2.5	3.6	39					
ρ_{emp}	0.159	0.186	0.108	−0.060	−0.540	−0.510	−0.342	−0.360	0.936

Table VII: Observed and Calculated Spin Densities for Lophine-x, L^-

	Positions											
	o-	*p*-	*o'*-	*m*-	C_1	C_2	C_3	C_4	N	*m'*-	*p'*-	Total
Obsd.	0.052	0.260	0.208									1.144
Calcd. A	0.061	0.072	0.023	0.002	0.023	0.186	0.071	0.009	0.095	0.018	0.166	1.000
Calcd. B	0.009	0.015	0.099	0.001	0.011	0.015	0.156	0.122	0.010	0.001	0.027	1.000

small for the latter group of positions. The positions *m'*, *p'*, and N were ignored because no experimental splitting can be assigned to these positions.

(*D*) *Lophine-x Negative Ion*, L^-. Since this compound itself is not paramagnetic if not irradiated with light, there will be two possible structural models for the negative ion. The one model, A, has a network of atomic nuclei slightly different from that of L·. This network has 23 electrons and will have different paired electron spin densities on the nitrogen or nitrogens. This model may correspond to a nonplanar dimer L:L^-, or at any rate to L_p discussed in the latter section existing if the compound is not illuminated with light. The calculated values, where $h_N = 2.0$ was chosen by the same reason as that discussed in section B, are listed in Table VII. The other model, B, is that where the negative ion has the same atomic network as that in L· but with 25 electrons (as 24 electrons are for a diamagnetic species or for a triplet state). The values calculated on these models are shown in Table VII.

The number of protons interacting with the unpaired electron is 4 + 2 + 2 = 8, while there are 15 protons in the structure, Fig. 5B. The group with four protons can be the *o*- or *m*-, while the groups with two protons can be the *p*-, *o'*-, or *m'*-protons. The *p'*-position should have approximately zero spin density in any case. Although the agreement between the observed and calculated spin densities is not good in any of these cases, it seems reasonable that the four equivalent protons are in the *o*-position and that the two groups of two equivalent protons are in the *p*- and *o'*-positions. The larger line widths in the spectrum of Fig. 4 than that of Fig. 2 may indicate some unresolved splitting from N, or from the *m*-, *m'*-, and *p'*-protons. It seems that model A gives a better fit.

Discussion

A simplest molecular orbital calculation for BPA (+) using $h_N = 0$, and $k_{C-N} = 1.0$ gives zero spin density on the *m*-position. In this respect a valence bond calculation gives a better result. However, a molecular orbital calculation in which the parameters α and β are varied properly yield fairly reasonable results except for these positions where negative spin densities[3] should be placed. An empirical procedure for Lophine-x, ρ_{emp}, gave a total spin density of 0.936. This may suggest that this type of fitting may have some meaning. However, it seems impossible to employ this kind of correction for L^- or for the spectrum in Fig. 4.

In case of the spin density calculations in nitrile anion radicals[14] and nitro-substituted anion radicals,[11] the results obtained by the approximate SCF-MO theory of McLachran[15] were more suitable than those by the simple molecular orbital theory. In this respect it will be worthwhile to carry out similar calculations for the present cases, though it was not attempted in this work. The e.s.r. spectrum from a solution gives only the isotropic splitting factors. In the case of irradiated creatinine hydrochloride, etc.,[16] the anisotropic proton hyperfine splitting factors were relatively smaller than the isotropic proton splitting factors. This may suggest that the actual spin densities can be smaller than the apparent spin densities obtained from

(14) P. H. Rieger and G. K. Fraenkel, *J. Chem. Phys.*, **37**, 2795 (1962).

(15) A. D. McLachran, *Mol. Phys.*, **3**, 233 (1960).

(16) H. Ueda, *J. Chem. Phys.*, **40**, 901 (1964).

the isotropic part of the splitting factors. Therefore, it seems that the disagreement among the nitrogen splitting constants presented by several researchers might have to be discussed from this point of view.

The mechanism of the phototropy of Lophine-x is still not clear. The structural model, Fig. 5B, has not been confirmed yet. The observed spin densities, on the other hand, show that the model Fig. 5B agrees fairly well with L·. Therefore, it can be said that the e.s.r. spectrum of Fig. 2 has given some structural information about L·. It can also be said that the spectrum of Fig. 4 is due to some structure which is not much different from Fig. 5B. There are 4, 2, 2 different types of protons in L^-. This instantly indicates that the unpaired electron spin should have densities on all the three phenyl rings. Accordingly, it should have spin densities on the central five-membered ring. The two possible mechanisms for the negative ion formation are

$$L_F + K \longrightarrow L^- + K^+ \qquad (I)$$

$$L\cdot + 2K \longrightarrow L^{2-} + 2K^+ \qquad (II)$$

$$L_p \text{—light} \longrightarrow L\cdot \qquad (III)$$

The results of Table VII would indicate that (I) is the more likely mechanism.

Since L_p is not paramagnetic, a singlet–triplet transitions or photoionization process might be considered for (III). To get some information about the possibility of a singlet–triplet transition, an e.s.r. signal at the half field was sought. No appreciable signal was found. However, this fact does not necessarily deny the existence of a triplet state because the half-field transition can be forbidden in such cases. However, if the species, Fig. 5B, has such low excited levels, then 2,3,5-triphenyltriazine, which has a hydrogen at N_1 position in Fig. 5B, will also have such a transition. The experimental result showed that no such phototropy was observed from this compound. It was also impossible to get a negative ion from 2,3,5-triphenyltriazine.[17] The photoionization mechanism must be ruled out also. A photoionization requires an electron accepter and the accepter should be the solvent in this case. There will be a reverse process, the rate of which is dependent on the structure of the solvent. No such solvent effect was found in the formation of L· in benzene and in dimethoxyethane.

The positive and negative ions of aromatic hydrocarbon ions give different spin densities for the same network of atomic nuclei.[2] In these cases, the two spectra due to positive and negative ions were quite similar except for their splitting factors. All the atomic wave functions contributing to the molecular wave function are 2p functions of carbon atoms in these aromatic hydrocarbons. Therefore, the change of exchange and coulomb integrals due to change of the electric charge will be almost equal for all the C–C bonds and C atoms. It will also be true that the two eigenfunctions corresponding to the $(N + 2)/2$ and $N/2$ lowest eigenvalues of the secular determinant have identical shape, where N is the even number of atomic orbitals contributing to the molecular orbital. However, if the network of atomic nuclei involves a heteroatom, the change of electric charge changes the coulomb integral for the heteroatom. This therefore, changes the spin density on the heteroatom greatly, and the resulting e.s.r. spectra for differently charged species will be remarkably different.

Carrington and Santos-Veiga[12] concluded that the nitrogen splitting constant has only one term. However, there is no reason to believe that the theoretical formulation with two terms is in error.[14] In the present problem in Table IV, the splitting constants $Q_1 = 21$ and $Q_2 = 7.0$ gauss seem to fit the observed values, -1, except at the C(a) and *m*-positions. This will be due to the negative spin densities of the *m*-position. The observed spin densities of -0.042 for *m*-positions seem to be correct. Then if it is assumed that this difference from the value computed by the HMO method, *i.e.*, -0.044, should be subtracted from the computed value at the C(a) position, the resulting spin density at C(a) position is 0.068. From these corrected spin densities, a relation for the nitrogen splitting constants can be derived

$$A = (Q_1 \times 0.494) - (2 \times 0.068Q_2)$$

The observed value is 9.2 gauss[4]; therefore

$$Q_1 = 18.7 + 0.275Q_2$$

If Q_1 is 20.9 gauss, Q_2 will be 9.0 gauss, and if Q_2 is 7.0, Q_1 will be 20.6 gauss.

Acknowledgment. The author thanks Professor C. A. McDowell and K. G. F. Paulus for their helpful suggestions to this problem. The author also thanks the National Research Council of Canada for grants.

(17) H. Ueda, unpublished result.

Solubility of Tetraphenylarsonium Periodate and the Equilibria between Periodate Species in Aqueous Solutions[1]

by S. H. Laurie, Jack M. Williams, and C. J. Nyman

Department of Chemistry, Washington State University, Pullman, Washington
(Received October 14, 1963)

The solubility in aqueous electrolyte solutions of tetraphenylarsonium periodate, $(C_6H_5)_4AsIO_4$, was determined over the temperature range 5–75°. Complete interpretation of the variation of solubility with pH required that equilibria between the species H_5IO_6, $H_4IO_6^-$, $H_3IO_6^{-2}$, and IO_4^- be established. Data obtained at 25° were: solubility product $K_{sp} = 3.88 \times 10^{-9}$; $\Delta H_s = 10.4$ kcal./mole; dehydration constant $K_d = a_{IO_4^-}/a_{H_4IO_6^-} = 43 \pm 17$; dissociation constants of H_5IO_6 were: $K_1 = (a_{H^+})(a_{H_4IO_6^-}/a_{H_5IO_6}) = (10 \pm 4) \times 10^{-4}$; $K_2 = (a_{H^+})(a_{H_3IO_6^{-2}}/a_{H_4IO_6^-}) = 3 \pm 1 \times 10^{-7}$; $\Delta H_1 = \Delta H_2$ *ca.* 0.

The use of tetraphenylarsonium chloride as an analytical reagent for the quantitative precipitation of periodate ion as $(C_6H_5)_4AsIO_4$ was suggested in 1935.[2,3] Recently, the method has been employed for the separation of free periodate ion from reaction mixtures containing both bound and free periodate ligand.[4,5] Surprisingly, however, no solubility measurements for $(C_6H_5)_4AsIO_4$ have been reported in the literature.

The pH range for the application of the precipitation method is somewhat uncertain when it is realized that the periodate ion may exist in one of several pH-dependent forms in aqueous solutions. Crouthamel, Hayes, and Martin[6] postulated the following equilibria in solution to account for the observed ultraviolet absorption of the periodate ion

$$H_5IO_6 \rightleftharpoons H^+ + H_4IO_6^- \quad (K_1 = 5.1 \times 10^{-4}) \quad (1)$$

$$H_4IO_6^- \rightleftharpoons H^+ + H_3IO_6^{-2} \quad (K_2 = 2.0 \times 10^{-7}) \quad (2)$$

$$H_4IO_6^- \rightleftharpoons 2H_2O + IO_4^- \quad (K_d = 40) \quad (3)$$

where K is the respective thermodynamic ionization or dehydration constant at 25°.

In the present study, the solubility of $(C_6H_5)_4AsIO_4$ has been determined in water over a wide temperature range by a radiotracer method using I^{131}-labeled periodate. The solubility has also been measured over the pH range 0 to 11 at 5, 25, and 40°, and the data obtained were interpreted in terms of the equilibria 1, 2, and 3.

Experimental

$(C_6H_5)_4AsI^{131}O_4$ was prepared by precipitation from a solution containing $Na_3H_2I^{131}O_6$. The method of preparation of the sodium paraperiodate was that outlined by Willard,[7] with slight modifications. The method consisted, briefly, of heating a mixture of excess (4.35 g.) $NaClO_3$, 2.95 g. of I_2, 0.1 mc. of NaI^{131} (obtained in basic sulfite solution, Atomic Corp. of America), and 0.5 ml. of concentrated HNO_3 in *ca.* 20 ml. of water at 60 to 70° until a clear solution remained. Then 4.5 g. of NaOH was added, the temperature was raised to 80°, and Cl_2 was bubbled through for 8 min. with vigorous stirring. The solution was finally made alkaline with NaOH to convert any $Na_2H_3I^{131}O_6$ to the less soluble $Na_3H_2I^{131}O_6$. The white precipitate was washed several times with small volumes of ice-cold water, the yield of 2 to 3 g. depending on the number of washings.

(1) Presented in part before the 18th Annual Northwest Regional Meeting of the American Chemical Society, Bellingham, Wash., June 16–18, 1963.

(2) H. Lamprey, Thesis, University of Michigan, 1935.

(3) H. H. Willard and G. M. Smith, *Ind. Eng. Chem., Anal. Ed.*, **11**, 186 (1939).

(4) C. J. Nyman and R. A. Plane, *J. Am. Chem. Soc.* **83**, 2617 (1961).

(5) J. M. Williams, M.S. Thesis, Washington State University, 1963.

(6) C. E. Crouthamel, A. M. Hayes, and D. S. Martin, *J. Am. Chem. Soc.*, **73**, 82 (1951).

(7) H. H. Willard, "Inorganic Syntheses," Vol. I, H. S. Booth, Ed., 1st Ed., McGraw-Hill Book Co., Inc., New York, N. Y., 1939, p. 170.

The radioactive periodate was dissolved in a 0.1 *M* HNO_3 solution and excess tetraphenylarsonium chloride (Eastern Chemical Co.) was added to precipitate the $(C_6H_5)_4AsI^{131}O_4$. After centrifuging and washing with water several times, the salt was recrystallized from a 4:1 methanol–water solvent. After standing, small particles were removed by decanting off the mother liquor and washing with water, leaving behind needle-shaped crystals of the desired product. These were washed successively with water, alcohol, and ether, and air dried. No weight loss was detected after 3 days at 125°. The crystals were analyzed by grinding weighed samples and suspending the powder in about 200 ml. of 0.05 *N* H_2SO_4. Reduction of periodate was achieved by bubbling in SO_2 gas. After removal of the excess SO_2 by boiling, $AgNO_3$ solution was added in excess to the hot solutions, from which the solid AgI was collected on a porcelain filter. This precipitate was dried and weighed. *Anal.* Calcd. for $(C_6H_5)_4AsIO_4$: I, 22.11. Found: I, 22.10.

The pH of the equilibrating solutions were adjusted with either a standard 1.0 *M* HNO_3 solution or a 0.1 *M* NaOH solution, and the ionic strength was maintained at 0.1 *M* by addition of $NaNO_3$. After saturation, accurate pH values were obtained, at the same temperature as the solubility measurements, with a Beckman pH meter. For the solutions of pH 0 and 0.5, the ionic strength was 1.0 *M*, and the pH was calculated from the stoichiometric acid concentration.

For the solubility determinations, the crystals were distributed among several tubes and each sample was washed with several small volumes of the solution with which it was to be equilibrated. About 40 ml. of the same solution was then added before the tubes were firmly stoppered and placed on a water-thermostated 16-r.p.m. rotating device to achieve saturation equilibria. Establishment of equilibrium was demonstrated by removing samples at different times and recording the activities of the solutions. Saturation equilibrium was found to have been achieved within 12–16 hr. at all temperatures investigated. For the solubility determinations at 5°, the samples were rotated a minimum of 3 days, and at the higher temperatures, they were rotated a minimum of 2 days to ensure saturation. Results of experiments using several different batches with differing specific activities of I^{131} gave solubilities under a given set of conditions which agreed within ±1%.

The saturated solutions at 5° were filtered, warmed to 25°, and then 25 ml. was taken for counting purposes. With alkaline samples at 5°, 1 drop of a concentrated NaOH solution was added from a capillary tube to stop any crystallization. For the saturated solutions at other temperatures, 25 ml. was withdrawn through a cotton–wool plug into a pipet which had been prewarmed to the same temperature as the sample. To each sample was added 1 drop of either a concentrated HNO_3 or concentrated NaOH solution from similar capillary tubes. The 25-ml. samples were pipetted into 5-cm. diameter weighing bottles, and the count rate of the 0.36 Mev. γ was obtained with a NaI(Tl) crystal scintillation counter (Nuclear Chicago Ltd.).

The solubility of each sample was obtained by comparing its count-rate to that of a standard sample, the background count-rate being subtracted from each. The standard sample was prepared by dissolving a known amount of $(C_6H_5)_4AsI^{131}O_4$ in 0.1 *M* NaOH and diluting to a known volume. Then 25 ml. of the standard was pipetted under the same conditions as the unknowns into similar 5-cm. bottles. The 0.36 Mev. γ count-rate of the standard was determined before and after the counting of each unknown.

A minimum of 20,000 counts was obtained in each case so that the statistical error was approximately 0.7%. With 25-ml. counting samples any reasonable error in pipetting would have had a negligible effect on the count-rate. Further, a 1% error in the total salt concentration would only result in *ca.* 0.1% deviation in the solubility. This, coupled with the observed reproducibility, would make ±1% a reasonable estimate for the experimental error in solubilities. The pH measurements were reliable to within ±0.02 pH unit.

Results and Discussion

From their spectral investigations, Crouthamel, *et al.*,[6] showed the absence of any polymeric species, such as $I_2O_9^{-4}$, in solution and proposed that equilibria 1, 2, and 3 were present. Their thermodynamic equilibrium constants are given by the expressions

$$(a_{H^+})(a_{H_4IO_6^-}/a_{H_5IO_6}) = K_1 \qquad (1a)$$

$$(a_{H^+})(a_{H_3IO_6^{-2}}/a_{H_4IO_6^-}) = K_2 \qquad (2a)$$

$$a_{IO_4^-}/a_{H_4IO_6^-} = K_d \qquad (3a)$$

where a denotes activity of the ion concerned.

The total periodate concentration, $[I_t]$, in solution may be expressed as

$$[I_t] = [IO_4^-] + [H_4IO_6^-] + [H_5IO_6] + [H_3IO_6^{-2}] \qquad (4)$$

Substituting (1a)–(3a) into (4) and reducing gives

$$[I_t] = \frac{a_{IO_4^-}}{K_d}\left\{(K_d + 1)/f_1 + (a_{H^+})/K_1 + K_2/(a_{H^+})f_2\right\} \qquad (5)$$

where f_1 and f_2 are the activity coefficients of univalent and bivalent ions, respectively. The solubility product, K_{sp}, is given by

$$K_{sp} = [(C_6H_5)_4As^+][IO_4^-]f_1^2 \quad (6)$$

For any saturated solution we may also put

$$[(C_6H_5)_4As^+] = [I_t] = S \quad (7)$$

where S is the solubility. Substituting (6) and (7) into (5), the final expression becomes

$$K_{sp} = S^2f_1^2 \left\{ \frac{K_d}{(K_d + 1) + \frac{(a_{H^+})f_1}{K_1} + \frac{K_2f_1}{(a_{H^+})f_2}} \right\} \quad (8)$$

Unfortunately, K_{sp} is not obtainable directly from solubility measurements without some prior knowledge of K_d, K_1, and K_2. The spectral investigations of Crouthamel, *et al.*,[6] however, show that the optical densities of sodium metaperiodate solutions of a given concentration approach a limiting value as the temperature increases above 60° and that the pH range of this limiting value also increases. This is consistent with a dehydration step approaching completion with increasing temperature, *i.e.*, $[IO_4^-] \rightarrow [I_t]$. If this is so, then K_d ought to be large above 60°, and the bracketed term on the right-hand side of expression 8 should approach unity. This also implies that the acid-dependent terms must be of negligible importance in determining the solubility in the pH range under investigation at the higher temperatures. This latter assumption can be justified as a first approximation by noting in Fig. 2 that as the temperature increases there is a widening of the pH range of minimum solubility, and hence, also for the range of existence of the monovalent ion. This assumption will be discussed later.

Thus, in the pH range 5.5 to 5.8, it is assumed as a first approximation that eq. 8 reduces to

$$K_{sp} = S_w^2f_1^2 \quad (9)$$

where S_w is the solubility of $(C_6H_5)_4AsIO_4$ in plain water with no added electrolyte. Data for S_w as a function of temperature are recorded in Table I, and values for $-\log S_w^2f_1^2$ are plotted *vs.* $1/T$ in Fig. 1. The necessary values for f were calculated from the Davies equation[8]

$$-\log f_i = Az_i^2\{\mu^{1/2}/(1 + \mu^{1/2}) - 0.3\mu\} \quad (10)$$

where μ is the ionic strength in moles per liter, z_i the charge on an ion i, and A is a constant at a given temperature in water.[9] If the specific heats of solid $(C_6H_5)_4AsIO_4$ and its ions in solution are constant over the temperature range 5 to 75°, *i.e.*, the heat of solution

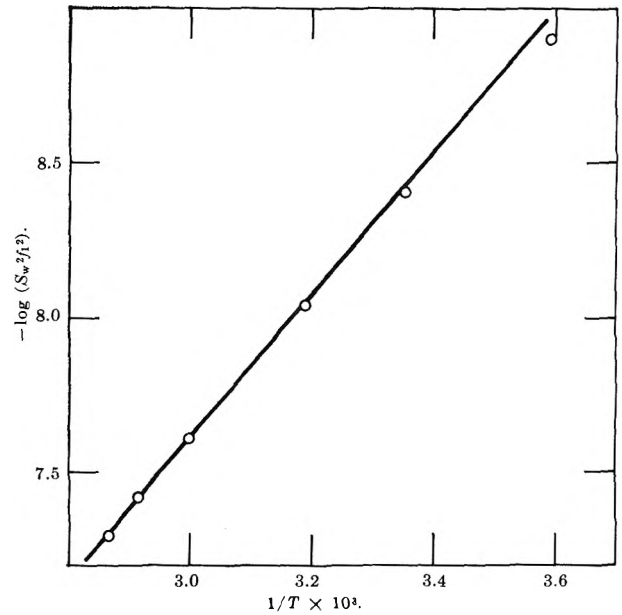

Figure 1. Plot of $\log (S_w^2f_1^2)$ *vs.* $1/T$ for tetraphenylarsonium periodate.

of the salt is constant over this range, then a plot of $-\log S_w^2f_1^2$ *vs.* $1/T$ should be linear at the higher temperatures where eq. 9 should be valid. Deviations from a straight line plot in the lower region due to increasing hydration and ionization of the $H_4IO_6^-$ should appear, and the experimental data showed the expected behavior. The values of K_{sp} at each temperature were obtained from the straight line plot and are recorded in Table I.

Table I: The Solubility (S_w) and K_{sp} of $(C_6H_5)_4AsIO_4$ in Water as a Function of Temperature at $\mu \simeq 0$

Temp., °C.	pH	$S_w \times 10^5$, moles/l.	$K_{sp} \times 10^9$
75.8	*ca.* 5.5	23.0 ± 0.2	50.9 ± 0.9
70.1	*ca.* 5.5	19.9 ± 0.1	38.2 ± 0.3
60.3	*ca.* 5.5	16.0 ± 0.1	24.8 ± 0.3
40.3	5.50	9.68 ± 0.05	9.01 ± 0.09
24.9	5.52	6.37 ± 0.02	3.88 ± 0.02
5.3	5.78	3.58 ± 0.02	1.06 ± 0.01

To obtain the values of K_d, K_1, and K_2, a series of successive approximations was employed. First, the deviation of the plot of $-\log S_w^2f_1^2$ *vs.* $1/T$ from a straight line was interpreted by assuming that the

(8) C. W. Davies, "Ion Association," Butterworths, London, 1962, p. 41.

(9) R. A. Robinson and R. H. Stokes, "Electrolyte Solutions," 2nd Ed., Butterworths, London, 1962, p. 468.

Table II: Final Values of K_d, K_1, and K_2 at Various Temperatures

Temp., °C.	K_d This work	K_d Previous[a] work	$K_1 \times 10^4$ This work	$K_1 \times 10^4$ Previous[a] work	$K_2 \times 10^7$ This work	$K_2 \times 10^7$ Previous[a] work
5.3	6.0 ± 0.2	*ca.* 11	6.9 ± 0.1	*ca.* 5.0	2.4 ± 0.1	*ca.* 3.0
24.9	43 ± 17	40	10 ± 4	5.1	3 ± 1	2.0
40.3	110 ± 30	*ca.* 95	10 ± 3	*ca.* 5.8	4 ± 1	*ca.* 2.3

[a] Values taken from data and graphs of ref. 6.

deviation was due to increasing hydration of IO_4^- to form $H_4IO_6^-$. For this purpose, eq. 8 simplified to

$$K_{sp} = S_w^2 f_1^2 \left(\frac{K_d}{K_d + 1}\right) \qquad (11)$$

From the K_{sp} and solubility data in Table I, first values of K_d were obtained. Since in Fig. 1, the deviations from a straight line were small, particularly at 40°, only estimates for K_d could be obtained. The first values of K_d from eq. 11 were 110 ± 30 at 40°, 40 ± 20 at 25°, and 8.5 ± 3.5 at 5°. First values of K_1 and K_2 were then obtained from the solubility data in Table III using eq. 8 with the first values of K_d and the values of K_{sp} obtained earlier. A second value of K_d was then obtained from the data in Table I by substitution of these first values of K_1 and K_2 back into eq. 8. The process of successive approximations was repeated until a self-consistent set of values of K_d, K_1, and K_2 was obtained. These final values at the various temperatures investigated are reported in Table II.

A justification of the assumption that the acid-dependent terms were negligible in estimating K_{sp} at the higher temperatures and also a justification of the method of obtaining the values of K_{sp} reported in Table I is the following. If the values of K_1, K_2, and K_d at 25 or 40° are substituted into eq. 8, the same values of K_{sp} are calculated as from eq. 11 wherein the acid-dependent terms involving K_1 and K_2 have been omitted. However, at 5°, the contributions of the acid-dependent terms are significant and must be included to obtain the proper values of K_{sp}, *i.e.*, K_{sp} at 5° cannot be estimated from an equation such as (9) or (11). Thus, with increasing temperature, $K_d/(K_d + 1)$ approaches unity, and the acid-dependent terms of eq. 8 do appear to become negligible at the pH of the saturated solutions of $(C_6H_5)_4AsIO_4$ and therefore at temperatures above 40°, K_{sp} can be calculated from eq. 9.

The solubility data listed in Table III are plotted in Fig. 2. The individual points represent the experimental data and the solid curves were calculated from eq. 8 using the constants reported in Tables I and II.

For the solubility measurements in Table III denoted by superscript *a*, the ionic strengths were 1.0 *M* in place of the usual 0.1 *M*. In order to correct these data for the ionic strength effect, the corresponding *hypothetical solubilities* $S_{0.1}$ (denoted in Table III by superscript *b*) of $(C_6H_5)_4AsIO_4$ in solutions whose pH values were 0.0 and 0.5 at $\mu = 0.1$ were approximated from the relationship

$$S_{0.1} = (S_{1.0})(f_{1.0}/f_{0.1})$$

$S_{1.0}$ is the measured solubility at pH 0.0 or 0.5 and the f's are the corresponding activity coefficients at the indicated ionic strengths. The value of $f_{0.1}$ was calculated from eq. 10, but $f_{1.0}$ was estimated from eq. 11 using the measured solubility of $(C_6H_5)_4AsIO_4$ (8.96 ×

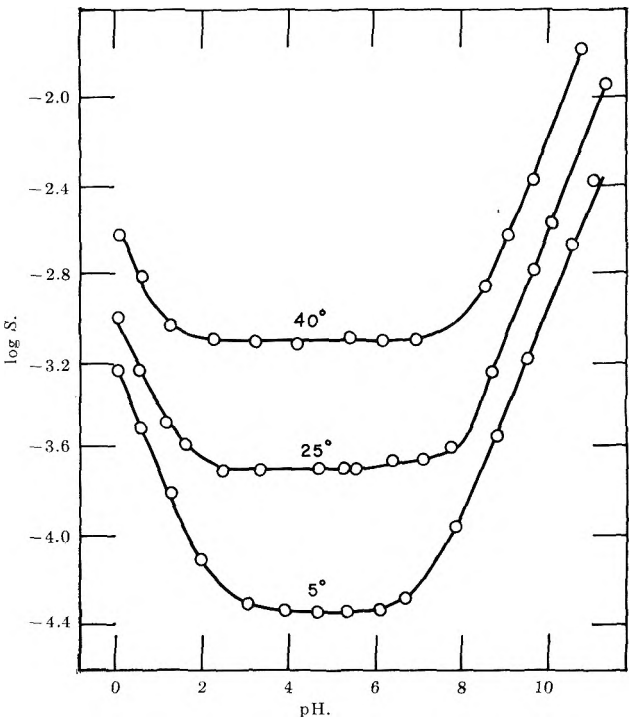

Figure 2. Plot of log solubility *vs.* pH for tetraphenylarsonium periodate at 5, 25, and 40°. *Left-hand scale is correct only* for data at 5°. Scale must be decreased by 0.4 unit for data at 25° and by 0.8 unit for data at 40°.

Table III: Solubility of Tetraphenylarsonium Periodate in Aqueous Solutions at an Ionic Strength of 0.1 *M*

	t = 5.3°			t = 24.9°			t = 40.1°	
	$S \times 10^4$, moles/l.			$S \times 10^4$, moles/l.			$S \times 10^4$, moles/l.	
pH	Obsd.	Calcd.	pH	Obsd.	Calcd.	pH	Obsd.	Calcd.
0	6.44[a]	...	0	4.46[a]	...	0	4.24[a]	...
(Calcd.)								
	5.80[b]	5.76		4.02[b]	3.78		3.82[b]	3.61
0.5	3.46[a]	...	0.5	2.53[a]	...	0.5	2.73[a]	...
(Calcd.)								
	3.13[b]	3.27		2.29[b]	2.23		2.47[b]	2.27
1.20	1.58	1.51	1.10	1.31	1.32	1.18	1.52	1.51
1.92	0.753	0.780	1.56	1.05	1.01	2.16	1.29	1.27
3.01	0.483	0.486	2.44	0.792	0.846	3.12	1.26	1.24
3.84	0.458	0.457	3.30	0.818	0.820	4.10	1.22	1.23
4.57	0.447	0.454	4.63	0.809	0.817	5.30	1.29	1.23
5.32	0.455	0.455	5.18	0.814	0.817	6.08	1.26	1.24
6.04	0.457	0.470	5.50	0.818	0.818	6.83	1.26	1.26
6.66	0.520	0.521	6.35	0.867	0.830	8.46	2.20	2.22
7.82	1.10	1.08	7.04	0.884	0.882	9.00	3.74	3.70
8.73	2.87	2.87	7.70	1.09	1.09	9.58	6.81	6.82
9.45	6.47	6.42	8.63	2.24	2.24	10.76	26.1	26.1
10.50	21.4	21.5	9.62	6.53	6.57			
11.08	41.7	41.8	10.06	10.8	10.8			
			11.30	45.8	45.1			

[a] μ = 1.0 *M*. [b] Calculated for μ = 0.1 *M*.

10^{-5} mole/l. at 25°) in 1.0 *M* $NaNO_3$ at pH 5.4. The necessary values of K_{sp} and K_d were taken from those reported in Table I. These hypothetical values of the solubility are very approximate, but they serve as a useful guide in estimating the values of K_1.

The mean K values in Table II are seen to be in fair agreement with the values of Crouthamel, *et al.*[6] Plots of log K ion *vs.* $1/T$ yield the results that $\Delta H \cong 0$ for the ionization processes. From the slope of the plot of Fig. 1 the heat of solution for $(C_6H_5)_4AsIO_4$ is 10.4 ± 0.1 kcal./mole.

From infrared measurements on several periodate salts, Keens and Symons[10] have proposed that the hydrated specie $H_4IO_6^-$ is the predominant specie in solution. Their results, however, do not rule out a hydration equilibrium being present. Such a hydration process will explain: (i) the precipitation of periodate ion in the form $(C_6H_5)_4AsIO_4$ independent of the species in solution; (ii) the variation of the periodate spectra with temperature[6]; and (iii) the observed rapid exchange of oxygen between water and periodate ion.[11,12] Furthermore, the variation in solubility of tetraphenylarsonium periodate with pH and temperature, as reported here, can be successfully accounted for by the ionization and hydration equilibria proposed by Crouthamel, *et al.*

From an analytical viewpoint, the reported solubility data support the use of $(C_6H_5)_4AsIO_4$ for the quantitative determination of periodate ion. However, it is suggested that the precipitation of periodate as $(C_6H_5)_4AsIO_4$ is best suited for gram quantities of periodate ion and that the pH of the original solution be in the region 3 to 7. The method is unsuitable for alkaline media, and certain other anions, as reported by Willard and Smith,[3] must be absent.

Acknowledgments. The authors are indebted to the National Science Foundation for financial support under Grant No. NSF-G 18826.

(10) N. Keens and M. Symons, *Proc. Chem. Soc.*, 383 (1960).

(11) A. I. Brodskii and N. A. Vyotskoya, *Dokl. Akad. Nauk SSSR*, **101**, 869 (1955).

(12) M. Anbar and S. Guttman, *J. Am. Chem. Soc.*, **83**, 781 (1961).

The Reaction of Methyl Radicals with Toluene

by Mark Cher

North American Aviation Science Center, Canoga Park, California *(Received October 22, 1963)*

Gas phase photolyses ($\lambda = 3660$ Å.) of mixtures of azomethane with toluene-α-d_3, toluene-d_8, and toluene-d_5 were carried out at 60°, and the isotopic composition of the product methane was determined in order to assess the importance of the methyl free radical reaction with the aromatic ring. It is concluded that methyl radicals abstract hydrogen directly from the aromatic ring in toluene at a rate which is 0.17 as fast as the rate of abstraction from the side chain. Deuterium isotope effects of about 6.4 for both the side chain and ring abstraction reactions are shown to be extremely important in determining the course of the reaction. Analyses by gas chromatography showed that ethylbenzene is a major nongaseous product, and xylene and bibenzyl are barely detectable. In the liquid phase photolysis, *o*-xylene is a major product, while *m*-xylene, *p*-xylene, and ethylbenzene are formed in smaller yield, and bibenzyl is found only in trace amount. The difference in the products implies that methyl radicals do not permanently add to the ring in the gas phase reaction, but they do so in the liquid phase reaction. These results are discussed in terms of the different mechanisms that operate in each phase.

Introduction

The reaction of methyl radicals with toluene is of particular interest because of the possibility of comparing relative rates of reaction with the aliphatic and aromatic parts of the toluene molecule. In the liquid phase, evidence has been presented for both addition of the free radical to the ring[1] and abstraction of hydrogen from the ring to form methane.[2,3] In the gas phase it is usually assumed,[4,5] on the basis of bond strength arguments, that methyl radicals do not interact with the ring to any great extent, but only abstract hydrogen from the side chain. However, the recent work of Meyer and Burr[6] suggests that in the gas phase at 750° abstraction from the ring may indeed be very important. Therefore, we have undertaken to test directly for the possibility of ring involvement in the reaction producing methane by photolyzing gaseous mixtures of azomethane and deuterated toluene and by studying the isotopic composition of the methane. We reasoned that if addition of methyl radicals to the ring were indeed occurring, the reaction would be favored at low temperatures. Consequently, we chose to work at 60°, where the vapor pressure of toluene is adequately high. The production of methyl radicals in the photolysis of azomethane has been well established.[7]

Experimental

Apparatus. A conventional glass vacuum line was used to handle gases. In order to prevent condensation of toluene vapor, the reaction cell, the toluene storage vessel, a mercury manometer, and a McLeod gage were enclosed within a heated box maintained at 60.0 ± 0.5°. Metal Hoke valves, Type 413, were used inside the box. The cylindrical Pyrex reaction cell (50 mm. i.d., 176 mm. long) had flat Pyrex windows and was provided with a magnetically operated stirrer for gas mixing. The gas pressures were measured directly with the McLeod gage or mercury manometer.

The light source was a Hanovia Type A medium pressure mercury arc. The light beam, which filled the entire cell, was collimated roughly with a quartz condensing lens. A Corning 7–83 glass filter was used to isolate the 3660 Å. region.

(1) M. Levy and M. Szwarc, *J. Am. Chem. Soc.*, **76**, 5981 (1954).

(2) S. H. Wilen and E. L. Eliel, *ibid.*, **80**, 3309 (1958).

(3) M. Levy, M. Steinberg, and M. Szwarc, *ibid.*, **76**, 3439 (1954).

(4) A. F. Trotman-Dickenson and E. W. R. Steacie, *J. Chem. Phys.*, **19**, 329 (1951).

(5) I. B. Burkley and R. E. Rebbert, *J. Phys. Chem.*, **67**, 168 (1963).

(6) R. A. Meyer and J. G. Burr, *J. Am. Chem. Soc.*, **85**, 478 (1963).

(7) M. H. Jones and E. W. R. Steacie, *J. Chem. Phys.*, **21**, 1018 (1953).

Analysis. After photolysis all vapors were transferred to a series of traps at −196°. The noncondensable fraction, composed mainly of nitrogen and methane, was transferred by means of a toepler pump into a calibrated volume where the pressure was read, transferred to a container, sealed, and subsequently analyzed with a C.E.C. 21-103 mass spectrometer. A second fraction volatile at −150° (isopentane slush) was similarly collected and the pressure–volume product measured. Analysis of a few early samples showed this fraction to be mainly ethane and so the mass spectral analysis in most cases was not performed. Qualitative analyses for nongaseous products were carried out in a Perkin-Elmer Model 226 gas chromatograph equipped with a flame ionization detector, using a 30-m. "R" capillary column. This column is very satisfactory for resolving the three xylenes and ethylbenzene from each other.

Materials. Azomethane was prepared from 1,2-dimethylhydrazine hydrochloride by the procedure of Renaud and Leitch.[8] It was dried by bulb-to-bulb distillations through a Drierite trap and a final distillation at −78°. Methyl chloride contamination was reduced to less than 1% by extended pumping at −150°. The azomethane was stored at −196°, and all operations involving its volatilization were carried out in a semidarkened room.

Toluene-α-d_3 and toluene-d_8 were purchased from Merck Sharp and Dohme of Canada, Ltd. Toluene-d_5 was prepared by J. G. Burr in our laboratory by methylation of benzene-d_6. Each of these compounds was purified by means of preparative gas chromatography. Their low voltage mass spectra showed 6–7% toluene-d_{n-1} impurity, where n is the number of D atoms in each of the parent compounds.

Carbon dioxide (Matheson, Bone Dry) was purified by bulb-to-bulb distillation at −78°.

Results

The results of the photolysis of mixtures of azomethane with toluene-α-d_3 ($C_6H_5CD_3$), toluene-d_8 ($C_6D_5CD_3$), and toluene-d_5 ($C_6D_5CH_3$) are summarized in Table I. In all cases the major gaseous products are nitrogen, ethane, methane, and methane-d_1. Trace quantities of hydrogen are also observed. The fraction of azomethane decomposed, based on the yield of nitrogen, ranged from 16 to 24%. Since ethane is the major hydrocarbon product, and toluene is present in very large excess, the fraction of toluene decomposed is less than 0.1%. Figure 1 shows the CH_4/CH_3D yield ratio plotted as a linear function of the initial azomethane–toluene concentration ratio for the photolyses involving toluene-α-d_3 and toluene-d_8. We notice that

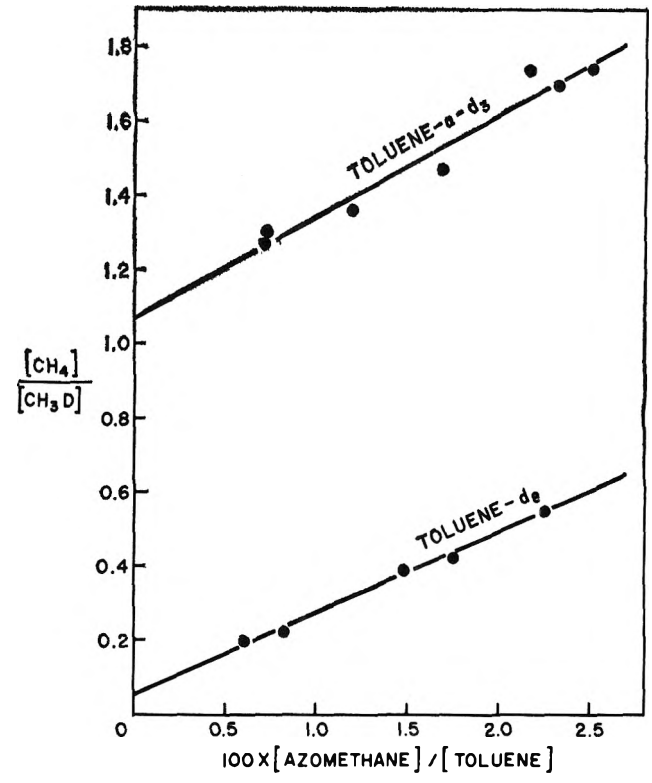

Figure 1. The isotopic composition of methane in the photolysis of azomethane–toluene mixtures.

the relative yield of CH_4 increases with increasing azomethane concentration, which is to be expected since a fraction of the methane originates *via* hydrogen abstraction from azomethane itself. In the case of toluene-d_5, the CH_4/CH_3D ratio is essentially independent of the azomethane–toluene concentration ratio within the range of concentrations studied, as shown in Table I. Addition of a large excess of CO_2 gas (last two runs in Table I) had no effect on the CH_4/CH_3D ratio, but resulted in a significant decrease in the $(C_2H_6 + CH_4 + CH_3D)/N_2$ ratio.

In view of the liquid phase findings[1] that methyl radicals add to the aromatic ring, it seemed worthwhile to examine the nature of the nongaseous products in the gas phase photolysis and compare them with the products of the liquid phase photolysis. For this purpose a mixture containing about 10% azomethane and 90% toluene was condensed and sealed into a small ampoule made of 6-mm. Pyrex tubing, the vapor phase region was masked off, and the exposed solution was photolyzed at room temperature for about 110 min. The total weight of liquid was comparable to the weight of gas in the gaseous experiments. A similar mixture

(8) R. Renaud and L. C. Leitch, *Can. J. Chem.*, 32, 545 (1954).

Table I: Photolysis of Azomethane–Toluene Mixtures—Gaseous Yields

Pressure, mm.			100 × [A]/[T]	Time,	μmoles				$\frac{CH_3D + CH_4 + C_2H_6}{N_2}$	$\frac{CH_4}{CH_3D}$
Azomethane	Toluene	CO_2		min.	N_2	CH_3D	CH_4	C_2H_6		
					Toluene-α-d_3					
0.57	79.9	...	0.71	121	2.33	0.044	0.056	1.97	0.89	1.27
0.59	81.0	...	0.73	133	2.44	0.053	0.068	1.78	0.78	1.30
1.01	83.9	...	1.20	131	3.93	0.071	0.095	3.65	0.97	1.36
1.42	84.2	...	1.69	116	4.21	0.075	0.110	3.90	0.97	1.47
1.66	76.9	...	2.16	120	5.98	0.066	0.113	5.59	0.96	1.74
1.11	47.9	...	2.32	136	3.75	0.060	0.120	3.80	1.06	1.70
2.00	79.8	...	2.51	97	6.02	0.071	0.124	5.45	0.94	1.74
					Toluene-d_8					
0.57	94.9	...	0.60	148	1.95	0.084	0.017	1.95	1.05	0.202
0.80	97.8	...	0.82	147	2.84	0.106	0.023	2.65	0.98	0.217
1.30	87.8	...	1.48	131	4.15	0.105	0.041	3.83	0.96	0.390
1.57	89.8	...	1.75	117	4.45	0.104	0.044	4.11	0.96	0.423
2.00	89.0	...	2.25	105	5.52	0.121	0.066	4.97	0.93	0.545
					Toluene-d_5					
1.29	71.5	...	1.80	126	4.07	0.016	0.648	3.96	1.14	40.5
1.47	81.7	...	1.80	123	4.01	0.023	0.896	3.03	0.99	39.0
2.26	83.6	...	2.70	80	3.92	0.019	0.730	3.12	0.99	38.4
1.51	84.2	297	1.79	126	4.21	0.025	0.969	2.18	0.75	38.8
1.49	83.3	641	1.79	130	4.00	0.023	0.919	1.62	0.64	40.0

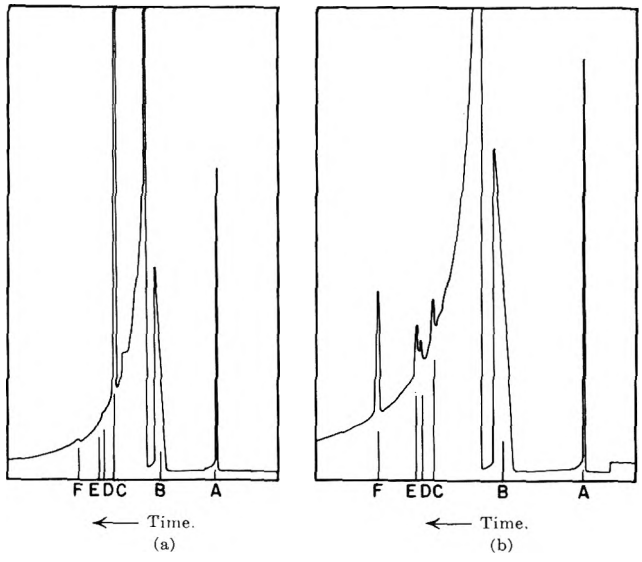

Figure 2. Gas chromatograms of liquid residues: (a) gas phase photolysis; (b) liquid phase photolysis. The identified peaks are: A, azomethane (×2000); B, toluene (×50,000 (a) and ×20,000 (b)); C, ethylbenzene; D, *p*-xylene; E, *m*-xylene; F, *o*-xylene. The attenuations of the product peaks are ×50 for (a) and ×5 for (b). The slight difference in retention times is due to the fact that (a) and (b) were run at different temperatures. The apparent peak between B and C is caused by the toluene tail as a result of the change in attenuation.

was also photolyzed at 60° for 104 min. in the gas phase in the usual manner. The condensable liquid residue in each experiment was analyzed by gas chromatography. The chromatograms obtained, Fig. 2, clearly show that in the liquid phase *o*-xylene is a major product, while *m*-xylene, *p*-xylene, and ethylbenzene are produced in smaller yield. In the gas phase, however, ethylbenzene is the only major nongaseous product, and the xylenes are barely detectable. Bibenzyl is observed only in trace quantities in both the gas phase and the liquid phase residues. Blank analyses of the nonphotolyzed material demonstrated absence of any of these products in the starting material. Except for smaller yields of products, analysis of the residue from a gas phase run involving toluene-α-d_3 gave similar results.

Discussion

The striking increase in the CH_4 yield relative to that of CH_3D in changing from toluene-d_8 to toluene-α-d_3 (Fig. 1) can only mean that hydrogen from the ring appears in the product methane, for otherwise the two lines would coincide. This conclusion is substantiated by the presence of CH_3D in the photolysis involving toluene-d_5. Although the yield of CH_3D in this case is quite small, about 2.5% of the total methane, it is nonetheless very significant in view of the isotope effect tending to retard reactions of deuterium relative to those of hydrogen, as discussed below.

In order to estimate the relative importance of ring abstraction *vs.* side-chain abstraction, we assume the

following simple mechanism for the formation of methane

$$CH_3NNCH_3 + h\nu \longrightarrow 2CH_3 + N_2 \quad (1)$$

$$CH_3 + A \xrightarrow{a} CH_4 + \cdot CH_2NNCH_3 \quad (2)$$

$$CH_3 + T \xrightarrow{s} CH_4 + \cdot CH_2C_6H_5 \quad (3)$$

$$CH_3 + T \xrightarrow{r} CH_4 + CH_3C_6H_4\cdot \quad (4)$$

where A and T denote azomethane and toluene, and a, s, and r are specific rate constants pertaining in the case of toluene to the reaction with the entire side chain or the entire aromatic ring. This mechanism leads to eq. 5–7 for the rates of production of CH_4 and CH_3D from each of the deuterated toluenes

$$\frac{R_{CH_4}}{R_{CH_3D}} = \frac{a}{s_d}\frac{[A]}{[T]} + \frac{r_h}{s_d} \quad \text{(toluene-}\alpha\text{-}d_3\text{)} \quad (5)$$

$$\frac{R_{CH_4}}{R_{CH_3D}} = \frac{a}{s_d + r_d}\frac{[A]}{[T]} \quad \text{(toluene-}d_8\text{)} \quad (6)$$

$$\frac{R_{CH_4}}{R_{CH_3D}} = \frac{a}{r_d}\frac{[A]}{[T]} + \frac{s_h}{r_d} \quad \text{(toluene-}d_5\text{)} \quad (7)$$

In these equations the subscript d or h indicates whether the abstraction involves deuterium or hydrogen. The justification for writing reaction 4 as a direct abstraction from the aromatic ring in place of a more complicated sequence of events involving a preliminary addition to the ring is given below. However, eq. 5, 6, and 7 are independent of this assumption. These equations predict straight lines when the CH_4/CH_3D yield ratio is plotted against the azomethane–toluene concentration ratio,[9] as shown in Fig. 1. The small intercept in the case of toluene-d_8 is due, of course, to the hydrogen impurity in the toluene-d_8. Equating the observed slopes and intercept in Fig. 1 to the corresponding ratio of rate constants, eq. 5 and 6, and using the observed CH_4/CH_3D yields in the toluene-d_5 experiments (Table I) in conjunction with eq. 7, we obtain after some simple algebraic manipulations the set of rate constant ratios shown in Table II, column (a).

The first two ratios are obtained more or less directly from the experimental measurements and are probably accurate to ±10%. The last four ratios depend on the small difference between the two slopes in Fig. 1; an error of ±10% in each slope could lead to an error of a factor of two in the calculation of these numbers. If we assume that the two isotope effect ratios r_h/r_d and s_h/s_d are equal within an uncertainty of, say, 10% then we obtain the values shown in Table II, column (b), in which case the limits of error are reduced to about 30%. We shall use these latter values for further discussion, as they are considered more reliable. (However, see below.)

Table II

Rate constant ratio	Calculated value (a)[a]	Calculated value (b)[b]	Remarks
r_h/s_d	1.07[c]		Toluene-α-d_3
r_d/s_h	0.026[c]		Toluene-d_5
s_h/s_d	11	6.4	Side chain isotope effect
r_h/r_d	3.8	6.4	Ring isotope effect
r_h/s_h	0.098[c]	0.17[c]	Toluene-d_0
$a/(r_h + s_h)$	2.3	3.3	

[a] Calculated from the slopes and intercept of Fig. 1 using eq. 5–7. [b] Calculated assuming equal isotope effects; *i.e.*, $r_h/r_d = s_h/s_d$. [c] These values are to be multiplied by the factor $^3/_5$ to obtain rate constants expressed in terms of "per C–H bond."

The significance of these ratios may be seen in the following summary. The ratios $r_h/s_d = 1.07$ and $r_d/s_h = 0.026$ are measures of the relative rates of abstraction from the ring and the side chain in toluene-α-d_3 and toluene-d_5, respectively. Thus with toluene-α-d_3, half of the methane originates *via* reaction with the ring, whereas with toluene-d_5 almost none comes *via* this process.

The ratio $r_h/s_h = 0.17$ indicates that about 15% of the time hydrogen abstraction from toluene occurs at the ring.[10] The activation energy difference between ring abstraction and side-chain abstraction corresponding to this ratio and assuming a steric factor ratio of $^5/_3$ is 1.5 kcal./mole, in very good agreement with the measured activation energy difference for the hydrogen abstraction reactions of methyl radicals with benzene[4] and toluene.[4,5] We note that this difference is nearly identical with the zero point energy difference between C–H and C–D bond stretching vibrations. It is not surprising, therefore, that the substitution of deuterium for hydrogen is so important in determining the course of the reaction, as is shown most vividly by comparing the cases of toluene-α-d_3 and toluene-d_5.

If we consider either Polanyi's universal linear relationship[11] or Johnston's recent calculations,[12] it be-

(9) Because the A/T concentration ratio changes with time, the proper procedure would have been to plot in Fig. 1 average A/T ratios rather than initial A/T ratios. The error introduced by making this simplification is relatively minor.

(10) This conclusion is not in conflict with previous observations[4,5] of straight lines in plots of ln $k_{abs}/k^{1/2}_{combination}$ *vs.* $1/T$. Over the temperature range available for study, a plot of the function ln $(A_1e^{-E_1/RT} + A_2e^{-E_2/RT})$ *vs.* $1/T$ shows no discernible curvature if E_1 and E_2 differ by 1–2 kcal./mole and A_1 and A_2 are of the same order of magnitude. Normal scatter in experimental data of this sort would completely obscure any curvature.

(11) N. N. Semenov, "Some Problems of Chemical Kinetics and Reactivity," Vol. I, Pergamon Press, New York, N. Y., 1958, p. 27.

(12) H. S. Johnston and C. Parr, *J. Am. Chem. Soc.*, **85**, 2544 (1963).

comes evident that this observed difference in activation energy of 1.5 kcal./mole is too small and not consistent with the difference of about 21 kcal./mole in the bond dissociation energies of the aromatic and side-chain C–H bonds in toluene. A plausible explanation is that the transition state for the ring reaction has a different geometrical configuration from that of the side-chain reaction, the latter corresponding most assuredly to the linear three-center type discussed by Johnston.[12] For aromatic systems, one may conceive a transition state such that the methyl radical is somehow directly attached to the ring, perhaps by the formation of a dimethylcyclohexadienyl radical, in which case Polanyi's relationship or Johnston's calculations would not necessarily apply.

The isotope effect ratios $r_h/r_d = 6.4$ and $s_h/s_d = 6.4$ are measures of the relative rates of abstraction of hydrogen and deuterium from the ring and the side chain, respectively. A detailed calculation of these ratios is not now feasible because of the uncertainty in the transition state for the ring reaction. Nonetheless, if we still apply the simplest possible theory and assume the loss of a C–H stretching mode and possibly the loss of two C–H bending modes in the transition state, we obtain,[13] using reasonable vibrational frequencies,[14] kinetic isotope effects of about 6 or 14, depending on whether we consider the bending modes or not, in fair agreement with our experimental results. The important consideration in these calculations is that if the kinetic isotope effects depend specifically on the shifts in the vibrational frequencies of C–H and C–D bonds of toluene, the two isotope effects should be of comparable magnitude, apart from the unknown tunneling corrections.[15] This would justify our previous assumption of equal isotope effects. However, because of the probable difference in transition states this question remains unsettled, pending the direct measurement of the temperature coefficient of the isotope effects.

Finally the ratio $a/(r_h + s_h) = 3.3$ refers to the relative rate of hydrogen abstraction by methyl radicals from azomethane and toluene. Using data compiled by Trotman-Dickenson,[16] we calculate $a/(r_h + s_h) = 3.6$ at 60°, in excellent agreement with our results.

By considering the rates of steps 2–4 as well as the known rate of recombination of methyl radicals, it is possible from our data to evaluate each of the rate constants on an absolute basis. For example, in the case of toluene-d_8

$$a = k_t^{1/2} R_{CH_4} / R_{C_2H_6}^{1/2} [A] \quad (8)$$

$$s_d + r_d = k_t^{1/2} R_{CH_3D} / R_{C_2H_6}^{1/2} [T] \quad (9)$$

where k_t is the rate constant for recombination of methyl radicals. Other rate constants are obtained in a similar manner by reference to the data from the other deuterated toluenes, except that in the calculations of s_h and r_h the previously computed value of $a/k_t^{1/2}$ (eq. 8) is utilized. The results using $k_t = 10^{13.34}$ cc. mole^{-1} sec.$^{-1}$ [17] are shown in Table III. Values of a and $s_h + r_h$ computed from data in the literature are also shown for comparison purposes. The excellent agreement displayed here, although very pleasing, must be considered to some extent fortuitous because the absolute rates of formation of methane and ethane were measured with considerably less precision than the CH_4/CH_3D ratios. Because of this reservation, we prefer not to compute ratios of rate constants from these data but use instead the values in Table II.

A question that arises now is whether the reaction of methyl radicals with the aromatic ring results in the immediate abstraction of a hydrogen atom or whether a permanent addition to the ring occurs, followed by hydrogen abstraction from the dimethylcyclohexadienyl radical *via* a second methyl radical, as postulated by Szwarc[3] for the liquid phase. The fact that the ratio $(C_2H_6 + CH_4 + CH_3D)/N_2$ is unity within experimental error (Table I)[18] and that xylene is not an important product of the reaction are convincing evidence that permanent addition of methyl radicals to the ring does not take place. We would propose instead that direct abstraction from the ring results in

Table III: Absolute Values of Rate Constants at 60°[a]

Rate constant	Calculated value: This work	Calculated value: Literature	Source of data
a	$(1.0 \pm 0.1) \times 10^6$	0.9×10^6[b]	Toluene-d_8
$s_d + r_d$	$(3.7 \pm 0.2) \times 10^4$	...	Toluene-d_8
s_d	$(2.6 \pm 0.2) \times 10^4$	...	Toluene-d_3
r_h	$(2.3 \pm 0.4) \times 10^4$	...	Toluene-d_3
r_d	$(1.0 \pm 0.2) \times 10^4$	...	Toluene-d_5
s_h	$(3.8 \pm 0.8) \times 10^5$	...	Toluene-d_5
$s_h + r_h$	$(4.0 \pm 0.8) \times 10^5$	4.7×10^5[c]	Toluene-d_3
		4.1×10^5[d]	Toluene-d_5

[a] All units are cc. mole^{-1} sec.$^{-1}$. The quoted error limits are average deviations. [b] See ref. 7. [c] See ref. 4. [d] See ref. 5.

(13) L. Melander, "Isotope Effects on Reaction Rates," Ronald Press Co., New York, N. Y., 1960, pp. 20–22.

(14) R. N. Jones and C. Sandorfy, "Technique of Organic Chemistry," Vol. IX, A. Weissberger, Ed., Interscience Publishers, Inc., New York, N. Y., 1961, pp. 387–398.

(15) H. S. Johnston, "Advances in Chemical Physics," Vol. III, Interscience Publishers, Inc., New York, N. Y., 1961, p. 131.

(16) A. F. Trotman-Dickenson, "Gas Kinetics," Butterworths Scientific Publications, London, 1955, pp. 201 and 202.

the short-lived tolyl free radical, which then undergoes a metathetical reaction with toluene to form the relatively stable benzyl radical. Recombination of the methyl radical with the benzyl radical produced in this way, as well as by direct abstraction from the side chain in toluene, accounts for the ethylbenzene product and also for the mass balance requirement that two methyl radicals be used up for each methane produced. Recombination of any radical R to form the dimer product R_2 (*e.g.*, bibenzyl) would cause the ratio $(C_2H_6 + CH_4 + CH_3D)/N_2$ to become greater than unity. Such a process is unlikely since the concentration of CH_3 radicals is large compared to that of any other R radical, as evidenced by the small yield of CH_4 relative to C_2H_6. Indeed no significant yield of bibenzyl was found.

The decrease in the $(C_2H_6 + CH_4 + CH_3D)/N_2$ ratio caused by the introduction of CO_2 may have to do with the competing reactions of methyl radicals with azomethane in abstraction and addition.[7] It is possible that the addition reaction requires a third body, and thus it is accelerated by the CO_2. This point requires further study.

Perhaps the most interesting facet of this system is the striking difference in the reaction mechanisms of the liquid and gas phases insofar as the participation of the aromatic ring is concerned. We can formally illustrate this difference by writing down the partial reaction scheme

$$CH_3 + C_6H_5CH_3 \rightleftharpoons [C_6H_5CH_3 \cdot CH_3]$$

free radical addition complex

$$\xrightarrow{R} CH_4 + CH_3C_6H_4\cdot \quad \text{(gas phase)} \qquad \text{(Ia)}$$

$$\xrightarrow{R} RH + \text{xylene} \quad \text{(liquid phase)} \qquad \text{(Ib)}$$

where R is a free radical. Reaction Ia is the unimolecular decomposition of the addition complex, and it represents the reaction path for the gas phase reaction which involves the ring. Reaction Ib is a bimolecular disproportionation reaction between free radicals, and it describes the predominant process in the liquid phase. Several factors may be suggested to explain the difference between the mechanisms in the two phases. Because of the lower recombination rate constant and much higher rate of initiation, the steady-state concentration of radicals R is higher in the liquid phase, and this undoubtedly accounts for the enhancement of reaction Ib in the liquid phase. A second consideration relates to the lower equilibrium constant between reactants and addition complex in the gas phase reaction, this being a free volume or entropy effect. Thus in the gas phase the addition complex is more likely to fly apart, and reaction 3 becomes the major process. An alternative but related point of view is that the initially highly excited addition complex has a longer lifetime in the liquid phase, because of efficient collisional deactivation, and thus the rate of reaction Ib is enhanced. However, an attempt to increase the yield of the ring reaction in the gas phase experiments by the addition of CO_2 so as to increase the lifetime of the complex was not successful, as shown by the constant CH_4/CH_3D yield ratio in the experiments with toluene-d_5.

Acknowledgment. The author is indebted to Prof. Harold S. Johnston for very helpful discussions, and to Mr. R. A. Meyer for the mass spectroscopic analysis.

(17) A. Shepp, *J. Chem. Phys.*, **24**, 939 (1956).

(18) A similar good material balance was obtained by Burkley and Rebbert[5] in their photolysis experiments with acetone as the source of methyl radicals.

Secondary Intermolecular Kinetic Isotope Effects in the Methylene Radical–*cis*-Butene-2-d_8–*cis*-1,2-Dimethylcyclopropane-d_8 System[1a]

by J. W. Simons[1b] and B. S. Rabinovitch

Department of Chemistry, University of Washington, Seattle, Washington (*Received October 29, 1963*)

A study of the geometric and structural isomerization reactions of chemically activated *cis*-1,2-dimethylcyclopropane-d_0 (DMC-d_0) and DMC-d_8 is reported. Activation was by addition of methylene, from the photolysis of ketene at 3200 Å. and 25°, to the double bond of *cis*-butene-2-d_0 and -d_8. The measured intermolecular isotope effects for the geometric isomerization ($k_g(H)/k_g(D) = 3.8$) and for one of the structural isomerization ($k_{sp}(H)/k_{sp}(D) = 4.3$) reactions are, for the most part, secondary quantum statistical-weight effects. The effect on other structural isomerization processes ($k_{sb}(H)/k_{sb}(D) = 5.2$) is a mixed primary–secondary isotope effect. Theoretical calculations of rates and of isotope effects are in fairly good agreement with experimental values. Anomalous high-pressure product compositions in both the -d_0 and -d_8 systems can be explained by the presence of ~29% triplet methylene radical reaction at high pressures. The addition of oxygen altered the product composition so as to indicate the removal of such triplet methylene reaction. Our earlier work on the isotope effects in singlet methylene radical C–H insertion and C=C addition reactions with *cis*-butene-2 has been extended. Calculations of the geometric isomerization rates of 1,2-cyclopropane-d_2 and 1,2-dimethylcyclopropane have been made and are compared to the existing data in thermal and chemical activation systems.

Introduction

The existence and measurement of large *normal* intermolecular secondary kinetic isotope effects in unimolecular decompositions of energized species, which take place in nonequilibrium systems, have been reported and discussed previously.[2-5] The origin of the isotope effect has been shown to be of a quantum statistical, rather than of a mechanistic, nature. The magnitude of this isotope effect depends on the total degree of isotope substitution and on the absolute and relative magnitudes of $\langle E \rangle$, the average energy of the energized species, and E_0, the critical energy for reaction. The magnitude of $\langle E \rangle$ is governed by E_{min}, the minimum energy of the activated species, and by $f(E)\,dE$, the nonequilibrium distribution function of energy states above E_{min}.

To date, the isotopic systems studied by chemical activation have involved critical energies E_0 in the region 30–35 kcal. mole^{-1}, with very small values (a few kcal. mole^{-1}) of the excess energy ($\langle E \rangle - E_0 = \langle E^+ \rangle$), as for ethyl radicals,[2a,4] or with somewhat larger values (around 8–10 kcal. mole^{-1}), as for butyl[2b] and propyl[5] radicals. The addition of singlet methylene radicals to the double bond of olefins produces vibrationally excited cyclopropanes.[6,7] This system offers the interesting possibility of studying these nonequilibrium normal secondary isotope effects at both a very high average energy $\langle E \rangle$, with minimum energy

(1) (a) This work was supported in part by NSF and in part by ONR; (b) General Electric Foundation Predoctoral Fellow; abstracted in part from the Ph.D. thesis of J. W. S.

(2) (a) B. S. Rabinovitch and J. H. Current, *Can. J. Chem.*, **40**, 557 (1962); (b) J. W. Simons, D. W. Setser, and B. S. Rabinovitch, *J. Am. Chem. Soc.*, **84**, 1758 (1962); (c) J. W. Simons and B. S. Rabinovitch, to be published.

(3) B. S. Rabinovitch and D. W. Setser, *J. Am. Chem. Soc.*, **84**, 1765 (1962).

(4) J. H. Current and B. S. Rabinovitch, *J. Chem. Phys.*, **38**, 783, 1967 (1963).

(5) W. E. Falconer, B. S. Rabinovitch, and R. J. Cvetanović, *ibid.*, **39**, 40 (1963).

(6) G. B. Kistiakowsky and K. Sauer, *J. Am. Chem. Soc.*, **78**, 5699 (1956).

(7) H. M. Frey and G. B. Kistiakowsky, *ibid.*, **79**, 6373 (1957).

$E_{min} \sim 100$ kcal. mole^{-1}, and also at high critical energy, $E_0 \sim 60$ kcal. mole^{-1}.[8]

The addition of methylene radicals, generated by the photolysis of ketene, to the double bond of *cis*-butene-2-d_0 and *cis*-butene-2-d_8, and the relative rates of the geometric and structural isomerization reactions of the energized *cis*-1,2-dimethylcyclopropane-d_0 and *cis*-1,2-dimethylcyclopropane-d_8 have been studied and are now reported. The effect of the deuterium substitution on the geometric isomerization rate is a secondary isotope effect; the effect on the structural isomerization rate involves mixed primary and secondary isotope effects[9]; both a hydrogen and deuterium atom may move to give different products.

During the course of this work, hydrogen–deuterium kinetic isotope effects in the addition of methylene radicals to the double bond of *cis*-butene-2-d_8, and in the insertion reactions into the vinylic and allylic carbon–deuterium bonds, were also determined. A preliminary account of these latter effects has appeared.[10] When oxygen is added to the systems, the magnitudes of these effects are somewhat altered. The effect of oxygen is interpreted, at least in part, as indicating the presence of some ground triplet state methylene radicals in the system.

Experimental

Materials. Ketene was prepared by pyrolysis of acetone and was purified by low temperature (−78°) gas chromatography on Fluoropak. The purified material contained 1.4% propylene and was stored at liquid nitrogen temperature.

Phillips research grade *cis*-butene-2 (purity 99.89%) was used without further purification, since gas chromatographic analysis indicated the presence of a trace of *trans*-butene-2 as the only impurity.

Phillips research grade ethylene (purity 99.9%) was used without further purification.

A mixture of butene-d_8 isomers containing minor impurities of propane, butane, butadiene, and some higher hydrocarbons was obtained from Merck of Canada, Ltd. This mixture contained 20–25% *cis*-butene-2-d_8 which was separated and purified by gas chromatography. The chemical purity was 99%, with *trans*-butene-2-d_8 as the major impurity. The isotopic purity of this isomer was checked mass spectrographically and found to be approximately 85% butene-d_8, 14% butene-d_7, and ~1% butene-d_6; correction for these impurities would amount to only a 3–4% effect on measured rates.

Apparatus and Procedure. All gas handling was performed with a conventional vacuum system. The filtered radiation of a G.E. AH-6 high-pressure mercury arc lamp was used for all photolyses. The filter was a 1–2-mm. Pyrex glass reactor wall and an aqueous solution of $NiSO_4 \cdot 6H_2O$ and $CoSO_4 \cdot 7H_2O$[11] circulating through a Corex D glass envelope, having a light path through the solution of about 5 mm. The transmission of the filter was measured, and from the known lamp output and variation of ketene quantum yields[12] and extinction coefficients[13] with radiation frequency, the average wave length for ketene decomposition was determined to be ~3200 Å.

Mixtures of ketene and *cis*-butene-2, with or without added oxygen, were photolyzed in Pyrex vessels of known volumes for reaction times varying between 30 and 90 min., depending upon the amount of ketene and the size of the reactor. The ratio of ketene to butene used was usually 1:15, and no significant variation in the product proportions of interest occurred as this ratio varied from 1:10 to 1:20. Systems without added oxygen will be designated as "pure." The entire condensable portion of the contents of a reactor was analyzed at the end of each run.

Analysis. Gas–liquid phase chromatography was used for all quantitative analyses. The analytical columns consisted of a 1-m. length of 20% hexamethylphosphoramide on firebrick followed by a 6-m. length of 20% $AgNO_3$–ethylene glycol (saturated solution) on firebrick. A mixture of known composition and components, similar in relative magnitudes to a reaction mixture, was used to calibrate the analytical columns. Since the products 2-methylbutene-1 and 3-methylbutene-1 were not resolved on these columns, only the total of these two components was determined. A correction to the 2-methylbutene-2 was determined for incomplete resolution of propylene from it; this correction was negligible at high pressures, but increased to 50–70% at the lowest pressures, particularly in the oxygen runs.

Results

Product Yields and Composition. Effect of Oxygen.[14] The pure systems will be considered first. The total

(8) D. W. Setser and B. S. Rabinovitch, *Can. J. Chem.*, **40**, 1425 (1962).

(9) D. W. Setser and B. S. Rabinovitch, *J. Am. Chem. Soc.*, **86**, 564 (1964).

(10) J. W. Simons and B. S. Rabinovitch, *ibid.*, **85**, 1023 (1963).

(11) W. A. Noyes and P. A. Leighton, "Photochemistry of Gases," Reinhold Publishing Corp., New York, N. Y., 1941.

(12) B. T. Connelly and G. B. Porter, *Can. J. Chem.*, **36**, 1640 (1958); *J. Chem. Phys.*, **33**, 81 (1960).

(13) J. Knox, R. G. W. Norrish, and G. Porter, *J. Chem. Soc.*, 1482 (1952).

(14) A. N. Strachan and W. A. Noyes, Jr., *J. Am. Chem. Soc.*, **76**, 3258 (1954); R. A. Holroyd and W. A. Noyes, Jr., *ibid.*, **78**, 4831 (1956).

yield of the C_5 products of interest, *cis*-1,2-dimethylcyclopropane (C), *trans*-1,2-dimethylcyclopropane (T), 2-methylbutene-2 (P_1), 2-methylbutene-1 (P_2) + 3-methylbutene-1 (P_3), *trans*-pentene-2 (P_4), and *cis*-pentene-2 (P_5), varied from ~20% of the ketene in the reaction mixture at the lowest pressures to ~60% at higher pressures, for both the $-d_0$ and $-d_8$ systems. The percentage of photolyzed ketene which these numbers represent is actually higher, since some ketene is diverted by secondary and simultaneous processes, such as undetected polymerization or attack by radicals. Variation of photolysis time in replicate experiments indicated incomplete photolysis of ketene (*i.e.*, lower product yields which increased with exposure times) at shorter times than those usually employed, and almost complete photolysis, under the actual run conditions at the higher of the pressures used.

Side reaction products of lower molecular weight, such as ethane, ethylene, propane, propylene, butane, etc., and an approximately equal amount of higher molecular weight hydrocarbon compounds (C_6–C_9 and largely unidentified) were ~20% of the ketene used at the lowest pressures in the pure systems. The amount of obvious alkyl radical side reaction products decreased considerably at higher pressures. Although the amount of this side reaction was large (equal to the total amount of C_5 products of principal interest, in the worst case), only very negligible amounts of these were C_5 hydrocarbons: *n*-pentane, isopentane, and pentene-1. It seems that the main C_5 products result essentially from the reactions represented in eq. a–d.[8] Some further decomposition of these will occur at lower pressures.

$$CH_2 + \textit{cis}\text{-butene} \xrightarrow{6k_a} P_5 \qquad \text{(a)}$$

$$\xrightarrow{2k_v} P_1 \qquad \text{(b)}$$

$$\xrightarrow{k_d} C^* \qquad \text{(c)}$$

$$\begin{array}{ccccc} & & (P_4,P_5)^* & \xrightarrow{\omega} & P_4,P_5 \\ & & k_{sp} \uparrow \quad \uparrow k_{sp'} & & \\ C & \xleftarrow{\omega} & C^* \underset{k_{g'}}{\overset{k_g}{\rightleftharpoons}} T^* & \xrightarrow{\omega} & T \\ & & k_{sb} \downarrow \quad \downarrow k_{sb'} & & \\ & & (P_1,P_2,(P_3))^* & \xrightarrow{\omega} & P_1,P_2,(P_3) \end{array} \qquad \text{(d)}$$

[8]

The addition of oxygen altered the product composition at each pressure (although not in the same way). The total yield of the C_5 products of interest was reduced to 40–50% of that in the pure systems. Even at the lowest percentage (1%) of oxygen, the amounts of lower molecular weight ($<C_5$), as well as some higher molecular weight ($>C_5$), side reaction products were reduced drastically, and large amounts of CO_2 were formed. Large amounts of the products which disappeared arose originally from conventional radical processes.[15,16] In the presence of 5–15% oxygen, the CO_2 and unidentified (presumably oxy en-containing) higher molecular weight compounds (having longer g.l.p.c. retention times), were the main side-reaction products. These side-reaction products amount to ~30% of the ketene used, at the lowest pressures. A visible fog was formed in the reactor at the highest oxygen percentages, undoubtedly due to the formation of high molecular weight oxygen-containing compounds.

The effect of varying percentages of added oxygen on the ($-d_0$) system (a similar behavior was observed for the ($-d_8$) system) is illustrated in Fig. 1 for two pressures. An explanation of an important change in C_5 product composition will be given in the section on

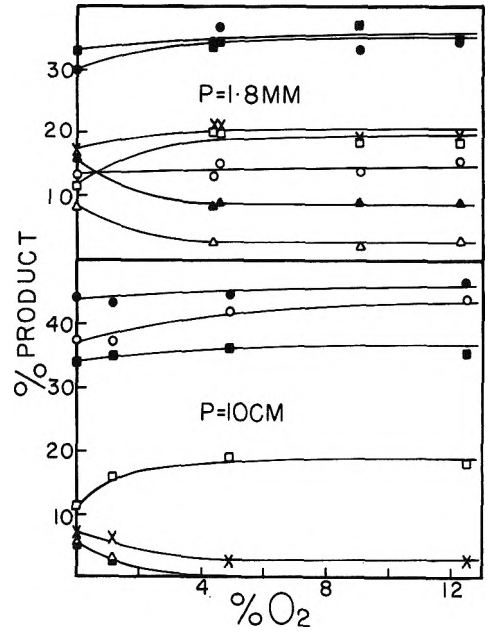

Figure 1. Variation of C_5 product composition in the ($-d_0$) system with % O_2 in the reaction mixture at two values of the total pressure; total 1,2-dimethylcyclopropane, C + T, ●; *cis*-1,2-dimethylcyclopropane, C, ○; *trans*-1,2-dimethylcyclopropane, T, ×; 2-methylbutene-2, P_1, □; 2- + 3-methylbutene-1, P_2 + P_3, △; *trans*-pentene-2, P_4, ▲; *cis*-pentene-2, P_5, ■.

(15) E. W. R. Steacie, "Atomic and Free Radical Reactions," 2nd Ed., Reinhold Publishing Co., New York, N. Y., 1954.

(16) H. M. Frey and G. B. Kistiakowsky, *J. Am. Chem. Soc.*, **79**, 6373 (1957); J. Bell and G. B. Kistiakowsky, *ibid.*, **84**, 3417 (1962).

triplet methylene reaction. It should be noted that, at both pressures, the oxygen effect on the product composition increased up to 5% oxygen, with virtually no further change, within experimental error, for larger percentages of oxygen.

Product Composition and Pressure Dependence. The pressure variation of the amounts of each of the C_5 reaction products, expressed as its percentage of the total of these products, is shown in Fig. 2–5 for both the pure system and the oxygen (5–15%) systems, with both butene-d_0 and -d_8. The variation of the total percentage of 1,2-dimethylcyclopropanes with the pressure is also shown. The collision frequency ω is proportional to pressure.

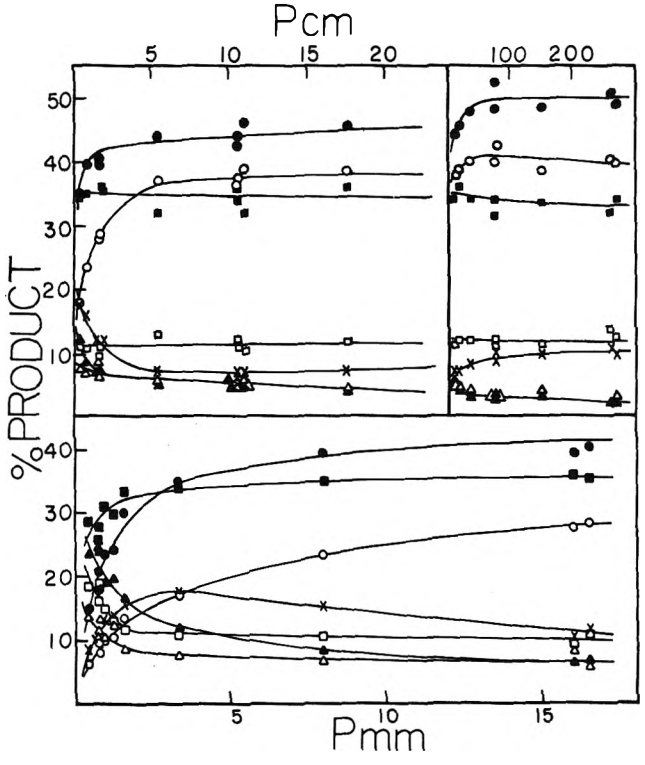

Figure 2. Variation of C_5 product composition with total pressure for the pure (-d_0) system, showing expanded presentations for different pressure regions. Smooth curves are shown through the data. The same symbols apply as in Fig. 1.

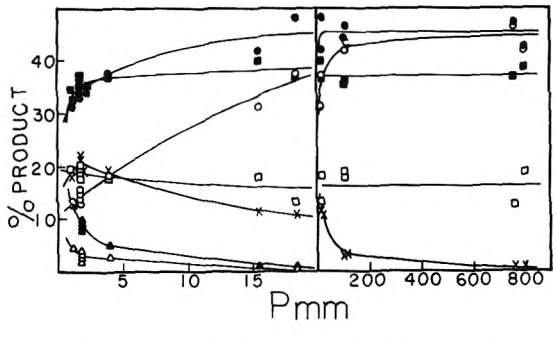

Figure 3. The same as Fig. 2 but with 5–15% O_2 added.

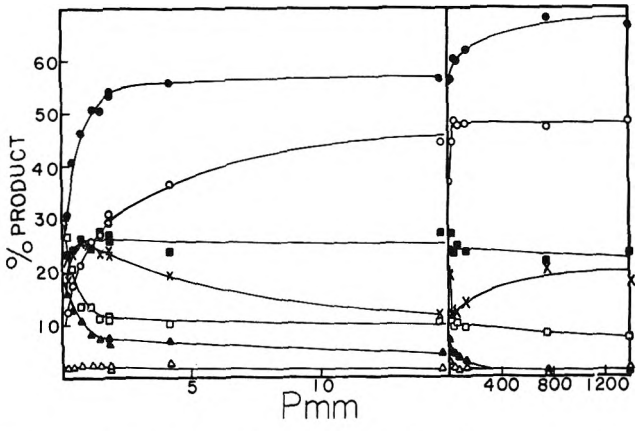

Figure 4. The same as Fig. 2 but for the pure (-d_8) system.

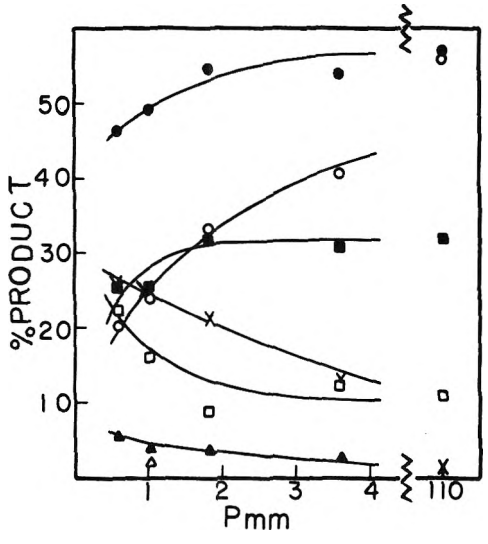

Figure 5. The same as Fig. 4 but with 5–15% O_2 added.

The Low Pressure Region. From Fig. 2–5 it is seen that the pressure variation of the product composition for all the systems in the low pressure region ($\lesssim$5 cm. for the -d_0 and $\lesssim$1 cm. for the -d_8 systems) is in qualitative agreement with the mechanism represented in eq. a–d, which is altered in nomenclature, only, from the generally accepted mechanism for the reactions of singlet methylene radicals with butene-2.[8,17] It is seen that for all the systems, as the pressure is decreased [C] decreases and [T] increases, due to geometric isomerization of [C*] to [T*], while [C + T] and

(17) H. M. Frey, *Proc. Roy. Soc.* (London), **A250**, 409 (1959); **A251**, 575 (1959).

Table I: Limiting High Pressure Product Composition (%) for Reaction of Singlet and Triplet Methylene Radicals with *cis*-Butene-2-d_0 and *cis*-Butene-2-d_8

	Triplet		Experimental[c]		Corrected[d] Singlet		O_2 results[e]	
	d_0[a]	d_8[b]	d_0	d_8	d_0	d_8	d_0	d_8
trans-1,2-Dimethylcyclopropane	31.3	64.6	9.2	19.4	0.6	0	0.6	0
cis-1,2-Dimethylcyclopropane	24.6	24	40.0	47.9	46.0	58.2	45.0	57.1
2-Methylbutene-2	3.7	0	12.0	7.9	15.3	11.3	16.5	10.9
trans-Pentene-2	12.3	3.3	2.6	1.0	−1.1	0	0	0
2,3-Methylbutene-1	8.8	3.3	3.1	1.1	0.8	0	0.4	0
cis-Pentene-2	19.3	5.3	33.3	22.9	38.8	30.3	37.5	32.0

[a] Data of Duncan and Cvetanović (for *cis*-butene-2-d_0). [b] Calculated from this work assuming 29% triplet methylene and comparing the pure-d_8 system with the O_2 system. [c] Experimental results for the pure systems in this work (ketene + *cis*-butene-2-d_0 and ketene + *cis*-butene-2-d_8). [d] Data for pure systems corrected for ~29% triplet methylene. [e] Experimental results from this work for ($-d_0$) and ($-d_8$) systems with 5–15% oxygen added.

the concomitant insertion products are essentially constant. As the pressure is further decreased, [C + T] decreases and the $\Sigma[P_i]$ increases as the slower structural isomerization increases in importance. The maximum in [T] occurs where the decrease in [T] due to structural isomerization of [T*] overtakes the increase in [T] due to the geometric isomerization of [C*] to [T*]. Quantitative agreement with expressions resulting from the mechanism is discussed in later sections.

The High Pressure Region. Equations a–c for the primary processes of singlet methylene interaction with *cis*-butene-2 predict that, at limiting high pressures, [T], [P_2 + P_3], and [P_4] go to zero, while [C], [P_1], and [P_5] go to constant values. This is the observed behavior in the presence of 5–15% oxygen. In both the ($-d_0$) and ($-d_8$) pure systems, at high pressures [T] goes through a minimum increasing to a constant value; [P_4], [P_2], and [P_3] approach finite constant values while [C], [P_1], and [P_5] either approach constant values or go through maxima and decrease slightly. The high pressure behavior of the pure systems indicates that, at least at high pressures, some other mechanism beside that shown in eq. a–c is operative. An added process in which reaction due to triplet methylene takes place at high pressures in the pure systems will now be discussed.

In Table I the observed high pressure product compositions are summarized for the four systems studied *in this work, along with the high pressure product* composition for triplet methylene reaction as obtained by Duncan and Cvetanović[18] from the Hg-photosensitization of ketene in the presence of *cis*-butene-2. The observed composition for the pure ($-d_0$) system was corrected for triplet methylene reaction by assuming that T, P_4, and P_3 + P_2 at high pressures arose solely from triplet methylene reaction. The corrected composition as shown in Table I agrees very well with the O_2 systems. The correction corresponded to 29% triplet methylene reaction. The propriety of using here the correction for triplet radical–butene-2 product composition as determined from a Hg-photosensitization system is supported by the fact that a similar product composition was also found by Frey,[19] who studied triplet methylene produced by inert gas collision-induced transitions to the ground state[20] of the singlet state radicals arising from diazomethane photolysis. Frey demonstrated the effect of added oxygen on the triplet methylene reactions by a result in which added oxygen restored the singlet methylene product composition.

The product composition from triplet methylene reaction with *cis*-butene-d_8 was calculated by a comparison of the pure and oxygen-containing systems and by assuming the same percentage of triplet radicals to be present as determined from the pure ($-d_0$) system.

Geometric Isomerization. Solution of the steady-state differential equation in [T*] (see eq. d) results in eq. 1, which has been given in previous work in a slightly different form[8,17]

$$\frac{[C]}{[T]} = \frac{\omega}{k_g} + \frac{k_g' + k_s'}{k_g} \qquad (1)$$

where

$$k_s' = k_{sb}' + k_{sp}' \qquad (2)$$

The value of k_g may be determined from a plot of [C]/[T] *vs.* ω, without a detailed knowledge of the

(18) F. J. Duncan and R. J. Cvetanović, *J. Am. Chem. Soc.*, **84**, 3593 (1962), and private communication.

(19) H. M. Frey, *ibid.*, **82**, 5947 (1960).

(20) G. Herzberg, *Proc. Roy. Soc.* (London), **A262**, 291 (1961).

structural isomerization products. The plot should be a straight line at all pressures, for a monoenergetic system (*i.e.*, k_g, k_g', and k_s' all constant, independent of pressure), or slightly curved for a system with only a small energy spread, such as the systems of this study. Figure 6 shows the straight line fit to the results for the

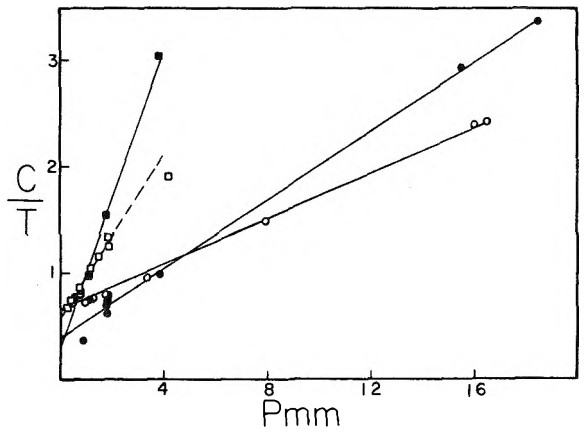

Figure 6. Plots of the ratio *cis*-/*trans*-dimethylcyclopropane at low pressures for all the systems: pure ($-d_0$) system, ○; 5–15% O_2 ($-d_0$) system, ●; pure ($-d_8$) system, □; 5–15% O_2 ($-d_8$) system, ■. The least-square lines (solid) through the data have these equations: ○, $[C/T] = 0.107P_{mm} + 0.67$; □, $[C/T] = 0.38P_{mm} + 0.59$; ●, $[C/T] = 0.16P_{mm} + 0.41$; ■, $[C/T] = 0.72P_{mm} + 0.30$. The dashed line is the extension of the corresponding least-square line.

($-d_0$) and ($-d_8$) systems, in the presence and the absence of added oxygen. The effect of added oxygen is to increase the slopes in Fig. 6 and reduce the rate constant k_g by a factor of 0.67 and 0.53 in the ($-d_0$) and ($-d_8$) cases, respectively, and to lower the intercepts by factors of 0.61 and 0.50, respectively. These results are from experiments in which 5–15% oxygen was added.

The average experimental rate constants and isotope effects are summarized in Table II. Experimental rate constants were calculated from the least-squares lines in Fig. 6. Although oxygen has a marked effect on the rate constants, the isotope effect is increased by only 20%.

The values of k_g' given in Table II were calculated from the intercepts, with use of the relation that $k_s' \sim 0.1k_g'$, which is a good assumption since the geometric isomerization rates in this and other related systems[8] are ~10 times faster than the structural isomerization rates; any error due to this assumption is negligible.

The low intercepts for the oxygen results in Fig. 6 may be the result of experimental error and the large extrapolation, but it seems more likely that the addition of oxygen has other effects on the system than can be accounted for solely by elimination of triplet methylene reaction.

Table II: Geometric Rate Constants (10^8 sec.$^{-1}$) and Isotope Effects for Activated Dimethylcyclopropane-d_0 and Dimethylcyclopropane-d_8

	No oxygen	5–15% oxygen[b]	Theoretical
k_g(H)	1.96 ± 0.05[a]	1.34 ± 0.04[a]	1.52
k_g(D)[c]	0.52 ± 0.03[a]	0.29 ± 0.01[a]	0.43
$\frac{k_g(H)}{k_g(D)}$	3.8 ± 0.25	4.5 ± 0.2	3.54
$\frac{k_g'(H) + k_s'(H)}{k_g(H)}$	0.67 ± 0.04[a]		0.80
$\frac{k_g'(D) + k_s'(D)}{k_g(D)}$	0.59 ± 0.03[a]		0.77
k_g'(H)	1.17 ± 0.08[a]		1.09
k_g'(D)	0.27 ± 0.02[a]		0.30
$\frac{k_g'(H)}{k_g'(D)}$	4.3 ± 0.4	(6.4 ± 1.8)	3.64
$\frac{k_g(H)}{k_g'(H)}$	1.68	(2.7)	1.40
$\frac{k_g(D)}{k_g'(D)}$	1.89	(3.8)	1.43

[a] Calculated from standard deviations of least-squares slopes and intercepts. [b] The values in parentheses are doubtful since the intercepts and therefore k_s/k_g' for the O_2 systems are out of line with what would be expected from thermal work[21] and other methylene work.[8,17] [c] (H) and (D) refer to light and deuterated molecules, respectively.

Structural Isomerization. The structural isomerization of 1,2-dimethylcyclopropane-d_0 and -d_8 follows two principal paths, corresponding to rupture of the two different types of ring bonds; the carbon atoms and their attached atoms, are labeled type a and b

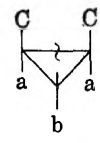

$\xrightarrow{k_{sp}}$ *cis*- and *trans*-pentene-2, (b → a) (e)

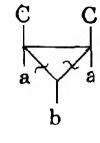

$\xrightarrow{k_{sb}}$ {2-methylbutene-2, (a → b); 2-methylbutene-1, (a → a)} (f)

The nature of the atom transfer is indicated in parentheses; there are two equivalent alternative rupture paths shown in (f). The deuterium isotope effect on k_{sp} is a secondary one since only H-atom transfer, (b → a), occurs in both isotopic systems.[9] The isotope effect on k_{sb} is a mixed primary and secondary effect;

an H-atom transfers in the ($-d_0$) system and a D atom transfers in the ($-d_8$) system.

The reacting cyclopropane is largely geometrically isomerized prior to structural isomerization, and the evaluation of the structural rate constants from the mechanism in eq. a–d was simplified by taking $k_{sb} = k_{sb}'$ and $k_{sp} = k_{sp}'$, which makes $k_s = k_s'$, also. This approximation is readily shown to be reasonable: Flowers and Frey have reported[21] that $k_{sb} = k_{sb}'$ in the thermal isomerization of 1,2-dimethylcyclopropane. Also, they obtained $k_{sp}/k_{sp}' = 1.4$, and a frequency factor ratio of 0.40. The average energy of the reacting molecules in the thermal system was less than in the present chemical activation system; for this energy increase, a ratio here of k_{sp}/k_{sp}' close to unity[22] is expected.

Application of the steady-state hypothesis to [C*] and [T*] and solution of the resulting differential equations gives these expressions

$$\frac{\sum_{j=1}^{3}[P_j]}{[C]+[T]} = \frac{1}{\omega}\left(k_{sp}\frac{2k_v}{k_d} + k_{sb}\frac{2k_v}{k_d} + k_{sb}\right) + \frac{2k_v}{k_d} \qquad (3a)$$

where $2k_v/k_d = \lim_{\omega\to\infty}[P_1]/[C+T]$; also

$$\frac{\sum_{j=4}^{5}[P_j]}{[C]+[T]} = \frac{1}{\omega}\left(k_{sb}\frac{6k_a}{k_d} + k_{sp}\frac{6k_a}{k_d} + k_{sp}\right) + \frac{6k_a}{k_d} \qquad (3b)$$

where $6k_a/k_d = \lim_{\omega\to\infty}[P_5]/[C+T]$; finally

$$\frac{\sum_{j=1}^{5}[P_j]}{[C]+[T]} = \frac{1}{\omega}\left(k_s + k\frac{k_i}{k_d}\right) + \frac{k_i}{k_d} \qquad (3c)$$

where $k_i = 6k_a + 2k_v$; $k_s = k_{sb} + k_{sp}$; and $k_i/k_d = \lim_{\omega\to\infty}([P_1]+[P_5])/([C]+[T])$.

In Fig. 7 and 8, the appropriate pentenes, as determined from eq. 3, are plotted *vs.* 1/pressure for the ($-d_0$) and ($-d_8$) systems, respectively. The high pressure behavior in the pure systems was discussed above and is not included. As is appropriate for systems with a narrow energy dispersion, the plots approximate straight lines, the slopes and intercepts of which give rate constants averaged over the whole pressure region. With use of the limiting extrapolated high pressure product compositions from Fig. 7 and 8, rate constants at any pressure may be calculated from eq. 3. Alternatively, to avoid this extrapolation, difference

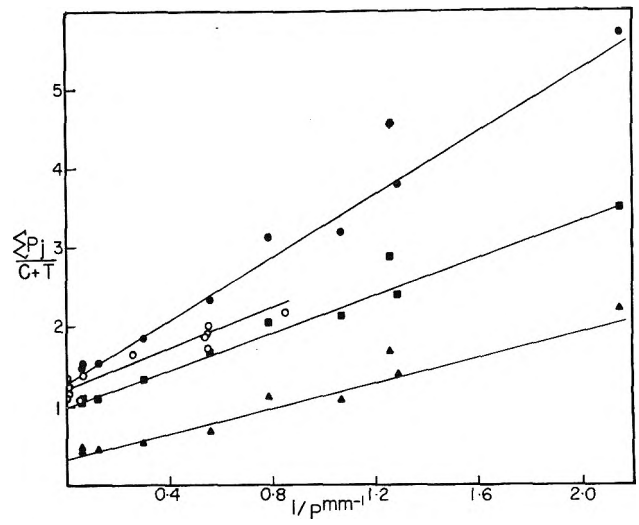

Figure 7. Variation of the ratio of the sums of various pentene products to total dimethylcyclopropane with inverse pressure for the pure and O_2 ($-d_0$) systems: $\sum_{j=1}^{5}[P_j]$, pure system, ●; $\sum_{j=4}^{5}[P_j]$, pure system, ■; $\sum_{j=1}^{3}[P_j]$, pure system, ▲; $\sum_{j=1}^{5}[P_j]$, O_2 system, ○. Only low-pressure data are included for the pure system. Solid lines are from the best fit curves of eq. 4.

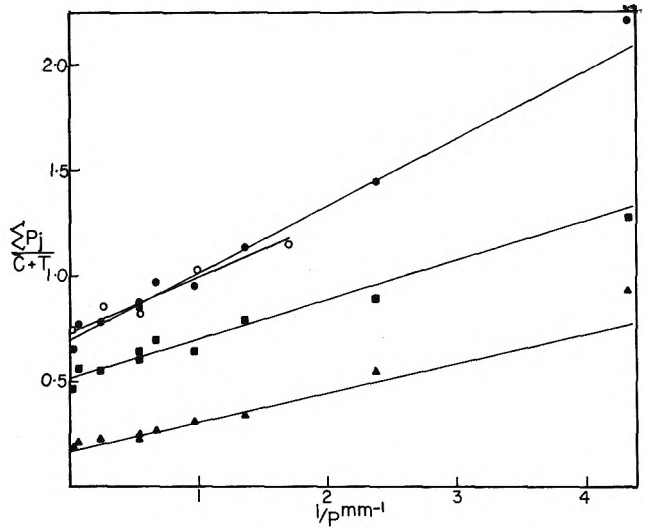

Figure 8. The same as Fig. 7 but for the ($-d_8$) systems.

expressions for the structural constants (eq. 4) were derived from eq. 3

$$k_{sb} = \omega_1\omega_2\frac{\left(\sum_{j=1}^{3}[P_{j1}] - \sum_{j=1}^{3}[P_{j2}]\right)}{[\omega_2([C]+[T])_1 - \omega_1([C]+[T])_2]} \qquad (4a)$$

(21) M. C. Flowers and H. M. Frey, *Proc. Roy. Soc.* (London), **A257**, 122 (1960); **A260**, 424 (1961).

(22) J. N. Butler and G. B. Kistiakowsky [*J. Am. Chem. Soc.*, **82**, 759 (1960)] found similar behavior for methylcyclopropane.

$$k_{sp} = \omega_1\omega_2 \frac{\left(\sum_{j=4}^{5}[P_{j1}] - \sum_{j=4}^{5}[P_{j2}]\right)}{[\omega_2([C] + [T])_1 - \omega_1([C] + [T])_2]} \quad (4b)$$

$$k_s = \omega_1\omega_2 \frac{[([C] + [T])_1 - ([C] + [T])_2]}{[\omega_1([C] + [T])_2 - \omega_2([C] + [T])_1]} \quad (4c)$$

In eq. 4, the structural rate constants, which vary only a little with pressure, may be taken constant over a small pressure range, p_1 to p_2, to which the subscripts 1 and 2 refer. In Fig. 9, the "low pressure" data for the pure ($-d_0$) and ($-d_8$) systems are fitted to eq. 4 by finding the rate constants which fit the data. From the rate constants so determined and from the expressions in eq. 3, limiting high pressure values of the percentages ([C] + [T]), $\sum_{j=1}^{3}[P_j]$, and $\sum_{j=4}^{5}[P_j]$ were calculated to be 43.7, 14.8, and 41.5, respectively, for the pure ($-d_0$) system, and 59.3, 11.1, and 29.6, for the pure ($-d_8$) system. These values are in fair agreement with the measured results given in Table I for the oxygen systems and with the results from the pure systems corrected for 29% triplet methylene reaction. This suggests, in line with some evidence above from *trans*-dimethylcyclopropane variation with pressure, that triplet methylene reaction is not as important at low pressure as at high.

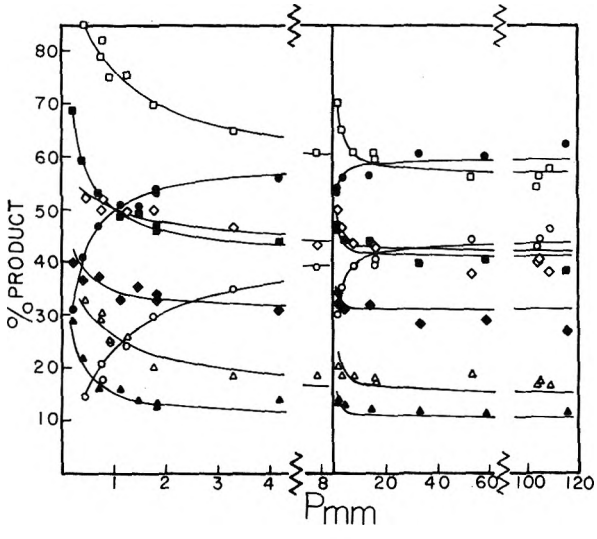

Figure 9. Plot of various C_5 product proportions *vs.* pressure at lower pressures showing the fit of eq. 4 (solid curves) to the pure systems data: open symbols for the ($-d_0$) system and solid symbols for the ($-d_8$) system; C + T, total dimethylcyclopropane, O; $\sum_{j=1}^{5}[P_j]$, total pentenes, □; $\sum_{j=1}^{3}[P_j]$, △; $\sum_{j=4}^{5}[P_j]$, ◇.

Average values of k_s for oxygen-containing systems were obtained in the same way (Fig. 7 and 8). No attempt was made to separate the total rates into individual k_{sb} and k_{sp} values since very few low pressure data were taken in the oxygen systems.

In Table III, the average experimental structural rate constants and isotope effects for the pure and oxygen systems are summarized. The agreement for the isotopic ratio, $k_s(H)/k_s(D)$, is excellent. There is an indication that k_s in the presence of oxygen is a little less than in the pure system. This apparent difference could simply be caused by some minor triplet reaction still occurring at low pressure in the pure system, or it could be due to some unspecified oxygen complications.

Table III: Rate Constants and Isotope Effects for Structural Isomerization of Activated 1,2-Dimethylcyclopropane-d_0 and -d_8[a]

	Pure systems	Oxygen added	Theoretical[c]
$k_s(H)$[b]	1.82	1.25	1.76
$k_{sb}(H)$[d]	1.09		0.821
$k_{sp}(H)$	0.73		0.939
$k_s(D)$	0.38	0.30	0.394
$k_{sb}(D)$[d]	0.21		0.130
$k_{sp}(D)$	0.17		0.264
$k_s(H)/k_s(D)$	4.8	4.2	4.47
$k_{sb}(H)/k_{sb}(D)$	5.2		6.32
$k_{sp}(H)/k_{sp}(D)$	4.3		3.56

[a] Rate constants are in units of 10^7 sec.$^{-1}$. [b] (H) and (D) refer to the light and deuterated molecules, respectively. [c] These are calculated k_E values and ratios for the processes involved, at an average energy based on those of ref. 8. [d] Calculated rate contains an error of ~7%.

Deuterium Isotope Effects on Methylene Insertion and Addition. In Table IV the results on methylene radical insertion into the C—H and C—D bonds, and addition to the C=C bonds of *cis*-butene-d_0 and *cis*-butene-d_8, at 25°, are summarized. The values for the pure systems are changed only slightly from the values of our preliminary report,[10] except in one respect. The present propylene correction to the 2-methylbutene-2 product (see description under Analysis) causes fairly large differences in k_v/k_a from the earlier report, since k_v is measured by the 2-methylbutene-2 formed at high pressures. The present ratios 1.07 and 1.13 make more sense, and agree better with related determinations in the literature,[8] than our previous values of 1.21 and 1.52, respectively. The results from the oxygen systems accord fairly well with the pure systems, in general. The principal difference, although not a serious one, is a decrease in the oxygen system of 20%

Table IV: Methylene Insertion and Addition Ratios

	Pure system[a]	Oxygen
$k_i(H)/k_d(H)$	1.29	1.22
$k_i(D)/k_d(D)$	0.69	0.74
$[k_i[H]/k_d(H)][k_d(D)/k_i(D)]$	1.87	1.65
$k_d[H]/k(E)$	0.99	0.79
$k_d(D)/k(E)$	0.97	0.75
$k_d(H)/k_d(D)$	1.02	1.05
$k_i(H)/k_i(D)$	1.91	1.73
$k_v(H)/k_a(H)$ (per bond)	1.07	1.32
$k_v(D)/k_a(D)$ (per bond)	1.13	1.02
$k_a(H)/k_a(D)$	1.94	1.61
$k_v(H)/k_v(D)$	1.84	2.08

[a] These ratios result from the limiting product composition, derived from curves fitting the low-pressure data in the pure systems, as described in the previous section. Only slightly different values result from the triplet corrected compositions in Table I.

in the ratios, $k_d(H)/k(E)$ and $k_d(D)/k(E)$ (a somewhat anomalous increase of 25% in $k_v(H)/k_a(H)$ is considered suspect); that some differences do occur, which are undoubtedly not all of fundamental sigficance, is not surprising in view of the varied effects caused by oxygen, not to mention the general difficulty of reproducing any value to within 10% in methylene gas phase systems. In any case, the ratios of ratios are found less sensitive both to complexities or changes of mechanism and the values for $k_d(H)/k_d(D)$ and $k_i(H)/k_i(D)$ agree with the earlier report.[10]

Discussion

Triplet Methylene Radical Reaction. Although the elucidation of the chemistry of these systems was not originally, nor indeed is, the major purpose of the present work, nonetheless, we have had to examine the chemical complications encountered.

The higher pressure C_5 product compositions and their change upon addition of oxygen is consistent with the increasing importance (25–30%) of triplet methylene radical reaction in the pure systems at higher pressures. This hypothesis is by no means proven for this complex system, but it provides a consistent explanation of the results.

The existing high pressure data in other methylene systems do not rule out the possibility of some triplet methylene reaction, although the thermal[8] and photolytic[17] decomposition of diazomethane in the presence of butenes at high pressures suggest only a few per cent, or less, of triplet reaction in those systems. In connection with this and other studies, systematic examination has been made, over a wide range of total reaction pressure in each, of the effect of added O_2 on a variety of systems, including ketene with ethylene, propylene, and butene-1; in the latter case, F. H. Dorer has found that the removal of oxygen perceptibly changes the proportions of products (at the high pressure limit) in the direction of the product composition found by Cvetanović and Duncan for butene-1 with triplet methylene.[18] In any case, the presence of oxygen affects these systems to some degree besides merely capturing alkyl radicals; no previous systematic studies are known of the effects due to O_2 in the presence of a variety of olefin substrates.

The mechanism for triplet radical formation, if it occurs, is unknown. At 3100 Å., it is possible[12] that it could involve collision-induced singlet–triplet intersystem crossing of the excited singlet ketene, although the occurrence of this process has not been shown.[12,14]

For purposes of the present isotopic investigations it appears, fortunately, that the complications designated as "triplet" in nature are relatively unimportant at lower pressures. The rate constants and isotope effects in both the pure and oxygen systems are nearly the same, and thus do not depend on the correctness of the preceding hypothesis.

Structural Isomerization. Theoretical calculations were made of the structural isomerization rate. To simplify the experimental calculations, the reactant cyclopropane was described earlier as a 1:1 *cis–trans* mixture. This is not quite the correct ratio that applies for all conditions, but the effect on the calculations of a variation from unity is small. An *average* critical energy for each of the combined reaction paths, defined by k_{sb} and k_{sp}, was recalculated for the *cis–trans* mixture from the thermal isomerization data of ref. 21; E_{0b} and E_{0p} differ by less than 0.1 kcal. mole^{-1} (see Appendix I). The initially formed excited molecules have an energy spread of ~10 kcal. mole^{-1} due to photolysis and thermal energy distributions in the formation reactions; but since the average excess energy, given by $\langle E^+ \rangle = \langle E \rangle - E_0 = 106 - 60 = 46$ kcal. mole^{-1}, is also large, the relative energy dispersion is small. Thus k_{sb} and k_{sp} are well represented by $k_{\langle E \rangle}$ values for the two reactions. The Marcus–Rice formulation of k_E was used[23]

$$k_E = \frac{I_r}{h} \frac{\sum_0^{E^+} P(E^+_{vr})}{N^*_E} \qquad (5)$$

where I_r is the partition function ratio for the adiabatic degrees of freedom (over-all rotations) of the activated

(23) R. A. Marcus and O. K. Rice, *J. Phys. Colloid Chem.*, 55, 894 (1951); R. A. Marcus, *J. Chem. Phys.*, 20, 359 (1952).

complex (+) and the energized molecule (*); $\Sigma P(E^+_{vr})$ is the sum of the degeneracies of internal energy states of the active degrees of freedom of the activated complex, over the range from zero to E^+; and N^*_E is the density of internal energy states for the active degrees of freedom of the energized molecule at the energy E^*.

Models for the molecule and decomposition activated complex were constructed from which values of $P(E^+_{vr})$ and N^*_E were obtained. The models for the ($-d_0$) species were fitted to the existing thermal isomerization data,[21] while conformity to the Teller–Redlich product rule was demanded of the ($-d_8$) models. Discussion of these calculational details is given in Appendix I.

The calculated specific rates and isotope effects are summarized in Table III. The agreement with experiment is good, being somewhat better for the pure systems than with oxygen added.

Calculations were also made (Appendix I) for structural isomerization of 1,2-cyclopropane-d_2. They give a calculated intramolecular primary isotope effect of $k_H/k_D = 2.5$ at 718°K. for the thermal structural isomerization; the experimental value[24] is 2.18. The calculated value at the energy of the present chemical activation systems is reduced to 1.58. Recent work on the thermal isomerization of methylcyclopropane-d_2[9] gives isotope effects in general agreement with those found for cyclopropane-d_2.

The ratio $k_{sp}(H)/k_{sp}(D)$ (Table III) is a measure of the secondary intermolecular isotope effect on structural isomerization in the present system, since an H atom transfers in both cases. Although this secondary effect is mechanistic[2a] in part, since the two D atoms which are on the ring carbons interact somewhat with the reaction coördinate, the largest part of the observed effect corresponds to a quantum statistical-weight effect due to the lowered vibration frequencies of the deuterated species. The magnitude of this nonequilibrium effect has been shown to decrease with increasing energy of the reactants above the critical threshold E_0, for a fixed value of the latter. In the present system, $\langle E^+ \rangle$ is fourfold greater than the largest value in previous work on butyl[2b] and propyl[5] radicals; together with a partially compensating twofold increase in E_0 (60 kcal. mole^{-1} relative to 31–33 in the radical studies) and resultant threefold increase in $\langle E \rangle = \langle E^+ \rangle + E_0$, this results in a reduced, but still large, statistical isotope effect predicted as 3.6 and measured as 4.3.

The ratio $k_{sb}(H)/k_{sb}(D)$ involves a mixed primary and secondary intermolecular isotope effect. The value should be larger than that for the secondary ratio above and this is found (Table III) both from experiment (5.2) and calculation (6.3). Although a separation of the two effects into separate contributions is not strictly accurate, the relative increase in the isotope effect for k_{sb} over that for k_{sp}, given as the quotient of the last two entries in Table III, may be taken as a rough measure of the intramolecular primary isotope effect. The calculated value is somewhat higher than that observed. The model used is related to that for cyclopropane-d_2. In view of the uncertainties in the experimental values, the agreement is considered satisfactory and no attempt was made to improve the model or the slightly arbitrary value[25] of $\Delta E_0 = 1.2$ kcal. mole^{-1}, between H and D atom transfer, assumed in the calculations.

Geometric Isomerization. The thermal and chemically activated geometric isomerization of 1,2-dimethylcyclopropane-d_0 and -d_8, and of 1,2-cyclopropane-d_2, provide good tests of theoretical calculations and of proposed activated complex models. Reference 9 describes the mechanism for both geometric and structural isomerization, but so far quantitative calculations for structural isomerization, only, have been presented in detail. We now consider the calculation of unimolecular rates and fall-off behavior for the geometric isomerization (Appendix I).

The fall-off curve for the thermal unimolecular geometric isomerization of dideuteriocyclopropane has been calculated according to the expression of RRKM theory[23]

$$k_{uni} = \frac{I_r e^{-E_0/RT}}{Q_{vr} h} \sum_{E'=0}^{\infty} \frac{\sum_{E^+_{vr}=0}^{E^+} P(E^+_{vr}) e^{-E^+/RT}}{1 + \frac{I_r}{\omega h} \frac{\sum_{E^+_{vr}=0}^{E^+} P(E^+_{vr})}{N^*_E}} \qquad (6)$$

where Q_{vr} is the molecule vibrational–internal rotation partition function, and other quantities were defined previously. The calculated curves have a fall-off shape (Fig. 10) corresponding to a Slater value of $n \simeq 12$–14, which is close to the experimental ($n \simeq 13.5$) value.[24] The absolute pressure discrepancy, $\Delta \log p$ is only 0.20 log p unit. The calculated value of $k_{g\infty}$ fits an experimental thermal value ($A_{calcd} = 10^{16.1}$ sec.$^{-1}$); the activation energy was arbitrarily set 1 kcal. mole^{-1} less than the value for structural isomerization (Table V). This energy difference was discussed in ref. 24.

(24) E. W. Schlag and B. S. Rabinovitch, *J. Am. Chem. Soc.*, 82, 5996 (1960).

(25) A. T. Blades [*Can. J. Chem.*, 39, 1401 (1961)] measured a similar magnitude in the decomposition of cyclopropane-d_0 and -d_6.

Table V: Calculated and Measured Values for Geometric Isomerization of Cyclopropane and Dimethylcyclopropane (DMC)

System	$\langle E \rangle$, kcal. mole^{-1}	k_g (exptl.), sec.$^{-1}$	k_g (calcd.), sec.$^{-1}$	k_g/k_s (exptl.)	k_g/k_s (calcd.)	Ref.
1,2-DMC-d_0, thermal, 715.4°K.		12.7×10^{-4}	12.2×10^{-4}	26.8	24.6	21
Ketene + *cis*-butene-2-d_0 (3200 Å.)	106	1.96×10^{8}	1.52×10^{8}	10.8	8.65	This work
CH_2N_2 + *cis*-butene-2-d_0 (250°)	109	3.5×10^{8}	2.31×10^{8}	8.1	8.13	8
CH_2N_2 + *cis*-butene-2-d_0 (300°)	112	4.4×10^{8}	3.47×10^{8}	7.5	7.94	8
CH_2N_2 + *cis*-butene-2-d_0 (400°)	116	11.5×10^{8}[d]	5.54×10^{8}	11.5	7.37	8
CH_2N_2 + *trans*-butene-2-d_0 (4358 Å.)	116	9.0×10^{8}	5.54×10^{8}	8.9	7.37	13
Ketene + *cis*-butene-2-d_8 (3200 Å.)	106	0.52×10^{8}	0.43×10^{8}	13.7	11.0	This work
Cyclopropane-d_2, thermal, 718°K.		2.0×10^{-4}[a]	1.95×10^{-4}	12.7	7.55[b]	24
Ketene + ethylene-d_2 (3340 Å.)	102	11.8×10^{10}[c]	3.06×10^{10}	18.7[c]	3.32[b]	26
Ketene + ethylene-d_2 (3200 Å.)	105	15.8×10^{10}[c]	4.63×10^{10}	14.2[c]	3.24[b]	26

[a] This value of k_g is one-half the constant as defined in ref. 24; k_g in this table represents the rate constant for formation of one isomer from the other. [b] Part of the difference between the theoretical and experimental ratios arises from a calculational model for structural isomerization which fits the values of A and E_a for cyclopropane given by Falconer, Hunter, and Trotman-Dickenson[27]; their k values are higher than those measured by Pritchard, Sowden, and Trotman-Dickenson, *Proc. Roy. Soc.* (London), **A217**, 517 (1963), and (roughly a factor of two) by Schlag and Rabinovitch. Since the experimental geometric isomerization values were also measured by the latter authors,[26] the calculated ratios must be multiplied by this factor to put them on a comparable basis; this makes the calculated and experimental values in the thermal case virtually coincide. [c] This is a large discrepancy above that mentioned in (*b*) and in view of the intuitively expected and theoretically calculated decline of k_g/k_s with increased energy, it is quite probable that the experimental result is in error. [d] The experimental value seems to have increased somewhat excessively relative to 300°.

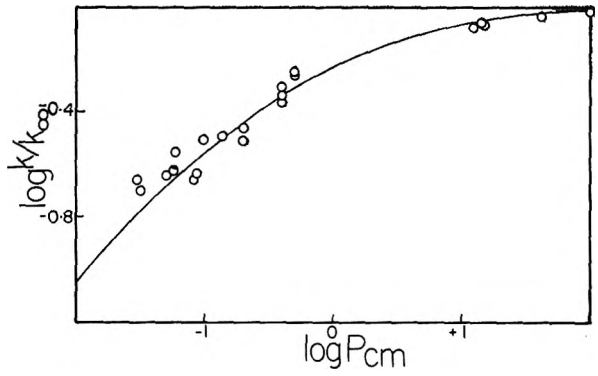

Figure 10. Unimolecular fall-off curve for geometric isomerization of 1,2-cyclopropane-d_2 at 718°K.: experimental data of Schlag and Rabinovitch, O; the solid curve is the theoretical curve from the present work shifted 0.20 log P unit to higher pressure; calculated fall-off curvature corresponds to Slater $n \simeq 12$, while experimental is $n \simeq 13.5$.

Values of $k_{\langle E \rangle}$ for geometric isomerization in chemical activation systems[26] were calculated from eq. 5 at the average energy of these systems. For the same reasons discussed for structural isomerization, these values are taken as good representations of the measured average k_g values.

The extension of the activated complex model for geometric isomerization from cyclopropane-d_2 to 1,2-dimethylcyclopropane involved replacement of the CHD group by $C(CH_3)H$ group frequencies. The models fit the experimental thermal high pressure rate constant[27] for the (-d_0) molecule (Table V). The models for the molecule and activated complex in the (-d_8) system have Teller–Redlich product rule agreement with their (-d_0) analogs. The calculated rates and isotope effects in the present chemical activation system are summarized in Table II. The agreement with the experimental results for the pure systems is good.

The origin of the isotope effects on k_g and k_g' is largely of a quantum statistical-weight nature; a smaller mechanistic effect, due particularly to the substitution in the ring near the reaction site, also appears from a straightforward application of the Teller–Redlich product rule and lowering of zero point energies per deuterium substitution and is automatically included ($E_{0D} = E_{0H} + 0.4$ kcal. mole^{-1}).

The results of these calculations as applied to a variety of systems in the literature are summarized and compared to experiment in Table V. In view of the neglect in the calculations of anharmonicity effects, of possible inefficient intermolecular energy transfer, and of experimental error which is always present in these systems, the agreement is extremely good. It can be

(26) B. S. Rabinovitch, E. Tschuikow-Roux, and E. W. Schlag, *J. Am. Chem. Soc.*, 81, 1081 (1959).

(27) W. E. Falconer, T. E. Hunter, and A. F. Trotman-Dickenson, *J. Chem. Soc.*, 609 (1961).

considered evidence in support of these activated complex models and of levels of energy which are consistent with those in ref. 8.

Appendix I

Rate Calculations

The molecule models were based on known, or transferred, frequency assignments. The activated complex models were assigned to fit the experimental high pressure frequency factors where these rate data were available. Teller–Redlich product rule agreement within 10% was accepted for the frequency assignments of deuterated models. The zero-point energy differences (ΔE_z) fall in the range 1.8–2.0 kcal. mole^{-1} per deuterium atom. In the application of the product rule to activated complexes, the groups which were defined to separate along the reaction coordinate (C–H or C–D stretch primarily for structural isomerization, and C–C stretch for geometric isomerization) were used in the reduced mass calculations; ref. 9 should be consulted for further discussion on this point. Moment of inertia ratios of the light and deuterated molecules are known for cyclopropane-d_0 and -d_6[28] and were closely estimated for dimethylcyclopropane species.

E_0 was calculated from the Arrhenius E_a values with use of the standard expressions.[29] The evaluation of $\Sigma P(E^+_{vr})$ and N^*_E from the models was done by direct summation or accurate approximation[30] at high energies using programs written by Mr. G. Z. Whitten for the IBM 709 computer; no frequency grouping was required for molecules. Vibrations were treated as harmonic. A modification[4,31] of the expression given by Marcus[23] for the density of free internal rotational states was used. Tabulations of energy sums and densities at various energies for all species described below may be found in ref. 31. The symmetry number ratio and number of reaction paths were included in I_r.

1,2-Cyclopropane-d_2. The vibrational frequencies for the molecule (Table VI) were deduced from those given by Cyvin[32] for cyclopropane-d_0 and -d_6. The observed fundamentals rather than the corrected frequencies are used, since the former provide a partial correction for anharmonicity.

The *geometric isomerization complex* for 1,2-cyclopropane-d_2 was derived from the molecule on the basis of the expanded ring model[9,24]; the frequencies of propane,[33] propylene,[34] butane,[33] and cyclobutane[35] were used as a guide. A ring mode was taken as the reaction coordinate; two methylene twisting vibrations became hindered internal rotations. Other changes in the molecule frequencies were very minor. There are two different complexes, one with two CHD rotors (reaction path weight of 1) and the other with one CHD and one

Table VI: 1,2-Cyclopropane-d_2 Frequencies[a]

Mode	ω, cm.$^{-1}$
C–H stretch	3103, 3082 (2), 3028
C–D stretch	2236, 2211
CH_2 def.	1442
CHD def.	1378, 1258
CH_2 twist	1188
CHD twist	1072, 970
Ring mode	1104, 982 (2)
CH_2 wag	869
CHD wag	870, 795
CH_2 rock	739
CHD rock	734, 633

[a] $E_z = \Sigma {}^1/_2 h\nu = 45.40$ kcal. mole^{-1}; $\Delta E_z = 1.97$ kcal. mole^{-1} per D atom.

CH_2 rotor (reaction path weight of 2); a weighted average of these was taken for the actual model. The grouped frequencies are (cm.$^{-1}$): 2973(4), 2160(2), 1260(4), 869(4), 702(3), hindered CHD rotor, hindered [$^2/_3CH_2$ + $^1/_3$CHD] rotor; $E_z = 39.82$ kcal. mole^{-1}. An internal rotation barrier of ~3.5 kcal mole^{-1} was used to fit the experimental thermal rate. Hindered internal rotational entropies were determined from the tables given by Pitzer.[36] A barrier of 5 kcal. together with some small terminal methylene frequency lowerings would also fit the data. The value of E_0 is 61.80 kcal. mole^{-1}, based on $E_a = 64.10$ kcal. mole^{-1} for geometric isomerization. The value of $(I^+_{ABC}/I_{ABC})^{1/2}$ used was 1.30, slightly larger than the value 1.21[28] which applies for the structural isomerization of cyclopropane-d_0. The reaction path degeneracy is 3 for this geometric isomerization. A 709 program written previously by D. W. Setser was used in the fall-off calculations.

The *structural isomerization complexes* for 1,2-cyclopropane-d_2 were based on the model given previously for cyclopropane-d_0.[8] A small difference in these models resulted from the use of Cyvin's[32] assignments of CH_2

(28) D. W. Setser, Ph.D. Thesis, University of Washington, 1961.

(29) S. Glasstone, K. J. Laidler, and H. Eyring, "The Theory of Rate Processes," McGraw-Hill Book Co., New York, N. Y., 1941.

(30) G. Z. Whitten and B. S. Rabinovitch, *J. Chem. Phys.*, **38**, 2466 (1963).

(31) For details, see J. W. Simons, Ph.D. Thesis, University of Washington, 1964.

(32) S. J. Cyvin, *Spectrochim. Acta*, **16**, 1022 (1960).

(33) J. H. Schactschneider and R. G. Snyder, *ibid.*, **19**, 85, 117 (1964).

(34) I. M. Sverdlov, *Proc. Akad. Sci. USSR, Chem. Sect.*, 106 (1956).

(35) G. N. Rathjens, Jr., N. K. Freeman, W. D. Gwinn, and K. S. Pitzer, *J. Am. Chem. Soc.*, **75**, 5634 (1953).

(36) K. S. Pitzer, "Quantum Chemistry," Prentice-Hall, Inc., New York, N. Y., 1958.

twist and rock vibrations as compared to those of Herzberg.[37] There are three *H transfer complexes:* (a) H atom transfer from CH_2 to a CHD group (reaction path weight of 4); (b) H atom transfer from a CHD to the CH_2 group (path weight of 2); (c) H atom transfer from a CHD to the other CHD group (path weight of 2). An average of these complexes was used: *3040(3), 2200(2), 1230(5), 880(3), 710(6), 510;* E_z = 38.72 kcal. mole^{-1}. The E_{aH} value for cyclopropane-d_0 was used,[27] which gave E_0 = 62.73 kcal. mole^{-1}. Apart from reaction path degeneracy, I_r is closely similar to the value for cyclopropane-d_0.

There are two activated complexes for *D transfer:* (a) a D atom transfers from a CHD to the other CHD group (path weight of 2); (b) a D atom transfers from a CHD to the CH_2 group (path weight of 2). An average was taken for the D transfer model; this model was deduced from the molecule in the same way as the H transfer model: 3050(4), 2190, 1230(5), 880(3), 712(6), 510; E_z = 39.97 kcal. mole^{-1}. Thus $E_{0D} - E_{0H}$ = 1.25 kcal. mole^{-1} was obtained; this is consistent with the measured value of the intermolecular critical energy difference for cyclopropane-d_0 and -d_6.[25] The moment of inertia ratio is virtually the same as for the H transfer complex.

1,2-Dimethylcyclopropane-d_0. The vibrational frequencies of the 1,2-dimethylcyclopropane-d_0 molecule are given in Table VII. The ring and skeletal motion frequencies were taken from those for cyclopropane and from a partial assignment for 1,1-dimethylcyclopropane.[38] The CH_2 group frequencies were those for cyclopropane. The $C(CH_3)H$ group frequencies were assigned to be consistent with those for *cis*-butene-2,[39] propylene,[34] and a model for methylcyclopropane given by Wieder.[40] This frequency assignment is partially altered from that used earlier,[8] but in view of the insensitivity of the calculations to the detailed assignments, the agreement is satisfactory.

The *geometric isomerization complex* is similar to that for cyclopropane-d_2. Different reaction paths were averaged into a single model. The grouped frequencies are (cm.$^{-1}$): 2982(10), 1350(10), 952(9), 682(3), 400(2), free CH_3 internal rotation (2), hindered $C(CH_3)H$ internal rotation, hindered $[^2/_3CH_2 + {}^1/_3C(CH_3)H]$ internal rotation; E_z = 78.60 kcal. mole^{-1}. An internal rotational barrier of ~20 kcal. mole^{-1} gave a fit of the observed thermal rate,[21] $10^{15.25}e^{-59,420/RT}$; the model gives E_0 = 57.80 kcal. mole^{-1}. A value of $(I^+_{ABC}/I_{ABC})^{1/2}$ was estimated at 1.15. The activated complex described is for the formation of a "biradical" intermediate; in order to represent k_g for the formation of the *trans* from the *cis* isomer, the rate must be multiplied by the fraction of biradicals that recyclize to the *trans* isomer. This fraction (which is one-half for cyclopropane-d_2) was estimated as 0.67 from the thermal *cis–trans* equilibrium constant[21] and from the equilibrium ratio in chemical activation systems (ref. 8 and Table II).

Table VII: 1,2-Dimethylcyclopropane-d_0 Frequencies[a]

Mode	ω, cm.$^{-1}$
(CH_2) C–H stretch	3103, 3083
(CH) C–H stretch	3038, 3028
(CH_3) C–H stretch	2990 (3), 2950 (2), 2900
CH_3 def.	1465 (2), 1450 (2), 1380 (2)
CH_2 def.	1442
C–H bend	1200 (2), 650 (2)
Ring def.	1120, 960 (2)
CH_3 rock	1040 (2), 960 (2)
CH_2 twist	1188
CH_3–C stretch	950, 890
CH_2 wag	869
CH_2 rock	740
CH_3–C– bend	700 (2), 400 (2)
CH_3–C– torsion	Free rotor (2)

[a] E_z = 82.39 kcal. mole^{-1}.

The *structural isomerization "b-complex"* for formation of 2-methylbutene-2 and 2-methylbutene-1 resembles the cyclopropane-d_2 complex in which the H atom transfers from a CHD group to the other CHD group or to the CH_2 group. The grouped frequencies are (cm.$^{-1}$): 2985(9), 1350(10), 946(10), 685(5), 400(2), free CH_3 internal rotations (2); E_z = 77.27 kcal. mole^{-1}. This model fitted the observed thermal rate, $10^{14.32}e^{-62,110/RT}$ and gives E_0 = 60.47 kcal. mole^{-1}. The ratio $(I^+_{ABC}/I_{ABC})^{1/2}$ used was 1.1, as in the earlier work.[8] The reaction pathways are 4 for the b-complex. The *structural isomerization "p-complex"* for formation of *cis*- and *trans*-pentene-2 is analogous to the cyclopropane-d_2 complex in which an H atom transfers from the CH_2 group to a CHD group. The grouped frequencies are (cm.$^{-1}$): 2985(9), 1327(11), 957(8), 679(6), 400(2), free CH_3 internal rotation (2); E_z = 77.10 kcal. mole^{-1}. The model fitted the thermal rate, $10^{14.39}e^{-62,040/RT}$; E_0 is calculated as 60.38 kcal. mole^{-1}. I_r is the same as for the b-complex.

1,2-Dimethylcyclopropane-d_8. The vibrational frequencies assigned to 1,2-dimethylcyclopropane-d_8 are

(37) G. Herzberg, "Infrared and Raman Spectra of Polyatomic Molecules," D. Van Nostrand and Co., Princeton, N. J., 1945.

(38) F. F. Cleveland, M. J. Murray, and W. S. Galloway, *J. Chem. Phys.*, **15**, 742 (1947).

(39) C. M. Richards and J. R. Nielsen, *J. Opt. Soc. Am.*, **40**, 442 (1950).

(40) G. M. Wieder, Ph.D. Thesis, Polytechnic Institute of Brooklyn, 1961.

given in Table VIII. The activated complexes for the ($-d_8$) system were derived in the same way as for the ($-d_0$) system. The I_r ratio is the same as for the ($-d_0$) system. The grouped frequencies for the *geometric isomerization complex* are (cm.$^{-1}$): 3043(2), 2231(8), 1440, 1043(9), 814(10), 500(2), 340(2), free CD_3 internal rotation (2), hindered $C(CD_3)D$ internal rotation, hindered [$^2/_3CH_2$ + $^1/_3C(CD_3)D$] internal rotation; E_z = 64.03 kcal. mole^{-1} and ΔE_z = 1.82 kcal. mole^{-1} per D atom. The critical energy difference is $E_{0D} = E_{0H}$ + 0.44 kcal. mole^{-1}.

Table VIII: 1,2-Dimethylcyclopropane-d_8 Frequencies[a]

Mode	ω, cm.$^{-1}$
(CH_2) C–H stretch	3103, 3083
(CD) C–D stretch	2264, 2256
(CD_3) C–D stretch	2246, 2236 (2), 2216 (2), 2179
CH_2 def.	1440
CH_2 twist	1150
CD_3 def.	1085 (s), 1070 (4)
Ring def.	1050, 890 (2)
C–D bend	950 (2), 500 (2)
CH_2 wag	860
CH_2 rock	740
CD_3 rock	856 (2), 770 (2)
CD_3–C stretch	813, 762
CD_3–C bend	610 (2), 340 (2)
CD_3–C– torsion	Free rotor (2)

[a] E_z = 67.38 kcal. mole^{-1}; ΔE_z = 1.88 kcal. mole^{-1} per D atom.

The *structural isomerization b-complex* for D transfer is analogous to the D transfer complex of cyclopropane-d_2. The grouped frequencies are (cm.$^{-1}$): 3043(2), 2218(7), 1440, 1020(11), 801(9), 550(4), 340(2), free CD_3 internal rotation (2); E_z = 63.42 kcal. mole^{-1}. We also obtain ΔE_0 for the intermolecular primary isotope effect of 1.16 kcal. mole^{-1}, slightly smaller than the value for the intramolecular effect for cyclopropane-d_2. The group frequencies for the *structural isomerization p-complex* are (cm.$^{-1}$): 3003, 2231(8), 1350, 1053 (10), 811(10), 555(5), 340(2), free CD_3 internal rotation (2), E_z = 62.17 kcal. mole^{-1} and ΔE_z = 1.88 kcal. mole^{-1} per D atom. E_0 is the same as in the ($-d_0$) system since E_z was lowered the same for the molecule and the activated complex.

A Study of Autophobic Liquids on Platinum by the Contact Potential Method

by C. O. Timmons and W. A. Zisman

U. S. Naval Research Laboratory, Washington, D. C. *(Received November 2, 1963)*

Several nonspreading liquids were investigated on a platinum surface using contact potential and contact angle measurements to determine whether or not their nonspreading behavior was caused by "autophobicity," *i.e.*, the property of a liquid being unable to spread upon its own adsorbed monolayer. The liquids studied were 1-octanol, 1-octanoic acid, tri-*p*-cresyl phosphite, mixed *meta* and *para* isomers of tricresyl phosphate, methylene iodide, and three chlorinated biphenyls. Each liquid was shown to be autophobic. Contact potential difference and contact angle data for adsorbed monolayers on platinum of each liquid are presented and discussed. Contact potential differences for the phosphate and phosphite were the same, indicating that the two types of molecules have different mechanisms of surface interaction with the metal surface. It was also found that raising the relative humidity affects the autophobic contact angle of liquid 1-octanoic acid, 1-octanol, and methylene iodide, but the effect is opposite in sign for the methylene iodide. This result sheds considerable light on the effect of water adsorption on the adsorptive properties of halogen derivatives of the hydrocarbons.

Introduction

In previous studies of wetting[1] it has been shown that several classes of pure liquids, including the branched and unbranched aliphatic acids and alcohols, are nonspreading on such high-energy surfaces as platinum, α-alumina, and fused silica because they adsorb unaltered to form low-energy surfaces upon which the bulk liquid will not spread; *i.e.*, the critical surface tension (γ_c) of the resulting coated surface is less than the surface tension (γ_{LV}) of the liquid. Liquids of this type were termed "autophobic" by Hare and Zisman.[1] The nonspreading liquids reported later[2] included certain phosphate esters and chlorinated aromatic hydrocarbons and ethers whose nonspreading property was not conclusively explained but was believed to arise from the same cause. In addition to nonspreading on high-energy surfaces due to autophobicity, nonspreading can be produced in all pure liquids investigated to date by the addition of an appropriate polar compound which preferentially adsorbs to form a suitable low-energy surface.[3-11]

It is conceivable, however, that the above conditions need not be the only ones sufficient for the occurrence of nonspreading on high-energy surfaces. Harkins and Feldman[12] defined the initial spreading coefficient (S) as

$$S = W_a - W_c$$

where W_a and W_c are the work of adhesion and cohesion for a given liquid. For spreading to occur spontaneously S must be positive; hence, if $W_c > W_a$, nonspreading will result. It was the purpose of this investigation to examine a number of types of nonspreading

(1) E. F. Hare and W. A. Zisman, *J. Phys. Chem.*, **59**, 335 (1955).

(2) H. W. Fox, E. F. Hare, and W. A. Zisman, *ibid.*, **59**, 1097 (1955).

(3) W. C. Bigelow, D. L. Pickett, and W. A. Zisman, *J. Colloid Sci.*, **1**, 513 (1946).

(4) W. C. Bigelow, E. Glass, and W. A. Zisman, *ibid.*, **2**, 563 (1947).

(5) E. G. Shafrin and W. A. Zisman, *ibid.*, **7**, 166 (1952).

(6) F. Shulman and W. A. Zisman, *ibid.*, **7**, 465 (1952).

(7) A. H. Ellison, H. W. Fox, and W. A. Zisman, *J. Phys. Chem.*, **57**, 622 (1953).

(8) E. F. Hare, E. G. Shafrin, and W. A. Zisman, *ibid.*, **58**, 236 (1954).

(9) H. W. Fox, E. F. Hare, and W. A. Zisman, *J. Colloid Sci.*, **8**, 194 (1953).

(10) W. A. Zisman, "Relation of the Equilibrium Contact Angle to Liquid and Solid Constitution," Advances in Chemistry Series, No. 43, American Chemical Society, Washington, D. C., 1963, p. 1.

(11) R. L. Cottington, C. M. Murphy, and C. R. Singleterry, "Effect of Polar–Nonpolar Additives on Oil-Spreading on Solids, with Applications to Nonspreading Oils," Advances in Chemistry Series, No. 43, American Chemical Society, Washington, D. C., 1963, p. 341.

(12) W. D. Harkins and A. J. Feldman, *J. Am. Chem. Soc.*, **44**, 2665 (1922).

liquids, including the phosphate esters and chlorinated aromatic liquids reported earlier, to determine whether each is autophobic or whether it is nonspreading simply because the spreading coefficient is negative. Similar studies were also made of 1-octanol and 1-octanoic acid, whose autophobic character had been firmly established earlier.[1]

Because of their sensitivity to the presence of an adsorbed monolayer, both contact potential and contact angle measurements were made after passage of a liquid drop over a polished, clean, metal surface to determine whether the liquid had or had not left behind a film adsorbed on the solid substrate. If the pure liquid was capable of exhibiting a nonzero contact angle without the formation of an adsorbed low-energy surface film, obviously there would be no contact potential difference (ΔV) before and after rolling the drop of liquid over the clean metal surface. If the liquid was autophobic, θ for that liquid on the monolayer-coated metal would be the same as the value manifested by that liquid on the bare metal, and the contact potential difference would indicate adsorption of the autophobic liquid.

Materials and Experimental Procedures Used

The following liquids were used in this investigation: 1-octanol, 1-octanoic acid, and tri-*p*-cresyl phosphite (Eastman Kodak Co.); methylene iodide and mixed *meta* and *para* isomers of tricresyl phosphate (Fisher Chemical Co.); and the chlorinated biphenyls, Aroclors 1242, 1248, and 1254 (Monsanto Chemical Co.). With the exception of the phosphorus-containing compounds, each of these liquids, immediately before use, was percolated repeatedly through an adsorption column of silica gel and activated alumina to remove polar impurities. The phosphorus-containing liquids were percolated through Florisil only.

A pure platinum disk, 0.95 cm. in diameter, was used as the solid substrate for observing the spreading behavior of each of the liquids studied. Before each experiment, it was polished on a wet Buehler Selvyt cloth with levigated alumina having an average particle size of 0.3 μ; it was then rinsed in hot concentrated C.P. nitric acid, rinsed in flowing, grease-free distilled water, heated briefly to red heat over a Bunsen flame, and finally cooled in clean air at 50% relative humidity.

A monolayer of each liquid was adsorbed on the platinum substrate by the repeated wiping technique described by Levine and Zisman[13] and also by the retraction method.[14] The criterion used for concluding that only a monolayer remained on the substrate was that the results of contact angle and contact potential measurements were the same, within experimental error, for both techniques of monolayer preparation. In addition, in using the wiping technique, a valuable indication that a monolayer had been formed was that further vigorous wiping with clean filter paper caused no further changes in either the contact angle or the contact potential difference.

Solvents for preparing solutions used in the retraction process were nitromethane or methylene iodide, each of which had been freshly percolated through an adsorption column of activated alumina and silica gel. Properties of the monolayers retracted from solutions in these two solvents were identical.

Contact potential differences were measured between the platinum surface, before and after coating it with the film being studied, and an aged reference electrode consisting of Ra-226 foil with a thin gold overlayer. Bewig's modification of the ionization method of measuring the contact potential difference was used because it allowed automatic recording.[15] All results reported here were reproducible within ± 0.015 v. or less.

The value of θ reported is the slowly advancing contact angle obtained by gradually increasing the volume of a sessile drop of a pure liquid resting on the horizontal surface of the solid. Contact angles were measured with a goniometer telescope and were reproducible to within $\pm 2°$.

All contact potential difference and contact angle results presented here are averages of a total of at least six results and were performed at 20 to 25° and 50% relative humidity unless otherwise stated.

Results and Discussion

Autophobic Behavior of the Phosphate and Phosphite Esters. The sample of mixed *meta* and *para* isomers of tricresyl phosphate studied exhibited a contact angle of 6° on the bare platinum substrate. After adsorbing a monolayer of this liquid on the platinum by the wiping method or by retracting a monolayer from a 1% by wt. solution in methylene iodide, the tricresyl phosphate exhibited the same 6° contact angle on that monolayer. On the same film-coated surfaces, sessile drops of water and methylene iodide exhibited contact angles of 62 and 25°, respectively (Table I). The measured contact potential difference for such a monolayer of tricresyl phosphate on platinum was 0.620 v. (Table II).

Tricresyl phosphate presumably adsorbs with the highly polar phosphate group nearest the metal surface. Inspection of a Stuart–Briegleb ball model of this com-

(13) O. Levine and W. A. Zisman, *J. Phys. Chem.*, 61, 1068 (1957).

(14) E. G. Shafrin and W. A. Zisman, *ibid.*, 64, 519 (1960).

(15) K. W. Bewig, "A Modification of the Ionization Method Especially Suitable for Continuously Recording Contact Potential Differences," NRL Report 5915, April 11, 1963.

Table I: Contact Angle (θ) for Various Liquids on Platinum and on Tricresyl Phosphate and Tricresyl Phosphite Monolayers Adsorbed on Platinum (20–25°; 50% Relative Humidity)

	Contact angle (θ) of test liquid			
Solid surface studied	Tricresyl phosphate	Tricresyl phosphite	Methylene iodide	Water
Bare platinum	6°	5°	11°	Spread
Tricresyl phosphate monolayer	6°	..	25°	62°
Tricresyl phosphite monolayer	..	5°	21°	62°

Table II: Contact Potential Differences Resulting from Monolayers Adsorbed on Platinum (20–25°; 50% Relative Humidity)

Adsorbed compound	Contact potential difference, ΔV (v.)	Calculated apparent perpendicular moment μ_p (D.)
Tricresyl phosphate	0.620	1.65
Tricresyl phosphite	0.619	1.65
Aroclor 1242	0.110	0.34
Aroclor 1248	0.053	0.18
Aroclor 1254	−0.020	−0.07
1-Octanol	0.140	..
1-Octanoic acid	0.120	..
Methylene iodide	0.120	0.11

pound indicates that the planar aromatic ring portions of the adsorbed molecule may orient at right angles to the solid surface. Fox, Hare, and Zisman[9] have reported water contact angles of from 92 to 95° on the solid surfaces covered with benzene rings when the planar ring was oriented perpendicular to the solid surface, and contact angles of from 55 to 58° when the planar ring was tilted slightly from the vertical. They also reported a contact angle of 37° for methylene iodide on a surface composed of benzene ring edges and faces. The contact angles obtained here are consistent with their results if we assume the benzene rings are nearly at right angles to the adsorbing solid surface.

The fact that θ for a drop of tricresyl phosphate was the same on bare platinum and on platinum coated with a tricresyl phosphate monolayer proves that it is an autophobic liquid. The cross-sectional area for the adsorbed tricresyl phosphate molecule was taken to be 100 Å.^{2} because (a) inspection of the ball model indicates the projected area to be about 115 Å.^{2}, and (b) Ries[16] obtained a molecular area of 95.0 Å.^{2} for a condensed monolayer of tri-*p*-cresyl phosphate adsorbed on water. Using this value and the fact that ΔV was equal to 0.620 v., the apparent perpendicular component (μ_p) of the dipole moment of the adsorbed molecule was computed from the Helmholtz equation

$$\Delta V = 4\pi n\mu_p$$

where n is the number of adsorbed molecules per unit area. In this case $\mu_p = 1.65$ D. Although no gaseous or dilute solution dipole moment data are available for this compound, it is a reasonable approximation to assume that the contribution of the methyl substituent on each benzene ring can be neglected and to compare this value with the dipole moment of 2.81 D. obtained for triphenyl phosphate in benzene at 25°.[17] One is left with the same situation reported recently by Bewig and Zisman[18] that the dipole moment of the molecule adsorbed on platinum as computed from contact potential data is much less than that measured in the gaseous state or in dilute solution by other methods. The probable causes are the neglect of the dipole induced by the proximity of the adsorbed molecules to the metal surface and to each other as well as the effect of any adjacent dipoles of adsorbed water present under the conditions of these experiments.

Table I also summarizes the results of measurements of θ for tri-*p*-cresyl phosphite on bare platinum and for several liquids on an adsorbed monolayer of tri-*p*-cresyl phosphite prepared by both the wiping method and by retraction from a 1% by wt. solution in methylene iodide. A sessile drop of tri-*p*-cresyl phosphite exhibited a 5° contact angle both on bare platinum and on platinum coated with the phosphite monolayer. Therefore, tri-*p*-cresyl phosphite is also an autophobic liquid. On the surface coated with the phosphite monolayer, θ for water and methylene iodide were 62 and 21°, respectively. Thus, the water contact angle is the same and the methylene iodide contact angle is 4° less than on the tricresyl phosphate monolayer. The near equality of the contact angles on the phosphate and phosphite monolayers is entirely consistent with our expectation that their outermost structures would be the same.

As indicated in Table II, the adsorbed monolayer of tri-*p*-cresyl phosphite caused nearly the same contact potential difference as tricresyl phosphate, although both compounds occupy essentially the same surface area per adsorbed molecule. This surprising result leads to the same apparent perpendicular component of the dipole moment, 1.65 D., which may be compared

(16) H. E. Ries, Jr., and H. D. Cook, *J. Colloid Sci.*, **9**, 535 (1954).
(17) G. L. Lewis and C. P. Smyth, *J. Am. Chem. Soc.*, **62**, 1529 (1940).
(18) K. W. Bewig and W. A. Zisman, *J. Phys. Chem.*, **67**, 130 (1963).

with the dipole moment of 2.02 D. (in benzene solution at 25°) for the analogous triphenyl phosphite.[17] One might expect both a greater contact potential difference and apparent dipole moment from the phosphate than the phosphite since the dipole moments from measurements on the dielectric constants of gases or dilute solutions are larger for the phosphates that have been studied than those of the analogous phosphites. However, it is probable that the unpaired electrons of the phosphite phosphorus atom are able to react or associate with oxygen atoms already adsorbed on the platinum surface. This would result in a molecular species identical with the phosphate, thereby resulting in the same apparent dipole moments.

Autophobic Behavior of the Chlorinated Biphenyls. Aroclors 1242, 1248, and 1254 are commercial mixed chlorinated biphenyls which, as stated by the manufacturer, have on the average three, four, and five chlorine atoms per molecule, respectively. However, in each liquid there are present molecules containing more or less chlorine. From inspection of Stuart–Briegleb molecular models and from the fact that chlorine substitution in biphenyl proceeds in the order *para*, *para'*, *ortho*, *ortho'*,[19] it can be seen that the two phenyl groups will not be coplanar.

Table III: Contact Angle (θ) for Various Liquids on Platinum and on Aroclor Monolayers Adsorbed on Platinum (20–25°; 50% Relative Humidity)

	Contact angle (θ) of test liquid				
Solid surface studied	Aroclor 1242	Aroclor 1248	Aroclor 1254	Methylene iodide	Water
Bare platinum	10°	10°	20°	11°	Spread
Aroclor 1242	11°	...	...	24°	68°
Aroclor 1248	...	12°	...	15°	67°
Aroclor 1254	...	...	21°	9°	69°

Table III summarizes the values of θ observed for each of the Aroclors on bare platinum and on its own adsorbed monolayer, prepared by the wiping technique and by retraction from methylene iodide solution. Contact angles of drops of methylene iodide and water on these monolayers are also given. It can be concluded from these results that the Aroclor liquids are autophobic since each exhibits the same contact angle on bare platinum and on platinum coated with the respective Aroclor monolayer.

Nearly identical water contact angles of from 67 to 69° were observed on each of the Aroclor films, but the methylene iodide contact angles decreased from 24 to 15 to 9° on monolayers of Aroclors 1242, 1248, and 1254, respectively. The planes of the phenyl groups of an adsorbed Aroclor molecule would lie in varying degrees of tilt with respect to the monolayer–air interface as chlorination progresses. The same argument used with tricresyl phosphate can be employed here, *i.e.*, that the contact angles of water and methylene iodide on an Aroclor monolayer should be somewhere between those found on adsorbed benzene rings when oriented perpendicular to the surface or tilted slightly from the vertical. These extremes, for water, are 55 and 95°; the methylene iodide contact angle is 37° for benzene rings tilted slightly from the vertical orientation.[9] The fact that chlorine atoms are present at the monolayer–air interface probably has little significance as far as contact angles are concerned, since the number of chlorine atoms is small compared to the number of aromatic groups, and since the critical surface tension of wetting (γ_c) of a partially chlorinated surface, such as polyvinyl chloride, is nearly the same as that for a surface of benzene rings oriented perpendicular to the surface.[14]

Although a methylene iodide contact angle of 24° is reasonable for Aroclor 1242, it is difficult to understand why θ decreases with the others. It is possible that as chlorination progresses, close packing becomes more difficult and hence methylene iodide exhibits a lower value of θ. That the lower methylene iodide contact angles were not caused by their solution of the monolayer was shown by using a sessile drop of methylene iodide containing a small amount of the Aroclor in question. Sessile drops of these solutions exhibited the same values of θ as did drops of pure methylene iodide.

Contact potential differences caused by the adsorption of a monolayer of each of these liquids, and the calculated perpendicular component of the apparent dipole moment, are given in Table II. The large decrease in the contact potential difference with increasing chlorination of the molecule can be explained in terms of the directed permanent dipole moment contributions of the individual C–Cl bonds. Assuming that chlorine substitution in biphenyl proceeds as indicated above, and that because they are so highly polarizable as many of the chlorine atoms as possible will adhere to the metal substrate, the end-view projections of the three Aroclors would be expected to appear as in Fig. 1. The arrows refer to the positive direction of the permanent C–Cl moment projected onto the plane of the paper, and "into" and "out" indicate whether the bond is directed at approximately 30° into the plane of the paper or 30°

(19) F. C. Whitmore, "Organic Chemistry," Vol. 2, 2nd Ed., Dover Publications, Inc., New York, N. Y., 1951.

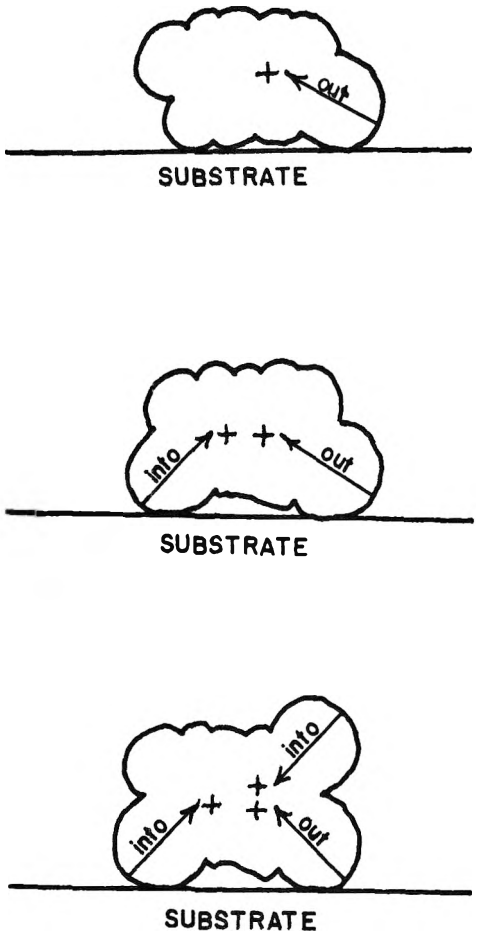

Figure 1. End-view projection of Aroclor molecules: top, Aroclor 1242; middle, Aroclor 1248; bottom, Aroclor 1254.

away from it. Not shown in Fig. 1 are the C–Cl moments at the *para* positions of the molecule; they are directed normal to the plane of the paper, and in opposite directions, thereby effectively canceling one another.

Figure 1a is the end-view projection of Aroclor 1242; the positive end of the C–Cl dipole pointing away from the metal substrate, together with whatever moments are induced in the molecule by the electric field of the metal, give rise to the measured contact potential difference of 0.110 v. In Aroclor 1248 (Fig. 1b) with the addition of the fourth Cl atom, two C–Cl dipoles are directed away from the metal substrate and, in the plane of the paper, toward each other. Although one dipole is directed into the plane of the paper, and the other away, they are located near the center of gravity of the molecule, and the fourth C–Cl dipole tends to reduce the molecule's net permanent moment. This may cause the reduction of the contact potential difference, in this case to 0.053 v. In Aroclor 1254 the addition of the fifth C–Cl dipole to the molecule (Fig. 1c) causes a reverse in sign of the measured contact potential difference (−0.020 v.) because now there is an oriented dipole with its negative end directed away from the substrate.

Autophobic Behavior of 1-Octanol and 1-Octanoic Acid. The results obtained in studying the autophobic properties of liquid 1-octanol and 1-octanoic acid are similar and will be discussed together. Table IV summarizes values of θ obtained for these liquids on bare platinum and on their own adsorbed monolayers, as well as the contact angles of methylene iodide and water on each monolayer. The monolayers were prepared by (a) the wiping method, (b) retraction from the melt, and (c) retraction from 0.1 wt. % solution in nitromethane.

Table IV: Contact Angle (θ) for Various Liquids on Platinum and on Several Kinds of Monolayers Adsorbed on Platinum (20–25°; 50% relative humidity)

	Contact angle (θ) of test liquid			
Solid surface studied	1-Octanol	1-Octanoic acid	Methylene iodide	Water
Bare platinum	35°[a]	35°[a]	11°[a]	Spread
1-Octanol monolayer	18°	..	37°	68°
1-Octanoic acid monolayer	..	22°	45°	75°
Methylene iodide monolayer	..	..	23°	73°

[a] Nonequilibrium value.

Both the acid and the alcohol exhibited an initial contact angle of 35° on bare flamed platinum, whereas Hare and Zisman[1] reported an angle of 42°. The reason for this anomaly is not clear since the platinum specimen used by Hare and Zisman also caused contact angles of 35° under the conditions of this experiment. However, it is believed that the 35° angle is the proper one because of the great care taken in the present study. This initial 35° contact angle is a nonequilibrium condition and, in both cases, the angle decreased to about 20° in the course of 2 hr. The contact angles of methylene iodide and water on the adsorbed 1-octanol monolayer were 37 and 68°, respectively. Since Levine and Zisman[13] obtained methylene iodide contact angles of 56 and 57° on close-packed monolayers of 1-octanol and 1-octanoic acid adsorbed on soda-lime glass, the 37° contact angle obtained here probably indicates that the 1-octanol molecules were unable to adsorb as closely together on flamed platinum. Similar results were observed with 1-octanoic acid monolayers upon which methylene iodide and water exhibited contact angles of

45 and 75°, respectively. Because of the higher contact angles obtained on the 1-octanoic acid monolayers, it can be concluded that the adsorbed 1-octanoic acid molecules are packed more closely than the 1-octanol molecules on flamed platinum, but not as closely as on soda-lime glass.

Although 1-octanol and 1-octanoic acid each exhibited an initial contact angle of 35° on bare flamed platinum neither liquid gave this contact angle on its own adsorbed monolayer. Instead the contact angles observed were 18 and 22°, respectively, which agree well with the equilibrium value of 20° obtained for these liquids on bare flamed platinum. It is probable that the lower contact angles (*ca.* 20°) are a result of a mixed film of water molecules, which are certainly present, and either alcohol or acid molecules. It is well known that an adsorbed monolayer has a high permeability to water unless it is close-packed and has very high intermolecular cohesion. Neither of these conditions are satisfied by the short-chain alcohol and acid studied here.

The 35° contact angle observed initially on flamed platinum is probably a result of relatively smaller amounts of water present initially on the platinum surface. If the flamed platinum is allowed to stand for as long as 1 hr. in room atmosphere before adding the test drop of acid or alcohol, the 35° contact angle no longer manifests itself and angles of 18 and 22° are observed. These results indicate that 1-octanol and 1-octanoic acid are autophobic when equilibrium with adsorbed water is complete and the autophobic contact angles, under these conditions, are 18 and 22°, respectively.

An interesting result, which further shows the effect and importance of the amount of adsorbed water present, is obtained when 1-octanol is studied on flamed platinum in an atmosphere maintained at less than 10% relative humidity. Under these conditions a 35° contact angle is observed for the alcohol on both the bare metal and on its own adsorbed monolayer. These contact angles are also much more stable than those measured at 50% relative humidity as no changes were observed until after 4 hr. At the same time a marked change in the methylene iodide contact angle resulted. In air at less than 10% relative humidity methylene iodide gave a 28° contact angle on the 1-octanol monolayer. At 50% relative humidity this angle was 37°. This is to be expected when one considers that the octanol monolayer under study contains some water molecules. Since methylene iodide is nonspreading on water it is reasonable to expect the methylene iodide contact angle to increase as the amount of included water increases.

The contact potential difference resulting from the adsorption of monolayers of 1-octanol and 1-octanoic acid were 0.140 and 0.120 v., respectively (Table II). (Interestingly, these same values were obtained when measured in air at less than 10% relative humidity.) The perpendicular component of the apparent dipole moment of each compound was not calculated because each monolayer was definitely not close-packed and it was not possible to determine reliably the value for the number of molecules occupying a unit area of surface and the inclination of the dipole axis from the vertical.

Autophobic Behavior of Methylene Iodide. The results obtained with methylene iodide are analogous to those obtained with 1-octanol and 1-octanoic acid. Methylene iodide exhibited an 11° contact angle on bare previously flamed platinum and, under ambient room conditions, a 23° contact angle on its own adsorbed monolayer. Water gave a 73° contact angle on methylene iodide monolayers (Table IV) prepared both by the wiping technique and by retraction from the melt.

The 11° contact angle of methylene iodide on bare flamed platinum was also a nonequilibrium condition and was found to increase gradually, approaching a value of 23° after 3 hr. When the experiment was repeated in air at less than 10% relative humidity, methylene iodide exhibited an 11° contact angle both on the bare metal substrate and on its own adsorbed monolayer.

These results indicate again the importance of adsorbed water included in a monolayer. In air at 50% relative humidity methylene iodide behaves as an autophobic liquid, after equilibration with water is complete, and exhibits an autophobic contact angle of 23°. In air at less than 10% relative humidity the effect of water is not immediately so pronounced and methylene iodide behaves as an autophobic liquid with an autophobic contact angle of 11°. It would seem likely that this contact angle, given enough time, would also finally equilibrate at 23°; however, no changes were observed over a course of 4 hr.

The measured contact potential difference resulting from the adsorption of a monolayer of methylene iodide was 0.120 v. (Table I); reduction of the relative humidity to less than 10% caused no change in this value. From measurement of the Stuart–Briegleb molecular model of this molecule one obtains a projected rectangular molecular area of about 36 Å.^{2}. Assuming closest molecular packing in the adsorbed film, the apparent perpendicular moment calculated from the Helmholtz relationship is 0.11 D. This value is considerably less than the reported dipole moments of this molecule measured in solution. These vary from 2.12 D. (in benzene at 25°)[20] to 1.1 D. (in benzene at 25°).[21]

However, it is again probable that our calculated moment is low as a result of the proximity of the metal surface and the neighboring methylene iodide atoms and the effect of included water molecules.

The differences in spreading behavior of methylene iodide on flamed platinum under varying conditions of relative humidity is remarkable and suggestive. It is well known that the liquid alkyl halides, as well as methylene iodide, are nonspreading on water or have negative spreading coefficients.[12] From the results reported here it appears possible that the *n*-alkyl halides could be made to spread over a noble metal surface and adsorb as more or less close-packed monolayers by eliminating the presence of water on the metal surface.

(20) P. C. Mahanti and R. N. Das-Gupta, *J. Indian Chem. Soc.*, 6, 411 (1929).

(21) H. Muller and H. Sack, *Z. Physik*, 31, 815 (1930).

Conductance Measurements of Solutions of Some Salts in Anhydrous Ethylenediamine and Propylenediamine

by G. W. A. Fowles

Department of Chemistry, The University, Southampton, England

and W. R. McGregor

Department of Chemistry, Brighton College of Technology, Brighton, England *(Received November 5, 1963)*

Conductance measurements are reported for solutions of $AgNO_3$, AgI, ethylenediamine monohydrochloride, and KI in ethylenediamine, and for $AgNO_3$, KI, and AgI in propylenediamine. Calculations of Fuoss plots have been made for these salts and the results compared with those previously reported.

Introduction

During a study of the general solvent properties of anhydrous diamines,[1,2] it became necessary to measure the conductance of a variety of salts in ethylenediamine and propylenediamine. There is some variation in the Λ_0-values reported in the literature for solutions in ethylenediamine,[3,4] and no conductivity data have previously been published on solutions in propylenediamine. We report here the experimental results and compare them with those already in the literature where appropriate.

Experimental

Materials. A.R. grade $AgNO_3$, KCl, and KI (British Drug Houses Ltd.) were recrystallized twice from doubly-distilled water and dried first at 110° and finally by pumping *in vacuo*. AgI was made by mixing equimolar solutions of A.R. grade $AgNO_3$ and KI, well washed with doubly-distilled water, and dried as were the other salts. Ethylenediamine dihydrochloride, which was prepared by the addition of excess concentrated HCl to aqueous solutions of the diamine, was recrystallized from aqueous ethanol and dried as before. Analysis showed that the dihydrochloride was formed.

(1) G. W. A. Fowles, W. R. McGregor, and M. C. R. Symons, *J. Chem. Soc.*, 3329 (1957).

(2) G. W. A. Fowles and W. R. McGregor, *ibid.*, 136 (1958).

(3) W. H. Bromley and W. F. Luder, *J. Am. Chem. Soc.*, 66, 107 (1944).

(4) B. B. Hibbard and F. C. Schmidt, *ibid.*, 77, 225 (1955).

Anal. Calcd.: Cl, 53.2. Found: Cl, 53.1. The dihydrochloride can be considered a uni-unielectrolyte, since it dissolves in an excess of amine to give the monohydrochloride. Anhydrous ethylenediamine and propylenediamine were purified as described previously.[1,2]

Dielectric Constant of Propylenediamine. This has not previously been reported. It could not be measured by the conventional condenser apparatus that was available because of the ready contamination of the diamine by moisture, carbon dioxide, and metal parts of the condenser. The dielectric constant of propylenediamine was measured by comparing its damping effect on the electric vector of a standing microwave in a wave guide with the effect of other liquids of known dielectric constant. The measurements were carried out in sealed Pyrex tubes so that contamination was eliminated. The dielectric constant was found to be 10.2 ± 0.3 at 25°.

Dielectric Constant of Ethylenediamine. The value 12.9 was used.[3]

Viscosity of Ethylenediamine and Propylenediamine. The value of 0.0154 poise was used for ethylenediamine.[3] A value of 0.0146 poise was determined for propylenediamine, using an Ostwald viscometer.

Apparatus and Procedure. Resistance measurements were made using a Jones and Josephs type a.c. bridge in conjunction with a battery-fed Hartley-type oscillator. Resistance measurements were normally made at a frequency of 1000 c.p.s., although periodic measurements were made at both higher and lower frequencies (using a Pye variable-frequency oscillator); the results did not differ significantly. The signal from the bridge was amplified by a 3:1 intervalve transformer, and the balance point detected by head-phones.

The conductance cells were constructed from a 500-ml. round-bottomed flask (*cf.* Fig. 1), together with a large-bore stopcock and ground joint for attachment to the vacuum apparatus; a side arm of the flask contained the platinum electrodes, which were lightly platinized. The cell constants were determined both directly with aqueous solutions of potassium chloride and indirectly by comparison with other cells of known constants. All measurements of resistance were carried out in an oil-filled thermostat at 25 ± 0.02°, (N.P.L. calibrated thermometer). Prior to use, the conductance cells were cleaned with "hydrogen fluoride–Teepol" solution, washed with distilled water, steamed out for 2 days, and dried by prolonged pumping and flaming on a vacuum line. The stopcock was greased with silicone high-vacuum lubricant; the presence of a small quantity of this grease did not materially alter the conductivity of the diamine solutions. The cell electrodes were short circuited by lengths of stout copper wire at all times except during the actual resistance measurements.

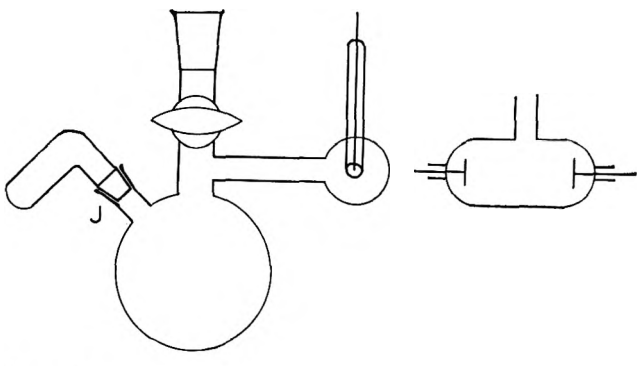

Figure 1.

Resistance measurements were made in the moderately dilute range 10^{-3}–10^{-4} M. The salt was weighed into a weighing bottle made from a B14 cone; the cone was lightly greased, and the bottle and its contents were attached to the conductance cell at J (*cf.* Fig. 1). Pure solvent was distilled directly into the (weighed) cell under vacuum, and the cell was detached and reweighed to determine the weight of solvent added. Solutions of increasing dilution were obtained by condensing fresh solvent into the cell.

Results and Discussion

Plots of Λ against $\sqrt{c}$, where c is the molar concentration, gave curves rather than straight lines in all cases, and values of Λ_0 and K (*cf.* Tables I–VII) were therefore obtained by the method of Fuoss and Kraus.[5] At the start of each experiment the specific conductance of the pure solvent was measured and the value obtained deducted from the measured conductance for

Table I: $AgNO_3$ in Ethylenediamine

$c \times 10^3$	Λ	$\frac{F(Z)}{\Lambda} \times 10^3$
2.24	30.9	27.1
1.17	36.1	24.3
0.723	40.1	22.4
.541	42.5	21.4
.464	44.0	20.8
.458	44.2	20.7
.321	47.3	19.6
.156	52.7	18.0
.0926	57.0	16.8

(5) C. A. Kraus and R. M. Fuoss, *J. Am. Chem. Soc.*, **55**, 476 (1933); **57**, 488 (1935).

Table II: KI in Ethylenediamine

$c \times 10^3$	Λ	$\frac{F(Z)}{\Lambda} \times 10^3$
1.62	34.6	24.8
1.11	37.8	23.4
1.05	38.7	22.9
0.747	41.2	21.9
.674	43.0	21.0
.581	43.4	21.0
.146	56.6	16.8
.115	58.9	16.2
.106	59.4	16.1

Table III: AgI in Ethylenediamine

$c \times 10^3$	Λ	$\frac{F(Z)}{\Lambda} \times 10^3$
3.48	5.54	16.0
1.46	8.56	10.7
1.19	9.25	9.92
0.656	11.9	7.89
0.262	16.8	5.64

Table IV: $NH_2CH_2CH_2NH_3Cl$ in Ethylenediamine

$c \times 10^3$	Λ	$\frac{F(Z)}{\Lambda} \times 10^3$
8.25	11.8	66.4
2.05	19.4	44.9
0.831	27.0	33.5
.508	32.1	28.7
.384	35.6	26.0

Table V: $AgNO_3$ in Propylenediamine

$c \times 10^3$	Λ	$\frac{F(Z)}{\Lambda} \times 10^3$
3.83	8.40	..
3.35	8.75	..
1.78	10.7	71.8
1.15	12.6	63.7
0.920	13.4	61.1
.552	16.2	52.4
.434	17.1	50.5
.313	19.7	44.5

each salt concentration. The specific conductances obtained for the solvents were in the ranges: ethylenediamine, 5×10^{-7}–2×10^{-6} mho; propylenediamine, 8×10^{-8}–3.5×10^{-7} mho. Plots of $F(Z)/\Lambda$ against

Table VI: KI in Propylenediamine

$c \times 10^3$	Λ	$\frac{F(Z)}{\Lambda} \times 10^3$
4.22	5.36	...
1.05	9.28	88.3
0.657	11.4	74.0
0.313	15.8	55.5
4.36	5.35	...
1.96	7.28	107.0
0.921	9.79	84.5

Table VII: AgI in Propylenediamine

$c \times 10^3$	Λ	$\frac{F(Z)}{\Lambda} \times 10^3$
1.93	1.27	...
1.48	1.77	...
1.20	1.86	...
1.09	2.06	...
0.558	2.71	291
.505	2.84	278
.298	3.59	229

Table VIII

		This work		—Ref. 3—		—Ref. 4—	
			K		K		K
Solvent	Salt	Λ_0	$\times 10^4$	Λ_0	$\times 10^4$	Λ_0	$\times 10^4$
Ethylenediamine	$AgNO_3$	65.8	4.61	61.4	8.07	63.5	5.74
	KI	71.9	4.8	69.2	6.02	..	...
	AgI	45.5	0.112	48.8	0.431	72.8	0.168
	$C_2H_9N_2Cl$	61.5	1.16	..	...	..	...
Propylenediamine	$AgNO_3$	53.1	0.82	..	...	..	...
	KI	50.0	1.51	..	...	..	...

$c\Lambda f^2/F(Z)$ gave straight lines and values of Λ_0 and K were obtained (*cf.* Table VIII).

Bearing in mind the relatively large correction that has to be made for the specific conductance of the solvent, the Λ_0-value for $AgNO_3$ in ethylenediamine agrees well with the two figures previously reported.[3,4] For AgI in ethylenediamine our Λ_0 value agrees well with that reported by Bromley and Luder,[3] but is considerably less than that measured by Hibbard and Schmidt.[4] Bromley and Luder suggested that the low conductance of AgI arose because of considerable ion pairing, which is reflected by the K value obtained. Ion pairing should be even more significant for solutions in propylenediamine with its lower dielectric constant, and we do indeed find that AgI has a markedly lower conductance than either $AgNO_3$ or KI, and in general both Λ_0 and K values for a given salt are lower in propylenediamine than in ethylenediamine. However, the viscosity of

propylenediamine is somewhat lower than that of ethylenediamine so the lower Λ_0-values found in the former indicate the formation of larger solvates. The opposing effects of lower dielectric constant and lower viscosity on conductance might explain why it is that although Λ_0 for KI is higher than for $AgNO_3$ in ethylenediamine, the order is reversed in propylenediamine. Bromley and Luder calculated that the ion sizes of $AgNO_3$ were slightly greater than those of KI, and it is possible that in propylenediamine the dominating factor is viscous drag rather than the degree of ion pairing, particularly at high dilutions.

Manganese Vapor Pressures in Equilibrium with Manganese–Iron–Nickel Solid Solutions

by J. H. Smith,

Applied Research Office, Ford Motor Company, Dearborn, Michigan

H. W. Paxton, and C. L. McCabe

Department of Metallurgical Engineering, Carnegie Institute of Technology, Schenley Park, Pittsburgh 13, Pennsylvania *(Received November 9, 1963)*

The partial pressure of manganese gas in equilibrium with manganese–iron–nickel solid solutions was measured as a function of concentration at 1232°K. by the Knudsen effusion technique coupled with a vacuum microbalance. The manganese–nickel system exhibits negative departures from an ideal solution with the exception of the β-phase alloys where the nonideality is slightly positive. These departures decrease as iron replaces nickel in solid solution. The Gibbs excess molal free energy was calculated for ternary concentrations from the ternary Gibbs–Duhem equation and estimated for the iron–nickel binary concentrations. Nonregular solution behavior exists in both binary and ternary concentrations.

Introduction

Thermodynamic information concerning substitutional solid solution behavior among transition metals of the first long period has been obtained for the chromium–iron,[1-4] manganese–iron,[5-9] iron–cobalt,[10] and iron–nickel[11-12] systems. These systems have been reported to exhibit only small departures from Raoult's law (somewhat larger departures have been reported for chromium–iron[2,4]) and on the basis of the physical and chemical properties of the components, they could perhaps be expected to conform closely to Raoultian behavior. The present study was undertaken to extend the information concerning metallic solid solutions and to investigate the general applicability of Raoultian behavior in additional transition metal solutions. Both

(1) C. L. McCabe, R. G. Hudson, and H. W. Paxton, *Trans. AIME*, 212, 102 (1958).

(2) E. Z. Vintaikin, *Dokl. Akad. Nauk*, 118, 977 (1958).

(3) O. Kubaschewski and G. Heymer, *Acta Met.*, 8, 416 (1960).

(4) Y. Jeannin, C. Mannerskantz, and F. D. Richardson, *Trans. AIME*, 227, 300 (1963).

(5) J. F. Butler, C. L. McCabe, and H. W. Paxton, *ibid.*, 221, 479 (1961).

(6) J. H. Smith, H. W. Paxton, and C. L. McCabe, *ibid.*, 221, 895 (1961).

a binary (manganese–nickel) and a ternary solution (manganese–iron–nickel) with a common solvent (manganese) were studied in which the properties of each component, such as electronegativity, atom radius, and cohesive energy were very similar and an extensive concentration range with the same crystal structure (f.c.c.) could be investigated.

Experimental

The Knudsen effusion technique[13] was employed to measure the vapor pressure of manganese in equilibrium with the solid solutions. The weight loss due to vaporization of manganese from the solid solutions was measured *in situ* by means of a quartz vacuum microbalance sensitive to 4 μg. The experimental apparatus has been described previously.[5] Appropriate choices of the cell geometry and orifice radii were made to ensure that the mean free path for molecular effusion was sufficiently long that any Whitman correction[14] would be insignificant. Nonequilibrium contributions to the effusion flux from surface diffusion along the cell walls as described by Winterbottom and Hirth[15a] were also insignificant since the magnitude of the manganese vapor pressures was large in relation to the range of orifice radii chosen.[15b] Techniques for condensate analysis were unnecessary because of the high vapor pressure of manganese.

Component materials [electrolytic manganese (99.9%), Ferrovac-E iron (99.9%), and Mond nickel (99.6%)] were induction melted in stabilized zirconia crucibles under a purified argon atmosphere. A total of 46 alloys was prepared, fourteen in the manganese–nickel binary and the remainder in the ternary system. The ternary alloys were chosen at five nickel–iron concentration ratios with the concentration of manganese varying from 20 to 100%. The maximum impurity limits as determined from chemical analyses are indicated in Table I.

Table I: Maximum Impurity Limits, wt. %

Al	C	Ca	Co	Cr	Cu	Fe
0.03	0.02	0.05	0.01	0.01	0.03	0.01
Mg	Mo	N	Ni	O	Si	Zr
0.01	0.01	0.01	0.03	0.03	0.05	0.02

For these experiments effusion cells were fashioned from 15-mil molybdenum sheet, and their lids were made from 5-mil molybdenum sheet. The orifices were obtained by making a point indentation in the center of the lid which could be sanded through to produce a knife-edged hole. The area of the hole was then obtained by making a 100× shadow graph profile. Arc welding in an argon atmosphere was used to seal the lids in place and complete the cell fabrication.

During effusion, the depletion of manganese from the surface of the solid solutions was minimized by maximizing the surface area of the powdered sample, minimizing both the effusion orifice radius and the initial time required to reach equilibrium temperature, and limiting each effusion cell to a single isothermal run.

The vapor pressures of pure iron and nickel are lower than that for pure manganese by factors of 10^{-5} [16] and 10^{-6},[17] respectively, at 1232°K. so that any contribution of the iron and nickel species to the effusing flux would be too small to detect by the experimental technique employed. No condensate analyses were made and manganese vapor was considered to be the sole source of the measured effusion flux. The mass spectrographic measurements of Drowart[18] give an upper limit of 1.5×10^{-5} molecule/atom for manganese vapor in equilibrium with solid manganese at 1180°K., thus providing experimental evidence for the existence of a nearly monatomic manganese vapor. Drowart's measurement permits unrestricted use of the atomic weight for manganese in Knudsen's molecular effusion equation

$$p_{Mn} = m/A_0\left(\frac{2\pi RT}{M_{Mn}}\right)^{1/2} \qquad (1)$$

where p_{Mn} is the effusing manganese equilibrium vapor pressure, m is the manganese weight loss per unit time through an orifice of area A_0, and M_{Mn} is the atomic weight of the effusing manganese species.

Results

The equilibrium manganese vapor pressures were calculated from eq. 1 using the measured rate of man-

(7) C. L. McCabe and R. G. Hudson, *J. Metals*, **9**, 17 (1957).

(8) A. P. Lyubimov, A. A. Granovskaya, and L. E. Berenshtein *Zh. Fiz. Khim.*, **32**, 1591 (1958).

(9) W. B. Kendall and R. Hultgren, *Trans. Am. Soc. Metals*, **53**, 199 207 (1961).

(10) T. Satow, S. Kachi, and K. Iwase, *Sci. Rept. Res. Inst. Tohoku Univ., Ser. A*, **8**, 502 (1956).

(11) O. Kubaschewski and O. von Goldbeck, *Trans. Faraday Soc.*, **45**, 948 (1949).

(12) R. A. Oriani, *Acta Met.*, **1**, 448 (1953).

(13) M. Knudsen, *Ann. Physik*, **28**, 999 (1909).

(14) C. I. Whitman, *J. Chem. Phys.*, **20**, 161 (1952).

(15) (a) W. L. Winterbottom and J. P. Hirth, *ibid.*, **37**, 784 (1962); (b) the orifice radii were chosen to coincide with the range of those orifice areas where the equilibrium vapor pressure of manganese has previously been shown to be independent of effusion cell orifice area.

(16) J. W. Edwards, H. L. Johnston, and W. E. Ditmars, *J. Am. Chem. Soc.*, **73**, 4729 (1951).

(17) H. L. Johnston and A. L. Marshall, *ibid.*, **62**, 1382 (1940).

(18) J. Drowart, Thesis, University of Brussels, 1957.

ganese weight loss. The pressure was independent of the orifice radius for the range of radii used. The data for β-manganese as a function of temperature are plotted in Fig. 1. These data served as a calibration

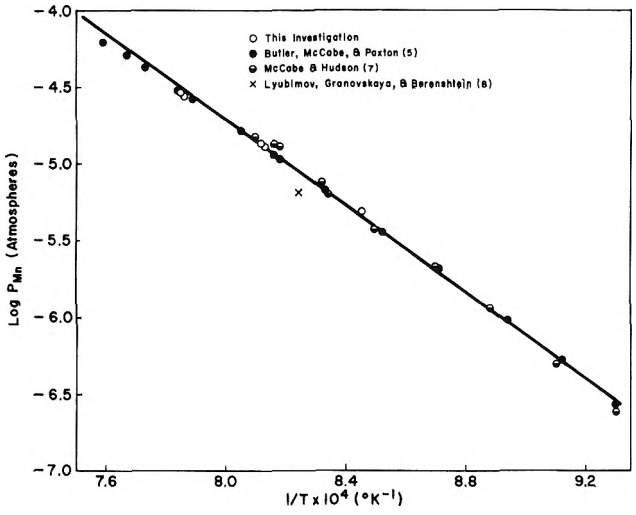

Figure 1. The pressure of manganese in equilibrium with β-Mn as a function of temperature.

for this investigation since they were consistent with the data from other investigations and agreed well with the equation previously obtained by Butler, *et al.*,[5] for the vapor pressure of pure β-manganese

$$\log p_{Mn}\ (\text{atm.}) = \frac{-14{,}190}{T} + 6.66 \qquad (2)$$

The departure of the measured values from the linear plot at higher temperatures is due to the failure to satisfy the necessary molecular flow conditions for Knudsen effusion, *i.e.*, the mean free path of the manganese atoms becomes less than ten times the cell dimensions.

The manganese vapor pressure data at 1232°K. for the manganese–nickel system are plotted as Raoultian manganese activities (a_{Mn}) in Fig. 2 with the range of values obtained from 46 measurements indicated by the height of the bars.[19] Previously determined activity curves for the manganese–iron system[5,6] are presented in Fig. 3. In order that the component activities in each phase might correspond to the crystal structures of the appropriate solid solutions, the β-phase (complex cubic) solid components in their β-phase, and the pure components in their γ-phase (f.c.c.) were chosen for the standard state of the γ-phase solutions. Pure solid γ_{Mn}, β_{Fe}, and β_{Ni} are not stable at 1232°K. so that these particular component standard states are nonphysical. For the manganese activity calculations, the

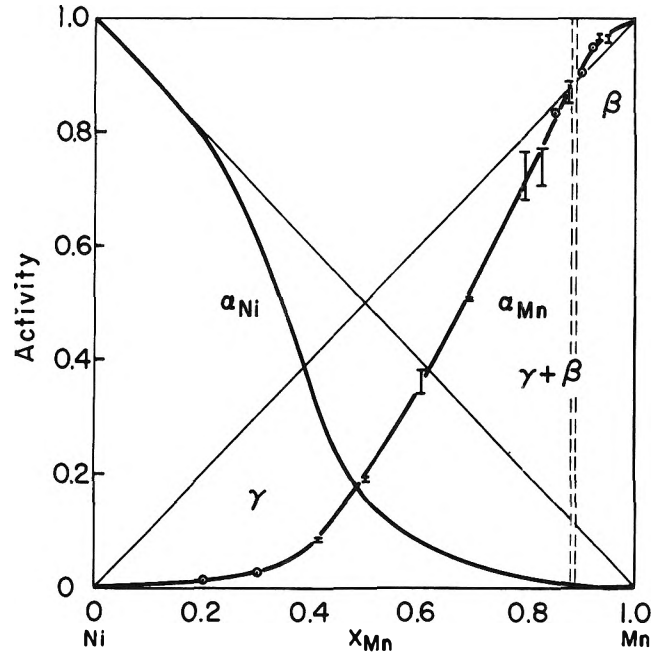

Figure 2. Activity of manganese and nickel as a function of atom fraction Mn (X_{Mn}) in the Mn–Ni system at 1232°K. Raoult's law is shown for the β-phase standard state for alloys in the β-phase while the γ-phase of the components is the standard state for all γ-phase alloys.

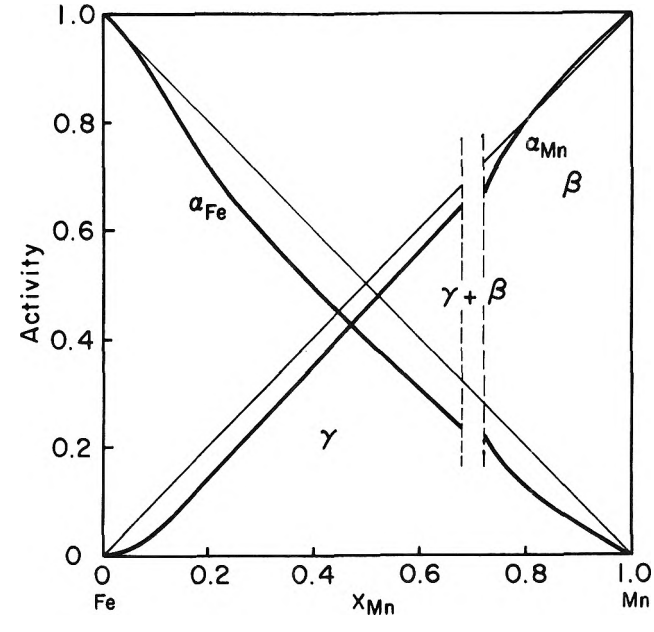

Figure 3. Activity of manganese and iron as a function of atom fraction Mn (X_{Mn}) in the Mn–Fe system at 1232°K. Raoult's law standard states are the same as those indicated for Fig. 2.

(19) J. H. Smith, Thesis, Carnegie Institute of Technology, Pittsburgh, Pa., 1960; the absolute values for the equilibrium manganese vapor pressures referred to in this article are given in this reference.

vapor pressure of pure γ-manganese was obtained by using the equations given by Kelley, *et al.*,[20] for the standard Gibbs free energy of sublimation of the β- and γ-manganese phases. The nickel activity curve in Fig. 2 was derived from the Gibbs–Duhem relationship in the form[21]

$$\ln \gamma_{Ni} = -\alpha_{Mn} X_{Ni} X_{Mn} - \int_{X_{Ni}=1}^{X_{Ni}} \alpha_{Mn}\, dX_{Ni} \quad (3)$$

where the Raoultian activity coefficient for nickel is $\gamma_{Ni} = a_{Ni}/X_{Ni}$, X_{Ni} is the atom fraction of nickel, and $\alpha_{Mn} = \ln \gamma_{Mn}/(1 - X_{Mn})^2$. Values for the iron activity curve in Fig. 3 were similarly determined in the manganese–iron system.

At low manganese concentrations in the manganese–nickel system the limit of experimental sensitivity was reached at $X_{Mn} \backsim 0.2$. This necessitates representing the more dilute manganese concentrations by a smooth continuation of the experimentally determined activity data. Since the manganese activity had decreased to 10^{-2} at $X_{Mn} \backsim 0.2$, this portion of the curve appears linear on the scale used; *i.e.*, this portion seems to obey Henry's law (although the validity of this behavior remains unproven). This linear representation renders Raoultian conformity to the nickel activity when the Gibbs–Duhem integration is performed over the same concentration range.

The constancy of manganese pressure in the range of the two phase equilibrium of this system located the equilibrium phase boundaries within 1 atom % of the concentrations indicated by Hansen.[22]

The manganese partial pressure for several binary manganese–nickel alloys was investigated as a function of temperature. However, the maximum temperature range was restricted by the mean free path length requirement for the manganese vapor while the minimum temperature was determined by the sensitivity of the evaporation determinations. Within this temperature range no change in the temperature coefficient of p_{Mn} relative to that for pure manganese could be detected, and thus the enthalpy of solution could not be evaluated for any concentration. The data were not sufficiently extensive to interpret this behavior as being indicative of zero enthalpy of solution.

Figure 4 summarizes the equilibrium manganese pressure data for the isothermal manganese–iron–nickel solid solutions at 1232°K. The extent of scatter in the data was similar to that shown for the manganese–nickel binary in Fig. 2. This section indicates the concentration of each of the ternary alloys investigated (circled numbers) and also their equilibrium manganese pressure when referred to the numerically identical isobaric curve. Manganese pressures for each of the

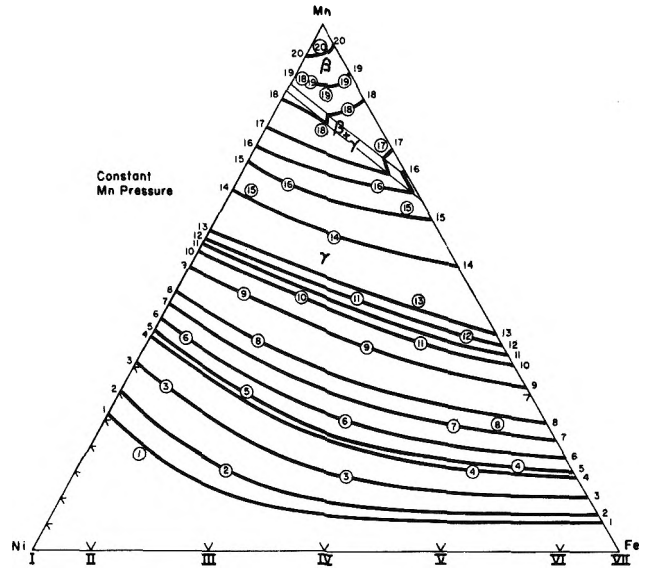

Figure 4. Scatter of the manganese pressure data as a function of concentration for the Mn–Fe–Ni system at 1232°K. The Roman numerals indicate X_{Fe}/X_{Ni} ratios chosen for thermodynamic calculations.

Table II: Data for Constant Mn Pressure Curves

Curve no.	Average Mn pressure, atm. × 10^{-6}
1	0.26
2	0.37
3	0.67
4	1.17
5	1.32
6	1.68
7	2.17
8	2.61
9	3.56
10	4.15
11	4.43
12	4.70
13	5.03
14	6.92
15	8.28
16	9.10
17	10.18
18	11.17
19	12.44
20	13.14

(20) K. K. Kelley, B. F. Naylor, and C. H. Shomate, U. S. Bureau of Mines Technical Paper No. 686, U. S. Govt. Printing Office, Washington, D. C., 1946.

(21) L. S. Darken and R. W. Gurry, "The Physical Chemistry of Metals," McGraw-Hill Book Co., New York, N. Y., 1953, p. 264.

(22) M. Hansen, "Constitution of Binary Alloys," McGraw-Hill Book Co., New York, N. Y., 1958, p. 939.

isobars are listed in Table II. The position of these isobars represents averaging of the data for internal consistency prior to thermodynamic calculations in the ternary system. The isobars were determined from smoothed curves of p_{Mn} *vs.* X_{Mn} in the manganese–nickel and manganese–iron systems and constructed to conform with the data in the ternary system. Manganese pressures at the concentrations where these isobars intersected lines of constant X_{Ni}/X_{Fe} (shown by the Roman numerals in Fig. 4) were plotted as a function of X_{Mn} in each of the pseudo-binaries represented by the X_{Ni}/X_{Fe} ratios and the best p_{Mn} curve again determined. Maintaining the p_{Mn} fixed in the binaries, a second family of isobars was then constructed using X_{Mn} values obtained from the pseudo-binary curves. The proximity of the experimental points (circled) to these averaged isobars gives an indication of the scatter caused by experimental error and the averaging procedure. In a few cases additional error was introduced into Fig. 4 by the use of a single isobaric representation for two or more alloys of widely different concentrations but approximately the same p_{Mn}. Their pressures were averaged to avoid unjustifiably close increments in p_{Mn}.

Utilizing the isobaric data in Fig. 4, manganese isoactivity curves were calculated for the ternary concentrations and appear in Fig. 5. The discontinuity in those curves crossing the two phase region is due to the change in standard states for the two solutions. Phase equilibria shown in Fig. 4 and 5 were not investigated for ternary concentrations but were taken from the work of Kurnakov and Troneva[23] and the compilation of Guertler.[24]

Darken's solution[25] to the ternary Gibbs–Duhem equation allows for the calculation of the free energy of the ternary system and two of the component activities if thermodynamic data for the remaining single component are measured throughout the ternary system. In this investigation the Gibbs excess molal free energy of solution (G^{xs}) was calculated with the aid of Darken's equation in the following form

$$G^{xs} = RT\Big\{(1 - X_{Mn})\Big[\int_{X_{Mn}=1}^{X_{Mn}} \alpha_{Mn}\, dX_{Mn}\Big]_{X_{Fe}/X_{Ni}} - X_{Fe}\Big[\int_{X_{Mn}=1}^{X_{Mn}=0} \alpha_{Mn}\, dX_{Mn}\Big]_{X_{Ni}=0} - X_{Ni}\Big[\int_{X_{Mn}=1}^{X_{Mn}=0} \alpha_{Mn}\, dX_{Mn}\Big]_{X_{Fe}=0}\Big\} \quad (4)$$

The first integral term was evaluated from a plot of α_{Mn} *vs.* X_{Mn} using the ternary manganese isoactivity curves in Fig. 5, while the last two terms were similarly determined from the binary activity data shown in Fig. 2 and 3. The results of these calculations are summa-

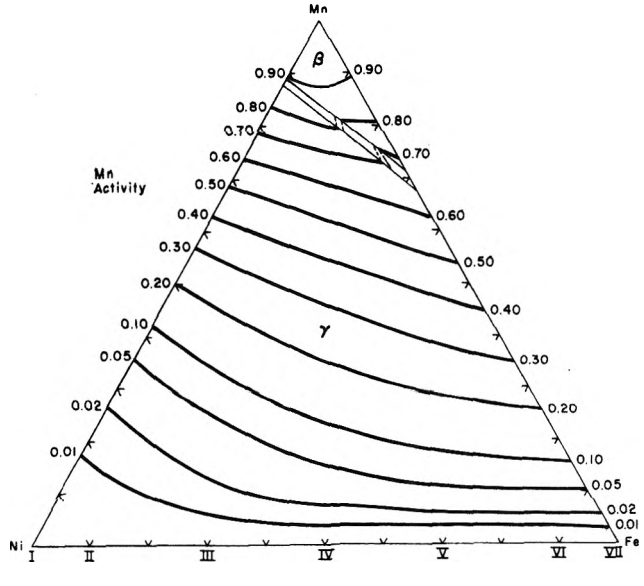

Figure 5. Mn activity as a function of concentration for the Mn–Fe–Ni system at 1232°K.

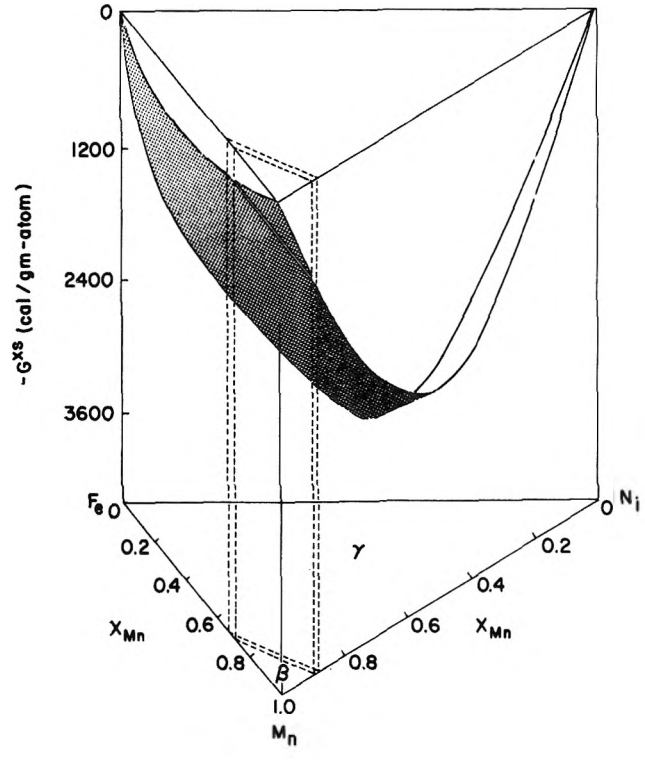

Figure 6. Gibbs excess molal free energy of solution (G^{xs}) as a function of concentration for the Mn–Fe–Ni system at 1232°K.

(23) N. N. Kurnakov and M. Y. Troneva, *Izv. Sektora Fiz. Khim. Analiza*, **24**, 132 (1953).

(24) W. Guertler, WADC Tech. Rpt. 58-615, Pt. I, ASTIA No. 210719, 80 (1959).

(25) L. S. Darken, *J. Am. Chem. Soc.*, **72**, 2909 (1950).

rized in Table III and the values plotted in Fig. 6. The maximum error in measuring p_{Mn} was determined to be $\pm 8\%$ which causes a maximum uncertainty of ± 175 cal./g.-atom for the binary G^{xs} data given in Table III. Additional errors introduced in averaging the ternary data increase the uncertainty to ± 225 cal./g.-atom for ternary concentrations.

Table III: Ternary G^{xs} Values, $-G^{xs}$ cal./g.-atom

	I	II	III	IV	V	VI	VII
	X_{Fe}/X_{Ni}						
X_{Mn}	0/1	1/9	3/7	1/1	7/3	9/1	1/0
0.0	0	979	2891	3660	2894	1760	0
0.10	727	1506	3038	3636	2908	1866	272
0.20	1420	2022	3180	3513	2788	1809	379
0.30	2025	2448	3217	3349	2593	1679	406
0.40	2441	2666	3092	3072	2353	1515	404
0.50	2551	2620	2850	2744	2081	1324	379
0.60	2402	2394	2495	2353	1763	1107	338
0.70	2056	2010	2034	1880	1395	867	...
0.80	1513	1466	1440	1307	...	610	220
0.90	791	744	708	617	453	291	108

The nickel activity for ternary concentrations may be calculated from the G^{xs} data by

$$\ln \gamma_{Ni} = \frac{(1 - X_{Ni})^2}{RT} \left[\frac{\partial \left(\frac{G^{xs}}{1 - X_{Ni}} \right)}{\partial X_{Ni}} \right]_{X_{Fe}/X_{Mn}} \quad (5)$$

The calculated values are summarized in Fig. 7. A similar treatment for the Fe component yielded the isoactivity curves plotted in Fig. 8.

Iron–nickel G^{xs} values may be estimated by evaluation of eq. 4 for the limiting case of $X_{Mn} = 0$ at each of the X_{Fe}/X_{Ni} ratios. Results of this evaluation have been included in Fig. 6. Application of eq. 5 at $X_{Mn} = 0$ for each X_{Fe}/X_{Ni} ratio permits calculation of the component activities in the Fe–Ni system and these are included in Fig. 7 and 8 as the termini of the isoactivity curves along the iron–nickel concentrations.

The limiting manganese activity coefficient (γ_{Mn}°) obtained from plots of α_{Mn} *vs.* X_{Mn} as $X_{Mn} \rightarrow 0$ are shown as a function of X_{Fe}/X_{Ni} in Fig. 9. This behavior is similar to that observed by Smith[26] for γ_c° at infinite carbon dilution in iron–nickel solutions at 1273°K., since the activity coefficients in both investigations show a strong concentration dependence in the region of $X_{Ni} = 0.7$. Smith noted that this was approximately the same concentration where the Curie point and the order–disorder transformation temperature show maxima and the liquid–solid equilibrium has a minimum. Thus, the behavior of γ_{Mn}° also indicates possible persistence over a significant temperature span of the factors responsible for these energetic relationships.

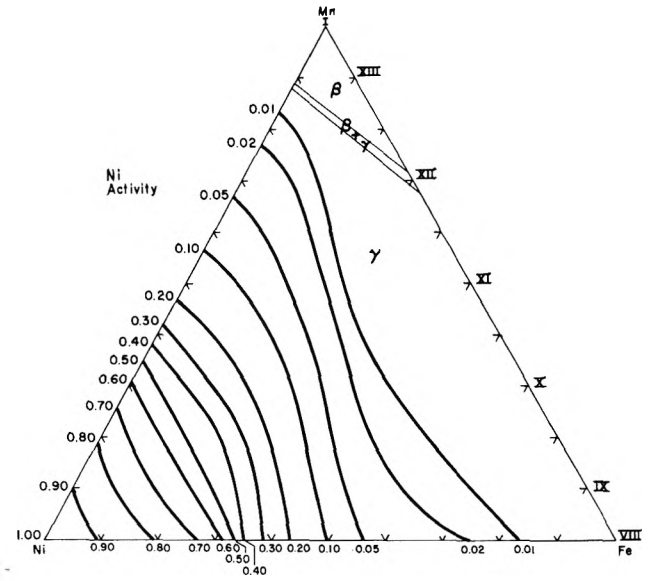

Figure 7. Nickel activity as a function of concentration for the Mn–Fe–Ni system at 1232°K.

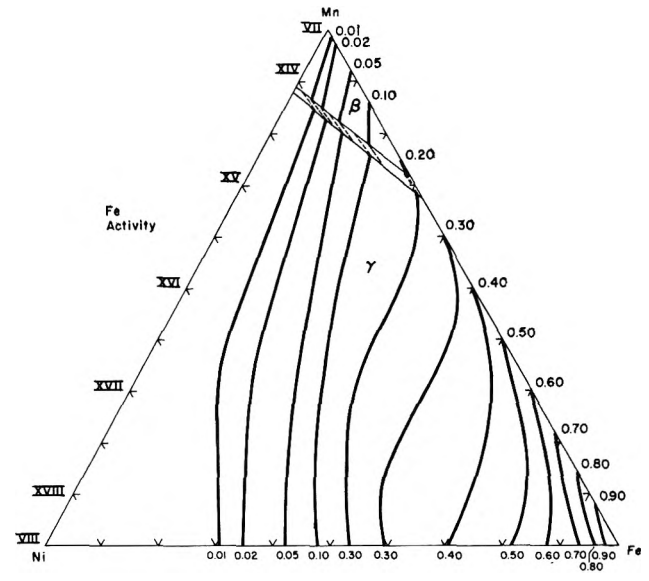

Figure 8. Iron activity as a function of concentration for the Mn–Fe–Ni system at 1232°K.

Discussion

Most metallic solution models are based on explicit enthalpy and entropy functions, and since enthalpy

(26) R. P. Smith, *Trans. AIME*, 218, 62 (1960).

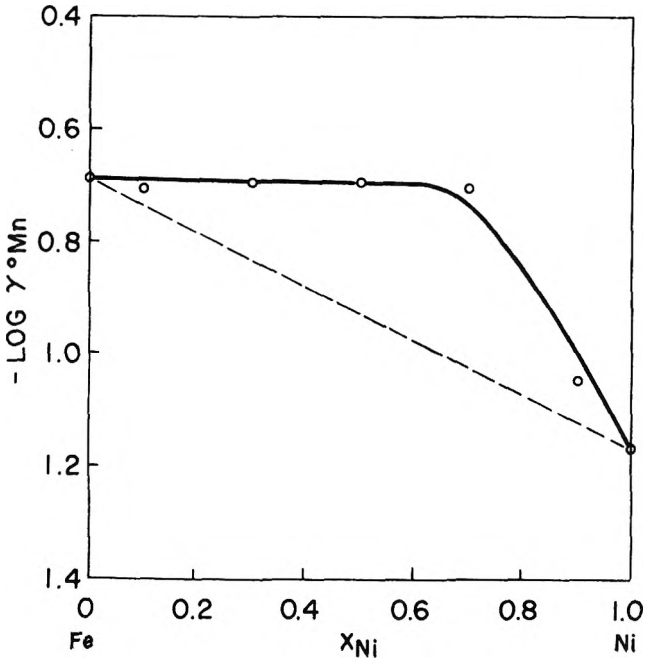

Figure 9. Manganese activity coefficient extrapolated to infinite dilution as a function of atom fraction Ni (X_{Ni}) for the Ni–Fe system at 1232°K.

data were not determined in this study, no apportionment of these contributions to the free energy of solution could be performed directly to test the usefulness of such models in describing the data. The only available enthalpy data are those of Kendall and Hultgren,[9] who have recently measured heat contents and heats of formation for two γ_{Mn-Fe} alloys. By combining their results with similar data for pure γ-Mn[20] and γ-Fe[27] the heat of solution (H^{xs}) has been calculated for each of these alloys. When used in conjunction with the Mn–Fe G^{xs} data, these calculations permit evaluation of the excess entropy of solution (S^{xs}) at the two concentrations. Table IV summarizes the calculated values. The entropy of mixing values are smaller by a factor of 3 or 4 than those required for the ideal entropy of mixing of a regular solution. This nonregular solution behavior was also indicated by the observed lack of constancy of the α_{Mn} function with composition when performing the Gibbs–Duhem integration, although the additional constants were not investigated for subregular conformity.[28]

Calculations of the heat of solution for the manganese–nickel system have been made from the phase diagram[29] on the assumption that this system is unsymmetrically regular, *i.e.*, the activity coefficients are unsymmetrical functions of the mole fraction. However, when these calculations are combined with the present G^{xs} data the resulting $-S^{xs}$ values were significantly larger than could be attributed to the error spread, thus leading to internal inconsistency with the assumption of $S^{xs} = 0$ for unsymmetrically regular solutions. Further evidence for the nonregular solution behavior in this system was obtained from the strong concentration dependence of the α_{Mn} function. The temperature of this investigation occurs nearly midway between a minimum in the liquidus (1291°K., $X_{Mn} \backsim 0.6$) and a congruent transformation (1183°K., $X_{Mn} \backsim 0.5$) and several hundred degrees above the $MnNi_3$ superlattice-ordering and magnetic transformations. None of the calculated thermodynamic functions indicated any influence of these phenomena in the manganese–nickel solutions as has been suggested for the iron–nickel solutions.

Table IV: Thermodynamic Quantities for Two Mn–Fe Alloys at 1232°K.

X_{Mn}	G^{*a} (cal./g.-atom)	G^{xs}	$H^{xs} = H^{*a}$ (cal./g.-atom)	S^{*a} (cal./g.-atom deg.)	S^{xs}
0.304	−1914	−411	−1538	+0.31	−0.92
0.488	−2081	−384	−1550	+0.43	−0.95

[a] G*, H*, and S* are the integral free energy, enthalpy, and entropy of solution, respectively.

Figure 6 shows that the nickel component exerts a dominant force in determining the G^{xs} values for ternary solutions, even for the low concentrations present in the β-phase. This interpretation can also be made from the partial quantities plotted in Fig. 5, 7, and 8. Similar observations made by Cigan[30] indicated that nickel solutions were much more non-Raoultian than iron solutions when zinc was used as a common solvent.

When any two of the component activities have been evaluated for a particular ternary solution concentration the third may be determined from

$$G^{xs} = RT[N_{Mn} \ln \gamma_{Mn} + N_{Fe} \ln \gamma_{Fe} + N_{Ni} \ln \gamma_{Ni}] \quad (6)$$

Equation 6 may be used to evaluate the internal consistency when evaluating the two component activities by the use of eq. 5. Eleven concentrations were chosen at different X_{Ni}/X_{Mn} for varying X_{Fe}, and iron activities were calculated using eq. 6 in conjunction with the previously calculated γ_{Mn} and G^{xs} values along with

(27) L. S. Darken and R. W. Gurry, *Trans. AIME*, **218**, 397 (1960).

(28) H. K. Hardy, *Acta Met.*, 1, 202 (1953).

(29) R. P. Rastogi and K. T. Rama Varma, *Proc. Indian Acad. Sci.*, **48A**, 336 (1958).

(30) J. M. Cigan, Thesis, Carnegie Institute of Technology, Pittsburgh, Pa., 1960.

γ_{Ni} values obtained by use of eq. 5. Iron activities determined in this manner varied a maximum of 24% from those evaluated by eq. 5 with a mean variance of 9%. This comparison demonstrates the inherent difficulty of accurate graphical construction for evaluation of eq. 5.

The Darken solution to the ternary Gibbs–Duhem equation was used in preference to the solutions developed by Schuhmann[31] and Wagner[32] because the errors arising from tangent evaluation are minimized. All three methods require both tangent evaluation and graphical integration. The techniques of Schuhmann and Wagner require two tangent evaluations which preceed the integral evaluation while Darken confined a single tangent determination to the calculation of the partial properties of each component following the previously calculated integral properties.

The maximum G^{xs} values as obtained from the Gibbs–Duhem relationship are seen to occur along the iron–nickel binary in Fig. 6. A direct investigation of G^{xs} for a portion of the iron–nickel system has been made independently by both Kubaschewski and von Goldbeck[11] and Oriani[12] between approximately 1000 and 1200°K. by means of gaseous equilibria techniques. *The results of the two investigations were similar; however*, the data obtained by Kubaschewski and von Goldbeck showed more scatter. A comparison of Oriani's data for G^{xs}/RT with the calculated values obtained here is shown in Fig. 10. The relative position of the two curves would not be anticipated from consideration of the usual behavior in which the excess values become smaller as the temperature is increased for a particular solution in which the equilibria remain approximately constant.

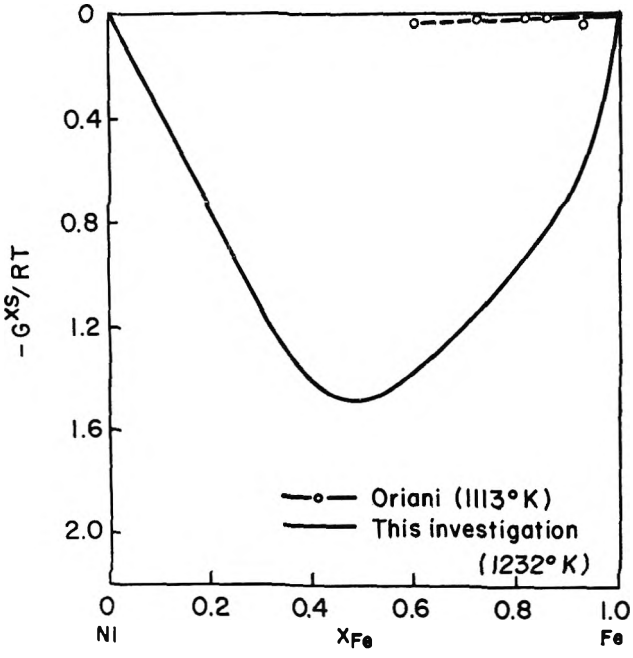

Figure 10. Gibbs excess molal free energy of solution (G^{XS}) as a function of atom fraction Fe (X_{Fe}) for the Ni–Fe system.

A detailed examination of the Gibbs–Duhem integration reveals that the large G^{xs} values calculated for the iron–nickel system were a consequence of the disproportionately large integration contribution provided from the data measurements in the β-phase concentrations of the ternary system. The extent of this contribution is apparent from a comparison of the relative β-phase and γ-phase contributions used in evaluation of the α_{Mn} integral at $N_{Fe}/N_{Ni} = 1$ (Fig. 11). To evaluate the contribution from the β-phase, the manganese activity coefficient (γ_{Mn}) may be set equal to unity throughout all of the β-phase concentrations. Such an assumption is not a strong contradiction of the experimental observations of $\gamma_{Mn} \geq 1$ for the β-phase solu-

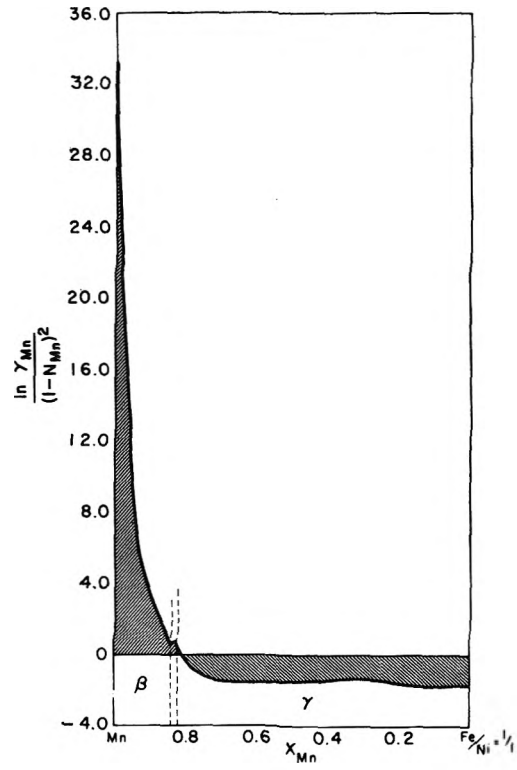

Figure 11. The α_{Mn} function $\left[\frac{\ln \gamma_{Mn}}{(1 - X_{Mn})^2}\right]$ *vs.* X_{Mn} at $X_{Fe}/X_{Ni} = 1/1$ on the Mn–Fe–Ni system at 1232°K.

(31) R. Schuhmann, Jr., *Acta Met.*, 3, 219 (1955).

(32) C. Wagner, "Thermodynamics of Alloys," Addison-Wesley Co., Cambridge, Mass., 1952, p. 19.

tions as plotted in Fig. 2, 3, and 5 although the data measurements show that the manganese activity coefficient is greater than unity for these concentrations. This modification raises the G_{xs} surface throughout the ternary concentrations with the maximum shift indicated in Fig. 12 by the G^{xs} values for the iron–nickel system. Although the magnitude of the curve decreases by approximately a factor of two, the G^{xs} values remain conspicuously negative. Figure 12 also indicates

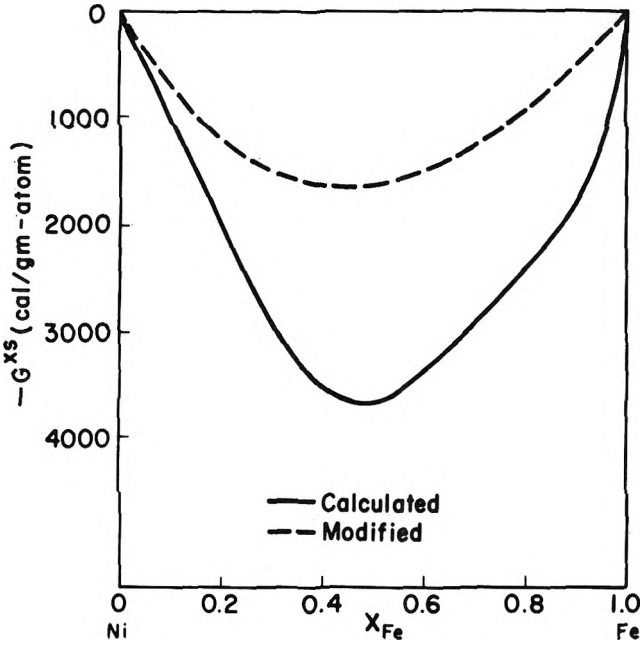

Figure 12. Calculated and modified values of the Gibbs excess molal free energy of solution (G^{xs}) as a function of atom fraction Fe(X_{Fe}) for the Fe–Ni system.

that the asymmetry present in the calculated curve was contributed entirely from the β-phase integration contribution. Thus, the assumption of Raoultian behavior for the solvent in the concentration region of the pure solvent should be used with the appropriate reservations suggested by Darken.[25]

The vapor pressure data of pure β_{Mn} and γ_{Mn}[20] indicate that β is stable relative to γ at 1232°K. by about 30 cal./g.-atom. This small instability is the order of magnitude to be anticipated for a transition which is displaced only a small amount from its equilibrium temperature.

Since the β-structure is nonphysical for nickel and iron at all temperatures, the evaluation of ΔG° for $\gamma \rightarrow \beta$ can be made in the manganese–nickel and manganese–iron systems by invoking the requirement of constant component activity in the two-phase equilibria. Within the two-phase equilibrium of the manganese–nickel system the following relation may be evaluated from Fig. 2

$$\frac{p_{Ni}/p^0_{Ni}(\gamma)}{p_{Ni}/p^0_{Ni}(\beta)} = \frac{a_{Ni}(\gamma)}{a_{Ni}(\beta)} = 1.04 \qquad (7)$$

Therefore

$$\Delta G^\circ_{Ni(\gamma\rightarrow\beta)} = RT \ln \frac{a_{Ni}(\gamma)}{a_{Ni}(\beta)} \approx +95 \text{ cal./g.-atom} \qquad (8)$$

A similar procedure for iron in the manganese–iron system yields

$$\Delta G^\circ_{Fe(\gamma\rightarrow\beta)} + 90 \text{ cal./g.-atom} \qquad (9)$$

Although the β-instabilities for both nickel and iron are indicated to be a factor of 3 larger than for manganese, additional interpretation does not seem warranted since their magnitude at this temperature is less than the limit of estimated error in the data.

No solid solution models have yet been developed which can adequately predict metallic solution behavior or describe the behavior in relation to physical structure. The current status of model development has been reviewed by Oriani and Alcock.[33] None of these models satisfactorily describes the present data. In the phenomenological approach advanced by Hume-Rothery, consideration must be given to the relative differences in atom size, valence, and electronegativity among the solution components. If atom radii comparisons are applicable,[34] then the data of Pearson[35] indicate less than 5% difference and mitigate the atom size difference criterion for the observed changes in solution behavior. Any large contribution to the enthalpy of solution from the strain energy associated with atom size differences is improbable.[36,37] Valence considerations in transition metals remain quite uncertain and since the electronegativity values are a function of valences, a similar uncertainty is also associated with this consideration.

Summary

Coupling of a vacuum microbalance with the Knudsen effusion technique has been used to obtain consistent equilibrium vapor pressures as low as 1×10^{-7}

(33) R. A. Oriani and C. B. Alcock, *Trans. AIME*, **224**, 1104 (1962).

(34) P. A. Flinn, B. L. Averbach, and M. Cohen, *Acta Met.*, **1**, 664 (1953).

(35) W. B. Pearson, "A Handbook of Lattice Spacings and Structures of Metals and Alloys," Pergamon Press, New York, N. Y., 1958, pp. 631, 636, 730.

(36) R. A. Oriani, *Acta Met.*, **4**, 15 (1956).

(37) B. L. Averbach, "Theory of Alloy Phases," American Society for Metals, 1956, p. 311.

atm. in the manganese–iron–nickel system. No dependence of the equilibrium p_{Mn} as a function of the effusion cell orifice area was found for any of the alloys.

The equilibrium manganese vapor pressures exhibit nonregular solution behavior in both the manganese–nickel and manganese–iron–nickel solutions at 1232°K. Application of the ternary form of the Gibbs–Duhem integration provided thermodynamic functions for the ternary solutions and an estimate of these functions for the iron–nickel binary concentrations, which were not investigated. Nickel exerts the strongest contribution to the concentration dependence of the thermodynamic functions for the solid solutions. All concentrations have component activity coefficients less than or equal to unity with the sole exception of those for manganese in portions of the β-phase concentration range. The solution behavior obtained is significantly different from other binary transition metal systems in which some degree of Raoultian behavior has been observed.

Acknowledgments. This investigation was supported by a grant from the American Iron and Steel Institute and a fellowship given by the Armco Steel Corp. Mr. Harold C. Brown of the Armco Steel Corp. very generously performed the chemical analyses. We are indebted to the Crucible Steel Co. and the International Nickel Co. for thermocouple calibrations and nickel metal, respectively.

The Chemical Thermodynamic Properties of Methyl Ethyl Ketone

by G. C. Sinke and F. L. Oetting

Thermal Research Laboratory, Dow Chemical Company, Midland, Michigan *(Received November 13, 1963)*

Heat capacities from 13 to 338°K., melting point, heat of fusion, and the heat of combustion of methyl ethyl ketone have been measured. The derived third-law entropy along with literature values for the vapor heat capacity and spectroscopic evidence for the existence of only one rotational isomer served to define a continuous potential function for the skeletal internal rotation. This potential function was used in the calculation of thermodynamic properties of the vapor to 1000°K. The heat of formation derived from the heat of combustion is significantly less negative than previous combustion values, but agrees well with a heat of hydrogenation result.

Introduction

A consistent table of thermodynamic properties of methyl ethyl ketone was desired for engineering calculations. A literature search revealed serious disagreement among several papers devoted to methyl ethyl ketone. The entropy based on parameters derived from vapor heat capacity measurements[1] was a full unit higher than the third-law value.[2] The heat of formation from the heat of combustion of the gas[3,4] was about 1 kcal. more negative than that derived from the heat of combustion of the liquid.[2] The latter in turn was over 1 kcal. more negative than a value which can be calculated from the heat of combustion of 2-butanol[5,6] and the heat of hydrogenation of methyl

(1) J. K. Nickerson, K. A. Kobe, and J. J. McKetta, *J. Phys. Chem.*, 65, 1037 (1961).

(2) G. S. Parks, W. D. Kennedy, R. R. Gates, J. R. Mosley, G. E. Moore, and M. L. Renquist, *J. Am. Chem. Soc.*, 78, 56 (1956).

(3) R. S. Crog and H. Hunt, *J. Phys. Chem.*, 46, 1162 (1942).

(4) R. S. Crog, Thesis, Purdue University, June, 1942.

(5) J. Chao, Thesis, Carnegie Institute of Technology, 1960.

(6) H. A. Skinner and A. Snelson, *Trans. Faraday Soc.*, 56, 1776 (1960).

ethyl ketone.[7,8] New measurements reported here yield consistent thermodynamic properties and more accurately define internal rotation characteristics of methyl ethyl ketone.

Experimental

Previous publications contain descriptions of methods and apparatus for low temperature calorimetry.[9,10] A rotating bomb calorimeter was available and was used for the combustion calorimetry, although rotation would not be necessary. The bomb had a volume of 348 ml. and was charged with 1 ml. of water and 30 atm. of oxygen in all experiments. Samples were enclosed in bags of polyester film as described by Good and Scott.[11] The film contained 62.20% carbon and 4.18% hydrogen and the remainder was assumed to be oxygen. Under the humidity conditions prevailing in the laboratory, the film had a heat of combustion, $-\Delta Ec/M$, of 5468.0 cal. g.$^{-1}$. The calorimeter was calibrated with NBS benzoic acid 39h and the calorimeter equivalent was found to be 3352.6 cal. deg.$^{-1}$. Corrections to standard states were made by the method of Prosen.[12] Both ignition energy and nitric acid formation were very small and were assumed to be constant.

Heat capacity and heat of combustion values are based on a molecular weight of 72.108. The ice point is taken as 273.15°K. and 1 cal. (defined) = 4.184 absolute joules.

Samples. For the low temperature studies, commercial methyl ethyl ketone was dried with calcium sulfate and distilled in a 100-plate column. The sample was 99.78 mole % pure as shown by the variation of melting point with the fraction melted. For combustion studies, commercial methyl ethyl ketone was dried with acetic anhydride and distilled. Freezing curve analysis showed a purity of 99.74 mole %. This sample was fractionally crystallized until it was 99.85 mole % pure. The heat of combustion of the two samples was the same within experimental error, which was taken as evidence that the impurities did not seriously affect the combustion values.

Low Temperature Data. The sample was degassed and distilled into a platinum sample container under vacuum and sealed with 20 mm. of helium at room temperature. The platinum container weighed 252.49 g. and the sample weighed 49.972 g. corrected to vacuum conditions. Three series of measurements were taken. The observed values are given in Table I. Three determinations of the heat of fusion gave ΔH_m = 2016.9 ± 1.4 cal. mole^{-1} where the uncertainty is the maximum deviation from the mean. The melting point was determined by the usual plot of the equilibrium temperature *vs.* the reciprocal of the fraction melted. Results are given in Table II, showing the extrapolated triple-point temperature and the mole fraction impurity, N_2*. Smoothed values for the heat capacity given in Table III were derived with the aid of a computer smoothing program. Extrapolation to 0°K. was by means of a Debye function for six degrees of freedom with θ = 124.7°, which fit the experimental data from 13.1 to 26.5°K. The smoothed values have been corrected for premelting effects.

Heat of Combustion. Results of six determinations of the heat of combustion are given in Table IV. The sample mass was based on direct weighing and corrections for buoyancy. The derived values of the molar heats of combustion and heat of formation include corrections to constant pressure and the use of −94.054 and −68.317 kcal. mole^{-1} for the heats of formation of carbon dioxide and liquid water, respectively.

Calculation of Internal Rotation Parameters

As discussed by Nickerson, Kobe, and McKetta[1] (hereafter designated N.K.M.) a reasonable choice of potential function for the skeletal internal rotation shows three minima per cycle, with two equal minima higher than the third. Tables of contributions to the thermodynamic functions for such potential functions have been published by Scott and McCullough.[13] In these functions, the potential energy is zero for the lowest minimum, V_2 is the potential energy at the higher minima, V_1 is the height of the lower barriers, and the height of the higher barrier is $V_1 + V_2$. The tables give contributions to thermodynamic functions for various combinations of V_1 and V_2. Conversely, if an experimental value for a thermodynamic function is available and the contributions from all other sources are subtracted, leaving an "experimental" skeletal rotation contribution, a V_1 and V_2 combination can be derived. Actually, for each such experimental datum, a number of pairs will be found to be satisfactory, and if plotted as V_1 *vs.* V_2 will give a line. If a number of

(7) M. Dolliver, A. T. L. Gresham, G. B. Kistiakowsky, E. A. Smith, and W. E. Vaughan, *J. Am. Chem. Soc.*, **60**, 440 (1938).

(8) A. H. Cubberley and M. B. Mueller, *ibid.*, **68**, 1149 (1946).

(9) F. L. Oetting and R. A. McDonald, *J. Phys. Chem.*, **67**, 2737 (1963).

(10) F. L. Oetting, *ibid.*, **67**, 2757 (1963).

(11) W. D. Good and D. W. Scott, "Experimental Thermochemistry," Vol. II, H. A. Skinner, Ed., Interscience Publishers, New York, N. Y., 1962, Chapter 2.

(12) E. J. Prosen, "Experimental Thermochemistry," Vol. I, F. D. Rossini, Ed., Interscience Publishers, New York, N. Y., 1956, Chapter 6.

(13) D. W. Scott and J. P. McCullough, U. S. Bureau of Mines Report of Investigations, No. 5930, Pittsburgh, Pa., 1962.

Table I: Experimental Molal Heat Capacity of Methyl Ethyl Ketone, cal. deg.$^{-1}$

T, °K.[a]	C_s[b]	T, °K.[a]	C_s[b]	T, °K.[a]	C_s[b]
Series I		292.87	37.76	208.45	35.88
(Crystal)		299.39	37.96	213.97	36.01
13.12	0.984	305.88	38.22	220.15	36.03
14.33	1.344	312.33	38.43	226.99	36.08
15.58	1.620	318.74	38.81	247.25	36.50
16.98	2.194	325.09	38.94	253.96	36.59
18.53	2.566	331.41	39.27	260.63	36.82
20.37	3.033			267.26	37.01
22.36	3.567	Series II		273.85	37.14
24.45	4.233	(Crystal)		280.41	37.32
26.53	4.772	13.21	0.941	286.93	37.58
28.75	*5.327*	*14.56*	*1.349*	*293.40*	37.90
31.17	6.012	16.20	1.745	299.84	38.08
33.79	6.709	17.86	2.283	306.24	38.22
36.73	7.559	19.59	2.833	312.60	38.55
40.11	8.421	21.37	3.412	318.92	38.79
43.97	9.289	23.29	4.025	325.19	39.04
48.21	10.00	25.27	4.592	331.44	39.33
52.93	10.97	27.24	5.098		
58.20	11.69	29.24	5.609	Series III	
64.10	12.65	31.26	6.110	(Crystal)	
70.28	13.43	33.43	6.782	140.57	20.62
75.94	14.17	35.84	7.271	147.34	21.25
81.27	14.92	38.55	8.013	153.78	21.88
86.35	15.57	41.74	8.779	160.08	22.48[c]
91.24	16.04	49.47	10.36	166.24	23.19[c]
97.03	16.60	54.06	10.99	172.25	23.96[c]
103.69	17.28	59.20	11.91	178.10	25.21[c]
110.10	17.92	64.96	12.77	183.11	38.38[c]
116.30	18.49	70.92	13.43		
122.34	18.99	77.46	14.34	(Liquid)	
128.22	19.54	84.37	15.28	192.08	35.64
133.96	20.06	90.86	15.99	197.73	35.75
139.57	20.56	97.07	16.58	203.35	35.82
145.06	21.05	103.04	17.20	208.95	35.93
150.45	21.55	108.80	17.78	214.53	36.01
155.74	22.00	114.38	18.28	220.08	36.07
161.48	22.65[c]	119.81	18.77	225.62	36.15
167.67	22.33[c]	125.11	19.26	242.03	36.35
173.71	24.22[c]	130.28	19.68	247.48	36.36
179.52	25.96[c]	135.34	20.20	252.90	36.53
183.88	46.68[c]	140.30	20.58	258.31	36.66
		145.16	21.01	263.68	36.89
(Liquid)		149.93	21.49	269.02	37.08
191.62	35.59	154.62	21.92	274.35	37.23
197.25	35.67	160.67	22.46[c]	280.24	37.39
202.85	35.68	168.03	23.39[c]	286.85	37.59
208.44	35.87	175.15	24.48[c]	293.42	37.92
213.99	35.92	181.69	30.27[c]	299.85	38.07
219.53	35.99	185.42	194.46[c]	306.45	38.22
225.74	36.07			312.91	38.57
259.70	36.77	(Liquid)		319.33	38.76
266.40	*36.97*	*191.74*	*35.75*	*325.71*	39.10
273.07	37.11	197.33	35.77	332.06	39.38
279.71	37.23	202.91	35.64	338.39	39.46
286.31	37.48				

[a] T is the average temperature of each determination. [b] C_s is the heat capacity of the condensed phase at saturation pressure. [c] Values not corrected for premelting.

Table II: Summary of Melting Point Study[a]

1/fraction melted	T, °K.
3.87	186.166
2.52	186.287
1.86	186.342
1.47	186.387
1.00 (this sample)	186.401
0.00 (100% pure)	186.477

[a] T_{tp} = 186.48°K.; N_2^* = 0.0022.

experimental points are available, ideally all the lines should intersect at a single point defining a unique potential function.

By interpolation and a short extrapolation of the smoothed entropies of Table III, it is possible to calculate the experimental liquid entropy at three of the five temperatures at which N.K.M. measured the heat of vaporization. Table V gives the calculated values of the ideal gas entropy at these temperatures. The gas imperfection correction and compression terms are based on data given by N.K.M. These three entropy values and the five vapor heat capacity values measured by N.K.M. can be used to give eight lines on a V_1 *vs.* V_2 plot. The molecular parameters and vibrational assignment selected by N.K.M. were used to calculate the contributions of all but the skeletal rotation. The methyl barriers of 1000 and 2400 cal./mole selected by N.K.M. did not give a plot yielding a point which simultaneously satisfied both entropy and heat capacity data. By trial and error, it was found that methyl barriers of 1200 and 2950 cal./mole gave the plot shown in Fig. 1. There is no unique point of intersection, but a range of approximate tangency which fits the data within experimental error. Infrared and Raman spectra show no evidence of rotational isomers other than the *trans* configuration.[1] A final selection for the skeletal rotation potential function was therefore made at $V_1 = V_2 = 1260$ cal./mole, values which eliminate any potential well at the skew position, thus implying no stable configuration other than the *trans*, and also fit the data within experimental error. Because of the many variables involved, it cannot be claimed that this is a unique solution, but the true shape of the potential function cannot be far from that derived and shown in Fig. 2. Employing the above parameters, the thermodynamic functions of methyl ethyl ketone were calculated and are compared with experimental values in Table VI.

From the results of N.K.M. the standard heat of vaporization at 298°K. is calculated as 8.34 kcal. mole^{-1}. Combined with the experimental heat of for-

Table III: Molal Thermodynamic Functions of Methyl Ethyl Ketone

T, °K.	C_p, cal./°K.	S, cal./°K.	$H_T - H_0/T$, cal./°K.	$F_T - H_0/T$, cal./°K.	$H_T - H_0$, cal.
13.00	0.940	0.345	0.259	0.086	3.4
15.00	1.472	0.517	0.385	0.132	5.8
20.00	2.966	1.146	0.844	0.301	16.9
25.00	4.415	1.965	1.415	0.550	35.4
30.00	5.761	2.891	2.029	0.862	60.9
35.00	7.114	3.882	2.660	1.222	93.1
40.00	8.358	4.914	3.296	1.618	131.8
45.00	9.453	5.963	3.920	2.043	176.4
50.00	10.41	7.010	4.522	2.487	226.1
60.00	11.99	9.053	5.641	3.412	338.5
70.00	13.42	11.01	6.651	4.359	465.6
80.00	14.74	12.89	7.580	5.309	606.4
90.00	15.89	14.69	8.441	6.252	759.7
100.00	16.91	16.42	9.237	7.183	923.7
110.00	17.91	18.08	9.981	8.099	1098
120.00	18.82	19.68	10.68	8.997	1282
130.00	19.69	21.22	11.34	9.878	1474
140.00	20.58	22.71	11.97	10.74	1676
150.00	21.51	24.16	12.57	11.59	1886
160.00	22.40	25.58	13.16	12.42	2106
170.00	23.20	26.96	13.73	13.23	2334
180.00	23.89	28.31	14.27	14.03	2569
186.48	24.30	29.16	14.62	14.54	2725
		Liquid			
186.48	35.60	39.98	25.43	14.54	4742
190.00	35.67	40.64	25.62	15.02	4868
200.00	35.79	42.47	26.13	16.35	5225
210.00	35.90	44.22	26.59	17.64	5583
220.00	36.02	45.90	27.01	18.88	5943
230.00	36.14	47.50	27.41	20.09	6304
240.00	36.31	49.04	27.78	21.27	6666
250.00	36.52	50.53	28.12	22.41	7030
260.00	36.77	51.96	28.45	23.52	7397
270.00	37.06	53.36	28.76	24.59	7766
280.00	37.37	54.71	29.06	25.65	8138
290.00	37.70	56.03	29.36	26.67	8513
298.15	37.98	57.08	29.59	27.49	8821
300.00	38.05	57.31	29.64	27.67	8892
310.00	38.42	58.56	29.92	28.65	9274
320.00	38.83	59.79	30.19	29.60	9660
330.00	39.23	60.99	30.46	30.53	10051
335.00	39.42	61.58	30.59	30.99	10247

mation of the liquid, the heat of formation of the ideal gas is calculated as -56.97 ± 0.30 kcal. mole^{-1}. Employing this value with calculated thermodynamic functions at even temperatures and properties of the elements from Stull and Sinke[14] gives the chemical thermodynamic properties listed in Table VII.

Table IV: Heats of Combustion and Formation of Methyl Ethyl Ketone

Sample purity, mole %	Total cal.	Mylar, cal.	Fuse, cal.	Wash-burn cor., cal.	Sample mass, g.	$-\Delta E_c°/M$, cal./g.
99.74	6647.3	426.2	9.2	2.5	0.76773	8088.0
99.74	6692.6	486.8	9.5	2.6	0.76576	8088.3
99.85	7129.3	481.6	10.5	2.8	0.82005	8090.2
99.85	6895.1	490.3	10.3	2.6	0.78942	8096.9
99.85	7274.9	495.6	9.4	2.8	0.83727	8082.3
99.85	7159.4	489.2	9.5	2.8	0.82315	8088.3
					Av.	8089.0
					σ =	1.9

$\Delta E_c°$ = −583.28 kcal./mole
$\Delta H_c°$ = −584.17 kcal./mole
$\Delta Hf°_{298}$ (l) = −65.31 ± 0.29 kcal./mole

Table V: Experimental Molal Entropy of Methyl Ethyl Ketone, cal. deg.$^{-1}$

	T, °K. 314.61	338.69	352.54
S (l)	59.132	62.017	63.613
$\Delta H_v/T$	25.647	22.749	21.206
Compression	−2.768	−0.933	−0.010
Gas imperf.	0.151	0.250	0.319
$S°$(g)	82.162	84.083	85.128

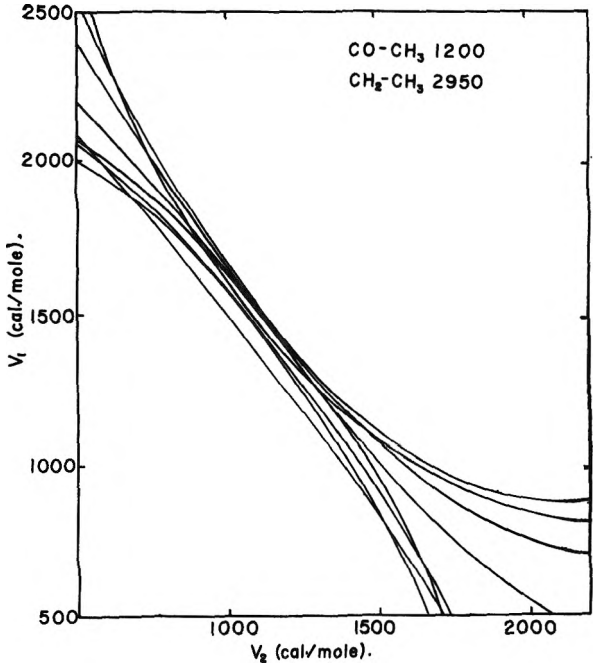

Figure 1. Plot to determine potential function for skeletal rotation.

Table VI: Comparison of Experimental and Calculated Values

T, °K.	S(calcd.)	S(exptl.)	Dev.
314.61	82.14	82.16	0.02
338.69	84.06	84.07	0.01
352.54	85.18	85.13	−0.05
	C(calcd.)	C(exptl.) (N.K.M.)	Δ
347.15	27.09	27.11	0.02
372.15	28.39	28.45	0.06
397.15	29.68	29.73	0.05
432.15	31.47	31.48	0.01
467.15	33.20	33.13	−0.07

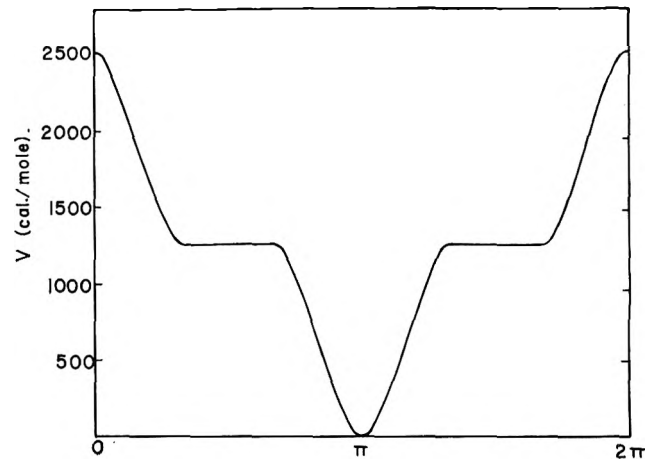

Figure 2. Potential function for skeletal rotation.

Comparison with Earlier Work

The heat capacities for the condensed phases reported by Parks and co-workers[2] are from 0.5 to 4.2% higher than the present work over the entire range. Their derived entropy at 298°K. of 57.7 cal. mole^{-1} °K.$^{-1}$ is therefore significantly higher than the present work (57.08 cal. mole^{-1} °K.$^{-1}$). When calculated to the gas phase, the present work gives 80.81 cal. mole^{-1} °K.$^{-1}$ as compared to 82.51 cal. mole^{-1} °K.$^{-1}$ reported by N.K.M. This discrepancy was resolved when it was learned that mathematical errors had been made in the vapor heat capacity calculations and the corrected entropy is 80.91 cal. mole^{-1} °K.$^{-1}$ in excellent agreement with the present result.[15] The heat of formation based on the heat of combustion of the liquid reported by Parks and co-workers[2] is 1.37 kcal. more negative than our result, while the flame calorimeter value of Crog[4] is 2.32 kcal. more negative. Two modern values for 2-butanol[5,6] are in excellent agreement at ΔHf_{298}(l) = −81.89 kcal. mole^{-1}. The measured heat of hydrogenation of methyl ethyl ketone by Dolliver, *et al.*,[7] and the heat of hydrogenation from equilibrium constants by Cubberley and Mueller[8] are also in excellent agreement at ΔH_{298} = −12.955 kcal. mole^{-1}. Combination of these results with the heat of vaporization of 2-butanol[16] yields for methyl ethyl ketone $\Delta Hf°_{298}$(g) = −56.90 kcal. mole^{-1}. This last value, which is judged the most reliable of the three earlier results, is in good agreement with the heat of combustion of this research.

Table VII: Molal Chemical Thermodynamic Properties of Methyl Ethyl Ketone[a]

T, °K.	$C_p°$, cal. deg.$^{-1}$	$S°$, cal. deg.$^{-1}$	$H° - H°_{298}$, kcal.	$\Delta Hf°$, kcal.	$\Delta Ff°$, kcal.	log Kf
298.15	24.59	80.81	0.000	−56.97	−34.92	25.595
300	24.68	80.96	0.046	−57.00	−34.78	25.338
400	29.81	88.76	2.769	−58.39	−27.16	14.840
500	34.76	95.96	6.002	−59.60	−19.21	8.397
600	39.09	102.69	9.700	−60.59	−11.04	4.022
700	42.83	109.00	13.800	−61.38	− 2.71	0.847
800	46.08	114.94	18.250	−61.99	+ 5.71	−1.560
900	48.90	120.53	23.001	−62.45	14.20	−3.448
1000	51.33	125.81	28.016	−62.74	22.73	−4.968

[a] To retain internal consistency, some values are given to one more decimal place than justified by the absolute accuracy.

(14) D. R. Stull and G. C. Sinke, "Thermodynamic Properties of the Elements," Advances in Chemistry Series, No. 18, American Chemical Society, Washington, D. C., 1956.

(15) J. J. McKetta and E. T. Beynon, Jr., personal communication, 1963.

(16) N. S. Berman and J. J. McKetta, *J. Phys. Chem.*, 66, 1444 (1962).

Radiolysis of Acid Aqueous Solutions of Aquopentaammine- and Hexaamminecobaltic Ions[1]

by D. Katakis[2] and A. O. Allen

Chemistry Department, Brookhaven National Laboratory, Upton, New York *(Received November 16, 1963)*

On irradiation with γ-rays in acid solution, the aquopentaammine and hexaammine complexes of Co(III) decompose to give Co(II) and nitrogen. The decomposition is inhibited by bromide, chloride, and bisulfate ions, but seems to require the presence of Co(II) ions. The reaction is thought to involve an attack on the complexes by OH radicals, catalyzed by Co(II).

Very little has been published on the radiation chemistry of the complex ions of metals other than iron. Egunov and Dolin[3] have made some qualitative observations on irradiation of solutions of nickel and cobalt ammines. The present results concern the irradiation with γ-rays of solutions of aquopentaamine- and hexaamminecobaltic ions in 0.1 N acid solutions.

Experimental

The irradiations were made with Co^{60} γ-rays. The dose rate was determined with the Fricke dosimeter using $G(Fe^{+3}) = 15.5$ and $\epsilon_{305} = 2180$ at 24°. $[Co(NH_3)_5CO_3]NO_3$ was prepared by the method described by Basolo and Murmann[4] and used further for the preparation of $[Co(NH_3)_5OH_2](ClO_4)_3$. The complex was recrystallized three times from triply distilled water.

Commercial $Co(NH_3)_6Cl_3$ (City Chemical Corp.) was used for the preparation of $[Co(NH_3)_6](ClO_4)_3$. The salt was again recrystallized and washed exhaustively with triply distilled water. Cobalt(II) perchlorate was prepared from the carbonate by treatment with $HClO_4$. Water used for the preparation of the solutions was triply distilled. All other reagents were analytical grade and used without further purification.

Co^{+2} was determined by extraction. Five ml. of the irradiated complex solution and 5 ml. of a NH_4SCN solution (566 g. of NH_4SCN/l.) were shaken for approximately 1 min. with 5 ml. of purified methyl isobutyl ketone and the optical density of the organic layer was measured at 6200 Å. The Co^{+2} concentration was estimated by reference to a calibration curve. At optical densities higher than 0.2 the Co^{+2} concentration is given by the empirical formula

$$(Co^{+2}) = 5.43 \times 10^2(O.D. - 0.022)\ \mu M$$

Solutions of the complex always contained some Co^{+2} ($\sim$20 μM) which was taken care of by the blank.

H_2O_2 in $Co(NH_3)_5OH_2^{+3}$ solutions was determined by the Ti method.[5] The extinction coefficient at 406 mμ was determined by comparison with the I^- method. It varies slightly for different preparations of the Ti solution. In our case it was found to be only 0.040 as much as that for the I^- method. Beer's law is obeyed. The complex, Co^{+2}, $HClO_4$, and $HClO_3$ do not interfere.

The low pressure combustion technique[6] was used for O_2 and H_2. N_2 was determined by difference.

Qualitative tests for NO_2^-, NO_3^-, NH_2OH, and NH_2-NH_2[7] in samples irradiated in the absence of air failed to reveal the presence of any of these species. In samples irradiated in the presence of air these compounds

(1) Research performed under the auspices of the U. S. Atomic Energy Commission.

(2) Nuclear Research Center "Democritus," Aghia Paraskevi Attikis, Athens, Greece.

(3) A. V. Egunov and P. I. Dolin, *Dokl. Akad. Nauk SSSR*, **142**, 1 (1962).

(4) F. Basolo and R. K. Murmann, *Inorg. Syn.*, **4**, 171 (1953).

(5) G. M. Eisenberg, *Ind. Eng. Chem., Anal. Ed.*, **15**, 327 (1943).

(6) E. R. Johnson and A. O. Allen, *J. Am. Chem. Soc.*, **74**, 4147 (1952).

(7) F. Feigl, "Qualitative Analysis by Spot Tests," Elsevier Publishing Co., New York, N. Y., 1946.

were also absent, except that the brucine test for NO_2^- and NO_3^- was inconclusive, perhaps due to interference by H_2O_2. Chlorate ion is formed from direct action of radiation on $HClO_4$.[8] At the low perchloric acid concentrations and doses used here, however, the amount is negligible.

Results

Air-Free Solutions of $[Co(NH_3)_5OH_2](ClO_4)_3$ *in 0.1 N* $HClO_4$. On irradiation, the concentrations of H_2, H_2O_2, and CO_2 (from impurities) reach a low and irreproducible steady state at concentrations of a few μM, a behavior reminiscent of that of pure water.[9] The cobalt, however, is reduced to Co^{+2}, as shown in Fig. 1. There is an induction period which is removed by addition of Co^{+2}. The decrease in complex concentration was checked in a few runs and found equal to the Co^{+2} formed. Absorption spectra of irradiated solutions showed nothing except the spectra of $Co(NH_3)_5OH_2^{+3}$ and Co^{+2}. After the induction period, $G(Co^{+2}) = 1.8$.

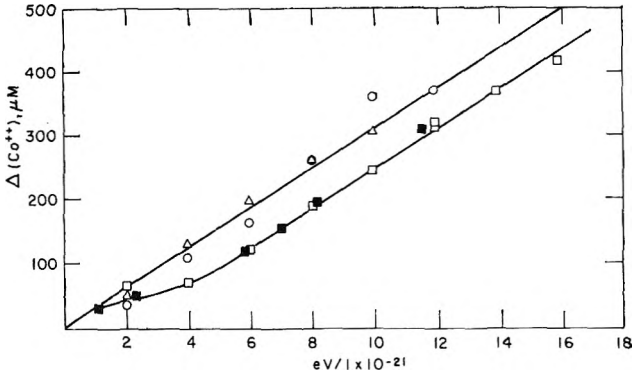

Figure 1. Formation of Co^{+2} in air-free aquopentaamminecobaltic solutions, 0.1 N in $HClO_4$, at a dose rate of 3.31 $\times$ 10^{20} e.v./l. min.: O, $Co(NH_3)_5OH_7^{+3}$ 5.66 $\times$ 10^{-4} M, Co^{+2} 10^{-4} M; △, $Co(NH_3)_5OH_2^{+3}$ 5.66 $\times$ 10^{-4} M, Co^{+2} 1.98 $\times$ 10^{-4} M; □, $Co(NH_3)_5OH_2^{+3}$ 5.66 $\times$ 10^{-4} M; ■, $Co(NH_3)_5OH_2^{+3}$ 1.68 $\times$ 10^{-3} M.

The oxidation product corresponding to the cobalt reduction is nitrogen gas. Five determinations at a dose of 56.5 $\times$ 10^{20} e.v./l. gave N_2 concentrations ranging from 12.2 to 20.3 μM; the Co^{+2} concentration at this dose is 112 μM. The over-all reaction appears to be

$$6Co(NH_3)_5OH_2^{+3} + 22H^+ = 6Co^{+2} + N_2 + 28NH_4^+ + 6H_2O$$

Air-Saturated Solutions of $[Co(NH_3)_5OH_2](ClO_4)_3$. The presence of air lowers $G(Co^{+2})$ to 0.8 (Fig. 2). The H_2O_2 yield is the same as in the absence of any

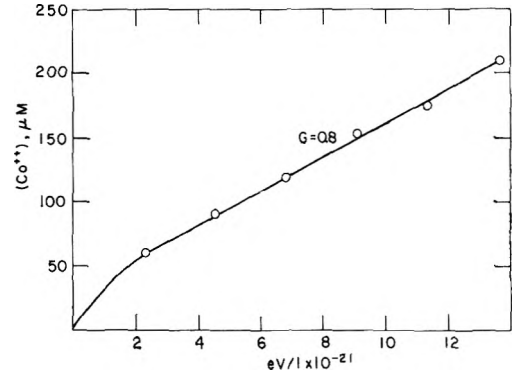

Figure 2. Formation of Co^{+2} in air-saturated 2.8 $\times$ 10^{-3} M aquopentaamminecobaltic solution, 0.1 N in $HClO_4$, at a dose rate of 3.7 $\times$ 10^{20} e.v./l. min.

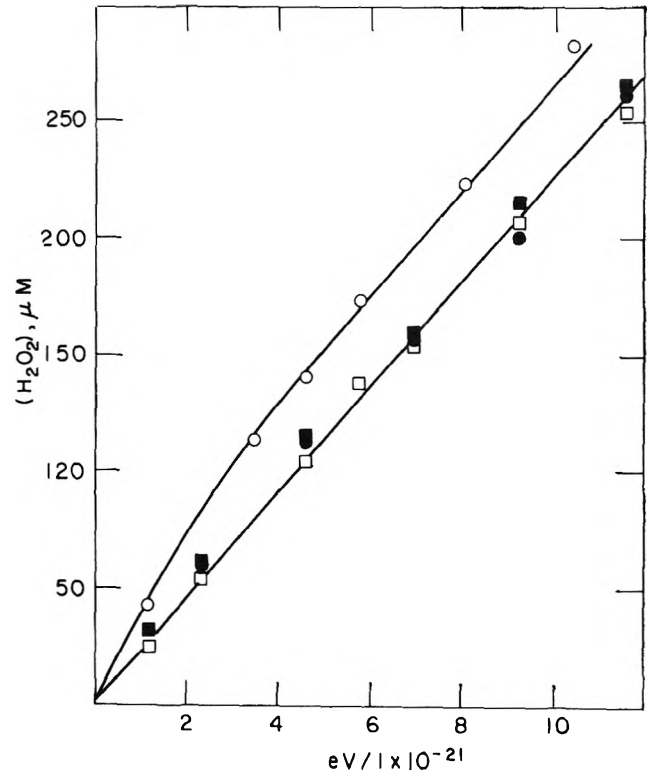

Figure 3. Peroxide formation in air-saturated solutions, 0.1 N in $HClO_4$, at a dose rate of 3.8 $\times$ 10^{20} e.v./l min.: O, $Co(NH_3)_5OH_7^{+3}$ 4.6 $\times$ 10^{-4} M; ●, $Co(NH_3)_5OH_2^{+3}$ 4.6 $\times$ 10^{14} M, Co^{+2} 2.3 $\times$ 10^{-4} M; □, no cobalt salt added; ■, Co^{+2} 2.3 $\times$ 10^{-4} M.

added salt, both in 0.1 M $HClO_4$ (Fig. 3) and 0.1 N H_2SO_4 (Fig. 4). The curves both of (Co^{+2}) and (H_2O_2) *vs.* dose have positive intercepts that are removed by

(8) D. Katakis and A. O. Allen, *J. Phys. Chem.*, submitted for publication.

(9) H. Fricke, E. J. Hart, and P. H. Smith, *J. Chem. Phys.*, 6, 229 (1938).

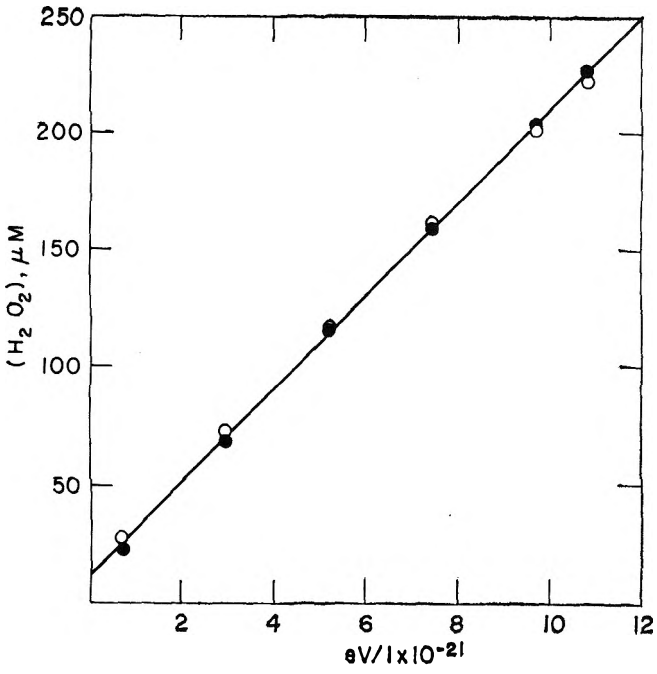

Figure 4. Peroxide formation in air-saturated solutions, 0.1 N in H_2SO_4, at a dose rate of 3.8×10^{20} e.v./l. min.: O, $Co(NH_3)_5OH_2^{+3}$ 4.6×10^{-4} M; ●, no cobalt salt added.

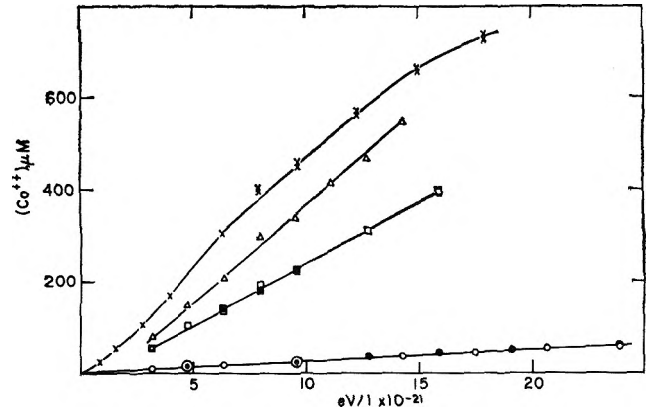

Figure 5. Formation of Co^{+2} in air-free 1 mM hexaammine-cobaltic solutions, 0.1 N in $HClO_4$: O, NaCl 10^{-2} M, dose rate 3.18×10^{20} e.v./l. min.; ●, KBr 10^{-2} M, dose rate 3.18×10^{20} e.v./l. min.; □, Na_2SO_4 10^{-2} M, dose rate 3.18×10^{20} e.v./l. min.; ■, Na_2SO_4 2×10^{-2} M, dose rate 3.18×10^{20} e.v./l. min.; Δ, only the complex, dose rate 3.18×10^{20} e.v./l. min.; ×, only the complex, dose rate 1.38×10^{19} e.v./l. min.

initial addition of Co^{+2} (data bearing on this point not shown here for Co^{+2}). These intercepts may be due to impurities introduced with the complex.[10]

Air-Free Solutions of 1 mM $Co(NH_3)_6(ClO_4)_3$ in 0.1 N $HClO_4$. Figure 5 summarizes the results. $G(Co^{+2})$ after the induction period is 2.5 at the higher dose rate. Addition of 10 or 20 mM Na_2SO_4 reduces $G(Co^{+2})$ to 1.6; addition of 10 mM NaCl or KBr reduces it to 0.15. At the lower dose rate the induction period is shorter, but the product–dose curve after the induction period appears less precisely linear. The reduction again appears to be balanced by the formation of nitrogen gas. In solutions with added chloride, hydrogen was found to appear with its normal G value of 0.45.

Discussion

We shall attempt to explain the above results in terms of reactions of H and OH radicals. It seems clear that the reduction of either complex is not due in any important measure to its reaction with H atoms. This is shown most clearly by the strong inhibition of the hexaammine complex decomposition by chloride or bromide ions which are known[11] to interfere with reactions of OH, but not of H. Since nitrogen is a product, we must assume that oxidizing radicals attack the complex, oxidizing an ammonia molecule and thereby breaking up the complex. The trivalent cobalt is left in a less stable form, which is attacked by H atoms and reduced to Co^{+2}. Thus, the reaction consumes one oxidizing radical and one reducing radical and the *difference* in the available numbers of reducing and oxidizing radicals (which governs the peroxide yield in aerated solutions[11]) remains unchanged—hence, the lack of effect of the pentaammine complex on $G(H_2O_2)$ in air. Ammonia is known to be oxidized by radiation (in the presence of an electron acceptor) in alkaline but not in acid aqueous solutions,[11] presumably because the NH_3 molecule can react with oxidizing radicals, while the NH_4^+ ion cannot. If the pentaammine complex were reduced directly by H atoms, the ammonia in these acid solutions would be liberated in the form of NH_4^+, and the excess oxidizing radicals would have to appear eventually in the form of peroxide or oxygen. The postulate of initial attack on the NH_3 in the complexes by oxidizing radicals is thus required for a consistent picture.

Now there is evidence that Co^{+2} is oxidized by OH radicals. Lefort reports[12] that Co^{+3} in 0.8 N H_2SO_4 is reduced by γ-rays with the same yield (measured in reducing equivalents) as Ce(IV), O_2, and other oxidizing agents (G = 2.4). But these yields depend on the difference of the H and OH yields, and the result implies that the OH radical acts to reduce the yield by reoxidiz-

(10) A. O. Allen and R. A. Holroyd, *J. Am. Chem. Soc.*, 77, 5852 (1955).

(11) (a) A. O. Allen, "The Radiation Chemistry of Water and Aqueous Solutions," Van Nostrand, Princeton, N. J., 1961; (b) T. Rigg, G. Scholes, and J. Weiss, *J. Chem. Soc.*, 3034 (1952); M. A. Proskurnin and Y. M. Kolotyrkin, *Proc. Intern. Conf. Peaceful Uses At. Energy, 2nd Geneva*, 29, 52 (1958).

(12) M. Lefort, *J. chim. phys.*, 54, 782 (1957).

ing the product, Co^{+2}. We might then expect that Co^{+2}, like Cl^-, Br^-, or HSO_4^- which also are oxidized by OH,[11,13,14] would reduce the yield of decomposition of the complex. This is not so; instead, the existence of an induction period suggests that presence of Co^{+2} at a concentration of at least 0.6×10^{-4} M is required for the decomposition to proceed with its full yield. To explain this, we may assume that OH does not attack the complex directly. Instead, it reacts with Co^{+2}; but the product, which we may write as $Co(OH)^{+2}$, does not immediately rearrange to the more stable $Co^{+3}(aq)$, which is known to be inert toward both aquopentaammine[15] and hexaammine[16] complexes. The $Co(OH)^{+2}$ remains for a finite time in a more active form and this form is able to attack the ammonia complexes, resulting in oxidation of an ammonia molecule. The oxidized nitrogen must go through a complicated series of steps before winding up as the final product, N_2. We have no evidence regarding the detailed nature of these steps.

In support of this mechanism, the yield of decomposition of the hexaammine complex, $G = 2.5$, is nearly equal to the accepted value of the yield of OH in acid solutions.[11] However, the yield is lower with the pentaammine complex. Here, we may assume that $Co(OH)^{+2}$ reacts slowly with this complex, so that some of it has time to rearrange to $Co^{+3}(aq)$, and attack on the complex is reduced. The further reduction in yield caused by the presence of oxygen may be due to oxygen catalysis of the rearrangement.

During the induction period, H and OH find little to react with and, as in pure water, some of them will eventually disappear by reacting with each other. Increasing the dose rate increases the dose required to go through the induction period by favoring radical–radical reactions relative to the reaction of OH with Co^{+2}.

Bromide and chloride ions react with OH to form Br and Cl atoms. Since both inhibit the reaction equally, it seems probable that neither Br nor Cl can bring about any reaction of the cobaltammine complex. The very small residual attack on the complex ($G = 0.15$) must arise through a different mechanism, perhaps an attack on the complex by solvated electrons in competition with their reaction with H^+ to form the H atoms.[17] The existence of this low-yield mechanism, which produces Co^{+2}, explains why the induction period is shorter than might otherwise be expected. Inhibition by HSO_4^- is less since the product of its reaction with OH, the radical HSO_4, probably has a higher free energy than Br or Cl atoms and can associate with Co^{+2} to bring about, to some extent, a reaction with the complex similar to that given by $Co(OH)^{+2}$.

The above mechanism is extremely speculative, but is the only one we can think of which will agree with all the observations. Further work is needed to test various features of the proposed mechanism.

Baxendale, Fielden, and Keene[18] find that in neutral solutions the solvated electron, which is the form taken by the reducing radical at neutral pH, reacts very rapidly with $Co(NH_3)_6^{+3}$, in an encounter-controlled reaction. We find that in acid solutions the H atom, which is formed there, reacts relatively slowly, if at all, with this complex. This result is in line with the greater reactivity of the solvated electron than of the H atom as a reducing agent, which has been shown in the cases of hydrogen peroxide[19] and ferric sulfate.[20] Dixon and Baxendale[17] have further demonstrated the competitive reaction between $Co(NH_3)_6^{+3}$ and H^+ for the electron, in the presence of 0.1 M methanol, and find that the H atoms resulting from the reduction of H^+ all attack the methanol in preference to the cobalt complex, as would be expected from the present work.

(13) H. Taube and W. C. Bray, *J. Am. Chem. Soc.*, **62**, 3357 (1940).

(14) C. J. Hochanadel, *Radiation Res.*, **17**, 286 (1962).

(15) A. Haim and H. Taube, *J. Am. Chem. Soc.*, **85**, 495 (1963).

(16) S. A. Hoshowsky, O. G. Holmes, and K. J. McCallum, *Can. J. Res.*, **B27**, 258 (1949).

(17) J. H. Baxendale, private communication.

(18) J. H. Baxendale, E. M. Fielden, and J. P. Keene, *Proc. Chem. Soc.*, 242 (1963).

(19) N. F. Barr and A. O. Allen, *J. Phys. Chem.*, **63**, 928 (1959).

(20) G. Dobson and G. Hughes, *Trans. Faraday Soc.*, **57**, 1117 (1961).

Absolute Rate Constants for H Atom Reactions in Aqueous Solutions[1]

by J. P. Sweet and J. K. Thomas

Argonne National Laboratory, Argonne, Illinois *(Received November 22, 1963)*

The radiolysis of ferric sulfate solutions in 10^{-2} N sulfuric acid saturated with hydrogen gas has been carried out with short 1-μsec. pulses on a linear electron accelerator and with larger 0.01-sec. pulses on a Van de Graaff electron accelerator. Examination of the results gave the rate constant for H atom recombination $2k_1 = 2.0 \times 10^{10}$ M^{-1} sec.$^{-1}$ and the rate constant for the H atom reaction with ferric ion under these conditions as $k_2 = 9.0 \times 10^7$ M^{-1} sec.$^{-1}$. The rate constant for the reaction of H atoms with hydrogen peroxide was also measured spectroscopically by following at 365 mμ the Cl_2^- transient formed *via* $H + H_2O_2 \xrightarrow{\text{rate determining}} OH + H_2O$, $OH + Cl^- \xrightarrow[\text{fast}]{H^+ + Cl^-} Cl_2^-$. This was found to be $0.90 \pm 0.1 \times 10^8$ M^{-1} sec.$^{-1}$. These results are discussed and related to other rate constants in solution and in the gas phase.

Introduction

In the past decade the extensive development in radiation chemistry has called more and more for further detail both in the mechanism of the radiolysis process and in the subsequent chemical reactions. With regard to the latter, the literature has contained[2-6] several attempts to estimate the absolute rate constants for the reactions in aqueous solutions of H atoms, OH radicals, and hydrated electrons, with themselves and with solutes. In the case of the solvated electron the problem is greatly simplified as this species absorbs strongly in the visible part of the spectrum and hence may be conveniently followed continuously during any of its reactions. However, H atoms and OH radicals have no strong absorption bands to enable us to observe them and only "kinetic" methods have been used in the measurement of their rate constants. These kinetic methods usually require some simplifying device, either chemical or mathematical, in order finally to elucidate their rate constants.

In the present work the choice of a suitable system greatly simplified the mathematical treatment and introduced no error into the calculations. The system used was ferric ion solutions supersaturated or saturated with 1 atm. of H_2 (0.8 mM H_2) at pH 2.1 (H_2SO_4) such that all the e_{aq}^- gave H atoms *via* $e_{aq}^- + H_3O^+$ ($\tau_{1/2} < 10^{-7}$ sec.). Two experimental conditions were used: (a) The solutions were irradiated with 1-μsec. pulses of 13-Mev. electrons in a linear accelerator, and (b) the solutions were irradiated for short irradiation times (0.002-0.01 sec.), with a steady 1-Mev. electron beam from a Van de Graaff generator.

In the linear accelerator radiations, approximately 10^{-7} M or less of H + OH radicals were produced per liter per 1-μsec. pulse. Hence, if we assume that previous work[2-4] is correct and k_{H+H} is $\sim 10^{10}$, then no significant reaction takes place during the pulse, the half-life of the radicals being 500 μsec. At the end of the pulse, knowing the dosimetry of the apparatus we then know the H + OH radical concentrations. It has been reported[2a] that $k_{OH+OH}/k_{OH+H_2} = 10^6$, hence, with 1 atm. of H_2 over the solution, all the OH radicals would react with the H_2 to give H atoms (half-life $\sim$ 20 μsec.). Hence, before any significant radical–radical reactions occurred, the OH radicals had reacted to produce H atoms raising the concentration to I-(G(H) + G(OH))/l. pulse where I is the radiation intensity/l. pulse.

The addition of ferric ion to this system tended to

(1) Based on work performed under the auspices of the U. S. Atomic Energy Commission.

(2) (a) H. A. Schwarz, *J. Phys. Chem.*, **66**, 255 (1962); (b) J. K. Thomas and E. J. Hart, *Radiation Res.*, **17**, 408 (1962).

(3) J. K. Thomas, *J. Phys. Chem.*, **67**, 2593 (1963).

(4) H. Fricke and J. K. Thomas, National Academy of Science, Conference on Basic Mechanisms in the Radiation Chemistry of Aqueous Media, Gatlinburg, Tenn., May, 1963; *Radiation Res. Suppl.*, 4 (1964).

(5) S. Gordon, *et al.*, *J. Am. Chem. Soc.*, **85**, 1375 (1963).

(6) S. Gordon, *et al.*, *Discussions Faraday Soc.*, **36**, 193 (1963).

remove the H atoms *via* $H + Fe^{3+} \rightarrow Fe^{2+} + H^+$ and ferrous ion was produced. Essentially a competition existed between

$$H + H \xrightarrow{k_1} H_2 \qquad (1)$$

and

$$H + Fe^{3+} \xrightarrow{k_2} Fe^{2+} + H^+ \qquad (2)$$

examination of which gave the ratio k_1/k_2 of the rate constants for the reactions.

Under continuous irradiation on the Van de Graaff a stationary state concentration of H atoms was produced in the above solutions. The concentration of H atoms depended on (a) the rate of production of H; (b) the rate of decay *via* reaction 1 and 2. Examination of the system now produced the absolute value of the rate constants for reactions 1 and 2.

Experimental

Triply distilled water was used to make up all the solutions; the hydrogen was Matheson high purity and the other materials used were all of reagent grade. All vessels used were washed with distilled water prior to heating at 500° for 3 hr.

Ferrous ion was analyzed by adding a 0.1% *o*-phenanthroline solution to the irradiated solution and measuring the resulting red color at 510 mμ in a 5- or 10-cm. cell in a Beckman DU spectrophotometer. Calibration of this method of analysis gave an extinction coefficient for the ferrous complex of 11,000 ± 150 in good agreement with the value in the literature.[7] Immediately after irradiation the ferrous solution was dumped into the *o*-phenanthroline solution. This eliminated any reaction of the ferrous ion formed with the molecular H_2O_2 which was produced, half-life greater than 30 min., the resulting ferrous complex being stable toward the H_2O_2.

The solutions were evacuated and saturated with H_2. They were then forced with excess H_2 pressure into the cells or syringes by a method due to Senvar and Hart.[8]

The procedure for irradiating the cells on the linear accelerator has been described together with the Van de Graaff irradiations when the solution flowed past the exit port of the accelerator.[3] Dosimetry was carried out by using the Fricke dosimeter (aerated 10^{-3} *M* Fe^{2+} in 0.8 *N* H_2SO_4); the number of ferric ions produced per 100 e.v., *i.e.*, $G(Fe^{3+})$ was 15.6 for the Linac and Van de Graaff experiments.[2b,3]

Results

Linear Accelerator. The results of the linear accelerator irradiations of 10^{-2} *N* H_2SO_4, saturated with H_2 and containing varying amounts of ferric ion is shown in Fig. 1. The $G(Fe^{2+})$ is plotted against $[Fe^{3+}]/I$ where the intensity I is expressed as the total H atom concentration at the end of the 1-μsec. pulse (this includes the contribution from the $OH + H_2 \rightarrow H + H_2O$ reaction also). The experimental results

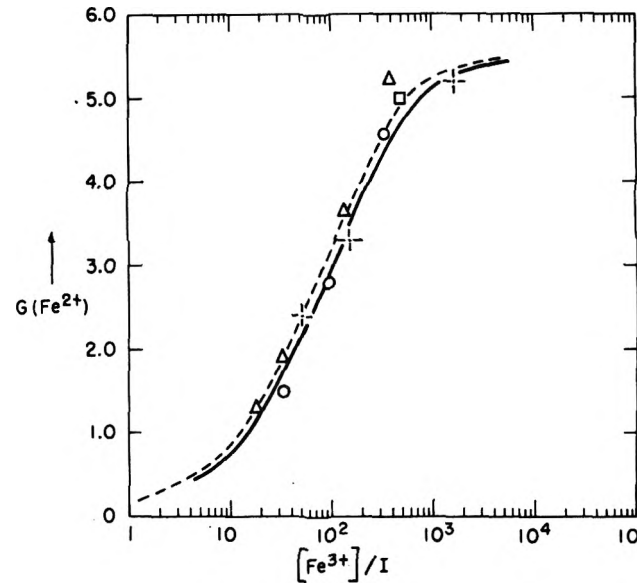

Figure 1. $I(\mu M H/P)$: ○, 0.314; △, 0.079; □, 0.20; +, 0.059; calculated k_1/k_2: – – – –, 100; ——, 125.

were obtained by varying I from 0.059 to 0.31 μ*M* of H/l. pulse. and also the ferric ion from 1.5×10^{-6} to 10^{-4} *M*, the $[H_2SO_4]$ being 10^{-2} *N* and the $[H_2]$ 0.8 m*M* (1 atm. of H_2). In most cases the amount of ferrous ion formed increased linearly with the radiation dose: in cases where this was not obeyed the extrapolation of the ferrous ion yield to zero dose was applied in order to calculate $G(Fe^{2+})$, the number of ferrous ions produced/100 e.v. of energy absorbed by the system.

This system may be described by the equations

$$H_2O \longrightarrow e_{aq}^- + H^+ + OH + H_2 + H_2O_2$$

$$e_{aq}^- + H^+ \longrightarrow H \qquad (a)$$

$$OH + H_2 \longrightarrow H + H_2O \qquad (b)$$

$$H + H \longrightarrow H_2 \qquad (1)$$

$$H + Fe^{3+} \longrightarrow Fe^{2+} \qquad (2)$$

Thus

(7) W. B. Fortune and M. G. Mellor, *Ind. Eng. Chem. Educ.*, **10**, 60 (1938).

(8) C. B. Senvar and E. J. Hart, *Proc. Intern. Conf. Peaceful Uses At. Energy, 2nd, Geneva*, **29**, 19 (1958).

$$\frac{d(H)}{dt} = -2k_1(H)^2 - k_2(H)(Fe^{3+})$$

$$(H) = \frac{k_2(Fe^{3+})(I)}{[2k_1(I) + k_2(Fe^{3+})]\exp[k_2(Fe^{3+})t] - 2k_1(I)}$$

where I is the H atom concentration at the end of the pulse, where $t = 0$, k_1 and k_2 being the rate constants for reactions 1 and 2, respectively. Then the fraction of H atoms combining with the Fe^{3+} is

$$\frac{k_2(Fe^{3+})}{2k_1(I)} \ln\left[1 + \frac{2k_1(I)}{k_2(Fe^{3+})}\right]$$

This predicts that for the experimental conditions that were used, a plot of $G(H_2)$ *vs.* $(Fe^{3+})/I$ should give one universal curve for all intensities; this is seen to be true for the present experiments. The dose rate I was calculated using the measured μM Fe^{3+}/l. pulse from the dosimetry together with a $G(H) + G(OH) = 5.8$. This value for $G(H) + G(OH)$ was taken as the $G(Fe^{2+})$ *vs.* $(Fe^{3+})/I$, extrapolated at high (Fe^{3+}) to 5.80. Also, irradiation of a solution of 10^{-4} M Fe^{3+}, 10^{-2} N H_2SO_4, 0.8 mM H_2 on a Co^{60} γ-ray source gave $G(Fe^{2+}) = 5.80$. The mechanism predicts that at the low intensity on the Co^{60} γ-source (10^{19} e.v. l.$^{-1}$ min.$^{-1}$) and at the extrapolated $G(Fe^{2+})$ in the linear accelerator runs should give $G(Fe^{2+}) = G(H) + G(OH)$. It is essential that no H atoms are lost during the pulse so that the I may be calculated as above. The fact that changing the I_0 by a factor of six had no effect on the position of the curve in Fig. 1 is confirmatory evidence that the H atom reactions are long lived compared with the time that is necessary for both their production processes *via* reactions a and b.

Figure 1 also shows various curves that were calculated assuming different values of k_1/k_2; it was decided that the best experimental fit of calculated to experimental data was obtained with a value of $2k_1/k_2$ of between 250/1 and 200/1. Hence from the present data $2k_1/k_2$ was found to be 225 ± 25.

Van de Graaff. Ferric ion solutions in 10^{-2} N H_2SO_4 under 1 atm. of H_2 were irradiated for short periods with a 1-Mev. electron beam from a Van de Graaff accelerator. The ferric ion concentration was varied from 10^{-5} to 10^{-4} M and the intensity from 3.10×10^{21} to 3.2×10^{22} e.v. l.$^{-1}$ sec.$^{-1}$. The solutions were flowed past the accelerator port through a 1- or 2-mm. diameter capillary tube at flow rates close to 1 ml./sec. A lead collimator determined the length of the irradiation period, *e.g.*, with a 2-mm. opening of the collimator, a 1-mm. diameter capillary, and a flow rate of 1 ml./sec., the solution was irradiated for approximately 0.002 sec. The exact flow rate varied within 10% depending on the particular 100-ml. syringe and the exact diameter of the flow tubes also varied from tube to tube. These differences were noted and the necessary corrections were always made. Various irradiation times were given to a solution by varying the lead collimator and in all cases the production of Fe^{2+} was proportional to the irradiation time indicating that no secondary back reactions of the products took place. The results are shown in Fig. 2 where $G(Fe^{2+})$ is plotted against $[Fe^{3+}]/I^{1/2}$, where I is the intensity expressed [H]/l. pulse.

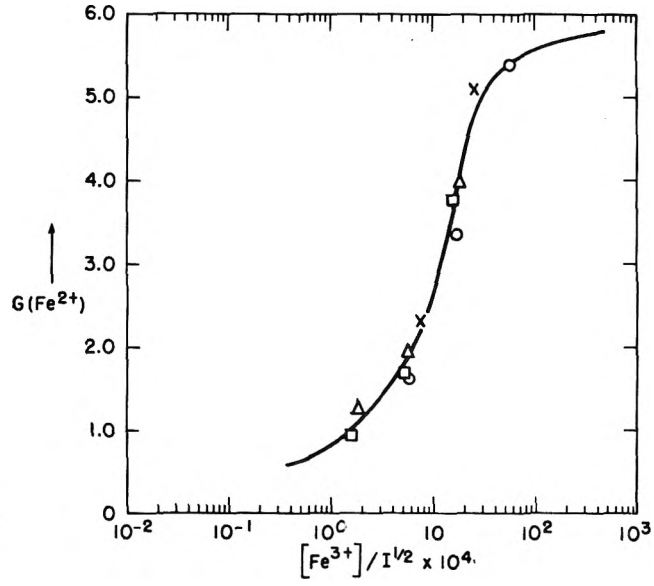

Figure 2. Intensity, mM H/S (G(H) = 5.8): O, 0.347; △, 2.65; □, 3.31; ×, 1.59.

Under these irradiation conditions in a time which was short (*e.g.*, 10% or less) compared to the irradiation period, a stationary concentration of H atoms was closely approximated and the following expression then can be written

$$\frac{d(H)}{dt} = 0 = I - 2k_1(H_s)^2 - k_2(H_s)(Fe^{3+})$$

where (H_s) is the stationary concentration of H atoms. If we denote

$$\frac{(H_s)}{(Fe^{3+})} = x$$

then

$$I = 2k_1x^2(Fe^{3+})^2 + k_2x(Fe^{3+})^2$$

$$= 225x^2k_2(Fe^{3+})^2 + k_2x(Fe^{3+})^2$$

i.e.

$$\frac{(Fe^{3+})^2}{I} = \frac{1}{k_2(225x^2 + x)}$$

At any $(Fe^{3+})^2/I$, the corresponding x may be calculated from the expression

$$G(Fe^{2+}) = (G(H) + (G(OH)) \times \frac{k_2(H_s)(Fe^{3+})}{k_2(H_s)(Fe^{3+}) + 2k_1(H_s)^2}$$

i.e.

$$\frac{(H_s)}{(Fe^{3+})} = x = \left(\frac{G(H) + G(OH)}{G(Fe^{2+})} - 1\right)\frac{k_2}{2k_1}$$

$$= \left(\frac{5.8}{G(Fe^{2+})} - 1\right)\frac{1}{225}$$

A plot of $(Fe^{3+})^2/I$ against $1/(225x^2 + x)$ is shown in Fig. 3, the slope of which gives $1/k_2$. A value of $9 \times 10^7\ M^{-1}$ sec.$^{-1}$ was obtained for k_2, *i.e.*, $2k_1 = 2.0 \times 10^{10}\ M^{-1}$ sec.$^{-1}$.

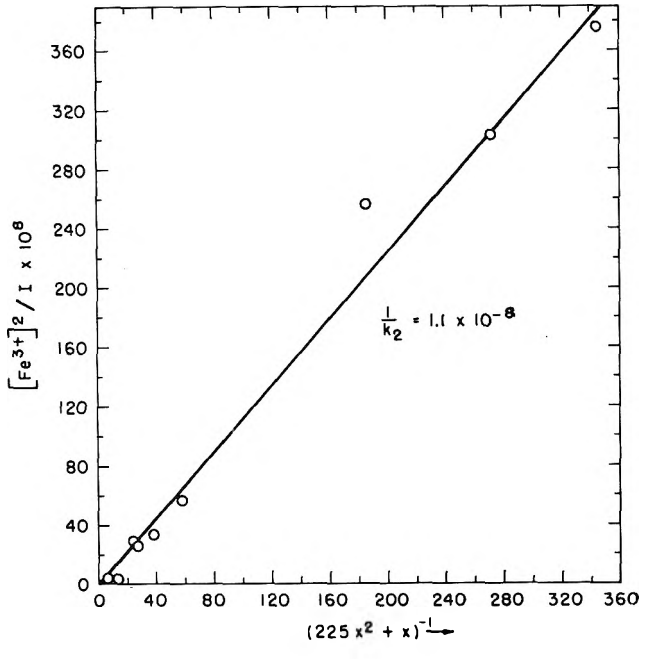

Figure 3. The results from Fig. 2 plotted as $([Fe^{3+}]^2/I) \times 10^8$ *vs.* $(225x^2 + x)^{-1}$.

Spectroscopic Estimate of $k_{H + H}$. In a previous publication[2] a value of $2k_1/k_3 = 250$ was obtained for the ratio of rate constants for the reactions of H atoms with themselves and with hydrogen peroxide. It has been possible to obtain $k_{H+H_2O_2}$ directly by the following pulse radiolysis method.

In 1.0 N sulfuric acid solutions containing 0.2 M NaCl, the reaction $OH + Cl^- \rightarrow Cl \xrightarrow{Cl^-} Cl_2^-$ is rapid and occurs in less than 0.1 μsec. On adding H_2O_2 to this system the reaction

$$H + H_2O_2 \longrightarrow OH + H_2O \qquad (3)$$

occurs and the resultant OH immediately gives Cl_2^-. It thus was possible to arrange the system so that the rate of production of Cl_2^- was governed entirely by the rate of reaction 3. The transient Cl_2^- has a strong absorption at 350 mμ and by using the pulse radiolysis technique described in ref. 5 and 6, it was possible to follow the appearance of the transient Cl_2^- with time. Briefly, a light beam is passed through the H_2O_2 solution and then into a photomultiplier tube. The species produced by the radiation, *i.e.*, Cl_2^- absorbs some of the light causing the output of the photomultiplier tube to change. This change is observed and photographed on a Tektronic oscilloscope.

Figure 4 shows the results obtained with a solution, 1.0 N H_2SO_4, 0.2 M NaCl, $2 \times 10^{-3}\ M$ H_2O_2. The top trace is obtained with no light falling on the photomultiplier and corresponds to a solution with an optical density of infinity. The bottom trace is that obtained with the full light intensity on the phototube; the distance between these lines is I_0. The intermediate trace is that given by the absorbing Cl_2^- species; the distance of this trace from the O.D. = ∞ line gives I_t. The optical density (O.D.) of the species at any time is thus given by $\log I_0/I_t$.

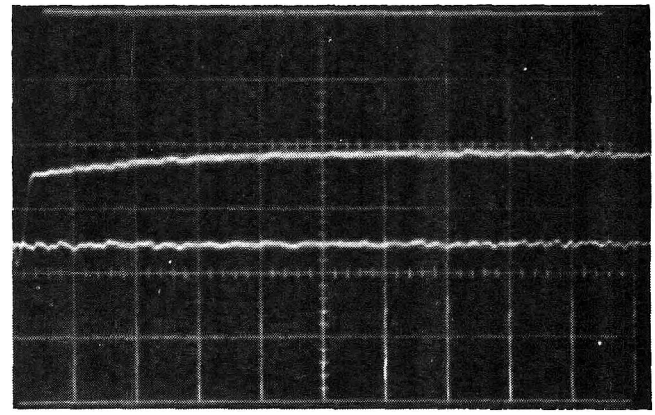

Figure 4. The transient Cl_2^- produced with a 1-μsec. pulse in the radiolysis of a deaerated solution of 1.0 N sulfuric acid, 0.2 M sodium chloride, and 2 mM hydrogen peroxide. The sweep time was 2 μsec. for each small square and approximately 1 μmole of H atoms was produced per liter per pulse. Under these conditions the decay of the Cl_2^- transient has a half-life greater than 100 μsec.

$$-\frac{d(H)}{dt} = \frac{d(Cl_2^-)}{dt} = k(H)(H_2O_2)$$

and

$$(H) = (Cl_2^-)_\infty - (Cl_2^-)$$

where $(Cl_2^-)_\infty$ is the (Cl_2^-) when all the H atoms have reacted and corresponds to the optical density given by the flat part of I_t to the far right of the curve. By substituting we obtain

$$\log\left[\frac{(Cl_2^-)_\infty}{(Cl_2^-)_\infty - (Cl_2^-)_t}\right] = k(H_2O_2)t$$

i.e

$$\log\left[\frac{(O.D.)_\infty}{(O.D.)_\infty - (O.D.)_t}\right] = k(H_2O_2)t$$

A plot of the results obtained from Fig. 4 is shown in Fig. 5. A good pseudo-first-order plot was obtained; the results are shown in Table I, $k_3 = 0.9 \pm 0.1 \times 10^8$ M^{-1} sec.$^{-1}$. In a previous communication[3] a value of 125 was given for $k_{H+H}/k_{H+H_2O_2}$. Hence, from the above value we can calculate k_{H+H} as $1.1 \pm 0.1 \times 10^{10}$ which is in good agreement with the value given by the kinetic method reported here.

Table I: Rate Constant for the Reaction of H Atoms with Hydrogen Peroxide

$[H_2O_2]$, M	$[H^+]$, N	$[Cl^-]$, M	$k \times 10^{-8}$
8.75×10^{-3}	0.8	0.1	0.8
1.72×10^{-2}	0.8	0.1	1.0
8.75×10^{-3}	0.8	0.3	0.8
2×10^{-3}	1.0	0.2	0.93

Discussion

The present values of $2k_1 = 2 \times 10^{10}$ M^{-1} sec.$^{-1}$ and 2.2×10^{10} for the rate constant for the recombination of H atoms in aqueous solution can be compared with the values of 1.2×10^{10} (*cf.* ref. 3), 2.6×10^{10},[4] and 3.0×10^{10}.[9] In the first two references the span in $2k_1$ from 1.2 to 2.6×10^{10} was obtained by the varying importance that was paid to the other reactions involved in the system. In ref. 9, the system, which was Fe^{2+}–H_2SO_4, was complicated by the presence of OH radicals and ferric hydride, $Fe^{2+}H$. The importance of the role of these species in the determination of $2k_1$ was minimized as much as possible by suitable choice of experimental conditions but nevertheless the $2k_1$ of 3×10^{10} which was estimated would tend to be too large. It is possible that the difference of 50% in the value for k_1 between ref. 9 and the present work is not important if the errors in both cases were large enough.

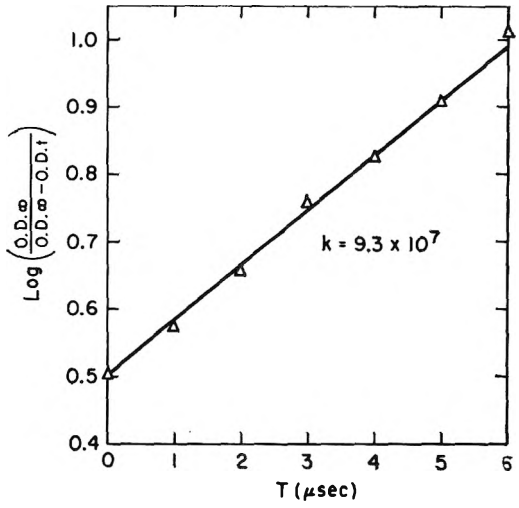

Figure 5. The results from Fig. 4 plotted as a pseudo-first-order reaction.

Riesz and Hart[10] have measured the ratio of rate constants for the reaction of H atoms with ferric sulfate in 10^{-2} N sulfuric acid and deuterium gas. They find a value of 120 in favor of the ferric species present. Combining this with the present value for H + ferric species in 10^{-2} N sulfuric acid gives $k_{H+D_2} = 7.5 \times 10^5$ M^{-1} sec.$^{-1}$. This rate constant has been measured in the gas phase[11-13] and is 0.4×10^5 M^{-1} sec.$^{-1}$ at 25°. The rate in aqueous solution thus seems to be about 20 times that in the gas phase. Previous opinions[14,15] have been in favor of a faster rate for a bimolecular reaction in solution than in the gas phase. To a good degree of approximation, the ratio of the rates for a bimolecular reaction is given by

$$R = \frac{V^\circ_s \times V^\circ_s}{V^\circ_{FH} \times V^\circ_{FD_2}} \frac{V^\circ_{jH-D_2}}{V^\circ_s} e^{-(2-1)}$$

where V°_s is the molar volume of the solvent and V°_{FH} and $V^\circ_{jH-D_2}$ are the free volumes per molecule at their boiling points of the H atom, deuterium gas, and the reaction complex, respectively. Since the specific

(9) H. A. Schwarz, *Radiation Res.*, 19, 181 (1963).

(10) P. Riesz and E. J. Hart, *J. Phys. Chem.*, 63, 858 (1959).

(11) G. Boato, G. Careri, A. Cimino, E. Molinari, and G. G. Volpi, *J. Chem. Phys.*, 24, 783 (1956).

(12) H. L. Friedman and A. H. Zeltmann, *ibid.*, 28, 878 (1958).

(13) J. Hirschfelder, H. Eyring, and B. Topley, *ibid.*, 4, 170 (1936).

(14) S. Glasstone, K. J. Laidler, and H. Eyring, "The Theory of Rate Processes," McGraw-Hill Book Co., Inc., New York, N. Y., 1941, p. 410.

(15) S. W. Bensen, "The Foundations of Chemical Kinetics," McGraw-Hill Book Co., Inc., New York, N. Y., 1960, p. 504.

gravity of liquid D_2 is about 0.1, its molar volume is about that of water. If it is then assumed that the molar volume of H atoms is similar to that of H_2 and D_2, and that the molar volume of the complex $H-D_2$ is the sum of those of the reactants, then on introducing the generalism that for most liquids the free volume is 1% of the molar volume, we have

$$R = \frac{100 \times 2}{e} \simeq 75$$

The present work roughly seems to bear out the above discussion on the influence of physical state on a bimolecular reaction. Studies of similar reactions both in the gas phase and in other solvents should provide a fruitful field of research.

Rothschild and Allen[16] have found that the ratio $k_{H+O_2}/k_{H+Fe^{3+}}$ in 10^{-2} N sulfuric acid is 208, and so it may be estimated that $k_{H+O_2} = 1.9 \times 10^{10}$ in agreement with the previous measurement[3] in the O_2–H_2O_2–H_2SO_4 system which gave 1.2×10^{10} M^{-1} sec.$^{-1}$. Czapski, *et al.*,[17] have determined that $k_{H+O_2}/k_{H+\text{ethanol}} = 1.3 \times 10^3$ while Baxendale and Smithies[18] have determined the relative rates of reaction of H atoms with a series of compounds, a few of which are listed in Table II.

Table II: Rates of Reaction of H Atoms with Solutes[a]

Compound	$k_{H+RH} \times 10^{-9}$
Oxygen	19.0
Benzoquinone	3.1
Cu^{2+}	5.8×10^{-3}
Ethanol	1.5×10^{-2}
Methanol	1.6×10^{-3}
Acetone	3.5
Acetic acid	1.0×10^{-4}

[a] $k_{H+O_2}/k_{H+\text{ethanol}} = 1.3 \times 10^3$ [17]; $k_{H+O_2} = 1.9 \times 10^{10}$ (present work).

Acknowledgment. J. P. S. wishes to thank the A. N. L. and A. M. U. for a Summer Studentship. The authors wish to thank Dr. E. J. Hart for constant support and discussion, Miss P. Walsh who helped in the work, Mr. B. Clifft who operated the Linear Accelerator, and Mr. R. Lowers who operated the Van de Graaff.

(16) W. G. Rothschild and A. O. Allen, *Radiation Res.*, 8, 101 (1958).

(17) G. Czapski, J. Rabani, and G. Stein, *Trans. Faraday Soc.*, 58, 1 (1962).

(18) J. H. Baxendale and D. Smithies, *Z. Physik. Chem.* (Frankfurt), 6, 242 (1956).

Reactions of Carbonyl Compounds with Amines and Derivatives

by R. Bruce Martin

Cobb Chemical Laboratory, University of Virginia, Charlottesville, Virginia *(Received November 26, 1963)*

The results of Cordes and Jencks on semicarbazone, Schiff base, and oxime formation may be described by one of two mechanisms which incorporate the pH–rate profiles and effects of general acid–base catalysis. The first mechanism, involving general acid-catalyzed attack of basic amine at the carbonyl group to yield a protonated tetrahedral addition intermediate followed by decomposition of this intermediate, accounts for the results of the weakly basic semicarbazide and aromatic amines to yield semicarbazones and aromatic Schiff bases, respectively. The second mechanism, involving apparent noncatalyzed attack of the basic amine nucleophile at the carbonyl carbon to yield a tetrahedral addition intermediate followed by general acid-catalyzed decomposition of this neutral intermediate, accommodates the results for the more strongly basic hydroxylamine and aliphatic amines to yield oximes and aliphatic Schiff bases, respectively. The two mechanisms may be combined into a single mechanism with general acid catalysis in both steps and all results for all four nucleophiles accommodated by appropriate Brønsted exponents.

In a noteworthy series of papers, Cordes and Jencks have studied the formation of semicarbazones,[1,2] Schiff bases,[3,4] and oximes[2] in aqueous solutions. They have presented convincing evidence that formation and hydrolysis of these compounds proceed by a two-step mechanism involving a tetrahedral carbon addition intermediate.

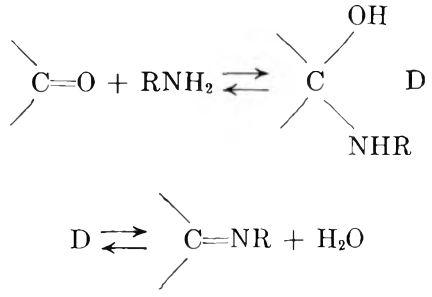

The evidence for a two-step mechanism is based upon maxima in pH–rate profiles obtained when observed first-order rate constants are plotted against pH, presence of general catalysis on only one side of the maxima indicating a change in rate-limiting step, and spectroscopic inference in the case of oximes and semicarbazones. Of the above two reactions, the first is rate limiting in acid solutions and the second in neutral solutions.[1-4]

Though presenting the results of general catalytic studies in these systems and indicating which step of the reaction is subject to catalysis, these workers have not derived the kinetic consequences of introduction of general catalysts into the above two-step mechanism. The pH–rate profiles are sufficiently complicated so that along with the requirements of general catalysts only a few mechanisms are kinetically permissible, and these may be further reduced in number by chemical arguments. It is the purpose of this paper to derive the kinetic consequences of the presence of general catalysts in the above two-step mechanism. The results of such a detailed analysis accommodate in a natural and simple way in a single rate equation the pH–rate profile and general catalytic effects. Most of the qualitative conclusions of Cordes and Jencks[1-4] are substantiated, some of the results are thrown into sharper focus, and a few quantitative differences appear. One striking result is the demonstration that Schiff base formation and hydrolysis occur by different mechanisms in aliphatic and aromatic Schiff bases.

(1) E. H. Cordes and W. P. Jencks, *J. Am. Chem. Soc.*, **84**, 4319 (1962).

(2) W. B. Jencks, *ibid.*, **81**, 475 (1959).

(3) E. H. Cordes and W. P. Jencks, *ibid.*, **84**, 832 (1962).

(4) E. H. Cordes and W. P. Jencks, *ibid.*, **85**, 2843 (1963).

Experimental

The rates of two reactions were studied in order to provide information for specific points in the discussion that follows.

The rate of reaction on the acid side of the maximum for oxime formation from acetone and hydroxylamine was studied in aqueous solution at 25.0° and ionic strength 0.32 maintained with KCl. The initial rates of oxime formation were followed at 220 mμ on a Cary 11 spectrophotometer. Table I presents for increasingly acid solutions observed first-order rate constants obtained at about 6×10^{-4} M acetone concentration and second-order rate constants.

Table I: Rate of Reaction of Acetone and Hydroxylamine in HCl Solutions

pH or M HCl	(NH_3OH^+) $\times 10^2$, M	k_{obsd} $\times 10^2$, min.$^{-1}$	$k_{obsd}/(NH_3OH^+)$, min.$^{-1}$ M^{-1}
2.13 (pH)	1.7	26.0	15
1.19 (pH)	1.7	3.8	2.2
0.10 (pH)	1.7	0.51	0.30
2.9 M	0.9	0.20	0.22
2.9 M	1.7	0.33	0.19
2.9 M	3.6	1.00	0.28
6.5 M	1.7	0.31	0.18

The second reaction studied was the hydrolysis rate in strong H_2SO_4 solutions of the Schiff base p-nitrobenzylidene-1,1-dimethylethylamine. It was prepared as described previously,[4] m.p. 76–78°, lit.[4] 72–75°.

Initial rates of hydrolysis of the Schiff base were followed on a Cary 14 spectrophotometer and observed first-order rate constants were calculated from initial slopes of the straight line portion of absorption at 280 mμ *vs.* time curves by the equation

$$k_{obsd} = \frac{dA}{dt} \times \frac{-1}{C(\epsilon_s - \epsilon_p)}$$

where A is the absorption at 280 mμ, C the molar concentration of Schiff base, ϵ_s and ϵ_p, the molar extinction coefficients at 280 mμ in H_2SO_4 solutions of Schiff base and p-nitrobenzaldehyde, are 22,500 and 12,500, respectively. In these acid solutions the Schiff base exhibits an absorption maximum at 280 mμ. Results for k_{obsd} values *vs* molarity of H_2SO_4 obtained at 25.0° are presented in Table II.

A plot of log k_{obsd} *vs.* log a_{H_2O} for the results recorded in Table II yields a curve with an initial slope of 11 or more in dilute acid solutions. It has been suggested[5] that such steep slopes are indicative of reactions inhibited by acid in acidic solutions and a more satisfactory presentation may be made by plotting log $k_{obsd} - H_0$ *vs.* log a_{H_2O} where $-H_0$ refers to the Hammett acidity function.[6] Since the most acid solution of Table II has $-\log a_{H_2O} = 0.38$, the values of the third column show that log $k_{obsd} - H_0$ is only weakly dependent upon log a_{H_2O} with a slope of less than unity. This result indicates that water is functioning neither as a nucleophile nor as a proton transfer acid in the rate determining step[5] for hydrolysis of this aliphatic Schiff base in strongly acid solutions. The significance of this conclusion will be mentioned later.

Table II: Hydrolysis of p-Nitrobenzylidene-1,1-dimethylethylamine in H_2SO_4 Solutions

Concn. of H_2SO_4, M	$k_{obsd} \times 10^4$, min.$^{-1}$	$-\log k_{obsd} + H_0$
2.19	150	0.89
2.91	58	0.92
4.02	14.9	1.01
5.11	5.1	0.96
6.51	0.6	1.18

Semicarbazones

The reaction of several aromatic aldehydes with semicarbazide is general acid catalyzed on the acid side of a pH–rate profile of observed second-order rate constant *vs.* pH and specific hydrogen ion catalyzed on the basic side.[1] A mechanism which can account for the general acid catalysis and pH dependence is mechanism I, where general acid HB

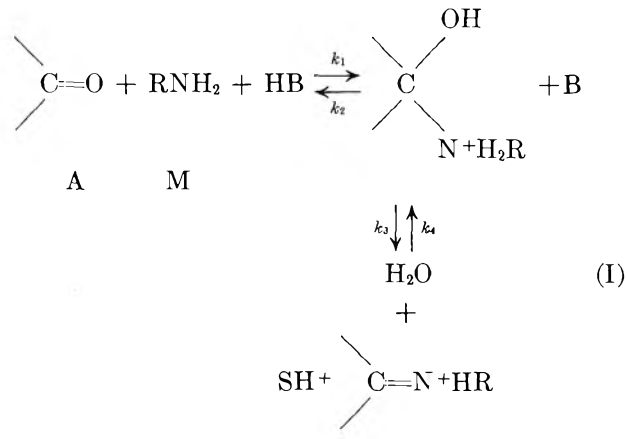

(I)

and general base B are related by the acid ionization constant $K_B = (H^+)(B)/(HB)$. In terms of the symbols assigned to the components in the mechanism, application of the steady-state approximation to the tetrahedral addition intermediate yields for the initial rate of semicarbazone formation

$$R = \frac{k_{obsd}}{C_M}\frac{(H^+) + K_1}{K_1} = \frac{(H^+) + K_1}{K_1 C_M(A)}\frac{d(S)}{dt} = \frac{k_1'(H_3O^+) + k_1''(H_2O) + k_1'''(HB)}{1 + [k_2'(H_2O) + k_2''(OH^-) + k_2'''(B)]/k_3} \quad (1)$$

where $K_1 = (M)(H^+)/(MH^+)$ and $C_M = (M) + (MH^+)$, the total concentration of amine in both acidic and basic forms. The ratio $K_1/[(H^+) + K_1]$, where $pK_1 = 3.65$, gives the fraction of semicarbazide in the free base form. Catalytic constants for several acid (k_1) and basic (k_2) catalysts are indicated in eq. 1. The single prime refers to the hydronium ion–water acid–base system, the double prime to water–hydroxide ion system, and the triple prime to other catalytic components that may have been added to the system.

Cordes and Jencks[1] have plotted the logarithms of the second-order rate constants given by the left-hand side of eq. 1 *vs.* pH. These curves exhibit a slope of -1 in the 2–4 pH range, a plateau from about pH 4 to 6, and again a slope of -1 at pH > 6. We now consider the application of eq. 1 to each of these regions in turn.

In the 2–4 pH range, eq. 1 reduces to

$$R_3 = k_1'(H_3O^+) + k_1''(H_2O) + k_1'''(HB) \quad (2)$$

indicating general acid catalysis of amine attack on the carbonyl group as the rate-limiting step. In the absence of buffers, R_3 is given by the first term on the right where for *p*-chlorobenzaldehyde[1] $k_1' = 9.0 \times 10^4\ M^{-2}\ \text{min.}^{-1}$.

In the plateau region from pH 4 to 6 eq. 2 is also applicable, but the first term on the right is no longer dominant. From this region in the absence of buffers, eq. 2 yields $k_1''(H_2O) = 26\ M^{-1}\ \text{min.}^{-1}$ for *p*-chlorobenzaldehyde. By studying the effect of added buffers in eq. 2 Cordes and Jencks[1] deduced a Brønsted exponent of 0.25.

At pH > 6 the $k_2''(OH^-)/k_3$ term in the denominator of eq. 1 becomes greater than unity and hence an equilibrium is established in the first step of the mechanism. We obtain

$$R_7 = k_3\Sigma k_1(HB)/\Sigma k_2(B) = k_3K_s(H^+) \quad (3)$$

where $K_s = (DH^+)/(M)(A)(H^+)$, and (DH^+) is the molar concentration of the tetrahedral addition intermediate in the mechanism. Equation 3 describes rate limiting apparent specific acid catalyzed dehydration of the tetrahedral addition intermediate. From the negative unit slope above pH 6 for *p*-chlorobenzaldehyde,[1] $k_3K_s = 1 \times 10^7\ M^{-2}\ \text{min.}^{-1}$. This value agrees well with one of 0.9×10^7 obtained from independent measurements[7] of the equilibrium constant for addition compound formation and its rate of decomposition in 25% ethanol at 25.0°. That the product k_3K_s is nearly independent of substituent in a series of substituted benzaldehydes is confirmed by its low Hammett ρ-value of 0.07[7] and the almost superimposable rate curves[1] for semicarbazone formation at pH > 6.

Only one of the general base terms in the denominator of eq. 1 need be greater than unity to establish an equilibrium in the first step of the mechanism. We are proposing to account for the negative slope and specific hydrogen ion catalysis at neutral pH by the predominance of the $k_2''(OH^-)/k_3$ term in the denominator in this pH region. For the H_2O–OH^- acid–base system, eq. 3 yields

$$k_2''/k_3 = k_1''(H_2O)/k_3K_sK_w$$

where K_w is the ion product constant for water. Substitution of the values already mentioned for *p*-chlorobenzaldehyde yields $k_2''/k_3 = 26 \times 10^7$.

To this point, the $k_2'(H_2O)/k_3$ term in the denominator of eq. 1 has been persistently ignored. It may be estimated by application of eq. 3 to obtain

$$k_2'(H_2O)/k_3 = k_1'/k_3K_s$$

Substitution of the values already mentioned for *p*-chlorobenzaldehyde yields $k_2'(H_2O)/k_3 = 9 \times 10^{-3}$. This value is much less than unity so that we are justified in assuming it negligible when applying eq. 1 to these systems. For the acetophenone reaction studied by Cordes and Jencks,[1] this term is about 0.1, closer to, but still less than, unity.

Evidently, the (H_2O) term in the denominator of eq. 1 is never significant while the (OH^-) term is important only at pH $>$ 5–6. Addition of buffers at lesser pH values should yield an initial straight line portion when R is plotted against buffer concentration corresponding to the results of eq. 2. If sufficient quantities of the basic component are eventually present at higher concentrations, eq. 3 would be applicable

(5) R. B. Martin, *J. Am. Chem. Soc.*, **84**, 4130 (1962). The appearance of water as a nucleophile in a pre-equilibrium step is incorrectly treated in this reference. Inferred w values do depend upon which step is rate-limiting in ester hydrolyses. The discussion given for the γ-butyrolactone enigma is valid only if the first step in ester hydrolysis is rate-limiting. Nucleophilic water should not appear explicitly in eq. III-3 and IV-2. The section on values of w from mechanism should be correspondingly modified. The p term should be deleted from eq. IV-3 and IV-4. Other changes are minor and no general arguments are significantly altered. In this paper two different correct ways for handling nucleophilic water in a pre-equilibrium step are presented in eq. 7 and 11.

(6) Values of the Hammett acidity function were interpolated from the tabulation of M. A. Paul and F. A. Long, *Chem. Rev.*, **57**, 1 (1957).

(7) B. M. Anderson and W. P. Jencks, *J. Am. Chem. Soc.*, **82**, 1773 (1960). Their k_2K_1 is equivalent to our k_3K_s. The mechanism of the addition reaction proposed in this reference is presumably superseded by that in ref. 1.

and a plot of R *vs.* buffer concentration should level off at a rate corresponding to this equation. This result is precisely that obtained by Cordes and Jencks[1] for acetophenone upon addition of propionic acid at pH 4.10. For this acid, they give $k_1''' = 9.6$ and we calculate $k_3K_s = 5 \times 10^4$ from their data at pH > 5 in the same way as indicated above. Applying eq. 3 and substituting the mentioned constants at pH 4.10, we obtain (HB) = 0.4 M for the concentration of propionic acid that yields $k_2'''(B)/k_3 = 1$ in the reaction with acetophenone. This propionic acid concentration is on the bend connecting the initial straight line and horizontal portions of the R *vs.* propionic acid concentration plot. This result substantiates the suggestion that the results at neutral pH can be explained by invocation of the $k_2''(OH^-)/k_3$ term and that eq. 3 is of general validity with a single k_3K_s value for a given aldehyde or ketone with all catalytic systems.

The leveling-off of a rate *vs.* buffer concentration plot at high buffer concentrations is presumptive evidence for a change in the rate-determining step. Such a leveling-off should be looked for wherever a change in rate determining step is suspected or if it is being sought.

Aromatic Schiff Bases

Formation. For the reaction of *p*-chlorobenzaldehyde with aniline[6] mechanism I and the equations already discussed for semicarbazone formation account adequately for the results. Instead of presenting plots of the left-hand side of eq. 1 *vs.* pH as they did for semicarbazones,[1] Cordes and Jencks[3] have plotted k_{obsd} *vs.* pH for the appearance of Schiff base from the above reactants. This kind of plot yields a maximum at about pH 4 and a leveling off at a constant rate below pH 2.

In acid solutions, eq. 1 may be written

$$k_{obsd}/C_M = \{K_1/[(H^+) + K_1]\}[k_1'(H_3O^+) + k_1''(H_2O) + k_1'''(HB)]$$

From the constant rate below pH 2, Cordes and Jencks[6] obtained $k_1' = 1.7 \times 10^6\ M^{-2}$ min.$^{-1}$. They also calculated a Brønsted exponent of 0.25 from a study of a series of buffers below pH 3. The rise in the k_{obsd} *vs.* pH plot from pH 2 to 4 is due to the increase in free base form of aniline, $pK_1 = 4.6$. Mechanisms with general catalysis in only the dehydration rather than the formation of the tetrahedral intermediate step cannot account satisfactorily for the leveling-off of the rate in acid solutions or general acid catalysis on the acid side of the maximum.

At about pH 4 the $k_2''(OH^-)$ term in the denominator of eq. 1 becomes significant, causing the formation rate to decrease with increasing pH. When the unity term in the denominator of eq. 1 is exceeded by any of the other denominator terms, there is an equilibrium for formation of the tetrahedral addition intermediate, and the reaction rate is determined by its decomposition to yield Schiff base. The term in brackets in eq. 1 may then be represented by $k_3K_s \cdot (H^+)$ to yield

$$k_{obsd}/C_M = K_1k_3K_s(H^+)/[(H^+) + K_1] \quad (4)$$

where $K_s(H^+) = \Sigma k_1(HB)/\Sigma k_2(B)$ for all general catalysts in the system. For $K_1 > (H^+)$, the value of eq. 4 increases with decreasing pH, predicting apparent specific acid catalysis on the basic side of the maximum in the pH–rate profile. From this pH region $k_3K_s \simeq 17 \times 10^6\ M^{-2}$ min.$^{-1}$.

The pH–rate profile presented by Cordes and Jencks[3] may be represented by insertion of the following values in eq. 1: $pK_1 = 4.56$, $k_1' = 1.7 \times 10^6$, $k_1''(H_2O) = 500$, $k_2''/k_3 = 3 \times 10^9$, and $k_2'(H_2O)/k_3 = 0.1$, the last term negligible compared to unity as above. Values are derived by arguments similar to those used in the semicarbazone section. All units are expressed in molarity and minutes. The value of k_1'' is consistent with the Brønsted exponent mentioned previously.

Inserting the above values in eq. 1 shows that some contribution of general acid catalysis to the formation rate is still expected at pH 5.10, accounting for the apparent catalytic constant of acetic acid being about $^1/_{10}$ that observed at pH 2.50. Application of Brønsted catalysis arguments to the above k_2 values indicates that catalytic systems with $pK_a > 3$, except water, ought to show a leveling-off of the catalytic rate as the concentration of basic catalytic component increases. As the catalyst concentration is increased, partitioning of the tetrahedral intermediate favors reactants rather than products. For hydroxide ion this crossover point is at about pH 5.5.

Similar pH–rate profiles have been observed for the reaction of pyridoxal derivatives and aminothiols.[8] In these aqueous systems formation of a thiazolidine ring serves to trap the unstable Schiff base much as semicarbazone formation was used in the study of Cordes and Jencks.[3] Since Schiff base formation was evidently the rate limiting step in some of the pyridoxal reactions, the explanation for the curves is similar to that presented here. The analysis is made more compli-

(8) M. V. Buell and R. E. Hansen, *J. Am. Chem. Soc.*, **82**, 6042 (1960).

cated, however, by additional acidic groups which ionize throughout the pH region studied.

Hydrolysis. From mechanism I, we obtain for the observed first-order rate constant for the initial rate of Schiff base disappearance

$$k_{obsd} = \frac{-1}{C_s}\frac{dC_s}{dt} = \frac{k_4(H_2O)(H^+)}{(H^+) + K_2} \times \left[\frac{1}{1 + k_3/[k_2'(H_2O) + k_2''(OH^-) + k_2'''(B)]}\right] \quad (5)$$

where $K_2 = (S)(H^+)/(SH^+)$ and $C_s = (S) + (SH^+)$, the total concentration of Schiff base in both acidic and basic forms. The hydrolysis rate exhibits a maximum at $0 < pH < 2$. As the pH is increased from this range, the rate decreases due to the decrease in the fraction of protonated Schiff base given by $(H^+)/[(H^+) + K_2]$ with $pK_2 = 2.8$. In terms of free Schiff base, hydrolysis is general acid catalyzed in agreement with observation. At about pH 5 a curious inflection should occur in the descending profile due to coming into play of the system with OH^- as base; the same k_3/k_2'' ratio obtained in formation also applies here and determines the inflection pH. Once the inflection point is passed, the term in brackets is unity, and since $K_2 > (H^+)$ in the region also, the hydrolysis reaction is specific acid catalyzed.

At $9 < pH < 12$, the pH–rate profile is horizontal,[3] probably due to the appearance of the direct reaction of $SH^+ + OH^-$. For CBA this reaction rate constant appears to be 3×10^5 times faster than $k_4(H_2O)$ for $SH^+ + H_2O$. A factor of about 10^7 has been found for the ratio of certain protonated thiazoline derivatives reacting with OH^- and H_2O at a carbon–nitrogen double bond.[9] The subsequent increase in rate at $pH > 12$ may be due to $S + OH^-$. If this is so, OH^- reacts about 10^{10} times faster with SH^+ than with unprotonated Schiff base.

In strongly acidic solutions, eq. 5 becomes

$$k_{obsd} = k_4(H_2O\left[\frac{1}{1 + k_3/k_2'(H_2O)}\right] \quad (6)$$

From our discussion of the formation reaction in this region, we have $k_3 > k_2'(H_2O)$ and eq. 6 becomes

$$k_{obsd} = k_4(H_2O)k_2'(H_2O)/k_3 = K_T k_2'(H_2O) \quad (7)$$

where $K_T = (DH^+)/(SH^+) = k_4(H_2O)/k_3$. General base catalysis of hydrolysis of protonated Schiff base is predicted in this region though it would be difficult to observe directly.

For CBA hydrolysis, the slope of a plot of log k_{obsd} *vs.* logarithm of activity of water is 3.1 in H_2SO_4.[3] This value is in the range 1 to 3.3 indicated for water acting solely as a nucleophile.[10] In eq. 7, water acts as a proton acceptor for which a slope of greater than 3.3 is suggested.[10] Evidently, we must reduce the 3.3 limit for the purposes of this reaction. A role for water acting as a proton transfer agent in this region is indicated, however, by a decrease in rate of hydrolysis by about one-half when D_2SO_4 is used in place of H_2SO_4.[3]

Oximes

Unlike the semicarbazone and Schiff base formation reactions just discussed which are general acid catalyzed on the acidic side of the maxima in a plot of observed first-order rate constant *vs.* pH, the formation of oximes is general acid catalyzed on the basic side of the maxima which occurs at about pH 4.[2] General acid catalysis of dehydration of tetrahedral addition intermediate is not consistent with the above mechanism and a new one is required for oxime formation.

A detailed mechanism which can account for oxime formation is mechanism II. Remembering that the

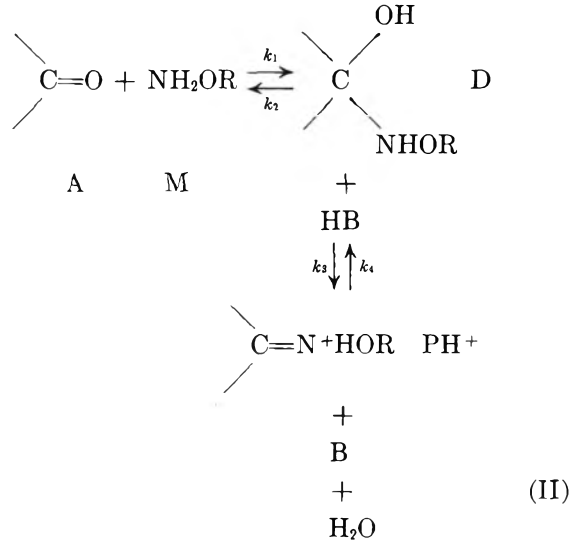

(II)

tetrahedral intermediate can exist in appreciable concentration under some conditions on the basic side of the maximum in the pH–rate profile, we nevertheless assume a steady-state approximation for D and obtain

$$\frac{k_{obsd}}{C_M} = \frac{+1}{C_M(A)}\frac{d(P)}{dt} = \frac{K_1 k_1}{(H^+) + K_1} \times \left[\frac{1}{1 + k_2/[k_3'(H_3O^+) + k_3''(H_2O) + k_3'''(HB)]}\right] \quad (8)$$

where $K_1 = (M)(H^+)/(MH^+)$ and $C_M = (M) + (MH^+)$, the total concentration of amine in both acidic and basic forms. Catalytic constants k_3 for several

(9) R. B. Martin and A. Parcell, *J. Am. Chem. Soc.*, **83**, 4830 (1961).
(10) J. F. Bunnett, *ibid.*, **83**, 4956, 4968 (1961).

acid catalysts are indicated in eq. 8. We show later that $k_3''(H_2O) << k_2$ and $k_3'(H_3O^+)$ up to pH 7, the highest studied.[2]

On the basic side of the maximum of the pH–rate profile in the absence of buffers, eq. 8 becomes

$$k_{obsd}/C_M = K_1k_1k_3'(H_3O^+)/k_2[(H^+) + K_1]$$

The midpoint of the descent is at pH = pK_1 (=6.0 for hydroxylamine) and the rate-limiting step is general acid catalyzed attack by a solvated proton on the tetrahedral addition intermediate. Addition of other general acids further increases the rate of dehydration of the tetrahedral intermediate. From a figure given by Jencks[2] the catalytic constant for dihydrogen phosphate ion, k_3''', is about 5 M^{-1} min.$^{-1}$.

At the maximum in the pH–rate profile, eq. 8 becomes

$$k_{max}/C_M = K_1k_1k_3'/k_2$$

From the observed $k_{max}/C_M = 1 \times 10^2$ for acetone and hydroxylamine,[2] $k_1k_3'/k_2 = 1 \times 10^8$. These values are identical with those given by Jencks.[2] From an estimate of an equilibrium constant for formation of the tetrahedral intermediate, Jencks obtains $k_1 = k_2$, so that $k_3' = 1 \times 10^8$. Comparison of this catalytic constant for the hydrated proton with that obtained above for dihydrogen phosphate ion indicates a high Brønsted exponent of about 0.85. Accordingly, the $k_3''(H_2O)$ term of eq. 8 should be about 10^{-5} min.$^{-1}$, which is negligible when compared with the values considered below for the catalytic constant for the solvated proton.

On the acid side of the maxima eq. 8 yields

$$k_{obsd}/C_M = K_1k/[k_2/k_3' + (H_3O^+)] \qquad (9)$$

From the experimental points of the descent on the acid side of the pH–rate profile for acetone and hydroxylamine,[4] we obtain $k_2/k_3' = 2 \times 10^{-3}$. Combination of this result with that in the previous paragraph yields $k_1 = 2 \times 10^5$ M^{-1} min.$^{-1}$, which is evidently also the value of k_2.

The treatment of the previous paragraph for the acid side of the maximum differs from that given by Jencks.[2] By not considering the k_2/k_3' term in eq. 9, he obtains a curve which is too steep to fit the experimental points. The experimental points form a sigmoid curve,[2] like a titration curve, and are much better accommodated by an equation of the form of (9) which fits the experimental points precisely. A consequence of this different approach is that our k_1 and k_2 values are about three times greater than those given by Jencks. Values of other constants are unchanged.

Jencks[2] ascribed the deviation of his experimental points from his theoretical curve to an acid-catalyzed reaction similar to the first step of the acid-catalyzed reaction of mechanism I for semicarbazone formation and assigned an acid-catalyzed rate constant for oxime formation corresponding to $k_1' = 1 \times 10^7$ min.$^{-1}$ M^{-2} in that mechanism. We have re-examined the acid catalyzed reaction, and the results are presented in Table I. Taking $k_{obsd}/(NH_3OH^+) = 0.20$ min.$^{-1}$ M^{-1} as the best value in strongly acid solutions and dividing by $K_a = 10^{-6}$ M for hydroxylamine, we obtain $k_1' = 2 \times 10^5$ min.$^{-1}$ M^{-2}. This value is only $^1/_{50}$ as much as that suggested by Jencks and indicates that his explanation for the lack of fit is unlikely.

In order to accommodate the bulk of the results for oxime formation, it is necessary to invoke mechanism II or some kinetic equivalent. Only for the formation reaction in strong acids must a small contribution from mechanism I be included. In more dilute acids, general acid catalysis is not observed and mechanism II describes completely the course of the reaction.

Aliphatic Schiff Bases

The pH–rate profiles for the rates of hydrolysis of a series of substituted benzylidene-1,1-dimethylethylamines exhibit[4] a constant rate of hydrolysis at 9 < pH < 13, due to reaction of protonated Schiff base SH^+ with OH^-. At 5 < pH < 7, reaction of SH^+ with water becomes of increasing importance, finally yielding a plateau at 4 < pH < 5 where the Schiff bases are predominantly in the protonated form. General base catalysis in terms of protonated Schiff base occurs in this region. At pH < 3, the rates decrease with increasing acidity. No inflection such as occurs in the hydrolysis of the aromatic Schiff base, N-*p*-chlorobenzylideneaniline, is observed.[4]

The results for the hydrolysis of aliphatic Schiff bases may be accounted for by the reverse of mechanism II to yield, with the usual steady-state approximation for the tetrahedral addition intermediate, for the observed first-order rate constant for the initial rate of Schiff base disappearance

$$R = k_{obsd} = \frac{-1}{C_S}\frac{dC_S}{dt} = \frac{k_2(H^+)}{(H^+) + K_2} \times \left[\frac{k_4'(H_2O) + k_4''(OH^-) + k_4'''(B)}{k_2 + k_3'(H_3O)^+) + k_3''(H_2O) + k_3'''(HB)}\right] \qquad (10)$$

where the symbols are the same as those used in formulating the hydrolysis of aromatic Schiff bases. The rate constants, however, designate reactions in mechanism II.

In acid solutions, pH < 3, the $k_3'(H_3O^+)$ term dominates the denominator term in brackets of eq. 10 so

that an equilibrium exists in the first step of the hydrolysis reaction, and we obtain

$$R_2 = k_2K_S/(H^+) \qquad (11)$$

where $K_S = (D)(H^+)/(SH^+)(H_2O)$ and (D) is the molar concentration of tetrahedral addition intermediate. From the observed rate for benzylidene-1,1-dimethylethylamine (BDA) at pH 1, $k_2K_S = 1.4 \times 10^{-3}$ min.$^{-1}$ M.

In the general base catalyzed plateau region $4 < pH < 5$ eq. 10 becomes

$$R_4 = k_4'(H_2O) + k_4''(OH^-) + k_4'''(B)$$

Cordes and Jencks give $k_4'(H_2O) = 0.41$ min.$^{-1}$ for BDA and from their Fig. 5 an approximate constant of $k_4''' = 5$ min.$^{-1}$ M^{-1} may be calculated for general base catalysis by acetate anion. Combination of the catalytic constants for water and acetate acting as general bases yields a Brønsted exponent of about 0.4 and predicts that for general base catalysis by hydroxide ion $k_4'' \simeq 4 \times 10^5$ min.$^{-1}$ M^{-1}. Since the observed rate of reaction of hydroxide ion with protonated Schiff base is 3.0×10^7 min.$^{-1}$ M^{-1}, almost 10^2 times greater than above, the rates in the plateau region at pH > 9 are interpreted as due to direct nucleophilic attack of hydroxide ion on protonated Schiff base. This conclusion is identical with that reached by Cordes and Jencks[4] by an entirely different line of reasoning. Thus the $k_4''(OH^-)$ term is never dominant in the numerator of eq. 10 but a separate equation must be written for direct nucleophilic attack by hydroxide ion

$$SH^+ + OH^- \xrightarrow{k_{OH^-}} D$$

where for BDA $k_{OH^-} = 3 \times 10^7$ min.$^{-1}$ M^{-1}. This equation is consistent with the absence of observable general base catalysis at pH > 9.

The preceding analysis has assumed that $k_3''(H_2O)$ in eq. 10 is always less than k_2. This assumption may be tested by noting that $k_3''(H_2O)/k_2 = k_4''K_W/l_2K_S$. This last fraction has a value of 2×10^{-4} even when the observed rate of hydroxide ion attack is substituted for k_4'', assuring that $k_3''(H_2O) << k_2$. The general equation for any catalytic system present is $k_3'''/k_2 = k_4'''K_B/k_2K_S$. Applying this result to acetic acid yields a value of 0.07 M^{-1} for the last fraction. For the k_3''' (HB) term to exceed k_2 in the denominator of eq. 10, a solution 14 M in acetic acid is required. Since the experiments in acetic acid–acetate mixture were performed to only 0.5 M in total acetate, the result of the calculation is consistent with no leveling-off of the k_{obsd} *vs.* total acetate concentration plots.

Mechanism II is consistent in every way with the results for hydrolysis of aliphatic Schiff bases. It cannot accommodate the inflection observed in the hydrolysis of the aromatic Schiff base N-*p*-chlorobenzylideneaniline. On the other hand, mechanism I proposed for the aromatic Schiff base cannot account for general base catalysis at pH 4 in the aliphatic Schiff bases. Thus the mechanisms of hydrolysis of aliphatic and aromatic Schiff bases exhibit different catalytic requirements.

This conclusion is substantiated by comparing the very different behavior of aromatic and aliphatic Schiff base hydrolysis in strongly acid solutions. As mentioned above, the slope of the log k_{obsd} *vs.* log a_{H_2O} plot for the aromatic Schiff base CBA is 3.1. As reported in the Experimental section, a similar plot for an aliphatic Schiff base yields a curve with a steep initial slope of 11 or greater. These data are well represented, however, by a reaction exhibiting acid inhibition in acid solutions with no involvement of water in the rate limiting step.[5] This latter result may be accommodated only by reaction 11 of mechanism II while the result for the aromatic Schiff base requires reaction 7 of mechanism I for its interpretation.

The hydrolysis of aliphatic Schiff bases exhibits similar pH–rate profiles and proceeds by a mechanism identical with that suggested for the hydrolysis of 2-methylthiazoline and 2-methyloxazoline.[11] In addition, the ratio of the rate of nucleophilic hydroxide ion attack to that of water-catalyzed attack of water is 10^7–10^8 M^{-1} in all cases.

Discussion

Two detailed mechanisms have been developed to account for the pH–rate profiles and general acid–base catalysis in reactions of carbonyl compounds with various amines to yield semicarbazones, Schiff bases, and oximes. These two detailed mechanisms are nearly the only possible ones that can accommodate the results discussed here. General catalysts must be introduced, and when combined with a reasonable chemistry, only the two mechanisms developed here can account for the maxima in pH–rate profiles. If these principles are accepted, our only task is to assign the various systems studied to one mechanism or the other, since in all cases mentioned general acid–base catalysis seems to predominate on only one side of the maxima in a pH–rate profile.

Other mechanisms kinetically equivalent to those suggested could be constructed. The mechanisms presented here are thought to be the simplest consistent

(11) R. B. Martin, R. I. Hedrick, and A. Parcell, in preparation.

with all the kinetic data and are formulated in terms of current ideas regarding the compounds involved. Other microscopic forms of the tetrahedral addition intermediates could be written. Some of our rate constants may therefore be combinations of equilibrium and other rate constants. From information currently available, these other constants cannot be evaluated separately, and there is no kinetic justification for writing these other forms. The arguments in this paper are developed on a primarily kinetic basis with structural considerations secondary. The mechanisms proposed or their kinetic equivalents are all that are kinetically justified to account for the results in the papers considered.

Mechanisms I and II are not equivalent; it has been pointed out in the Results section why one or the other is more suitable in any particular case. Semicarbazone and aromatic Schiff base formation and hydrolysis follow mechanism I, while oxime and aliphatic Schiff base formation and hydrolysis are best described by mechanism II. Analysis of the catalytic requirements in both aliphatic and aromatic Schiff base systems points up the apparently fundamentally different mechanisms required to accommodate the results for the two kinds of Schiff bases.

Since in the case of oxime formation at least features of both mechanisms I and II must be invoked, the question arises whether the two mechanisms might be combined. It may be shown that mechanism III accounts

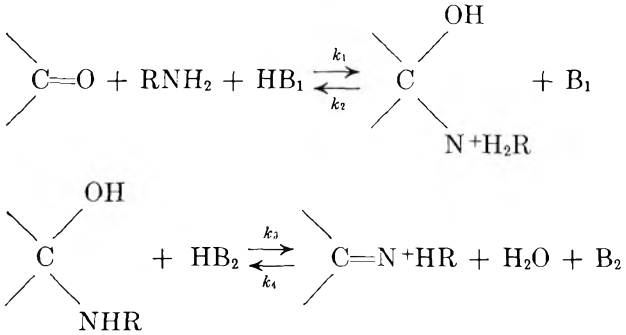

(III)

for all the results discussed in this paper. In this mechanism both steps of the formation reactions are general acid catalyzed, but the Brønsted exponents for the two reactions are such that mechanisms I and II are special cases of mechanism III. The rate constants of mechanism III in some cases acquire a different significance than in the previous mechanisms. For instance, k_3 of mechanism I becomes k_3K_D in mechanism III, where K_D is the acid ionization constant of the tetrahedral carbon addition intermediate. Since this ionization constant cannot be determined by a steady-state analysis, no new information is gained by factoring it from an apparent rate constant. K_D can be determined in principle, however, in some cases such as oxime formation, where high concentrations of intermediate can be obtained in neutral solutions. Also, the k_4 constants of mechanisms I and II are replaced by $k_4K_{B_2}$ in mechanism III where K_{B_2} is the acid ionization constant of the general catalytic components appearing in the second reaction. Although all the results discussed here may be described in terms of mechanism III, it is more convenient, in most cases, to consider either mechanism I or II depending upon which is applicable to the case under study.

In the above discussion of oxime formation, rate constants were obtained that applied to both mechanisms I and II. The Brønsted exponent for general acid catalysis in the second step of mechanism III was evaluated as 0.85. The Brønsted exponent for general acid catalysis of oxime formation in the first step of mechanism III may be estimated by considering $k_1' = 2 \times 10^5$ min.$^{-1}$ M^{-2} for hydronium ion catalysis and the value of $k_1 = 2 \times 10^5$ min.$^{-1}$ M^{-1} from mechanism II to represent $k_1''(H_2O)$ where k_1'' is the catalytic coefficient for water acting as a general acid. Combination of these results yields a low Brønsted exponent of 0.10 for general acid catalysis in the first step of mechanism III for oxime formation.

Granting a slight oversimplification, the four nitrogen-containing reactants, when listed in order of increasing pK_a values, divide so that the two most acidic belong to the class of mechanism I and the two most basic to the class of mechanism II. In Table III the nitrogen bases are listed in order of increasing basicity and also tabulated are the Brønsted exponents for general acid catalysis in the first, α_1, and second, α_2, steps of mechanism III as mentioned or deduced in this paper.

Table III: Brønsted α-Values for First and Second Steps of Mechanism III

	pK_a	α_1	α_2
Semicarbazide	3.6	0.25	~1.0
Aniline	4.6	0.25	~1.0
Hydroxylamine	6.0	0.10	0.85
Aliphatic amines	~10.0	~0.0	~0.6

In Table III, values of α near zero imply that water is the dominant general acid catalyst, usually swamping the effects of other general acids. General acid catalysis by hydronium ion appears, if at all, only in strongly

acid solutions. Unless the solutions are fairly acid, the reverse reaction will exhibit apparent specific base catalysis. On the other hand, values of α near unity mean that hydronium ion catalysis predominates and the reaction appears only specific acid catalyzed, except for fairly basic solutions where the hydronium ion concentration is low. Unless the solutions are fairly basic, the reverse reaction will appear uncatalyzed because water is the dominant base. Application of these principles to mechanism III for the first two nucleophiles of Table III yields a mechanism kinetically indistinguishable in aqueous solvents under most conditions from mechanism I and for the last two nucleophiles a mechanism equivalent to mechanism II.

Table III reveals only a gradual progression in the α-values of the nitrogen bases for the reactions discussed here. Thus the division of the four bases into two groups is not sharp, so that we might expect aniline and hydroxylamine especially to exhibit dual behavior under approximate conditions. This effect has already been described above for hydroxylamine. Hydrolysis in neutral solutions of some aromatic Schiff bases seems to be general base catalyzed in terms of protonated Schiff base[12] in accord with mechanism II. Semicarbazones exhibit similar behavior.

Though the α_1-values of Table III apply to proton transfer reactions that are concerted with bond making, they have been determined with a variety of general acid catalysts for each nucleophile and carbonyl substrate. The α_1-value of 0.25 obtained when semicarbazide attacks each of several substituted benzaldehydes[1] provides an indication of the extent of proton transfer from general acid catalyst in the transition state of the first reactions of mechanisms I or III. When the general acid catalyst is water, a plot[13] of log $k_1''(H_2O)$ *vs.* the logarithm of the equilibrium constant for formation of the tetrahedral intermediate from semicarbazide and several substituted benzaldehydes[7] yields a slope of 0.47. Since this value is greater than $\alpha_1 = 0.25$ for the same reaction, nucleophilic attack at carbonyl carbon is evidently further advanced in the transition state to addition intermediate than is proton transfer from general acid catalysts.

By writing out detailed mechanisms and their corresponding rate equations, a complete account may be given of the reactions discussed. The differences between our interpretation and those of Cordes and Jencks derive ultimately from explicit consideration of general catalytic terms arising from solvent components. Thus we are able to account in a natural way for apparent specific acid catalyzed dehydration of tetrahedral addition intermediates in semicarbazone and aromatic Schiff base formation and to provide a more satisfactory description of hydroxylamine attack at a carbonyl carbon. These differences lead to the formulation of different transition states.

In the reaction of hydroxylamine with O-acetylhydroxylamine, the observed pH–rate profile with a maximum is wider than that calculated theoretically.[14] Consideration of general catalysis by solvent components will broaden the theoretical curve to give better agreement with experiment.

When metal ions such as divalent transition metal ions are added to the systems discussed here, their effect on the tetrahedral addition intermediate as well as upon reactants and products must be considered in evaluating their effects upon reaction rates. An analysis of this kind has not yet been performed. The analysis presented here in the metal-free systems is an essential first step in incorporating the data we are obtaining in systems with added metal ions.

Acknowledgment. This research was supported by grants from the National Science Foundation.

(12) A. Willi and R. F. Robertson, *Can. J. Chem.*, **31**, 361 (1953); R. L. Reeves, *J. Am. Chem. Soc.*, **84**, 3322 (1962).

(13) J. E. Leffler and E. Grunwald, "Rates and Equilibria of Organic Reactions," John Wiley and Sons, Inc., New York, N. Y., 1963, p. 161.

(14) W. P. Jencks, *J. Am. Chem. Soc.*, **80**, 4585 (1958).

Application of the Archibald Ultracentrifugal Method for the Study of Dilute Polymer Solutions. III. Effects of Polydispersity and Nonideality

by Yoshinori Toyoshima and Hiroshi Fujita

Department of Polymer Science, Osaka University, Osaka, Japan *(Received December 3, 1963)*

Sedimentation measurements of the Archibald type were performed on methyl ethyl ketone (MEK) solutions at 25° and cyclohexane solutions at 35° of two polystyrene samples. One sample was a conventional polydisperse polystyrene, and the other a narrow distribution one prepared by anionic polymerization, but both had comparable weight-average molecular weights M_w. The apparent molecular weight $M_{app}(t)$, evaluated at the meniscus of the solution, changed with time t in the qualitative fashion predicted by a theory of Fujita, *et al.* That is, (i) $M_{app}(t)$ was independent of time when the solute was monodisperse and its solution was under θ-conditions; (ii) $M_{app}(t)$ increased with time when the solute was monodisperse and its solution was positively nonideal (*i.e.*, the second virial coefficient was positive); (iii) $M_{app}(t)$ decreased with time when the solute was polydisperse and its solution was under θ-conditions. In cyclohexane at 35°, plots of M_{app}^{-1} *vs.* c_0 were horizontal over the range of c_0 studied, regardless of the heterogeneity of solute, where M_{app} is the value of $M_{app}(t)$ at $t = 0$ and c_0 is the initial concentration of the solution. This plot for the polydisperse solute in MEK at 25° gave a curve of upward curvature, but the corresponding plot for the monodisperse solute in the same solvent was linear over the entire range of c_0 studied (<1.2 g./dl.). From these results we are tempted to conclude that the upswing nature of M_{app}^{-1} *vs.* c_0, which has been observed in many previous studies of dilute polymer solutions by the Archibald method, may be attributed to polydispersity in molecular weight of a given solute. Values of M_w and light scattering second virial coefficient A_2' were determined from intercepts and initial slopes of the plots of M_{app}^{-1} *vs.* c_0 obtained, by applying the series expansion of Fujita, *et al.* The results accorded well with the values deduced from light scattering measurements. For a fixed M_w the value of A_2' appeared to increase as the polydispersity of the solute was decreased.

Introduction

In part I of this series, Fujita, *et al.*,[1] developed a theory of the Archibald ultracentrifugal method[2] for dilute polymer solutions, with polydispersity in molecular weight of the solute and thermodynamic nonideality of the solution taken into account. It was shown that the quantity M_{app}^{-1} can be expanded in terms of the initial concentration of the solution c_0 as

$$1/M_{app} = 1/M_w + 2A_2'c_0 + \text{higher terms in } c_0 \quad (1)$$

where M_{app} is the value at time $t = 0$ of an apparent molecular weight $M_{app}(t)$ defined by eq. 15 of ref. 1, M_w is the weight-average molecular weight of the solute, and A_2' is the light scattering second virial coefficient of the given solution. According to eq. 1, the values of M_w and A_2' may be obtained from the intercept and initial slope of a plot for M_{app}^{-1} *vs.* c_0.

(1) H. Fujita, H. Inagaki, T. Kotaka, and H. Utiyama, *J. Phys. Chem.*, 66, 4 (1962).

(2) H. K. Schachman, "Ultracentrifugation in Biochemistry," Academic Press, Inc., New York, N. Y., 1959; H. Fujita, "Mathematical Theory of Sedimentation Analysis," Academic Press, Inc., New York, N. Y., 1962.

Preliminary experiments with polystyrene fractions in methyl ethyl ketone (MEK) at 25°, reported in part I, checked the validity of this procedure. Similar verification has been given in part II of this series by Inagaki, *et al.*,[3] who examined two solution systems polystyrene–cyclohexane and polymethyl methacrylate–*n*-butyl chloride in the vicinity of the θ-temperature characteristic of each. They found that in both systems the plots for M_{app}^{-1} *vs.* c_0 were horizontal at the respective θ-temperatures, but showed appreciable upward or downward curvatures, depending on whether the temperature was above or below the characteristic one. Similar deviations of M_{app}^{-1} *vs.* c_0 from linearity had often been observed by previous workers[1,4,5] since the early study on the system polyvinyl chloride–tetrahydrofuran by Kegeles, *et al.*[4] However, the reason for this phenomenon remains unknown.

The following predictions have been given in part I for the variation of the apparent molecular weight $M_{app}(t)$ with time t. (i) If the solute is monodisperse and the solution is positively nonideal (*i.e.*, the second virial coefficient is positive), $M_{app}(t)$ evaluated at the meniscus of the solution increases with increasing time of centrifugation; (ii) If the solute is polydisperse and the solution is ideal (*i.e.*, the solute is dissolved in a θ-solvent), $M_{app}(t)$ at the meniscus is a decreasing function of time. The reverse should be the case with $M_{app}(t)$ measured at the bottom of the cell.

As far as we are aware, no definitive experimental evidence to support these predictions have as yet been obtained. Rather, Inagaki, *et al.*,[3] have shown data which appeared to contradict the prediction (ii). However, there are reasons to believe that the Phywe ultracentrifuge they used is not very advantageous for sedimentation measurements of the Archibald type to be performed with precision. Probably it is due to such instrumental drawbacks that Inagaki, *et al.*, failed to confirm the theoretical prediction. With regard to prediction (i), their data are of no use, because they used polydisperse samples.

The study reported below is concerned with an experimental check of the above predictions and also with a discussion of the cause responsible for the curvature of the plot for M_{app}^{-1} *vs.* c_0. To this end, we chose a conventional polystyrene as a sample of polydisperse solute and an anionically polymerized polystyrene as an approximate model of monodisperse solute, and studied these samples both in MEK at 25° and in cyclohexane at 35°; the latter is a well-known θ-solvent for this polymer.

Experimental

Materials. The polydisperse polystyrene, designated as SMI, was obtained from the Committee on Molecular Weight Study of the Society of Polymer Science, Japan. Its weight-average molecular weight M_w was determined, by the light scattering method, in a cooperative research project organized by the Committee. Its reliable number-average molecular weight M_n is not yet available but the osmotic pressure measurements by Matsuo[6] indicate that its M_w to M_n ratio is about 2.5. To know the extent of polydispersity, Toyoshima[7] evaluated its molecular weight distribution $f(M)$ by the sedimentation–transport method with cyclohexane at 35° as solvent, following the procedure described by Homma, *et al.*[8] The result obtained is shown in Fig. 1. The anionically polymerized polystyrene used

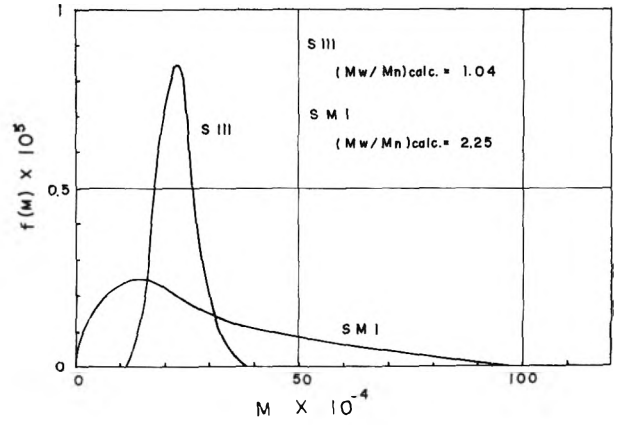

Figure 1. Differential distributions of molecular weight in polystyrenes S111 and SMI. Both were determined from sedimentation–transport measurements in cyclohexane at 35°, following the procedure described by Homma, *et al.*[8]

was obtained from the Commission of Macromolecules of the International Union of Pure and Applied Chemistry, through the courtesy of Professor J. Furukawa of Kyoto University. It was designated as S111 by the Commission. Data for its M_n, M_w, $f(M)$, and osmotic and light scattering second virial coefficients in various solvents are available in the table accompanying distribution of sample. Figure 1 includes the $f(M)$ of this sample determined ultracentrifugally by Homma, *et al.*,[8] who used the same solvent as in Toyoshima's work on sample SMI. One can observe a marked differ-

(3) H. Inagaki, S. Kawai, and A. Nakazawa, *J. Polymer Sci.*, **A1**, 3303 (1963).

(4) G. Kegeles, S. M. Klainer, and W. J. Salem, *J. Phys. Chem.*, **61**, 1286 (1957).

(5) W. Scholtan and H. Marzolph, *Makromol. Chem.*, **57**, 52 (1962).

(6) T. Matsuo, personal communication.

(7) Y. Toyoshima, M.S. Thesis, Osaka University, 1963.

(8) T. Homma, K. Kawahara, H. Fujita, and M. Ueda, *Makromol. Chem.*, **67**, 132 (1963).

ence in molecular weight heterogeneity between the two samples. Comparing with SMI, S111 may be regarded as being effectively "monodisperse." In what follows, therefore, we shall refer to S111 as monodisperse sample for convenience of description. Table I lists appropriate averages of the reported M_n and M_w, and our measurements of the limiting viscosity numbers in cyclohexane at 35° of these two polystyrenes.[9] It should be noted that the M_w values of the two samples are comparable, though their polydispersities are markedly different from one another.

Table I: Characteristics of Polystyrenes Studied

Sample	$M_n \times 10^{-4}$	$M_w \times 10^{-4}$	$[\eta]$ (dl./g.)[a]	Remarks
SMI	...	28.9	0.393	Polydisperse
	(13.0)[b]	(29.3)[b]		
S111	23.0	23.8	0.385	Nearly monodisperse

[a] Limiting viscosity number in cyclohexane at 35°. See Appendix for the reason that $[\eta]$ values of the two samples having different M_w are nearly the same. [b] The values calculated from the molecular weight distribution curve shown in Fig. 1.

Before use, sample S111 was dried *in vacuo* at 80° for 8 hr., while sample SMI was first precipitated into methanol from a benzene solution and then dried *in vacuo* at 80° for 10 hr.

Both MEK and cyclohexane were dried and fractionally distilled before use, and appropriate cuts (b.p. 79.5–79.6° for MEK and b.p. 80.6–80.9° for cyclohexane) were collected.

Ultracentrifugation. A Spinco Model E ultracentrifuge with a temperature controlling unit was used with schlieren optics and a phase plate. Both a standard 12-mm. cell and a 30-mm. cell were used, depending on the initial concentration of the solution to be examined. Rotor speeds employed were 9945–11,272 r.p.m. with fluctuations less than 0.5%. In view of these relatively low rotor speeds used it is expected, with fair confidence, that both MEK and cyclohexane solutions would have behaved as incompressible systems at all concentrations and temperatures studied, *i.e.*, all pressure effects were negligible. In each experiment the temperature was kept to within ±0.3°. The constant of the optical system was determined by using a synthetic boundary cell. The analysis of each schlieren photograph was made in the manner described previously,[1] after it had been magnified by a factor of 20 and traced on transparent millimeter graph paper by means of a Universal Contour projector of Nippon Kogaku Co. (Tokyo). For the partial specific volumes $\bar{v}$ of polystyrene in MEK and in cyclohexane and also the densities ρ_0 of these solvents, the following numerical values were deduced from relevant sources: $\bar{v}$ in MEK = 0.907 ml./g.,[10] $\bar{v}$ in cyclohexane = 0.940 ml./g.,[11] ρ_0 of cyclohexane at 35° = 0.7650 g./ml.,[12] and ρ_0 of MEK at 25° = 0.7995 g./ml.

Light Scattering. To confirm the reported values of M_w and A_2', light scattering measurements on sample SMI were made both in MEK at 25° and in cyclohexane at 35° by using the photometer and the experimental procedure entirely similar to those described in part I. No such study was made on sample S111, since the amount of sample available was very limited.

Results and Discussion

Apparent Molecular Weight $M_{app}(t)$. Since no satisfactory liquid was available for both MEK and cyclohexane to form a sharp liquid–liquid interface in the region near the cell bottom, data for $M_{app}(t)$ were taken only at the meniscus of the solution. Figures 2 to 5 illustrate $M_{app}(t)$ as a function of time t at three representative initial concentrations c_0, for the four combinations of polymer and solvent studied, *i.e.*, (i) S111 in cyclohexane at 35° (Fig. 2); (ii) S111 in MEK at 25° (Fig. 3); (iii) SMI in cyclohexane at 35° (Fig. 4); (iv) SMI in MEK at 25° (Fig. 5). Here, in accordance with Trautman,[13] t was taken to be $t' + t_f/3$, where t_f is the time until the rotor attains the desired operational speed from rest, and t' is the time elapsed after the full speed has been attained; in our experiments, t_f was of the order of 2 min. The preceding four systems may be classified as: (i) an ideal solution of a monodisperse solute; (ii) a nonideal solution of a monodisperse solute; (iii) an ideal solution of a polydisperse solute; and (iv) a nonideal solution of a polydisperse solute. Thus, in accordance with the theory developed in part I,[1] plots for $M_{app}(t)$ *vs.* t in these four systems should exhibit the following behavior: (i) $M_{app}(t)$ is independent of t for any low value of c_0; (ii) $M_{app}(t)$ increases with increasing t for any low value of c_0; (iii) $M_{app}(t)$ decreases with increasing t for any low value of c_0; (iv) $M_{app}(t)$ increases or decreases with time, depending on the value of c_0, *i.e.*, on the relative importance of polydispersity and nonideality ef-

(9) The average M_w of SMI has been calculated from data compiled by the Committee on Molecular Weight Study; *Kobunshi Kagaku*, 17, 216 (1960).

(10) G. V. Schulz and M. Hoffmann, *Makromol. Chem.*, 23, 220 (1951).

(11) B. Rosen, *J. Polymer Sci.*, 17, 559 (1955).

(12) International Critical Tables, Vol. 3, 1st Ed., 1928, pp. 28, 29.

(13) R. Trautman, *J. Phys. Chem.*, 60, 1211 (1956).

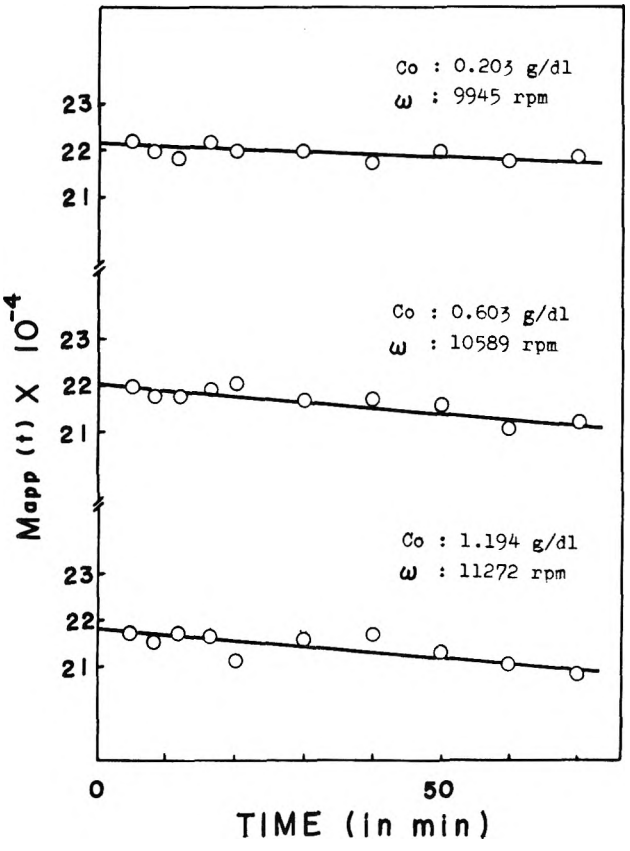

Figure 2. Time dependence of apparent molecular weight at the meniscus, $M_{app}(t)$, for monodisperse polystyrene S111 in cyclohexane at 35° (θ-solvent).

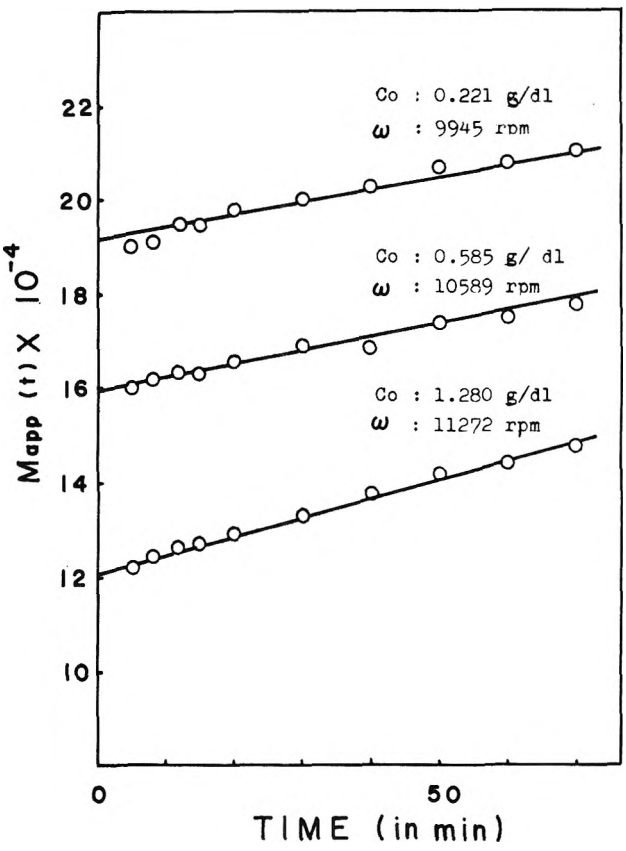

Figure 3. Time dependence of apparent molecular weight at the meniscus, $M_{app}(t)$, for monodisperse polystyrene S111 in methyl ethyl ketone at 25° (nonideal solvent).

fects. At some c_0, it may become sensibly constant over a range of time. The data shown in Fig. 2 to 5 are seen to demonstrate, at least qualitatively, these theoretical predictions, although some uncertainty remains concerning the verification of prediction (iv) in terms of the data of Fig. 5. One may notice the plots of Fig. 2 to exhibit a slight negative slope. Although it is not certain whether this behavior is real or not, theoretically it is not unexpected, since S111 is not perfectly monodisperse. In their study, reported in part II of this series, on systems polystyrene–cyclohexane and polymethyl methacrylate–*n*-butyl chloride, Inagaki, *et al.*,[3] observed $M_{app}(t)$ at the respective θ-temperatures to increase slightly with time. Considering that the polymer samples they used were doubtlessly polydisperse, such data are not in accordance with prediction (iii). The reason they were led to this contradiction remains unresolved. Summarizing, it may be concluded that the time dependence of $M_{app}(t)$ (at the meniscus of the solution) predicted theoretically in part I has been checked, at least qualitatively, by experiment. It is hoped that experiments to examine this conclusion will be undertaken with other systems of polymer and solvent.

The evaluation of $M_{app}(t)$ requires extrapolation of an experimentally determined curve for refractive index gradient *vs.* radial distance r to either the position of the meniscus r_1 or the cell bottom r_2. In part I we pointed out that no satisfactory theory to guide this extrapolation had been established. This unfortunate situation still remains unchanged, and we have to resort to an appropriate empirical procedure to effect the extrapolation. Probably this is the weakest point in current applications of the Archibald ultracentrifugal method. In this study, recourse again has been made to an empirical method proposed and applied with success in our previous studies[1,3]: plots for the logarithm of $[\partial n_c(r)/\partial r]/rn_c(r)$ *vs.* r are extrapolated to $r = r_1$. Here $n_c(r)$ is the excess refractive index of the solution at the position r and $\partial n_c(r)/\partial r$ is its gradient at the same position.[14] This procedure worked fairly well in most cases treated, but this does not warrant the reliability of the extrapolated values and hence of the resulting $M_{app}(t)$, since the method is purely empirical.

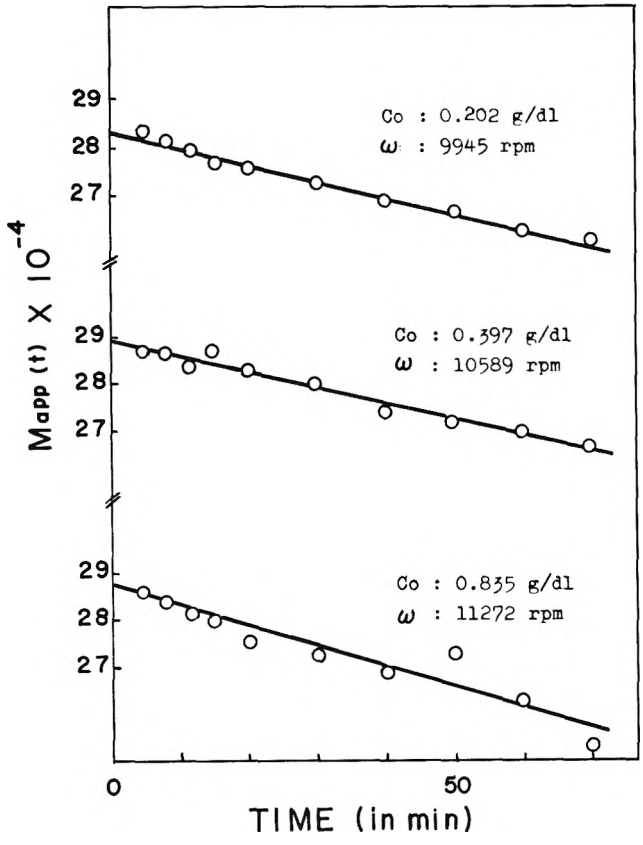

Figure 4. Time dependence of apparent molecular weight at the meniscus, $M_{app}(t)$, for polydisperse polystyrene SMI in cyclohexane at 35° (θ-solvent).

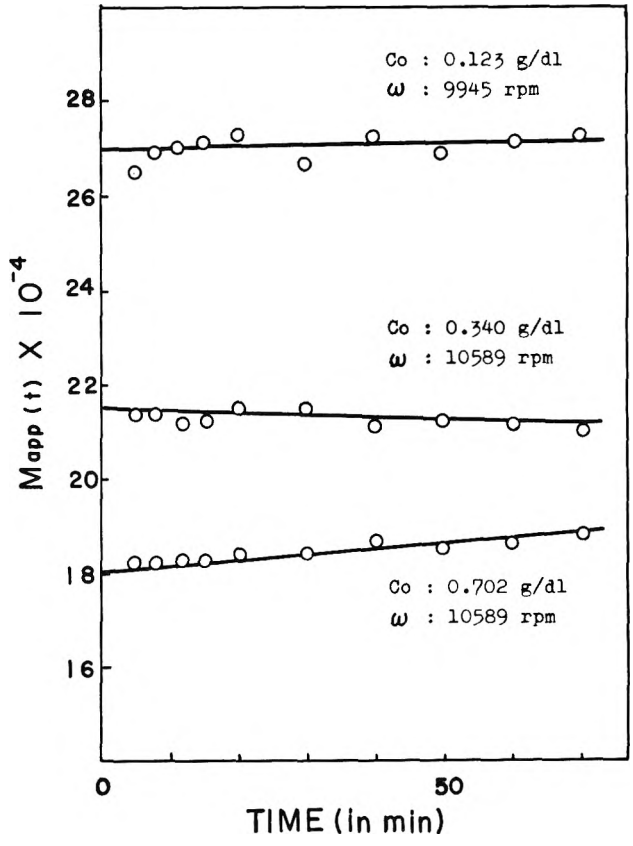

Figure 5. Time dependence of apparent molecular weight at the meniscus, $M_{app}(t)$, for polydisperse polystyrene SMI in methyl ethyl ketone at 25° (nonideal solvent).

Plots for M_{app}^{-1} vs. c_0. Figure 6 shows M_{app}^{-1} as a function of c_0 for S111 in MEK at 25° and in cyclohexane at 35°. The corresponding plots for SMI are given in Fig. 7. It is seen that these plots for S111 and SMI in cyclohexane at 35° are horizontal, within experimental error, over the range of c_0 studied. This suggests that under θ-conditions, not only the term in c_0 but also at least the term in c_0^2 in series 1 may vanish, regardless of polydispersity of the solute. The fact that the term in c_0 becomes zero under θ-conditions is consistent with our current concept of dilute polymer solutions, in which A_2' is zero when the system is at the θ-temperature. The plots for M_{app}^{-1} in MEK at 25° converge, at the limit of zero concentration, to the same intercepts as those of the corresponding cyclohexane plots. This is the behavior expected from eq. 1. The values of M_w obtained from these common intercepts in terms of eq. 1 are listed in Table II. The plot for S111 in MEK is essentially linear over the concentration range indicated, while that for SMI in the same solvent shows a definite upward curvature. This curvature is, however, not as noticeable as those we observed in previous studies[1,3] on polystyrene fractions in MEK. The difference may deserve a further investigation, but it would be of some significance to remark that our previous data were taken with a Phywe ultracentrifuge, while those reported here were with a Spinco Model E ultracentrifuge; the schlieren photographs taken with the latter machine were apparently much sharper and allowed more accurate tracing of the refractive index gradient curves than did those obtained with the former machine. Further demonstrations of the upward curvature of M_{app}^{-1} *vs.* c_0 have been reported by Inagaki[15] for a polystyrene

(14) The equations for $n_c(r)$ given in the footnote on p. 8 of ref. 1 were misprinted. For example, the equation appropriate for r near the meniscus should read

$$n_c(r) = (n_c)_{t=0} - (1/r_1^2)\int_r^{r_p} r^2(\partial n_c/\partial r)dr - \int_{r_1}^{r} [(r/r_1)^2 - 1](\partial n_c/\partial r)dr$$

(15) H. Inagaki, *Makromol. Chem.*, **64**, 215 (1963).

Table II: Comparison of Data between Archibald Method and Light Scattering Method

Sample	Solvent	Sedimentation $M_w \times 10^{-4}$	Sedimentation $A_2' \times 10^4$ (c.g.s.)	Light-scattering $M_w \times 10^{-4}$	Light-scattering $A_2' \times 10^4$ (c.g.s.)
SMI	MEK, 25°	28.2	1.37	27.9	1.45
SMI	Cyclohexane, 35°	28.2 (29.3)[a]	0	28.9	0
S111	MEK, 25°	22.2	1.75	20.4[b]	2.1[b]
S111	Cyclohexane, 35°	22.2	0	26.5[b]	0

[a] Calculated from the molecular weight distribution curve shown in Fig. 1. [b] Values given in the table accompanying distribution of sample.

fraction in toluene, and by Inagaki, *et al.*,[16] for polyacrylonitrile fractions in dimethyl formamide and in dimethyl sulfoxide. These previous data appear to suggest that the upswing nature of the plot for M_{app}^{-1} *vs.* c_0 may be inherent to the Archibald method applied to polymer solutions and that, because of the resulting difficulty of extrapolating the plot to infinite dilution, this feature diminishes the practical value of the method.[17] From comparison of Fig. 5 and 6, with the notice that SMI is quite polydisperse and S111 is approximately monodisperse, we are tempted to conclude that the molecular weight heterogeneity of the given solute would primarily be responsible for the deviation of a plot for M_{app}^{-1} *vs.* c_0 from linearity. The fact that such a deviation was common in previous studies may not be due to the inherent nature of the Archibald method but rather a consequence of the situation that polymer samples used were polydisperse.

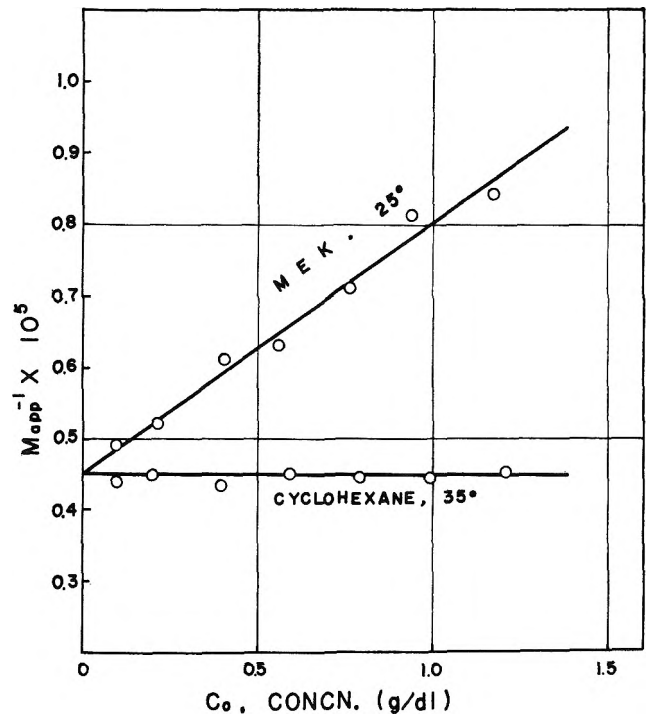

Figure 6. Plots for M_{app}^{-1} as a function of initial concentration c_0 for monodisperse polystyrene S111 in methyl ethyl ketone at 25° and in cyclohexane at 35°.

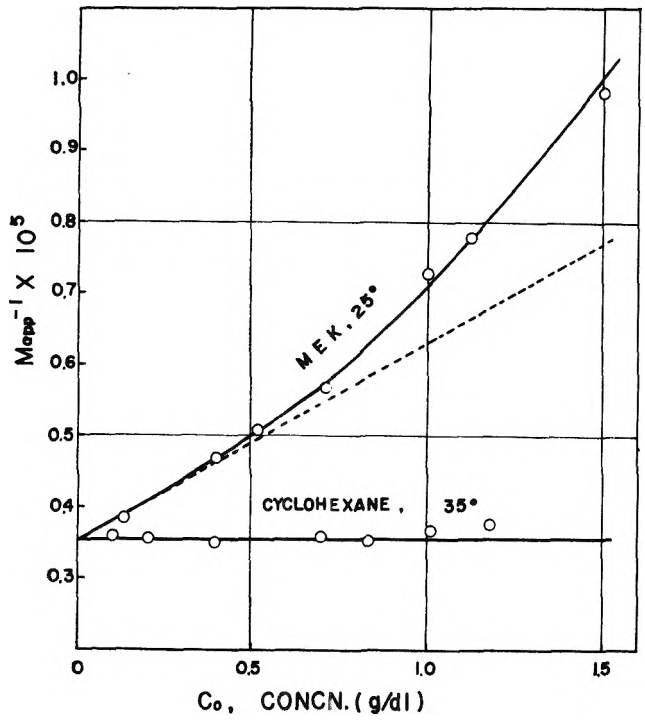

Figure 7. Plots for M_{app}^{-1} as a function of initial concentration c_0 for polydisperse polystyrene SMI in methyl ethyl ketone at 25° and in cyclohexane at 35°.

The values of A_2' estimated from the initial slopes of the solid lines of Fig. 6 and 7 are given in Table II. The A_2' value so obtained for the system S111–MEK is about 25% larger than that for the system SMI–MEK. Although it is likely that the light scattering second virial coefficient is affected by polydispersity of a given solute, it is not yet certain whether this appreciable difference is realizable or at least is in the right direction expected by theory when the marked difference in polydispersity between these two samples is taken into account.

(16) H. Inagaki, T. Matsuo, and K. Hayashi, Paper read at the 12th Polymer Symposium, Nagoya, Japan, November, 1963.

(17) This difficulty may be more or less reduced by using an empirical procedure proposed by Inagaki,[16] who showed that a linear extrapolation may be made when log M_{app}^{-1} is plotted against c_0.

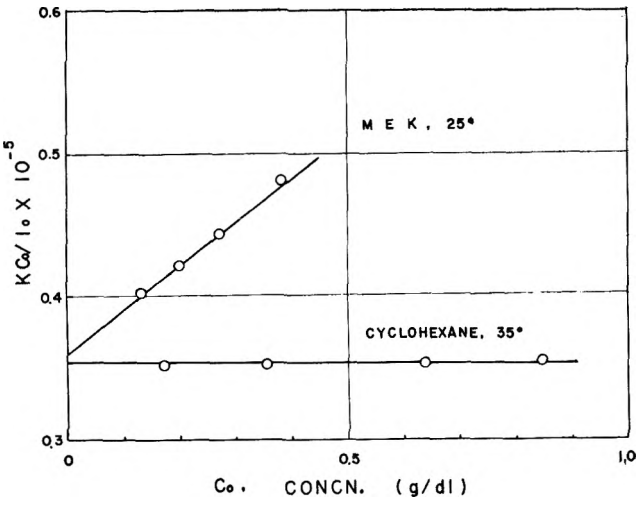

Figure 8. Kc_0/i_0 as a function of polymer concentration c_0 for polydisperse polystyrene SMI in methyl ethyl ketone at 25° and in cyclohexane at 35°. Here i_0 is the reduced intensity of scattered light at zero angle, and K is the familiar constant in the theory of light scattering. Data were taken with the unpolarized blue light from mercury.

Comparison with Light Scattering Data. Figure 8 shows plots for Kc_0/i_0 *vs.* c_0 on sample SMI in MEK at 25° and in cyclohexane at 35°. Here i_0 is the excess turbidity of the solution over that of the solvent and K is the familiar constant appearing in the theory of light scattering. These plots were obtained by treating experimental data in terms of the Zimm procedure. The values of M_w and A_2' deduced from the intercepts and initial slopes of these plots are recorded in Table II. This table also includes the corresponding values for sample S111 taken from the table accompanying distribution of sample.

Comparison of data summarized in Table II indicates that, as expected, eq. 1 yields the same information as does the method of light scattering. It is seen that for both M_w and A_2' the agreement between the Archibald and light scattering measurements is better with sample SMI than with sample S111, in either of the two solvents studied. However, even in S111 the average of the M_w from light scattering measurements in the two solvents comes close to our Archibald value. Of interest is the result that the A_2' value for S111 in MEK from light scattering experiment is even about 50% larger than the corresponding light scattering value for SMI in the same solvent. This difference is more appreciable than that found here between the Archibald A_2' values of the two systems. However, both results are qualitatively consistent, and we are tempted to consider that the value of A_2' may increase as polydispersity of the solute is decreased.

Acknowledgment. The study reported in this paper was made possible by a grant-in-aid (G21512) from the National Science Foundation, Washington, D. C. The principal investigator (H. F.) thanks the Foundation for its confidence in him.

Appendix

The result of Table I that the values of $[\eta]$ for SMI and S111 in cyclohexane at 35° are nearly the same may be accounted for by the difference in polydispersity between the two samples. For a series of perfectly monodisperse polystyrene samples in this θ-solvent one may write

$$[\eta] = KM^{1/2} \qquad (1')$$

where M is the molecular weight of a given (monodisperse) polystyrene, and K is a constant characteristic of the system. For K one may substitute a value of 8.0×10^{-4} which has recently been obtained by Homma, *et al.*,[8] from measurements on "living" polystyrene samples. In fact, if the value of 0.385 given in Table I is substituted into $[\eta]$ in eq. 1′, together with this K value, one obtains $M = 23.1 \times 10^4$, which is quite close to the M_w value of S111, an almost monodisperse polystyrene. Both sides of eq. 1′ are multiplied by the differential molecular weight distribution $f(M)$ and integrated over the entire range of M, giving

$$[\eta] = K \int_0^\infty f(M)(M)^{1/2}dM \qquad (2')$$

Here $[\eta]$ denotes the limiting viscosity number of a polystyrene sample having the molecular weight distribution $f(M)$ in cyclohexane at 35°. Substitution of the $f(M)$ curve for sample SMI shown in Fig. 1 into eq. 2′, along with $K = 8.0 \times 10^{-4}$, yields, after numerical integration, $[\eta] = 0.404$. This compares well with the experimental value of Table I.

The Nature of Residual OH Groups on a Series of Near-Faujasite Zeolites

by J. L. Carter, P. J. Lucchesi, and D. J. C. Yates

Process Research Division, Esso Research and Engineering Company, Linden, New Jersey
(Received December 4, 1963)

The infrared spectra of a series of ion-exchanged zeolites of the faujasite family have been measured. The exchanged materials contained the ions: sodium, lithium, potassium, silver, cadmium, calcium, barium, and strontium. It is shown that these faujasites retain OH (and OD) groups on their surface, even after evacuation at 450°. These spectra are compared and contrasted with those of alumina, silica, and titania. It is considered that some of the OH groups are attached to "alumina-like" parts of the lattice, and some to the "silica-like" part of the lattice. Finally, a third type of OH groups is related to the presence of exchangeable cations.

Introduction

Despite the importance of zeolites or so-called molecular sieves, very little infrared spectroscopic work has been done on the surface properties of these materials. It has been considered that, as their highly crystalline nature ensures that the valencies of most of the ions are satisfied, zeolites would not contain any residual OH groups after evacuation at elevated temperatures. Such surface OH groups on oxides have infrared absorption bands which vary characteristically with the oxide: *e.g.*, alumina,[1] silica,[2,3] and titania.[4] It is of obvious interest and importance to determine whether or not zeolites contain similar residual OH groups.

The earliest work appears in a note by Frohnsdorff and Kington,[5] who used a mull technique and studied zeolites with relatively large amounts of adsorbed water. The mull technique is unsatisfactory in studying the spectra of adsorbed species, as discussed elsewhere.[6] A study by Szymanski, Stamires, and Lynch[7] gave considerably more information. However, they used a spectrometer with a NaCl prism which has extremely poor resolution in the OH stretching region, and no spectra were presented of dehydrated zeolites having residual OH groups. Since this work was begun, a paper by Bertsch and Habgood[8] has appeared in which very low coverages of adsorbed water and carbon dioxide were studied. They did not, however, find any residual OH groups on the evacuated sieves.

We have recorded the infrared spectra of a series of ion-exchanged faujasite-like molecular sieves evacuated at several temperatures. The results obtained show that all sieves studied had three residual OH groups (with little, if any, residual water) and that two of these bands are probably associated with OH groups which are part of the aluminosilicate structure, while the third OH band appears associated with the varying cationic part of the structure.

Experimental

Materials. The starting material in this work was pure, powdered Linde 13X sieve (containing no binder), which has a near-faujasite[9] type of structure. The majority of the work, and all of the ion-exchanged preparations, was done using Linde Lot No. 13961, but some work was done with Na-13X, Linde Lot No. 133692-R. The sodium to aluminum ratio was determined in our laboratories for both batches. For Lot No. 13961, our data gave a molecular ratio varying from 0.94 to 0.97 from four separate determinations,

(1) J. B. Peri, *Actes Congr. Intern. Catalyse, 2e, Paris, 1960*, 1, 1333 (1961).

(2) A. N. Terenin, *Mikrochim. Acta*, 2, 467 (1955).

(3) R. S. McDonald, *J. Phys. Chem.*, 62, 1168 (1958).

(4) D. J. C. Yates, *ibid.*, 65, 746 (1961).

(5) G. J. C. Frohnsdorff and G. L. Kington, *Proc. Roy. Soc.* (London), A247, 469 (1958).

(6) R. P. Eischens and W. A. Pliskin, *Advan. Catalysis*, 10, 2 (1958).

(7) H. A. Szymanski, D. N. Stamires, and G. R. Lynch, *J. Opt. Soc. Am.*, 50, 1323 (1960).

(8) L. Bertsch and H. W. Habgood, *J. Phys. Chem.*, 67, 1621 (1963).

(9) R. M. Barrer, F. W. Bultitude, and J. W. Sutherland, *Trans. Faraday Soc.*, 53, 1111 (1957).

the average being 0.96. On Lot No. 133692-R, two determinations were done, values of 0.95 and 0.97 being obtained, again giving an average of 0.96.

From this material, the sodium was removed by ion exchange with metal salts using procedures similar to those of Barrer and Bratt.[10] Deuterium was obtained from the General Dynamics Corp. and was stated to have a purity of at least 99.5%. Before use, it was dried by passage through a trap at 77°K.

The degree of ion exchange was determined by analyzing the zeolite for the amount of residual Na and was greater than 90% in all cases. To check that the ion-exchange processes had not destroyed the crystal structure, X-ray analyses were run on all samples, using a Philips diffractometer with a Gieger counter detector. They showed the samples to be crystalline, with only traces of amorphous material present. In addition, X-ray data were obtained for the Na material (Lot No. 13961), both on the powder as received, and after pressing at 10,000 p.s.i. As expected, no significant differences could be found either in line intensities, positions, or widths, and it is concluded that no changes are induced in the samples by the pressing procedure.

To put the powders in a form suitable for spectroscopic examination, quantities of the powders were pressed in a 1-in. die at 10,000 p.s.i. The "thicknesses" used ranged from 15 to 35 mg./cm.^{2}. Pieces about 0.5 cm. wide and 2 cm. long were cut from the disk to fit in the cell.

Apparatus. The apparatus used consisted of a dual cell, in which the compressed zeolite flakes were placed for spectroscopic examination. One end of the cell which was used for the high temperature evacuation of the samples was made of silica. The Pyrex end of the cell had two barium fluoride windows, attached with Glyptal cement. Other details of the apparatus have been published elsewhere.[11]

A Beckman IR-7 double beam grating spectrometer was used, with two mirror systems providing external foci. The samples used had quite high light losses, mostly due to scattering, so that slits had to be used which were wider than normal. Details are given (from the maker's handbook) in Table I of the resolution of the instrument, in cm.$^{-1}$, for a slit width of 1 mm. at the given frequencies. The actual slit widths used, in mm., are noted in the figure legends. For the slit widths used here, the effective resolving power under the given experimental conditions can be obtained by multiplying the resolution given in the table by the slit widths actually used.

Procedure. After the samples were inserted in the cell, they were evacuated and then heated to 100°. When a dynamic vacuum in the region of 10^{-4} torr was obtained, the temperature was increased slowly to 200°. After reaching the same vacuum again, the temperature was further increased until the highest temperature needed for the particular experiment was reached. This is necessary because some of these zeolites are damaged[12] by water at temperatures above 200°. Pumping then continued until vacua in the region of 5×10^{-6} torr were obtained. The cell was then isolated from the vacuum system and the spectrum of the sample run after cooling to room temperature.

Table I: Resolution in cm.$^{-1}$/mm. of Slit Width

Frequency, cm.$^{-1}$	Resolution, cm.$^{-1}$
3800	8.4
3700	7.8
3600	7.4
3500	6.9
2800	6.1
2700	5.6
2600	5.2
2500	4.7

In the cases where deuteration was to be carried out, the above steps were followed initially, and the spectrum of the OH groups was determined. After this, the sample was reheated and evacuated to the desired deuteration temperature, and then the deuterium was added. Pressures in the region of 20–40 cm. were used. After the desired time of deuteration had elapsed, the sample was evacuated while still hot and then cooled down to room temperature *in vacuo*.

Results

The variation of residual water and OH groups on the Na zeolite as a function of temperature of evacuation is shown by the spectra of Fig. 1. The thickness of this particular sample was not measured, but it was about 15 mg./cm.^{2} as calculated by comparison of the optical densities of curve d of Fig. 1 with the comparable curve in Fig. 5.

Figure 2 shows the OH stretching bands of the near-faujasite substituted with the monovalent cations silver, lithium, and potassium.

Figure 3 shows the spectra of the near-faujasite substituted with the divalent cations of cadmium and cal-

(10) R. M. Barrer and G. C. Bratt, *J. Phys. Chem. Solids*, 12, 130 (1959).

(11) D. J. C. Yates and P. J. Lucchesi, *J. Chem. Phys.*, 35, 243 (1961).

(12) R. M. Barrer and W. I. Stuart, *Proc. Roy. Soc.* (London), A249, 464 (1959).

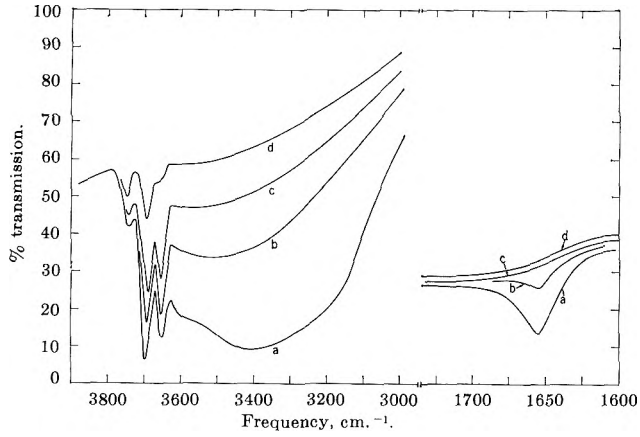

Figure 1. Transmission spectra of Na–X faujasite after evacuation at: (a) 150°; (b) 300°; (c) 450°; and (d) 600°. Slit widths in mm. at 3800, 3700, and 3600 cm.$^{-1}$ are 1.90, 1.63, and 1.43.

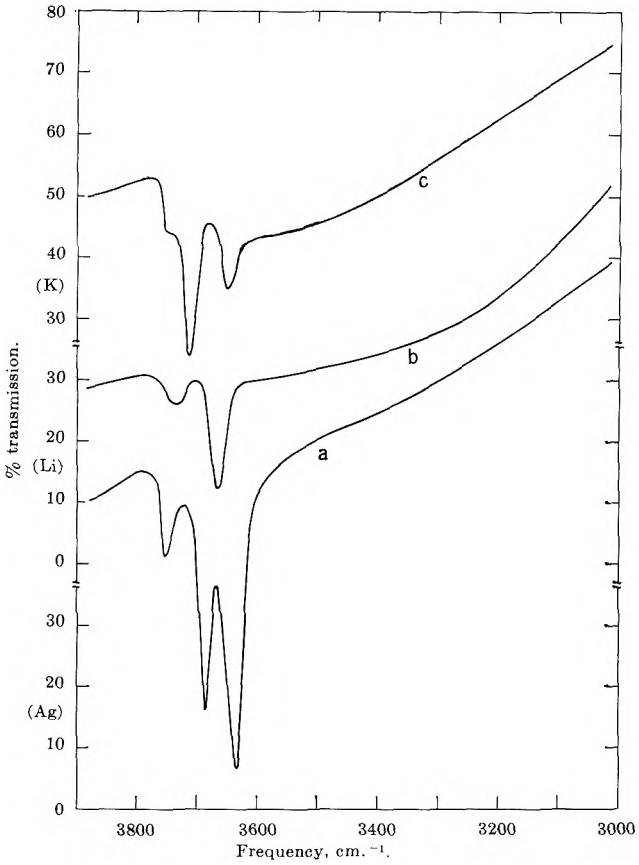

Figure 2. Transmission spectra, after evacuation at 450°, of (a) Ag–X; (b) Li–X; and (c) K–X. Slit widths in mm. for a, at 3800, 3700, and 3600 cm.$^{-1}$ are: 1.65, 1.40, and 1.25. Slit widths for b and c at the same frequencies are b, 1.55, 1.36, 1.20; c, 1.80, 1.55, 1.36.

cium and Fig. 4 shows spectra obtained with the strontium and barium samples.

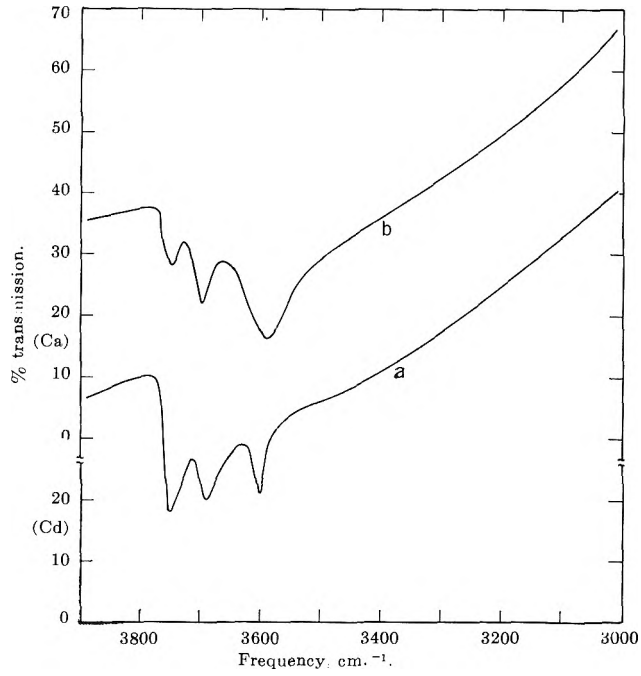

Figure 3. Transmission spectra, after evacuation at 450°, of (a) Cd–X and (b) Ca–X. Slit widths in mm. for (a) at 3800, 3700, and 3600 cm.$^{-1}$ are: 1.90, 1.63, and 1.43. For (b) at the same frequencies: 1.70, 1.46, and 1.30.

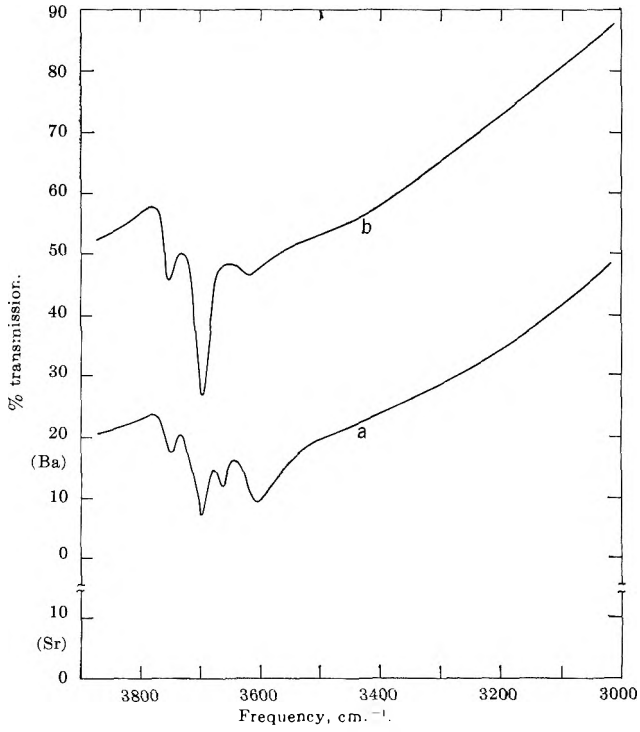

Figure 4. Transmission spectra, after evacuation at 450°, of (a) Sr–X and (b) Ba–X. Slit widths for both (a) and (b) in mm. at 3800, 3700, and 3600 cm.$^{-1}$ are 1.65, 1.40, and 1.25.

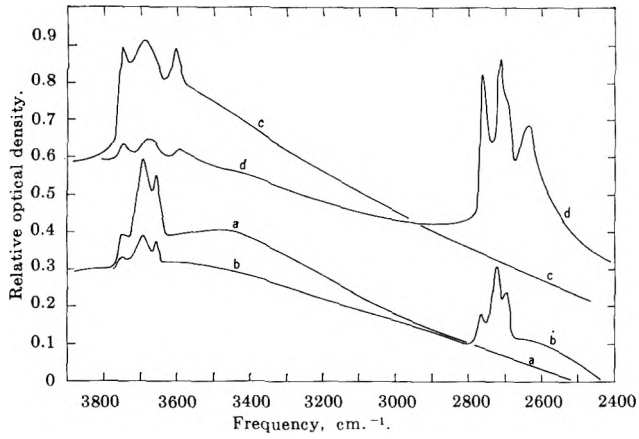

Figure 5. Absorption spectra of Na–X (a and b) of thickness 31.5 mg./cm.^{2} for Cd–X (c and d) thickness 29.9 mg./cm.^{2}. Slit widths in mm. for all spectra at 3800, 3700, 3600, 2800, 2700, and 2600 cm.$^{-1}$ are: 2.8, 2.4, 2.1, 2.2, 2.1, and 2.1, respectively. Treatments: (a) evacuation at 600°; (b) same sample after deuteration with 16.1 cm. of D_2 for 10 min. at 450°; (c) evacuation at 450°; (d) same sample after deuteration with 16.7 cm. of D_2 for 10 min. at 450°.

Figure 5 shows spectra, presented in absorbance, of samples of known thickness of the sodium and cadmium forms of the material.

Table II contains a summary of the frequencies found of the residual OH and OD groups (after evacuation at 450°) for all the samples studied.

Table II: Frequencies (cm.$^{-1}$) of Residual OH and OD Groups on Near-Faujasites

Cation	Band positions, cm.$^{-1}$			
Li (OH)	3740		3660	
Na (OH)	3750	3695	3655	
Na (OD)	2765	2725	2700	
K (OH)	3750	3715	3650	
K (OD)	2760	2735	2690	
Ag (OH)	3750	3685	3630	
Ba (OH)	3750	3695	3620	
Ca (OH)	3750	3695	3590	
Sr (OH)	3750	3700	3660	3605
Cd (OH)	3750	3690	3600	
Cd (OD)	2760	2715	2640	

Discussion

Nature of Residual Water on Na-13X. Some controversy appears in the published literature concerning the presence or absence of residual OH groups (as distinct from water) on the Na zeolite (Linde 13X). Szymanski, *et al.*,[7] considered that residual OH groups were present on this material, while Bertsch and Habgood's observations[8] indicated the absence of structural surface hydroxyls.

While we agree with Szymanski, *et al.*, in concluding that residual OH groups are present, we do not consider that their published spectra showed this at all. In fact, the bands which they assigned to isolated OH groups are almost certainly due to water, and this point has been discussed elsewhere.[8]

Figure 1 shows that an extremely broad band, centered at about 3400 cm.$^{-1}$ is observed after evacuation at 150° together with three sharp bands at 3750, 3695, and 3655 cm.$^{-1}$. At 300°, there is little change in the intensity of the three high frequency bands, and no change in their frequencies, but the 3400 cm.$^{-1}$ band moved to about 3500 cm.$^{-1}$ and became much weaker. At 450°, the broad band became weaker and appeared to move to higher frequencies. At 600°, the three high frequency bands were considerably reduced in intensity, although unaltered in frequency, and the broad band was absent. Even without confirming evidence from the 1600-cm.$^{-1}$ region, it can be stated that the spectra in Fig. 1 are due to two types of residual OH groups, one giving the broad band and the other giving the three sharp bands.

The broad band at about 3400 cm.$^{-1}$ is undoubtedly due to a hydrogen-bonded species: it is a well-known characteristic of such systems that extremely broad, intense, bands are formed, with half-widths of several hundreds of wave numbers.[13] For instance, van Thiel, Becker, and Pimentel,[14] showed that polymeric water, in a solid nitrogen matrix, had a stretching band at 3355 cm.$^{-1}$ with a half-width of 365 cm.$^{-1}$. We cannot accurately measure the half-width of our 3400-cm.$^{-1}$ band, but it is probably of the same order of magnitude as that found in the matrix work. The matrix studies also showed that broad bands are not found in the bending vibration of water; the half-width of the 1633-cm.$^{-1}$ band in the polymeric species is only 35 cm.$^{-1}$. The half-width of the band which we find at 1655 cm.$^{-1}$ is 25 cm.$^{-1}$. In addition, it was shown in the matrix work[14] that the stretching band of the monomer had a half-width of only 25 cm.$^{-1}$.

Based on the above studies with water, it is considered that the broad band in Fig. 1 at about 3400 cm.$^{-1}$ and the narrow band at 1655 cm.$^{-1}$ are due to residual hydrogen-bonded "polymeric" water.

(13) G. C. Pimentel and A. L. McClellan, "The Hydrogen Bond," W. H. Freeman and Co., San Francisco, Calif., 1960.

(14) M. van Thiel, E. D. Becker, and G. C. Pimentel, *J. Chem. Phys.*, 27, 486 (1957).

The OH groups of the other type are responsible for the three high-frequency bands. They are isolated OH groups and are not hydrogen bonded to any significant degree. At temperatures of 450° and above, the 1655 cm.$^{-1}$ bending band disappears and the broad 3400 cm.$^{-1}$ band is very weak indeed. Hence, the water on this particular sieve is substantially all removed at 450°, while strong bands due to isolated OH groups remain. As the intensity of the 1655 cm.$^{-1}$ band is much less than that of the 3400–3600 cm.$^{-1}$ band, it is difficult to use the absence of the 1655 cm.$^{-1}$ band to indicate the removal of water. No doubt, if thicker samples were used, it would be found that higher temperatures had to be used to remove all the water. However, with our thickness, and the vacua and pumping times we used, all the water seemed to be removed at 450° and above.

It is of interest to note that the only workers[8] who used resolution similar to ours did not find the three high-frequency OH bands on dehydration of the Na–X sieves. This is difficult to understand. It is possible that this discrepancy is due to differences in sodium to aluminum ratio in the particular samples used. Bertsch and Habgood[8] state that their analyses showed a Na:Al ratio of 1.01, with values varying from 0.96 to 1.07. Our analyses on Lot No. 13961 give an average of 0.96, with values varying from 0.94 to 0.97. However, it should be pointed out that there seems to be a considerable amount of conflicting data on the Na:Al ratio for Linde 13X. The earliest reported analyses seem to be by Barrer, Buser, and Grütter,[15] who reported a Na:Al ratio of unity, with only a 1% variation in the ratio. The only other workers who have found ratios close to unity are Bertsch and Habgood.[8] Several other workers have reported values considerably less than this; Howell,[16] for example, reported 0.92, and Szymanski, Stamires, and Lynch[7] reported 0.91. In an effort to clear up this disagreement, we asked the manufacturers of the material what they considered to be a typical value of this ratio. They told us[17] that the majority of the lots they make have a ratio of about 0.9, with approximate limits 0.85 and 0.95. It would thus appear that the majority of the Linde 13X which has been used is somewhat sodium deficient, and it is possible that the workers who obtained unity Na:Al ratio had unusual samples. As a check on this point, we have measured infrared spectra on a sample of Lot No. 133692-R after evacuation at 450°. Spectra were obtained which were very similar indeed to those shown in Fig. 1, the three OH groups having similar intensities and frequencies. The only significant difference seemed to be that the ratio of the peak optical density of the 3750 cm.$^{-1}$ band, relative to the 3695 cm.$^{-1}$ band, was about 0.3 for Lot No. 13961 and 0.45 for Lot No. 133692-R. The peak optical densities of the 3695 cm.$^{-1}$ band were 0.46 for Lot No. 13961 (thickness 28.0 mg./cm.^{2}) and was also 0.46 for Lot No. 133692-R (thickness 30.7 mg./cm.^{2}). This shows that the coverage of the surface with OH groups, after evacuation at 450°, is similar for the two lots of 13X.

If the difference in Na:Al ratio for our samples (ratio 0.96, Lot No. 13961) and those used by Bertsch and Habgood (ratio 1.01, Lot No. not given) is significant, this might explain the strong bands which we found. If the lattice is sodium-deficient, it will become stable, in aqueous systems, either by hydronium ions[7] or possibly by hydrogen ions. The question of residual hydronium ions will be considered later, but if the lattice is stabilized by the presence of strongly adsorbed hydrogen ions, it is possible that these would transform into OH groups on heating and evacuating the material.

Although it is difficult to compare OH intensities due to complications of hydrogen bonding, it is of interest to note that the spectra of the Na–X sample (of thickness 31.5 mg./cm.^{2}) in Fig. 5 has an optical density of the most intense band (at 3690 cm.$^{-1}$) of 0.30 after evacuation at 600°. With an alumina of thickness 32.2 mg./cm.^{2} after evacuation at 600°, the most intense band (at 3720 cm.$^{-1}$) had an optical density[18] of 0.68. Figure 3 in ref. 19 gives an illustration of the relative OH intensities on the same alumina as that mentioned above. This suggests that the OH coverage of the surface of Na–X after evacuation at 600° is about one-seventh as great as that on alumina, as the surface area of the alumina used is 295 m.^{2}/g.,[19] while that of the Na–X is about 1000 m.^{2}/g., both being calculated on the sample weight after evacuation at 450°. The latter area was calculated from argon isotherms measured in this laboratory, and is in good agreement with that published by Barrer and Sutherland.[20]

This relatively low coverage of Na–X surface with residual OH groups, compared with the much less crystalline alumina, is in agreement with earlier ideas of the nature of zeolitic surfaces. However, the statement of earlier workers[8] that "There is an absence of structural surface hydroxyls to any detectable extent," while it may have been correct under their experi-

(15) R. M. Barrer, W. Buser, and W. F. Grütter, *Helv. Chim. Acta*, **39**, 518 (1956).

(16) P. A. Howell, *J. Phys. Chem.*, **64**, 364 (1960).

(17) R. W. Alexis, Linde Co., private communication.

(18) D. J. C. Yates, unpublished results.

(19) P. J. Lucchesi, J. L. Carter, and D. J. C. Yates, *J. Phys. Chem.*, **66**, 1451 (1962).

(20) R. M. Barrer and J. W. Sutherland, *Proc. Roy. Soc.* (London), **A237**, 439 (1956).

mental conditions, is not always correct when other samples are used. The results obtained in this work show that the surfaces of molecular sieves are complex and contain OH groups as impurities in common with surfaces of other less well-crystallized oxides. The view has been fairly widely held in the past that the internal surfaces of zeolites could be understood solely in terms of their crystallographic structure, but it is now evident that the effect of residual OH groups will have to be considered when the surface properties of these materials are under discussion.

Finally, we examined our spectra for the presence of residual H_3O^+. Spectra of H_3O^+ in crystals[21] show that a very broad band exists in the region from 2900 to 3300 cm.$^{-1}$, and that this band varies in frequency with the surroundings of the H_3O^+ ion. However, a band at about 1690–1750 cm.$^{-1}$ seems to be characteristic of these ions, both for solids[21] and in solutions.[22] We have found no trace of a band under any conditions in the 1700 cm.$^{-1}$ region in this work (Fig. 1) on Na–X. If any such ions are left, even after evacuating the material at low temperatures (150°), they must be present at low concentrations.

Variations in Frequency and Intensity of Residual OH Groups with Change of the Cations. From Fig. 1 to 4, it will be seen that there is a very considerable variation in the nature of residual OH group on one type of zeolite, namely near-faujasite, when the exchangeable cations are varied. Even when only one type of cation is changed (*e.g.*, monovalent, Fig. 1 and 2) there is a considerable change in the spectrum. In the most general sense, this must indicate that the oxygen atoms which are part of these OH groups are affected in some way by the cations, but a detailed interpretation of these effects cannot be undertaken with the data presently available.

Some oxides, such as silica, only have one OH stretching frequency[3]; others have two (anatase[4]) and three (alumina[1]). In the case of alumina, no explanation of the origin of these three bands has been given, and it is extremely difficult to do so without additional nonspectroscopic information.

However, as zeolites are essentially aluminosilicates in which electrical neutrality is ensured by the exchangeable cations, it is reasonable to try to determine if any of the OH bands found on the zeolites can be correlated with those found on the component oxides. Silica, being the simplest, is considered first. Here, all forms of silica, whether prepared under anhydrous conditions (*e.g.*, Cabosil[3]), or as silica powders under aqueous conditions,[3] or as porous glass[2,23] made in aqueous acid solutions,[24] give a sharp band at 3750 cm.$^{-1}$ when evacuated at high enough temperatures.[23,25] Examination of Table II shows that, in all cases, the highest frequency of the three bands found on 13X is between 3750 and 3740 cm.$^{-1}$. It is possible that this band is caused by OH groups, the oxygen of which is part of the "silica" portions of the zeolite.

With alumina, in contrast, three bands are found at frequencies of about[19] 3785, 3740, and 3710 cm.$^{-1}$. These vary a little[1,18] from alumina to alumina in frequency and relative intensity, but in most cases three bands are obtained, the two lower frequency ones being the most intense.[26] Examination of Table II shows that the OH band of intermediate frequency is in the region 3715 to 3685 cm.$^{-1}$. While this band is clearly not as well defined (a spread of 30 cm.$^{-1}$) as the higher frequency band (a spread of 10 cm.$^{-1}$) it still seems reasonable that this band has a common origin, probably independent of the exchangeable cation. It is suggested that the band near 3700 cm.$^{-1}$ on these near-faujasites is due to OH groups, the oxygen of which is part of the "alumina" portions of the zeolite.

The lowest frequency band in Table II, in marked contrast with the other two bands, varies widely in frequency, from 3660 to 3590 cm.$^{-1}$ as the cations are changed. The only oxide for which OH bands have been found at frequencies below 3700 cm.$^{-1}$ is titania, where bands at 3680 and 3675 cm.$^{-1}$ were observed.[4] Because of their wide variation in frequency, and because these frequencies are all substantially lower than those reported on alumina, silica, and titania, we consider that these bands are connected with the presence of the lattice cations. It is unlikely that the oxygen of these OH groups is directly attached to the cation, but rather that it is close to the cation. If it were directly attached to the cation, bands might be expected with relative frequencies similar to those found[27] with solid LiOH and KOH. The latter occur at 3678 and 3611 cm.$^{-1}$, while the bands on the respective near-faujasites occur with much smaller frequency differences at 3660 and 3650 cm.$^{-1}$ (Table II). Further evidence comes from experiments[8] where water was added back to dehydrated 13X. Under these conditions, sharp bands were found at 3720 and 3648 cm.$^{-1}$ for the Li–X and K–X sieves, and these bands were plausibly assigned[8] to water molecules adsorbed directly on the cations.

(21) C. C. Ferisco and D. F. Hornig, *J. Chem. Phys.*, 23, 1464 (1955).

(22) M. Falk and P. A. Giguere, *Can. J. Chem.*, 35, 1195 (1957).

(23) D. J. C. Yates, *Advan. Catalysis*, 12, 265 (1960).

(24) M. E. Nordberg, *J. Am. Ceram. Soc.*, 27, 299 (1944).

(25) T. H. Elmer, I. D. Chapman, and M. E. Nordberg, *J. Phys. Chem.*, 66, 1517 (1962).

(26) J. L. Carter and D. J. C. Yates, unpublished results.

(27) R. A. Buchanan, *J. Chem. Phys.*, 31, 870 (1959).

As well as a wide variation in frequency, these bands vary even more in intensity. Figure 4 shows that the 3620 cm.$^{-1}$ band on Ba–X is very weak, while the 3590 cm.$^{-1}$ band on Ca–X (Fig. 3) is very strong. The 3630 cm.$^{-1}$ band on Ag–X (Fig. 2) is also extremely strong, but the most telling comparison is that between the barium and calcium zeolites, in view of the chemical similarity of these cations.

In addition to the data given in Fig. 5, more detailed experiments have been done on the rate of exchange of OH groups and the rate of formation of OD groups. The Na, K, and Cd samples were studied and were deuterated for 10 min. at 150, 300, and 450°.

It was thought that if the low frequency OH groups were directly associated with the cations, there would be a marked variation in the rate of exchange of these groups as the cation was changed. This was not found to occur. In all cases (Na, K, Cd) the intermediate frequency OH groups disappeared to exactly the same extent as did the low frequency groups at all the temperatures used. These observations are thus consistent with the idea that these low frequency OH groups are attached to the lattice close to the cations rather than directly to the cations.

No other attempt will be made here to interpret the varying frequencies and intensities of these 3660 to 3590 cm.$^{-1}$ bands in these near-faujasites. It is considered that such an attempt should wait until a systematic spectroscopic survey has been made of a whole range of ion-exchanged near-faujasites. A further point is that the position of the cations is only known for the sodium form[28] of the 13X material, and even then 48 of the 80 cations per unit cell could not be located. In addition, these X-ray data were obtained with the crystals containing about 25–35% adsorbed water, as they were left in equilibrium with air[28] while under examination, and there is evidence that some of the cations are mobile in hydrated Na–X.[29] Hence, X-ray data on dehydrated near-faujasites, kept under vacuum, with a series of cations, would be needed to enable the present data to begin to be interpreted in terms of crystallographic structure.

Acknowledgments. We wish to thank Mr. P. H. Corneil for his assistance in performing the deuteration experiments, and Mr. W. R. Epperly for helpful discussions.

(28) L. Broussard and D. P. Shoemaker, *J. Am. Chem. Soc.*, 82, 1041 (1960).

(29) R. M. Barrer and G. C. Bratt, *J. Phys. Chem. Solids*, 12, 154 (1959).

Mercury-Photosensitized Decomposition of Propane, Isobutane, and *n*-Pentane at 1849 Å.[1]

by Richard A. Holroyd and Timothy E. Pierce

Radiation Research Laboratories, Mellon Institute, Pittsburgh, Pennsylvania
(Received December 5, 1963)

The relative radical yields from the reaction of excited mercury ($^1P_1$) atoms (produced by the 1849-Å. line of Hg) with propane, isobutane, and *n*-pentane have been determined by use of the ethyl-C^{14} radical scavenger. The 1849-Å. line was isolated with a preirradiated (with γ-rays) LiF filter. The primary dissociation of propane by Hg($^1P_1$) atoms yields 50% *n*-propyl and 50% isopropyl radicals. Similarly the dissociation of isobutane yields 42% isobutyl and 58% *t*-butyl radicals, and the dissociation of *n*-pentane yields 28% *n*-pentyl, 43% 1-methylbutyl, and 29% 1-ethylpropyl radicals. Carbon–carbon bonds are not dissociated at this wave length. The relative rates of removal of tertiary, secondary, and primary hydrogen atoms by Hg($^1P_1$) atoms are in the ratio 12:3:1 contrasting with sensitization of hydrocarbons by Hg($^3P_1$) atoms for which this ratio is 350:65:1. The mechanism of quenching of Hg($^1P_1$) atoms by aliphatic hydrocarbons is formation of radicals by the direct interaction with, and cleavage of, a carbon–hydrogen bond. The ratios, D/R, of disproportionation (in which C_2H_6 and an olefin are formed) to combination are estimated: for $C_2H_5 + n\text{-}C_3H_7 \rightarrow$, D/R = 0.06; for $C_2H_5 + i\text{-}C_4H_9 \rightarrow$, D/R $\sim$ 0; for $C_2H_5 + n\text{-}C_5H_{11}$, D/R = 0.08.

Introduction

In a study of the mercury-photosensitized decomposition of hydrocarbons at 2537 Å. in which radical yields were determined it was shown that tertiary and secondary hydrogen atoms are much more readily abstracted by Hg($^3P_1$) atoms than primary hydrogen atoms.[2] Further it was shown that there was a correspondence between primary radical yields and quenching cross sections for individual carbon–hydrogen bonds. In the course of that investigation it was observed that for *n*-pentane the relative yield of *n*-pentyl radicals was greater when the unfiltered light (2537- and 1849-Å. lines both present) from a low-pressure mercury arc was used than when the 2537-Å. line was used alone. It was suggested that mercury ($^1P_1$) atoms, formed by 1849-Å. excitation, are more effective than ($^3P_1$) atoms in breaking primary carbon–hydrogen bonds. Until this time the reactions of paraffins with excited singlet metal atoms has received little attention. The present study is concerned with the reaction of Hg($^1P_1$) atoms with propane, isobutane, and *n*-pentane.

The 1849-Å. line of mercury may be isolated with a LiF filter.[3] When LiF is irradiated with γ-rays this filter absorbs strongly at 2537 and allows the shorter 1849- and 1942-Å. mercury lines to pass.

Sensitization with mercury ($^1P_1$) atoms is of interest both for comparison with the mercury ($^3P_1$) atom sensitization results and to help establish the mechanism of the sensitization with excited singlet mercury atoms. Although more energy, 6.7 e.v., is available at 1849 Å., it is not expected that excited electronic levels of the hydrocarbon will be reached in the sensitization since if spin is to be conserved a singlet state would be formed which for simple hydrocarbons is at higher energies for a vertical transition.

The technique used to determine radical yields was

(1) This investigation was supported, in part, by the U. S. Atomic Energy Commission; presented at the 146th National Meeting of the American Chemical Society, Denver, Colo., January, 1964.

(2) R. A. Holroyd and G. W. Klein, *J. Phys. Chem.*, 67, 2273 (1963).

(3) J. L. Weeks, S. Gordon, and G. M. A. C. Meaburn, *Nature*, 191, 1186 (1961).

identical with that used earlier.[2] A low concentration of ethylene-C^{14} is present to generate the $C^{14}{}_2H_5$ radical scavenger. Labeled hydrocarbons are produced from which the radical yields in reaction 1 may be determined. The precision and higher sensitivity of this C^{14}

$$Hg(^1P_1) + RH \longrightarrow R_i + H + Hg \qquad (1)$$

tracer technique was useful because the 1849-Å. line in the arc employed was relatively weak.

Experimental

Light Source. The source of 1849-Å. radiation was a conventional low pressure mercury arc mounted 3 cm. above the front window of a quartz reaction cell (220 cc.). The space between the arc and filter was flushed with N_2. A 3-mm. thickness of LiF crystal which had been irradiated with γ-rays was used to isolate the 1849-Å. line. This filter was found to be quite satisfactory if certain precautions are observed. Since the intensity of the 1849-Å. line is ~5% of the 2537-Å. line, which also sensitizes the decomposition efficiently, the filter must reduce the 2537-Å. intensity at least to 0.1%. In actual practice the LiF filter was placed in the γ-source until its O.D. at 2537 Å. was >4.0. The optical density was determined on a Cary Model 14 recording spectrophotometer; measurements up to an O.D. of 4 were possible by using a reference solution whose O.D. at 2537 Å. is about 2.0. The filter was checked after each photolysis. Photobleaching of the absorption band occurred but in every case the O.D. at 2537 Å. after the photolysis was greater than 3.5. Thus, the intensity of the 2537-Å. line was reduced to ~0.01%. This filter passed approximately 20% of the 1849-Å. line (measurements actually made at 1950 Å.). After each experiment the LiF filter was returned to the γ-source and subjected to a dose of ~0.2 Mrad before reuse. The filter gradually darkened at 1849 Å. after repeated irradiations but could be cleared by heating to a high temperature. The efficiency of the filter in removing the 2537-Å. line was demonstrated by carrying out a photolysis in the usual manner utilizing the irradiated LiF filter and also a Corning 7910 filter (which cuts out the 1849-Å. line). No products whatsoever were formed in this blank experiment.

The photolysis cell was mounted vertically so that it could be immersed in a cooling bath. In the case of propane most of the results are for 25° but in later work on isobutane and *n*-pentane the cell was cooled to approximately 0° so that the mercury concentration in the cell would be reduced and the effective reaction volume increased. It was noted that sensitization occurred (at a reduced rate) even at −78° with 1849 Å.[4] Approximately 1 hr. was allowed prior to each photolysis to ensure equilibration and to allow mixing of the $C^{14}{}_2H_4$ and the hydrocarbon. The temperature in the reaction volume, which is close to the front window, may have been somewhat above the temperature of the bath since the front window was not actually immersed in the bath.

The hydrocarbons were Phillips research grade. The ethylene-C^{14} was obtained from New England Nuclear Corp. The purification of these materials and details of the analytical technique have already been described.[2]

Results and Discussion

The results obtained for propane, isobutane, and *n*-pentane are summarized in Tables I, II, and III, respectively. The products in every case are the same as those observed in the mercury sensitization[2] at 2537 Å., namely, ethane-C^{14}, butane-C^{14}, and from two to three labeled hydrocarbons formed by reaction of an ethyl-C^{14} radical with the parent radicals. In general, substantial yields of radicals resulting from the scission of a primary carbon–hydrogen bond are observed, in contrast to sensitization at 2537 Å. Fragment radicals are not observed.

Kinetic Considerations. Mercury sensitization of hydrocarbons with 1849-Å. light is expected to satisfy the requirements of applicability of the $C^{14}{}_2H_5$ radical scavenging technique. Hydrogen atoms must be available from the primary decomposition to generate $C^{14}{}_2H_5$ radicals. That this occurs is indicated by the results which show that labeled hydrocarbons are produced. Also high intensities prevail because of the high value of the extinction coefficient of mercury vapor at 1849 Å.; thus, radical combination reactions are favored.

Therefore, it is reasonable to assume that the same secondary reactions, 2–8, follow the primary decomposition, reaction 1, as were shown to occur at 2537 Å.

$$H + C^{14}{}_2H_4 \longrightarrow C^{14}{}_2H_5 \qquad (2)$$

$$H + RH \longrightarrow H_2 + R_i \qquad (3)$$

$$C^{14}{}_2H_5 + R_i \longrightarrow R_i\text{–}C^{14}{}_2H_5 \qquad (4)$$

$$C^{14}{}_2H_5 + R_i \longrightarrow C^{14}{}_2H_6 + R_i(-H) \qquad (5)$$

$$C^{14}{}_2H_5 + R_i \longrightarrow C^{14}{}_2H_4 + RH \qquad (6)$$

$$C^{14}{}_2H_5 \longrightarrow C^{14}{}_4H_{10} \qquad (7)$$

$$2C^{14}{}_2H_5 \longrightarrow C^{14}{}_2H_4 + C^{14}{}_2H_6 \qquad (8)$$

If even higher light intensities are employed, the reac-

(4) This was expected since the vapor pressure of mercury at −78° is sufficient to absorb completely the 1849-Å. line in a few centimeters; *cf.* "The Photochemistry of Gases" by W. A. Noyes, Jr., and P. A. Leighton, Reinhold Publishing Co., New York, N. Y., 1941, p. 218.

Table I: Propane

C_2H_6, mmoles	$C^{14}{}_2H_4$, μmoles	Rate, picomoles/sec. C_2H_6	n-C_4H_{10}	i-C_5H_{12}	n-C_5H_{12}	k_5/k_4[a]	$k_5/k_2 \times 10^3$
			Temp. = 24°				
1.02	8.43	9.17	19.0	27.0	24.5	0.05	1.54
1.08	3.11	7.18	10.7	25.4	17.9	0.03	1.51
1.05	1.91	11.0	9.96	29.4	18.9	0.19	1.46
1.08	1.38	7.18	6.56	25.9	14.8	0.06	1.41
1.04	0.87	2.96	2.22	11.9	7.0	0.03	1.58
1.11	0.78	4.46	2.68	19.6	10.4	0	1.63
			Temp. = −78°				
1.05	1.40	1.89	2.36	5.9	3.9	0.09	...

[a] Here reaction 5 is $C_2H_5 + n\text{-}C_3H_7 \rightarrow C_2H_6 + C_3H_6$, k_5/k_4 for the reaction of C_2H_5 with $i\text{-}C_3H_7$ is taken as 0.21.

Table II: Isobutane (0°)

i-C_4H_{10}, mmoles	$C^{14}{}_2H_4$, μmoles	Rate, picomoles/sec. C_2H_6	n-C_4H_{10}	2,2-Dimethylbutane	Isohexane	k_5/k_4[a]	$k_5/k_2 \times 10^3$
1.13	13.1	...	6.10	13.0	12.2	...	...
1.09	5.53	6.63	2.77	11.5	9.41	0.05	8.6
1.12	3.39	5.35	2.03	10.0	7.62	0.00	7.0
1.12	2.75	4.09	0.98	7.76	5.60	0.00	8.4
1.02	1.84	3.04	0.57	5.67	3.97	0.02	7.9

[a] Here reaction 5 is C_2H_5 + isobutyl → $C_2H_6 + i\text{-}C_4H_8$.

Table III: Pentane (0°)

n-C_5H_{12}, mmoles	$C^{14}{}_2H_4$, μmoles	Rate, picomoles/sec. C_2H_6	n-C_4H_{10}	3-Methylhexane	3-Ethylpentane	n-Heptane	k_5/k_4[a]	$k_5/k_2 \times 10^3$
0.9	14.4	6.12	9.77	10.4	5.93	7.29	0.12	2.5
0.9	6.42	6.36	8.86	12.3	7.35	8.00	0.05	2.3
0.9	2.93	5.56	5.65	11.6	6.71	6.63	0.04	2.2
0.9	2.00	6.25	4.51	12.5	7.09	6.81	0.12	2.4
0.9	1.44	3.68	2.45	8.22	4.72	4.06	0.04	2.2
0.9	1.28	4.67	3.00	9.65	5.54	5.23	0.10	1.9

[a] Here reaction 5 is $C_2H_5 + n\text{-}C_5H_{11} \rightarrow C_2H_6 + i\text{-}C_5H_{10}$.

tion $H + R_i \rightarrow$ occurs, but here it is assumed to be unimportant.

In general, reaction 1 will produce several radicals R_1, R_2, etc.; α_i is the fraction of dissociations which gives radical, R_i. It has been shown[2] that the ratio of radical yields is obtained from the yields of the corresponding labeled hydrocarbons from the relationship

$$\frac{\phi_{R_i}}{\phi_{R_j}} = \frac{\phi_{R_j\text{-}C^{14}{}_2H_5}(1 + k_5/k_4 + k_6/k_4)}{\phi_{R_i\text{-}C^{14}{}_2H_5}(1 + k_5/k_4 + k_6/k_4)}$$

where k_5/k_4 and k_6/k_4 are the appropriate disproportionation ratios for the radicals R_i and R_j. Further, the mechanism predicts that eq. I should

$$\frac{R_i\text{-}C^{14}{}_2H_5}{C^{14}{}_4H_{10}} = \frac{2\alpha_i(1 + k_8/k_7)}{(1 + k_5/k_4 + k_6/k_4)} + B\frac{(RH)}{(C^{14}{}_2H_4)} \quad (I)$$

be obeyed, where B is a constant. Plots of $R_i\text{-}C^{14}{}_2H_5/C^{14}{}_4H_{10}$ *vs.* $(RH)/(C^{14}{}_2H_4)$ are linear (Fig. 1–4) and the values of α_i were evaluated from the values of the intercepts, as obtained by the least-squares method, and the

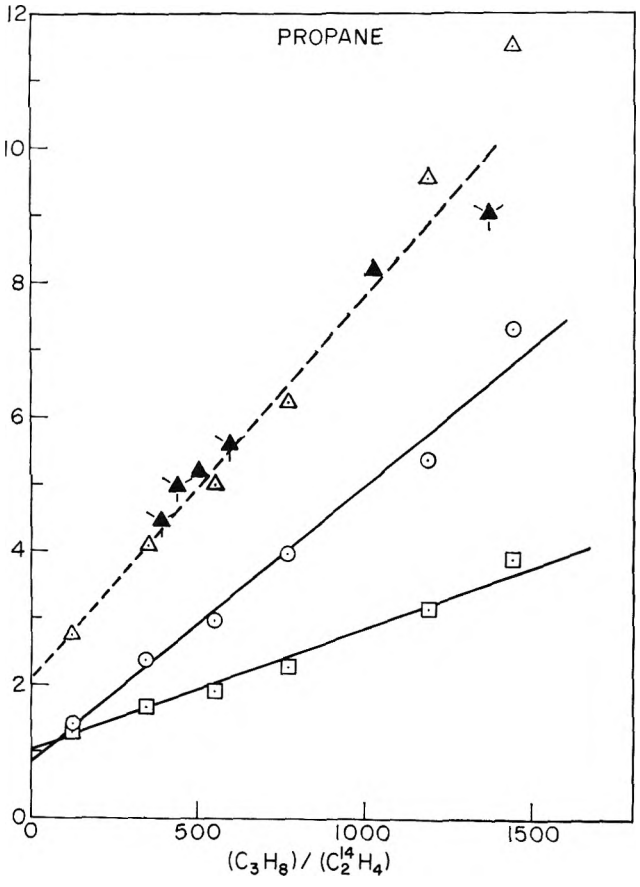

Figure 1. Propane (25°). The lower two solid lines connect observed values of the ratios isopentane-C^{14}/n-$C^{14}_4H_{10}$, ⊙; and n-pentane-C^{14}/n-$C^{14}_4H_{10}$, ⊡. The triangular points are values of the quantity $[\Sigma R\text{-}C^{14}_2H_5(1 + k_5/k_4)]/1.12\ C^{14}_4H_{10}$ at 1849 Å., △; and at 2537 Å., ▲ (flagged points are data from ref. 2).

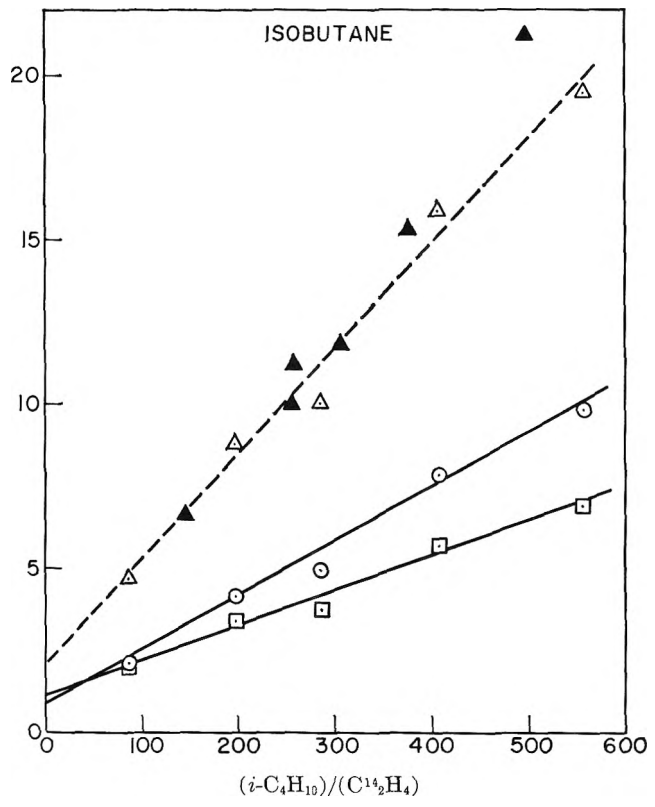

Figure 2. Isobutane. The lower solid lines connect observed values of the ratios: 2,2-dimethylbutane-C^{14}/n-$C^{14}_4H_{10}$, ⊙; and isohexane-C^{14}/n-$C^{14}_4H_{10}$, ⊡. The triangular points are values of the quantity $[\Sigma R\text{-}C^{14}_2H_5(1 + k_5/k_4)]/1.12C^{14}_4H_{10}$ at 1849 Å. and 0°, △; and at 2537 Å. and 25°, ▲ (ref. 2).

appropriate disproportionation to combination ratios, the determination of which will be discussed below.

Values of k_3/k_2 were calculated from plots of eq. II

$$\frac{\sum_i R_i\text{-}C^{14}_2H_5(1 + k_5/k_4)}{C^{14}_4H_{10}(1 + k_8/k_7)} = 2 + \frac{4k_3}{k_2}\frac{(RH)}{(C^{14}_2H_4)} \qquad \text{(II)}$$

which is obtained by summing the above equation for all radicals, R_i. The values of k_3/k_2 obtained in this study from plots of eq. II in Fig. 1, 2, and 3 for propane, isobutane, and n-pentane were 0.0015, 0.0081, and 0.0022, respectively, in good agreement with the values obtained by Holroyd and Klein.[2]

Since eq. II does not contain any α's, it can be used to test if the same mechanism is applicable at both 2537 and 1849 Å. by plotting the quantity on the left-hand side *vs.* $(RH)/(C^{14}_2H_4)$. It is found that the data at 2537 Å. (Fig. 1–3, filled triangles) lie on the same line as determined by the 1849-Å. data (Fig. 1–3, open triangles). Thus, although the primary dissociation is shown to be wave length dependent, the secondary reactions are essentially the same at the two wave lengths. It can also be seen from the figures that no significant fraction of the hydrogen atoms produced are "hot" since if they were formed with excess kinetic energy and abstracted hydrogen forming H_2, the intercepts of the plots of eq. II would be much larger than 2. Further, it is observed that in a 1% solution of $C^{14}_2H_4$ in propane the $C^{14}_2H_4$ will scavenge 83% of the hydrogen atoms generated at 1849 Å.

Propane. The observed products from propane are n-pentane-C^{14} and isopentane-C^{14}. Thus, only n-propyl and isopropyl radicals are produced; but in this case the yield of n-pentane-C^{14} is nearly equal to that of isopentane-C^{14} at high ethylene-C^{14} concentration. A least-squares analysis of the data plotted according to eq. I (lower two lines in Fig. 1) gave intercepts for n-pentane-C^{14}/butane-C^{14} and isopentane-C^{14}/butane-C^{14} of 1.01 and 0.83, respectively. Thus, the ratio of the relative yields of radicals from reaction 1 is

$$\alpha_{t\text{-Pr}}/\alpha_{n\text{-Pr}} = \frac{0.83}{1.01} \times \left(\frac{1 + 0.21 + 0.19}{1 + 0.06 + 0.08}\right) = 1.01$$

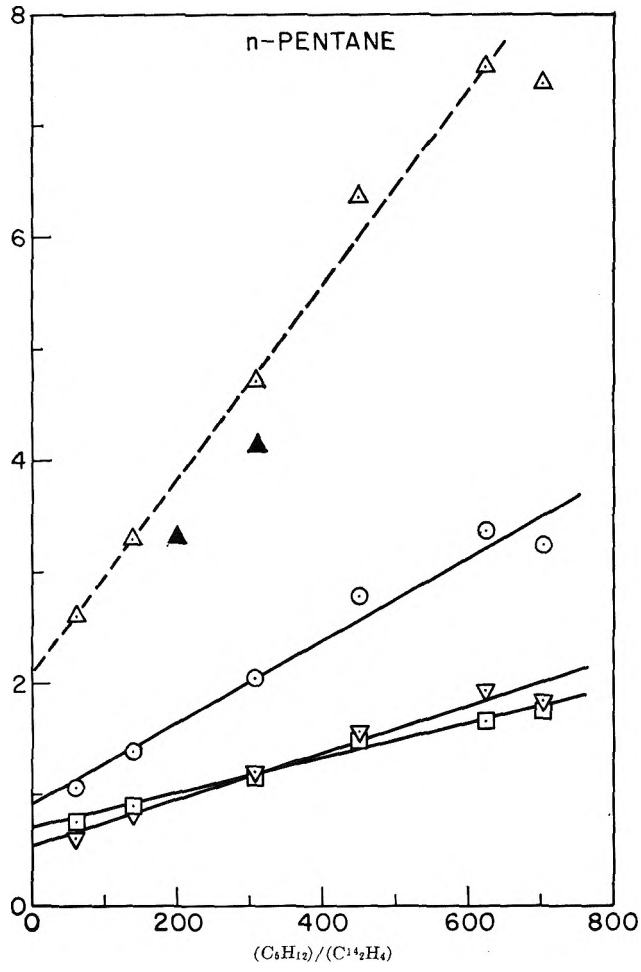

Figure 3. *n*-Pentane (0°). The lower three solid lines connect observed values of the ratios: 3-methylhexane-C^{14}/*n*-$C^{14}_4H_{10}$, ⊙; 3-ethylpentane-C^{14}/*n*-$C_4{}^{14}H_{10}$, ▽; and *n*-heptane-C^{14}/*n*-$C^{14}_4H_{10}$, ⊡. The triangular points are values of the quantity $[\Sigma R\text{-}C^{14}_2H_5(1 + k_5/k_4)]/1.12C^{14}_4H_{10}$ at 1849 Å., △; and at 2537 Å., ▲.

The disproportionation ratios used are: for R = isopropyl, $k_5/k_4 = 0.21$[2] and $k_6/k_4 = 0.19$[5]; and for R = *n*-propyl, $k_5/k_4 = 0.06$ (see Table IV) and $k_6/k_4 = 0.08$.[6]

The primary decomposition at 1849 Å. is

$$Hg(^1P_1) + C_3H_8 \longrightarrow Hg + H + n\text{-}C_3H_7\ (50\%)$$
$$\longrightarrow Hg + H + i\text{-}C_3H_7\ (50\%)$$

Thus, the secondary hydrogen atoms are three times as reactive as the primary hydrogen atoms. These results contrast sharply with the 2537-Å. results, obtained by this same technique,[2] which showed that the primary decomposition is[7]

$$Hg(^3P_1) + C_3H_8 \longrightarrow Hg + H + n\text{-}C_3H_7\ (10\%)$$
$$\longrightarrow Hg + H + i\text{-}C_3H_7\ (90\%)$$

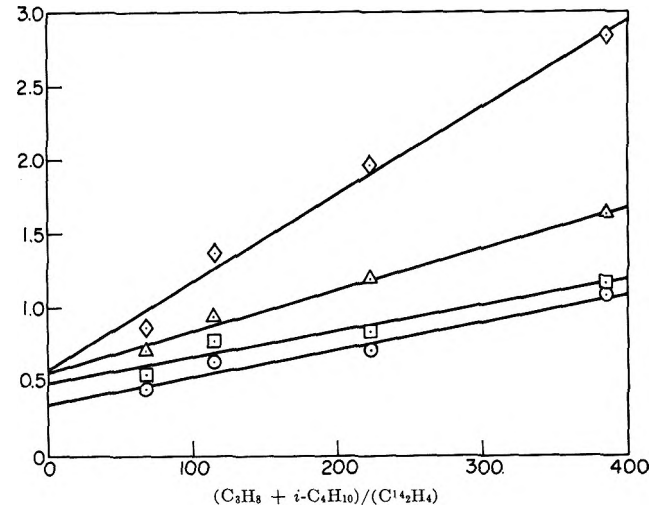

Figure 4. Propane and isobutane (1:1) 0°. The lines connect observed values of the following ratios: isopentane-C^{14}/*n*-$C^{14}_4H_{10}$, ⊙; *n*-pentane-C^{14}/*n*-$C^{14}_4H_{10}$, ⊡; isohexane-C^{14}/*n*-$C^{14}_4H_{10}$, △; 2,2-dimethylbutane-C^{14}/*n*-$C^{14}_4H_{10}$, ◇. Abscissa is $(C_3H_8 + i\text{-}C_4H_{10})/(C^{14}_2H_4)$.

It would be valuable to know quantum yields at 1849 Å. No attempt was made to measure the light flux accurately; however, the quantum yields may be estimated if the ratio of intensities of the 1849- and 2537-Å. lines are known. From an experiment with propane the absorbed light intensity of the 2537-Å. line was calculated to be ~5 nanoeinsteins/sec. assuming $\phi_H{}^{2537} = 0.9$. The rate of formation of $C^{14}_2H_5$, the sum of the rates of all labeled hydrocarbons, is 0.10 nanomole/sec. in a typical run at 1849 Å. (top row of Table I). The rate of formation of hydrogen atoms, R_H, is given by $R_{C^{14}_2H_5}[1 + k_3(C_3H_8)/k_2(C^{14}_2H_4)]$, which is equal to 0.12 nanomole/sec. Since ϕ_H cannot be larger than unity this places a minimum on the intensity of the 1849-Å. line of 0.60 nanoeinstein/sec., (the filter absorbed 80% at 1849 Å.). Thus, for unfiltered light from the lamp, the intensity of the 1849-Å. line reaching the cell is >7% of the intensity of the 2537-Å. line. If the relative intensity of the 1849-Å. line is not much larger than 7% the quantum yield of hydrogen atoms is close to unity.

Isobutane. The labeled products from isobutane, besides C_2H_6 and C_4H_{10}, are 2,2-dimethylbutane and isohexane. From the plots of eq. I (Fig. 2) the intercepts for 2,2-dimethylbutane-$C^{14}/C^{14}_4H_{10}$ and isohexane-$C^{14}/C^{14}_4H_{10}$ are 0.90 and 1.13, respectively.

(5) J. A. G. Dominguez, J. A. Kerr, and A. F. Trotman-Dickenson, *J. Chem. Soc.*, 3357 (1962).

(6) Predicted from eq. III, ref. 2.

(7) There is, however, some controversy regarding the relative yields of *n*-propyl and isopropyl radicals from the primary decomposition of propane at 2537 Å.; *cf.* ref. 2 for details.

As above the ratio $\alpha_{t\text{-butyl}}/\alpha_{\text{isobutyl}}$ is given similarly by

$$\frac{0.90}{1.13} \times \frac{1 + 0.51 + 0.31}{1 + 0.02 + 0.05} = 1.4$$

The disproportionation ratios used are: for R = *t*-butyl, $k_5/k_4 = 0.51$ (see below) and $k_6/k_4 = 0.31$[5]; and for R = isobutyl, $k_5/k_4 = 0.02$ (Table IV) and $k_6/k_4 = 0.05$.[6] The primary reaction in the 1849-Å. sensitized decomposition of isobutane is

$$\text{Hg}(^1\text{P}_1) + i\text{-C}_4\text{H}_{10} \longrightarrow \text{Hg} + \text{H} + \text{isobutyl (42\%)}$$
$$\longrightarrow \text{Hg} + \text{H} + t\text{-butyl (58\%)}$$

The tertiary hydrogen atom is thus 12 times as reactive as the primary hydrogen atoms. Again these results contrast sharply with the 2537-Å. results obtained by this same technique which showed that only 3% of the radicals in the initial dissociation are isobutyl.

n-Pentane. The results in Table III show that three radicals: R_1 = *n*-pentyl, R_2 = 1-methylbutyl, and R_3 = 1-ethylpropyl, are formed from *n*-pentane. The values of α as determined from the intercepts of the lower three lines in Fig. 3 are: $\alpha_1:\alpha_2:\alpha_3 = 0.69\ (1 + 0.08 + 0.09):0.91\ (1 + 0.25 + 0.11):0.54\ (1 + 0.25 + 0.29) \cong 1:1.5:1$. The initial dissociation of *n*-pentane at 1849 Å. is therefore

$$\text{Hg}(^1\text{P}_1) + n\text{-C}_5\text{H}_{12}$$
$$\longrightarrow \text{Hg} + \text{H} + \cdot\text{CH}_2\text{CH}_2\text{CH}_2\text{CH}_2\text{CH}_3\ (28\%)$$
$$\longrightarrow \text{Hg} + \text{H} + \text{CH}_3\dot{\text{C}}\text{HCH}_2\text{CH}_2\text{CH}_3\ (43\%)$$
$$\longrightarrow \text{Hg} + \text{H} + \text{CH}_3\text{CH}_2\dot{\text{C}}\text{HCH}_2\text{CH}_3\ (29\%)$$

The disproportionation ratios used are: for R_1 (*n*-pentyl), $k_5/k_4 = 0.08$ (Table IV) and $k_6/k_4 = 0.09$[6]; for R_2 (1-methylbutyl), $k_5/k_4 = 0.25$[2] and $k_6/k_4 = 0.11$[6]; for R_3 (1-ethylpropyl), $k_5/k_4 = 0.25$[2] and $k_6/k_4 = 0.29$.[6] These results confirm the earlier observation that when the unfiltered light of a low pressure mercury arc is used, inordinately high yields of *n*-pentyl radicals are observed as a result of photosensitization by the 1849-Å. line of Hg. Only 2% of the radicals formed with 2537 Å. are *n*-pentyl radicals.

Propane–Isobutane (1:1). The sensitization of an equimolar mixture of propane and isobutane was studied to compare directly the relative reactivity of these two compounds toward $\text{Hg}(^1\text{P}_1)$ atoms and to give some measure of the relative quenching cross sections of the two substances at 1849 Å. Further, this study provides an additional measurement of the primary radical yields for the individual hydrocarbons. In the mixture thermal hydrogen atoms preferentially attack isobutane; thus, the ratio of the yields of isopentane-C^{14} and *n*-pentane-C^{14} is largely a measure of the ratio of the primary radical yields from propane. The average value of this ratio for the four points in Fig. 4 is 0.86, in good agreement with the extrapolated ratio of the intercepts, 0.83, in Fig. 1.

The primary radical yields, determined from the intercepts in Fig. 4, are 18% isopropyl, 21% *n*-propyl, 39% *t*-butyl, and 22% isobutyl. The ratio of the total yield of butyl radicals to the total yield of propyl radicals, which is 1.6, is the over-all quenching efficiency of isobutane, relative to that of propane. The effective quenching cross section of isobutane is obtained from this ratio by taking into account the difference in molecular weights and is found to be 1.8 times that for propane. It is assumed in arriving at this value that the quantum yield of radicals, R, is the same for both propane and isobutane. Unfortunately absolute values of quenching cross sections for $\text{Hg}(^1\text{P}_1)$ atoms are not available for comparison. From theoretical considerations it is expected that quenching cross sections at 1849 Å. should be greater than at 2537 Å.[8,9]

Relative Reactivity of Carbon–Hydrogen Bonds. The propane and pentane results indicate that the average rate of removal of a secondary hydrogen atom by a $\text{Hg}(^1\text{P}_1)$ atom is 2.8 times the rate of removal of a primary hydrogen atom. Similarly, the isobutane data show that the rate of removal of the tertiary hydrogen atom is 12 times that of a primary hydrogen atom.[10] These values contrast with sensitization of hydrocarbons by $\text{Hg}(^3\text{P}_1)$ atoms for which the ratio of reactivities of tertiary, secondary, and primary hydrogen atoms was found to be 360:65:1. The excited singlet mercury atom is less selective in its reactions with hydrocarbons than the triplet, an effect which probably results from the increase in exothermicity of the quenching reaction.

Mechanism of Quenching. The results obtained by 1849-Å. sensitization contrast with the results of the direct photolysis of hydrocarbons at 1470 Å. In the vacuum ultraviolet photolysis of propane[11] and *n*-butane[12] at 1470 Å. molecular detachment of H_2 and CH_4 are primary processes of major importance. This contrast is to be expected since as was pointed out

(8) J. L. Magee, *J. Chem. Phys.*, **8**, 687 (1940).

(9) K. J. Laidler, *ibid.*, **15**, 712 (1947).

(10) It is interesting to note that the 1849-Å. results on radical yields are similar to radiolysis data. For example, in the radiolysis of saturated hydrocarbon liquids, parent radicals are formed, and further a secondary hydrogen atom is two to three times and a tertiary hydrogen is ~16 times (R. A. Holroyd and G. W. Klein, unpublished results) more likely to be removed than a primary hydrogen atom. However, in contrast, radiolysis leads to fragment radicals and molecular products and the "primary processes" in radiation chemistry are entirely different.

(11) H. Okabe and J. R. McNesby, *J. Chem. Phys.*, **37**, 1340 (1962).

(12) M. C. Sauer, Jr., and L. M. Dorfman, *ibid.*, **35**, 497 (1961).

earlier the optically allowed excited electronic state of the hydrocarbon may not be formed by sensitization with $Hg(^1P_1)$ atoms.

These results suggest that the quenching of $Hg(^1P_1)$ atoms by saturated hydrocarbons leads to radicals by interaction with and scission of a carbon–hydrogen bond as was predicted by Laidler[9,13] from theoretical considerations several years ago.

Disproportionation to Combination Ratios. Since normal type radicals are formed in substantial yields at 1849 Å., the present data may be used to estimate disproportionation (in which $C^{14}{}_2H_6$ and an olefin are formed) to combination ratios, k_5/k_4, for reactions of $C^{14}{}_2H_5$ with these normal radicals. The results are shown in Table IV. For this calculation the amount of ethane-C^{14} formed in reaction 8 is assumed to be 0.12 as much as the butane-C^{14} yield; and, in the case of propane, the ethane-C^{14} formed in the disproportionation of $C^{14}{}_2H_5$ and isopropyl radicals is taken as 21% of the isopentane-C^{14} yield.[2] For R = *n*-propyl, the value obtained here for k_5/k_4 is 0.06 ± 0.04, which is somewhat lower than the value of 0.14 reported by Thynne,[14] based on a single experiment.

In a similar fashion k_5/k_4 for R = isobutyl is estimated to be 0.02 ± 0.02. In this case the amount of ethane-C^{14} formed in the disproportionation reaction of $C^{14}{}_2H_5$ and *t*-butyl radicals is taken as 0.51 as much as the 2,2-dimethylbutane-C^{14} yield, a value which is the average of the two values reported: 0.54 (ref. 2) and 0.48 (ref. 6). The value of k_5/k_4 obtained where R is *n*-pentyl is 0.08 ± 0.04.

Apparently, for reactions of ethyl radicals with normal type radicals, combination predominates as is the case for reactions of methyl and various normal-type radicals.[15]

Table IV: Disproportionation to Combination Ratio, k_5/k_4, for Normal Radicals

	Obsd.	Lit. ref.	Calcd.[a]
$C_2H_5 + n\text{-}C_3H_7$	0.06 ± 0.04	0.14[b]	0.14
$C_2H_5 + i\text{-}C_4H_9$	0.02 ± 0.02	...	0.10
$C_2H_5 + n\text{-}C_5H_{11}$	0.08 ± 0.04	...	0.14

[a] Ref. 2, eq. III. [b] See ref. 14.

(13) K. J. Laidler, *J. Chem. Phys.*, **10**, 43 (1942).

(14) J. C. J. Thynne, *Proc. Chem. Soc.*, 68 (1961).

(15) M. H. J. Wijnen, *J. Am. Chem. Soc.*, **83**, 3752 (1961).

Derivation of Two Equations for the Estimation of Vapor Pressures[1]

by Donald G. Miller

Lawrence Radiation Laboratory, University of California, Livermore, California
(Received December 7, 1963)

Two new vapor pressure equations are derived which exhibit the known curvatures of log P *vs.* $1/T$ plots. One is obtained from numerical integration of the Clapeyron equation using the empirical equations of Watson for ΔH and Haggenmacher for ΔZ. The result is $\log P_{atm} = k(I - I_b)$, where k depends on the input data (either T_b, T_c, ΔH_b or else T_b, T_c, P_c). The numerically evaluated integral I is a function of the reduced temperature T_r and a characteristic parameter of liquids $a = T_{rb} \ln P_c/(1 - T_{rb})$, and can be represented by a simple empirical equation whose coefficients are functions of a. A simpler form for the average a (= 6.87) is especially good for estimating vapor pressures from 10 to 1500 mm. with input data T_b, T_c, ΔH_b. The second equation, $\log P_r = -(G/T_r)[1 - T_r^2 + k(1 - T_r)^3]$, is in reduced form and is derived from a four-constant empirical equation by exploiting known properties of liquids. The constant G correlates linearly with the characterizing parameter a. The only input data needed are T_b, T_c, P_c, since k may be evaluated at T_b when G is known. Best results are obtained if one intercept of the linear equation for G is chosen for the region 10–1500 mm., and another for the region T_b–T_c. In this case, predicted vapor pressures are better than from other reduced equations. The calculations are also considerably easier, as a value of $\log P_r$ can be obtained in one pass on a calculator capable of repeated and accumulative multiplications. Regions of best utility with appropriate input are discussed briefly.

I. Introduction

Many attempts have been made to represent the vapor pressure of an arbitrary liquid as a function of temperature.[2-4] However, most common vapor pressure equations are of little value for any large fraction of the liquid range because they do not reproduce the actual curvatures of a log P *vs.* $1/T$ plot, where P is the pressure and T is the absolute temperature in °K. Although the plot is practically a straight line over a considerable temperature range, a careful look at precise data reveals the behavior[5,6] shown in exaggerated form in Fig. 1. The curve is slightly concave downward over most of the range from the triple point up, but close to T_c the curvature becomes slightly convex with an inflection point usually found around T_r = 0.80–0.85 (0.7 for methane, near 1.0 for ethanol). The subscript c refers to the critical point, and the reduced temperature T_r is T/T_c.

We are interested in obtaining vapor pressure equations requiring a minimum of input data to characterize the vapor pressure curve, having the proper curvatures, and from which calculated vapor pressures will be within 10% of experimental ones. Such estimation equations will be called predictors.

Two general types of predictors are derived in this paper. Both exhibit the proper curvatures, and their regions of best utility are discussed. Greater detail of derivations, variants, utility, and comparisons with other equations is available elsewhere.[7,8]

(1) This work was performed under the auspices of the U. S. Atomic Energy Commission.

(2) For a large number of early references, see J. R. Partington, "Advanced Treatise of Physical Chemistry," Vol. 2, Longmans, Green and Co., Inc., London, 1951, paragraph VIII J. 18.

(3) A. Lydersen, R. Greenkorn, and O. Hougen, "Generalized, Thermodynamic Properties of Pure Fluids," Wisconsin University Engineering Experimental Station, Report No. 4, Madison, Wis., 1955.

(4) R. Reid and T. Sherwood, "The Properties of Gases and Liquids," McGraw-Hill Book Company, Inc., New York, N. Y., Chapter 4, 1958.

(5) G. Thodos, *Ind. Eng. Chem.*, **42**, 1514 (1950).

(6) W. Waring, *ibid.*, **46**, 762 (1954).

(7) D. G. Miller, Report UCRL-7287, Lawrence Radiation Laboratory, Livermore, Calif., 1963.

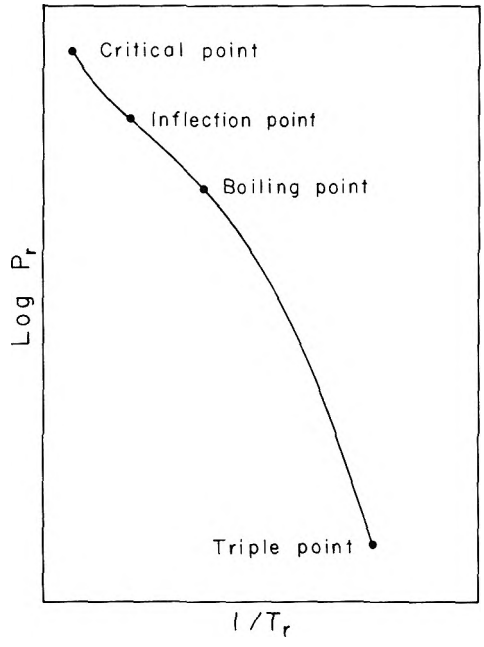

Figure 1. The log P_r *vs.* $1/T_r$ vapor pressure plot exaggerated to show the various curvatures. (Adapted with permission from ref. 5, courtesy of *Ind. Eng. Chem.*)

The first predictor is obtained by numerically integrating the Clapeyron equation using empirical approximations for the heat of vaporization and the compressibility factor difference. This predictor may be used with reduced input (T_b, T_c, P_c) or semireduced input (T_b, T_c, ΔH_b) where ΔH is the heat of vaporization; subscript b refers to the normal boiling point, and subscript c refers to the critical point.

The second is obtained by exploiting the known properties of liquids to reduce the number of constants of an appropriate empirical vapor pressure equation and then correlating the remaining ones with critical point data. This reduced predictor characterizes vapor pressures with a knowledge only of T_b, T_c, and P_c.

II. Numerical Integration of the Clapeyron Equation

A. The Form of the Integral. The Clapeyron equation

$$\frac{dP}{dT} = \frac{\Delta H}{T\Delta V} \tag{1}$$

may be written in the more convenient form

$$\frac{d(\ln P)}{dT} = \frac{\Delta H}{\Delta Z}\left(\frac{1}{RT^2}\right) \tag{2}$$

where $\Delta V = V_v - V_l$, V is the volume, subscripts v and l refer to the vapor and the liquid, R is the gas constant, and Z is the compressibility factor

$$Z = PV/RT \tag{3}$$

Both ΔH and ΔZ must be zero at the critical point, but $\Delta H/\Delta Z$ has a finite limiting value of about $7RT_c$. A typical plot of $\Delta H/\Delta Z$ *vs.* T_r is shown in Fig. 2. Between T_b and T_c, $\Delta H/\Delta Z$ has nearly the average

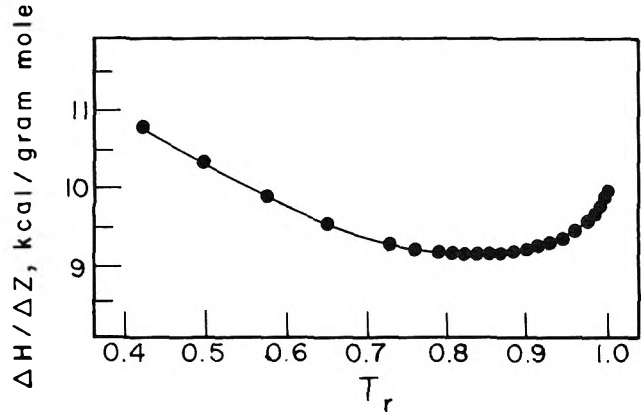

Figure 2. Plot of $\Delta H/\Delta Z$ *vs.* T_r for water, showing the minimum between T_b and T_c and the upward curvature below T_b. (Adapted with permission from ref. 6, courtesy of *Ind. Eng. Chem.*)

value owing to the cancellation of large effects, and the minimum (at $T_r \simeq 0.8$) occurs at the inflection point of log P_r *vs.* $1/T_r$ plots. The reduced pressure P_r is P/P_c. Below T_b, ΔZ is nearly 1 so that the temperature dependence of ΔH predominates. Because of the curvature, the common assumption that ΔH = constant is a poor approximation; nor is a linear dependence correct.

To obtain a more precise integration of eq. 1, better expressions for the temperature dependence of ΔH anp ΔZ are necessary. A very good empirical equation for ΔH, due to Watson[9] and many others,[10] is

$$\Delta H = \Delta H_0\left(\frac{1 - T_r}{1 - T_{r0}}\right)^{0.38} \tag{4}$$

where ΔH_0 and T_{r0} refer to a temperature where ΔH is known. Although the value of the constant is 0.38 ± 0.06, deviations from experimental data of values calculated from eq. 4 average only 2% with a maximum of 3 or 4% up to within about 10° of T_c for a variety of compounds.[11] Similarly there is a widely used

(8) D. G. Miller, Report UCRL-7292, Lawrence Radiation Laboratory, Livermore, Calif., 1963.

(9) K. M. Watson, *Ind. Eng. Chem.*, **35**, 398 (1943).

(10) W. R. Gambill, *Chem. Eng.*, **64**, No. 12, 261 (1957), gives many references going back to 1895.

(11) See ref. 4, p. 97.

empirical equation for ΔZ, due to Haggenmacher,[12] which is also good except near T_c

$$\Delta Z = \left[1 - \frac{P_r}{T_r^3}\right]^{1/2} \tag{5}$$

Substitution of eq. 4 and 5 in 1 and changing the variable to T_r yields

$$\frac{d(\ln P)}{dT_r} = \frac{\Delta H_0}{RT_c(1 - T_{r0})^{0.38}}\left[\frac{(1 - T_r)^{0.38}}{T_r^2\left(1 - \frac{P_r}{T_r^3}\right)^{1/2}}\right] \tag{6}$$

Because of P_r in the right-hand side, integration in this form is impossible. We therefore approximate P_r as a function of T_r with the reduced Kirchhoff equation

K
$$\ln P_r = a\left(1 - \frac{1}{T_r}\right) \tag{7}$$

where a is a constant characteristic of the substance. (For convenience, predictors are given a boldface letter designation.) This equation is equivalent to assuming that $\Delta H/\Delta Z$ is constant for the substance. Between T_b and T_c, where P_r becomes important in eq. 5, this approximation is quite good (see Table I). Below T_b, where eq. 7 is poor, the P_r term is small. Since the error is a correction to a correction term, eq. 5 will still be a good approximation over the entire liquid range.

Substitution of eq. 7 in eq. 6, integration, and changing to base 10 logarithms yields

$$\log P/P_1 = \left(\frac{\Delta H_0}{LRT_c(1 - T_{r0})^{0.38}}\right) \times \int_{T_{r1}}^{T_r}\left[\frac{(1 - T_r)^{0.38}}{T_r^2\left(1 - \frac{\exp[a(1 - 1/T_r)]}{T_r^3}\right)^{1/2}}\right]dT_r = kI_{T_{r1}}^{T_r} \tag{8}$$

where $L = 2.3025851$, k is the term in parentheses, and $I_{T_{r1}}^{T_r}$ is the integral.

Thomas[13] was the first to employ the general ideas which lead to eq. 8. He used eq. 4 with exponent 0.4 and a different expression for ΔZ. Kordes[14] subsequently employed eq. 4 but ignored ΔZ. Their integrals, like eq. 8, have no closed forms. They were content to use series expansions which, unfortunately, are not valid much above the boiling point. On the other hand, Frost and Kalkwarf[15] took ΔH as a linear function of T and used van der Waals' equation to evaluate ΔV. Their resulting semiempirical equation is better than would be expected from these approximations (*e.g.*, ΔZ_{FK} is not zero at T_c).

We evaluate the integral I by means of numerical integration using Simpson's rule. However I depends parametrically on a, which must be known before numerical work can begin.

An expression for a may be obtained by comparing the derivative of eq. 7 with eq. 2 in reduced form. It contains $\Delta H/\Delta Z$, whose average value between T_b and T_c is close to ΔH_b.[16] Using this fact we obtain

$$a = \frac{\Delta H_b}{RT_c} \tag{9}$$

Alternatively, a may be obtained from

$$a = \frac{T_{rb} \ln P_c}{1 - T_{rb}} \tag{10}$$

which is a consequence of eq. 7.

B. Integration with the Average a. Consider an "average" liquid, *i.e.*, one which has the average Trouton constant $\Delta H_b/T_b = 20.67$, and the average Guldberg–Guye constant $T_{rb} = 0.6600$. These values in eq. 9 yield an average $a = 6.867$.[16]

We may now proceed with the integration. For tabulation purposes, T_{r1} is conveniently chosen as a fixed but arbitrary lower limit of integration. Because no substance is liquid below $T_r = 0.3$, with the exception of liquid metals such as Hg, the choice $T_{r1} = 0.3$ will avoid negative signs in the table. Therefore, values of $I_{0.3}^{T_r}$ were computed by an IBM 650 and tabulated from $T_r = 0.31$ up to 1.0.

Equation 8 can be written in terms of this tabulated integral because the reference limit cancels out, *i.e.*, for any two vapor pressures P and P'

$$\log P/P' = kI_{T_r'}^{T_r} = \log P/P_1 - \log P'/P_1 = k[I_{0.3}^{T_r} - I_{0.3}^{T_r'}] \tag{11}$$

Equation 11 may now be written in the simplified notation

$$\log P/P' = k(I - I') \tag{12}$$

If T_r' is chosen as the normal boiling point, then $P' = 1$ atm. and eq. 12 becomes

MR
$$\log P_{atm} = k(I - I_b) \tag{13}$$

(12) J. E. Haggenmacher, *J. Am. Chem. Soc.*, **68**, 1633 (1946).

(13) L. Thomas, *J. Chem. Soc.*, 3415 (1949).

(14) E. Kordes, *Z. Elektrochem.*, **58**, 424 (1954).

(15) A. Frost and D. Kalkwarf, *J. Chem. Phys.*, **21**, 264 (1953).

(16) The average value of $\Delta H/\Delta Z$ is about 0.96–0.97 less than $\Delta H_b/\Delta Z_b$, but because ΔZ_b is also about 0.96–0.97, this factor cancels, leaving ΔH_b.[17]

(17) See ref. 4, p. 93.

Note that k may be calculated from its definition in eq. 8

$$k_h = \frac{\Delta H_0}{LRT_c(1 - T_{r0})^{0.38}} \quad (14)$$

which depends on ΔH_0 and T_c, but not on P_c. Therefore, a knowledge of T_b, T_c, and ΔH at some temperature (usually but not necessarily at the boiling point) together with a single table of $I(T_r)$ permits characterization of the vapor pressure. This combination of parameters is a happy one because T_c is often available when P_c is not. In this case, eq. 13 is a "semireduced" vapor pressure equation since only one of the critical parameters is used.

An alternative expression for k is found by setting $P = P_c$ (in atm.) in eq. 13, whence

$$k_r = \frac{\log P_c}{I_c - I_b} \quad (15)$$

Therefore, a knowledge of T_c, P_c, and T_b together with the $I(T_r)$ table should also be sufficient to characterize the vapor pressure curve. Note also that from eq. 12 we may obtain the reduced form

$$\log P_r = k(I - I_c) \quad (16)$$

Examination of the tabulated integral showed that it reflects the curvature below T_b quite accurately. Even more important, the inflection point of the log P *vs.* $1/T$ plot is predicted at $T_r = 0.815$, close to the average of observed values. Moreover, the limiting value of $\Delta H/\Delta Z$ is finite, as it should be. However, an appropriate plot of experimental data *vs.* tabular entries for compounds with a near 6.87 showed deviations from the expected straight line near T_c. This is where both Watson's and Haggenmacher's equations are less accurate. Therefore, tabular entries between $T_r = 0.91$ and 1.0 were adjusted to fit the experimental data. This adjustment did not change the general shape of the curve or the position of the inflection point.

It would be convenient to have the table in analytical form. Therefore, since I contains all the temperature-dependent part of the vapor pressure, a number of common vapor pressure equations known[6] to reproduce both the inflection point and appropriate curvatures were fitted to the adjusted table ($0.35 \leq T_r \leq 1.0$) by least squares. The equation

$$I = A + C(T_r - 1/T_r) + D(T_r^2 - 4/T_r) \quad (17)$$

fitted the table very well and fortunately is very easy for hand calculations. For this reason, the adjusted table has not been included in this paper.

By substituting eq. 17 (with A omitted because it always cancels) into eq. 13, we obtain

$$\textbf{MRA} \quad \log P_{atm} = \frac{k}{T_r}[T_r^2(0.60706T_r - 1.44779) - I_bT_r - 0.98045] \quad (18)$$

where k is obtained from either eq. 14 or eq. 15 depending on available data, and I_b by solving eq. 18 after setting $P = 1$ atm. and $T_r = T_{rb}$. **MRA** (denoted by **MRA1** in ref. 7) predicts the inflection point at $T_r = 0.795$. It is a reduced equation if P_c is used; semireduced if ΔH is used. It also yields a vapor pressure in one pass on a hand calculator capable of repeated and accumulative multiplications.

Comparison[7] with data (described in more detail elsewhere[18]) for a large number of compounds showed that when k_h (ΔH, T_b, T_c) was used, the predicted vapor pressures were extremely close to experimental values in the region 10–1500 mm., but in general were not too good between 1500 mm. and the critical point. On the other hand, when k_r (T_c, P_c, T_b) was used, results were good between T_b and T_c, but not too good below T_b. Hence, a hope that better approximations for ΔH and ΔZ would compensate for the use of an average a was not realized.

C. Integration with Different a. It was found that for substances with a near 6.87, **MRA** was a good predictor over the entire liquid range; for a markedly different from 6.87, the results were notably poorer. Values of a for various compounds are between 4 and 10. All but hydrogen and helium are above 5, all but alcohols and organic acids below 8.5, and the average near 7 (as predicted in the previous section). It seemed reasonable, therefore, to expect better results if the correct a were used in the integration.

Since a numerical integration for each compound is impractical, a set of additional tables of I were computed for $a = 4, 4.5, 5, \ldots, 9, 9.5$.

The problem of adjusting all 12 tables above $T_r = 0.90$ was avoided as follows. Analysis of the $a = 6.867$ table had shown that the adjusted values (*i.e.*, from $T_r = 0.91$ to 1.00) were reproduced quite well when only entries below $T_r = 0.91$ were used for the fit. On the rather arbitrary assumption that this would hold true for all a, each of the six a tables (4, 5, . . ., 9) was fitted from $T_r = 0.35$ to 0.90 with several common vapor pressure equations by least squares. The form

$$I = A + B/T_r + CT_r + DT_r^2 \quad (19)$$

(18) D. G. Miller, *Ind. Eng. Chem.*, **56**, No. 3, 46 (1964).

gave the best over-all fit on balance. It was then used to fit each of the remaining six a tables for T_r from 0.35 to 0.90, and the calculated values from 0.91 to 1.00 were taken as adjusted values for each corresponding table.

A few typical compounds were tested using the a table closest to the value calculated from eq. 10. The results with k_h (ΔH, T_c, T_b) were not much different from those using eq. 18 (or the original table). However with k_r (P_c, T_c, T_b), the improvement, especially below T_b, was great enough that the k_r form appeared competitive with other reduced equations and hence warranted further testing.

To avoid the use of 12 tables (or 12 equations) and perhaps interpolation, it is desirable to represent them by a single analytical equation.

Plots of the coefficients of form 19 for each table as a function of a showed reasonable regularity. Consequently, the equation

$$I(a, T_r) = A(a) + B(a)/T_r + C(a)T_r + D(a)T_r^2 \quad (20)$$

where

$$A(a) = \Sigma\alpha_k a^k,\ B(a) = \Sigma\beta_k a^k, \text{ etc.}\ldots \quad (21)$$

was fitted by least squares to the entries of all 12 tables for all T_r from 0.35 to 0.90 inclusive using an IBM 7090. Equations 13, 20, and 21 together are denoted by **MRD**. A number of variations were tried in an attempt to find the best fit to the tables and best prediction of vapor pressures compatible with the least computation. Comparison with experiment showed that using

$$a^* = (a + \text{constant}) \quad (22)$$

gave better results with all fits to the tables, the value of the constant depending on the input data and pressure region. The final choice was a fit to the tables of $5 \leq a \leq 8.5$ with terms up to a^2.

The resulting equation is

$$\log P_{atm} = \frac{k}{T_r}\left[B - T_r^2(C + DT_r) - I_b T_r\right] \quad (23)$$

MRD

$$\begin{Bmatrix} B = -0.80344 - 0.04772a^* + 0.00346(a^*)^2 \\ C = -0.82365 - 0.22436a^* + 0.02181(a^*)^2 \\ D = 1.34422 - 0.13486a^* + 0.00270(a^*)^2 \end{Bmatrix} \quad (24)$$

where A has been omitted because it always cancels. Equations 14 or 15 are used to obtain k, and the coefficients B, C, and D are obtained from a^*, which in turn comes from eq. 22 and either eq. 9 or 10. I_b is then determined as with eq. 18. **MRD** also yields a value of log P in one pass on a hand calculator.

D. Comparison with Experiment and Regions of Utility. The comparison of various alternate fits and various values of the constant in eq. 22, as well as comparisons with other predictors, are given in detail elsewhere.[7,18] The conclusions are as follows:

Low Pressure Region. With semireduced input (T_b, T_c, ΔH_b), **MRA** (eq. 18) is an extremely good predictor in this range and is better than any other predictor known to the author. The average *maximum* error[19] is only 3% for 71 organic and inorganic compounds not associated in the vapor, and predicted vapor pressures for 70 of the 71 (including alcohols and other polar compounds) are within 10%. Even the extreme case of the liquid metal Hg (not considered in the 71 compounds) is within 12%. Since eq. 23 is not significantly better and is more complicated, **MRA** is to be preferred for this input–pressure region combination.

Equation 23 with reduced input (T_b, T_c, P_c) and the best $a^* = a + 0.2$, denoted by **MRDL** (by **MRD6B** in ref. 7), is about as good (average maximum error 5–6% as well-known reduced equations such as Riedel's[20–23] or Frost–Kalkwarf's[24,25] but is handier for computation. However, it is not quite as good nor as easy to calculate with as the reduced predictor derived in the next section.

High Pressure Region (T_b–T_c). Using semireduced input, eq. 23 with the best $a^* = a + 0.5$, denoted by **MRDH** (by **MRD6D** in ref. 7), is better than other known equations, but is not as good as might be desired. The average maximum error for 24 inorganic compounds is 7.3% and one-fourth do not fit within 10%.

Equation 23 with reduced input and the best $a^* = a + 0.7$, denoted by **MRDU** (by **MRD6E** in ref. 7), is about the same as **MRA** in spite of the correction factor a, both being well within the 10% criterion and with respectably low average maximum errors (3%). Surprisingly, however, neither one is substantially better than the simple reduced Kirchhoff equation

(19) The average error is about half the average maximum error.

(20) L. Riedel, *Chem. Ingr.-Tech.*, 26, 83 (1954).

(21) L. Riedel, *Kaltetech.*, 9, 127 (1957).

(22) Ref. 4, p. 76.

(23) J. Hirschfelder, R. Buehler, H. McGee, Jr., and J. Sutton, *Ind. Eng. Chem.*, 50, 375 (1958); corrections, *Ind. Eng. Chem. Fundamentals*, 1, 224 (1962).

(24) E. Reynes and G. Thodos, *ibid.*, 1, 127 (1962).

(25) E. Reynes and G. Thodos, *A.I.Ch.E. J.*, 8, 357 (1962).

K (eq. 7), and both are definitely inferior to other reduced equations.

In view of the improved way we took the temperature dependence of ΔH and ΔZ into account, and the fact that the inflection point was reproduced so well, it is rather surprising the **MRD** equations are not much better than **K** nor at least as good as the Frost–Kalkwarf equation in the high pressure region. Two explanations are possible, both related to the facts that (1) k_r is strongly affected by the value of I_c, and (2) that the tabular I depends more strongly on the behavior of ΔH and ΔZ as T_c is approached. The first explanation is that the approximations for ΔH and ΔZ are not as good in combination in the T_b–T_c range as they are individually, and quite unexpectedly are worse than the Frost–Kalkwarf combination. In this case, the weaker link is probably the Haggenmacher equation. However, we attempted to account for such effects by adjusting the tables between $T_r = 0.90$ and 1.0. Hence, the second and perhaps most likely explanation is that our adjustment method (fitting to $T_r = 0.90$ and extrapolating to 1.0) is in fact not adequate. Moreover, the improvement obtained from using a^* instead of a may be a result of basing the original adjustment of the $a = 6.867$ table on the data of Stull[26] which is known to have systematic errors between T_b and T_c.[27] Unfortunately, not only is the adjustment using experimental data tedious, but good data[28] did not become available until this study was nearly completed.

III. Correlation of the Constants of a Simple Reduced Vapor Pressure Equation

A. Preliminaries. Waring[6] has shown that to reproduce the proper curvatures and the inflection point of Fig. 1, an empirical equation must have at least four constants and satisfy certain other requirements on the signs of $\Delta H/\Delta Z$ derivatives. He listed several common empirical equations, three of which satisfied all his requirements.

$$\log P = A + B/T + C \log T + DP/T^2 \qquad \text{Frost–Kalkwarf} \quad (25)$$

$$\log P = A + B/T + C \log T + DT^n \qquad \text{Riedel } (n = 6) \quad (26)$$

$$\log P = A + B/T + CT + DT^2 \quad (27)$$

Reynes and Thodos[24,25] considered the reduced form of eq. 25 and correlated experimentally determined constants, obtaining the result

$$\textbf{FK} \quad \log P_r = \left[\frac{5}{9}\gamma - \frac{40}{27}\right]\left[\frac{1}{T_r} - 1\right] + \gamma \log T_r + 0.1832\left[\frac{P_r}{T_r^2} - 1\right] \quad (28)$$

where γ is a constant determinable at T_b when T_c and P_c are known.

Riedel[20–23] obtained the reduced equation

$$\textbf{R} \quad \ln P_r \approx \alpha_c \ln T_r - 0.0838(\alpha_c - 3.75)[36/T_r - 35 - T_r^6 + 42 \ln T_r] \quad (29)$$

from the reduced form of eq. 26 by eliminating one of the constants by means of an empirical property of liquids and correlating the remaining ones. The empirical property, known as the Plank–Riedel[29,30] condition, is

$$\left(\frac{d\alpha}{dT_r}\right)_{T_r=1} = 0 \quad (30)$$

where Riedel's α is defined as

$$\alpha = \frac{d(\log P_r)}{d(\log T_r)} \quad (31)$$

This condition was discovered by examining plots of α *vs.* T_r (see Fig. 3) for substances with good data. The value of α at the critical point, α_c, is a characteristic constant of a liquid (values are 7 ± 2.5) and appears in eq. 29. It also may be determined at T_b given T_c and P_c.

Predictors **FK** and **R** are good, but are somewhat inconvenient for hand calculation because of their log terms; **FK** is still worse because the presence of P_r on the right-hand side of eq. 28 requires as many as four iterations near T_c to get a value of $\log P_r$.[15]

B. Derivation. We choose to analyze eq. 27,[31] for which hand calculation is somewhat easier, and we too will make use of the Plank–Riedel condition.

The constant A of eq. 27 in reduced form may be eliminated because $P_r = 1$ when $T_r = 1$, yielding

(26) D. R. Stull, *Ind. Eng. Chem.*, **39**, 517, 1684 (1947).

(27) G. W. Thomson in "Techniques of Organic Chemistry," Vol. I, part 1, A. Weissberger, Ed., 3rd Ed., Interscience Publishers, Inc., New York, N. Y., 1959, p. 516.

(28) D. G. Edwards, Report UCRL-7167, Lawrence Radiation Laboratory, Livermore, Calif., 1963.

(29) R. Plank and L. Riedel, *Ingr.-Arch.*, **16**, 255 (1948).

(30) R. Plank and L. Reidel, *Texas J. Sci.*, **1**, 86 (1949).

(31) Waring[6] pointed out that eq. 27 does not satisfy the experimental criteria for $\Delta H/\Delta Z$ derivatives at T less than $-C/6D$ (his coefficient 4 is a misprint). In terms of the constants G and k found further on, this is a T_r of between 0.33 and 0.43. Since this is at the lowest limits of the liquid range (0.5–1 mm.), it is not a serious concern here. These limits may be reducible even further by choosing higher powers of T for the D term. This possibility is being reserved for a subsequent study.

$$\log P_r = B(1/T_r - 1) + C(T_r - 1) + D(T_r^2 - 1) \quad (32)$$

From eq. 32 and 31, we find that

$$\alpha = L(-B/T_r + CT_r + 2DT_r^2) \quad (33)$$

and that

$$\alpha_c = L(-B + C + 2D) \quad (34)$$

The Plank–Riedel condition (eq. 30) is now used to eliminate a second constant: by differentiating eq. 33, substituting $T_r = 1$, and setting the result equal to zero, one obtains

$$B + C + 4D = 0 \quad (35)$$

which may be used to eliminate any one of the three constants B, C, and D from eq. 32, leaving only two constants.

Similarly any two of B, C, D, and α_c can be eliminated by means of eq. 34 and 35. Because α_c is a characteristic parameter, it is certainly reasonable to consider combinations which contain it. The simplest form of all these possibilities turns out to involve α_c and D and is found by solving for B and C in eq. 34 and 35, substituting them in eq. 32, collecting terms, and rearranging. The result is eq. 36.

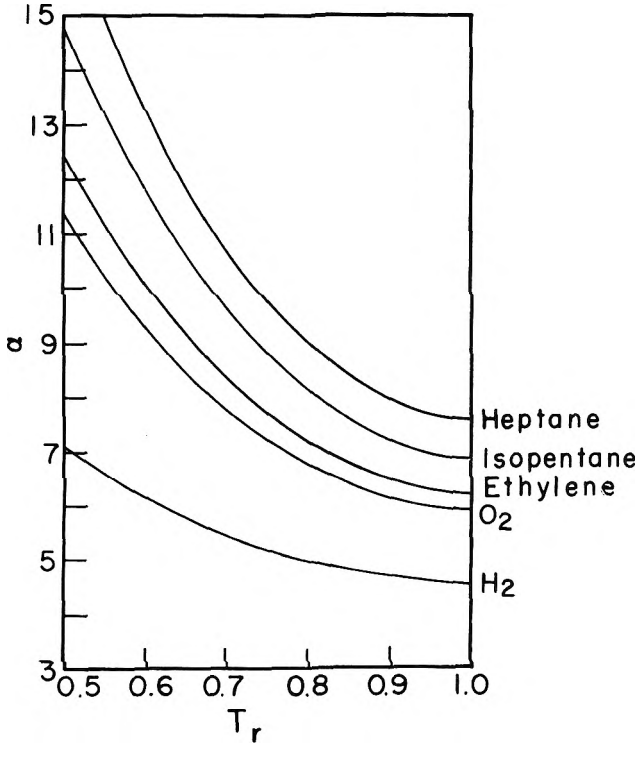

Figure 3. Plot of Riedel's α *vs.* T_r. (Adapted with permission from Fig. 1 of ref. 20.)

$$\log P_r = \frac{-\alpha_c}{2LT_r}\left[1 - T_r^2 + \frac{2DL}{\alpha_c}(1 - T_r)^3\right] \quad (36)$$

It is convenient to write eq. 36 as

$$\textbf{RPM} \quad \log P_r = \frac{-G}{T_r}[1 - T_r^2 + k(1 - T_r)^3] \quad (37)$$

where

$$G = \alpha_c/2L,\ k = 2DL/\alpha_c \quad (38)$$

With these abbreviations, $\Delta H/\Delta Z$ and α become

$$\frac{\Delta H}{\Delta Z} = LRT_cG[1 + T_r^2 + k(1 - T_r)^2(1 + 2T_r)] \quad (39)$$

$$\alpha = \frac{LG}{T_r}[1 + T_r^2 + k(1 - T_r)^2(1 + 2T_r)] \quad (40)$$

With one other vapor pressure point (such as the normal boiling point), either G or k can be obtained in terms of the other. However, the remaining constant must be eliminated either (1) by another experimental condition analogous to the Plank–Riedel condition, (2) by still another piece of experimental data such as $\Delta H/\Delta Z$ or another vapor pressure point, or (3) by correlation of G or k with each other or with the critical and normal boiling points.

A possible experimental condition is the minimum in the curve of $\Delta H/\Delta Z$ *vs.* T_r that most substances have at T_r between 0.8 and 0.85 (Fig. 2). Differentiating eq. 39 with respect to T_r and setting the result equal to zero yields

$$k = \frac{2DL}{\alpha_c} = \frac{1}{3(1 - T_{rm})} \quad (41)$$

where T_{rm} is the reduced temperature at the minimum. Substitution of 0.80 and 0.85 for T_{rm} gives k values of 1.7 and 2.2, respectively. Sample calculations showed that k was different for different compounds, the average being about 1.7–1.8 (corresponding to a T_{rm} of 0.81, which is essentially that found for the average compound in section II). However, eq. 37 with $k = 1.7$ or $k = 1.8$ as a "universal" constant was not as good a predictor as either **R** or **FK**.[8]

Using another vapor pressure point to eliminate a constant would be all right except that, for reasons given below, low pressure points are most suitable but are most often lacking. The use of $\Delta H/\Delta Z$ has the disadvantage that even if ΔH is available, ΔZ usually is not. Although ΔZ can be estimated by eq. 5, the expressions for G and k (obtained by solving eq. 37 and 39 simultaneously) are found to be too

sensitive to small errors in ΔZ to be useful. There remains the possibility of correlating the constants.

C. Correlation of the Constants.—Expressions for G and k can be obtained by solving for them simultaneously using one eq. 37 for the normal boiling point and another for any other vapor pressure point i of interest. To aid in correlating the constants, k_t and G_t were computed for a given compound at a number of vapor pressure points. This was done on an IBM 650 for 80 compounds of different types in the 10–1500 mm. range and 28 inorganic compounds in the T_b–T_c range.

It was found that k and hence G are not exactly constant for a given compound. With increasing T_r, k increases (typically about 20% between 10 mm. and P_c) and G decreases (typically about 5%). (The trend is so smooth that any irregularity indicates a bad experimental point.) This implies that either the Plank–Reidel condition is not strictly true, or the original four-constant equation does not adequately represent the data, or both.

However, the kind of equation being sought, whose constants are determined from the boiling and critical points, *interpolates* between T_b and T_c and *extrapolates* below T_b. Thus, an error in k is less important between T_b and T_c but becomes dominant at low temperature, not only because of extrapolation but because the $k(1 - T_r)^3$ term becomes larger there relative to the $1 - T_r^2$ term. Therefore, a better over-all fit will come from a k representative of the low pressure region.

A low pressure k and its corresponding G were chosen for each of the 80 compounds mentioned above. The k's varied between 0.04 (He) and 4.4 (SO_3) with an average of about 1.75; most of them were between 1.5 and 2.0. The G's varied between 0.84 (He) and 2.4 (N_2O_4) with most between 1.4 and 1.7.

There were definite trends among the k as well as the G values with boiling point, T_{rb}, and P_c. Therefore, G and k were plotted against a number of combinations of T_{rb} and P_c, such as

$$f_n = T_{rb}^n \log P_c \qquad (42)$$

and the parameter a (eq. 10), as well as against each other.

The best correlation was that of G with a, shown in Fig. 4. The least-square line for the low pressure range G's is

RPML $$G = 0.2471 + 0.19654a \qquad (43)$$

It is not surprising that G is well correlated with a because $G = \alpha_c/2L$, and α_c in turn correlates well with a.[32]

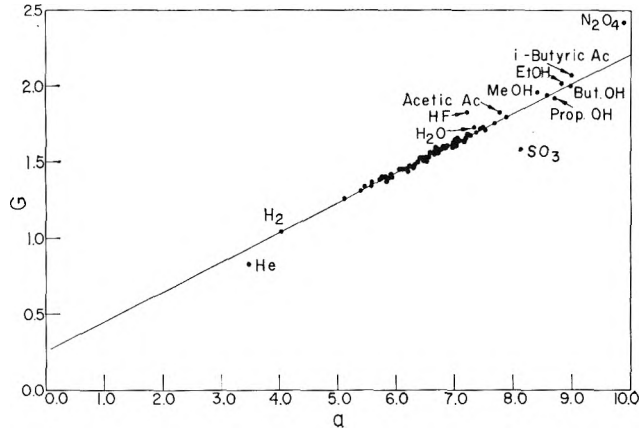

Figure 4. Plot of low temperature G *vs.* $a = (T_{rb} \ln P_c)/(1 - T_{rb})$. Solid line is least-squares fit.

Thus, with G calculated from eq. 43 and 10 in terms of T_{rb} and P_c, the third constant is obtained. The last one, k, is now determined using the normal boiling point, thereby specifying the entire vapor pressure curve with only two pieces of data, the critical point and the normal boiling point.

The Riedel and Frost–Kalkwarf equations are of this type also, but are more complex and as noted earlier involve computational problems. Equation 37, however, is very well suited to hand calculation: First a is calculated from T_b, T_c, and P_c by eq. 10; next G is obtained from a; and then k is obtained from eq. 37 evaluated at the normal boiling point. The further calculation of vapor pressures is now very easy as a value of log P_r is obtained in one pass on any hand calculator capable of repeated and cumulative multiplications. For substances like acetylene and CO_2, whose triple points are *above* one atmosphere, a can be computed from

$$a = \frac{-T_{rt} \ln P_{rt}}{1 - T_{rt}} \qquad (44)$$

where t refers to the triple point.

Comparison with experimental data, discussed more fully elsewhere,[8,18] showed that **RPML** (denoted by **RPMD** in ref. 8) is a very good predictor in the 10–1500 mm. range, and quite acceptable in the T_b–T_c range in spite of using the empirical equation for low temperature G's. However, owing to their slight temperature dependence, slightly higher values of k and slightly lower values of G should be more appropriate for the T_b–T_c region.

Therefore, for each compound an "average" G and k were selected from the sets of G_t and k_t calculated

(32) D. G. Miller, *Ind. Eng. Chem. Fundamentals*, **2**, 78 (1963).

from experimental vapor pressures in the high temperature region. These selected values were plotted against various functions of T_{rb} and P_c. Again the best correlation was G with a as shown in Fig. 5. The straight line shown has the same slope as the low temperature line but an intercept 0.02 less; *viz.*

RPMH $G = 0.2271 + 0.19654a$ (45)

A compromise equation for the entire liquid range is

RPMA $G = 0.2421 + 0.19654a$ (46)

D. Comparison with Experiment. Comparison of the above predictors with alternate correlations and other reduced equations is given in detail elsewhere.[8] The conclusions are as follows:

Low Pressure Region. **RPML** is a good reduced predictor in this range. The average maximum per cent deviation for the 71 organic and inorganic compounds[18] not associated in the vapor is only 5.2%[33] and

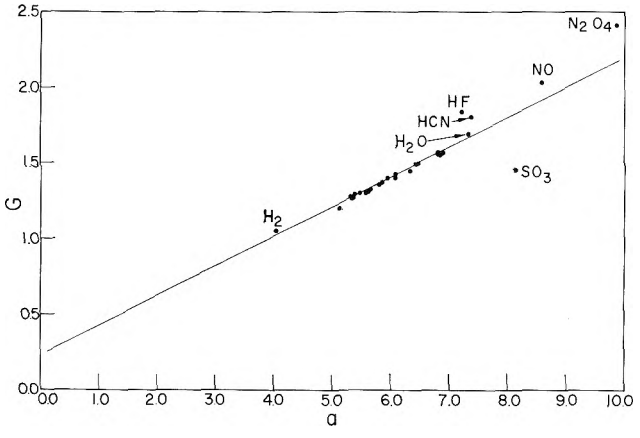

Figure 5. Plot of high temperature G *vs.* a. Solid line is eq. 45.

predicted vapor pressures are within 10% for 85% of these compounds. **RPML** is also better than **MRDL**, slightly better than **R** and **FK**, and considerably simpler than any of them for hand calculations.

High Pressure Region. All the **RPM** equations are good. **RPMH** (denoted by **RPMD2** in ref. 8) is the best and better than the other reduced predictors, with all 24 compounds not associated in the vapor within the 10% criterion and with an average maximum deviation of only 1.5%. Moreover the calculations with **RPMH** are again considerably simpler than with **R** or **FK**, especially for **FK** for which the number of iterations increases as T_c is approached.

The best single equation for both regions is **FK**, followed closely by **R**, and then reasonably closely by the compromise **RPMA** (denoted by **RPMD5** in ref. 8). **RPMA** can certainly be considered competitive with the other two if ease of calculation is balanced against goodness of prediction. However, the best reduced predictors are **RPML** from 10 to 1500 mm. and **RPMH** from T_b to T_c. Even with the slight inconvenience of two equations instead of one, the computations are still much easier than with **R** or **FK**. Consequently these two predictors are proposed for use with reduced input.

In general, reduced equations are not too good at low pressures with pathological liquids such as alcohols, carboxylic acids, associated substances like HF, or dissociating ones like N_2O_4. However, all but **R** are good to within 15% for the liquid metal Hg (10% if the rather uncertain critical temperature is raised 2.5%).

IV. Remarks and Recommendations

To aid in assessing the relative merit of various predictors, abbreviated results of comparison with

Table I: Comparison of Predictors with Experimental Data

			71 compounds		
	Predictor	Equations	10^3S	Number not within 10%	Average maximum % error
	Reduced input (T_b, T_c, P_c)				
10–1500 mm.	**MRDL**	24, 15, 22	86.8	11	5.7
	RPML	37, 43	70.7	11	5.2
	RPMA	37, 46	80.7	11	5.9
	R	29	73.4	12	5.3
	FK	28	74.5	12	5.1
	K	7	2073	62	40.4
	Semireduced input (T_b, T_c, ΔH_b)				
	MRA	18, 14	22.1	1	2.9
			24 compounds		
	Predictor	Equations	10^4S	Number not within 10%	Average maximum % error
	Reduced input				
T_b–T_c	**MRA**	18, 14	104.2	0	3.06
	MRDU	24, 15, 22	132.2	1	2.90
	RPML	37, 43	55.4	0	2.34
	RPMH	37, 45	25.7	0	1.54
	RPMA	37, 46	42.7	0	2.08
	R	29	36.6	0	1.67
	FK	28	29.1	0	1.54
	K	7	108.4	0	3.20
	Semireduced input				
	MRDH	24, 15, 22	854	6	7.3

(33) The maximum deviation is almost always at the lowest pressure where the extrapolation from T_b is the longest.

experiment are given in Table I. The values of S, the number of compounds not fit within 10%, and the average maximum % deviation are included for the predictors derived in this paper, as well as for the reduced Riedel **R**, Frost–Kalkwarf **FK**, and Kirchhoff **K** equations. S is defined as

$$S = \sum_{\text{compounds}} \left(\frac{\sum_{\text{points}} \delta^2}{n} \right) \qquad (47)$$

where n is the number of experimental vapor pressure points for each compound and δ is the per cent residual in P divided by 100.

Owing to the remarkably good predictions of **MRA**, it is recommended for rapid estimation of vapor pressures in the 10–1500 mm. region using semireduced input (T_b, T_c, ΔH_b). Owing to their superior fit and simplicity of calculation, the reduced predictors **RPML** and **RPMH** are proposed for rapid estimation of vapor pressures in the low and high pressure regions, respectively, using only the normal boiling point and critical point as input data.[34]

Finally we draw attention to the fact that the parameter a defined by eq. 10 appears in a decisive role not only in the two types of vapor pressure equations of sections II and III, but also in an expression for α_c,[32] in the Giacolone approximation for $\Delta H_b/RT_c$,[35] and in Edmister's estimate[36] of the acentric factor ω.[37] It would appear therefore that a is a fundamental characteristic parameter of liquids analogous to α_c, the critical compressibility factor Z_c, and the acentric factor ω.

Acknowledgments. The author wishes to thank Mr. Nick Clecak for aid with some of the calculation and Dr. David Edwards for permitting the prepublication use of his smoothed vapor pressure data in the T_b–T_c region. The author is especially indebted to Mr. Robert Carpenter of the Computation Division who handled all the electronic computer aspects of this problem.

(34) Preliminary calculations indicate that substituting the G and k of **RPMA** in eq. 39 and using ΔZ from eq. 5 gives a good estimate of ΔH_b (~1.5% average).

(35) See ref. 4, p. 93, eq. 4–37.

(36) W. C. Edmister, *Petrol. Refiner*, **37**, No. 4, 173 (1958).

(37) K. S. Pitzer, D. Z. Lippmann, R. F. Curl, Jr., C. M. Huggins, and D. E. Petersen, *J. Am. Chem. Soc.*, **77**, 3433 (1955).

The Mass Spectral Fragmentation of 1,3-Butadiene and 1,3-Butadiene-1,1,4,4-d_4

by A. Bruce King

Gulf Research & Development Company, Pittsburgh, Pennsylvania *(Received December 14, 1963)*

The mass spectral patterns of 1,3-butadiene and 1,3-butadiene-1,1,4,4-d_4 are compared. The appearance potentials of the principal ions and the metastable transitions that are observed are reported. Complete equilibration of the hydrogen atoms in the partially deuterated compound takes place before fragmentation occurs. It is suggested that this may arise from isomerization to 1,2-butadiene. A fragmentation mechanism is proposed, and the principal features are discussed.

Introduction

In recent years, the mass spectra of several lower molecular weight hydrocarbons have been investigated using partially deuterated compounds. These studies demonstrate the extent of exchange between hydrogen atoms on the different skeletal atoms prior to skeletal fragmentation. In the simple paraffins, the degree of exchange is generally not large, as exemplified by the reported spectra of partially deuterated ethane,[1,2] propane,[1,3,4] *n*-butane,[1,5] and isobutane.[1,4] As suggested by Stevenson and Wagner,[1] the olefinic compounds exhibit a higher degree of exchange before the skeletal break occurs. The point is illustrated by the exchange observed in the ionic fragment formed by loss of a methyl radical from partially deuterated propylene[6] and 1-butene.[7]

The purpose of this paper is to supplement the existing information on hydrogen atom exchange prior to fragmentation by presenting similar data obtained in our laboratory for 1,3-butadiene-1,1,4,4-d_4.

Experimental

The mass spectra and appearance potential measurements were made on a C.E.C. 21-103C equipped with a room temperature inlet system. The ion source was maintained at 250°. Appearance potential measurements were made using krypton as an internal standard. The ion intensity scales of the ionization efficiency curves of the ion under study and the calibrating ion were adjusted to make the slopes of the linear regions equal. The ionization efficiencies were then plotted on a semilog scale and the ionization potential determined from the displacement of the curves.[8] For the fragment ions the curves were not identical in shape; and hence, the minimum threshold was estimated from the displacement of the interpolated semilog plots of the ionization efficiencies at ion currents slightly above the noise level. This procedure essentially gives results equivalent to the vanishing current method. Positive identification of some of the minor metastable transitions was made possible with spectra obtained on a C.E.C. 21-102 (modified) that was equipped with a metastable suppressor to give comparison spectra with and without the metastable contributions.

The 1,3-butadiene used was Phillips research grade. The 1,3-butadiene-1,1,4,4-d_4 was prepared by Dr. Dale E. Van Sickle of Stanford Research Institute by repetitive exchange of 2,4-dihydrothiophene 1,1-dioxide with deuterium oxide following the procedure of Cope, *et al.*[9] The low voltage mass spectrum indicated the

(1) D. P. Stevenson and C. D. Wagner, *J. Chem. Phys.*, **19**, 11 (1951).

(2) D. O. Schissler, S. O. Thompson, and J. Turkevitch, *Discussions Faraday Soc.*, **10**, 46 (1951).

(3) F. E. Condon, *J. Am. Chem. Soc.*, **73**, 4675 (1951).

(4) F. E. Condon, H. L. McMurray, and V. Thornton, *J. Chem. Phys.*, **19**, 1010 (1951).

(5) W. H. McFadden and A. L. Wahrhaftig, *J. Am. Chem. Soc.*, **78**, 1572 (1956).

(6) W. H. McFadden, *J. Phys. Chem.*, **67**, 1077 (1963).

(7) W. A. Bryce and P. Kebarle, *Can. J. Chem.*, **34**, 1249 (1956).

(8) J. W. Warren, *Nature*, **165**, 810 (1950).

(9) A. C. Cope, G. A. Berchtold, and D. L. Ross, *J. Am. Chem. Soc.*, **83**, 3849 (1961).

Table I: Fragmentation Patterns of 1,3-Butadiene and 1,3-Butadiene-1,1,4,4-d_4 at 70 e.v.

m/e	Total ionization (C^{13} cor.), %: $CH_2CHCHCH_2$	Total ionization (C^{13} cor.), %: $CD_2CHCHCD_2$
2	0.100	0.501
3	0.006	0.040
4		0.023
12	0.591	0.495
13	0.550	0.116
14	0.817	0.523
14.5		0.012
15	0.586	0.154
16	0.004	1.037
17		0.391
18		0.109
19	0.024	0.004
19.5	0.007	0.019
20	0.002	0.009
24	0.176	0.185
25	1.019	0.246
25.5	0.693	0.094
26	5.64	1.009
26.5	0.079	0.322
27	13.41	3.11
27.5		0.245
28	8.34	3.92
28.5		0.034
29	0.009	9.19
29.5		0.008
30		5.92
31		4.21
32		0.871
36	0.366	0.336
37	1.661	0.511
38	1.773	1.258
39	20.47	1.158
40		4.97
41		13.87
42		3.904
48	0.378	0.219
49	1.918	0.249
50	5.68	1.224
51	4.64	1.693
52	2.072	3.20
53	12.31	2.020
54	16.67	2.001
55		1.186
56		6.08
57		4.91
58		17.09

only isotopic impurity to be 2.1% $C_4H_3D_3$. The assignment of the position of the deuterium atoms solely to the terminal carbon atoms is assured by the method of preparation and the lack of d_5-component.

Table II: Metastable Transitions

Observed mass	Approximate intensity (% total ionization at 70 e.v.)	Transition	Calculated mass
	$CH_2CHCHCH_2$		
13.8	0.01	53 → 27	13.8
24.2	0.01	28 → 26	24.2
28.2	0.06	54 → 39	28.2
29.1	~0.006	55 → 40	29.1
35.1	0.008	39 → 37	35.1
49+	0.08	53 → 51	49.1
52+	0.04	54 → 53	52.1
	$CD_2CHCHCD_2$		
14.8	0.006	57 → 29	14.8
15.9	0.004	57 → 30	15.9
~23.6	0.001	31 → 27	23.5
24.3	0.004	30 → 27	24.3
25.3	0.01	31 → 28	25.3
27.7	~0.04	58 → 40	27.6
~29	~0.03	58 → 41	29.0
30.4	0.04	58 → 42	30.4
33.9	0.004	40 → 37	34.2
		42 → 38	34.4
35.1	0.005	41 → 38	35.2
		56 → 52	48.2
		56 → 53	50.1
~51 (very broad)	~0.03	56 → 54	52.0
		57 → 53	49.1
		57 → 54	51.1

Results

The 70-v. spectra for 1,3-butadiene and 1,3-butadiene-1,1,4,4-d_4 are listed in Table I as per cent of total ionization. Both spectra are corrected for the C^{13} contributions, but no attempt was made to correct the entire deuterated spectra for the $C_4H_3D_3$ impurity. The metastable transitions observed for these two compounds are listed in Table II. It should be noted that all of the transitions observed in the deuterated compound represent the principal isotopic analogs of all of the metastable transitions observed in the unlabeled compound.

The results of the appearance potential measurements on the principal ions of the unlabeled butadiene are listed in Table III along with the literature data. Quite reasonable agreement is found in all cases except $m/e = 26$. The observation of an ionization potential that is greater than the photoionization value[10] is presumably due to the difference between the adiabatic and the vertical transition energies. The other electron impact results for the 1,3-butadiene ionization potential

(10) K. Watanabe, *J. Chem. Phys.*, 22, 1564 (1954); 26, 542 (1957).

Table III: Appearance Potential Measurements on 1,3-Butadiene

m/e	Ion	This work (probable uncertainty ±0.10 e.v.)	Literature	Ref.
54	$C_4H_6^+$	9.33 e.v.	9.18 e.v.	14
			9.24	*a*
			9.13	21
			9.2	*b*
		Photoionization:	9.070 e.v.	10
53	$C_4H_5^+$	12.03	12.1	21
39	$C_3H_3^+$	11.65	11.9	*b*
			11.71	14
			11.99	21
28	$C_2H_4^+$	13.10	13.4	21
27	$C_2H_3^+$	15.53	15.72	14
			16.2	21
26	$C_2H_2^+$	~14.6	16.3	21

[a] J. D. Morrison and A. J. C. Nicholson, *J. Chem. Phys.*, **20**, 1021 (1952). [b] R. E. Fox and A. Langer, *ibid.*, **18**, 460 (1950).

equilibrium carbon–carbon bond distances for 1,3-butadiene and the 1,3-butadiene ion show significant change on ionization which would be expected to be reflected in differences between the adiabatic and vertical ionization potentials.

Spectra of both compounds were also obtained for several values of the electron energy near the ionization potential. The unlabeled compound gave typical curves of fraction of total ionization *vs.* electron energy. Following the earlier notation of the author,[12] the parent ion was the only ion to exhibit a type I dependence, *i.e.*, a continuous asymptotic decrease with electron energy in excess of the ionization potential. m/e = 28, 39, 52, and 53 exhibited a rapid rise at very low energies with a distinct maxima in the 20–25 e.v. range, followed by a decrease at higher energies (type II). The ions at m/e = 15, 26, 27, 50, and 51 showed the type III curves, that is a gradual increase commencing at a threshold above those for the type II ions

Table IV: Summary of Abundances of the Principal Ions of $CD_2CHCHCD_2$ at Various Electron Energies

		Uncorrected electron energies							
m/e	Ratio	10 e.v.	12 e.v.	15 e.v.	20 e.v.	25 e.v.	30 e.v.	40 e.v.	70 e.v.
				C_4H_5					
57 (less 0.0214 × m/e = 58)			2.15	3.78	6.15	6.32	5.71	5.53	4.54
56			2.62	4.80	8.15	8.15	7.72	7.28	6.076
	56/57		(1.219)	1.270	1.325	1.290	1.352	1.316	1.338
								mean	1.315 ± 0.028
				C_3H_3					
42		0.77	2.87	3.89	5.08	4.86	4.57	4.33	3.90
41		2.38	9.24	12.20	16.88	16.27	15.86	15.10	13.87
40		0.79	3.01	4.02	5.38	5.33	5.30	5.24	4.97
	42/(42 + 41 + 40)	0.195	0.190	0.193	0.186	0.184	0.178	0.176	0.172
	41/(42 + 41 + 40)	0.604	0.611	0.607	0.618	0.615	0.616	0.612	0.610
	40/(42 + 41 + 40)	0.201	0.199	0.200	0.197	0.201	0.206	0.212	0.218
				C_2H_4					
32			0.13	0.32	0.74	0.78	0.79	0.74	0.871
31			0.72	1.59	3.55	3.65	3.74	3.47	4.21
30			0.54	1.32	4.14	5.14	5.36	4.69	5.92
	32/31		0.181	0.201	0.208	0.214	0.211	0.213	0.207
								mean	0.209
	30/31		0.75	0.818	1.166	1.408	1.433	1.352	1.408
				C_2H_3					
30 (less 0.784 × m/e = 31)				0.07	1.36	2.28	2.43	1.97	2.63
29				0.12	3.49	6.51	7.51	7.37	9.19
28 (less 0.75 × m/e = 27)				0.032	0.79	1.26	1.55	1.52	1.58
	38/(28 + 29 + 30)			0.32	0.240	0.227	0.212	0.181	0.196
	29/(28 + 29 + 30)			0.54	0.620	0.648	0.653	0.679	0.686
	28/(28 + 29 + 30)			0.14	0.140	0.125	0.135	0.140	0.118

show values in excess of the spectroscopic result (see Table III). A recent theoretical calculation[11] of the

(11) D. A. Hutchison, *Trans. Faraday Soc.*, **59**, 1695 (1963).
(12) A. B. King and F. A. Long, *J. Chem. Phys.*, **29**, 374 (1958).

and continuing to rise over the entire voltage range. The type II curve shape is generally associated with important primary products, while the type III indicates high activation energy primary products or secondary and higher order modes of formation.

The spectra of the deuterated compound *vs.* electron energy is summarized very briefly in Table IV. These data represent the isotope distribution at various electron energies for the principal ions discussed below.

Discussion

The most striking feature of the mass spectrum of the deuterated compound is the complete equilibration of the hydrogen atoms as is exhibited by the skeletal fragmentation reactions. These reactions are discussed in detail below, but one may examine the isotope distribution of the $C_3H_3^+$ given in Table IV as an example. The distribution $d_1:d_2:d_3$ is calculated to be 1.0:0.0:0.0 if the methyl group is from a terminal methylene and a hydrogen atom from the other terminal carbon (1–4 transfer). Similarly for a 1–3 hydrogen atom transfer without previous exchange, a 0.0:1.0:0.0 distribution is predicted. The calculated distribution, if complete equilibration of hydrogen atoms occurs, is 0.2:0.6:0.2 and this closely corresponds to the observed distribution. The $C_3H_3^+$ is formed by the lowest energy primary reaction and involves loss of a methyl radical. Thus, an intermediate involving a hydrogen atom rearrangement is readily formed.

The heats of formation of 1,3-butadiene ion and other isomeric ions were calculated from the heats of formation of the neutral species[13] and the ionization potential of each compound. The heats of formation thus calculated are ΔH_f(1,3-butadiene ion) = 10.21 e.v.,[10] ΔH_f(1,2-butadiene ion) = 11.25 e.v.,[14] ΔH_f(1-butyne ion) = 11.9 e.v.,[11] and ΔH_f(2-butyne ion) = 11.4 e.v.[15] Since the appearance potential of the lowest transition is 2.58 e.v. above the ground state of the 1,3-butadiene ion, all of the other three isomeric ions listed above may exist at this energy level, and the activation energy for the isomerization process, especially to 1,2-butadiene, which requires only one hydrogen atom to migrate, would probably be low enough to permit the complete equilibration of the hydrogen atoms before fragmentation can take place. The similarities of the mass spectral patterns for the four isomers listed above[16] would suggest that similar intermediate precursors to fragmentation exist for the other compounds. It should be emphasized that the possibility of hydrogen atom exchange without concurrent isomerization is not ruled out. The exchange mechanism based on an isomerization reaction to 1,2-butadiene is suggested by the ease with which methyl radicals are lost from the 1,3-butadiene parent ion. Although methylcyclopropene ion is another possible isomerization intermediate which may lose a methyl group, the $C_3H_3^+$ that would be formed is not of the propargyl structure indicated from thermochemical evidence.[14]

On the basis of the above observations, the metastable transition and appearance potential data in Tables II and III, and the low voltage dependence of the relative ion intensities, a mechanism for the fragmentation of 1,3-butadiene is suggested in Fig. 1. The activation energies in electron volts are given for the principal reactions. The activation energies for the primary processes are referred to the adiabatic ionization potential. The details of the formation of the principal fragment ions are discussed below.

$C_4H_5^+$. The activation energy for loss of a hydrogen atom is 2.96 e.v., and a metastable transition is observed for the reaction although the loss of a methyl radical has an activation energy lower by 0.38 e.v. Since the difference in activation energy is only 15% of the lower activation energy, a competition between these two processes at the upper threshold must exist in order to explain the metastable transitions, and this would seem to be reasonable. It is worth noting in this regard that the formation of $m/e = 28$ from the parent ion at 4.03 e.v. is not seen as a metastable transition. From the observed threshold for the $C_4H_5^+$, $\Delta H_f(C_4H_5^+) \leq 10.96$ e.v. is calculated.[10,13]

The parent-D and parent-H ion intensities for 1,3-butadiene-1,1,4,4-d_4 are listed in Table IV as a function of the electron energy. The $m/e = 57$ peak is corrected for the $C_4H_3D_3$ impurity, but no correction was attempted for the minor C_4D_4 contribution at $m/e = 56$. Except for a minor difference at the lowest electron energy, the ratio is constant throughout the voltage range indicating there is no effect of electron energy on the relative rates of these two reactions. Using the conventional definition of the primary isotope effect (π), namely, the ratio of the probability of the loss of a deuterium atom to the probability of the loss of a hydrogen atom,[17] $\pi = 1.315/2 = 0.66$. One could also determine the secondary isotope effect (Γ) defined as

(13) (a) F. D. Rossini, *et al.*, "Selected Values of Physical and Thermodynamic Properties of Hydrocarbons and Related Compounds," American Petroleum Institute, Carnegie Press, Pittsburgh, Pa., 1953; (b) F. D. Rossini, *et al.*, "Selected Values of Chemical Thermodynamic Properties," National Bureau of Standards Circular 500, U. S. Govt. Printing Office, Washington, D. C., 1952.

(14) J. Collin and F. P. Lossing, *J. Am. Chem. Soc.*, **79**, 5848 (1957).

(15) F. H. Coats and R. C. Anderson, *ibid.*, **79**, 1340 (1957).

(16) American Petroleum Institute, Research Project 44, Agricultural and Mechanical College of Texas, College Station, Texas.

(17) M. W. Evans, N. Bauer, and J. Y. Beach, *J. Chem. Phys.*, **14**, 701 (1946).

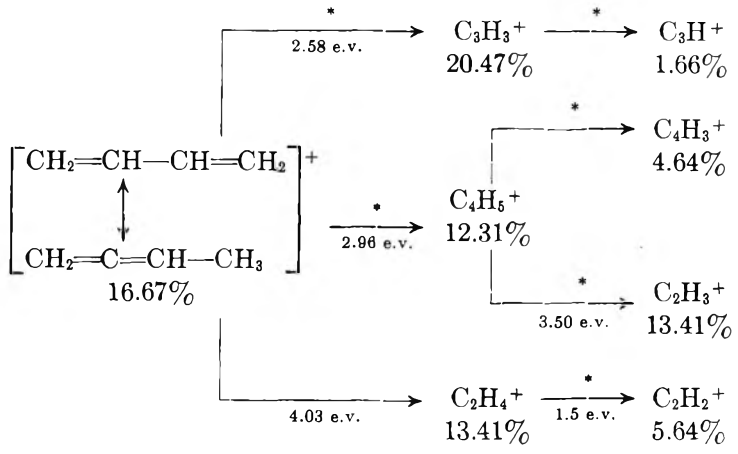

Figure 1. Fragmentation mechanism for 1,3-butadiene. Asterisks refer to metastable transitions observed, and the percentages refer to percentage of total ionization at 70 e.v.

the ratio of the rate of removal of an individual hydrogen atom from the deuterated compound to the undeuterated compound. Based on the fractional intensities of $m/e = 53$ and 57, in the respective compounds, one calculates $\Gamma = 4.91 \times 3/12.31 = 1.20$. It should be emphasized that in the calculation of Γ based on relative ion yields in the spectra of two different molecules, one is in effect making assumptions with regard to the comparative mechanisms and rate constants for not only the ionic species of interest but also the competing and successive reactions of this species. Unless one can justify these assumptions, the meaning of the secondary isotope effect (Γ) that is frequently reported is open to serious question. In addition, the complete equilibration of all the hydrogen atoms in the 1,3-butadiene spectra removes the need for distinguishing between the different types of C–H bonds in defining the isotope effect and the values thus obtained represent a weighted average of the two bond types present.

$C_3H_3^+$. The $C_3H_3^+$ ion, which has been suggested to have the structure of the propargyl ion,[14] is found with the lowest primary activation energy. As previously discussed the ease with which a methyl radical is lost is indicative of the rearrangement to the 1,2-butadiene-type structure. The appearance potential of $C_3H_3^+$ agrees well with the earlier value of Collin and Lossing,[14] and this is reflected in the good agreement of the calculated[13] $\Delta H_f(C_3H_3^+) \leqslant 11.40$ e.v. with the list of values tabulated by them for the formation of $C_3H_3^+$ from several compounds.[14]

The isotope distribution of $C_3H_3^+$ for the labeled compound is shown in Table IV. The slight increase in $m/e = 40$ with electron energy is attributed to increasing contribution from $C_3D_2^+$. The distribution at the lower electron energies agrees very well with the statistical distribution of 0.2:0.6:0.2. These results clearly demonstrate the complete randomization of the hydrogen atoms prior to skeletal break. The lack of a detectable isotope effect suggests that the activated complex does not involve a hydrogen atom transfer in the rate-determining step, but rather originates from a species in which the hydrogen transfer has already occurred, *e.g.*, 1,2-butadiene. The slight decrease of the $C_3D_3^+$ at the higher voltages is suggestive of the lack of complete equilibration of the hydrogen atoms for the very short-lived reactants, but this suggestion is only tentative.

$C_2H_4^+$. The formation of the ethylene ion requires the greatest activation energy of the three primary processes. The calculated appearance potential for the ethylene ion according to the over-all reaction

$$CH_2CHCHCH_2 + e \longrightarrow C_2H_4^+ + C_2H_2 + 2e \quad (1)$$

is 12.26 e.v. based on heats of formation of the neutral species[13] and the ionization potential of ethylene.[18] This indicates an excess energy requirement for reaction 1, *i.e.*, an activation energy of the reverse reaction, of 0.8 e.v. There are several possible factors that might be cited to explain the relatively high yield of the ethylene ion when there are several competing reactions of much lower activation energy. The frequency factor, or the rate of change of the rate constant with internal energy, for reaction 1 may be sufficiently larger than for the competing reactions, or the distribution of internal energies of the butadiene ion is such as to favor the higher energy region where all three of the primary reaction rates are more comparable. Another possibility is

(18) W. C. Price and W. T. Tutle, *Proc. Roy. Soc.* (London), **A174**, 207 (1940).

that an excited state of butadiene is formed which favors the formation of ethylene ion over the other primary ions. This explanation is equivalent to stating that the quasi-equilibrium assumption[19] is not applicable to the butadiene ion. The complete scrambling of the hydrogen atoms prevents further elucidation of the reaction at this time. A C^{13}-labeled compound might be of value for this point.

The isotope ratios of the ethylene ions are also shown in Table IV. Above 15 e.v., significant contributions to $m/e = 30$ from $C_2D_3^+$ are encountered. Based on the low voltage ratio of 30/31 and the average 32/31 ratio given, the isotopic distribution observed is $d_2:d_3:d_4::0.393:0.502:0.105$ compared with the statistical distribution 0.40:0.533:0.067. The constancy of the 32/31 ratio with electron energy is contrasted by the minor trend observed for the 42/41 ratio for $C_3H_3^+$.

$C_2H_3^+$. The most striking feature about the vinyl ion is the observation of a metastable transition for its formation from $C_4H_6^+$ rather than the parent ion. The calculated appearance potential for this over-all process

$$CH_2CHCHCH_2 + e \longrightarrow C_2H_3^+ + C_2H_2 + H + 2e \quad (2)$$

is 15.62 e.v. (based on $\Delta H_f(C_2H_3^+) = 12.15$ e.v.[20]). This agrees quite well with the observed appearance potential clearly proving that $C_2H_3^+$ is formed *via* reaction 2 and not directly from the parent ion by

$$CH_2CHCHCH_2 + e \longrightarrow C_2H_3^+ + C_2H_3 + 2e \quad (3)$$

which has a calculated threshold of 13.45 e.v. It is worth noting that Collin and Lossing had previously observed that the $\Delta H_f(C_2H_3^+)$ was too high when calculated from this appearance potential assuming the process was reaction 3.[14] The isotopic distribution for the vinyl ion in the deuterated spectra is based on major corrections for contributions at $m/e = 30$ and 28 for $C_2D_2H_2^+$ and $C_2D_2^+$. The distributions found at the lower voltages agree well with the calculated value of $d_3:d_2:d_1::0.230:0.600:0.170$ based on statistical distribution from the precursors $C_4H_2D_3$ and C_4HD_4 in a 1.315:1.0 ratio. The change of this distribution at the higher voltages may be the result of higher energy processes or may be due to incorrect estimation of the other contributions at $m/e = 30$ and 28.

$C_2H_2^+$. The appearance potential measured for this ion is only approximate and is significantly lower than the value reported by Barker, *et al.*[21] The calculated value[13,22] of the appearance potential for the over-all process

$$CH_2CHCHCH_2 + e \longrightarrow C_2H_2^+ + C_2H_2 + H_2 + 2e \quad (4)$$

is 14.97 e.v. which agrees fairly well with our value. If this assignment is correct, the excess energy in reaction 1 is available for the subsequent decomposition to $C_2H_2^+$, which is observed as a metastable transition.

Acknowledgment. The author wishes to express this thanks to Dr. Dale E. Van Sickle for supplying the sample of 1,3-butadiene-1,1,4,4-d_4. He also wishes to thank Dr. John C. Schug for his comments and H. T. Best and J. P. Klems for obtaining the mass spectral data.

(19) H. M. Rosenstock, M. B. Wallenstein, A. L. Wahrhaftig, and H. Eyring, *Proc. Natl. Acad. Sci. U. S.*, **38**, 667 (1952).

(20) F. H. Field and J. L. Franklin, "Electron Impact Phenomena," Academic Press, Inc., New York, N. Y., 1957.

(21) R. Barker, W. H. Hamill, and R. R. Williams, Jr., *J. Phys. Chem.*, **63**, 825 (1959).

(22) W. C. Price, *Phys. Rev.*, **47**, 444 (1935).

Photolysis and Radiolysis of Propargyl Bromide

by M. Trachtman

John Harrison Laboratory, University of Pennsylvania[1] *and Frankford Arsenal, Philadelphia, Pennsylvania* *(Received December 13, 1963)*

The radiation and photochemistry of propargyl bromide in the liquid phase was studied in the presence and absence of free-radical scavengers at 25°. The gaseous products from radiolysis were hydrogen, acetylene, and methylacetylene, whereas only methylacetylene was observed in photolysis. The failure of oxygen and diphenylpicrylhydrazyl to inhibit acetylene formation was attributed to its formation *via* an ion-molecule reaction suggested by a study of the pressure dependence of the mass spectrum of propargyl bromide. The data do not permit any conclusions regarding the extent of formation of acetylene *via* hot radical and excited molecule reactions.

Much work has been done on the irradiation of acetylene in the gas phase,[2-4] but there is little information in the literature relating to the radiolysis of more complex compounds containing a triple bond. Except for a technical research report,[5] no radiolysis studies of propargyl compounds have been reported. This research reports an investigation of the photochemistry and radiation chemistry of propargyl bromide in the liquid phase. Propargyl bromide was chosen as a likely substance for comparison of radiolysis and photolysis. Photolysis would be expected to involve a scission of the C–Br bond; the radiolysis might be expected to follow a similar path since high energy deposition would be localized on the bromine atom.

Experimental

Materials. Propargyl bromide was purified by passage through a column of silica gel followed by fractional distillation in an 46-cm. Vigreux column. A middle cut boiling at 79.1° (759 mm.) was water-white and was stored in the dark at 5°. Iodine was resublimed after grinding with potassium iodide. 2,2-Diphenyl-1-picrylhydrazyl, Eastman Kodak Co., was used as received. Commercial oxygen was used directly from a Liquid Carbonic Co. cylinder after passage through calcium sulfate to remove moisture.

Apparatus. The light source was a Hanovia SC 2537 low pressure mercury resonance lamp constructed of a Vycor envelope shaped into a four-coil helix which was 12.5 cm. in diameter and 10.5 cm. long. Its output is 90% at 2537 Å. with small intensities at longer wave lengths. The filter solution used in all photolysis experiments was 0.20% solution of 2,7-dimethyl-3,6-diazocyclohepta-1,6-diene perchlorate as described by Kasha.[6] This solution restricted the actinic radiation to the mercury lines at 2537 and 2652 Å. Uranyl oxalate was employed as the actinometer. Propargyl bromide was found to absorb 3.2×10^{16} quanta ml.$^{-1}$ sec.$^{-1}$ in the region transmitted by the filter solution by means of the principle of equivalent optical densities.[7]

All the rate studies were carried out in a vessel consisting of a quartz tube closed at one end and surrounded by a Vycor jacket which contained the filter solution. The inner tube was connected to a Pyrex Vycor graded seal. The volume of this vessel was 9.8 ml. Propargyl bromide was found to absorb all of the incident light at 2537 Å. Since this resulted

(1) This work is in part a contribution from the Laboratory for Research on the Structure of Matter, University of Pennsylvania, supported by the Advanced Research Projects Agency, Office of the Secretary of Defense, and by the Army Material Command under Project No. OMS 5010.11.838, "Basic Research in the Physical Sciences."

(2) S. C. Lind, C. J. Hochanadel, and J. A. Ghormley, "Radiation Chemistry of Gases," Reinhold Publishing Corp., New York, N. Y., 1961.

(3) G. J. Mains, H. Niki, and M. H. J. Wijnen, *J. Phys. Chem.*, **67**, 11 (1963).

(4) D. J. Leroy and E. W. R. Steacie, *J. Chem. Phys.*, **12**, 117 (1944).

(5) Astia AD No. 297177, Monsanto Research Corporation, "Radiation Polymerization of Acetylene Derivatives," 1962.

(6) M. Kasha, *J. Opt. Soc. Am.*, **38**, 429 (1948).

(7) D. H. Volman and J. C. Chen, *J. Am. Chem. Soc.*, **81**, 756 (1959).

in a very inhomogeneous distribution of photoexcited molecules, quantum yields are subject to considerable uncertainty. The photolysis experiments were performed at 25°.

γ-Irradiations. Samples for irradiation were contained in 35-mm. o.d. Pyrex tubes, equipped with break seals, which could be reproducibly positioned in the 600-c. Co^{60} source. The volume of liquid varied from 50 to 60 ml. and was measured to ±0.5 ml. at the conclusion of each experiment.

The dose rate for the samples during the period of this work was approximately 1×10^{19} e.v./g./hr. (2×10^5 r./hr.). The exact values were determined using the Fricke dosimeter as described by Miller.[8] All of the irradiations were conducted at room temperature (25 ± 2°).

Procedure. In all the experiments, propargyl bromide was degassed using the method of Newton[9] after which it was distilled into the reaction vessel. The reaction vessels were sealed off while the propargyl bromide was frozen at −196°. After warming to room temperature, the reaction vessel was positioned in the center of the light helix except where noted otherwise in the subsequent text. Photolysis periods ranged from 30 to 120 min., whereas radiolysis periods ranged from 1 to 168 hr. After irradiation, the gaseous products were removed by distilling the solution from the reaction vessel through a bath at −64°. Trap to trap distillation was employed for the removal of the gaseous products which were finally transferred to a pressure–volume apparatus using a Toepler pump. Two line traps between the Toepler pump and the sample trap were cooled with Dry Ice–acetone to remove any escaping propargyl bromide. After pressure–volume measurements, the entire gaseous sample was collected in a bulb and analyzed using a Consolidated Electrodynamics Type 21-130 mass spectrometer. The liquid samples were analyzed using a C.E.C. 21-103C mass spectrometer because of its higher mass range. Pure samples of the liquid products were not available and quantitative determination of these was not possible.

An attempt was made to analyze the liquid products using the Perkin-Elmer Model 154 gas chromatograph. Flash pyrolysis occurred at the injection block (temperature 125°) leading to the formation of a polymer which obstructed the carrier gas channel. A similar phenomenon occurred when the liquid products were injected into the *heated* inlet system of the C.E.C. 103C mass spectrometer for analysis. An examination of the spectrum indicated the presence of pyrolysis products in such large quantities that the parent peaks m/e = 118 and 120 were greatly reduced. This would indicate that the pyrolysis products, mainly polymeric, were formed in the heated inlet block.

The absence of HBr and Br_2 in the products does not exclude the possibility that these compounds are formed during the radiolysis and photolysis. If these molecules were formed, they would readily react with the unsaturated parent or product compounds present.

Results

Effect of Total Dose. Mass spectrometric analyses showed the gaseous radiolysis products to be mainly methylacetylene, hydrogen, acetylene, and methyl bromide, with trace amounts of diacetylene, vinylacetylene, bromoacetylene, and butadiene. The yields of methylacetylene, hydrogen, and acetylene increased linearly with time, indicating a constant "G" value. The results are listed in Table I and are expressed as μmoles of product per mole of propargyl bromide. The "G" values obtained for these products are as follows: methylacetylene G = 0.26; hydrogen G = 0.018; acetylene G = 0.013.

Table I: Yield of Major Products upon Radiolysis of Propargyl Bromide, Expressed as μmoles of Product/Mole of Propargyl Bromide

Time, hr.	Methylacetylene	Acetylene	Hydrogen
6	47	3.0	2.7
18	126	6.5	5.6
24	177	8.0	9.5
48	425	21.4	29.5
51	457	23.2	30.4
92	835	40.3	45.8
168	1420	70.0	113.5

In the mass spectrum of the liquid radiolysis products (introduced at room temperature), peaks at m/e = 78, 156, and 160 indicated the presence of $(HC{\equiv}C{-}CH_2)_2$, C_6H_5Br, and C_6H_7Br. The mass spectrum also contained groups of peaks with intensity ratios 1:2:1; at m/e = 196, 198, and 200 indicating the presence of $HC{\equiv}C{-}CHBr_2$, at m/e = 234, 236, and 238 indicating the presence of $HC{\equiv}C{-}CH_2{-}CBr_2{-}C{\equiv}CH$, and finally a group of peaks with intensity ratios of 1:3:3:1 at 276, 278, 280, and 282 indicating the presence of $BrCH_2CBr{=}CHBr$. As noted previously, these products could not be determined quanti-

(8) N. Miller, "Introduction a la Dosimetrie des Radiations," Chemical and Biological Actions of Radiations II, H. Haissinsky, Ed., Masson et Cie., Paris, 1956.

(9) A. S. Newton, *Anal. Chem.*, **28**, 1214 (1956).

tatively owing to the unavailability of the pure compounds.

The only gaseous product obtained during the photolysis of propargyl bromide was methylacetylene. The yield of methylacetylene was linear with time during the 2-hr. photolysis period. This result was similar to that obtained during the radiolysis; yields are given in Table II. The estimated quantum yield for methylacetylene is 9.3×10^{-3}.

Table II: Photolysis of Propargyl Bromide

Time, min.	Methylacetylene, μmoles/mole of propargyl bromide
30	50.4
60	100.7
90	153.0
120	215.8

The examination of the mass spectra obtained from the liquid products of photolysis indicated that the products were identical with the liquid products obtained during radiolysis differing only in relative amounts formed.

Effect of Additives. Several radiolysis experiments were performed in the presence of the radical scavengers oxygen and 10^{-2} *M* 2,2-diphenyl-1-picrylhydrazyl (DPPH). In all cases, the yield of methylacetylene decreased, whereas the yield of acetylene remained unchanged. Oxygen was found to decrease the yield of methylacetylene by 45%, whereas the yield of hydrogen and acetylene remained essentially unchanged. Using DPPH as the scavenger, the yield of methyl acetylene was reduced 60–65% and H_2 was reduced 60%. However, the yield of acetylene remained constant in the presence of DPPH. The different yields obtained in the presence of the two scavengers can be attributed to the greater scavenging efficiency of DPPH. It seems reasonable to suppose that the scavenging efficiency of the oxygen molecule is limited by its low solubility.

The photolysis of propargyl bromide was also performed in the presence of oxygen as the scavenger. DPPH cannot be used as a scavenger in the photolysis as it absorbs in the same region as the propargyl bromide. Preliminary experiments indicated that the yield of methylacetylene in the presence of oxygen was reduced but not eliminated. The failure of the scavenger to eliminate completely methylacetylene was attributed to the high concentration of propargyl radicals at the walls which rapidly depleted the oxygen concentration. When the sample tube which was normally placed at the center of the helix was placed 30 cm. away from the light source and photolyzed for 30 min., 3 μmoles of methylacetylene/mole of propargyl bromide were produced, but when the photolysis was carried out in the presence of oxygen, no methylacetylene was detected.

Polymer Formation. Five milliliters of the radiolysis products of the liquid solution (7.6 g. of starting material) was pipetted into a weighing bottle and the excess propargyl bromide was removed under vacuum. A viscous material remained. The yield of this polymer increased linearly with increasing dose as shown in Table III. The *G* yield of monomer consumption as polymer was 29.9 in excellent agreement with the value of 30 found at Monsanto.[5]

Table III: Yield of Polymer Remaining after Radiolysis

Time, hr.	Yield, g.
24	0.2004
48	0.3534
92	0.6993
168	1.2255

The same technique was employed to determine the quantum yield of polymer in photolysis as that used in the determination of polymer in radiolysis. The quantum yield of polymer formation was 8.08×10^{-2}. Polymer yield was not studied as a function of photolysis time.

Discussion

Photolysis. Photolysis of propargyl bromide produced methylacetylene and polymer as the main products. Smaller yields of $(HC{\equiv}C{-}CH_2)_2$, C_6H_5Br, C_6H_7Br, $HC{\equiv}C{-}CHBr_2$, $(HC{\equiv}C{-}CHBr)_2$, and $BrCH_2{-}CBr{=}CHBr$ were also observed. A mechanism consistent with the formation of these products is

Primary process

$$HC{\equiv}C{-}CH_2Br + h\nu \longrightarrow HC{\equiv}C{-}CH_2^{\cdot} + Br^{\cdot} \quad (1)$$

Methylacetylene formation

$$HC{\equiv}C{-}CH_2Br + HC{\equiv}C{-}CH_2^{\cdot} \longrightarrow HC{\equiv}C{-}CH_3 + HC{\equiv}C{-}\dot{C}HBr \quad (2)$$

C_6H_5Br and C_6H_7Br formation

$$HC{\equiv}C{-}CH_2^{\cdot} + HC{\equiv}C{-}CH_2Br \longrightarrow HC{\equiv}C{-}CH_2{-}CH{=}\dot{C}{-}CH_2Br \quad (3)$$

$$HC{\equiv}C-CH_2-CH{=}\dot{C}-CH_2Br + HC{\equiv}C-CH_2Br \longrightarrow HC{\equiv}C-CH_2-CH{=}CH-CH_2Br + HC{\equiv}C-\dot{C}HBr \quad (4)$$

$$HC{\equiv}C-\dot{C}HBr + HC{\equiv}C-CH_2 \longrightarrow HC{\equiv}C-CH_2-CHBr-C{\equiv}CH \quad (5)$$

Bromine atom reactions

$$Br\cdot + HC{\equiv}C-CH_2Br \longrightarrow \underset{\displaystyle Br}{\overset{\displaystyle |}{HC{=}\dot{C}-CH_2Br}} \quad (6)$$

$$Br\cdot + R\cdot \longrightarrow RBr \quad (7)$$

where R· is any of the free radicals postulated in reactions 1–6.

No C–C cleavage is assumed in the photolysis mechanism because no acetylene or CH_3Br has been observed. Also, additional support for the postulated free-radical mechanism in the photolysis experiments was obtained by studying scavenging effects of oxygen. In the presence of oxygen, no methylacetylene was detected indicating that the C–Br cleavage in photolysis involves exclusively free radicals.

Radiolysis. Radiolysis of propargyl bromide gave evidence for C–CH_2Br and C–H rupture even though the energy is mainly absorbed by the bromine atom. Inasmuch as radiolysis does not involve exclusively the lowest excited electronic state as in photolysis, there is the possibility that ions or higher excited states are produced either directly or *via* ion neutralization and are responsible for product formation.

The use of oxygen and DPPH as free-radical scavengers indicates that all of the acetylene, 35–40% of the methylacetylene, and 40% of the hydrogen are not scavenged. Therefore, it seems reasonable to conclude that 60–65% of the methylacetylene is produced by a free-radical reaction similar to that proposed for the photolysis in reaction 2. The remaining methylacetylene and all of the acetylene are produced by some nonscavengeable precursor. The possible reactions which may be involved are ion–molecule, molecular decomposition of higher excited states, and hot radical reactions.

An examination of the mass spectrum of propargyl bromide as a function of pressure resulted in the observation that the sensitivity of the peaks at m/e = 25 and 39 decreased with increasing pressure, implying that they are being consumed by ion–molecule reactions. Thus, acetylene and methylacetylene may be formed by reactions of the following type in the mass spectrometer.

$$C_3H_3^+ + C_3H_3Br \longrightarrow C_3H_4 + C_3H_2Br^+ \quad (8)$$

$$C_2H^+ + C_3H_3Br \longrightarrow C_2H_2 + C_3H_2Br^+ \quad (9)$$

Similar reactions might be postulated for the liquid phase radiolysis experiments. While the validity of quantitative extrapolation of observations from the low gas pressures in a mass spectrometer to the condensed phase is indeed subject to question, qualitative extrapolation does not appear unreasonable. These ion–molecule reactions do not preclude the possibility of product formation by excited molecule or hot radical reactions about which little quantitative data are available. If all the acetylene and 40% of the methylacetylene are assumed to be produced by ion–molecule reactions (eq. 8 and 9), the extent of inhibition of these products then reflects the relative importance of $C_3H_3^+$, C_2H^+, and $C_3H_3\cdot$ in the liquid phase radiolysis.

No quantitative conclusions can be reached regarding the mechanism of hydrogen formation. The failure of oxygen to scavenge any of the H_2 may be due to the low solubility of O_2. On the other hand, the observation that DPPH decreases the H_2 yield by 60% may be attributed to its ion-scavenging ability.

In both the photolysis and the radiolysis, there is evidence for the formation of HC≡C—CH_2—CHBr—C≡CH. While the low energy photolysis reaction would favor free-radical formation, this product in the radiolysis could also arise *via* an ion–molecule reaction involving $C_6H_6Br^+$ followed by neutralization.

In conclusion, the photolysis of progargyl bromide can be explained assuming a free-radical mechanism involving a C–Br scission as the primary process. The radiolysis is reasonably accounted for by both ionic and free-radical mechanisms of almost equal importance. Some products, notably acetylene, are assumed to be produced *via* an exclusively ionic mechanism because quantitative information regarding excited molecule and hot radical mechanisms are unavailable. The main product from both radiolysis and photolysis is polymer, indicating that the intermediates produced by both types of radiation can initiate a chain polymerization.

Acknowledgment. The author wishes to thank Prof. Gilbert Mains of the Carnegie Institute of Technology who made available his 21-103 mass spectrometer for the liquid studies, and who provided constant advice and encouragement which very tangibly aided the course of this research. Thanks are also due to Prof. John G. Miller for providing the author with the opportunity to undertake this work and

encouragement in carrying it out. Mr. Stephen Weininger helped with the mass spectrometry, and he and Dr. Robert Witonsky earned the author's appreciation for many stimulating discussions. Grateful acknowledgment is also expressed for the aid given by the Research Institute of the Frankford Arsenal.

Lattice Constants and Thermodynamic Parameters of the Hydrogen–Platinum–Palladium and Deuterium–Platinum–Palladium Systems

by Arnulf Maeland and Ted B. Flanagan

Chemistry Department, University of Vermont, Burlington, Vermont (*Received December 20, 1963*)

Absorption isotherms (25°) and thermodynamic parameters of absorption of deuterium by several platinum–palladium alloys have been determined. Relationships between the relative resistance of the alloys and their deuterium content have been established (25°). Results have been compared to the previously obtained data on the hydrogen–platinum–palladium system. The experimental differences between the heats of absorption of deuterium and hydrogen in palladium and several platinum–palladium alloys have been compared to predicted values for these differences. Lattice constants of the f.c.c. platinum–palladium alloys have been determined as a function of both the hydrogen and deuterium content of the alloys. Phase boundaries have been established using X-ray diffraction techniques.

Introduction

Direct absorption of hydrogen by palladium from hydrogen-stirred acidic water solutions has been shown to occur readily.[1,2] It has been demonstrated that electrode potentials of the palladium specimen during the course of absorption from solution have thermodynamic significance, *i.e.*, the hydrogen is approximately uniformly distributed throughout each phase of the nonstoichiometric hydrides during absorption.[2,3] Absorption of hydrogen from solution is a useful technique for the determination of absorption isotherms below 100° because direct equilibration in the absence of solution is slow below 100°. Carson, *et al.*,[4] have employed this technique to investigate the absorption of hydrogen by a series of palladium-rich platinum–palladium alloys. The equilibrium solubilities (25°, 1 atm.) of hydrogen in these alloys were found to decrease with increasing platinum content. Absorption isotherms revealed the existence of pressure-invariant regions for alloys with at least 8.80% platinum (25°, 1 atm.). In analogy with the behavior of pure palladium,[5] these pressure invariant regions correspond to the coexistence of the α- and β-nonstoichiometric hydride phases. The two-phase region was said to disappear when the platinum content had reached 12 ± 1.5%, but the isotherm obtained for the 12.03% platinum–palladium alloy was inconclusive.[4]

A large difference in the equilibrium isotopic solu-

(1) T. B. Flanagan and F. A. Lewis, *Trans. Faraday Soc.*, **55**, 1400 (1959).

(2) R. J. Fallon and G. W. Castellan, *J. Phys. Chem.*, **64**, 4 (1960).

(3) T. B. Flanagan and F. A. Lewis, *Trans. Faraday Soc.*, **55**, 1409 (1959).

(4) A. W. Carson, T. B. Flanagan, and F. A. Lewis, *ibid.*, **56**, 363, 371, 1332 (1960).

(5) D. P. Smith, "Hydrogen in Metals," Chicago University Press, Chicago, Ill., 1948.

bility of hydrogen and deuterium in certain platinum–palladium alloys has been recently reported.[6] In order to understand this difference in isotopic solubilities and for comparison with earlier results obtained on the H–Pt–Pd system,[4] the absorption isotherms and thermodynamic parameters of absorption of the D–Pt–Pd system have been examined in some detail.

Platinum–palladium forms a continuous series of f.c.c. solid solutions with no evidence of superstructure.[7] The addition of small amounts of platinum to palladium results in only a small change in the lattice constants. The lattice constants of the nonstoichiometric platinum–palladium hydrides and deuterides have not been measured previously. The lattice constants are of interest *per se* and are a valuable aid in the establishment of the phase boundaries more exactly than can be estimated from the absorption isotherms.

Experimental

Materials. The alloys were prepared from metals of 99.98% purity melted under argon. These were used in the form of wires of 0.027 and 0.012 cm. diameter. Deuterium gas was >99.5% pure and was passed through platinized asbestos (300°) and a liquid nitrogen trap before using.

Apparatus and Procedure. The apparatus has been described.[1] The specimens (15-cm. lengths) were mounted in soft glass, vacuum-tight holders.[1] The absorption runs were performed in dilute DCl solutions (~0.02 *N*). Resistance measurements were carried out by passing a constant, known d.c. current (~5 ma.) along the specimen and measuring the *iR* drop. The temperature of the reaction vessel was maintained to ±0.2° by a surrounding water bath. Deuterium contents were determined by outgassing (300°) the specimens in a vacuum system of known volume. Electrode potentials were measured with reference to a platinized platinum electrode in the same solution. At temperatures above approximately 25° the vapor pressure of water in the deuterium (hydrogen) gas may significantly reduce the deuterium (hydrogen) partial pressures to values below 1 atm. The procedure used to correct for this occurrence was to determine the electrode potentials of a Ag, $AgCl|Cl^-||H^+|H_2$, Pt cell as a function of temperature under conditions of hydrogen flow, etc., identical with those used for the determination of the potentials of the cell composed of the alloy and the hydrogen electrode. By comparison with data for a fully saturated and appropriately corrected Ag, $AgCl|Cl^-||H^+|H_2$, Pt cell,[8] it was possible to determine empirically the correction to be applied to the data obtained under the operating conditions of the cell formed between the alloy and the hydrogen electrode. Using the results obtained for the hydrogen system, similar corrections were applied to the deuterium system. The maximum corrections were approximately 0.7 mv. (50°) for deuterium and 1.5 mv. (60°) for hydrogen.

On some occasions deuterium (hydrogen) was introduced into the specimen electrolytically. The specimen was made cathodic with respect to an inert platinum electrode and electrolysis was performed with a constant current (1 ma.).

X-Ray Diffraction Studies. A number of X-ray diffraction patterns were taken at various deuterium (hydrogen) contents. In order to obtain a pattern, the wire was removed from the reaction vessel after the attainment of the desired deuterium (hydrogen) content and immersed in acetone with added sulfur. A small section was removed and immediately immersed in polymethacrylate solution to prevent deuterium (hydrogen) loss. To ensure further against loss of absorbed gas, the sample was sealed into 0.3-mm. glass capillaries. Occasional checks were made which indicated that loss of deuterium (hydrogen) had not occurred if the above procedure was employed; *e.g.*, sample contents were determined by degassing after exposure to X-rays and X-ray diffraction patterns on the sample were run over a period of several weeks. After removal of a small section of wire the remainder of the specimen was degassed, resealed to the holder, and reused.

With Cu Kα radiation, the penetration into the sample is approximately 20 μ and the X-ray pattern, therefore, corresponds to layers adjacent to the surface.[9] In order to help in the detection of a second phase which may be in the interior of the specimen, the 0.012-cm. wires were employed with Mo Kα radiation near phase boundaries. However, all lattice parameters quoted were obtained with Cu Kα radiation and a 114-mm. Norelco camera.

Results and Discussion

Relationships between R/R_0 and Deuterium Content. In order to obtain a convenient measure of the deuterium content of each alloy specimen, relationships between relative resistance (R/R_0) and deuterium content (D/M, expressed as atomic ratio of deuterium to metal) were established. Results are given in Table I. The R/R_0 *vs.* D/Pd relationship has been previously es-

(6) T. B. Flanagan, *J. Phys. Chem.*, **67**, 203 (1963).

(7) E. Raab, *J. Less-Common Metals*, **1**, 3 (1959).

(8) R. Bates and V. Bower, *J. Res. Natl. Bur. Std.*, **53**, 283 (1954).

(9) P. C. Aben and W. G. Burgers, *Trans. Faraday Soc.*, **58**, 1989 (1962).

Table I: Relationship between R/R_0 and D/M (Atomic Ratio) at 25°

2.79% Pt		5.73% Pt		8.80% Pt		12.03% Pt	
R/R_0	D/M	R/R_0	D/M	R/R_0	D/M	R/R_0	D/M
1.059	0.020[a]	1.047	0.016[a]	1.005	0.003[a]	1.007	0.002[a]
1.081	0.039[a]	1.079	0.032[a]	1.009	0.005[a]	1.011	0.005[a]
1.101	0.059[a]	1.097	0.047[a]	1.013	0.009[a]	1.012	0.007[a]
1.109	0.062	1.125	0.071[a]	1.020	0.011[a]	1.015	0.009[a]
1.115	0.074	1.108	0.071	1.025	0.014[a]	1.027	0.015[a]
1.120	0.079[a]	1.162	0.102[a]	1.035	0.018[a]	1.032	0.017[a]
1.136	0.082	1.210	0.142[a]	1.041	0.020[a]	1.042	0.022[a]
1.131	0.090	1.242	0.152	1.049	0.023[a]	1.046	0.024[a]
1.151	0.108[a]	1.373	0.233	1.055	0.026[a]	1.046	0.021
1.198	0.147[a]	1.452	0.270	1.062	0.029[a]		
1.316	0.211	1.543	0.300	1.076	0.033		
1.397	0.281	1.669	0.385				
1.475	0.308	1.632	0.386				
1.519	0.347	1.676	0.391				
1.563	0.356						
1.622	0.419						
1.688	0.453						
1.789	0.505						
1.796	0.506						

[a] Deuterium introduced by electrolysis and D/M obtained from the total coulombs of electricity passed.

tablished.[10] Smooth curves have been drawn through the data of Table I; these curves have been used as calibration curves from which deuterium contents could be obtained. The majority of the calibration points were determined after introduction of deuterium by direct absorption from solution. It may be seen from Table I and ref. 4 and 10 that the resistance of the specimens is increased more per atom of deuterium than per atom of hydrogen in both pure palladium and in these alloys.

Absorption Isotherms. Changes occurring in the electrode potential and relative resistance during absorption are shown in Fig. 1 for a typical run (2.79% platinum, 25°, 1 atm. of D_2, ~0.02 *N* DCl). The first descending portion of the potential–time curve is due to the solution of deuterium in the α-phase. The region of constant potential (plateau potential) corresponds to the coexistence of two nonstoichiometric deuteride phases called the α- and β-phases in analogy with pure palladium and hydrogen.[5] The minimum in the electrode potential which occurs immediately before the establishment of the plateau potential has been explained[3,9,11] as being due to the supersaturation of the α-phase before the surface layers are converted to the β-phase.

The electrode potential represents the nonstoichiometric reaction

$$^1/_2D_2 + xD{:}yPt{:}zPd = (x + 1)D{:}yPt{:}zPd \quad (1)$$

where x, y, and z represent actual numbers of atoms in the nonstoichiometric deuteride. Equilibrium deuterium pressures were calculated from the corrected electrode potentials by

$$P = e^{-2FE/RT} \quad (2)$$

and the corresponding D/M values were obtained from R/R_0 using Table I. Absorption isotherms are shown in Fig. 2 (25°).

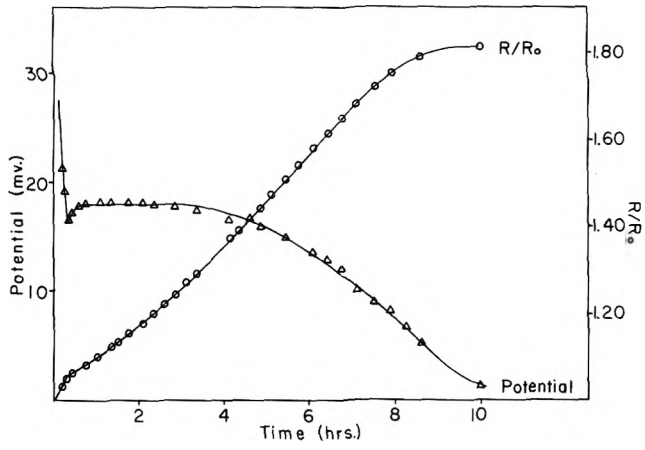

Figure 1. Absorption of deuterium by the 2.79% Pt alloy at 25°, 0.02 *N* DCl, 1 atm. of D_2.

(10) T. B. Flanagan, *J. Phys. Chem.*, **65**, 280 (1961).

(11) R. J. Ratchford and G. W. Castellan, *ibid.*, **62**, 1123 (1958).

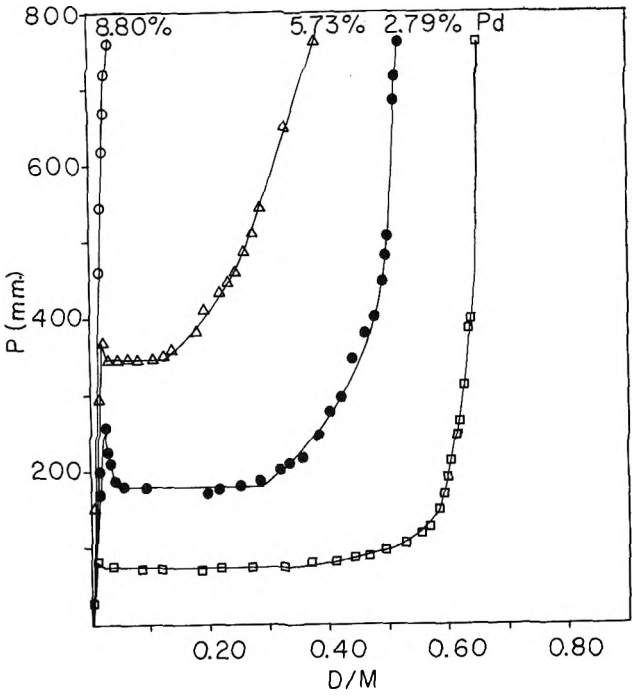

Figure 2. Pressure–concentration isotherms at 25°.

It should be pointed out that the deuterium plateau pressures for the platinum–palladium alloys at 25° are considerably greater than those found with hydrogen absorption for the alloy of corresponding composition.[4] In fact, in the deuterium system a two-phase region is not found in alloys of >8.80% platinum (25°, 1 atm. of D_2). However, when the effective deuterium pressure was increased above 1 atm. by electrolytic introduction of deuterium, a two-phase region was detected in the 8.80% platinum alloy as shown by the X-ray diffraction pattern (see below). Also, upon reduction of the temperature from 25 to 5° a plateau potential (~5 mv.) indicative of a two-phase region was observed in the 8.80% platinum alloy.

Thermodynamic Parameters. Heats of absorption in the two-phase region have been determined from the variation of the two-phase electrode potential (corrected to 1 atm. of deuterium) with temperature (0–50°).[3,11] The procedure employed was to use a recently degassed specimen and initiate an absorption run which was stopped after approximately 1 hr. The electrode potential was chosen as the maximum value after the supersaturation minimum; this maximum appeared at closely similar values of R/R_0 for a given alloy. Heats of absorption and the other thermodynamic quantities, representing reaction 1 in the two-phase region, are shown in Table II. The free energy change was calculated directly from the two-phase electrode potential (corrected to 1 atm.) and the entropy change was calculated from ΔH° and ΔG°.

Table II: Thermodynamic Parameters for Absorption of Deuterium (Hydrogen) in the Two-Phase Region of Platinum–Palladium Alloys (25°, 1 atm.)

Hydrogen isotope	Alloy % Pt	$-\Delta G^\circ$, cal./mole of D_2 (H_2)	$-\Delta H^\circ$, cal./mole of D_2 (H_2)	$-\Delta S^\circ$, e.u.	Ref.
H_2	0	2318	9546	24.2	[a]
D_2	0	1435	8551	23.9	10
H_2	2.79	1809	8226	22.5	4
D_2	2.79	886	7526	22.3	[a]
H_2	5.73	1283	7462	20.7	4
D_2	5.73	487	6828	21.3	[a]
H_2	8.80	572	6549	20.0	4

[a] This work.

Because of the large range of values obtained for the heat of absorption of hydrogen in the two-phase region of pure palladium (see ref. 11 and 12 for brief reviews), it was decided to redetermine this heat using the technique of direct absorption from solution. The primary purpose of this determination was to assure that the values of Table II should be internally consistent, *i.e.*, that all values are determined by the same method. Our value for this heat of absorption is 266 cal./mole more exothermic than the value obtained by a similar method (not identical) by Fallon and Castellan.[2] The value given in Table II is, however, only 59 cal./mole less exothermic than the most recent (and most reliable) calorimetric value.[12] We believe that this close agreement with the calorimetric value fully justifies the technique of direct absorption from solution *provided that proper experimental precautions* are exercised, *i.e.* (1) the determinations at each temperature are performed under as closely similar conditions as possible; (2) the electrode potentials are nearly constant (±0.1 mv.) during a considerable range of absorption; and (3) corrections are applied for variations of water vapor pressure with temperature if such a correction is required. The values for the heats of absorption of deuterium by pure palladium previously obtained[10] have now been corrected for the heavy water vapor pressure using results from the hydrogen system (see Experimental) and allowing for the smaller heavy water vapor pressure. This changes the previously obtained heat from −8795 to −8551 cal./mole; this change is slightly larger than the expected experi-

(12) D. M. Nace and J. G. Aston, *J. Am. Chem. Soc.*, **79**, 3619 (1957).

mental error. The heats and other thermodynamic parameters of absorption of hydrogen and deuterium by the platinum–palladium alloys have all been determined using electrode potentials which have been corrected for water vapor pressures. These corrections usually amounted to 200 to 300 cal./mole for the heats of absorption and only slight differences in the free energies and entropies of absorption.

The equilibrium solubility of deuterium in these platinum–palladium alloys are shown in Fig. 3 in comparison with earlier results for hydrogen[4] (25°, 1 atm. of D_2 (H_2)). It may be noted that there is a large isotopic solubility difference between hydrogen and deuterium at about 9% platinum (25°, 1 atm.).

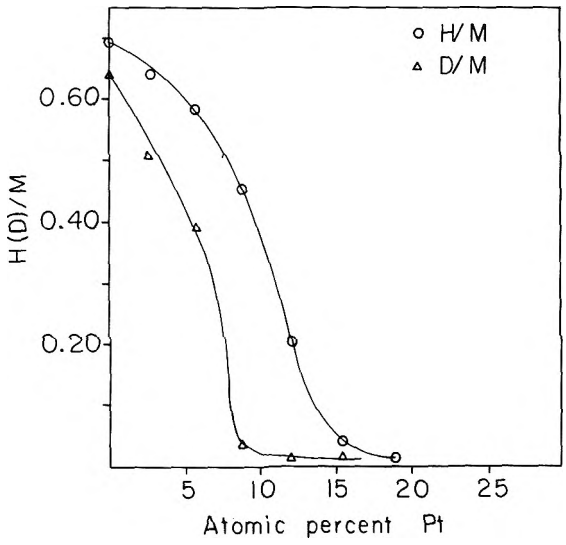

Figure 3. Equilibrium solubilities of deuterium and hydrogen in Pt–Pd alloys at 25°, 1 atm. of D_2 (H_2).

As pointed out earlier,[6] a separation of hydrogen and deuterium based upon pure palladium is not particularly promising in the vicinity of 25° (1 atm.) because of their closely similar solubilities. However, as Sieverts and Danz[13] pointed out many years ago, a separation may be feasible above 80° because the deuterium–palladium system no longer forms a two-phase region above 80° (1 atm.), whereas a second phase may still be formed in the hydrogen–palladium system (1 atm.). (A large increase of solubility accompanies two-phase formation.) This may be predicted from the thermodynamic parameters for pure palladium (Table II). The addition of platinum to palladium lowers the critical temperature for two-phase formation, so that a selective isotopic solubility can exist at room temperature for the alloy of the proper composition. It should be pointed out that in addition to being dependent upon the separate isotopic solubility differences of hydrogen and deuterium (Fig. 3), equilibrium separation factors will be dependent upon additional factors introduced by the simultaneous presence of hydrogen and deuterium in the alloys, *e.g.*, entropy of mixing.

From Table II we see that the heats of absorption of hydrogen are greater than those for deuterium, whereas the change of entropy upon absorption of either hydrogen or deuterium is approximately the same. Both the absolute magnitudes of the heat and entropy of absorption fall with increase of platinum content. The negative free energy change, therefore, becomes progressively smaller as the percentage of platinum increases, because the absolute magnitude of the heat of absorption falls more rapidly than the positive ($-T\Delta S°$) term. Since the negative enthalpy change is considerably lower for deuterium absorption, two-phase formation ceases at a smaller platinum content for absorption of deuterium. This leads to the result that the 8.80% platinum–palladium alloy no longer forms a two-phase region at 1 atm. of deuterium (25°).

Calculation of the Difference of the Heats of Absorption of Hydrogen and Deuterium. It is of interest to inquire as to the origin of the difference in the heats of absorption of hydrogen and deuterium in palladium and these platinum–palladium alloys since this thermodynamic parameter is largely responsible for the observed difference in isotopic solubilities. The difference in the heat of absorption of 1 mole of deuterium and 1 mole of hydrogen in pure palladium is given at temperature T as

$$\Delta H°_{T,f,(D)} - \Delta H°_{T,f,(H)} = \Delta H°_{0,f,(D)} - \Delta H°_{0,f,(H)} + \int_0^T C_{p(D)}\,dT - \int_0^T C_{p(H)}\,dT + \int_0^T C_{p(H_2)}\,dT - \int_0^T C_{p(D_2)}\,dT \quad (3)$$

where all terms refer to 1 mole of hydrogen (deuterium) and $\Delta H°_{T,f,(D)}$ is the heat of formation of the nonstoichiometric β-phase deuteride at temperature T, $\Delta H°_{0,f,(D)}$ is its heat of formation at 0°K., $C_{p(D)}$ is the heat capacity of the same species, and $C_{p(D_2)}$ is the heat capacity of 1 mole of deuterium gas; similar definitions hold for the hydrogen system. The heat capacity of pure palladium cancels.

The fifth and sixth terms on the right-hand side of eq. 3 may be obtained for normal hydrogen and deuterium from the literature[14] and the value, +24.5 cal./mole, includes the rotational contribution of orthohydrogen and paradeuterium to the enthalpy at

(13) A. Sieverts and W. Danz, *Z. physik. Chem.*, **38**, 46 (1937).

(14) H. W. Wooley, R. B. Scott, and F. G. Brickwedde, *J. Res. Natl. Bur. Std.*, **41**, 379 (1948).

0°K. The first and second terms of the right-hand side may be expressed as

$$\Delta H^\circ_{0,f,(D)} - \Delta H^\circ_{0,f,(H)} = \Delta E^\circ_{(H_2 - D_2)} - \Delta E^\circ_{((H)-(D))} \quad (4)$$

where $\Delta E^\circ_{(H_2 - D_2)}$ is the zero-point energy difference between gaseous hydrogen and deuterium. The term $\Delta E^\circ_{((H)-(D))}$ refers to the zero-point energy difference between the β-phase hydride and deuteride. The value of $\Delta E^\circ_{((H)-(D))}$ may be estimated from recent cold neutron scattering experiments of Bergsma and Goedkoop.[15] They find a single rather sharp optical mode, $\nu_H = 13.54 \times 10^{12}$ sec.$^{-1}$, which results from hydrogen vibrations. The Einstein model therefore would be expected to be a reasonably good approximation for the contribution of the hydrogen to the total heat capacity of the β-phase lattice. The value of $\Delta E^\circ_{((H)-(D))}$ is calculated (using $\nu_H = 13.54 \times 10^{12}$ and $\nu_D = \nu_H/\sqrt{2}$) as 567.5 cal./mole of hydrogen and deuterium atoms in $PdH_{0.6}$ ($PdD_{0.6}$) or 1135.0 cal./mole of H_2 (D_2) in $PdH_{0.6}$ ($PdD_{0.6}$). The value of $\Delta E^\circ_{(H_2-D_2)}$ is taken from the literature as 1780 cal./mole.

The temperature dependence of the hydrogen and deuterium contributions to the heat capacities of $PdH_{0.6}$ and $PdD_{0.6}$ (the third and fourth terms on the right-hand side of eq. 3) can either be calculated from the Einstein model $\int_0^{300} C_{v(D)}\,dT - \int_0^{300} C_{v(H)}\,dT = 506.4$ cal./mole of D_2 (H_2), or from graphical integration of Nace and Aston's data,[12] *i.e.*, $\int_0^{300} C_{p(D)}\,dT - \int_0^{300} C_{p(H)}\,dT \cong 420.0$ cal./mole. There is a gap in Nace and Aston's data for the deuterium system (152 to 279°K.) which introduces some uncertainty into the value determined from their data; for this reason and also for consistency with the calculated results for the 2.79 and 5.73% platinum–palladium alloys, the value from the Einstein model will be employed. It is expected that to a good approximation any differences in C_p and C_v will cancel when subtracting values of hydrogen from deuterium; therefore, 506.4 cal./mole will be taken as equal to the third and fourth terms in eq. 3. Substituting these values into eq. 3 and 4, we obtain for the difference in the heats of formation of the β-phase deuteride and hydride from pure palladium and 1 mole of D_2 (H_2) at 300°K.

$$\Delta H^\circ_{300,f,(D)} - \Delta H^\circ_{300,f,(H)} = 1126 \pm 40 \text{ cal./mole}$$

where the error is based upon the error in ν_H[14] and does not include an estimate of the error from employment of the Einstein model.

The result is in reasonably good agreement with the value of 995 cal./mole obtained from Table II. The calculated value refers, however, to the difference in the heats of formation of the β-phase from pure palladium, whereas the heats of absorption in Table II refer to the formation of the β-phase from α-phase. It would not be expected that there would be much difference between these two quantities, *e.g.*, Nace and Aston[12] find a value of +1226 cal./mole for absorption corresponding to the $\alpha \rightarrow \beta$ transition and a value of +1282 cal./mole for absorption by pure palladium to form β-phase. (There is an insignificant change in the calculated value of $\Delta H^\circ_{T,f(D)} - \Delta H^\circ_{T,f,(H)}$ as the temperature changes from 298 (Table II) to 303°K.[12]) The calculated value is approximately half-way between the value obtained from this work (Table II) and the calorimetric value of Nace and Aston.[12]

The progressive decrease in the value of $\Delta H^\circ_{300,f,(D)} - \Delta H^\circ_{300,f(H)}$ with increase of platinum content (Table II) is too large to be attributed to experimental error. Using the experimental values for $\Delta H^\circ_{300,f,(D)} - \Delta H^\circ_{300,f,(H)}$ for the 2.79 and 5.73% platinum–palladium alloys, 700 and 634 cal./mole, respectively, a value of ν_H can be calculated using a similar approach as was employed for pure palladium. The calculated frequencies are $\nu_H = 19.1 \times 10^{12}$ sec.$^{-1}$ (2.79%) and $\nu_H = 19.8 \times 10^{12}$ sec.$^{-1}$ (5.73%). The force constant increases with platinum content and the mean displacement of the hydrogen from its equilibrium position decreases with increase of platinum content. It may be pointed out that Bergsma and Goedkoop[15] found excellent agreement between the root mean square displacement of hydrogen in $PdH_{0.6}$ calculated from the Einstein frequency and that observed independently from thermal neutron scattering experiments.

Lattice Constants. X-Ray diffraction patterns have been obtained for a number of platinum–palladium alloys of varying deuterium and hydrogen contents. Upon absorption of hydrogen or deuterium the lattice remains f.c.c. with a slight expansion in the α-phase and a considerably larger expansion in the β-phase. Above the β_{min} composition the lattice constant of the alloys appears to increase in direct proportion to the hydrogen (deuterium) content as for pure palladium.[5]

From earlier work[4] on the hydrogen–platinum–palladium system it was not apparent from the shape of the isotherm of the 12.03% platinum alloy whether a two-phase region was formed (25°, 1 atm.). In Fig. 4 we have plotted the lattice constants for $\alpha_{H(max)}$ and $\beta_{H(min)}$ as a function of platinum content. Examination of Fig. 4 reveals that two phases are formed in the 12.03% platinum alloy at 25° and that the two-phase

(15) J. Bergsma and J. A. Goedkoop, *Physica*, **26**, 744 (1960).

Table III: Lattice Constants of the H–Pt–Pd and D–Pt–Pd Systems (25°)

Alloy, % Pt	Pure alloy, a_0 (Å.)	$\alpha_{H(max)}$	$\alpha_{D(max)}$	$\beta_{H(min)}$	$\beta_{D(min)}$
0	3.889 ± 0.001	3.895 ± 0.001	3.893 ± 0.001	4.025 ± 0.001	4.027 ± 0.001
2.79	3.890	3.895	3.894	4.013	4.020
5.73	3.891	3.896	3.895	4.010	4.008
8.80	3.892	3.905 ± 0.005	[a]	3.970 ± 0.005	[a]
12.03	3.893	3.900	[a]	3.960	[a]

[a] Two phases are not formed at 25°, 1 atm.

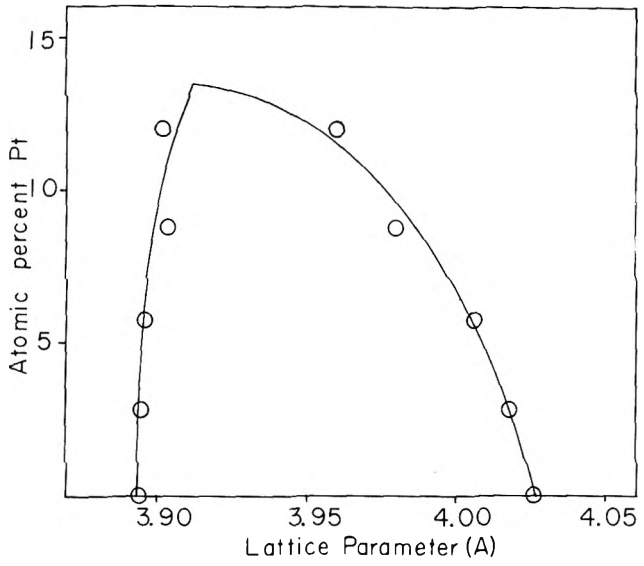

Figure 4. Lattice parameters for $\alpha_{H(max)}$ and $\beta_{H(min)}$ as a function of Pt content at room temperature.

region persists up to approximately 14% platinum. These parameters are shown in Table III in comparison with values for the deuterium–platinum–palladium system.

There have been many determinations of the lattice constants of the hydrogen–palladium system.[5] Our values for hydrogen–palladium are in excellent agreement with one of the most recent studies.[9] Ubbelohde[16] has measured the parameters of the deuterium–palladium system (20°). Our results differ slightly from Ubbelohde's which he has presented as expansions relative to pure palladium: $\alpha_D = 0.0028$ (ref. 15), $\alpha_D = 0.004$ (Table III); and $\beta_D = 0.1327$ (ref. 15), $\beta_D = 0.138$ (Table III).

The lattice expansion per deuterium atom is larger than per hydrogen atom, *e.g.*, the lattice constants of β_{min} for pure palladium are 4.025 (H/Pd = 0.58) and 4.027 (D/Pd = 0.56). The greater resistivity increase caused by deuterium as compared to hydrogen may be partly due to this greater relative lattice expansion. Using the constants in Table III for pure palladium, d ln V/dm = 0.18 for the hydride and 0.19 for the deuteride where V is the volume and m is the concentration of hydrogen (deuterium) atoms. Bridgman[17] has found that the resistance of palladium increased with volume, *i.e.*, d ln R/d ln V = 4.0 at room temperature. If we combine these two expressions we obtain d ln R/dm = (d ln R)/d ln V × (d ln V)/dm and for palladium we can calculate d ln R/dm = 0.72 for the hydride and 0.76 for the deuteride. This simplified treatment shows that the lattice expansion is an important factor in the observed difference in the resistivity of the β-phase hydrides and deuterides.

Determination of Phase Boundaries by X-Ray Diffraction. Phase boundaries have been located using X-ray diffraction patterns. The low content phase boundary, α_{max}, has been determined as the content corresponding to the point of appearance of the second phase. Alternatively, the early change of slope in the R/R_0 *vs.* H/M relationship corresponds to the composition of α_{max}. Both of these approaches yield values close to those estimated from the isotherms. Table IV shows the results and it may be noted that α_{max} is approximately independent of the percentage of platinum, although as for the β-phase the content of α_{max} is slightly smaller for the deuteride.

The β-phase boundary, β_{min}, was determined by two methods. The first method was to estimate the content at which the second phase (α) disappeared. The second approach was to obtain lattice constants at compositions greater than β_{min} and since these constants are a linear function of content, they may be extrapolated against content to the lattice constant characteristic of β_{min}. The second, more precise approach, was employed for the 2.73% platinum alloy and gave results in good agreement with the first method (Table IV).

Although values for β_{min} (25°) have often been em-

(16) A. R. Ubbelohde, *Proc. Roy. Soc.* (London), **A159**, 306 (1937).
(17) P. W. Bridgman, *Proc. Am. Acad. Sci.*, **79**, 125 (1951).

Table IV: Phase Boundaries of the H–Pt–Pd and D–Pt–Pd Systems (1 atm., 25°)

Alloy	$\alpha_{H(max)}$	$\alpha_{D(max)}$	$\beta_{H(min)}$	$\beta_{D(min)}$
0	0.030 ± 0.005	0.015 ± 0.005	0.58 ± 0.02	0.56 ± 0.02
2.79	0.020	0.015	0.51	0.46
5.73	0.02	0.015	0.45 ± 0.05	0.35 ± 0.05
8.80	0.03	[a]	0.35	[a]
12.03	0.02	[a]	0.20	[a]

[a] Two phases not formed (25°, 1 atm.).

ployed for the hydrogen–palladium system, there was considerable disagreement as to the proper value in 1948.[5] There appear to have been no X-ray determinations of this value since before 1948. The value determined here agrees with that employed by von Stackelberg[18] and agrees reasonably well with that estimated from absorption isotherms.[5] The corresponding value for the deuterium system has not been previously determined by X-ray diffraction.

Examination of the absorption isotherms in Fig. 2 and those of ref. 4 indicates that the β-phase boundaries established by X-ray diffraction and by estimation from the absorption isotherms are comparable for *all systems except the H–Pt (12.03)–Pd, D–Pt (2.79)–*Pd, and D–Pt (5.73)–Pd systems. Jost[19] has shown that diffusion of deuterium in palladium is slower than hydrogen. Since the addition of platinum would be expected also to reduce the rate of diffusion it is suggested that the absorption isotherms for deuterium absorption by the 2.79 and 5.73% platinum alloys are in error near the β_{min}-phase boundary because of slow diffusion within the specimen.

Acknowledgments. Support for this research by U.S.A.E.C. Contract AT(30-1)-3000 is gratefully acknowledged.

(18) M. von Stackelberg and H. Bischoff, *Z. Elektrochem.*, **59**, 467 (1955).

(19) W. Jost, "Diffusion," Academic Press, New York, N. Y., 1952.

The Standard Entropies of the Aqueous Lithium and Fluoride Ions and the Heat of Solution of Lithium Fluoride[1]

by Clark C. Stephenson,

Department of Chemistry, Massachusetts Institute of Technology, Cambridge 39, Massachusetts

Harry P. Hopkins, and Claus A. Wulff

Department of Chemistry, Carnegie Institute of Technology, Pittsburgh 13, Pennsylvania
(Received December 20, 1963)

The literature contains two discordant values, 4.7 ± 1.0 and 2.5 ± 0.3 cal./mole °K., for the standard entropy of the aqueous lithium ion, based on the solution thermochemistry of Li_2CO_3 and LiOH, respectively. Confirmation of the latter value would determine the standard entropy of the aqueous hydroxide ion and permit a choice between the two values reported for the heat of ionization of water. Reported herein are a calculation of the standard entropy of the aqueous lithium ion, from literature data for $LiCl \cdot H_2O$, as 2.5 ± 0.3 cal./mole °K., and a value of 3.0 ± 0.4 cal./mole °K. based upon a calorimetrically measured heat of solution of LiF: $\Delta H°_{298} = 1070 \pm 50$ cal./mole.

Introduction

The standard entropy of the aqueous lithium ion at 25° given by Latimer, Pitzer, and Smith[2] is 4.7 ± 1.0 cal./mole °K., and is derived from a study of the reaction $Li_2CO_3(s) = 2Li^+(aq) + CO_3^{-2}(aq)$. The value, 3.4 cal./mole °K., is tabulated in Circular 500, National Bureau of Standards[3]; however, it is difficult to ascertain how this value was calculated. Johnston and Bauer[4] find 2.5 ± 0.3 cal./mole °K. for the entropy of the aqueous lithium ion from a study of the reaction $LiOH \cdot H_2O(s) = Li^+(aq) + OH^-(aq) + H_2O$. An independent confirmation of the result obtained by Johnston and Bauer is of considerable interest because the calculations can then be reversed to establish the standard entropies of the aqueous carbonate and hydroxide ions. The entropy of the hydroxide ion is based on thermodynamic data for the equation $H_2O(aq) = H^+(aq) + OH^-(aq)$; however, two different values for the heat of ionization of water are frequently quoted. One of these, 13,510 cal./mole,[5] leads to the value −2.0 cal./mole °K. for the standard entropy of the hydroxide ion, whereas the other, 13,360 cal./mole,[6] gives −2.5 cal./mole °K. The result given by Johnston and Bauer for the lithium ion is based on the latter value for the hydroxide ion.

$S°_{Li^+(aq)}$ from $LiCl$–$LiCl \cdot H_2O$. A recent value[7] of the entropy of LiCl(s) at 25°, 14.17 ± 0.02 cal./mole °K., in conjunction with data concerning $LiCl \cdot H_2O(s)$, can be utilized to obtain a value for the entropy of $Li^+(aq)$. Solubility measurements[8] of the monohydrate are in good agreement at 19.95 ± 0.05 at 25°. The tabulations of Robinson and Stokes[9] give the mean activity coefficient and the activity of water in the saturated solution as 62.1 and 0.1105, respectively. For the change in state

$$LiCl \cdot H_2O(s) = Li^+(aq) + Cl^-(aq) + H_2O(aq) \quad (1)$$

(1) Presented at the 146th National Meeting of the American Chemical Society, Denver, Colo., January, 1964.

(2) W. M. Latimer, K. S. Pitzer, and W. V. Smith, *J. Am. Chem. Soc.*, **60**, 1829 (1938).

(3) National Bureau of Standards Circular 500, U. S. Govt. Printing Office, Washington 25, D. C., 1952.

(4) H. L. Johnston and T. W. Bauer, *J. Am. Chem. Soc.*, **73**, 1119 (1951).

(5) H. S. Harned and R. A. Robinson, *Trans. Faraday Soc.*, **36**, 973 (1940).

(6) K. S. Pitzer, *J. Am. Chem. Soc.*, **59**, 2365 (1937).

(7) D. A. Shirley, *ibid.*, **82**, 3841 (1960).

(8) M. P. Applebey, F. H. Crawford, and K. Gordon, *J. Chem. Soc.*, 1665 (1934).

(9) R. A. Robinson and R. H. Stokes, "Electrolyte Solutions," Butterworth and Co., Ltd., London, 1959.

the standard free energy change at 25° is $\Delta G^\circ_{298} = -1364 \log (62.1 \times 19.95)^2(0.1105) = -7130$ cal.

Dissociation pressures for the monohydrate[10-12] can be represented by the relation $\Delta G^\circ = 14{,}520 - 34.2T$, and $\Delta G^\circ_{298} = 4320$ cal./mole for the change in state

$$LiCl \cdot H_2O(s) = LiCl(s) + H_2O(g) \qquad (2)$$

The vapor pressure of water at 25° is 23.75 mm., leading to a value of $\Delta G^\circ_{298} = 2055$ cal./mole for

$$H_2O(aq) = H_2O(g) \qquad (3)$$

The standard free energy for the solution of lithium chloride, *i.e.*

$$LiCl(s) = Li^+(aq) + Cl^-(aq) \qquad (4)$$

can be computed from the above data as $\Delta G^\circ_{298} = -7130 - 4320 + 2055 = -9395$ cal./mole.

According to Lange and Dürr,[13] the heat of solution, at infinite dilution, of anhydrous LiCl is −8850 cal./mole. Hence, for eq. 4, $\Delta S^\circ_{298} = (-8850 + 9395)/298 = 1.8$ cal./mole °K.

Kelley[14] tabulates the entropy of $Cl^-(aq)$ as 13.5 ± 0.1 cal./mole °K., that value being the mean of three experimental determinations in good agreement. The entropy of $Li^+(aq)$ can now be computed as $S^\circ_{Li^+(aq)} = 14.17 - 13.5 + 1.8 = 2.5 \pm 0.3$ cal./mole °K., in excellent accord with the value of Johnston and Bauer.

$S^\circ_{F^-(aq)}$ from NaF. The entropy of the lithium ion may also be obtained from data concerning lithium fluoride, but first a more reliable value for the standard entropy of the aqueous fluoride ion is required. The value of −2.3 ± 2 cal./mole °K. given by Latimer, Pitzer, and Smith[2] and quoted in Circular 500[3] may be superseded by that derived in the following manner from the unusually reliable data concerning NaF. The entropy of NaF(s) at 25° is 12.26 ± 0.07 cal./mole °K.[15] From the activity coefficient of sodium fluoride in its saturated solution,[9] 0.575, and the solubility,[16] 0.983 *m*, the standard free energy of solution is $\Delta G^\circ_{298} = -1364 \log (0.575 \times 0.983)^2 = 675$ cal./mole. The standard enthalpy of solution is *213 ± 10* cal./mole[17] and $\Delta S^\circ_{298} = (210 - 675)/298.15 = -1.56$ cal./mole °K. The standard entropy of the aqueous fluoride ion at 25° is then 12.26 − 14.3 − 1.56 = −3.6 ± 0.2 cal./mole °K. A value in accord with −3.6 can be derived from an appropriate choice of thermodynamic data concerning KF and $KF \cdot 2H_2O$, but the limits of error are larger.

Heat of Solution of LiF. The heat of solution of lithium fluoride was determined calorimetrically in an apparatus that has been described previously.[18] All samples, Fisher Certified reagent LiF, were dissolved into 950 ml. of distilled water at 25.0 ± 0.1° and gave satisfactory rates of dissolution for concentrations between 0.02 and 0.04 *m*.

A least-squares analysis of the data as a function of concentration leads to an extrapolated value of 1070 ± 50 cal./mole for the standard enthalpy of solution of lithium fluoride. The observed concentration dependence is in good accord with the heats of dilution obtained by Lange and Leighton.[19] Measurements of the heats of solution of sodium fluoride and lithium fluoride in hydrochloric acid using a simpler apparatus,[20] and the assumption that their heats of dilution are equal, gave a result of 1100 ± 100 cal./mole for the standard enthalpy of solution of LiF.

A recent paper[21] reports a result for the heat of solution of LiF(s) at 21.5°, to give $LiF \cdot 3800(aq)$, as 1.25 ± 0.02 kcal. The heat of dilution[19] and an appropriate choice for the partial molar heat capacity of $Li^+(aq) + F^-(aq)$ [*i.e.*, −13 cal./mole °K.[22]] can be utilized to convert the above datum to $\Delta H^\circ_{298} = 1110 \pm 50$ cal./mole

$S^\circ_{Li^+(aq)}$ from LiF(s). The solubility of lithium fluoride, 0.0513 *m* at 25°,[16,23] is sufficiently low that its activity coefficient in the saturated solution may be estimated without serious error. Hence, $\Delta G^\circ_{298} = -1364 \log (0.82 \times 0.0513)^2 = 3784$ cal./mole. From the above results $\Delta S^\circ_{298} = (1070 - 3784)/298.15 = -9.1$ cal./mole °K. for the equation

$$LiF(s) = Li^+(aq) + F^-(aq) \qquad (5)$$

The entropy of the aqueous lithium ion can be calculated from the preceding results and the entropy of LiF(s), 8.52 cal./mole °K.,[24] as 8.52 + 3.6 − 9.1 = 3.0 ± 0.4 cal./mole °K.

(10) A. Lannung, *Z. physik. Chem.*, **A170**, 134 (1934).

(11) G. F. Huttig and F. Reuscher, *Z. anorg. allgem. Chem.*, **137**, 155 (1924).

(12) C. Slonim and G. F. Huttig, *ibid.*, **181**, 55 (1929).

(13) E. Lange and F. Dürr, *Z. physik. Chem.*, **121**, 361 (1926).

(14) K. K. Kelley and E. G. King, "Entropies of the Elements and Inorganic Compounds," U. S. Bureau of Mines, Bulletin 592, U. S. Govt. Printing Office, Washington, D. C., 1961.

(15) E. G. King, *J. Am. Chem. Soc.*, **79**, 2056 (1957).

(16) J. H. Payne, *ibid.*, **59**, 947 (1937).

(17) L. G. Hepler, W. L. Jolly, and W. M. Latimer, *ibid.*, **75**, 2809 (1953).

(18) C. Wu, M. M. Birky, and L. G. Hepler, *J. Phys. Chem.*, **67**, 1202 (1963).

(19) E. Lange and A. L. Robinson, *Chem. Rev.*, **9**, 89 (1931).

(20) C. A. Wulff, Ph.D. Thesis, Massachusetts Institute of Technology, 1962.

(21) V. P. Kolesov and S. M. Skuratov, *Russ. J. Inorg. Chem.*, **6**, 889 (1961).

(22) C. M. Criss, Ph.D. Thesis, Purdue University, 1961.

(23) M. A. Klochko and K. T. Batova, *Zh. Neorgan. Khim.*, **5**, 2325 (1960).

Table I: The Entropy of the Aqueous Lithium and Fluoride Ions[a]

		$S^\circ_{Li^+(aq)}$
$Li_2CO_3(s)$	$= 2Li^+ + CO_3^{-2}$	4.7 ± 1.0
$LiOH(s)$	$= Li^+ + OH^-$	2.5 ± 0.3
$LiCl(s)$	$= Li^+ + Cl^-$	2.5 ± 0.3
$LiF(s)$	$= Li^+ + F^-$	3.0 ± 0.4
		$S^\circ_{F^-(aq)}$
$NaF(s)$	$= Na^+ + F^-$	-3.6 ± 0.2

[a] Units: cal./mole °K.

The values for the entropy of the aqueous lithium ion are summarized in Table I. The obvious discrepancy in the value from the data concerning lithium carbonate may be attributed in part to inaccuracies in the solubility products used in the calculations, and in part to the correction necessary for hydrolysis in the estimation of ΔH°. The good agreement shown by the other three values substantiates the choice of -2.5 cal./mole °K. for the standard entropy of the hydroxide ion, and therefore, the lower of the two values quoted for the heat of ionization of water is preferred.

Acknowledgment. The authors acknowledge their debt to Professor L. G. Hepler, of the Carnegie Institute of Technology, for the use of his laboratory and its facilities, and to Dr. C. Wu for her assistance with the measurements. The partial financial support of the National Science Foundation is gratefully acknowledged.

(24) K. Clusius, J. Goldman, and A. Perlick, *Z. Naturforsch.*, **4a**, 424 (1949).

The Radiation-Induced Chain Reaction between Nitrous Oxide and Hydrogen in Aqueous Solutions[1]

by C. H. Cheek and J. W. Swinnerton

U. S. Naval Research Laboratory, Washington 25, D. C. *(Received December 21, 1963)*

The radiation chemistry of solutions containing mixtures of nitrous oxide and hydrogen has been studied. Nitrous oxide oxidizes hydrogen by a radiation-induced chain reaction which proceeds moderately in neutral solution and quite efficiently in strongly alkaline solution. Oxygen inhibits the chain reaction in neutral solution, but has no effect in strongly alkaline solution. The lack of a dose-rate dependence is attributed to chain-terminating reactions with impurities which predominate over radical–radical combination. Mechanisms are proposed to account for the observations. The results account in part for an alternate interpretation of the sigmoid increase in $G(N_2)$ at high pH in irradiated nitrous oxide solutions.[2]

Introduction

Recent reports on the yields of the radiolysis products of water in strongly alkaline solution are in disagreement. In an interpretation of the radiation chemistry of nitrous oxide solutions, Dainton and Watt[2] have proposed that $G_{e_{aq}^-}$ and G_{OH} increase sigmoidally by about one unit in the range above pH 11, whereas a re-

(1) Presented in part at the 144th National Meeting of the American Chemical Society, Los Angeles, Calif., April, 1963.

(2) F. S. Dainton and W. S. Watt, *Nature*, **195**, 1294 (1962).

cent kinetic analysis of the radiation chemistry of alkaline hypobromite solutions[3] purports to show that the yields of the radiolysis products of water are essentially constant in pH range 4 to 14.

The radiation chemistry of aqueous nitrous oxide solutions is being studied at this laboratory in an effort to resolve the discrepancy. Exploratory experiments revealed that, in the absence of gas space, $G(H_2) = 0$ in γ-irradiated nitrous oxide solutions at pH above 3. Dainton and co-workers,[2,4] however, reported positive values for $G(H_2)$ throughout the pH range. Their positive values may be due to escape of radiolytic hydrogen into the gas space above their solutions. The disagreement afforded a clue which led to the work described here. In order to obtain additional information, we have studied the radiation chemistry of solutions containing mixtures of nitrous oxide and hydrogen.

Experimental

Reagent grade chemicals were used without further purification. Solutions of the nongaseous constituents in triply distilled water were saturated with the desired gaseous mixture and transferred to the irradiation cells in a manner such that no gas space remained above the solutions. The apparatus and procedure for sample preparation have been described.[5] The relative amounts of gases in the mixture were controlled by the use of flow meters, and mixing occurred at the entrance to the purging vessel.

The Co^{60} γ-ray source was calibrated by ferrous sulfate dosimetry. Dissolved gases were determined by a gas chromatographic method which has been described.[6]

Results and Discussion

Figure 1 shows the chain disappearance of hydrogen with dose in a typical experiment at pH 13.5. Figure 2 presents the variation of $G(-H_2)$ and $G(N_2)$ with pH for solutions initially containing ~0.5 mM H_2 and ~6 mM N_2O. The results show that no chain reaction occurs in strongly acid solution, a moderate chain reaction occurs in neutral solution, and a more efficient, strongly pH-dependent chain reaction occurs in the range above pH 12. $G(N_2)$ parallels $G(-H_2)$ in the chain reactions, and no oxygen is formed. Hydrogen peroxide quickly reaches a steady-state concentration ≤ 2 μM in neutral solution and at pH > 12, but rises to higher steady-state concentrations at 10 < pH < 12, with a maximum value of 40 μM at pH 10.5.

Variation of the dose rate does not affect the yields in neutral or alkaline solutions.

A trace of added oxygen causes a brief induction period before the chain reaction begins in neutral solution, but appears to have no effect on the chain reaction in strongly alkaline solution.

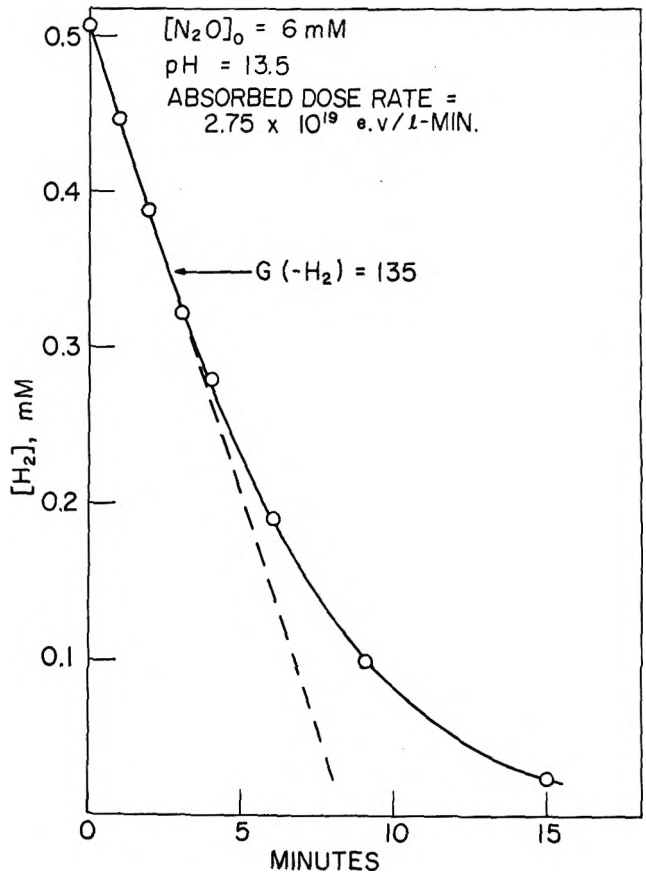

Figure 1. Chain disappearance of hydrogen in strongly alkaline solution.

The following mechanism is proposed to account for the results in neutral solution.

$$H_2O \rightsquigarrow e_{aq}^-, H^+, OH, H_2, H_2O_2 \quad (0)$$

$$N_2O + e_{aq}^- \longrightarrow N_2 + OH + OH^- \quad (1)$$

$$H_2 + OH \longrightarrow H + H_2O \quad (2)$$

$$N_2O + H \longrightarrow N_2 + OH \quad (3)$$

$$H_2O_2 + H \longrightarrow H_2O + OH \quad (4)$$

$$H + M \longrightarrow \text{term} \quad (5)$$

Essentially all the e_{aq}^- and OH are assumed to disappear by reactions 1 and 2 under the experimental condi-

(3) C. H. Cheek and V. J. Linnenbom, *J. Phys. Chem.*, **67**, 1856 (1963).

(4) F. S. Dainton and D. B. Peterson, *Proc. Roy. Soc.* (London), **267**, 443 (1962).

(5) C. H. Cheek, V. J. Linnenbom, and J. W. Swinnerton, *Radiation Res.*, **19**, 636 (1963).

(6) J. W. Swinnerton, V. J. Linnenbom, and C. H. Cheek, *Anal. Chem.*, **34**, 483 (1962); *ibid.*, **34**, 1509 (1962).

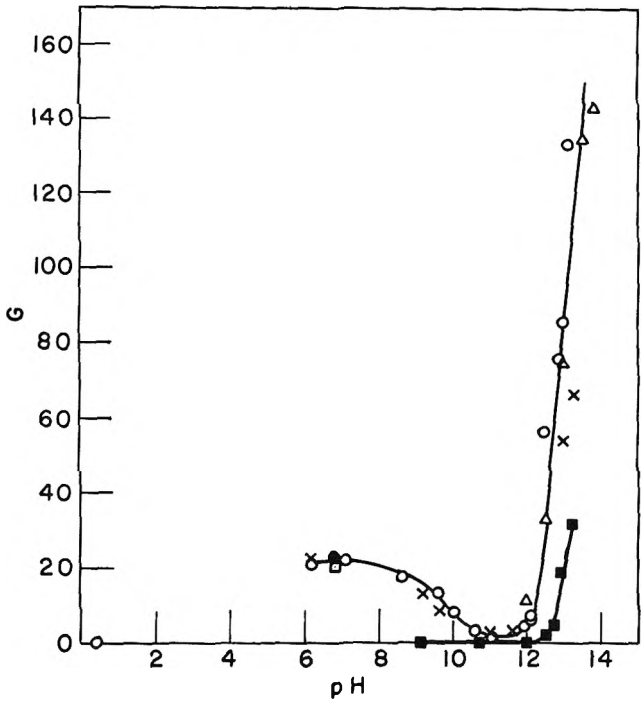

Figure 2. Effects of pH, dose rate, and carbonate on $G(-H_2)$ and $G(N_2)$. Initially ~0.5 mM H_2 and ~6 mM N_2O. Dose rate, 3.11×10^{20} e.v./l. min.: ×, $G(N_2)$; ○, $G(-H_2)$; ■, $G(-H_2)$ with 0.01 M carbonate present. Dose rate, 2.75×10^{19} e.v./l. min.: △, $G(-H_2)$. Dose rate, 1.75×10^{21} e.v./l. min.: ●, $G(N_2)$; □, $G(-H_2)$.

tions. Reactions 2 and 3 comprise the chain oxidation of hydrogen by nitrous oxide. In a similar manner, hydrogen peroxide is reduced to water by reactions 2 and 4. The absence of a dose-rate effect shows that chain termination occurs principally by processes other than radical–radical combination. The reaction

$$H_2O_2 + OH \longrightarrow HO_2 + H_2O \qquad (6)$$

leads to chain termination, but it occurs much too infrequently to account for the chain length of ~4, since $k_2 = k_6$[7] and $(H_2) >> (H_2O_2)$. No additional decomposition products have been found, and it is assumed that chain termination is effected by impurities. The principal chain-termination process is represented schematically by eq. 5.

The results in strongly alkaline solution are accountable by the following sequence.

$$H_2O \xrightarrow{OH^-\ \sim\sim} e_{aq}^-,\ OH,\ H_2,\ HO_2^- \qquad (0')$$

$$N_2O + e_{aq}^- \longrightarrow N_2 + OH + OH^- \qquad (1)$$

$$H_2 + OH \longrightarrow H + H_2O \qquad (2)$$

$$H + OH^- \longrightarrow e_{aq}^- \qquad (7)$$

$$e_{aq}^- + HO_2^- \longrightarrow 2OH^- + OH \qquad (8)$$

$$e_{aq}^- + M \longrightarrow \text{term} \qquad (9)$$

Reactions 1, 2, and 7 constitute a chain sequence in which the oxidation of hydrogen by nitrous oxide is strongly augmented as the pH becomes high enough for reaction 7 to compete effectively for H atoms. Chain termination is considered to occur principally by the action of impurities, as discussed below.

The observed decrease in reaction yield in the pH range 8 to 12 is not expected on the basis of the mechanisms proposed above, and the effect is attributed to reaction of reducing radicals with bicarbonate or carbonate introduced as an impurity in the sodium hydroxide. The lower curve in Fig. 2 shows that 0.01 M carbonate completely suppresses the chain reaction up to pH 12. The pH dependence of the carbonate effect suggests that the impurity competes effectively with reaction 3 for hydrogen atoms, but not with reaction 7 above pH 12. It appears that bicarbonate (pK = 10.2) is much more effective than carbonate. This is in agreement with the report[8] that the absorption spectrum of the hydrated electron has been observed in carbonate solution, but is suppressed completely in bicarbonate solution.

There can be little doubt that impurities played a major role in chain termination in neutral and alkaline solutions. Experiments with carbonate-free solutions are clearly desirable and are being pursued. A value of $G(N_2)$ = 10 was obtained at pH 11.2 in a very recent experiment in which the carbonate concentration was ~5 μM. This suggests that the depression in reaction yields at pH 8 to 12 may be eliminated by the use of carbonate-free solutions and provides further credence to the assignment of chain termination to bicarbonate.

It is noteworthy that the maximum steady-state concentration of peroxide is obtained in the pH range of maximum suppression of the chain reaction, as is to be expected if the chain-terminating reaction also suppresses the removal of peroxide by reaction 8.

The increased efficiency of the chain reaction at high pH is attributable to the large difference between the rate constants of reactions 1 and 3. Dainton and Peterson[4] estimated $k_1 \sim 10^8$–10^9 M^{-1} sec.$^{-1}$, and Czapski and Jortner[9] reported $k_3 \sim 10^3$–10^4 M^{-1} sec.$^{-1}$.

The occurrence of reaction 7 has been demonstrated unequivocally.[10]

Inhibition of the chain reaction by oxygen in neutral

(7) A. O. Allen, "The Radiation Chemistry of Water and Aqueous Solutions," D. Van Nostrand Co., New York, N. Y., 1961, p. 86.

(8) E. J. Hart and J. W. Boag, *J. Am. Chem. Soc.*, 84, 4090 (1962).

(9) G. Czapski and J. Jortner, *Nature*, 188, 50 (1960).

(10) J. Jortner and J. Rabani, *J. Am. Chem. Soc.*, 83, 4868 (1961).

solution is attributed to competition of reaction 10 with reaction 3.

$$H + O_2 \longrightarrow HO_2 \qquad (10)$$

Taking[11] $k_{10} = 1.2 \times 10^{10}\ M^{-1}$ sec.$^{-1}$, one obtains $k_{10}/k_3 \geq 10^6$, which indicates that as little as $10^{-6}\ M$ oxygen will suppress reaction 3 completely. The chain reaction commences as the oxygen is depleted. Small amounts of oxygen, however, do not compete effectively with the very efficient chain sequence in strongly alkaline solution. These observations suggest that oxygen produced in the radiolysis of N_2O solutions prevents the net reaction between N_2O and H_2 in neutral solution, but permits G_{H_2} to contribute to $G(N_2)$ in strongly alkaline solution, thereby accounting in part for the observed increase in $G(N_2)$ at high pH. This point and additional details will be considered in a publication on the radiation chemistry of N_2O solutions.

Acknowledgment. The authors are grateful to E. O. Davis and G. R. Gauvin for technical assistance.

(11) A. R. Anderson and E. J. Hart, *J. Phys. Chem.*, **66**, 70 (1962).

Adsorption from Nonelectrolyte Solutions on Porous 96% Silica (Vycor) Glass

by Robert L. Cleland

Department of Chemistry, Dartmouth College, Hanover, New Hampshire *(Received December 21, 1963)*

Adsorption studies on porous (Vycor) glass for the binary liquid systems: (I) $C_6H_6(1)$–CCl_4, (II) $C_6H_6(1)$–C_6H_{12}, and (III) $CCl_4(1)$–C_6H_{12} showed that component 1 was preferentially adsorbed at all compositions. The difference, Δw, between the potential energies of adsorption of a given component pair estimated from a linear plot of a Langmuir isotherm is too large when the surface shows normal heterogeneity of site–adsorbate interaction energy. Estimated surface compositions indicate that Δw is smaller on a porous glass surface than on silica gels of larger specific surface area. The difference is ascribable to larger adsorption potentials in the smaller pores of silica gels and to partial thermal dehydration of the porous glass surface.

Introduction

The supposition that transport properties of binary liquids in porous 96% silica (Vycor) glass[1] (hereafter referred to as porous glass) were affected by selective adsorption led to an experimental study of adsorption from binary solutions of interest. The data are compared with similar results for adsorption on silica gels having smaller pores.

Reduction in pore size in silica gels has been shown[2] to cause an increase of total adsorption of benzene and *n*-hexane vapors at low surface coverage. Similar effects occurred when the gel surface was dehydrated by heating.[2] The effect of reduction in pore size was attributed to an increased adsorption potential in smaller pores. The dehydration effect was explained by Kiselev as due to decreased interaction of the π-electron system of benzene with surface hydroxyl groups as the latter were removed. An increase in the adsorption of benzene per unit surface from benzene–*n*-heptane solutions also occurred with decreasing pore size in silica gels.[3] This effect was ascribed to a greater increase

(1) R. L. Cleland, "Binary Liquid Flow in Porous 96% Silica (Vycor) Glass," to be published.

(2) A. V. Kiselev, *Proc. Intern. Congr. Surface Activity, 2nd, London*, **2**, 179 (1957).

in the adsorption potential of benzene than of *n*-heptane in smaller pores.

Adsorption from nearly ideal nonelectrolyte solutions has been treated[4-6] in terms of a Langmuir model, which assumes constancy of site–adsorbate interaction and ideal behavior in the region of adsorption. The applicability of the model to adsorbents with polar surfaces is of doubtful validity.[7] A discussion of this question is possible on the basis of the present work.

Experimental

Reagents. Porous glass was kindly supplied by the Corning Glass Works as a 200-mesh powder. Benzene and carbon tetrachloride were Mallinckrodt reagent grade materials. Cyclohexane was Eastman Spectro grade. All reagents were dried over silica gel for several days before use.

Procedure. Before adsorption experiments the porous glass powder was heated at 500° for several hours in the atmosphere to remove adsorbed organic matter. The hot adsorbent was cooled in a desiccator containing silica gel. Samples of adsorbent were weighed into 60 ml. glass-stoppered bottles. Aliquots of initial solutions prepared by mixing pipetted volumes of reagents were added to the adsorbent. Liquid and solid reagents were thoroughly mixed with a glass rod. The system was allowed to equilibrate at room temperature (25–30°) for at least 24 hr. Preliminary experiments showed that no change occurred in the bulk liquid composition at longer times. Before samples were withdrawn for analysis, the mixing operation was repeated. The adsorbent was permitted to settle, a portion of the supernatant liquid was filtered, and the filtrate was compared refractometrically with the original solution in a Zeiss laboratory interference refractometer. Calibration of this instrument had been carried out over the entire composition range by direct comparison of solutions of known difference of volume fraction. Refractometric analyses were verified for some benzene–carbon tetrachloride experiments by density of the filtered liquid.

The heating procedure described above was varied in a study of the effect of dehydration on selective adsorption. Samples of porous glass were heated for periods of at least 12 hr. at various temperatures to 1000°. The loss in weight was determined as a function of temperature. Adsorption measurements on heated samples were performed as described above, except that adsorption systems were kept in a thermostat at 25°.

Results and Discussion

The quantities determined directly in the adsorption experiments were φ_1' and φ_1, the volume fraction of component 1 in the initial mixture added to the adsorbent and in the equilibrium liquid mixture, respectively, V' the volume of liquid mixture added to the adsorbent, and m the weight of the adsorbent. In each binary system studied a single component was preferentially adsorbed at all concentrations. The preferred component in each system was designated component 1, so that the quantity $\Delta\phi = \varphi_1' - \varphi_1$ was always positive.

The values of $\Delta\varphi$ were converted to $\Delta x = x_1' - x_1$, where x_1' and x_1 are the mole fractions of component 1 in the original mixture and the equilibrium liquid phase, respectively. The "apparent adsorption" on a mole basis may be defined by $n_0\Delta x/m$, where n_0 is the total number of moles of solution added initially to m grams of adsorbent; the symbol Ω of Siskova and Erdös[6] will be used for $n_0\Delta x/m$. Ostwald and de Izaguirre[8] showed that Ω could be written

$$\Omega = n_1^s x_2 - n_2^s x_1 = n^s(x_1^s - x_1) \qquad (1)$$

$$x_1^s = n_1^s/n^s$$

where, in the notation of Kipling and Tester,[9] n_1^s and n_2^s represent the number of moles of components 1 and 2 in the adsorbed surface layer per gram of adsorbent, and $n^s = n_1^s + n_2^s$ the total moles adsorbed per gram of adsorbent. The values of Ω obtained on powdered porous glass are plotted in Fig. 1 as a function of x_1 for the binary systems: (I) benzene(1)–carbon tetrachloride, (II) benzene(1)–cyclohexane, and (III) carbon tetrachloride(1)–cyclohexane, where (1) indicates component 1 for each system.

We may compare our results with data for adsorption from these binary systems on silica gel, which should have a surface chemically similar to that of porous glass for samples of identical thermal history. A suitable basis for comparison of adsorbents of different specific surface is the surface excess $\Gamma_1^{(N)}$ of Guggenheim and Adam,[10] which they defined by the relation

$$\Gamma_1^{(N)} = \Omega/S \qquad (2)$$

where S is the specific surface area of the adsorbent. Elimination of Ω from (2) by use of the second equality of (1) gives eq. 3.

(3) A. V. Kiselev and Y. A. El'tekov, *Dokl. Akad. Nauk SSSR*, **100**, 107 (1955).

(4) G. A. H. Elton, *J. Chem. Soc.*, 3813 (1954).

(5) A. Klinkenberg, *Rec. trav. chim.*, **78**, 83 (1959).

(6) M. Siskova and E. Erdös, *Collection Czech. Chem. Commun.*, **25**, 1729 (1960); **26**, 3086 (1961).

(7) G. Delmas and D. Patterson, *J. Phys. Chem.*, **64**, 1827 (1960).

(8) W. Ostwald and R. de Izaguirre, *Kolloid-Z.*, **30**, 279 (1922).

(9) J. J. Kipling and D. A. Tester, *J. Chem. Soc.*, 4123 (1952).

(10) E. A. Guggenheim and N. K. Adam, *Proc. Roy. Soc.* (London), **A139**, 218 (1933).

$$\Gamma_1^{(N)} = n^s(x_1^s - x_1)/S \qquad (3)$$

Reports of adsorption data for the binary systems of interest on silica gel of known surface area have been found in the literature only for the benzene–cyclohexane system. The values of $\Gamma_1^{(N)}$ calculated from these data are plotted as a function of x_1 in Fig. 2 and are seen to be distinctly larger for silica gel than for porous glass. A similar effect was observed in the benzene–*n*-heptane system,[3] where $\Gamma_1^{(V)}$, the volume excess of component 1 (benzene), was found to be larger in fine-pore (S = 440 m.²/g.) silica gel than in a coarse-pore (S = 340 m.²/g.) gel at low x_1; no differences in the gel data were observed at values of x_1 above the maximum value of $\Gamma_1^{(V)}$. The explanation by Kiselev and El'tekov of this effect, as well as that of the parallel increase in the initial part of the vapor-phase adsorption isotherm of benzene, was based on the expectation that a higher average adsorption potential would occur at the surface of the smaller pores. The increase in adsorption potential in going from larger to smaller pores would be expected to be greater for the more strongly adsorbed component. The increase in adsorption potential in smaller pores is due to the smaller distances, on the average, between adsorbed molecules of the liquid and the adsorbing atoms of the solid. A similar explanation may be expected to hold for the increased adsorption shown in Fig. 2 by the silica gels ($S \sim 700$ m.²/g.) over that of porous glass ($S \sim 150$ m.²/g.[11,12]).

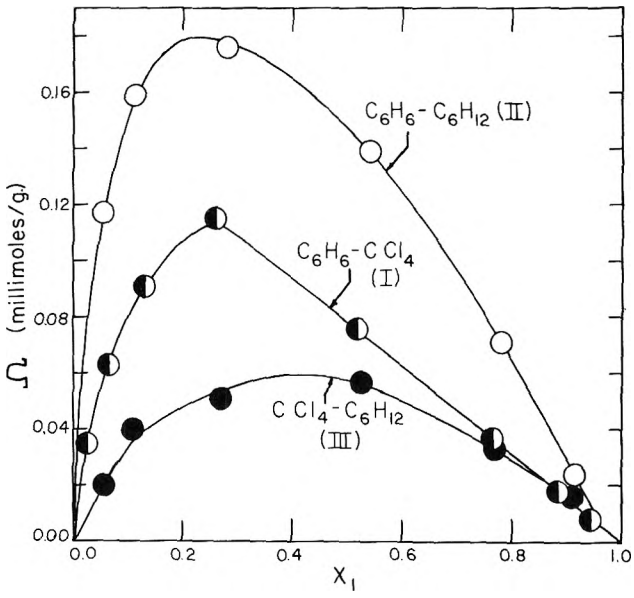

Figure 1. Experimental values of the apparent adsorption Ω as a function of the mole fraction of component 1 in the *equilibrium liquid*. Adsorbent: porous (Vycor) glass, preheated to 500°.

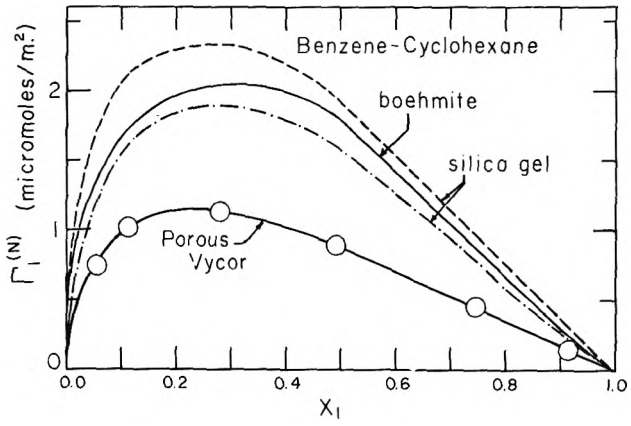

Figure 2. Molar surface excess (N-convention) for system II: C_6H_6–C_6H_{12} on various adsorbents: porous (Vycor) glass (this work), silica gels (upper curve, ref. 23; lower curve, ref. 21), and boehmite (ref. 24).

Estimation of Adsorption Parameters. The thermodynamic treatments of surface adsorption from solution have often used as a starting point either the concept of the adsorption potential due to Polanyi[13] or the quasi-crystalline model developed principally by Guggenheim.[14] Application of the Polanyi concept to adsorption from solution was made by Hansen and Fackler.[15] The quasi-crystalline model of surfaces was applied to adsorption from ideal solutions by Elton[4] and was extended to provide expressions for adsorption from "regular" solutions by Delmas and Patterson.[7] A chemical equilibrium approach to the problem[16] gave essentially similar results to those of Elton.

The advantage of the adsorption potential method, as applied by Hansen and Fackler,[15] is its natural introduction of heterogeneity of the various surface sites with respect to adsorbent–adsorbate interaction energy. Their method requires a knowledge of the experimental vapor-adsorption isotherms for each component. In the absence of such data, the quantitative application of both the potential method[6] and the results of the quasi-crystalline model[4,7] has usually been preceded by simplification to what is best termed a Langmuir model. The characteristic assumptions of this model are (1) that the solution is ideal, both in the surface

(11) H. Brumberger and P. Debye, *J. Phys. Chem.*, 61, 1623 (1957).

(12) A. Ron, M. Folman, and O. Schnepp, *J. Chem. Phys.*, 36, 2449 (1962).

(13) M. Polanyi, *Verhandl. Deut. physik. Ges.*, 18, 55 (1916).

(14) E. A. Guggenheim, "Mixtures," Oxford University Press, London, 1952.

(15) R. M. Hansen and W. V. Fackler, *J. Phys. Chem.*, 57, 634 (1953).

(16) O. M. Dzhigit, A. V. Kiselev, M. G. Terekhova, and K. D. Shcherbakova, *Zh. Fiz. Khim.*, 22, 107 (1948).

layer and the bulk phase, and (2) that molecular interactions with the surface may be assumed constant independent of site location in the first monolayer and may be neglected in the second and further layers.

For the treatment of our experimental data the Langmuir model would appear to be a reasonable first approximation to the physical situation. The binary solutions studied in our work have been shown[17] to have thermodynamic properties approximately corresponding to those of ideal solutions. The assumption of homogeneity of molecular interactions with the surface is crude, however. It has been demonstrated by measurement of differential heats of adsorption of water vapor[18] and organic vapors[2] on silica gel as a function of surface coverage that considerable heterogeneity of adsorbent–adsorbate site interaction occurs.

For the Langmuir model in which a square lattice of N^s sites is assumed to be randomly and completely covered by N_1^s molecules of kind 1 and N_2^s molecules of kind 2, the adsorption isotherm is given, essentially in Elton's notation, by

$$\frac{x_1^s}{x_1}\frac{x_2}{x_2^s} = \frac{q_1^s}{q_1}\frac{q_2}{q_2^s}\exp\left(\frac{w_2^s - w_1^s}{RT}\right) \qquad (4)$$

where $x_i^s = N_i^s/N^s$ represents the surface mole fraction of component i, q_i and q_i^s are, respectively, the bulk liquid and adsorbed phase molecular partition functions, which are supposed mutually independent in this approximation. The quantity w_i^s is the increase in potential energy per mole of component i upon transfer from the bulk liquid phase to the surface layer. The Langmuir form of the adsorption isotherm is obtained by assuming that the ratio q_i^s/q_i is given by $\exp(w_i'/RT)$, where w_i' is a constant. Equation 4 then becomes

$$\alpha = \frac{x_1^s}{x_1}\frac{x_2}{x_2^s} = \exp(\Delta w/RT)$$
$$\Delta w = w_2 - w_1 \qquad (5)$$
$$w_i = w_i^s + w_i'$$

where α is introduced as a convenient adsorption parameter.

Equations 1 and 5 may be combined to yield a straight-line form for plotting experimental data, as shown by Siskova and Erdös,[6] to give

$$\frac{\Omega}{1 - x_1} = -\frac{1}{\alpha}\frac{\Omega}{x_1} + n^s\left(\frac{\alpha - 1}{\alpha}\right) \qquad (6)$$

The slope and intercept of a linear plot of $\Omega/(1 - x_1)$ against Ω/x_1 may then be used to evaluate n^s, α, and, by use of (5), $\Delta w/RT$. The linearity obtained in plots of actual data according to (6) is indicated for adsorption from the benzene–cyclohexane system on various adsorbents in Fig. 3. Slopes and intercepts derived from this and similar plots have been used to estimate the values of $\Delta w/RT$ and n^s presented in Table I.

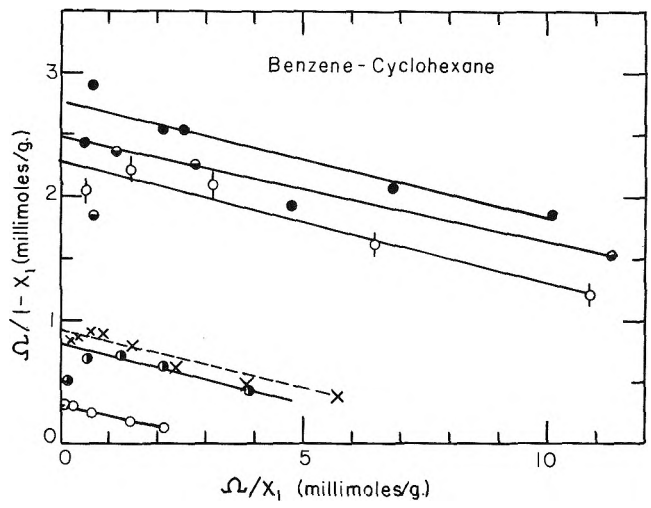

Figure 3. Experimental adsorption data for system II: C_6H_6–C_6H_{12} plotted according to eq. 6. Adsorbents: ○, porous (Vycor) glass, this work; ◑, silica gel[19]; ◇, silica gel[21]; ●, silica gel[22]; ◒, silica gel[23]; – – – –, boehmite.[24]

Table I: Adsorption Parameters from Langmuir Model

Adsorbent[a]	S, m.²/g.	$\Delta w/RT$	n^s, mmoles/g.	a, m.²/μmole	Reference
System I: $C_6H_6(1)$–CCl_4[b]					
PG	150	2.2	0.20	0.8	c
SG		1.8	1.3		6
SG		1.8	1.4		19
SG		2.0	1.7		20
System II: $C_6H_6(1)$–C_6H_{12}[b]					
PG	150	2.4	0.36	0.43	c
SG		2.3	0.90		19
SG	700	2.3	2.5	0.28	21
SG		2.4	3.1		22
SG	630	2.5	2.7	0.23	23
B		2.4	2.4	1.0	24
System III: $CCl_4(1)$–C_6H_{12}[b]					
PG	150	1.1	0.24	0.65	c
SG		1.4	0.77		19

[a] PG = porous glass, SG = silica gel, B = boehmite (activated alumina). [b] Adsorption temperatures varied from 20 to 33°. [c] This work.

(17) G. Scatchard, S. E. Wood, and J. M. Mochel, *J. Am. Chem. Soc.*, **62**, 712 (1940) (system I); *J. Phys. Chem.*, **43**, 119 (1939) (system II); *J. Am. Chem. Soc.*, **61**, 3206 (1939) (system III).

(18) W. A. Patrick and C. E. Greider, *J. Phys. Chem.*, **29**, 1031 (1925).

Data for adsorption of the three binary systems of interest on a silica gel sample[19] showed increases in Ω in the order found for porous glass, *i.e.*, $\Omega_{III} < \Omega_I < \Omega_{II}$ at a given x_1.

Evaluation of adsorption parameters of the Langmuir model by means of the linear form (6) gives satisfactory agreement among the various silica gel samples for a given binary system. Insofar as values of $\Delta w/RT$ are concerned, a rather surprising agreement occurs between porous glass and silica gel. The best straight line through the data for system II on boehmite (activated alumina)[24] also gives a value of $\Delta w/RT$ which agrees with that found for the silicaceous adsorbents.

The values of n^s, the molar surface coverage per gram of adsorbent, derived from (6), may be converted to a more suitable basis for comparison of adsorbents of different specific surface S by calculating $a = S/n^s$, the molar area of the adsorbate. Values of a are estimated in the fifth column of Table I where values of S are available, and are seen to depend rather strongly on the adsorbent.

The conclusion derived from the Langmuir model is that lower values of Ω must be due principally to a larger molar area a of the adsorbate, or, equivalently, to a smaller adsorption n^s. The result is clearly at variance with the expectation that the adsorption potential difference Δw is larger in the finer pores of the silica gels. The result must also be considered to indicate fewer adsorption sites per unit area for porous glass than for silica gel. This conclusion is basically unreasonable in view of the generally accepted view that a wetting liquid completely covers a solid surface. We conclude that variation in values of a implies that some sites show less preferential adsorption than others, or that Δw varies from one site to another. This conclusion is in basic disagreement with the Langmuir model assumed.

Surface Composition: The Kipling–Tester Method.[9] For adsorption on a heterogeneous surface the experimentally definable quantity is $\langle x_i^s \rangle = n_i^s/n^s$, the average mole fraction of component i in the adsorption region. The adsorption parameter $\bar{\alpha}$ may then be defined by an obvious extension of (5)

$$\bar{\alpha} = \frac{\langle x_1^s \rangle}{x_1} \frac{x_2}{\langle x_2^s \rangle} \equiv \exp(\overline{\Delta w}/RT) \qquad (5a)$$

where $\overline{\Delta w}$ is defined by the second equality. Without knowledge of the details of the distribution of surface sites as a function of Δw, the quantities $\bar{\alpha}$ and $\overline{\Delta w}$ cannot be explicitly related to average values of α and Δw for such a distribution. Changes in $\bar{\alpha}$ and $\overline{\Delta w}$ will, however, reflect changes in the respective averages.

Kipling and Tester[9] observed weight changes in adsorbents suspended in the equilibrium vapor of solutions as well as composition changes in the bulk solution phase. From these data they were able to determine experimental values of n_1^s and n_2^s for a binary liquid on a given adsorbent. The same authors showed further that with a certain set of assumptions, the experimental values could be calculated with good accuracy from the vapor-phase isotherms for the pure components and the "apparent adsorption" Ω from solution. The assumptions were (1) that adsorption occurred only in a liquid monolayer which completely covered the surface and (2) that the molar surface area a_i of component i in a mixture was identical with that of the pure component. These assumptions may be written for a binary mixture

$$\begin{aligned} n_1^s a_1 + n_2^s a_2 &= S \\ (n_i^s)_m a_i &= S \quad (i = 1,2) \end{aligned} \qquad (7)$$

where $(n_i^s)_m$, the number of moles of i adsorbed per gram in a monolayer of pure i, was further assumed to be the monolayer coverage given by the BET isotherm for the pure component. Values of a_i determined from such isotherms permitted the calculation of n_1^s and n_2^s from values of Ω for a given adsorption system by simultaneous use of (1) and (7).

Comparison of Langmuir and Surface Composition Models. Values of $x_1^s = n_1^s/(n_1^s + n_2^s)$ were calculated for the adsorption from benzene–cyclohexane solutions on boehmite by Kipling and Peakall[24] in the manner described above. The values of $\overline{\Delta w}/RT$ calculated from (5a) for their data are plotted as the dashed line in Fig. 5. The value of $\Delta w/RT = 2.4$ given in Table I for the plot (Fig. 3) of their data according to eq. 6 is clearly larger than the values of $\overline{\Delta w}/RT$ shown in Fig. 5 at all compositions.

A similar result may be demonstrated for an artificial adsorbent–adsorbate system for which we assume $\bar{\alpha} = 15 - 10x_1$. Values of $\langle x_1^s \rangle$ may be calculated as a function of x_1 for this system from (5a) and the relations $x_1 + x_2 = 1$, $\langle x_1^s \rangle + \langle x_2^s \rangle = 1$. The quantity Ω/n^s may be calculated from the $\langle x_1^s \rangle$ values so obtained when $\langle x_1^s \rangle$ is substituted for x_1^s in (3), and (2) is used. The slope of a plot of $\Omega/n^s(1 - x_1)$ against

(19) G. F. Lesokhina, K. A. Gol'bert, and A. A. Zhukovitskii, *Zh. Fiz. Khim.*, **22**, 363 (1948).

(20) B. S. Rao, *J. Phys. Chem.*, **36**, 616 (1932).

(21) E. B. Stuart and J. Coull, *A.I.Ch.E. J.*, **4**, 383 (1958).

(22) B. J. Mair, J. W. Westheimer, and F. D. Rossini, *Ind. Eng. Chem.*, **42**, 1279 (1950).

(23) S. Eagle and J. W. Scott, *ibid.*, **42**, 1287 (1950).

(24) J. J. Kipling and D. B. Peakall, *J. Chem. Soc.*, 4828 (1956).

$\Omega/n^s x_1$ is $-1/\alpha$ and the intercept $(\alpha - 1)/\alpha$ according to (6). When such a plot is made, linearity at least as good as that shown by the majority of the data of Fig. 3 is found. The value $\alpha = 19$ is derived from the slope of this plot and $\alpha = 8.7$ from its intercept. The slope thus clearly leads to a larger value for α than the maximum value (15) assumed for the artificial system. This result is evidently typical for systems in which $\bar{\alpha}$ decreases with increasing x_1, as in the benzene–cyclohexane system on boehmite. The adsorption data, expressed as Ω values, which would be observed for the artificial system would, nevertheless, be reproduced by the linear plot within normal experimental error (about 2%) throughout the composition range. Adequate reproduction of adsorption data by a plot of eq. 6 is thus no guarantee that the value of α derived from the slope of the line through the points will be a representative value. The use of plots based on the Langmuir model as a means of estimating values of Δw would appear to be unjustified in general, although such plots may represent convenient graphical methods for presenting adsorption data.

Estimate of Surface Compositions and $\Delta w/RT$ Values for Adsorption on Porous Glass. If the reasonable assumption is made that adsorption on porous glass follows the model of Kipling and Tester, only estimates of the molar areas a_i are required in order to estimate surface compositions from solution adsorption data. A value of $(n_1^s)_m$ from a B.E.T. treatment of a vapor-adsorption isotherm has been reported[12] as 0.66 mmole/g. for benzene on porous glass of specific surface S = 156 m.²/g. The value of a for benzene computed from this result is 238 m.²/mmole. This value agrees closely with that of 240 m.²/mmole for benzene adsorbed on silica gel, which was derived from the adsorption from benzene–*n*-heptane solutions.[3]

It would appear reasonable and it considerably simplifies calculations to take a values equal for C_6H_6, CCl_4, and C_6H_{12}. Molar surface areas for these adsorbates are usually similar on a given adsorbent, although they may differ for a given adsorbate from one adsorbent to another. For example, Kipling and Tester[9] found $a = 167$ for C_6H_6 and $a = 184$ for CCl_4 on a charcoal surface, while Smith, Pierce, and Cordes[25] reported $a = 247$ for C_6H_6 and $a = 229$ for C_6H_{12} on graphite, where all units of a are in m.²/mmole. Values of a calculated for the three adsorbates at 25° from the assumption that the molecules are arranged on a cubic lattice and that the surface density is equal to the bulk liquid density are: C_6H_6, 201 m.²/mmole; CCl_4, 204 m.²/mmole; C_6H_{12}, 208 m.²/mmole.

Values of $\langle x_1^s \rangle$ were calculated as a function of x_1 from Ω values by means of eq. 1 and 7 with a_i taken equal to 240 m.²/mmole for all components. The calculated surface compositions were then converted to values of $\Delta\bar{w}/RT$ by means of (5a). The results are plotted in Fig. 4 for the three systems studied on porous glass and in Fig. 5 for system II (C_6H_6–C_6H_{12}) on various adsorbents. The resemblance in shape of the curves in Fig. 5 is evident.

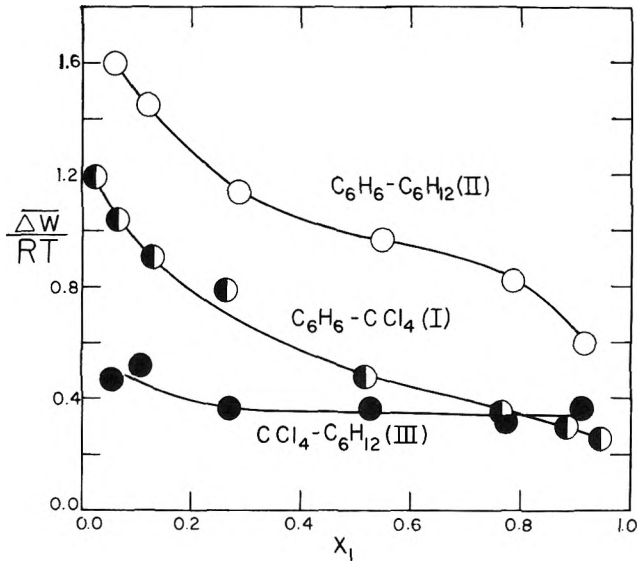

Figure 4. Average values of $\overline{\Delta w}/RT$ for the binary systems studied on porous (Vycor) glass as a function of equilibrium liquid composition. The molar surface areas of all components were assumed to be 240 m.²/mmole.

The influence of change in the magnitude of the value of a chosen was investigated, retaining the assumption that all adsorbates had equal a values. The result obtained was that the curves of Fig. 4 are shifted in roughly parallel fashion upward for larger and downward for smaller values of a. For example, $\overline{\Delta w}/RT$ for the C_6H_6–C_6H_{12} system on porous glass increases at $x_1 = 0.5$ from 0.78 at $a = 200$ m.²/mmole to 0.97 at $a = 240$ m.²/mmole and to 1.30 at $a = 300$ m.²/mmole.

For a given value of a the results shown in Fig. 5 clearly indicate that $\overline{\Delta w}/RT$ for a given binary system is smaller on porous glass than on silica gel or boehmite, in contrast to the result obtained from the Langmuir model, which showed no observable difference between the adsorbents (Table I). The plot of the latter model according to eq. 6 or 6a has been previously shown to be untrustworthy for the estimation of Δw values; the present technique appears preferable for that

(25) R. N. Smith, C. Pierce, and H. Cordes, *J. Am. Chem. Soc.*, **72**, 5595 (1950).

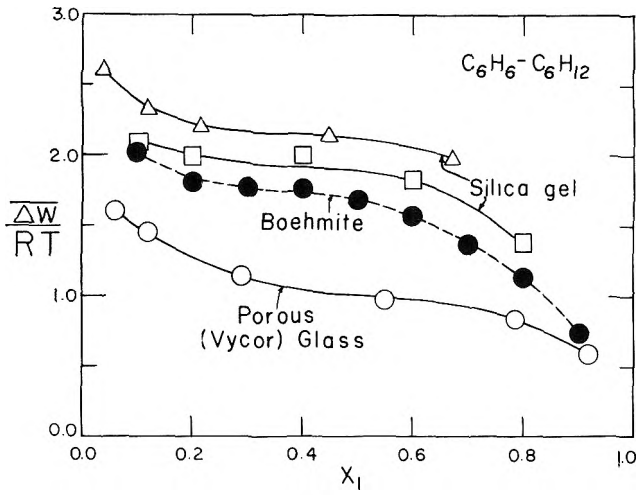

Figure 5. Average values of $\overline{\Delta w}/RT$ estimated from surface mole fractions as a function of equilibrium liquid composition for system II: C_6H_6–C_6H_{12}. Molar areas of both components were assumed to be 240 m.²/mmole (except for boehmite). Adsorbents: O, porous (Vycor) glass, this work; □, silica gel[21]; △, silica gel[23]; ●, (dashed line) boehmite.[24]

purpose, since it takes into account in an empirical way heterogeneity in site–adsorbate interaction.

The similarity in the composition behavior of the C_6H_6–C_6H_{12} system on different adsorbents demonstrated by Fig. 5 together with the greater magnitude of $\overline{\Delta w}/RT$ for the adsorbents of larger specific surface suggests that the interpretation of the greater selective adsorption of the latter in terms of larger adsorption potentials is correct.

Effect of Surface Dehydration. In view of the fact that silica surfaces are dehydrated upon ignition,[26] experiments were performed to determine whether loss of chemically-bound water during the heat treatment of porous glass before experimental use (see Experimental) might be responsible for the differences in $\overline{\Delta w}/RT$ observed between unheated silica gel and heated porous glass. It has been demonstrated experimentally that heating silica gels at temperatures to 500° does not affect the structure of the pores,[27] and a similar result may be expected for porous glass.

The weight loss on heating to successively higher temperatures was determined for a sample of porous glass. The sample lost little weight between 925 and 1000° and can be assumed free of surface hydroxyl groups at the latter temperature, in agreement with a similar result for silica gel.[26] The water content values given in Table II have been calculated with this assumption. Values of the density of surface hydroxyl groups given in this table have been calculated with the assumption that the surface area is 156 m.²/g. throughout, although some pore consolidation undoubtedly occurs at temperatures above about 500°. The values of surface hydroxyl density thus obtained resemble those for silica gels.[28]

Table II: Surface Water Content and Selective Adsorptivity of Ignited Porous Glass

t, °C.[a]	% water	Surface–OH density, no./mμ^2	$(\Omega_t/\Omega_{475})_{\varphi_1 = 0.25}$ System I	System II
No heating	4.35	...	1.11	
120	2.24	9.5	1.13	1.35
185	1.86	7.9	1.15	1.33
300	1.54	6.5	1.09	
475	1.12	4.7	1.00	1.00
825	0.64	2.7		
925	0.18	0.8		
1000	0.0[b]	0.0[b]		

[a] All heating periods were at least 24 hr., except at 1000° (12 hr.). [b] Assumed values.

The changes observed in the apparent adsorption Ω for systems I and II at $\varphi_1 = 0.25$, near the adsorption maxima for these systems, are reported in Table II as the ratio, Ω_t/Ω_{475}, of the apparent adsorption of samples heated at temperature t to that of samples heated at $t = 475°$. The adsorption selectivity of the systems studied decreases somewhat as dehydration occurs. This result agrees qualitatively with that expected on the basis of considerable decreases in vapor-phase adsorption,[2] heat of adsorption from the vapor phase,[2] and heat of wetting[29] for benzene upon surface dehydration of silica gels, effects which are either very slight or absent for paraffin hydrocarbons.[2,29]

The maximum effect on $\overline{\Delta w}/RT$ at $\varphi_1 = 0.25$ for an assumed a value of 240 m.²/mmole is an increase from 0.79 at $t = 475°$ to 0.96 at $t = 185$ for system I (C_6H_6–CCl_4) and from 1.14 at $t = 475°$ to 1.54 at $t = 120°$ for system II (C_6H_6–C_6H_{12}). The values of $\overline{\Delta w}/RT$ for silica gels at $\varphi_1 = 0.25$ for system II were 1.90 (data of Stuart and Coull) and 2.12 (data of Eagle and Scott).

Thus, for the benzene–cyclohexane system a part of the differences in $\overline{\Delta w}/RT$ between porous glass and silica gel can be attributed to greater dehydration of the porous glass surface due to the heating procedure used. The remainder can be ascribed to the larger average adsorption potential in the small pores due to the smaller average adsorbate molecule-site distance.

(26) I. Shapiro and I. M. Kolthoff, *J. Am. Chem. Soc.*, **72**, 776 (1950).

(27) W. W. Milligan and H. H. Rachford, *J. Phys. Colloid Chem.*, **51**, 333 (1947).

(28) R. K. Iler, "The Colloid Chemistry of Silica and Silicates." Cornell University Press, Ithaca, N. Y., 1955, pp. 235–237.

(29) J. W. Whalen, *J. Phys. Chem.*, **66**, 511 (1962).

Mass Spectrometric Observation of Secondary Ions in *n*-Pentane, *n*-Hexane, *n*-Heptane, and *n*-Octane

by L. M. Draper and J. H. Green

Department of Nuclear and Radiation Chemistry, University of New South Wales, Kensington, Sydney, Australia *(Received December 23, 1963)*

Secondary ions of mass $M - 1$ and $M - 2$ (where M is the mass of the parent ion) have been observed in the high pressure mass spectra of n-C_5H_{12}, n-C_6H_{14}, n-C_7H_{16}, and n-C_8H_{18}. Secondary ions of mass $M - 3$ have been observed in n-C_6H_{14} and n-C_8H_{18}. Similar observations have been made in mixtures of these hydrocarbons with several alkyl halides. Reaction cross sections calculated for "hydride ion transfer" reactions continue the unexplained decreasing trend with increasing molecular weight previously observed in lighter paraffins.

Introduction

The formation of secondary ions of mass $M - 1$ by hydride ion transfer has been reported by Field and Lampe[1] in C_2H_6, C_3H_8, n-C_4H_{10}, i-C_4H_{10}, neo-C_5H_{12}, and neo-C_6H_{14}. Pinkerton[2] has studied the formation of similar ions in n-C_5H_{12} and i-C_5H_{12}; and Boelrijk and Hamill[3] report secondary ions of mass 71, *i.e.*, $(M-1)$ in mixtures of a variety of additives with neopentane. This paper reports the formation of secondary ions in n-C_5H_{12}, n-C_6H_{14}, n-C_7H_{16}, and n-C_8H_{18} and in mixtures of these paraffins with alkyl halides.

Experimental

Experiments were conducted with a Metropolitan Vickers MS2-SG mass spectrometer. Reservoir pressures were measured with a mercury manometer and cathetometer in the range 5–20 mm., which corresponds roughly to ion source pressures from 2×10^{-4} to 7×10^{-4} mm. The molecular concentrations in the ionization chamber were estimated by collecting on the negatively biased ion repeller the total ion current in a gas of known ionization cross section (argon). The ionization chamber field strength was calculated from the ion repeller voltage and the dimensions of the chamber.

Results and Discussion

Pressure studies, in which changes in the ratios I_{M-X}/I_M (where I is the mass spectral ion intensity) are observed as the reservoir pressure (P_R) is increased, where carried out for each n-paraffin. Figures 1 and 2 show typical results for n-C_5H_{12} and n-C_8H_{18}, respectively. Table I lists the slopes of the plots I_{M-X}/I_M *vs.* P_R for each n-paraffin using 70 e.v. electrons at 2 μa. and a field strength of 0.8 v./cm. The stationary value of I_{M+1}/I_M (the ratio of two primary ions, $M + 1$ being an isotopic peak) over the pressure range used, indicates that the changes in the other ratios are real and not merely instrumental effects. Ion repeller studies, in which changes in the ratios I_{M-X}/I_M are observed as the ion repeller voltage is increased, were

Table I: Slopes ($I_{M-X}/I_M \times 10^3$ *vs.* P_R) from Pressure Studies at 0.8 v./cm. Field Strength in n-Paraffins Using a 70 e.v. Ionizing Electron Current of 2μa.

Paraffin	$\frac{I_{M+1}}{I_M}$	$\frac{I_{M-1}}{I_M}$	$\frac{I_{M-2}}{I_M}$	$\frac{I_{M-3}}{I_M}$
n-C_5H_{12}	0	7	3	...
n-C_6H_{14}	0	7	2	2
n-C_7H_{16}	0	1.4	0.5	...
n-C_8H_{18}	0	1.8	1.5	0.8

(1) F. H. Field and F. W. Lampe, *J. Am. Chem. Soc.*, **80**, 5587 (1958).

(2) D. M. Pinkerton, Ph.D. Thesis, University of New South Wales, Sydney, Australia, 1962.

(3) N. Boelrijk and W. H. Hamill, *J. Am. Chem. Soc.*, **84**, 730 (1962).

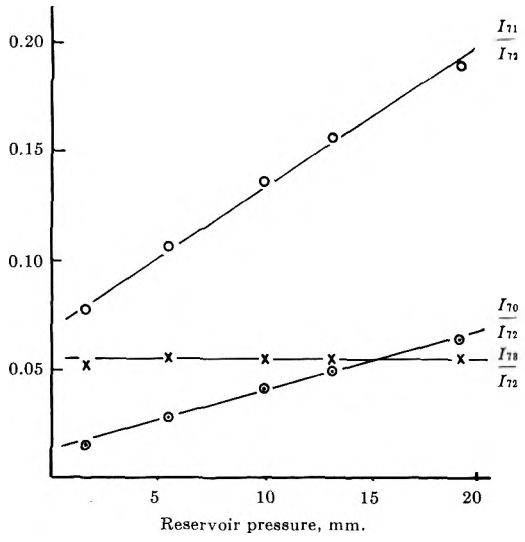

Figure 1. Pressure study in *n*-pentane: electron energy 70 e.v., electron current 2μa., and ion-repeller voltage 0.25 v. (0.8 v./cm.).

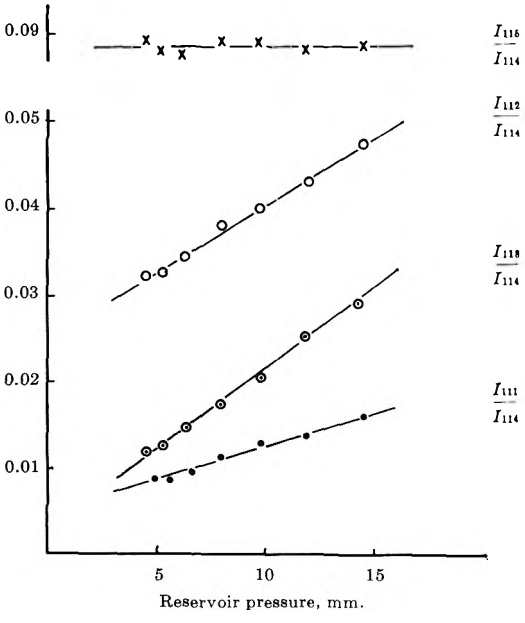

Figure 2. Pressure study in *n*-octane: electron energy 70 e.v., electron current 2μa., and ion-repeller voltage 0.25 v. (0.8 v./cm.).

also made. Pressure and ion repeller studies mutually confirm the formation of the following secondary ions: $C_5H_{11}^+$ and $C_5H_{10}^+$ in *n*-pentane; $C_6H_{13}^+$, $C_6H_{12}^+$, and $C_6H_{11}^+$ in *n*-hexane; $C_7H_{15}^+$ and $C_7H_{14}^+$ in *n*-heptane; $C_8H_{17}^+$, $C_8H_{16}^+$, and $C_8H_{15}^+$ in *n*-octane.

The simple electron accelerating system in the ion source prevents an accurate comparison of primary and secondary ion appearance potentials. The selection of primary reactant ions on thermodynamic grounds is also difficult because of lack of data and doubts about the structures of ions from the heavier paraffins. Using available data for *n*-pentane the values of ΔH_R for various reactant ions in the reactions

$$C_5H_{12} + R^+ \longrightarrow C_5H_{11}^+ + RH \qquad (I)$$

$$C_5H_{12} + R^+ \longrightarrow C_5H_{10}^+ + RH_2 \qquad (II)$$

have been calculated. This information is shown in Fig. 3. Reaction I tends to be endothermic and reaction II tends to be exothermic when R = C_xH_{2x}. The $C_xH_{2x}^+$ primary ions could well be involved in the formation of secondary ions at $M - 2$, while the remaining ions, with doubts about some of the heavier ones, are involved in hydride ion transfer reactions. The erroneous inclusion or exclusion of $C_4H_7^+$ and $C_4H_9^+$ as

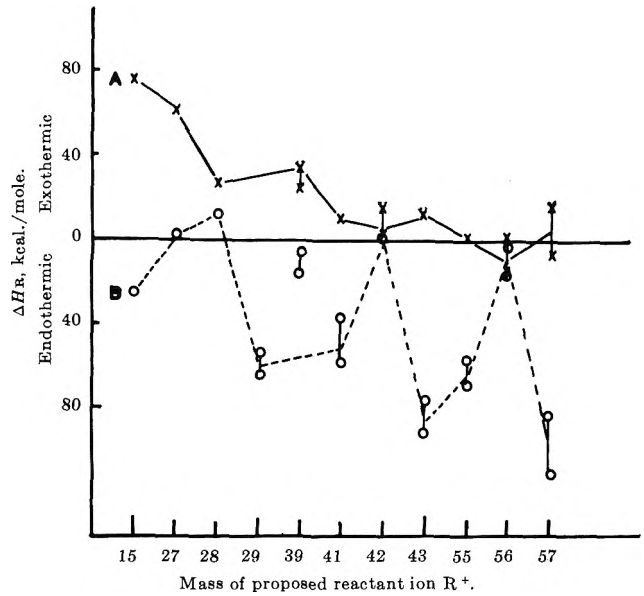

Figure 3. ΔH_R for some proposed ion–molecule reactions in *n*-pentane. (A) $C_5H_{12} + R^+ \rightarrow C_5H_{11}^+ + RH$. (B) $C_5H_{12} + R^+ \rightarrow C_5H_{10}^+ + RH_2$.

reactants will only slightly alter the calculated reaction cross section and rate. In the absence of sufficient thermodynamic data for the heavier paraffins, reactant ions have been selected for them by analogy with *n*-C_5H_{12}. The origin of $M - 3$ secondary ions in *n*-C_6H_{14} and *n*-C_8H_{18} will be mentioned later.

Table II lists the reaction cross sections and rate constants calculated for various ion source conditions using the formulas

$$Q_R = \frac{\lambda b_M}{\gamma d} \qquad (1)$$

where Q_R = composite reaction cross section consisting

Table II: Reaction Cross Sections and Rate Constants for Hydride Ion Transfer in Paraffins

	70 e.v., 2μa., 5.7 v./cm.[a]		This research, 70 e.v., 2μa.				
	Q_R, Å.²/molecule		5.7 v./cm.		0.8 v./cm.; Q_R, Å.²/molecule		
Paraffin	Pure subst.	Mixture with methane	Q_R, Å.²/molecule	$k \times 10^{10}$, ml./mole/sec.	Pure subst.	Av. all additives	Av. *n*-alkyl additives
C_2H_6	264	171	150	...	..	..	..
C_3H_8	66	107	...	...	..	..	..
n-C_4H_{10}	32	60	...	...	..	..	..
i-C_4H_{10}	34	101	...	...	..	..	..
n-C_5H_{12}	...	...	12.6	1.5	34	31	30
i-C_5H_{12}	...	...	...	...	...	..	..
neo-C_5H_{12}	14	12	17	...	..	..	..
n-C_6H_{14}	...	...	6.9	0.94	24	25	24
neo-C_6H_{14}	7	16	...	...	..	..	..
n-C_7H_{16}	...	...	3.2	0.34	9	11	8
n-C_8H_{18}	...	...	1.6	0.2	4	6	4

[a] Ref. 1.

of the sum of the reaction cross sections of individual reactant ions, λ = slope of plot I_{M-1}/I_M *vs.* P_R, $b_M = I_M/\Sigma I$ (primary reactants), $\gamma = [M]/P_R = 7.9 \times 10^{11}$ molecules/ml./mm., d = path length of primary ions, and

$$k = Q_R\left(\frac{Eed}{2\bar{m}_i}\right)^{1/2} \qquad (2)$$

where k = rate constant, E = field gradient, e = ionic charge, and $\bar{m}_i$ = weighted average mass of reactant ions. The results of Field and Lampe[1] are also included in Table II, together with reaction cross sections for hydride ion transfer in C_2H_6 and neo-C_5H_{12} found in the present research. Field and Lampe[1] have drawn attention to the unexplained decrease in reaction cross section with increasing molecular weight. They point out that the increasing polarizability and decreasing carbon–hydrogen bond dissociation energies with increasing molecular weight would lead one to expect the reverse behavior. They have dismissed the possibility of rapid decomposition of the heavier $M - 1$ ions and admit to "not at all understanding" the effect. One comment we can offer is that in spite of thermodynamic indications, perhaps one, rather than many primary ions, is in fact the reactant ion. It might then be found that the cross section increases with molecular weight.

In discussing some ion reactions in oxygen- and nitrogen-containing organic compounds, Beynon, *et al.*,[4] draw attention to some features which may be relevant to our problem. In the first place, the collision rate for the formation of the ion–molecule complex will decrease as the molecular weight increases. The lifetime of the complex will increase as the number of degrees of freedom increases. This would mean that the chance of extracting and measuring the decomposition products of the complex would be decreased and a lower apparent formation cross section would be calculated. As well as the numerical effect on the calculation noted already, one might suppose that, if $C_3H_7^+$ ions were the sole reactants in pentane, say, rather than $C_4H_9^+$ or heavier ions, the complex would have a shorter lifetime and the cross section for $C_5H_{11}^+$ would be greater than at present listed. Another feature which we have examined without success is the effect of varying asymmetry of the molecule on the rearrangement mode which provides the observed secondary ion. Our observation of $M - 1$ secondaries in the four paraffins, $M - 2$ secondaries from all four, but $M - 3$ secondaries from the even number carbon paraffins only and our feeling that the $M - 1$ and $M - 3$ ions are of common origin may point the way to an explanation which we cannot attempt just yet.

Mixtures containing a fixed partial pressure of *n*-paraffin ($P_R \sim 5$ mm.) and variable partial pressures of alkyl halide ($P_R < 15$ mm.) were used in pressure and ion-repeller studies. Care was constantly exercised to detect interference by primary ions of the additive at the masses at which ion intensities were being measured. Cross sections were calculated using the formula

$$Q_R = \frac{\lambda I_M Q_M}{I_M Q_A g_A \gamma d} \qquad (3)$$

where I_M = sum of the intensities of all ions in mass spectrum, Q_M and Q_A = total ionization cross section for paraffin and additive, respectively, and g_A = frac-

(4) J. H. Beynon, G. R. Lester, R. A. Saunders, and A. E. Williams, *Trans. Faraday Soc.*, **57**, 1259 (1961).

tion of reacting ions in mass spectrum of additive. The results are listed in Table III. In spite of con-

Table III: Reaction Cross Sections (Å.²/molecule) at Field Strength 0.8 v./cm. from Mixture Studies Using a 70 e.v. Ionizing Electron Current of 2 μa.

	Paraffin			
Additive	n-C_5H_{12}	n-C_6H_{14}	n-C_7H_{16}	n-C_8H_{18}
n-C_3H_7I	27.0	23.9	8.8	5.2
n-C_3H_6Br	17.8	14.0	6.4	2.5
n-C_3H_7Cl	43.1	33.3	11.7	5.4
n-C_4H_9Cl	30.8	23.8	6.0	2.5
Av. for n-alkyl additives	30	24	8	4
i-C_3H_7I	35.9	30.0	22.4	10.1
i-C_3H_7Br	47.1	31.0	19.7	10.6
i-C_3H_7Cl	34.9	28.6	15.7	8.6
sec-C_4H_9Cl	34.6	27.2	10.9	5.3
t-C_4H_9Cl	17.6	13.7	3.2	1.5
i-C_4H_9Cl	23.8	21.8	9.5	5.7
Av. for all additives	31	25	11	6

siderable variations for some additives, the averages of the Q_R values for mixtures are approximately equal to those found in pure substances. The average Q_R values for mixtures with the n-alkyl additives only gives even better correlation.

Where primary ions are formed with initial kinetic energy, the various parameters calculated from mass spectral cracking patterns are likely to be in considerable error, due to possible significant differences between relative ion intensities in the mass spectrum and the relative ion concentrations in the ion chamber. As part of the present investigation the relative total ionization cross sections of the additives were found by two different methods; (i) by summing all the ion intensities of the mass spectrum; (ii) by collecting and measuring the total ion current in the ion chamber. Method (i) gave low values for isopropyl iodide and bromide (Table IV). Ryan[5] showed that fragment ions from isopropyl alcohol are formed with initial kinetic energy while those from n-propyl alcohol are not. The high Q_R value found in mixtures with isopropyl bromide may possibly be explained in similar terms.

Boelrijk and Hamill[3] showed that charge exchange reactions occur in mixtures of neo-C_5H_{12} with CH_3Br and C_2H_5Br (but not with the corresponding chlorides and iodides) with which ions of mass 72 are formed. In this research, evidence from pressure and ion re-

Table IV: Cross Sections for Total Ionization in Propyl Halides

Substance	a	b	c
n-C_3H_7I	17.8	0.98	0.75
i-C_3H_7I	17.4		
n-C_3H_7Br	15.7	1.01	0.82
i-C_3H_7Br	15.9		
n-C_3H_7Cl	14.1	1.01	1.0
i-C_3H_7Cl	14.3		

[a] Cross section (Å.²/molecule) from measurement of total ion current using argon value of 3.52 Å.²/molecule. [b] Ratio of cross sections of iso- and n-propyl halides from a. [c] Ratio of cross sections of iso- and n-propyl halides as determined from summation of mass spectral peaks.

peller studies was found for the formation of ions of mass M in mixtures of n-C_3H_7Br with n-C_5H_{12} and n-C_7H_{16} (n-C_6H_{14} and n-C_8H_{18} were not investigated) but not for the other additives. Since the parent ion mass M was used as the primary reference ion in the observation of secondary ion formation, this explains the low Q_R value found in mixtures with n-C_3H_7Br. However, the equally low value in t-C_4H_9Cl remains unexplained.

The repetition of the order of the slopes for various additives with each n-paraffin suggests a common selection of primary reactant ions in the formation of secondary ions $M - 1$. This same order is again repeated for the $M - 3$ secondary ions and suggests a common origin for $M - 1$ and $M - 3$ ions. The decomposition

$$C_nH_{2n+1}^+ \longrightarrow C_nH_{2n-1}^+ + H_2$$

appears to be endothermic. However, it is possible that some $M - 1$ secondary ions are formed with sufficient excitation energy to overcome this endothermicity.

A different common order among the additives is observed for the formation of $M - 2$ secondary ions. Attempts to explain this order in terms of the abundance of $C_nH_{2n}^+$ ions in the various cracking patterns of the additives have been unsuccessful.

Acknowledgment. We are grateful for the assistance of J. Mason in this research.

(5) K. Ryan, Ph.D. Thesis, University of New South Wales, Sydney, Australia, 1963.

Gaseous Boroxine: Infrared Spectrum and Structure[2]

by Satish K. Wason and Richard F. Porter[2]

Department of Chemistry, Cornell University, Ithaca, New York *(Received December 23, 1963)*

Gaseous boroxine ($B_3O_3H_3$) has been isolated from the reaction of $H_2O(g)$ with elemental boron at temperatures near 1400°K. The gas at pressures between 1.0 and 2.0 torr can be maintained for a period up to 2 hr. at room temperature in the presence of excess argon. The infrared spectrum of the gas is similar to that for the isoelectronic molecule, borazine, and is consistent with a planar, D_{3h} structure. Spectral changes due to isotope substitution with ^{10}B and deuterium have also been observed. Boroxine reacts with oxygen in the gas phase to form $B_2O_3H_2(g)$. Traces of oxygen increase the rate of disappearance of $B_3O_3H_3(g)$ over that from its normal decomposition to $B_2H_6(g)$ and B_2O_3.

Introduction

Mass spectrometric studies[3] have shown that gaseous boroxine is produced at high temperatures in the reaction

$$1.5H_2(g) + B(s) + B_2O_3(s) = B_3O_3H_3(g) \quad (1)$$

Recently, Lee, Bauer, and Wiberley[4] have observed boroxine as a product in the explosive oxidation of B_5H_9 with oxygen. The product of reaction 1 may be trapped as a solid at liquid nitrogen temperatures. When this solid is warmed to room temperature, it partially decomposes to B_2H_6 and boron oxide. Lee, *et al.*, also noted decomposition of their product to B_2H_6 and B_2O_3 by monitoring the infrared spectrum of the gas over a time interval of about 1 hr. An analysis of the infrared spectrum of $B_3O_3H_3(g)$, however, has not been reported. We have recently observed that the rate of decomposition of gaseous boroxine is decreased notably in the presence of excess argon. The gas is stable under these conditions for a sufficient time for spectral observations and perhaps for study of its chemical behavior.

Experimental

The gas may be prepared by reaction 1 in a method similar to that outlined earlier.[3] A Vycor reaction tube is heated in a horizontal resistance-type furnace as shown in Fig. 1. One end of the tube is joined by a stopcock to a 10-cm. infrared cell and the other end is joined by separate stopcocks to a source of water vapor and a large bulb of argon at atmospheric pressure. A sample of 10–20 g. of a mixture of B and B_2O_3 in a molar ratio of about 1:1 is placed in a molybdenum shield which is enclosed in the central section of the reaction tube. The system, including the infrared cell, is pumped until the reaction temperature reaches about 1350°K. The stopcock between the furnace tube and the cell is then closed and water vapor at room temperature is introduced into the reaction chamber through a glass frit. Reaction is allowed to proceed for about 20 min. when the water source is cut off. The stopcock joining the cell to the Vycor tube is then opened as the reaction chamber is swept with argon. The stopcock is then immediately closed to entrap a sample of gaseous product in the cell.

Infrared Spectra. Infrared spectra of gaseous $B_3O_3H_3$ and $B_3O_3D_3$ with normal boron isotope abundances were first obtained with a Perkin-Elmer Infracord spectrophotometer for rapid scanning. Deuterated samples were prepared by replacing D_2O for H_2O in the reaction scheme. Spectra were also recorded for samples of $^{10}B_3O_3H_3$ and $^{10}B_3O_3D_3$ which were prepared by replacing the reactant mixture in the furnace with elemental boron containing 92% ^{10}B.[5] Spectra are illustrated in Fig. 2. Wave length measurements were obtained with a Beckman spectrophotometer Model IR7. These measurements are given in Table I.

(1) Supported by the Advanced Research Projects Agency.

(2) Alfred P. Sloan Fellow.

(3) W. P. Sholette and R. F. Porter, *J. Phys. Chem.*, **67**, 177 (1963).

(4) G. H. Lee, W. H. Bauer, and S. E. Wiberley, *ibid.*, **67**, 1742 (1963).

(5) Isotope Development Center, Oak Ridge National Laboratory, Oak Ridge, Tenn.

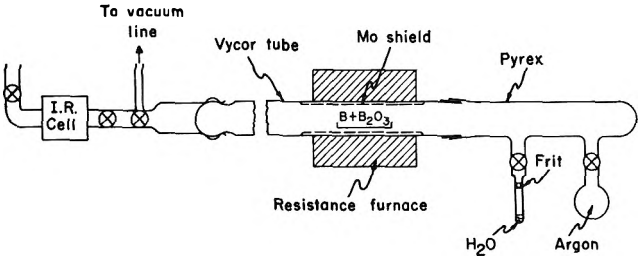

Figure 1. Apparatus for the preparation of gaseous boroxine.

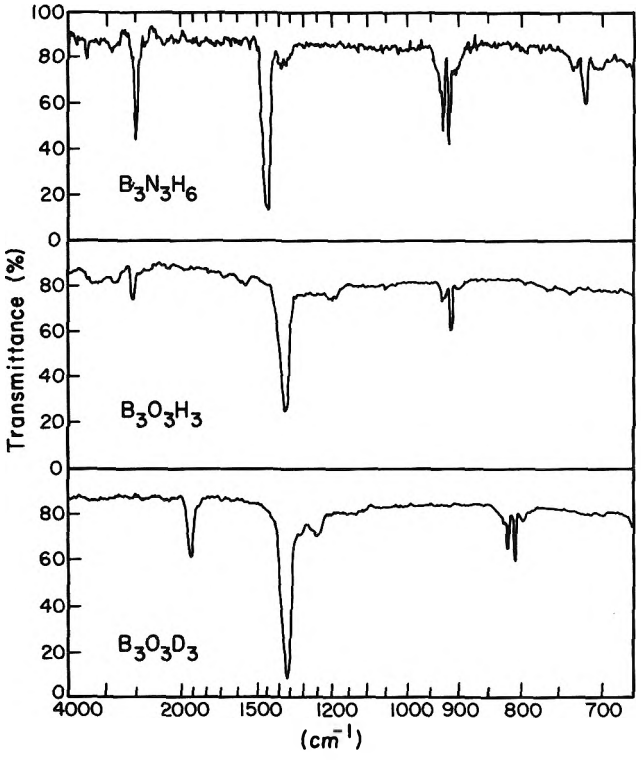

Figure 2. Comparison of the infrared spectra of gaseous $B_3O_3H_3$ and $B_3O_3D_3$ with that of borazine.

In Fig. 2, we also show for comparison purposes a spectrum of gaseous borazine recorded at a pressure of 1.4 torr in the same cell used for boroxine samples. Similarities in the spectra of $B_3N_3H_6$ and $B_3O_3H_3$ support the supposition that the two molecules have similar structures (*i.e.*, planar, D_{3h} symmetry), but differ mainly by the substitution of oxygen atoms for NH groups. From a comparison of absorption intensities we estimate that the pressure of boroxine in the cell was usually between 1.0 and 2.0 torr. The bands at 2530, 1465, and 918 cm.$^{-1}$ in borazine[6,7] apparently correspond to 2620, 1394, and 918 cm.$^{-1}$ in boroxine. The first two of these in borazine have been assigned to class E′ fundamentals and correspond to an in-plane B–H stretch and ring stretch, respectively. The third band has also been assigned to class E′. This involves an in-plane B–H, N–H bending motion. An alternative for the band at 918 cm.$^{-1}$ in boroxine is to assign it to class A_2'', an out-of-plane B–H bend. Band structure associated with the B–H bending mode is complicated in spectra of boroxine samples prepared from materials containing the natural abundances of ^{10}B and ^{11}B. A similar effect is observed with the corresponding band in borazine.[7] This structure is simplified in spectra of $^{10}B_3O_3H_3$ and $^{10}B_3O_3D_3$ (see Fig. 3). With $B_3O_3D_3$ prepared from natural boron three peaks are observed. This effect is probably due to the presence of isotopically substituted species $^{11}B_3$, $^{11}B_2{}^{10}B$, $^{10}B_2{}^{11}B$, and $^{10}B_3$ which are in a ratio of 64:48:12:1 for a natural $^{10}B/^{11}B$ ratio of 1/4. In the spectrum of $B_3O_3H_3$ prepared from natural boron the peak corresponding to $^{11}B_2{}^{10}BO_3H_3$ is apparently missing and is split into two components that accidentally

Table I: Infrared Spectra of Gaseous Boroxines

$B_3O_3H_3$[a]		$B_3O_3D_3$[a]	
Frequency, cm.$^{-1}$	Intensity[b]	Frequency, cm.$^{-1}$	Intensity[b]
2630 (sh)	...	1957 (sh)	...
2620	s	1948	s
1415[c]	...	1935[d]	...
1394	v.s.	1400 (sh)	...
1384	v.s.	1378	v.s.
1213	m	1368	v.s.
937[c]	m	827[c]	w
918	s	822[c]	m.s.
		811	s
$^{10}B_3O_3H_3$		$^{10}B_3O_3D_3$	
Frequency, cm.$^{-1}$	Intensity[b]	Frequency, cm.$^{-1}$	Intensity[b]
2630	s	1987 (sh)	...
2618	s	1974	s
1434	v.s.	1960[d]	...
1422	v.s.	1416	v.s.
1220	m	1404	v.s.
947[d]	...	832	s
935	s	827[e]	w
922[d]	...		

[a] Sample contains boron with natural isotope abundances. [b] v.s., very strong; s, strong; m, medium; w, weak; sh, shoulder. [c] Band apparently due to species containing ^{10}B. [d] Refers to P or R branch of the band. [e] Due to species containing ^{11}B.

(6) B. L. Crawford, Jr., and J. T. Edsall, *J. Chem. Phys.*, **7**, 223 (1939).

(7) W. C. Price, R. D. Fraser, T. S. Robinson, and H. C. Longuet-Higgins, *Discussions Faraday Soc.*, **9**, 131 (1950).

Table II: Partial Vibrational Assignments for Gaseous Boroxines

Fundamental	Symmetry species[a]	$^{11}B_3O_3H_3$, cm.$^{-1}$	$^{11}B_3O_3D_3$, cm.$^{-1}$	$^{10}B_3O_3H_3$, cm.$^{-1}$	$^{10}B_3O_3D_3$, cm.$^{-1}$
γ_6 (asymmetric B–H stretch)	E′	2620	1948	2624	1974
γ_7 (ring stretch)	E′	1389	1373	1428	1410
γ_8 (ring stretch)	E′	1213	...	1220	...
γ_{11} (out-of-plane B–H bend)	A_2''	918	811	935	832

[a] Classification based on assignments for $C_3N_3H_3$ (see ref. 8).

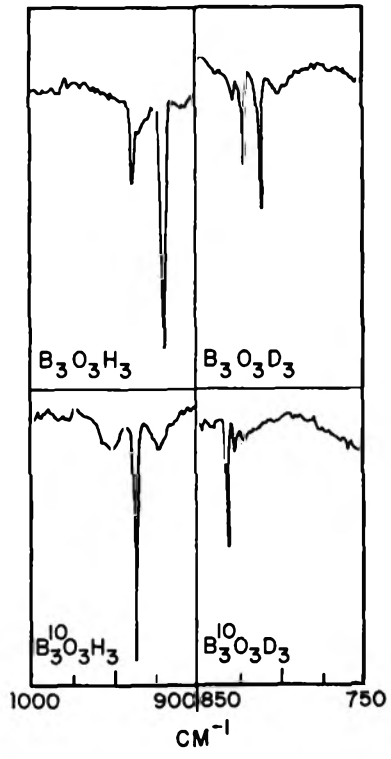

Figure 3. Effect of isotope substitution on the infrared absorption bands for the B–H bending vibration in boroxines.

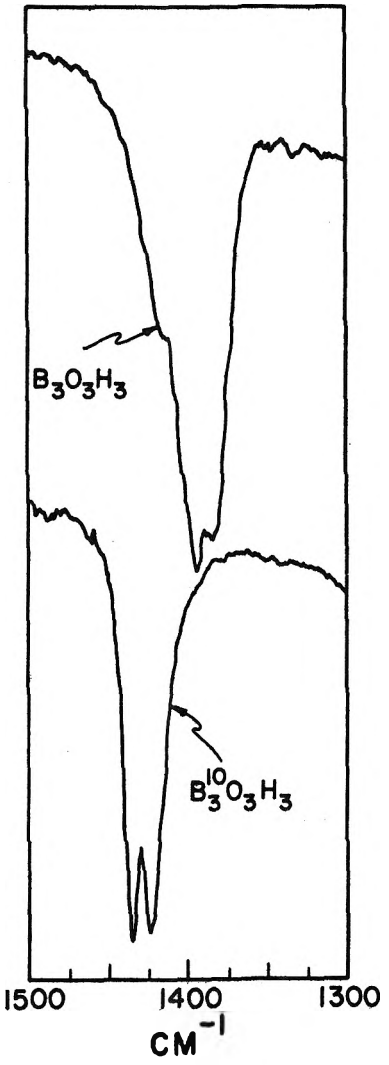

Figure 4. Effect of ^{10}B substitution in the infrared absorption band for the ring stretching vibration in boroxine.

overlap the peaks from $^{11}B_3O_3H_3$ and $^{10}B_2{}^{11}BO_3H_3$. The structure of the strong band near 1400 cm.$^{-1}$ is also simplified in the $^{10}B_3$ molecule (see Fig. 4). Band assignments are given in Table II. The band at 1213 cm.$^{-1}$ is tentatively assigned to E′ and is assumed to be a ring vibration. It was difficult to locate the position of this band in the deuterated spectra because of its low intensity.

Boroxine is also isoelectronic with $C_3N_3H_3$. A detailed infrared analysis[8] of the latter molecule indicates that it has D_{3h} symmetry. Seven fundamentals should be infrared active for the boroxine molecule with this symmetry. Three or at most four bands are observed at the low sample pressures in our experiments. Other bands may be below our spectral cutoff at about 650 cm.$^{-1}$.

(8) J. E. Lancaster, R. F. Stamm, and N. B. Colthup, *Spectrochim. Acta*, 17, 155 (1961).

The reaction of oxygen with gaseous boroxine was studied by observing spectral changes as the two reactants were mixed together. A bulb joining the infrared cell was filled with a mixture of argon and oxygen in a molar ratio of about 10:1 at a total pressure of 1 atm. After the spectrum of a freshly prepared sample of $B_3O_3H_3(g)$ was obtained, a small quantity of reactant gas was let into the cell and the spectrum was again recorded. The spectrum of the reaction products was similar to that reported by Ditter and Shapiro[9] for $B_2O_3H_2(g)$. A second product, which appears as a film on the cell window, has a strong absorption band at about 1260 cm.$^{-1}$ (see Fig. 5). This latter

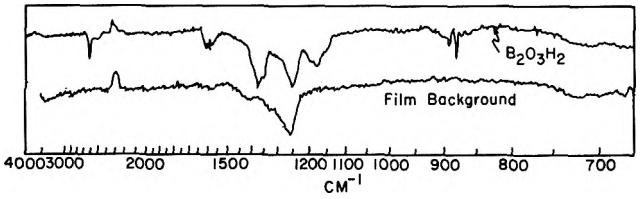

Figure 5. Spectrum of gaseous products formed by the reaction of oxygen and boroxine.

band is probably due to amorphous $B_2O_3(s)$.[10,11] A new band at approximately 1600 cm.$^{-1}$ may be attributed to $B_2H_6(g)$. The over-all reaction may then be assumed to be

$$3B_3O_3H_3(g) + 1.5O_2(g) = 3B_2O_3H_2(g) + B_2O_3(s) + 0.5B_2H_6(g)$$

The reaction is quite rapid; thus, a small air leak in the cell will enhance the rate of disappearance of $B_3O_3H_3$ over that observed in the normal decomposition reaction. In the absence of oxygen a gaseous sample of $B_3O_3H_3$ could usually be maintained for 1.5–2 hr.

Discussion

Similarities in the spectra of $B_3O_3H_3(g)$ and $B_2O_3H_2(g)$ are noteworthy. In Table III we have summarized spectral data for these two molecules. The most probable structure for $B_2O_3H_2(g)$ proposed by Ditter and Shapiro is the highly symmetrical D_{3h} model (*i.e.*, trigonal bipyramid)

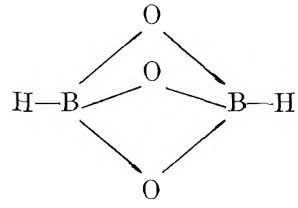

However, in view of the correspondence of the infrared bands of $B_3O_3H_3$ and $B_2O_3H_2$, the C_{2v} model

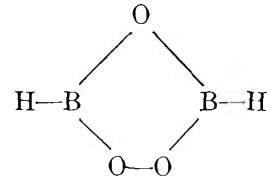

also suggested by Ditter and Shapiro, is perhaps even more plausible. A simple correspondence of isotope shifts on deuterium substitution is also evident. For the B–H stretching vibration $\nu_{^{11}B-D}/\nu_{^{11}B-H}$ = 0.743 and 0.745 for $^{11}B_2O_3H_3$ and $^{11}B_2O_3H_2$, respectively. For the B–H bending frequency the respective ratios are $\nu_{^{11}B-D}/\nu_{^{11}B-H}$ = 0.883 and 0.870. It is also difficult to explain the high B–H stretching frequency (2667 cm.$^{-1}$) for the D_{3h} model of $B_2O_3H_2(g)$ since it seems unlikely that the B–H bond in the tetracoordinated boron structure would be strengthened relative to that in the tricoordinated structure in boroxine.

Table III: Comparison of Fundamental Frequencies of $B_3O_3H_3(g)$ and $B_2O_3H_2(g)$

$^{11}B_3O_3H_3$ frequency, cm.$^{-1}$	$^{11}B_2O_3H_2$[a] frequency, cm.$^{-1}$	Intensity[b]
2620	2667	s
1389	1370	v.s.
1213	1175	v.s.
918	885	s

[a] Data of ref. 9. [b] Estimated from spectrum in Fig. 5.

Table IV: Comparison of Infrared Spectra of Solid and Gaseous $B_3O_3H_3$

$B_3O_3H_3(s)$[a] Frequency, cm.$^{-1}$	Intensity	$B_3O_3H_3(g)$ frequency, cm.$^{-1}$
2620	m	2620
2530	m.s.	...
1560	w	...
1404	s	1394
1335	s	...
1195	m.s.	1213
1115	s	...
903	s	918

[a] Data from ref. 10.

(9) J. F. Ditter and I. Shapiro, *J. Am. Chem. Soc.*, **81**, 1022 (1959)
(10) S. K. Gupta and R. F. Porter, *J. Phys. Chem.*, **67**, 1286 (1963).
(11) W. H. Bauer and S. E. Wiberley, Advances in Chemistry Series, No. 32, American Chemical Society, Washington, D. C., 1961, p. 115.

The spectrum of gaseous boroxine is similar to that for the solid[10] although several of the bands in the latter are quite broad. A comparison of the solid and gas spectra is shown in Table IV. The broad peak with maximum absorption at 1115 cm.$^{-1}$ in the solid is missing from the gas spectrum.[12] Bands in the solid corresponding to a B–H stretch at 2530 cm.$^{-1}$ and to a ring stretch at 1335 cm.$^{-1}$ are also absent in the gas. These bands must be allowed in the infrared through distortion of molecular symmetry due to interactions in the solid phase. Only the asymmetrical B–H stretching frequency (E′) at 2620 cm.$^{-1}$ is allowed in the gas spectrum. The band at 1335 cm.$^{-1}$ in the solid probably results from the splitting of the E′ fundamental that also accounts for the strong component at 1404 cm.$^{-1}$. The second ring stretching fundamental (E′) is likely the band at 1195 cm.$^{-1}$ which corresponds more closely to the band at 1213 cm.$^{-1}$ in the gaseous molecule.

Acknowledgment. We wish to thank Mr. W. Rysz for a sample of borazine and Dr. R. Pohl and Mr. V. Narayanamurti of the Department of Physics for assistance with spectral measurements.

(12) The shift in this band on deuterium substitution was misprinted as 1202 cm.$^{-1}$ in ref. 10. The correct value should be 1020 cm.$^{-1}$.

Adsorption and Oxidation of Formic Acid on Smooth Platinum Electrodes in Perchloric Acid Solutions

by S. B. Brummer and A. C. Makrides

Tyco Laboratories, Inc., Waltham, Massachusetts *(Received December 23, 1963)*

The adsorption and oxidation of formic acid on smooth platinum electrodes were studied in $HClO_4$ solutions by anodic and cathodic chronopotentiometry and by potentiostatic techniques. The oxidation rate at each potential was determined as a function of electrode preparation, pH, and formic acid concentration. Anodic pretreatment activates an electrode for the subsequent oxidation of HCOOH. However, the oxidation rate at any given potential declines with time because of the slow adsorption of a substance which interferes with the oxidation of HCOOH. The kinetics of adsorption and the extent of adsorption of the blocking substance were determined at a series of potentials. The equilibrium adsorption decreases with potential above 0.35 v. and is essentially zero at 0.70 v. The rate of oxidation of HCOOH is first order with respect to the free surface, the HCOOH concentration, and the pH. The oxidation rate increases with potential according to a Tafel type relation (slope $\sim$ 60 mv.) up to potentials of about 0.4 v., but the rate is independent of potential thereafter. The current plateau is not controlled by diffusion. A mechanism for oxidation is suggested in which the slow step is a nonelectrochemical dissociative reaction of HCOOH.

Introduction

The electrochemical conversion of formic acid to CO_2, one of the simpler organic electrooxidations, is of considerable interest because formic acid appears either as an intermediate or a by-product in the oxidation of methanol and formaldehyde. Despite this interest, the mechanism of the reaction is not well understood.

One of the first extensive investigations of the oxidation of formic acid was made by Müller and his coworkers who found[1-3] virtually 100% coulombic efficiency for the reaction

$$HCOOH \longrightarrow CO_2 + 2H^+ + 2e \qquad (1)$$

They also found that the current on smooth and black noble metal electrodes increased with potential at low potentials, declined somewhat as the potential was further raised, and again increased at about the oxygen evolution potential. The limiting current at intermediate potentials was not controlled by diffusion of HCOOH to the electrode surface. Müller and coworkers[1-3] also observed potential oscillations during anodic galvanostatic experiments in solutions containing *HCOOH*.

To account for these results, Müller and Tanaka[3] proposed the following mechanism: at low potentials the sequence of reactions

$$HCOOH_{soln} \longrightarrow HCOOH_{ads} \qquad (2)$$

$$HCOOH_{ads} \longrightarrow H_2 + CO_2 \qquad (3)$$

$$H_2 \longrightarrow 2H^+ + 2e \qquad (4)$$

was postulated and reaction 3 was assumed to be the slow step. At more positive potentials platinum oxide was presumed to be formed on the surface and the rate of (3) declined due to the lesser catalytic efficiency of the oxide. Eventually, another process, the direct discharge of formate ions, *viz.*

$$HCOO^- \longrightarrow HCOO_{ads} + e \qquad (5)$$

$$HCOO_{ads} \longrightarrow H_{ads} + CO_2 \qquad (6)$$

(1) E. Müller, *Z. Elektrochem.*, **29**, 264 (1923).

(2) E. Müller, *ibid.*, **33**, 561 (1927).

(3) E. Müller and S. Tanaka, *ibid.*, **34**, 256 (1928).

$$H_{ads} \longrightarrow H^+ + e \qquad (7)$$

took over and the current again increased with potential.

The potential oscillations were explained[3] by assuming that the current can be supported at a lower potential as soon as H_{ads} becomes available (see reaction 6). However, it is difficult to see why the above mechanism should lead to oscillations unless the concentration of H_{ads} were suddenly raised. Normally, one would expect this concentration to be very low since reaction 7 is fast. Another difficulty with the proposed mechanism is that the decline in the current on platinum commences at about +0.45 v. *vs.* H_2/H^+ (in the same solution), which is well below the potential at which even monolayers of oxide are formed on platinum.[4] Therefore, inhibition of reaction 3 due to oxide formation is unlikely at these low potentials.

Herasymenko[5] did not observe a maximum in the current–potential curve as found by Müller, *et al.*,[1-3] but he did find a limiting current. The initial rise in the current at low potentials was assumed[5] to be due to the oxidation of adsorbed formic acid molecules on active sites on the electrode, and it was postulated that the current stops increasing when the rate of electrochemical oxidation exceeds the rate of formic acid adsorption, this last being a nonelectrochemical step. This implies that the formic acid coverage decreases as the potential is raised. It was also suggested that formic acid may be oxidized at high positive potentials without prior adsorption.

Herasymenko[5] found lower currents in the presence of chloride and bromide ions and attributed this effect to the replacement of HCOOH on the electrode by these anions. Schwabe[6] has also suggested that the exclusion of formic acid from the double layer by anion adsorption is responsible for the potential-independent limiting current.

However, the results of Conway and Dzieciuch[7] suggest a possible difficulty with this interpretation. They studied the anodic process using pure HCOOH as solvent and also found a limiting current in the intermediate potential region. In this case only formate ion is present in the solution. If this ion is preferentially adsorbed at positive potentials, the existence of a limiting current implies that the discharge of the formate ion is not as easy as the oxidation of the HCOOH molecule. That this may be the case is suggested by the observation that in basic solution (where HCOOH dissociates) methanol is converted almost quantitatively to $HCOO^-$ which does not easily react further,[8] whereas in acid solution the yield is almost entirely CO_2.

Conway and Dzieciuch[7] do not, in fact, attribute the limiting current to anion displacement of adsorbed HCOOH. Instead, they assume a mechanism of the type shown in eq. 5–7. They account for the limiting current by postulating that reaction 6 is rate-determining and that the coverage by $HCOO\cdot$ radicals increases to unity at the start of the current plateau and stays at this value until an alternative reaction takes over at a higher potential. The presence of numerous side products in Kolbe electrolyses[9,10] supports the theory of free radical intermediates in the oxidation.

Schwabe[6] studied the decomposition of formic acid to CO_2 and H_2 and found a maximum in the rate at about pH 4.2. From this he concluded that HCOOH itself, and not $HCOO^-$, is the reacting species although the situation must be more complex to account for the maximum. He also found that the reaction is self-poisoning. He found no evidence for the reaction

$$HCOOH \longrightarrow CO + H_2O \qquad (8)$$

which suggests that the poisoning agent is not CO. However, a monolayer of adsorbed CO, which has been postulated in connection with the self-poisoning observed during anodic oxidation of HCOOH (see below), could not have been detected in these experiments. Schwabe suggested that the rate-limiting step for the anodic oxidation is the decomposition to H_2 and CO_2 (reaction 3). The current falls in the intermediate potential region due to exclusion of HCOOH from the double layer by anion adsorption and then increases due to an alternative process, *viz.*

$$2OH^- + HCOOH \longrightarrow 2H_2O + CO_2 + 2e^- \qquad (8a)$$

Another possibility is that the formate ion is discharged directly at high, positive potentials.

Breiter[11] studied the oxidation of HCOOH in 1 *N* $HClO_4$ on bright platinum using cyclic voltametry and chronopotentiometry. The chronopotentiometry (both anodic and cathodic) was performed during a slow (30 mv./sec.) potential sweep with sufficiently high current densities to eliminate diffusional effects. Thus, he was able to measure the extent of adsorption

(4) H. A. Laitinen and C. G. Enke, *J. Electrochem. Soc.*, **107**, 773 (1960).

(5) P. Herasymenko, *Ukr. Khim. Zh.*, **4**, 439 (1929).

(6) K. Schwabe, *Z. Elektrochem.*, **61**, 744 (1957).

(7) B. E. Conway and M. Dzieciuch, *Can. J. Chem.*, **41**, 21, 38, 55 (1963).

(8) M. J. Schlatter, "Fuel Cells," Vol. 2, G. J. Young, Ed., Reinhold Publishing Co., New York, N. Y., 1963, p. 200.

(9) K. Clusius and P. Holeman, *Z. physik. Chem.*, **B35**, 261 (1937).

(10) K. Clusius and W. Schanzer, *ibid.*, **A190**, 241 (1941); **A192**, 223 (1943).

(11) M. W. Breiter, *Electrochim. Acta*, **8**, 447, 457 (1963).

of an organic species (he suggests that this is HCOOH) on the electrode. He found a maximum adsorption of 260 μcoulombs per true cm.^{2} (210 μcoulombs for H atom adsorption[12]). He also found that in the anodic sweep, with (HCOOH) = 1 M, the adsorbed charge was constant up to ~0.8 v. but declined rapidly with further increase in potential. It will be shown below that these measurements involve a kinetic displacement of the adsorption equilibria and, therefore, are not directly pertinent to the steady-state oxidation of HCOOH.

Buck and Griffith[13] have also investigated the oxidation of formic acid by cyclic voltammetry and with anodic chronopotentiometry. Their most important result was the discovery that the chronopotentiogram is a function of the time the electrode has been in contact with the solution, but they did not make a detailed investigation of this phenomenon.

Slott[14] investigated the reaction with chronopotentiometry and also examined open circuit potentials. He found that after anodic pretreatment, the open circuit potential of the platinum electrode went through a minimum which was close to the hydrogen potential. He assumed that this was due to the decomposition of HCOOH to H_2 and CO_2. After the minimum, the potential rose in such a way as to suggest displacement of adsorbed hydrogen produced by reaction 3 by another species. He also found a "wait-time" effect in which the amount of oxidation possible decreased with increase of wait-time. He suggested that the adsorbed species which caused poisoning of the electrode was CO, but offered no proof of this.

Recent results[15] using cyclic voltammetry indicate that the peaks for the oxidation of CO and of HCOOH are similar and that the extent of adsorption during the oxidation of these two substances is also comparable. On the basis of these results it was concluded[15] that the poisoning agent is CO.

Munson[16] used chronopotentiometry to study the HCOOH oxidation and observed that the rate-limiting step is a pre-electrochemical reaction. The rate of this step reaches a maximum at a pH just less than 5, which suggests a mechanism similar to the decomposition to H_2 and CO_2, as observed by Schwabe.[6] However, Munson discounted the possibility that oxidation involved the direct oxidation of H_2, formed from the HCOOH by decomposition, because the HCOOH oxidation rate is much less than the H_2 oxidation rate at the same potential. He suggested that some other step, common between the two reactions, must be responsible for the observed pH correlation.

From the foregoing, it is clear that despite considerable interest in this important reaction, our understanding of its mechanism is still incomplete. The only adsorption measurements are those of Breiter[11] which, unfortunately, do not refer to steady-state conditions. The kinetics of adsorption have not been investigated and, indeed, some basic information on the steady-state current–potential behavior is not available. In the present study, measurements have been made of current–potential curves as a function of electrode preparation, pH, and HCOOH concentration. Also, studies of the adsorption kinetics and of steady-state adsorption have been made with anodic and cathodic chronopotentiometry.

Experimental

The electrochemical cell was constructed of Pyrex glass and was of conventional design. The central compartment contained the working electrode and had sufficient volume to minimize concentration changes during an experiment. The reference electrode was a platinized platinum cylinder immersed in the test solution which was saturated with purified hydrogen. Potentials were measured through a Haber–Luggin capillary, with a 0.15-cm. o.d. The counter electrode was also a platinized platinum cylinder and was connected to the main compartment *via* a coarse-fritted disk. All electrodes were mounted in such a way that only glass and Teflon came into contact with the solution. The platinum working electrodes were of 99.98% purity and were cylinders with an apparent area of 1–2 cm.^{2}. They were polished on silk with wet α-Al_2O_3 of particle size 0.3 μ, and were then washed with chromic–sulfuric acid, triply distilled water, and portions of the test solution.

The electrode area was estimated by cathodic charging in 1 N $HClO_4$ solution (at ~50 ma./cm.^{2}), from +0.5 v. *vs.* H_2/H^+ in the same solution, while on the anodic part of a slow triangular sweep (0.3 to 1.25 v.). This method has been used by Breiter[11] and gives excellent reproducibility if the solution is not stirred. All results are reported per real cm.^{2} on the basis of a H-atom coverage of 210 μcoulombs/cm.^{2} at 0.0 v.[12]

Solutions were made up with triply distilled water (once from alkaline permanganate) and were usually 1 M with respect to ClO_4^-. Different acidities (in the pH range −0.33 to +1.55) were obtained by adding

(12) F. G. Will and C. A. Knorr, *Z. Elektrochem.*, **64**, 258 (1960).

(13) R. P. Buck and L. R. Griffith, *J. Electrochem. Soc.*, **109**, 1005 (1962).

(14) R. Slott, Doctor of Science Thesis, Massachusetts Institute of Technology, January, 1963.

(15) California Research Corp., Richmond, Calif., "Investigative Study Relating to Fuel Cells," Report No. 10, Jan. 1–April 30, 1963, Contract DA-49-186-ORD-929.

(16) R. A. Munson, General Electric Research Labs, Schenectady, N. Y., Summary Report No. 1, March 31, 1962, Contract DA-44-009-ENG-4853.

appropriate quantities of NaOH to 1 M $HClO_4$ (both Baker A.R. grade). The working and counter electrode compartments were flushed with a continuous slow stream of purified N_2. Connections were made with Teflon tubing, and the stopcocks, required to control the rate of gas flow, had Teflon barrels. The formic acid was Baker A.R. grade.

Potential control was maintained with a Wenking fast-rise potentiostat. Switching to a galvanostatic circuit, for cleaning and for chronopotentiometry, was achieved with a Western Electric 275 C mercury-wetted relay, activated by a microswitch. Current transients were measured across a 0.1% General Radio Co. decade-resistance box with a Sargent SR recorder. Potential transients were observed on a Tektronix Type 535A oscilloscope using a Type D vertical preamplifier.

Unless otherwise stated, all measurements were made in an oil-filled bath maintained at 40 ± 0.2°. Potentials are reported *vs.* H_2/H^+ in the relevant solution.

Results and Discussion

Current–Potential Curves. Current–potential curves for the oxidation of HCOOH have been determined for platinum,[1-3,5,7] but a careful quantitative study in acid solutions, particularly on the bright metal, is not available. Most of the reported work is qualitative in nature and/or has been performed with black electrodes. Thus, simple information for the order of the oxidation with regard to pH and HCOOH has not been firmly established, nor has any quantitative treatment been made of the Tafel line observed at low potentials. The major stumbling block in obtaining such information, despite reports to the contrary,[7] is the irreproducibility of the current–potential behavior.

Preliminary experiments indicated that variations in current–potential behavior up to one order of magnitude (in current) are possible and that the system responds sluggishly to changes of potential. It was believed that the reason for this sluggishness and irreproducibility was the slowness of the adsorption characteristics of the system and, therefore, at each potential under study, one should adsorb from the solution onto a clean electrode.

To test this idea, the electrode was "cleaned" anodically (1–5 sec. at real current densities of 25–200 ma./cm.^{2}) and then returned to potentiostatic control. Its behavior was then observed as a function of time. After this electrode pretreatment, the rate of oxidation declined with time, at first rapidly and then more slowly. The rate of decline, during the initial period of decay (1 min.), was not affected by stirring the solution, but at longer times (1–10 min.) the current decreased somewhat more when the solution was stirred. The cleaning current density and the duration of the pulse did not affect the subsequent decline of the current.

A standard cleaning procedure was selected as 50 ma./cm.^{2} for ~1 sec., with stirring during the anodic pulse and for 10 sec. afterward. By this procedure, results reproducible to ~10% were obtained from run to run in freshly prepared solutions. The reproducibility tended to be better in the more acid solutions. It was observed (Fig. 1) that the rate of decline of the current was a function of the potential and was greatest at the lower potentials.

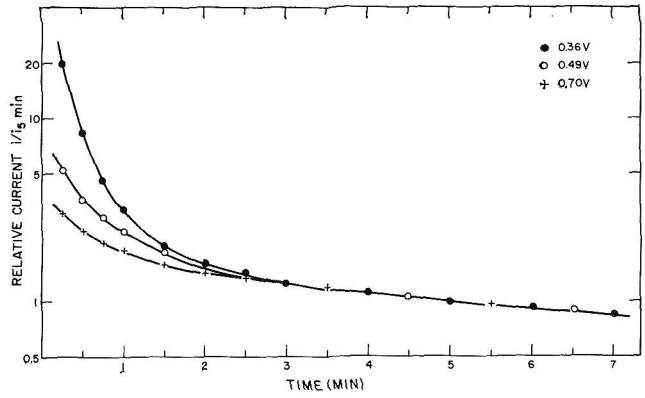

Figure 1. Decline of rate of oxidation, at various potentials, as function of time since cleaning for 1 M HCOOH in 2 M $HClO_4$.

Experiment showed that cleaning the electrode by cathodizing it with large current densities gave results similar to those obtained by anodic cleaning, providing that care was taken to remove the evolved H_2. At 0.7 v. the electrode was cleaned both anodically and cathodically. The agreement between the subsequently observed oxidation rates was sufficiently good to permit use of cathodic pretreatment for potentials above 0.7 v., where anodic pretreatment leaves a heavy surface oxide.

In Fig. 2, the current–potential curves, taken at different times, are plotted for 1 M HCOOH in 1 M ClO_4^- at pH 1.0. It is observed that, during the first 3 min., the apparent Tafel slope, b, decreases from a value of 106 mv. to ~60 mv. and, thereafter, remains constant. In Table I, data for a number of systems are presented. Notwithstanding that the current is still decreasing slowly, little variation is seen in b, as determined at 5 and 10 min. after activation. It is reasonable to assume that the slope at 10 min. is essentially the limiting slope, *i.e.*, b_t at $t \rightarrow \infty$. In molar HCOOH, $b_{t\rightarrow\infty}$ tends toward 60 mv. In more dilute solutions, some-

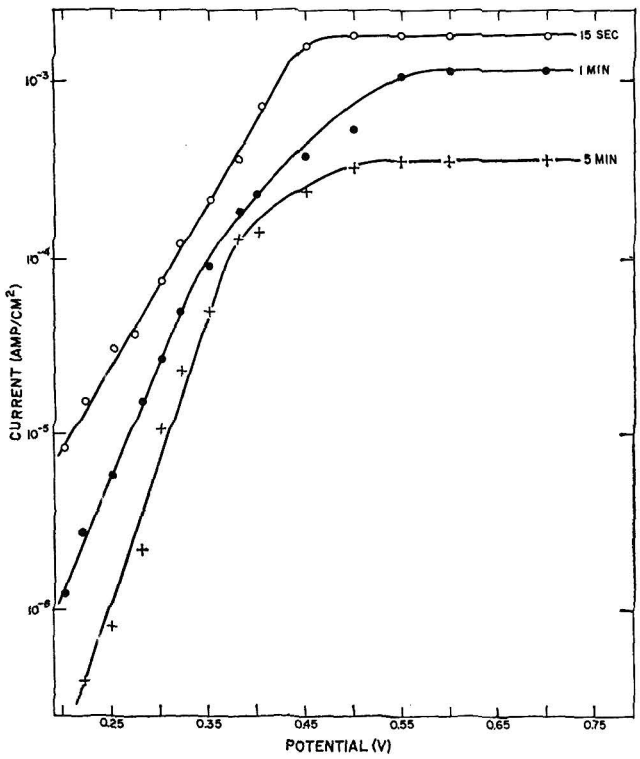

Figure 2. Log current vs. potential for oxidation of 1 M HCOOH at pH 1.0.

what larger Tafel slopes are observed; in 0.01 *M* HCOOH, the plot is so curved as to preclude the meaningful evaluation of a Tafel parameter.

Table I: Tafel Slope (in mv.) at Various Times after Activation

pH	Concn. of HCOOH, *M*	15 sec.	30 sec.	1 min.	2 min.	5 min.	10 min.
−0.33	1.0	62	64	70	80	60	63
−0.33	0.1	43	45	50	70	83	87
−0.33	0.01	Indeterminate slope (plot not linear)					
+0.05	1.0	73	78	75	85	75	..
+1.0	1.0	106	109	77	72	59	58
+1.45	1.0	85	70	75	65	58	61
+1.55	1.0	70	65	58	63	60	57

Whatever the reason for the apparent change in the current during the decay after activation (the change of Tafel slope suggests, *inter alia*, a change of the reaction mechanism), it may be postulated that $b_{t\to\infty}$ refers to the mechanism of the reaction in steady state of the electrode surface. The general observation is made, in general agreement with previous observations,[1-3,5,7] that a limiting current, independent of potential, is observed at potentials higher than about 0.45 v. This plateau is not directly affected by stirring (not a diffusion-limited current) nor is the potential of its commencement a significant function of pH or of time since activation.

Table II gives the pH dependence, (∂ log i/∂ pH), of the oxidation rate in 1 *M* HCOOH at 0.25 v. *vs.* n.h.e., a potential which falls within the Tafel region at all pH values. An example of a plot of log *i vs.* pH is presented in Fig. 3; it is seen that the linearity of the

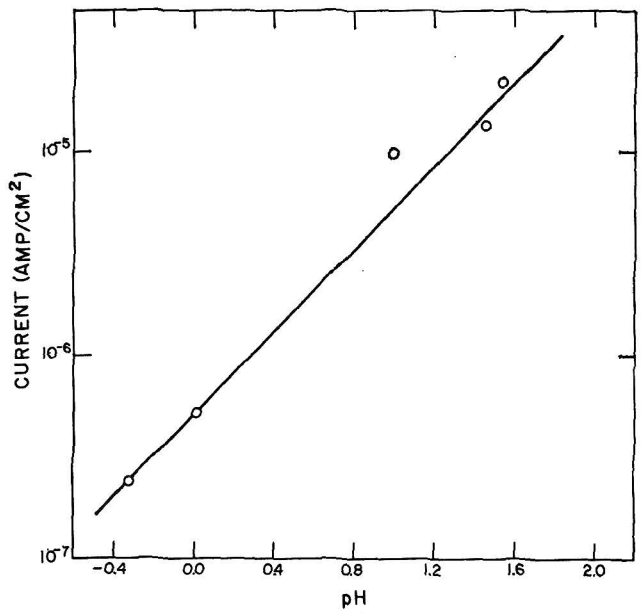

Figure 3. Log current *vs.* pH for 1 *M* HCOOH at 0.25 v. *vs.* N.H.E. Currents refer to 5 min. after cleaning the electrode.

plot is reasonably good. From Table II, it is apparent that (∂ log i/∂ pH) is about +1.0 and is only slightly dependent on the time after activation. In the limiting current region, (∂ log i/∂ pH) is independent of the time from activation, and is about +0.2; however, the plots show considerable scatter.

The order of the reaction with respect to formic acid, in the concentration range 0.01–1.0 *M*, and at times

Table II: (∂ log i/∂ pH)$_{0.25\text{ v.}}$ at Various Times after Activation

Time	∂ log i/∂pH
15 sec.	+1.35
30 sec.	+1.30
1 min.	+1.23
2 min.	+1.10
5 min.	+1.03
10 min.	+1.10

after activation in excess of ~2 min., is close to unity over the whole potential region.

Before discussing the electrochemical parameters, b and $(\partial \log i/\partial \text{pH})$, and their variation at short times after the activation, the extent and kinetics of the adsorption process on the platinum electrode from formic acid solutions will be considered in detail.

Steady-State Adsorption

The extent of adsorption of oxidizable species may, in principle, be determined by passing a large anodic current through the electrode and by estimating the charge corresponding to any transition periods which may appear in the chronopotentiogram. A potential–time curve in 1 M HCOOH is presented in Fig. 4. This curve, obtained by switching rapidly from a potentiostatic to a galvanostatic circuit, is seen to comprise four regions. During AB, the electrode potential rises steeply, corresponding to double layer charging.

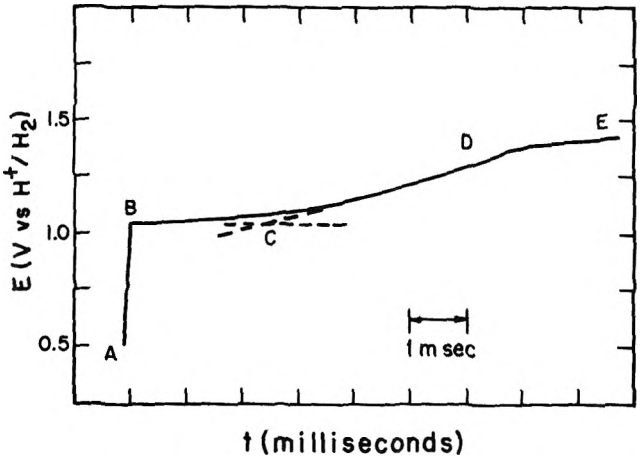

Figure 4. Anodic chronopotentiogram for oxidation of HCOOH adsorbed from 1 M $HClO_4$ at 0.2 v.

In the region BC, the potential is almost independent of time, although the exact point at which it merges into the more steeply rising part CD is rather indefinite. Finally, the potential becomes steady, no doubt as a result of the evolution of O_2 and the oxidation of HCOOH on an oxide-covered electrode.

The shape of the anodic time–potential curve is similar to that reported by Breiter.[11] Presumably, the region BC corresponds to the oxidation of adsorbed species on the electrode. It may also include a contribution from surface oxidation and from oxidation of species diffusing to the electrode. That the latter is not important is shown by the fact that charge, q_{BC}, is independent of the anodic current density. The indistinctness of the arrest and the possibility of concomitant surface oxidation pose some difficulties in evaluating the extent of adsorption from the charge corresponding to the BC region.

In order to overcome these difficulties, Breiter[11] compared the anodic trace he obtained in pure $HClO_4$ with that in HCOOH. The two curves coincided in the potential region DE and thus, by comparing the transition times for the region AD for the two cases, the adsorbed charge for HCOOH can be calculated.[11] The major assumption here is that the total extent of surface oxidation of platinum is the same in the presence and in the absence of HCOOH. This assumption was supported from measurements,[11] carried out by cathodic chronopotentiometry, of the extent of surface oxidation at various potentials during the anodic triangular sweep.

In our experiments, we did not observe the coincidence of the parts DE of the traces; this suggests that the assumption about the extent of oxidation of platinum in the two cases is probably not justified. We estimated the extent of adsorption directly from the region BC of the trace, applying no correction for surface oxidation. There may be a small contribution to q_{BC} from surface oxidation, but the evidence on this point, as presented by Breiter,[11] is not conclusive. His determinations of surface oxidation were made during a slow (30 mv./sec.) anodic voltage sweep and, by his own account, the electrode was (a) already bare when it reached platinum oxide potentials, and (b) was at these high potentials for some seconds before the cathodic charge determination. These conditions are far removed from those holding during the initial parts (AB and BC) of an anodic galvanostatic pulse. In the latter case, the electrode is covered with adsorbed material which must be largely removed before surface oxidation can commence. Furthermore, the regions AB and BC of the anodic pulse refer to times of the order of a few milliseconds, whereas the experiments quoted in ref. 11 deal with a surface which had been at these high potentials for a few seconds. Therefore, it is probable that surface oxide formation can be neglected during the stage corresponding to BC and that this arrest can be attributed entirely to the oxidation of an adsorbed organic species.

The surface coverage can also be determined by cathodic galvanostatic pulses. This method relies on the observation that essentially a monolayer of H is adsorbed before hydrogen evolution begins.[12,17] Hydrogen adsorption commences at ~0.35 v. and is complete in acid solution at ~0.0 v. The extent of adsorption

(17) A. N. Frumkin, "Advances in Electrochemistry and Electrochemical Engineering," Vol. 3, John Wiley and Sons, Inc., New York, N. Y., 1963.

of an organic substance can be determined from the difference between the charge corresponding to a monolayer of hydrogen and the charge actually observed, by assuming that H adsorbs only onto free surface during a cathodic pulse in HCOOH, *i.e.*, that H does not displace the adsorbed organic substance. This assumption is supported by the observation of θ_H values ranging, under various conditions, from $\theta_H \rightarrow 0$ to $\theta_H = 1$. If there were a marked tendency for the adsorbed organic molecules to be displaced, one would expect to see discontinuities in the range of θ_H observed; specifically, one would expect $\theta_H \rightarrow 1$ independently of the initial state of the electrode. The question whether an organic molecule (HCOOH or some other organic molecule resulting from its decomposition or reaction at the electrode) or H adsorbs onto bare sites as the potential decreases is answered by the observation that on a bare surface, *i.e.*, one formed by anodization at high potentials, the H coverage is the same as that found in the absence of HCOOH.

Therefore, it is possible to obtain two independent measurements of the extent of adsorption of organic molecules, one directly from q_{BC} and the other from the cathodic-pulse experiments. In order to compare these, some assumption must be made about the area (or number of equivalent hydrogen sites) occupied by each adsorbed molecule and about the number of electrons involved in the oxidation of each adsorbed molecule. The results suggest that the following possibilities can be entertained for the adsorbed species: (a) adsorption of formate radicals (one-electron oxidation), one radical per site; (b) adsorption of formic acid or of formate ion (two-electron oxidation), one molecule or ion per two sites; (c) adsorption of formic acid (two-electron oxidation), each molecule occupying an area of 14 Å.[2,7,11]; (d) adsorption of some other organic substance resulting from formic acid with a ratio of 1 electron (for anodic oxidation) per surface site.

Adsorption of formate radicals is unlikely since the maximum observed charge (q = 210 μcoulombs/cm.[2]) from anodic pulses would imply that a formate radical occupied an area of about 7 Å.[2], a value considerably less than the estimated cross-sectional area of a formic acid molecule (~14 Å.[2]). Since it is not possible to arrive at a choice between the remaining possibilities on the basis of the adsorption data alone, the question of the identity of the adsorbed species will be deferred until data on the kinetics of adsorption are presented. It will be assumed for the moment that a charge of 230 μcoulombs/cm.[2] corresponds to a monolayer, this being approximately the value obtained under assumptions (b) through (d). Thus, we take $\theta = q_{BC}$ (μcoulombs/cm.[2])/230 from the anodic runs and $\theta = 1 - \theta_H$ from the cathodic runs.

Because the coverage was a function of the time the electrode was kept at a fixed potential (see below), it was necessary to adopt a standard technique in measuring θ. The electrode was prepared with an anodic pulse in the usual way and returned to the potential of study. The solution was vigorously stirred with N_2 during this pretreatment and for 2–3 sec. afterward to remove any O_2 evolved during anodization. The θ measurement with an anodic pulse was made 2 min. after the electrode had been kept at the chosen potential. For the cathodic determinations of θ, the final coverage was estimated from the θ *vs.* t curve and also from an extrapolation of the equation describing the adsorption kinetics (see below) to infinite time. The agreement between these values was good (5–15%); but generally, for reasons which are discussed later, it was preferred to use the latter.

The results of these determinations are presented in Fig. 5 which shows that θ is close to unity at low potentials, begins to decrease at about 0.3 v., and decreases essentially to zero at about 0.7 v. This is in contrast to the observation of Breiter[11] that θ remained close to unity up to about 0.8 v. in 1 *M* HCOOH.

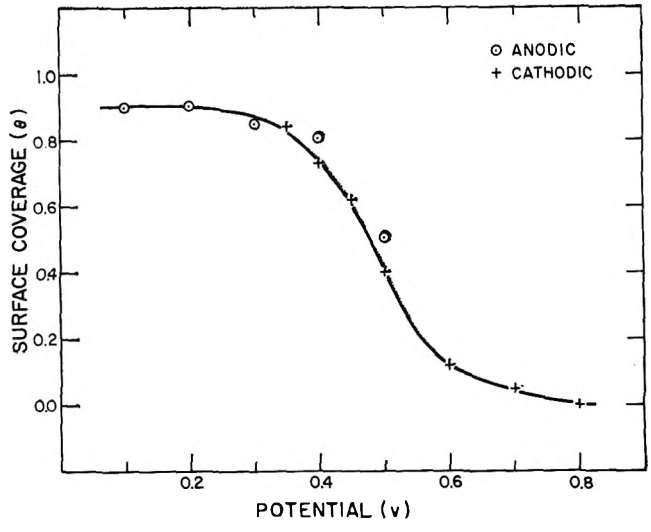

Figure 5. Coverage as a function of potential for 1 *M* HCOOH in 1 *M* $HClO_4$ at 40°.

Figure 5 also shows that suggested mechanisms of the reaction which account for the limiting current in terms of a limitingly high coverage of an adsorbed species (in particular, $HCOO^{\cdot}$; see, *e.g.*, Conway and Dzieciuch[7]) cannot be correct. It also seems likely that the adsorbed species is not an anion (*viz.* $HCOO^-$) since the

extent of adsorption decreases as the potential becomes more positive. However, if the source of the anion were an uncharged species (*e.g.*, HCOOH), its surface concentration might still decline at anodic potentials.

A further point of interest is that the values of θ determined at 0.40 and 0.45 v. were constant in the concentration range 0.05–1.0 *M*. At 0.01 *M* the coverage is lower, but only by a few per cent. This insensitiveness of θ with respect to HCOOH in this concentration range will be of importance in interpreting the mechanism of the reaction.

Adsorption Kinetics

It was thought that an explanation of the decline in rate as a function of time after activation might be found in terms of slow adsorption onto the electrode, particularly since the initial rate of decline is much greater in the potential region where the total extent of adsorption is highest (Fig. 1). Adsorption kinetics were determined by measuring θ as a function of time after activation by using the cathodic-charging method. Measurements were taken in the region 0.35–0.70 v.

Adsorption is indeed slow (see, *e.g.*, Fig. 6), the total extent of adsorption at a given potential being scarcely reached at 2 min. after electrode cleaning. It was also found that the extent of adsorption increased more rapidly, and to a somewhat higher final value (~0.05–0.10 unit of θ), if the solution was stirred. The effect of stirring becomes important only about 45 sec. after cleaning. It is thought that this effect arises from the presence of small amounts of impurity in the solution which, at longer times, can successfully compete for the remaining free surface. The major known impurity is CH_3COOH (0.3 mole %), but independent experiments showed that this material is not significantly adsorbed, even when present at concentrations far in excess of its concentration in the formic acid solutions. The results presented in the figures refer to unstirred solutions which probably represent more accurately the behavior of the HCOOH system itself.

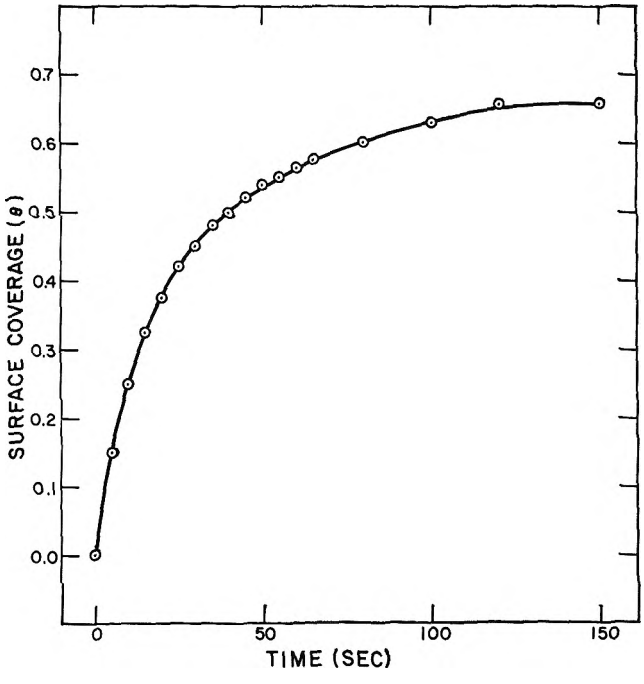

Figure 6. Adsorption of HCOOH from 1 *M* $HClO_4$, at 0.45 v., as a function of time.

It is seen (Fig. 6) that adsorption increases, at first rapidly and then more slowly, in the first 150 sec. after cleaning of the electrode. The fact that adsorption is so slow demonstrates strikingly the necessity of controlling carefully the time for which the electrode is in contact with the solution before a measurement is made. It also indicates clearly that the results obtained from cyclic voltammetry[11,13,15,18] are only qualitative and may be misleading.

The adsorption kinetics were tested with an equation of the type

$$\frac{d\theta}{dt} = k(1 - \theta) - k'\theta \qquad (9)$$

Equation 9 leads, at long times, to a Langmuir-type isotherm. Integration of eq. 9 yields

$$\log (1 - \alpha\theta) = \frac{-\beta t}{2.30} + \gamma \qquad (10)$$

where

$$\alpha = \left(1 + \frac{k'}{k}\right) \qquad (11)$$

$$\beta = k + k' \qquad (12)$$

and γ is a constant.

A typical example of the fitting of eq. 10 to the adsorption data is given in Fig. 7. This figure shows that over most of the range of time and θ, the data are represented well by this equation, although at times less than 15 sec. after activation, a systematic curvature is observed. This could be due to oxygen evolved in the activation process which may interfere with the adsorption process. However, the deviation is probably more fundamental than this since the main plot does not extrapolate to $\theta = 0$ at $t \rightarrow 0$.

At times in excess of about 80 sec. after cleaning, positive deviations are observed. It is probable that the influence of impurities becomes important at such

(18) A. L. Juliard and H. Shalit, *J. Electrochem. Soc.*, **110**, 1002 (1963).

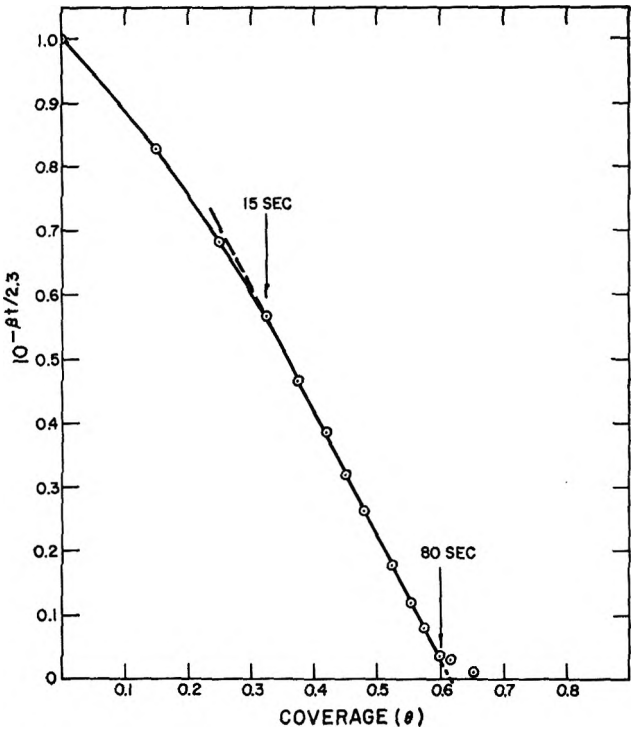

Figure 7. Fitting of eq. 10 to adsorption data for 1 *M* HCOOH in 1 *M* $HClO_4$ at 0.45 v.

long times and, therefore, that the most reliable value for $\theta_{t\to\infty}$ is obtained by extrapolating the plot in the manner indicated.

The plot fitted the data, within the above limitations, for adsorption at 0.35, 0.40, and 0.45 v. It is not possible to examine the equation below 0.35 v. because hydrogen adsorption on platinum is appreciable in this range. At 0.5 v. the equation apparently was not obeyed. The good fit obtained with eq. 10, which may extend right through the Tafel region of potential, suggests the validity of Langmuir conditions for the adsorbate. Thus, the adsorbate almost certainly is not charged since a significant change in kinetics with coverage, expected for a charged species, is not observed.

Constants for eq. 10 are given in Table III. The desorption constant, k', is sensibly independent of the concentration of HCOOH and, more surprisingly, of potential. It might have been supposed that the main desorption process is *via* oxidation, in which case its rate should be potential dependent. If we take a mean rate of 1.2×10^{-2} sec.$^{-1}$ and assume that a monolayer is about 200 μcoulombs/cm.^{2}, we find a desorption rate (at a monolayer) equivalent to 2.4 μa./cm.^{2}. It is interesting to note that this is considerably higher than the rate of oxidation under the same conditions of CO, which has been suggested[14,15] as the (blocking) adsorbed species in the HCOOH system.

The adsorption constant, k, decreases a little as the potential rises (as indeed it must if θ is to approach zero at high potentials), but by no means is the decrease sufficient to suggest that a cathodic discharge reaction is the rate-limiting step in adsorption. The adsorption constant increases approximately logarithmically with increase of HCOOH concentration.

Table III: Constants for Eq. 10 in 1 *N* $HClO_4$ at 40°

Potential, v.	HCOOH concn., *M*	β, $\times 10^{-2}$	α	γ	$k \times 10^{-2}$, sec.$^{-1}$	k' $\times 10^{-2}$ sec.$^{-1}$
0.35	1.0	9.2	1.19	−0.38	7.8	1.4
0.40	1.0	5.7	1.37	−0.19	4.2	1.5
0.40	0.1	3.3	1.36	−0.26	2.4	0.9
0.40	0.05	4.3	1.35	−0.16	3.2	1.1
0.40	0.01	3.2	1.57	−0.13	2.1	1.1
0.45	1.0	3.8	1.61	−0.07	2.4	1.4
0.45	0.1	3.2	1.76	−0.08	1.8	1.4
0.45	0.05	2.5	1.85	−0.05	1.3	1.2
0.45	0.01	1.95	2.38	−0.05	0.85	1.1

Relationship between Extent of Adsorption and Rate of Oxidation

The relationship between i and θ is shown in Fig. 8. It is a general observation that the oxidation current falls as the coverage increases. This indicates that the adsorbed species is not electrochemically active but rather that it poisons the main reaction. At 0.40 and 0.45 v. the current is directly proportional to the free surface $(1 - \theta)$ in the range investigated, $0.2 \leqslant \theta \leqslant 0.8$. It also seems that at 0.35, 0.40, and 0.45 v. the intrinsic rate of the reaction per unit of bare surface is the same. The observed ultimate rate of the reaction is higher at 0.45 v. than 0.40 v. because the coverage ultimately attained at 0.45 v. is lower. At 0.50 v., i still varies linearly with θ over most of the range investigated, but at low values of θ, i decreases more rapidly with increasing θ. At 0.60 v., where the i–θ relation was observed in the region $0 < \theta \leqslant 0.2$, i decreases very rapidly with increase in θ. This rapid variation would be expected if the most active sites for oxidation were blocked first.

A result, which is at first surprising, is that at a given θ, the activity of the electrode is higher at 0.35, 0.40, and 0.45 v. than at 0.50 and 0.60 v. That this is necessary to maintain the self-consistency of the data follows from the fact that whereas θ^{equilib} declines with increase of potential, the rate of oxidation (in the potential region above ~0.50 v.) is independent of the potential. The apparent decrease in the activity of

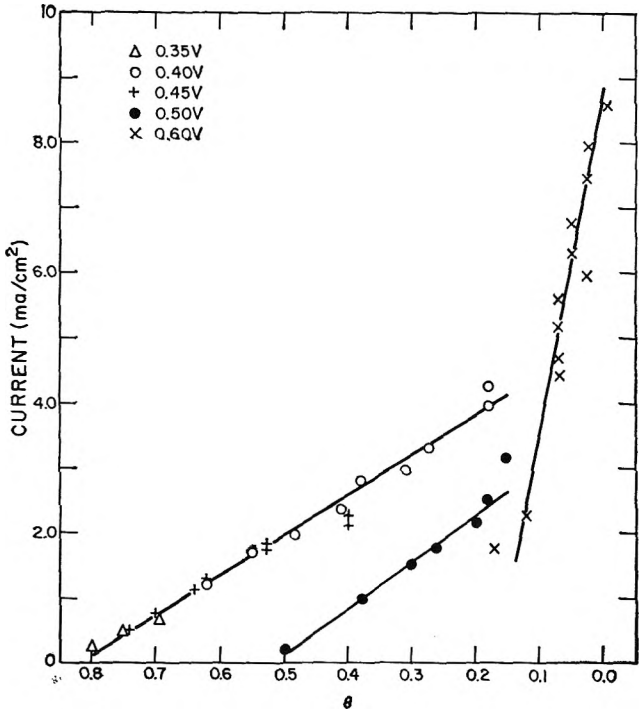

Figure 8. Oxidation of HCOOH in 1 M $HClO_4$ at various potentials as a function of the coverage of the electrode.

the electrode with increase in potential may be explained by assuming that as the potential rises, the (uncharged) active species is excluded from the double layer by ClO_4^- adsorption. This would also account for the fact that the total extent of adsorption decreases as the potential rises.

It is clear from Fig. 8 that the explanation for the long term current–time transients after the electrode cleaning, reported above, lies in the slow adsorption of a blocking material on the electrode. The fact that this effect is still important at higher potentials, where $\theta^{equilib}$ is small, is probably due to the much greater activity of the very first sites on which adsorption occurs (Fig. 8).

The suggestion[19] that the activity of the platinum electrode is related to a half-reduced oxide, which acts as an "electron bridge" for oxidation, does not seem to be applicable here. This suggestion cannot be reconciled with the substantial activation of the electrode observed from cathodic treatment nor with the dependence of the reaction rate on the coverage of the electrode by an adsorbed organic species.

Identity of the Adsorbed Species

Some controversy exists about the identity of the adsorbed species. The possibilities which readily come to mind are HCOOH itself, CO, the $HCOO\cdot$ radical, the $HCOO^-$ ion, an impurity from solution, or a by-product of the reaction. On the basis of the anodic charge determinations of q made by Breiter[11] and of those reported here, we can reject the $HCOO\cdot$ radical (or for that matter oxalic acid which might be formed from this radical).

Carbon monoxide, formed from the catalytic decomposition

$$HCOOH \longrightarrow CO + H_2O \qquad (13)$$

has been proposed[14,15] and is thermodynamically reasonable.[6] The evidence in favor of CO includes the observations[15] that during cyclic voltammetry with CO and HCOOH the charges corresponding to adsorption are similar and the oxidation peaks for the adsorbed material are found at about the same potential for both substances.

The evidence given in ref. 15 is thought to be incomplete. The fact that the oxidation peaks during cyclic voltammetry almost coincide is not really surprising since this potential is in the region of surface oxidation of the electrode. Adsorbed species are almost invariably oxidized in this potential region if they have not already been oxidized at a lower potential. The reported coincidence of the charges may be due to an admitted arbitrariness in the charge determination.[15]

In the present work it has been observed, using anodic transients, that the charge corresponding to complete coverage with CO (~340 μcoulombs/cm.²) is higher than for adsorption from HCOOH solutions (210 μcoulombs/cm.²). In addition, the anodic trace has a grossly different shape (*cf.* Fig. 4 and 9). Other

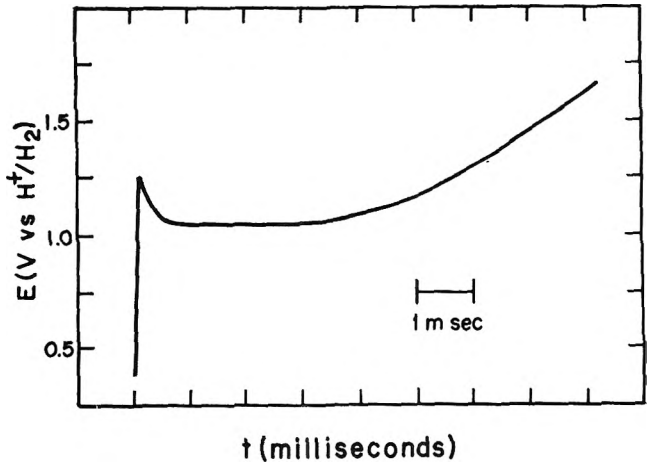

Figure 9. Anodic chronopotentiogram for oxidation of CO adsorbed from 1 M $HClO_4$ at 0.2 v.

(19) S. W. Feldberg, C. G. Enke, and C. E. Bricker, *J. Electrochem. Soc.*, 110, 826 (1963).

arguments against CO as the blocking species are less conclusive: θ_{CO} does not decline until the potential tends to ~0.8 v. (*cf.* Fig. 5) and the rate of its adsorption is much faster than the adsorption rate observed here. Gilman[20] has shown that the CO adsorption kinetics are controlled by diffusion. Neither of these arguments is conclusive if the source of the CO is HCOOH itself, decomposing on the electrode.

Another argument against CO is the value of the constant k' in eq. 10. This specific rate constant is higher than one expects for the nonelectrochemical desorption of CO, even at very low partial pressures, and is also much higher than the rate of oxidation of CO at the relevant potentials.

The possibility that $HCOO^-$ may be the blocking agent is suggested by its known unreactivity (albeit in alkaline solutions)[8,21] and also because infrared spectra[22] indicate that HCOOH is adsorbed from the gas phase on platinum as $HCOO^-$. The arguments against it are that θ tends to zero as the potential rises, which would not be expected for anion adsorption, and that eq. 10, which contains no interactive terms, appears to account satisfactorily for the kinetics of adsorption. The first of these arguments would fail if HCOOH were excluded from the double layer, as it evidently is, at higher potentials. In addition, one may doubt the sensitiveness of eq. 10 to detect interactions in the adsorbate and, thus, to exclude the possibility of $HCOO^-$ adsorption. However, it is still difficult to understand why adsorption from solution would be so slow if the adsorbed species were the formate ion.

The possibility that the adsorbed material is an impurity is also not supported by the experimental observations. The main impurity, CH_3COOH, did not adsorb. In addition, the impurity concentration is expected to be proportional to that of HCOOH, and yet the constant k depends approximately on the logarithm of the concentration.

Blocking of the surface by adsorption of HCOOH itself is unlikely. It can be postulated that HCOOH is adsorbed in two different modes: in the first, it oxidizes very rapidly; in the second, it is firmly held and does not oxidize. We might consider that the former involves dissociative adsorption with splitting of the C–H bond, while the latter mode involves adsorption through the carbon–oxygen double bond. However, if this were the case, we would also expect CH_3COOH to be adsorbed firmly, whereas in fact it is adsorbed very weakly.

The most likely possibility, then, is a product of a side reaction which is adsorbed to a coverage of ~200 μcoulombs/cm.^{2} This product is not charged and is difficult to oxidize but is removable under drastic oxidizing conditions. For example, one might suggest

$$2HCOOH \longrightarrow \underset{\displaystyle COOH}{\overset{\displaystyle CHO}{|}} + H_2O \qquad (14)$$

Experiment shows that this compound is strongly adsorbed from dilute solution, does not oxidize below about 0.50 v., and, even at high potentials, oxidizes very sluggishly. Its maximum surface coverage is ~170 μcoulombs/cm.^{2}.

Mechanism and Conclusions

All the electrochemical parameters derived in the Tafel region change with time since the kinetics of adsorption are different at different potentials. In this event, it seems justified for purposes of obtaining mechanistically-significant information to wait until the electrochemical parameters have become time-invariant (3–5 min. after cleaning), even though the current is still decreasing slowly with time. Accordingly, the mechanism suggested below refers to the steady state which is approached after about 5 min. from cleaning the electrode surface.

It is useful, at this point, to summarize the main findings of the present research and to indicate the experimental observations which must be explained by any useful mechanism of the reaction: (1) cleaning the electrode anodically (and to a large extent cathodically) results in a greater rate of oxidation of HCOOH; (2) the decline of the rate of oxidation with time thereafter is greatest at lower potentials; (3) at any potential, the rate of oxidation is in direct proportion to the clean surface area of the electrode; (4) the adsorption of a blocking agent is slow; (5) the identity of the blocking agent is not clearly established, but it seems likely that it is not CO, HCOOH, $HCOO^{\cdot}$, or $HCOO^-$; (6) the extent of adsorption decreases as the potential rises and is essentially zero at 0.70 v.; (7) different sites on the electrode are grossly different in their activities toward HCOOH oxidation; (8) the extent of adsorption is not very sensitive to HCOOH concentration; (9) $b_{t\to\infty}$ is ~60 mv.; (10) $(\partial \log i/\partial \mathrm{pH})$ is ~1.0 in the Tafel region; (11) $(\partial \log i/\partial \mathrm{pH})_E$ is ~0.2 in the limiting current region; (12) the order of the oxidation with respect to HCOOH is first over the whole region.

The following mechanism may be suggested to account for these observations

(20) S. Gilman, *J. Phys. Chem.*, **67**, 78 (1963).

(21) T. O. Pavela, *Ann. Acad. Sci. Fennicae*, **A59, II**, 1 (1954).

(22) K. Hirota, K. Kuwata, and S. Asai, *Nippon Kagaku Zasshi*, **80**, 701 (1959).

$$HCOOH^{soln} \rightleftharpoons HCOOH^{double\ layer} \quad (15)$$

$$HCOOH^{double\ layer} \xrightarrow{slow} H_{ads} + COOH^{\cdot}_{ads} \quad (16)$$

$$COOH^{\cdot}_{ads} \xrightarrow{fast} CO_2 + H^+ + e \quad (17)$$

$$H_{ads} \xrightarrow{fast} H^+ + e \quad (18)$$

If it is assumed that the active surface area, θ_A, is divided between free sites, θ_F, those covered with hydrogen atoms, θ_H, and those covered with some adsorbed blocking substance, θ_P, then

$$\vartheta_F = \theta_A - \theta_H - \theta_P \quad (19)$$

From (16)

$$i = \vec{k}(HCOOH)^{double\ layer}\theta_F \quad (20)$$

where $\vec{k}$ is a rate constant, and reaction 16 is assumed to take place only on free, active sites. θ_A is taken to be independent of potential, and θ_P was shown above to be independent of potential in the Tafel region, although not at higher potentials. If θ_H is determined by the equilibrium

$$H^+ + e \rightleftharpoons H \quad (21)$$

and if, in HCOOH solutions, it is given by

$$\theta_H = K(H^+) \exp -\left(\frac{\psi F}{RT}\right) \quad (22)$$

where K is the equilibrium constant of reaction 21 and ψ is the potential of the electrode with respect to a hydrogen electrode in the same solution, then

$$i = \vec{k}(HCOOH)^{d.l.}[\theta_A - \theta_P - K(H^+) \exp -\left(\frac{\psi F}{RT}\right)] \quad (23)$$

It is clear that eq. 23 offers an approximate explanation of all the presently known facts. The Tafel slope, $dE/d \log i$, is approximately 60 mv., and $(\partial \log i/\partial\ pH)_\psi$ is about 1.0 in the Tafel region. In addition, when $\theta_H \to 0$, as it is for $E_\psi \gtrsim 0.35$ v., a limiting current is observed. The order of the reaction with respect to HCOOH is unity, *via* eq. 15, and this equation also accounts for the apparent decline of the surface activity as the potential increases. The slowly adsorbing substance is formally included as θ_P, and the fact that θ_P is not very sensitive to concentration indicates why an order of unity with respect to HCOOH is observed even in the Tafel region. In the limiting current region, the pH dependence is small and may reflect some second-order effect on the rate of reaction 16. Substantiation is given to the postulate that reaction 16 is the rate-limiting step from the observation of Munson[16] that the rate-limiting step is pre-electrochemical, and that it reaches a maximum at about the same pH (5) as for reaction 3. Therefore, the mechanism given by eq. 15–18 appears to summarize satisfactorily all the observations which have been made on the electrooxidation of HCOOH in acid solutions.

Acknowledgment. The authors thank Miss J. I. Ford for her skillful experimental assistance. The authors are grateful to the Office of Naval Research for financial support under contract Nonr-3765(00).

The Sonolytic Decomposition of Organic Solutes in Dilute Aqueous Solutions. I. Hydrogen Abstraction from Sodium Formate

by M. Anbar[1] and I. Pecht

The Weizmann Institute of Science, Rehovoth, Israel (*Received December 30, 1963*)

Deuterated formate ions were sonolyzed in dilute aqueous solutions and the HD produced was determined. The yield of HD was found to be independent of solute concentration from 0.005 to 0.1 *M*. The yield of HD was diminished in both strongly acid and alkaline solutions. The results indicate the formation of hydrogen atoms under sonolytic conditions. The yield of "molecular" hydrogen formed under the same conditions is 50 times greater than that of hydrogen atoms.

The analogy between the behavior of radiolyzed and sonolyzed aqueous solutions has been pointed out in several studies.[2,3a] Molecular hydrogen was detected,[3b] and it was suggested that hydrogen atoms are also formed during sonolysis.[4] It was of interest to find out whether hydrogen atoms are formed under sonolytic conditions and to determine their yield.

The hydrogen abstraction from organic solutes was applied in radiation chemistry as an indicator for the presence of hydrogen atoms.[5,6] Quantitative information on the yield of hydrogen atoms in aqueous solutions was recently obtained by determining the yield of HD produced from deuterated organic solutes.[7-9] In the present study the sonolytic formation of hydrogen atoms was investigated by following the dehydrogenation of deuterated formate ions.

Experimental

Materials. Deuterated sodium formate (>98% D) was supplied by Volk Radiochemicals Co; $MgSO_4$ and NaOH were Fluke Puriss grade; NaF was Baker Analyzed Reagent. Distilled water was redistilled from alkaline permanganate and then from phosphoric acid. Argon of highest purity (Matheson Co.) was used. The pH of the solutions was determined using a Metrohm Kompensator Type E 148 C with an accuracy of 0.05 pH unit.

Ultrasonic Irradiation. A Model T 200 (Lehfeldt and Co. GMBH) ultrasonic generator with a water-cooled quartz transducer operating at 800 kc./sec. and an energy output of 1.6 ergs/cm.^{2} sec. was adapted to focus the ultrasonic energy to a limited volume. The irradiation vessel was thermostated by circulating water at 20 ± 1°. A small Pyrex bulb (10.5 ml.) connected to an inlet tube was used as the irradiation vessel. The bulb, which was of minimal thickness in order to reduce sonic absorption, was fitted at a constant position in the focus of the ultrasonic concentrator. In all experiments 4.0 ml. of water or aqueous solution were sonolyzed. The yield of H_2O_2 under these conditions was 4.2×10^{-6} mole/l./min.

Analysis. After sonolysis, the gas was introduced into a mass spectrometer (CEC Model 21-401) and the masses 2, 3, and 4 were determined, as well as masses 28 and 32 to check on air contamination. The masses 2, 3, and 4 were measured in the sequence $\overline{2}$, $\overline{3}$, $\overline{4}$, $\overline{3}$, $\overline{2}$, $\overline{3}$, $\overline{4}$, $\overline{3}$, $\overline{2}$. From the mean values of the three parts of the measured sequence, the ratio $R = (\overline{3} + 2 \times \overline{4})/(\overline{3} - \overline{4})$ was calculated. The values obtained showed a standard deviation of ±4%.

(1) Chemistry Division, Argonne National Laboratory, Argonne, Ill.

(2) A. Weissler, *J. Am. Chem. Soc.*, 81, 1077 (1959); *J. Acoust. Soc. Am.*, 32, 283 (1960).

(3) (a) M. Haissinsky and R. O. Prudhomme, *J. chim. phys.*, 47, 925 (1950); (b) P. Grabar and R. O. Prudhomme, *ibid.*, 44, 145 (1947).

(4) P. Rivayrand and M. Haissinsky, *ibid.*, 59, 623 (1962).

(5) J. T. Allan and G. Scholes, *Nature*, 187, 218 (1960).

(6) G. Scholes and M. Simic, *ibid.*, 199, 276 (1963).

(7) G. Lifshitz and G. Stein, *J. Chem. Soc.*, 3706 (1962).

(8) M. Anbar and D. Meyerstein, Israel AEC Report IA-901 (1963); *J. Phys. Chem.*, in press.

(9) M. Anbar and I. Pecht, *J. Chem. Phys.*, 40, 608 (1964).

The absolute yield of hydrogen was determined from the value of the $\bar{2}$ peak compared with known mixtures of H_2 and argon (5–15% H_2), measured under the same conditions.

Results and Discussion

The rate of formation of "molecular" hydrogen (H_2) from the water and of HD from the deuterated formate under different conditions, is given in Table I. It can be seen that the yield of "molecular" hydrogen (Y_{H_2}) in neutral solutions of sodium formate is independent of the concentration of the solute. As formate ions are most efficient scavengers of H atoms in solution,[10] it may be implied that H_2 is not formed by recombination of H atoms in solution but is produced in the cavities, in complete analogy to the formation of H_2O_2.[11] Y_{H_2} was found to be slightly diminished in 1 *M* solutions of NaF, probably owing to changes in water structure.[12] Oxygen, even at low concentrations (2.5%), was found to diminish Y_{H_2} by about 60%.

Table I: The Formation of HD from Sonolyzed Formate-*d* in Aqueous Solutions under Argon (1 atm.)[a]

Sodium formate	pH	Additive	[Additive], *M*	$R \times 10^2$	H_2 produced, μmoles/l. min.	HD produced, μmole/l. min.
....	6.0			....	25.0	....
0.005	6.0			1.75	25.0	0.44
0.01	6.0			1.95	22.0	0.43
0.025	6.0			2.2	24.5	0.54
0.05	6.0			2.7	23.0	0.53
0.1	6.0			2.6	25.0	0.65
0.05	0.6	H_2SO_4	0.25	1.75	16.2	0.27
0.05	3.0	H_2SO_4	0.0025	2.62	22.6	0.59
0.05	12.1	NaOH	0.01	2.35	25.0	0.59
0.05	14.0[b]	NaOH	1.0	0.43	28.5	0.12
0.05	7.0	NaF	1.0	1.91	18.4	0.35
0.05	7.0	$MgSO_4$	1.0	2.3	24.0	0.53
0.05	6.0	H_2O_2	0.05	2.00	23.4	0.47
0.05	6.0	$NaNO_3$	0.01	2.68	25.8	0.69
0.05	6.0	$NaNO_3$	0.05	2.68	22.6	0.61
0.05	6.5	O_2	2.6%	0.86	9.4	0.08

[a] Time of irradiation was 60–70 min. [b] By definition.

The effect of O_2 may be interpreted by the scavenging of H atoms and the formation of HO_2. The HO_2 radicals may form $H_2O_2 + O_2$. The yield of H_2O_2 originating from O_2, compared with the scavenging effect of O_2 on Y_{H_2} is, however, small.[11] It has to be assumed therefore, that O_2 interacts with a precursor of the H atoms in the cavity or that, at the given high transient temperatures, HO_2 decomposes according to $2HO_2 \rightarrow H_2O + O_2 + O$.

The yield of HD given in Table I was found to be almost independent of the concentration of formate ions, which implies its formation by indirect action. The per cent HD in the evolved hydrogen was found to be independent of the time of sonolysis; this excludes an isotopic exchange between hydrogen and water under our experimental conditions. In analogy to radiation chemistry,[7] the limiting value of HD may be taken as a measure for the yield of hydrogen atoms Y_H. Y_H was found to be diminished in acid solution. This effect is due to acidity and is not a salt effect, as is evident from the experiment with $MgSO_4$. The effect of acidity must be due to the penetration of formic acid into the cavities causing a decrease in Y_H. A parallel decrease in Y_{H_2} is also observed, and a reduction in $Y_{H_2O_2}$ in the presence of formic acid has been previously reported.[2] If electrons would be formed under sonolysis, one would expect an increase in Y_H with increasing acidity.[13]

The absence of electrons as precursors of H atoms in our system is corroborated by the finding that H_2O_2 or NO_3^-, both most effective electron scavengers,[14,15] do not affect Y_H to any appreciable extent. The slight decrease in Y_H in the presence of H_2O_2 is probably due to the oxygen formed from its decomposition. Oxygen acts as an effective scavenger of H atoms and diminishes Y_H far better than Y_{H_2}.

In strongly alkaline solutions, Y_H is diminished to a much greater extent than expected for a salt effect. This is due to the interaction of H atoms with OH^- resulting in the formation of hydrated electrons.[16]

It is of interest to compare the over-all yield of H_2O_2 under our conditions, $Y_{H_2O_2} = 4.9/\mu$moles/l. min.[11] with $Y_{H_2} = 25$ μmoles/l. min. The stoichiometry of the decomposition of water would require the formation of oxygen with a yield $Y_{O_2} = 10$ μmoles/l. min. The proportions between $H_2O_2:H_2:O_2::5:25:10$ are different from those obtained by Haissinsky, *et al.*,[17] at much lower ultrasonic intensities, namely 7:9:1.4. The relatively low yield of H_2O_2 under high ultrasonic intensities may imply that most of the H_2O_2 produced by the $2H_2O \rightarrow H_2O_2 + H_2$ reaction is decomposed at the high transient temperatures involved.[18] An alter-

(10) J. Rabani, *J. Phys. Chem.*, 66, 361 (1962).
(11) M. Anbar and I. Pecht, *ibid.*, 68, 352 (1964).
(12) M. Haissinsky and A. Mangeot, *Nuovo Cimento*, 4, 1086 (1954).
(13) E. Hayon and A. O. Allen, *J. Phys. Chem.*, 65, 2181 (1961).
(14) G. Czapski and A. O. Allen, *ibid.*, 66, 762 (1962).
(15) S. Nehari and J. Rabani, *ibid.*, 67, 1609 (1963).
(16) J. Jortner and J. Rabani, *J. Am. Chem. Soc.*, 83, 4868 (1961).
(17) M. Haissinsky, R. Klein, and P. Rivayrand, *J. chim. phys.*, 59, 611 (1962).
(18) M. E. Fitzgerald, V. Griffing, and J. Sullivan, *J. Chem. Phys.*, 25, 926 (1956).

native explanation could be the decomposition of water under high ultrasonic intensities to H and O atoms, forming H_2 and O_2 without H_2O_2 as intermediate. The absence of any deuterium isotope effect in the sonolytic formation of H_2 under high intensities[9] makes the second interpretation rather likely. On the other hand, it should be noted that the yield of hydrogen atoms in solution, Y_H, is only about $^1/_{50}$ of Y_{H_2}. This means that less than 2% of the hydrogen atoms produced in the cavity diffuse into solutions.

The Sonolytic Decomposition of Organic Solutes in Dilute Aqueous Solutions. II. The Sonolysis of Isopropyl Alcohol

by M. Anbar and I. Pecht

The Weizmann Institute of Science, Rehovoth, Israel *(Received December 30, 1963)*

The sonolytic decomposition of isopropyl alcohol in aqueous solutions under argon has been investigated following the evolution of hydrogen and the formation of acetone. It has been found that the yield of hydrogen produced significantly exceeds the yields of molecular and atomic hydrogen. The sonolytic decomposition of isopropyl alcohol is not scavenged by nonvolatile hydrogen atom scavengers. It was concluded that the sonolytic decomposition of isopropyl alcohol takes place in the cavities, where the high transient temperatures induce the monomolecular dehydrogenation of the alcohol. Hydrogen abstraction by a bimolecular process has been observed at high concentrations of isopropyl alcohol (>0.1 *M*).

Organic solutes in sonolyzed aqueous solutions have been shown to undergo extensive decomposition.[1-4] Certain organic solutes in aqueous solutions were found to affect the sonolytic formation of hydrogen peroxide[5-7] and the sonolytic oxidation of iodide ions.[5,8] It has been pointed out that the chemical effect of volatile organic solutes on the formation of H_2O_2 differs significantly from that of nonvolatile free-radical scavengers.[7] It was of interest to compare the sonolytic decomposition of volatile and nonvolatile organic solutes under similar conditions. The hydrogen abstraction from formate ions was investigated and was found to be induced by hydrogen atoms.[9] The sonolytic dehydrogenation of isopropyl alcohol in dilute solutions was chosen as a model reaction for the behavior of volatile solutes.

Experimental

Solutions of isopropyl-2-*d* alcohol (>99% deuterium, Merck Sharp and Dohme Ltd.) in triple-distilled water were sonolyzed under argon and the isotopic

(1) M. E. Fitzgerald, V. Griffing, and J. Sullivan, *J. Chem. Phys.*, **25**, 926 (1956).

(2) D. L. Currell and L. Zechmeister, *J. Am. Chem. Soc.*, **80**, 205 (1958).

(3) S. C. Srivastava, *Nature*, **182**, 47 (1958).

(4) B. H. Jennings and S. N. Townsend, *J. Phys. Chem.*, **65**, 1574 (1961).

(5) A. Henglein and R. Schulz, *Z. Naturforsch*, **8b**, 277 (1953).

(6) A. Weissler, *J. Am. Chem. Soc.*, **81**, 1077 (1959).

(7) M. Anbar and I. Pecht, *J. Phys. Chem.*, **68**, 352 (1964).

(8) N. Ellfolk and A. Virtanen, *Acta Chem. Scand.*, **11**, 230 (1957).

(9) M. Anbar and I. Pecht, *J. Phys. Chem.*, **68**, 1460 (1964).

Table I: The Sonolytic Formation of Hydrogen from Isopropyl Alcohol-Containing Solutions under Argon (1 atm., pH 6–7)[a]

	Isopropyl alcohol		Water isotopic composition		Hydrogen evolved	
	Isotopic composition	M		Additive	μmoles/l. min.	Atom % H
1.1	2-D *i*-PrOH	0.04	H_2O	...	140	92
1.2	2-D *i*-PrOH	0.02	D_2O	...	88	80
1.3	2-D *i*-PrOH	0.06	D_2O	...	135	74
1.4	2-D *i*-PrOH	0.30	D_2O	...	135	68
1.5	2-D *i*-PrOH	1.30	D_2O	...	131	63
1.6	2-H *i*-PrOH	0.03	D_2O	...	96	..
1.7	2-H *i*-PrOH	0.10	D_2O	...	151	83
1.8	2-D *i*-PrOH	0.04	H_2O	O_2 2.5%	60	92
1.9	2-D *i*-PrOH	0.04	H_2O	O_2 30%	6.8	90
1.10	2-D *i*-PrOH	0.04	H_2O	HCOONa 0.1 M	135	92
1.11	2-D *i*-PrOH	0.04	H_2O	$Mg(ClO_4)_2$ 1 M	100	91

[a] Time of irradiation, 30–60 min.

composition of the hydrogen evolved was determined. D_2O 99.8% (Norsk Hydro Electrisk) was triple distilled before use. The sonolysis and analysis were carried out as described in the previous article of this series.[9]

Acetone was determined spectrophotometrically according to the method of Berntsson.[10] To 2 ml. of the sonolyzed solution in a 5-ml. volumetric flask was added 0.2 ml. of 10 M NaOH. Then 0.06 ml. of salicylaldehyde (Fluka puriss) was added, followed by 2 ml. of 10 M NaOH; the solution then was diluted to the mark. After standing for 2.5 hr., the solution was transferred to an optical cell (1-cm.) and the optical density at 474 mμ was measured against a blank which contained an identical nonsonolyzed sample. The concentration was determined from a calibration curve which was linear between 1.0 and 20 $\times 10^{-5}$ M acetone with $\epsilon = 1.8 \times 10^5\ M^{-1}$ cm.$^{-1}$.

Results and Discussion

The sonolytic decomposition of isopropyl alcohol in aqueous solution was investigated using isotopic tracer techniques and examining the yield and isotopic compositions of the hydrogen evolved; the results are summarized in Table I. The sonolytic yield of hydrogen evolved over solutions of isopropyl alcohol is significantly higher (4–5-fold) than that produced in isopropyl alcohol-free or in formate-containing solutions.[9] A comparison of experiments 1.2, 1.6, 1.1, 1.3, 1.7, 1.4, and 1.5 shows that this effect is proportional to isopropyl alcohol concentration up to about 0.05 M, where a limiting value of about 140 μmoles of hydrogen/l. min. is reached. This implies the formation of hydrogen by a mechanism different from that producing molecular hydrogen,[9,12] or the hydrogen abstraction by hydrogen atoms.[9]

This decomposition is independent of hydrogen atoms, as it is not scavengable by formate ions (*cf.* 1.1 and 1.10). On the other hand, it is strongly dependent on the presence of O_2, which is found to diminish the yield of hydrogen (*cf.* 1.1, 1.8, and 1.9). The effect of $MgSO_4$ on the yield of hydrogen may be attributed to an effect on water structure.[11] It is suggested, therefore, that isopropyl alcohol decomposes in the cavities by a thermal process.[1,12–14] The isotopic tracer experiments corroborate this conclusion.

In all isotopic experiments a total isotopic equilibrium was attained, $[HD]^2/([H_2][D_2]) = 4$. This result implies a fast H_2–D_2 exchange in the cavities, most probably *via* H atoms and H_3 radicals as intermediates. In order to evaluate the isotopic experiments, one had to check on the isotopic exchange between hydrogen and water. This was examined as follows: 7% D_2 in argon (0.5 atom % H) was sonolyzed for 33 min. over 4 ml. of H_2O, yielding hydrogen which contained 12.4% H. From this, the rate of change in isotopic composition of the hydrogen was calculated, giving 15.4 μmoles/l. min. This value is lower than the amount of H_2 produced in H_2-free solutions (25 μmoles/l. min.) As hydrogen was shown to diminish the yield of H_2O_2[15] it is plausible that it also decreases the yield of H_2 from the

(10) S. Berntsson, *Anal. Chem.*, **28**, 1337 (1956).

(11) M. Haissinsky and A. Mangeot, *Nuovo Cimento*, **4**, 1086 (1954).

(12) M. Anbar and I. Pecht, *J. Chem. Phys.*, **40**, 608 (1964).

(13) B. E. Noltingk and E. A. Neppiras, *Proc. Phys. Soc.* (London), **B63**, 674 (1950).

(14) E. A. Neppiras and B. E. Noltingk, *ibid.*, **B64**, 1032 (1951).

(15) A. Henglein, *Z. Naturforsch.*, **44**, 179 (1957).

water. It thus may be concluded that no significant isotopic *exchange* between H_2 and H_2O, takes place under our experimental conditions.

The isotopic composition of the hydrogen evolved from solutions of isopropyl alcohol provides further information on the mechanism of its decomposition. From experiment 1.7 it is evident that most of the hydrogen evolved originates from the alcohol. About 17% of the hydrogen was found to originate from the water, amounting to 25.5 μmoles/l. min. This is equal to the molecular yield Y_{H_2} under our conditions, reported in the previous paper.[9] From experiment 1.2 it is evident that most of the hydrogen formed from isopropyl alcohol in dilute solutions originates from the methyl groups and at first approximation one obtains a statistical distribution of the hydrogens (1:6) as present in the alcohol. At higher concentrations of the alcohol, hydrogen derived from the α-position becomes more predominant (experiments 1.2, 1.3, 1.4, and 1.5), reaching a limiting value (after correction for the molecular hydrogen) of D:H of approximately 1:3 for hydrogens originating from α- and β-positions, respectively. This value is quite different from the ratio $\alpha:\beta = 2.5:1$ found under radiolytic conditions in aqueous solutions.[16] The per cent of D atoms abstracted from isopropyl-2-*d* alcohol in H_2O is not affected oxygen and $Mg(ClO_4)_2$, which inhibit the formation of the over-all yield of hydrogen (experiments 1.1, 1.11, 1.8, and 1.9).

Further information on the chemical decomposition of isopropyl alcohol can be inferred by following the formation of its major product of oxidation, namely acetone. The yield of acetone has been determined under different conditions and the results are given in Table II. From these data, it is evident that acetone is formed at a yield of about 10 μmoles/l. min. irrespective of the pH. The slight decrease in the yield in 1 *M* NaOH is a salt effect, which is analogous to the effect of KF in neutral solutions. The yield of acetone is in good agreement with the yield of hydrogen abstraction from the α-position as found in the sonolysis of dilute isopropyl-2-*d* alcohol in H_2O (experiments 1.1 and 1.10) which is approximately 11 μmoles/l. min. It has to be inferred that under these sonolytic conditions, the formation of a hydrogen molecule in the cavity which includes the α-hydrogen, leads to the formation of acetone. The formation of HD is in this case an intramolecular process. If the α-hydrogen would be abstracted by a hydrogen atom or by an organic free-radical followed by the formation of a CH_3COHCH_3 radical, one would expect the yield of acetone to be equal to half the yield of HD, as has been observed under radiolysis.[17]

Table II: The Effect of pH on the Formation of Acetone from Isopropyl Alcohol under Argon[a]

	pH	Yield of acetone, μmoles/l. min.
2.1	0.6	8.8
2.2	1.3	9.2
2.3	2.9	10.0
2.4	4.7	9.5
2.5	6.4	11.2
2.6	9.3	10.0
2.7	10.5	10.3
2.8	11.7	10.7
2.9	13.0	10.3
2.10	1 *M* NaOH	8.9
2.11	7.0 + 1 *M* KF	8.1

[a] *i*-PrOH = 0.05 *M*; time of irradiation, 5–10 min.

The effect of isopropyl alcohol concentration on the yield of acetone given in Table III shows an increase in its yield parallel to the increase in α-hydrogen abstraction described above. A quantitative comparison

Table III: *The Effect of Isopropyl Alcohol Concentration* on the Yield of Acetone[a]

	i-PrOH	Yield of acetone, μmoles/l. min.
3.1	1×10^{-3}	6.3
3.2	1×10^{-2}	9.4
3.3	5×10^{-2}	10.3
3.4	5×10^{-1}	14.0
3.5	1	19.0

[a] pH 5.0; time of irradiation, 5–10 min.

of experiments 1.5 and 3.5 shows the yield of HD from the α-hydrogen (after correction for the molecular yield) to be 26 μmoles/l. min. compared with 19 μmoles/l. min. of acetone. Subtracting the yield of HD or acetone at low isopropyl alcohol concentrations, namely 10 μmoles/l. min., one obtained 8 μmoles/l. min. of acetone produced for 15 μmoles/l. min. of HD abstracted; this suggests the formation and disproportionation of the CH_3COHCH_3 radical under these conditions.[17]

It may be concluded that isopropyl alcohol undergoes sonolytic decomposition in the cavities at a rate which is much higher than the rate of production

(16) M. Anbar and D. Meyerstein, to be published.

(17) J. T. Allan and G. Scholes, *Nature*, **187**, 218 (1960).

of molecular hydrogen, hydrogen peroxide, or hydrogen atoms. The decomposition of isopropyl alcohol results in the formation of hydrogen. At low concentrations of isopropyl alcohol the dehydrogenation seems to be an intramolecular process in which any two hydrogen atoms have an equal probability to be eliminated. The intramolecular production of a hydrogen molecule which involves the α-hydrogen of isopropyl alcohol yields mainly acetone. The decomposition of isopropyl alcohol at high concentrations involves an additional bimolecular reaction with a preferential abstraction of the α-hydrogen. These findings may be interpreted by the thermal decomposition of the alcohol inside the cavities in contrast to chemical changes of nonvolatile solutes which take place by "indirect action." The sonolytic behavior of volatile solutes cannot therefore be correlated with the sonochemistry of water and is a function of their volatility and thermal stability.

The Effect of Oxygen on the Electrical Resistance of Evaporated Silver Films

by A. W. Smith

Parma Research Laboratory, Union Carbide Corporation, Parma 30, Ohio *(Received January 2, 1964)*

The electrical resistance of thin films of silver was determined in the presence of various gases between 200 and 300°. Oxygen increased the resistance as a quadratic function with time. Reducing gases such as hydrogen, ethylene, or carbon monoxide returned the resistance of the film to its normal value. The effect is interpreted not as due to electronic interactions but as due to recrystallization of the film under the influence of the various gases.

Introduction

There have been two investigations reported in the literature on the effect of oxygen and other gases on the electrical resistance of silver films.[1,2] Both of these authors used chemically deposited silver on glass fibers. The measurement of resistance was made in both investigations by pressing a mat of these fibers between silver plates. In both studies the work was related to the oxidation of ethylene on silver. More recently, Dixon and Longfield[3] suggested that more work be done with this system.

Because of experience here in the determination of electrical resistance and the effect of adsorption on evaporated films on copper oxide, it was decided to study the effect of adsorption on the electrical resistance of evaporated silver films. The advantage of using evaporated films is that the uncertain contacts between fibers which were present in the previous studies would not be present.

Experimental

The experimental apparatus was that reported previously for studies on copper oxide films[4] with the exception of the evaporation tube and the equipment for measuring resistance. The evaporation tube was constructed as follows. A four-wire tungsten-through-glass "press" was cut perpendicular to the tungsten leads through the glass and the leads, and then this end was polished. Two coats of "bright platinum" and then two coats of chemically deposited silver covered this end of the press including the ends of the four tungsten leads. This metallic coating was removed

(1) G. H. Twigg, *Trans. Faraday Soc.*, 42, 657 (1946).

(2) G. D. Lyubarskii, *Dokl. Akad. Nauk Fiz. Khim.*, 1, 112 (1956).

(3) J. K. Dixon and J. E. Longfield in "Catalysis," Vol. VII, P. H. Emmett, Ed., Reinhold Publishing Corp., New York, N. Y., 1960, p. 183.

(4) A. W. Smith, *Actes Congr. Intern. Catalyse, 2e, Paris, 1960*, 1711 (1961).

from the space between the middle leads. This press was then installed in a Pyrex tube, and silver was evaporated from a filament onto the end of the press. The filament was prepared by winding three strands of 0.38-mm. molybdenum wire and one strand of 0.18-mm. silver wire. The resistance was measured by the four probe method. A constant current of 1 ma. was passed through the outer two leads and the voltage was measured across the center two leads with a Leeds and Northrup microvolter.

Results and Discussion

The increase in resistance upon admission of oxygen to silver-plated fibers was held by Lyubarskii[2] to be due to removal of electrons from the silver by the oxygen. Twigg,[1] on the other hand, held that oxygen interpolated itself between the contacts of one fiber to the next. Dixon and Longfield[3] assume that this is an electronic effect in suggesting that this measurement be used in studying the oxidation of ethylene on silver. The use of evaporated films can help to decide between these different mechanisms for this effect because the evaporated films form a continuous path and a four probe method may be used to eliminate contact effects.

Evaporated silver films of appropriate thickness showed large increases in resistance when exposed to oxygen at temperatures above about 200°. Films which were too thick showed only a small effect while films which were too thin lost metallic conductivity after one or more oxygen and hydrogen treatments. By comparing the temperature coefficient of resistance of the films with the data of Baker and Caldwell,[5] a value of 300–400 Å. was obtained for the thickness of appropriate films.

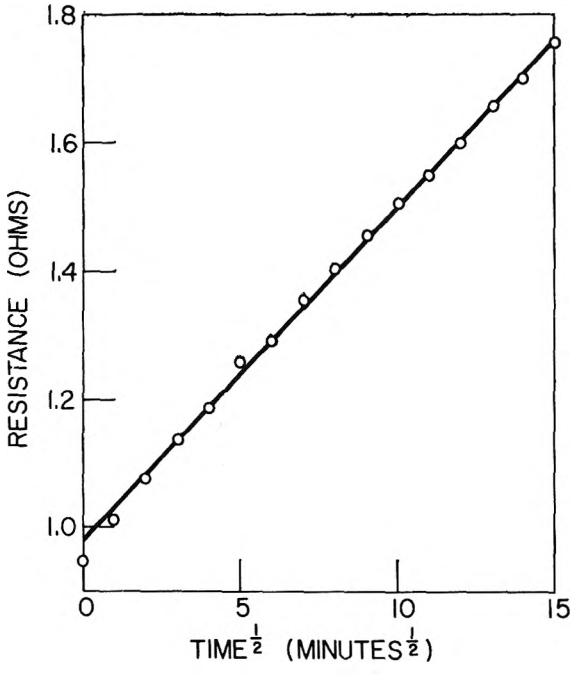

Figure 1. Increase in resistance of 350-Å. evaporated silver film when exposed to 100 torr pressure of oxygen at 254°.

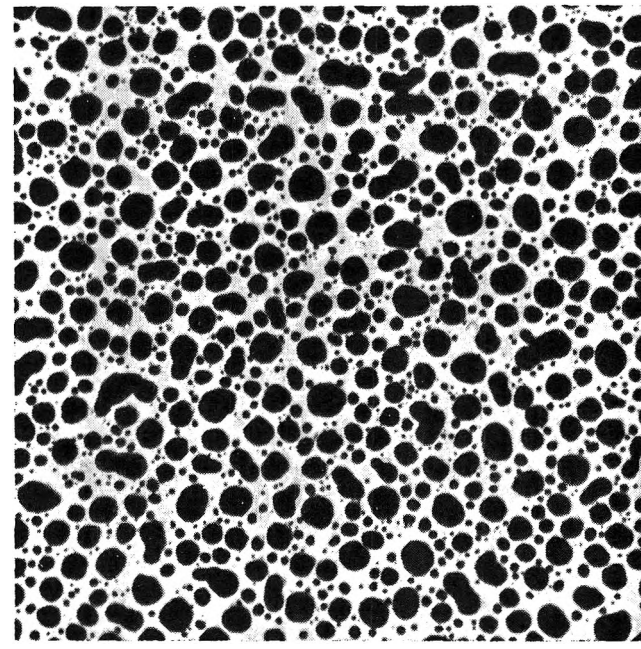

Figure 2. Electron micrograph of stripped silver film (magnification ×20,000).

There is no correlation between the rate of oxygen adsorption and the resistance changes. The adsorption of oxygen on silver above 200° is virtually complete in a matter of minutes.[6] The electrical resistance of these films, however, increased steadily, proportional to the square root of time, for long periods. In one attempt to observe saturation the resistance was followed for a week. At the end of this period the resistance was still increasing according to this function. Figure 1 shows a typical result for these films. During this run the resistance approximately doubled.

Treatment with reducing gases returns the resistance to its original value in a matter of minutes with a nearly exponential function. In one series of experiments at 300°, after a 15-min. exposure to hydrogen, 99% of the resistance change was restored, whereas after a 45-min. exposure to carbon monoxide only 70% of the change was restored. The effect of ethylene was intermediate between that of carbon monoxide and hydrogen. The oxygen–hydrogen cycle has been repeated many times with nearly identical resistance changes on each cycle.

(5) B. B. Baker and W. C. Caldwell, Ames Laboratory, 15C-215, U. S. Atomic Energy Commission, March 20, 1952.

(6) W. W. Smeltzer, E. L. Tollefson, and A. Cambron, *Can. J. Chem.*, **34**, 1046 (1956).

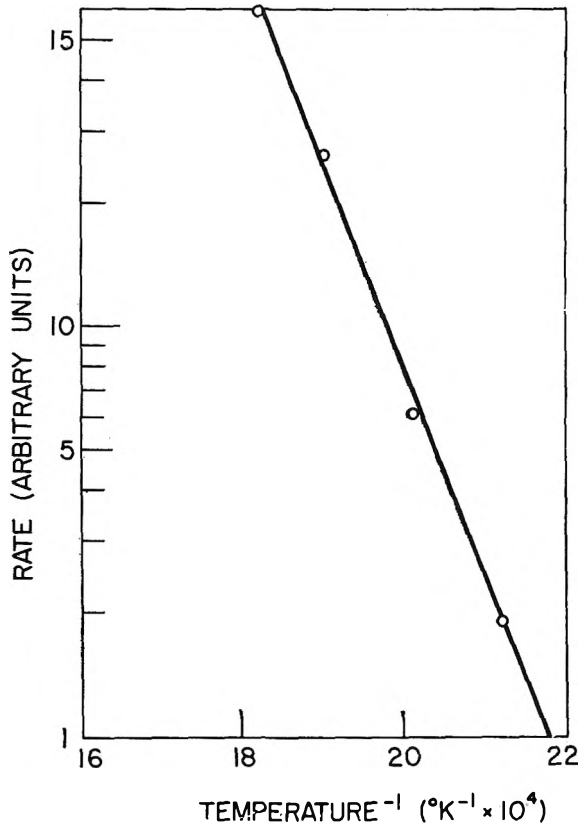

Figure 3. Arrhenius plot of rate of resistance increase *vs.* temperature for 350-Å. evaporated silver film exposed to 100 torr pressure of oxygen.

It is known that the alternate exposure to oxygen and hydrogen causes rapid roughening and faceting of many metal surfaces. Wilson, *et al.*,[7] have shown extensive recrystallization of silver when exposed to a mixture of ethylene and oxygen. Observation of the films used here with the electron microscope shows that, after much treatment, the originally smooth film formed agglomerated to separate particles. This is shown in Fig. 2. Under moderate treatments these particles are probably still connected by necks as shown for copper films.[4]

From the magnitude of the resistance change and from the lack of correspondence with the oxygen uptake, it seems obvious that this effect is not electronic. The observation that treatment with oxygen causes crystal growth indicates that the correct reason for this resistance change is crystallite growth with the removal of silver from the necks between crystallites. The role of oxygen is to provide a change in surface energy for the different crystal faces making such growth possible. A small electronic effect may also be present, but it would be hidden by the large nonelectronic effect.

The rate of grain boundary diffusion for silver has been determined to be 20 kcal./mole.[8] The rate constant K for the resistance change due to oxygen obtained from the expression, $dR/dt = K/R$, was determined at a number of temperatures. An Arrhenius plot of this data is shown in Fig. 3. This leads to an activation energy of 24 kcal./mole. This value indicates that the activation energy of the process responsible for the resistance change is of a reasonable magnitude for a diffusion-controlled process. Apparently the diffusion process is slower on an oxygen-covered surface than on a reduced surface. The fact that "resintering" goes at a different rate depending on the reducing gas used shows that the actual rate of oxygen removal may be important. Chalmers, King, and Shuttleworth[9] show that, at higher temperatures, oxygen causes striations produced by the exposure of 111 planes and that these disappear in a nitrogen atmosphere. This is strong evidence that the mechanism of recrystallization is responsible for the increase in resistance of evaporated silver films and presumably for plated fibers as well.

(7) J. N. Wilson, H. H. Voge, D. P. Stevenson, A. E. Smith, and L. T. Atkins, *J. Phys. Chem.*, **63**, 463 (1959).

(8) D. Turnbull in "Atom Movements," American Society of Metals, Cleveland, Ohio, 1951, p. 129.

(9) B. Chalmers, R. King, and R. Shuttleworth, *Proc. Roy. Soc.* (London), **A193**, 465 (1948).

Heats of Mixing of Polymers with Mixed-Solvent Media

by G. Delmas, D. Patterson,[1] and S. N. Bhattacharyya

Département de Chimie, Université de Montréal, Montréal, Canada *(Received January 2, 1964)*

Heats of mixing have been obtained for polydimethylsiloxane in dilute solution in the following mixed-solvent media: benzene–cyclohexane (I), benzene–heptane (II), benzene–carbon tetrachloride (III), benzene–chlorobenzene (IV), cyclohexane–carbon tetrachloride (V), and carbon tetrachloride–methylcyclohexane (VI), and for polyisobutylene in I, II, chlorobenzene–heptane (VII), and dodecane–hexane (VIII). The experimental values throughout the composition range of the solvent mixtures are compared with theoretical results based on the rigid lattice model with random mixing, and assuming the same contact energies between the solvents in the binary and ternary solutions. The calculated heats using mixtures I, II, and VII are considerably lower than observed. Such a discrepancy might be caused by a perturbation by the polymer of contacts between nonspherical molecules. On the other hand, such a discrepancy is also predicted by the Prigogine "deformable" lattice theory to occur for ternary solutions containing a polymeric component. No firm conclusion as to the source of the discrepancy seems possible at present.

Introduction

Measurements of thermodynamic properties of polymer–mixed solvent systems have been restricted to the free energy as found from studies of intrinsic viscosities, light scattering, phase relationships, etc. It seems possible to predict the thermodynamics of ternary systems which do not contain a polymer from the properties of the binary systems of the components. When a polymer is present, however, the free energy does not provide a very convenient test of such a prediction. This is because the combinatorial contribution to the free energy of mixing must be calculated and is sensitive to the particular approximation used. It seemed interesting, therefore, to measure heats of mixing of high polymeric liquids with mixed-solvent media, and to compare the results with values predicted from a knowledge of the heats of mixing of the three pairs of components.

Experimental

The polymers were polyisobutylene (PIB) and polydimethylsiloxane (PDS). The former was a fraction of $\bar{M}_v \backsim 30{,}000$ obtained from a commercial sample of Enjay Vistanex LM-MH-225, while the latter was a commercial Dow Corning DC 200 silicone of 60,000 centistokes viscosity ($\bar{M}_v \backsim 100{,}000$). No attempt was made to neutralize the small amount of residual catalyst in the PDS. The mixed-solvent media were as follows, the references giving the calorimetric excess heats: benzene–cyclohexane[2a] (I), benzene–heptane[3] (II), benzene–carbon tetrachloride[2a] (III), benzene–chlorobenzene[2b] (IV), cyclohexane–carbon tetrachloride[2a] (V), cyclohexane–methylcyclohexane (VI), chlorobenzene–heptane (VII), and dodecane–hexane[4] (VIII). Heats of mixing at 25° for VI and VII were obtained in this present study. The solvents were dried and fractionally distilled, except for the benzene and cyclohexane which were of "spectrograde" quality. All solvents were stored over calcium sulfate.

A Tian–Calvet microcalorimeter was used to obtain the heats of mixing at 25°, the apparatus and experimental technique being as previously described.[5]

(1) Address to which correspondence should be sent: Centre de recherches sur les macromolécules, Strasbourg, France.

(2) (a) J. R. Goates, R. J. Sullivan, and J. B. Ott, *J. Phys. Chem.*, **63**, 589 (1959); (b) J. Canning and G. H. Cheesman, *J. Chem. Soc.*, 1230 (1955).

(3) C. P. Brown, A. R. Mathieson, and J. C. J. Thynne, *ibid.*, 4141 (1955).

(4) J. H. van der Waals, *Rec. trav. chim.*, **70**, 101 (1951).

(5) G. Delmas, D. Patterson, and T. Somcynsky, *J. Polymer Sci.*, **57**, 79 (1962).

Small quantities of the polymers, which were highly viscous liquids, were dissolved in the mixed-solvent media, the final concentrations being ~1 g./100 ml. The heats of mixing observed at this concentration were then corrected to infinite dilution by dividing by $1 - \varphi_3'$ where φ_3' is the volume fraction of polymer 3 in the ternary solution. The change is less than 2%. The above method of correction ignores the lack of homogeneity in the polymer solution at great dilution and hence is only exact for a solution at the θ-point, *e.g.*, PIB–benzene. For the other solvents and mixtures, however, the difference in the correction brought about by using dilute solution theory would be well within experimental error. Repeated experiments using the microcalorimeter for heats of solution in pure solvents showed[5] a precision of ±2% for large heats of ~4 cal./g. and ±5% for heats of ~0.5 cal./g. The scatter of points in the present work seems to be usually less than this. Accuracy is estimated to be of the same order as above, and sources of error have been discussed elsewhere.[5] The excess heats of the mixed-solvent media VI and VII were found using a modification of the same apparatus, and will be taken up later.

Results and Discussion

The heats of mixing per gram of polymer and corrected to infinite dilution are shown in Fig. 1–10 as a function of the volume fraction, φ, of the second component of the solvent mixture. In each case the uppermost curve gives ΔH_{12} of eq. 6 as a function of the volume fraction of the second component of the mixed-solvent medium, the ordinate being on the right-hand side of the diagram. A full curve is drawn through the experimental points for ΔH_M, the ordinate being on the left-hand side, and similarly for the other full curve which is predicted using eq. 6 of the rigid lattice theory.

The heats of mixing arise from a dilution of the pure polymer down to the infinitely dilute solution. In the high concentration range, the Flory "concentrated solution" theory[6] would give an adequate description, but at great dilution the Flory–Krigbaum dilute solution theory[7] would be appropriate. However, since only a very small part of the total heat arises from dilution in this concentration range, it is a valid approximation to compare the whole heat with "concentrated solution" theory, which would in fact be completely correct at the θ-point. If, for instance, the solution enters the dilute region at ~5 g./100 ml., only ~5% of the total heat is absorbed in the dilute region and the error in the total calculated heat effect incurred by using the "concentrated solution" theory throughout has been calculated to be less than 2% for even a system as far removed from its θ-point as PIB–cyclohexane. (We have used eq. 32 of ref. 7 for $\Delta\bar{H}_1$ in the dilute range.)

Rigid Lattice Theory. Thus, using the usual rigid lattice theory and neglecting preferential adsorption of either solvent on the polymer, *i.e.*, using the random mixing or zeroth approximation, the heat of mixing[6] of N_3r_3-mers with a mixed-solvent medium containing N_1r_1-mers and N_2r_2-mers may be found to be

$$\Delta H_M = \frac{zN_3r_3(N_1r_1 + N_2r_2)}{N_1r_1 + N_2r_2 + N_3r_3} \times \{(1 - \varphi)w_{13} + \varphi w_{23} - \varphi(1 - \varphi)w_{12}\} \quad (1)$$

Here z is the lattice coordination number and φ, the volume fraction of component 2 in the mixed solvent, is given by

$$\varphi = N_2r_2/(N_1r_1 + N_2r_2) \quad (2)$$

The interchange energy, w_{ij}, is given by

$$w_{ij} = {}^1/_2(\epsilon_{ii} + \epsilon_{jj}) - \epsilon_{ij} \quad (3)$$

$-\epsilon_{ij}$ being the interaction potential of segments of types i and j. The Flory approximation has been used in eq. 1 for convenience, *i.e.*, $q = r$ in Guggenheim's terminology. For a dilute polymer solution, $N_3r_3 << N_1r_1 + N_2r_2$ and eq. 1 becomes

$$\Delta H_M = zN_3r_3\{(1 - \varphi)w_{13} + \varphi w_{23} - \varphi(1 - \varphi)w_{12}\} \quad (4)$$

For comparison with experiment we use

$$\Delta H_M(\varphi)/(\text{g. of polymer}) = zv_3/v\{(1 - \varphi)w_{13} + \varphi w_{23} - \varphi(1 - \varphi)w_{12}\} \quad (5)$$

$$\equiv (1 - \varphi)\Delta H_M(0) + \varphi\Delta H_M(1) - \Delta H_{12}(\varphi) \quad (6)$$

where v_3 is the specific volume of the polymer and v is the volume of a segment. The first two terms of expression 6 give a linear interpolation between the heats of mixing of the polymer with the pure liquids 1 and 2, thus the dotted lines in Fig. 1–10. The third term is the heat of mixing the liquids 1 and 2 to form a volume of mixed-solvent medium equal to that of the polymer. The figures show curves of $\Delta H_{12}(\varphi)$ which, save for VI and VII, were taken from published empirical equations[2-4] giving the excess heat as a function of composition. For systems II and VIII, such an equation is given at 20° instead of 25° and a small correction was applied using heat data at 70° for II and 30° for VIII and assuming the excess heat capacity to be independent

(6) P. J. Flory, "Principles of Polymer Chemistry," Cornell University Press, Ithaca, N. Y., 1953, p. 497.

(7) P. J. Flory and W. R. Krigbaum, *J. Chem. Phys.*, 18, 1086 (1950).

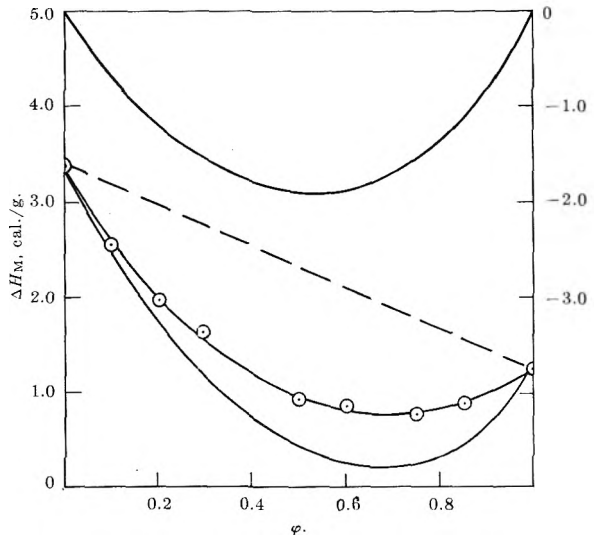

Figure 1. PDS–benzene–cyclohexane (I).

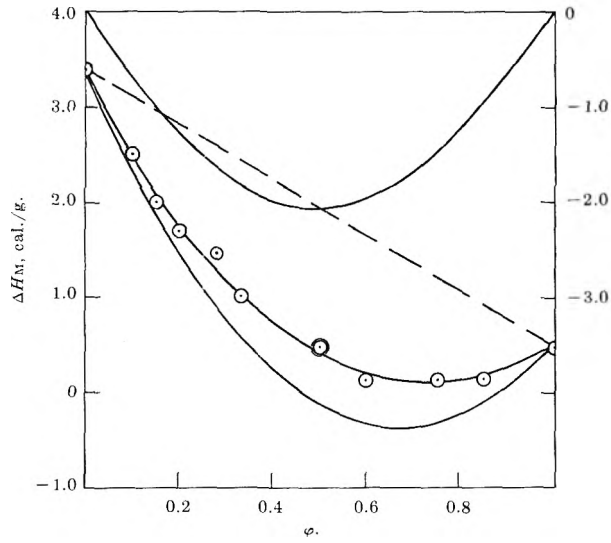

Figure 2. PDS–benzene–heptane (II).

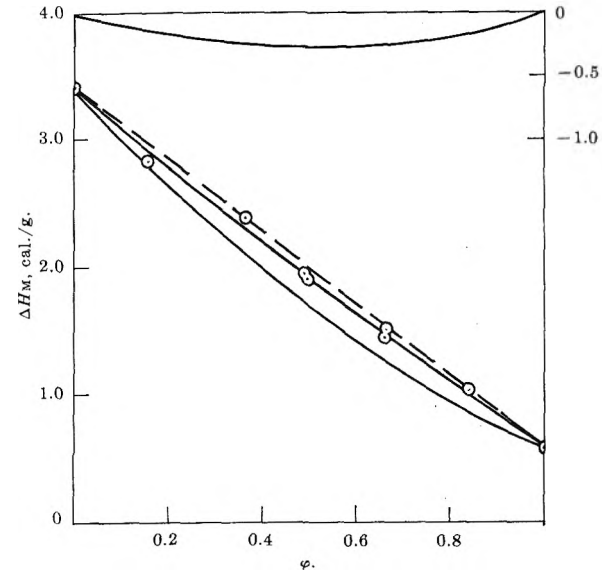

Figure 3. PDS–benzene–carbon tetrachloride (III).

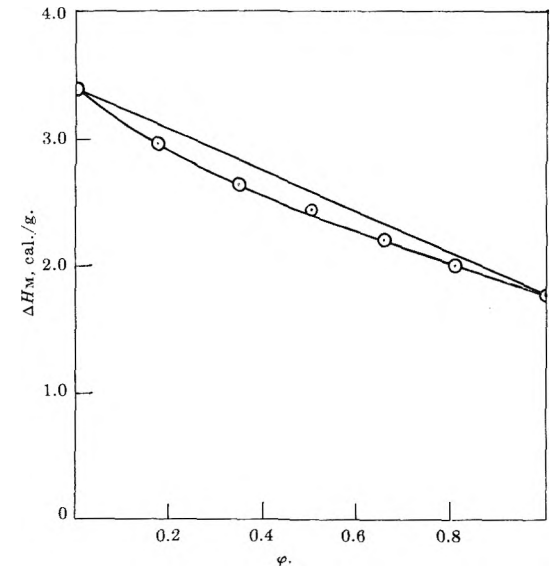

Figure 4. PDS–benzene–chlorobenzene (IV).

of temperature. The curve shown for ΔH_{12} for VI was drawn through nine experimental points over the concentration range, the accuracy being estimated to be $\pm 3\%$. For VII, three points near the equimolar composition were used to draw the curve of Fig. 6 assuming a composition dependence symmetrical in φ. The specific volumes of PDS and PIB at 25° for the appropriate molecular weights were calculated from the results of Fox and Loshaek[8] to be 1.03 and 1.10 ml., respectively.

Values of $\Delta H_M(\varphi)$ calculated from eq. 6 are shown in the figures and there is qualitative agreement with experiment in all systems. However, the predicted heats are considerably lower than those observed for about half the systems, *i.e.*, those containing I, II, and VII. This contrasts with the situation for nonpolar ternary mixtures not containing a polymer where the heat of mixing of the three components together may be calculated quite adequately from the heats of the three binary mixtures.[2a,3,9]

The Quasi-chemical Approximation. It would seem reasonable to suppose that the use of higher approximations than that of random mixing would only serve

(8) T. G Fox and S. Loshaek, *J. Polymer Sci.*, 15, 379 (1955).

(9) A. R. Mathieson and J. C. J. Thynne, *J. Chem. Soc.*, 3713 (1956).

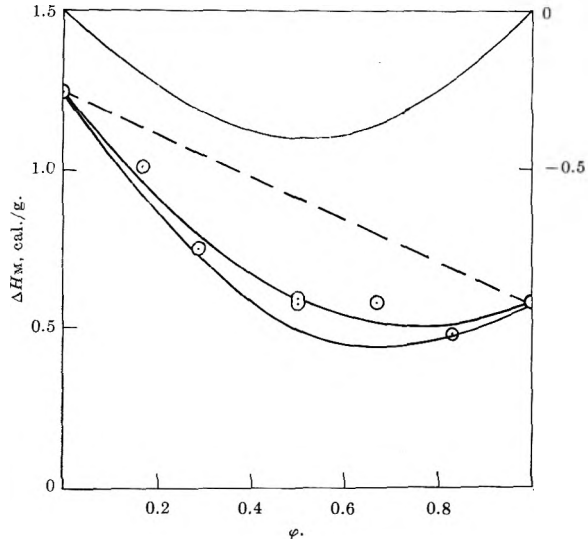

Figure 5. PDS–cyclohexane–carbon tetrachloride (V).

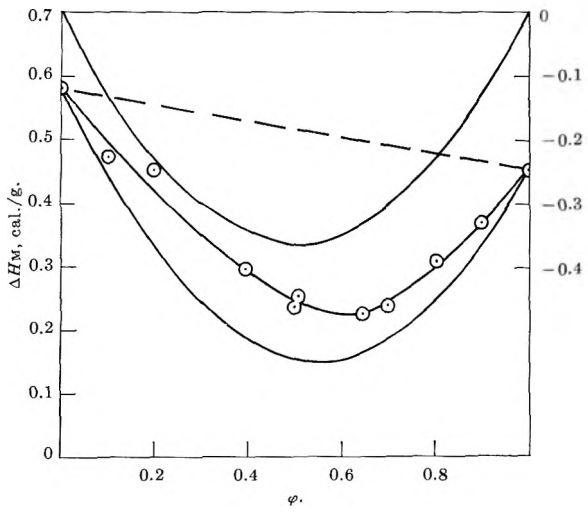

Figure 6. PDS–carbon tetrachloride–methylcyclohexane (VI).

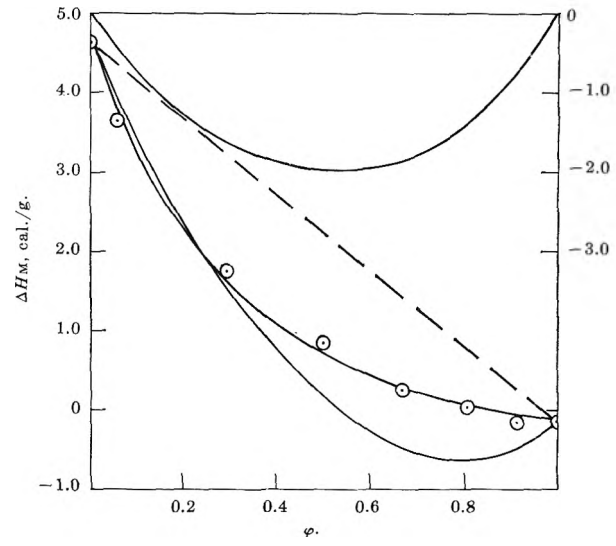

Figure 7. PIB–benzene–cyclohexane (I).

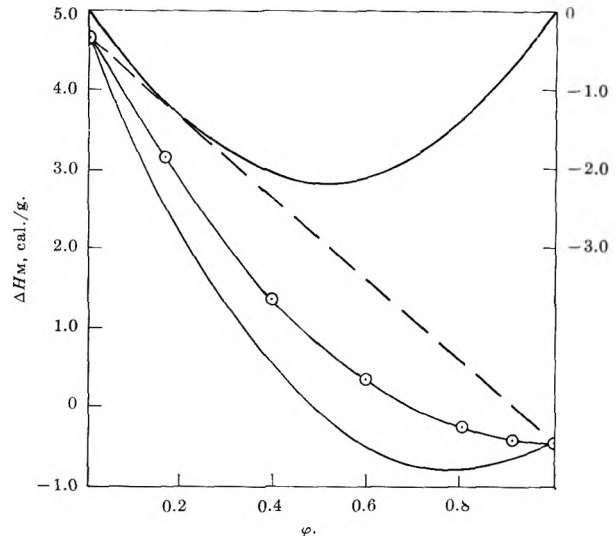

Figure 8. PIB–benzene–heptane (II).

to lower the calculated values of ΔH_M since the polymer would be allowed to "adsorb" the better of the two solvents. This may be checked conveniently by using the work of Tompa on the thermodynamics of binary mixtures in which the interaction energies of the two molecules may depend on their mutual orientation. In particular, using a square lattice and the quasi-chemical approximation, Tompa[10] calculates the heat of mixing a spherical molecule component with a component whose molecules are capable of two orientations of different energy with respect to a neighbor. This problem is formally identical with that of finding the heat of mixing of polymer segments with an equimolar binary mixture with $r_1 = r_2 = 1$, and using the quasi-chemical approximation for both the binary mixture and the resulting solution. The heat of mixing turns out to be given by eq. 6 save for the addition of the term $-(zv_3/v)kT\{(w_{13} - w_{23})/RT\}^2$ terms of higher order in w/kT being neglected. The extra term accounts for the adsorption of the better solvent by the polymer. The resulting further lowering of the calculated heat is small, ~0.05 cal./g. for PIB with I, and has been neglected since it would be further reduced for z larger than 4.

The Mixing Process. In discussing possible explanations of the discrepancy between predicted and observed values of ΔH_M, it is helpful to consider the mixing proc-

(10) H. Tompa, *J. Chem. Phys.*, 21, 50 (1953).

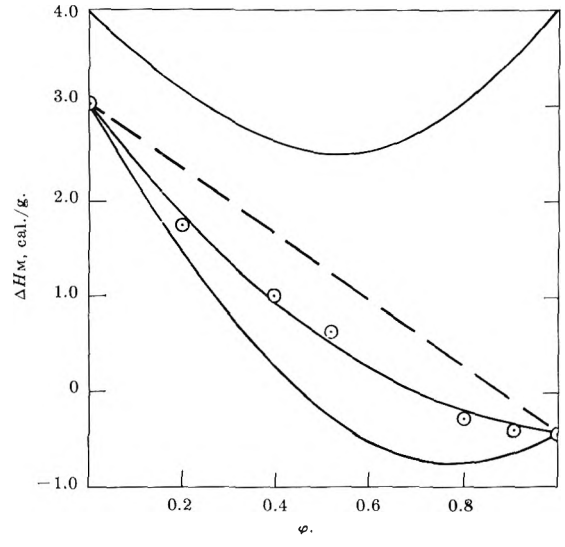

Figure 9. PIB–chlorobenzene–heptane (VII).

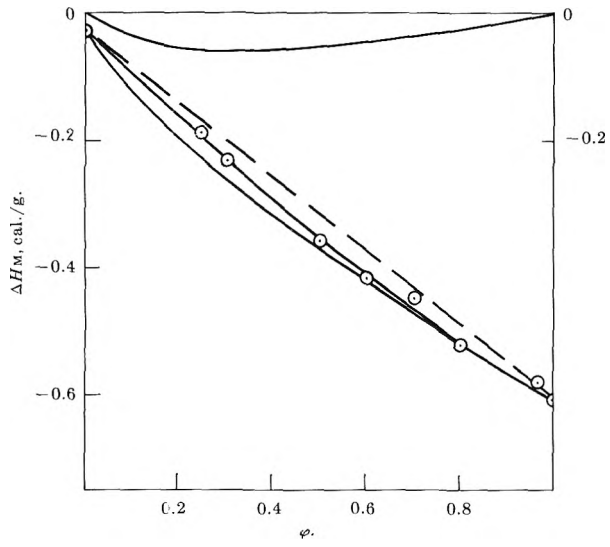

Figure 10. PIB–dodecane–hexane (VIII).

ess as the result of the following steps: (a) the mixed-solvent medium is separated into the pure liquids 1 and 2; (b) portions $1 - \varphi$ and φ of the polymer are mixed with the pure liquids 1 and 2 to produce in each a polymer volume fraction φ_3'; and (c) the resulting solutions are mixed to form the final ternary mixture without changing the polymer concentration and hence without any new polymer–solvent contacts. The heat effect associated with step b is seen to give the first two terms of eq. 6. In step a, $z(N_1r_1 + N_2r_2)\varphi(1 - \varphi)$ contacts of type 1–2 are replaced by 1–1 and 2–2 contacts. Of these, a fraction φ_3' or $zN_3r_3\varphi(1 - \varphi)$ contacts are never remade in step c. They contribute the third term of eq. 6. The remaining fraction $1 - \varphi_3'$ of the 1–2 contacts is remade in step c, and in the theory the accompanying heat effect cancels that entailed by breaking these contacts in step a. However, the 1–2 contacts are remade in the presence of the polymer and it is conceivable that the change of energy associated with making a 1–2 contact may be influenced by a neighboring polymer molecule.

For instance, if 1 is a plate-like aromatic molecule while 2 is spherical, the polymer might orient 1 so as to produce 1–1 and 1–2 interactions of a special type. In order to explain the sign of the discrepancy between theory and experiment, one would have to assume the axes of the benzene molecules parallel to the length of the polymer molecule. Then the formation of a 1–2 contact would entail breaking the relatively strong interaction of two aromatic molecules in contact over their "flat surfaces," enhancing the energy to form a 1–2 contact in step c of the mixing operation. This speculation accounts fairly well for the observed facts with I, II, and VII, but might also predict a similar discrepancy with III and IV. It is just possible that the relative success of eq. 6 for III and IV is due to the benzene–CCl_4 complex formation in III and the similar shape of the components of IV. However, there does not seem to be independent evidence for any ordering of aromatic molecules around the polymer chain. Rather, it has been suggested that polyisoprene[11] and PDS[12] may destroy an order already existing in a pure benzene solvent.

Effect of Volume Changes. It should now be pointed out that eq. 6 does not consider any effect of volume change in the mixing, and excess heats at constant pressure are often converted to excess energies at constant volume for comparison with the rigid lattice theory[13a] by use of an expression of form

$$\Delta E_v^M = \Delta H_p^M - \alpha T \Delta V^M/\beta \qquad (7)$$

α and β being the thermal expansion coefficient and compressibility of the solution. The only possibility of this change eliminating the discrepancy would lie in a ternary term in the volume of mixing, *i.e.*, that due to the presence of the polymer; the volume of mixing of components 1 and 2 in part c of the mixing process is different from that in part a. A calculation of the type of eq. 7 would be impractical for a ternary solution and in any case it is unlikely that this procedure is the correct one for comparing results with the rigid lattice theory.[13b]

(11) A. Münster, *Trans. Faraday Soc.*, **49**, 1 (1953).

(12) M. J. Newing, *ibid.*, **46**, 613 (1950).

(13) (a) J. H. Hildebrand and R. L. Scott, "The Solubility of Non-Electrolytes," Reinhold Publ. Corp., New York, N. Y., 1950, p. 138; (b) R. L. Scott, *J. Phys. Chem.*, **64**, 1241 (1960).

Results of the "Deformable Lattice" Theory. Instead, we choose to take volume changes into account using the Prigogine "deformable lattice" approach[14] which directly predicts excess functions at constant pressure, and which has already been applied to binary polymer solutions.[5] In this and similar theories, the energy of an intermolecular contact depends on the sizes of the cells in which the two molecules are located, and cell sizes are a function of the composition of the solution surrounding a cell. Thus a 1–2 contact can be influenced by the presence of a neighboring polymer molecule.

In the theory, thermodynamic functions of a liquid depend on a reduced temperature, T^*, given for an r-mer liquid by

$$T^* = \frac{kT(c/r)}{2z\epsilon^*} \tag{8}$$

ϵ^* is the minimum of the interaction potential between segments which occurs at a distance, r^*, and $3c$ is the number of external degrees of freedom of the r-mer. For the particular case of free rotation between successive segments, the "structural factor," c/r, is given by

$$\frac{c}{r} = \frac{1}{3} + \frac{1}{r} \tag{9}$$

and depends on the length of the molecule, tending to $^1/_3$ for infinite molecular weight. On the other hand, for a monomeric liquid, $c/r = 1$. A single T^* also exists for a solution, namely

$$\langle T^* \rangle = \frac{kT\langle c/r \rangle}{2z\langle \epsilon^* \rangle} \tag{10}$$

where the $\langle c/r \rangle$ and $\langle \epsilon^* \rangle$ are averages over the solution components

$$\langle c/r \rangle = \sum \varphi_i'(c/r)_i$$
$$\langle \epsilon^* \rangle = \sum \varphi_i' \epsilon_{ii} - 2\sum_{j>i} \varphi_i' \varphi_j' \omega_{ij} \tag{11}$$

(The prime superscripts indicate volume fractions in the ternary solution.) The heat of mixing is determined by the difference in "structural factor," c/r, between the component, and by differences in force fields and sizes. These latter are characterized by the parameters δ and ρ, defined by

$$\delta_{ij} = \epsilon_{jj}^*/\epsilon_{ii}^* - 1; \quad \rho_{ij} = r_{jj}^*/r_{ii}^* - 1 \tag{12}$$

and give positive heats of mixing.

We shall consider first the particular extreme case where both solvents have the same value of c/r, *i.e.*, $c_1/r_1 = c_2/r_2 = c_s/r_s$, but $\neq c_3/r_3$ and $\delta_{ij} \neq 0$. Returning to the description of the mixing process given above, the deformable lattice theory differs from the rigid lattice theory in that the energy associated with breaking 1–2 contacts in step a is now different from that associated with remaking them in step c. This is because of the polymer in step c which lowers the reduced temperature of the solutions by lowering $\langle c/r \rangle$ and hence $\langle T^* \rangle$ through eq. 10.

We have calculated the heat of mixing of a polymer with a mixed solvent medium using (a) the deformable lattice theory, (b) the geometric mean rule for contact energies, and (c) the simplifying assumption that $\rho_{ij} = 0$. Some straightforward but lengthy algebra shows that the heat of mixing is now given by eq. 6 plus the term

$$-T\left(1 - \frac{c_3/r_3}{c_s/r_s}\right)\Delta C_{p,12} \tag{13}$$

where $\Delta C_{p,12} \equiv \partial \Delta H_{12}/\partial T$ is the excess heat capacity of an amount of mixed solvent equal in volume to the polymer. The excess heat capacity is negative for most nonpolar binary mixtures so that (12) gives a positive contribution to the predicted heat as required by experiment. The above contribution vanishes when $c_3/r_3 = c_s/r_s$ and is only predicted when a component is polymeric. Although the calculation has not been performed in detail when restrictions (b) and (c) are relaxed and when the average potential theory instead of deformable lattice theory is used, it appears likely that the same results would be obtained.

System I has a negative value of $\Delta C_{p,12}$ which is found experimentally to be much larger than predicted by the Prigogine theory using the methods of ref. 14a. In either case, however, the contribution (12) is positive. Using the experimental value[2a] of $\Delta C_{p,12}$, from (13), would be much too large, but using the predicted value gives rough agreement for PIB and PDS with I. Similarly system II has a large negative $\Delta C_{p,12}$ and presumably also VII. For systems III–VI there appear also small discrepancies between eq. 6 and experiment which are just outside possible experimental error. Small negative values of $\Delta C_{p,12}$ and hence positive discrepancies are predicted for these systems although the excess heat capacity of IV appears to be zero[15] and that of III positive. V and VI were chosen because the molecules of the components are spherical and hence no effect would be predicted due to an orientation of the

(14) (a) I. Prigogine (with A. Bellemans and V. Mathot), "The Molecular Theory of Solutions," North-Holland Publ. Co., Amsterdam, and Interscience Publishers, Inc., New York, N. Y., 1957, Chapter 17; (b) A. Bellemans and C. Naar-Colin, *J. Polymer Sci.*, 15, 121 (1955).

(15) S. N. Bhattacharyya, A. V. Anantaraman, and S. R. Palit, *Physica*, 28, 633 (1962).

molecules. The discrepancy between experiment and eq. 6 is thus in favor of the deformable lattice theory.

System VIII has a large negative excess heat capacity[4] which is also predicted by theory.[16] However, this system is quite different from the others in that $\delta = \rho = 0$ and $c_1/r_1 \neq c_2/r_2$. The negative excess heat capacity arises in fact from this difference in the structural factors between components 1 and 2. In this case expression 13 no longer holds, and in fact one can show that ΔH_M should be correctly given by eq. 6 as is found experimentally.

Our final conclusion is that the source of the discrepancy between theory and experiment cannot be ascribed with confidence to either the volume effect on mixing or an orientation by the polymer of one of the components. However, the effect of volume changes on excess thermodynamic properties is established. One might hope to find this interpretation borne out by more accurate experimental work which would be of interest after more is known on this effect in binary solutions of polymers and on excess heat capacities of solutions.

Acknowledgments. We wish to thank the Paint Research Institute for their support enabling us to do this work, and the National Research Council of Canada for their general support of this laboratory. We are grateful for the gifts of polymers from Enjay Co. and from Dow Corning Silicones, Ltd., and we also wish to acknowledge the contribution of Prof. Marcel Rinfret and Mr. Patrick Picker who built the microcalorimeter installation.

(16) S. N. Bhattacharyya, D. Patterson, and T. Somcynsky, to be published.

Nuclear Magnetic Resonance Studies of Adsorption on Thorium Oxide[1]

by Wallace S. Brey, Jr., and Kenneth D. Lawson

Department of Chemistry, University of Florida, Gainesville, Florida *(Received January 3, 1964)*

Nuclear magnetic resonance line widths and relaxation times have been measured for water, methyl alcohol, ethyl alcohol, and butylamine adsorbed on thorium oxide. The source of the thorium oxide and the conditions of its activation influence the relaxation times of the adsorbate. Temperature dependence studies of the relaxation times of adsorbed water permit an estimate of the activation energy for the motions producing relaxation of the adsorbed molecules. Similar studies for the organic molecules lead to a quite different sort of information: it is possible to see in the line width thermal transitions corresponding to the successive loss of motional freedom of various parts of the molecule. Line width behavior seems also to be related to the ratio of molecular diameter to pore size.

Introduction

Nuclear magnetic resonance techniques appear to hold some promise as tools for investigating the interaction of adsorbed molecules with a substrate surface and with one another. The nature of the nuclear resonance spectrum is sensitive to, among other things, the particular magnetic environment of the hydrogen or fluorine atoms producing the absorption peak, as well as to the correlation times for nuclear magnetic

(1) Presented at the 145th National Meeting of the American Chemical Society, New York, N. Y., Sept., 1963.

dipoles in the adsorbed phase. A number of measurements have been made of line widths or relaxation times for various systems.[2-11] However, it has not been in general possible to differentiate between the behavior of various portions of the adsorbed molecule. For hydrogen atoms, the usual range of chemical shifts is 500–1000 cycles at 60 Mc., and the line widths of interest are of the order of several hundred to several thousand cycles, so that the absorption peaks of nuclei of different chemical shifts overlap one another. Furthermore, not much attention has been paid to the relationship between the history and structure of the adsorbent and the n.m.r. parameters of adsorbates on its surface.

In the present work, temperature dependence studies have led to results which can only be interpreted in terms of varying behaviors of different parts of the adsorbate molecule. Line width measurements for methanol, ethanol, and *n*-butylamine adsorbed on thorium oxide, carried out over the range from room temperature down to $-100°$ show that restriction of motion of part of the molecule, presumably the polar group attached to the surface, occurs not far below room temperature, while a narrow absorption band continues to appear at very much lower temperature. The latter must be associated with persistence of the free motion of the alkyl portions of the molecules at the lower temperatures.

Samples of thorium oxide prepared by dehydration of the hydroxide have also been compared with those obtained by thermal decomposition of the solid oxalate. As it will be shown below, not only does this difference in origin make a considerable difference in the behavior of the adsorbate, but also conditions of activation of the material from any one source, such as the temperature, modify the n.m.r. behavior of the adsorbate.

Experimental

Precipitation of the hydroxide was carried out by adding concentrated aqueous ammonia to a stirred solution of thorium nitrate. The nitrate was used as obtained from Fisher Scientific Co. The rate of addition of the ammonia was controlled, since this has been found to affect drastically the properties of the resulting oxide. The precipitate was then filtered with suction, washed, and dried at 120° for 24 hr. The granular material was powdered to pass 100 mesh and was activated by heating for 6 hr. under vacuum in a Vycor tube. Details of precipitation and activation conditions are given in Table I, along with the surface areas of the resulting oxides as determined from nitrogen isotherms at liquid nitrogen temperature by the B.E.T. method. Two thoria samples were prepared by heating Fisher thorium oxalate at 600° in an open-end tube in an electric furnace; circulation of air during decomposition was necessary to avoid deposition of carbon.

Table I: Thorium Oxide Sample Preparation

Sample number	Thorium nitrate, g.	Solution volume, ml.	Ammonia volume, ml.	Time of ammonia addition, min.	pH of final wash water	Activation temp., °C.	Surface area, $m.^2/g.$
1	40	500	50	0	...	600	14.4
2A	210	1250	250	0	7	600	14.1
2B	210	1250	250	0	7	500	28.9
3A	40	500	50	1.6	5	600	9.4
3B	40	500	50	1.6	5	500	31.1
4	40	500	50	0	7	550	20.7
5	40	500	50	0	9	500	2.0
6	Made by heating oxalate					600	12.5
7	Made by heating oxalate					600	37.0

The n.m.r. samples were held in 5-mm. tubes fitted with vacuum stopcocks. Increments of adsorbate were added from a vacuum line containing a buret of known volume. The amount adsorbed was checked after each addition by weighing the tube plus contents. Spectra were obtained with a Varian dual-purpose n.m.r. spectrometer, recording the derivative of the absorption peak with use of 80 c.p.s. modulation. The amplitude of the audio sweep field was kept at the lowest value for which a suitable signal could be obtained. The input power level was adjusted until onset of saturation was noted and then reduced several decibels below this level.

The temperature of the samples was controlled with the aid of a Varian Model V-4340 variable temperature probe unit. The thermocouple near the sample was calibrated against the reading of a thermocouple inside the empty sample tube. Each line width point reported corresponds to the average of five or more spectral sweeps. Time was allowed for the sample to come

(2) N. Fuschillo and J. G. Aston, *J. Chem. Phys.*, **24**, 1277 (1956).

(3) T. W. Hickmott and P. W. Selwood, *J. Phys. Chem.*, **60**, 452 (1956).

(4) J. R. Zimmerman and W. E. Brittin, *ibid.*, **61**, 1328 (1957).

(5) J. R. Zimmerman and J. A. Lasater, *ibid.*, **62**, 1157 (1958).

(6) J. R. Zimmerman, B. G. Holmes, and J. A. Lasater, *ibid.*, **60**, 1157 (1956).

(7) H. Winkler, *Z. Naturforsch.*, **16a**, 780 (1961).

(8) G. T. Barnes, *Z. Angew. Math. Phys.*, **13**, 533 (1962).

(9) K. Hirota, K. Fueki, and T. Sakai, *Bull. Chem. Soc. Japan*, **35**, 1545 (1962).

(10) V. I. Kvlividze, N. M. Ievskaya, T. S. Egorova, V. F. Kiselev, and I. D. Sokolov, *Kinetika i Kataliz*, **3**, 91 (1962).

(11) J. G. Aston and H. W. Bernard, *J. Am. Chem. Soc.*, **85**, 1573 (1963).

to constant temperature before these measurements were made, and line widths were determined both for increasing and for decreasing series of temperatures.

Spin–spin relaxation times, T_2, were taken as inversely proportional to the line width. Spin–lattice relaxation times, T_1, for the adsorbed molecules were estimated from the value of H_1 at which the signal intensity was a maximum, along with the calculated value of T_2. The lines were assumed to obey the Bloch equations, for which the shape is Lorentzian. To test the assumption of shape, the method of Pake and Purcell[12] was employed, in which there is measured the ratio of the maximum to the minimum in the derivative presentation of the dispersion curve. The ratios found varied from 4.9 up to 7.5; the Gaussian value is 3.5, and the Lorentzian value is 8. The average of the ratios determined was 6.2, which indicates that the lines are at least closer to Lorentzian than to Gaussian in shape.

The line widths as determined also have contributions from two other factors for which allowance has not been made in the data presented here. One is the inhomogeneity of the magnetic field produced by the solid at the sample: a suspension of thoria in liquid water gave a line width of about 60 c.p.s. as determined by high-resolution techniques. The other is sweep broadening from the modulation field which is about 70 c.p.s. for a narrow line and decreases to the point where it is negligible for lines with widths in excess of 350 c.p.s.

Results and Discussion

Figure 1 shows the line widths, measured at room temperature, for water adsorbed on four different samples of thorium oxide, numbers 3A, 3B, 4A, and 4B, all prepared from the hydroxide, as a function of amount of water adsorbed. In computing V_m, the amount of adsorbate equivalent to a "monolayer," the surface area occupied by one water molecule has been taken as 14.0 Å.^{2}. This value may in practice vary as much as 20% from sample to sample, but a variation of this magnitude would not affect the qualitative comparisons to be made. The two samples of larger surface area were activated at 500°, the two of smaller area at 600°. To a small degree, the positions of the curves may be dependent upon the amount of water remaining in the sample after activation. However, the isotherms were all continued to the point where any further addition of water was occurring with negligible rate, and the samples of high area did not adsorb readily an amount of water nearly as great, in terms of ratio to surface area, as did the low area samples, so that there appears to be a fundamental difference in behavior. The isotherm on the sample of 28.9 m.^{2}/g. was interrupted for about 30 days at the point where there is a break in the plot. The values in the short additional portion of the curve were determined following this interruption, and it will be observed that the adsorbate in the interim became more intimately associated with the solid, either by an activated adsorption process or by diffusion into interior, less accessible sites. A similar effect was not observed in samples activated at 600°, but was observed in other samples made at 500°.

Figure 2 shows the relaxation times for water adsorbed on sample 3B. Points obtained on desorption show an appreciable hysteresis in T_2 (which is inversely proportional to the line width shown in Fig. 1), while the value of T_1 is almost independent of surface coverage. The line width behavior of water adsorbed on two samples prepared from thorium oxalate is plotted

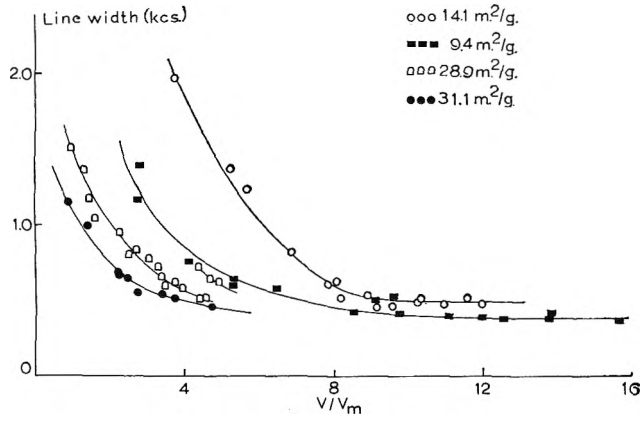

Figure 1. Variation of line width of adsorbed water with surface coverage for four samples of thorium oxide prepared from thorium hydroxide; surface areas cited were measured by N_2 adsorption.

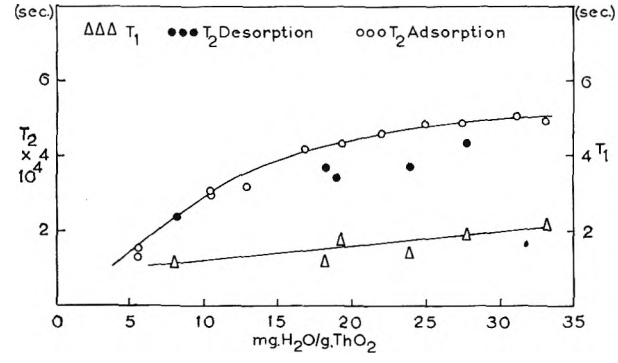

Figure 2. Relaxation times as a function of amount adsorbed for water on thoria sample 3B, prepared from thorium hydroxide.

(12) G. E. Pake and E. M. Purcell, *Phys. Rev.*, **74**, 1184 (1948).

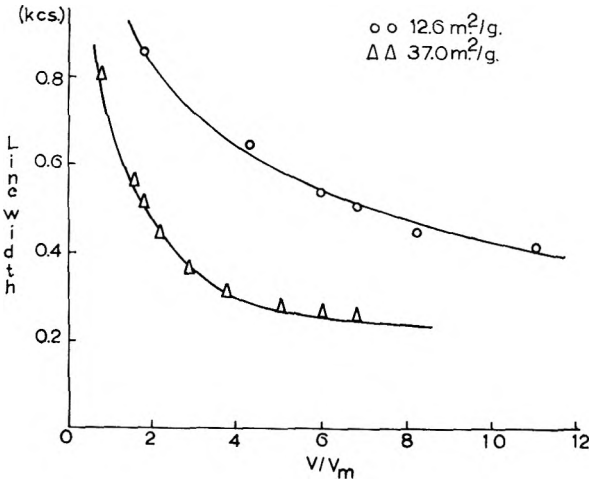

Figure 3. Variation of line width of adsorbed water with surface coverage for two samples of thorium oxide, of different surface area, prepared from thorium oxalate.

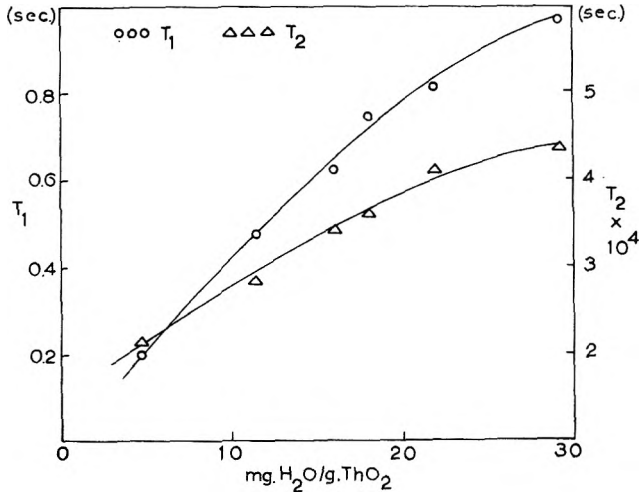

Figure 4. Relaxation times as a function of amount adsorbed for water on thoria sample 6, prepared from thorium oxalate.

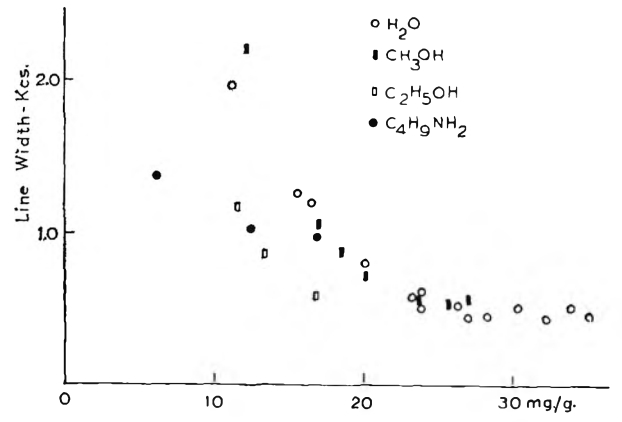

Figure 5. Line widths as a function of amount adsorbed for various adsorbates on thoria sample 2A, prepared from thorium hydroxide.

in Fig. 3. The lines are much narrower, especially at low coverages. This indicates, in a general way, that the interaction of water with the surface is weaker for these materials than when the hydroxide is the parent compound. The larger area sample again gives the narrower line for the same relative amount of water. The longitudinal relaxation times, T_1, for water on sample 6, from the oxalate, as shown in Fig. 4, exhibit a much stronger dependence on surface coverage than those on oxides from the hydroxide, and the relaxation is much more rapid. This suggests that the surface is acting as a very effective agent for longitudinal relaxation and is acting only on that fraction of the water held immediately adjacent to the surface. This could be the result of the presence of paramagnetic centers in the solid. It is interesting that the results are rather similar to those found for water adsorbed on γ-alumina.[3]

The line widths resulting when various other molecules are adsorbed on sample 2A, from the hydroxide, are compared with those for water in Fig. 5. Methanol and water have nearly the same widths at lower coverages, in contrast to ethanol and *n*-butylamine, which have narrower lines, although there should be an appreciable chemical shift contribution to line width for the latter two. The differences would be accentuated if the abscissa scale were based on moles rather than weight of adsorbate. One possible explanation is that the longer molecules have their organic tails free of the surface, with correspondingly longer relaxation times. An alternative possibility is that the larger molecules cannot fit into small pores; and thus, the lower effective area of the surface causes them to build up multilayers at a lower coverage than would be found for smaller molecules. On a sample activated at 500°, the behavior of methanol and ethanol is almost identical, indicating that perhaps both are excluded from the smaller pores, while the line width of the water resonance is still somewhat greater.

The transverse and longitudinal relaxation times as measured at room temperature for adsorbates other than water are compiled in Table II. These values are, of course, averaged over all the protons in the adsorbate molecule. The magnitude of T_1 is in some cases much larger than for water; moreover, it sometimes decreases with increasing surface coverage, rather than increasing as for water. This implies that the relaxation is not always produced by the surface, but receives contributions from interadsorbate effects.

Table II: Relaxation Times for Protons in Molecules Adsorbed on Thorium Oxide

Adsorbate, mg./g. of ThO_2	$T_2 \times 10^4$, sec.	T_1, sec.
	Methanol on sample 2A	
12.4	0.825	...
17.1	1.73	20.0
18.9	2.06	19.3
20.3	2.51	19.0
23.9	3.06	15.6
26.0	3.30	12.5
27.2	3.22	12.8
	Methanol on sample 2B	
10.9	1.40	3.0
14.5	1.82	11.6
17.7	2.40	11.2
	Methanol on sample 6	
8.6	2.54	3.4
13.8	3.94	6.8
	Ethanol on sample 2A	
11.4	0.59	36.4
13.4	2.13	5.9
16.9	3.09	0.86
	Ethanol on sample 2B	
4.7	1.05	...
10.1	1.37	7.8
12.8	1.86	11.4
16.7	2.62	16.0
	n-Butylamine on sample 2A	
6.1	1.33	3.18
12.9	1.76	3.81
16.9	1.85	5.74
16.9	1.95	5.44
	n-Butylamine on sample 3A	
5.3	1.25	6.72
8.2	2.07	2.04

Figure 6 shows typical data for the temperature dependence of the line width for water at three different coverages on sample 2B, from the hydroxide. The lowest coverage is just less than two monolayers. The highest coverage seems sufficient so that one might anticipate the formation of ice as the temperature is lowered, but the line width is only about one-tenth that of ice, even at -80 to $-90°$. Relaxation times for a coverage of 16.7 mg. of water per gram on sample 3B are shown as a function of temperature in Fig. 7. As expected, increasing temperature causes T_2 to increase; at the same time T_1 decreases as the components of molecular motions with frequencies in the vicinity of the resonance frequency increase in importance.

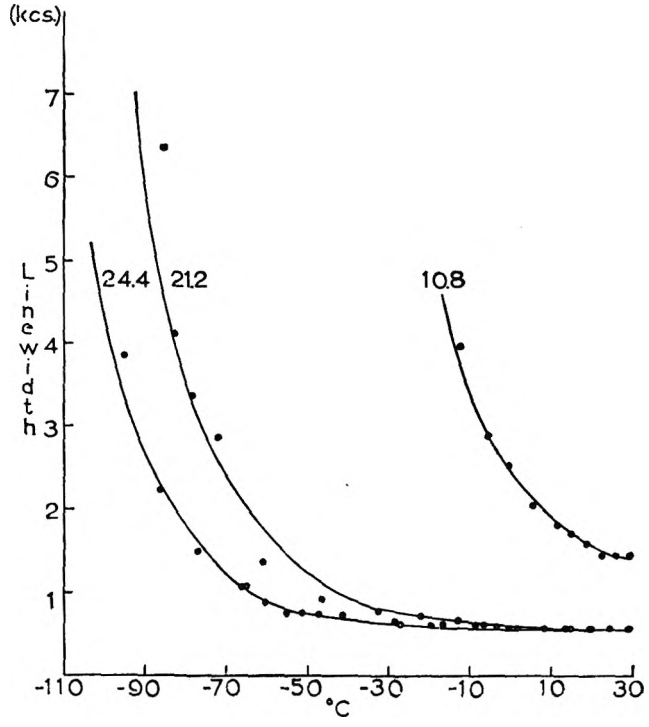

Figure 6. Temperature dependence of the line width for water adsorbed on thoria sample 2B, prepared from thorium hydroxide; numbers on the curves give the number of milligrams of water adsorbed per gram of thoria.

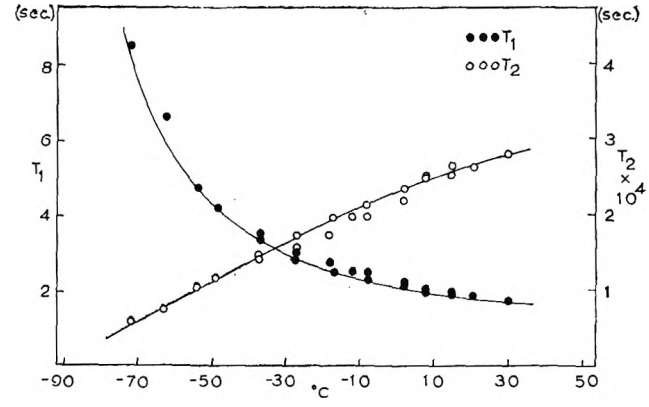

Figure 7. Temperature dependence of relaxation times for 16.7 mg. of water per gram of thoria on sample 3B.

Figures 8 and 9 are Arrhenius-type plots of the logarithm of the line width for water adsorbed on sample 3A, prepared from hydroxide, and on sample 6, prepared from oxalate, respectively. The apparent activation energy calculated from the slopes of the plots increases monotonically as the temperature decreases for the first sample, and the plots display three linear regions for all but the lowest coverage. If the slopes do represent

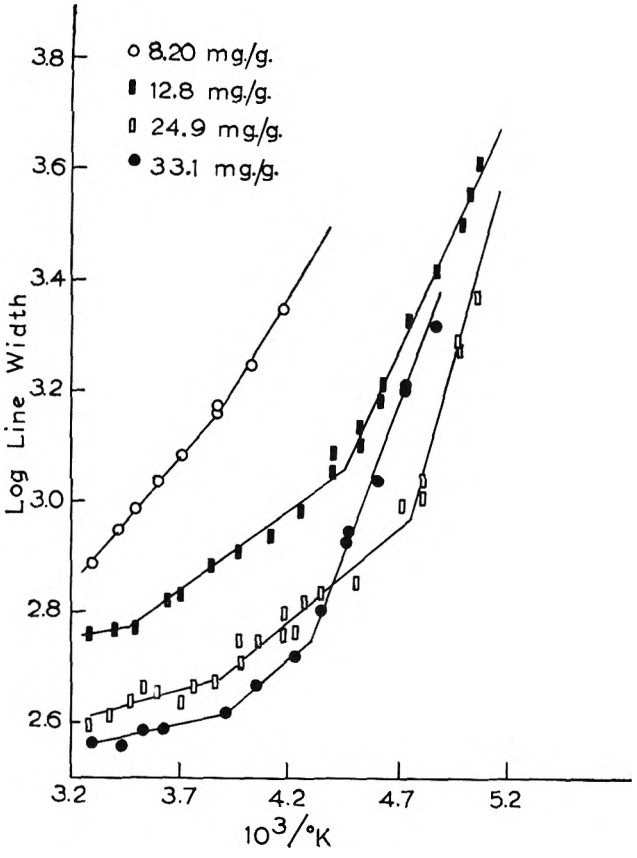

Figure 8. Logarithm of line width against reciprocal of the absolute temperature for various amounts of water adsorbed on thoria sample 3A, prepared from thorium hydroxide.

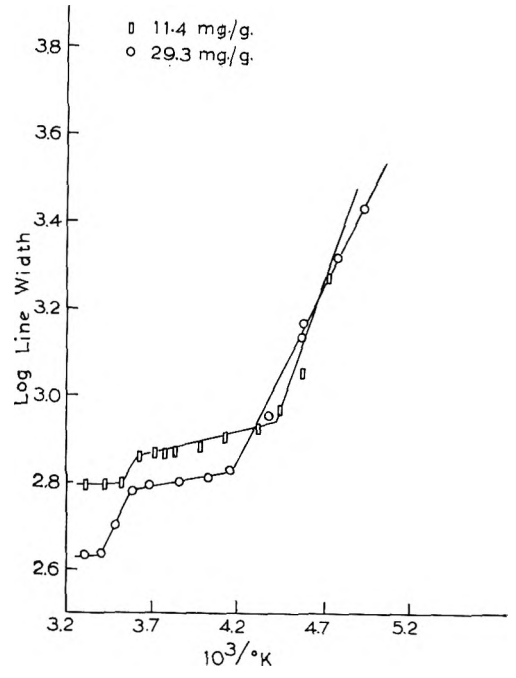

Figure 9. Logarithm of the line width against reciprocal temperature for two different amounts of water adsorbed on thoria sample 6, from the oxalate.

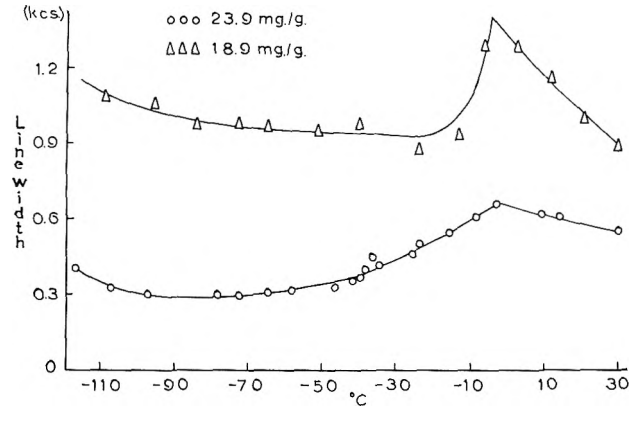

Figure 10. Temperature dependence of the line width of adsorbed methanol, for two different amounts adsorbed.

activation energies for molecular reorientation, this behavior is unreasonable. It appears, rather, that only the middle portion has a slope which may be so interpreted. For the region of narrow lines, the artificial broadening discussed above contributes an appreciable amount to the observed line width. In the low-temperature, wide line region, the large apparent activation energy is attributed to the formation of an incipient ice-like structure. The larger the coverage, the greater the fraction of the adsorbed water which is free to participate in this structure and the steeper the slope of the plot. For the sample from oxalate, the same explanations apply to the linear portions at the extremes of the curve. There are now, however, two middle portions with slopes increasing with increasing temperature, which correspond to two kinds of molecular motions. These behave in a reasonable way: the one with higher activation energy occurs appreciably only at higher temperatures.

The temperature dependence of the line width of methanol adsorbed on sample 2A, from the hydroxide, is shown in Fig. 10. For both coverages the line width shows an apparent maximum near 0° and then decreases to, or even below, the value observed at room temperature. In the region from about −30 to −90°, the width remains essentially constant. Below this it again begins to increase. The maximum near 0° is attributed to the loss of motion of the hydroxyl group at about this temperature, resulting in broadening of the hydroxyl contribution to the line to the point where it is not observable. That the maximum is more pronounced at lower coverage of the surface indicates that the effect results primarily from the interaction of the

adsorbent and adsorbate, rather than from cooperative effects in the adsorbate. If we assume that the molecules are primarily adsorbed by attachment through the hydroxyl group, the narrow resonance line at lower temperatures is then explained as the result of free rotation of the methyl groups, which persists to temperatures slightly below the bulk freezing point of methanol. Similar results are observed for methanol adsorbed on a sample of thoria derived from the oxalate.

In Fig. 11 there is shown the temperature dependence of the line width of ethanol adsorbed on sample 2B. The line width maximum appears at a somewhat higher temperature than for methanol. There is, at lower temperatures, a gradual increase in line width which seems to be occurring in two stages, such as one might expect if the methylene protons lost mobility before the methyl group, in consequence of the closer proximity of the methylene group to the site of attachment of the molecule to the surface.

The temperature dependence of the line width of *n*-butylamine adsorbed on sample 2A, from the hydroxide, is plotted in Fig. 12. Here again the behavior is similar to that of the alcohols. At higher coverages there are two reasonably well-defined maxima in the line width, one at about 10° and one at about −50°. In an attempt to verify that the results were reproducible, the measurements were repeated a number of times, and the scatter was found to be well within the experimental error. However, at low coverage it was found that in the temperature range corresponding to that between the two maxima at the higher coverage, the results were not reproducible. Close examination of the resonance line indicated that it is unsymmetrical, and in the temperature range in which difficult reproducibility was observed, the components of the line can be distinguished, as shown in Fig. 13. As the temperature is decreased, the part of the line belonging to the amino group broadens out still more and the sharp components due to the alkyl group predominate. The uncertainty of the line width in the transition region results from the inability to resolve completely the various components. At higher coverages, the contribution of the broad line resonance of the amino group is relatively less important since many of these groups are now not bonded to the solid, and the components of the line can be more easily resolved. Again, this is evidence that the effects observed include, at least in part, the interactions between the solid and the adsorbate.

The maximum in the line width curve for the amine at a lower temperature must now be explained. This may be the result of loss of motional freedom for the protons in the methylene group adjacent to the amino group. A second possibility is that this maximum represents loss of motional freedom for only those molecules not strongly under the influence of the solid. It is striking that the bulk freezing point for *n*-butylamine

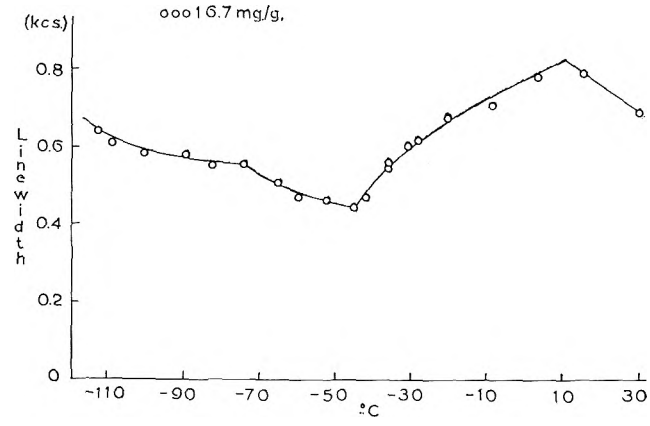

Figure 11. Temperature dependence of the line width of adsorbed ethanol.

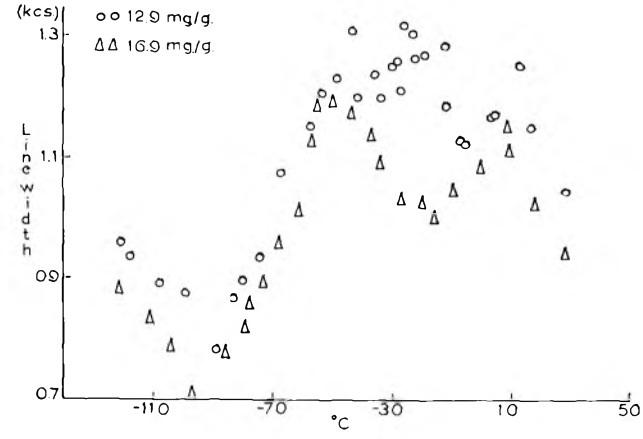

Figure 12. Temperature dependence of the line width of adsorbed butylamine; the two sets of points are for two different amounts adsorbed.

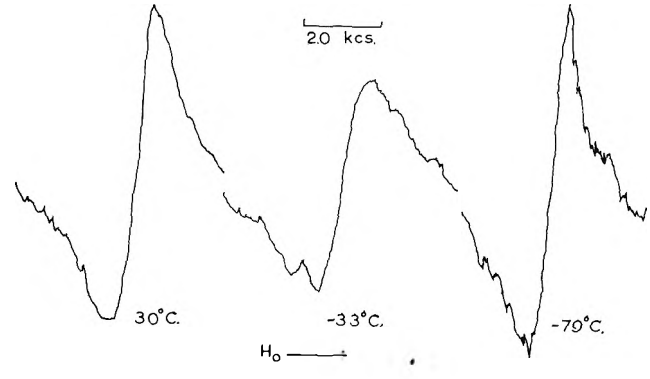

Figure 13. Derivative n.m.r. curves for adsorbed butylamine; the sweep rate is the same at all three temperatures.

is about $-50°$, so that the narrow line below that temperature must represent a contribution from molecules which are prevented from undergoing the freezing process.

The results of this investigation indicate some of the potentialities of n.m.r. as a tool to be added to those previously available for studying adsorption on solids. Measurements of the temperature dependence of relaxation times add greatly to the information about motions of adsorbed molecules which can be gained by this technique. Further work is in progress in these laboratories in an effort to relate the data obtained for specific samples of thorium oxide as adsorbent with other aspects of the surface structure of the oxide.

Acknowledgment. Financial support by the United States Atomic Energy Commission of this research is gratefully acknowledged.

Reaction of Oxygen with Evaporated Films of Lead

by J. R. Anderson and V. B. Tare

Chemistry Department, University of Melbourne, Parkville N.2, Victoria, Australia
(Received January 6, 1964)

The reaction of oxygen with evaporated films of lead has been studied in the range 90–548°K. and 10^{-2} to 10^{-5} mm. The only oxidation product that could be identified by electron diffraction was orthorhombic lead monoxide. At 548 and 503°K., the rate of oxidation was independent of oxide layer thickness (linear law) and proportional to the first power of oxygen pressure, while in the range 195–373°K. a direct logarithmic growth law was obeyed. Limiting oxygen uptakes varied from ~11 Å. at 90°K. to ~87 Å. at 373°K. Electrical resistance and thermal e.m.f. measurements have been made on thin polycrystalline layers of orthorhombic lead monoxide at oxygen pressures in the range 10^{-1} to 10^{-3} mm. The results are consistent with a model in which the lead oxide retains n-type bulk behavior over the whole of this range, but the measured over-all resistance is dominated by a p-type surface layer at oxygen pressures $>\sim10^{-2}$ mm. It is considered that in the principal mode of *bulk* nonstoichiometry there are present anion vacancies and electrons. The observed oxidation kinetics have been interpreted on the basis of the dissociation of oxygen being rate controlling, while the exact form of the oxidation kinetics depends on the way in which the concentration of adsorption sites varies in the course of the reaction. If at high temperatures the degree of surface coverage by adsorbed oxygen is low, a linear law results. If at lower temperatures a substantial fraction of adsorption sites is occupied and if adsorbed oxygen is present both as neutral pairs and as field-creating ions with the former in large excess, it is shown that the concentration of adsorption sites may decrease approximately exponentially with increasing oxide layer thickness, leading to an approximate direct logarithmic growth law. The oxidation theory of Grimley and Trapnell has been extended to include systems where anion vacancies are involved.

Introduction

Although the oxidation of lead has previously been studied in detail at temperatures approaching or exceeding the melting point (*e.g.*, Pilling and Bedworth[1] and Bircumshaw and Preston[2]), there are very few data available for lower temperatures, despite the long history of the practical use of lead as a protective device in the atmosphere. The present paper describes a study of the kinetics of oxidation of evaporated lead films in the temperature range 90–548°K. Ancillary to this, studies have been made of the structure of the product layer by electron diffraction and of the electrical properties of the orthorhombic modification of lead monoxide as a function of oxygen pressure and of temperature.

Experimental

Measurements with Lead Films. Lead films were evaporated onto the inside wall of a 250-ml. spherical vessel from a centrally situated source. The latter consisted of a coil of 0.35-mm. diameter tungsten wire which held a lead bead (54 mg.). The average rate of evaporation was about 5.4 mg. min.$^{-1}$, and the entire bead was evaporated. Prior to evaporation, the bead was outgassed for about 2 hr. at a temperature just insufficient to cause appreciable evaporation.

A conventional high-vacuum system was used with mercury diffusion pumps. The reaction vessel and final liquid-air trap could be baked and a residual pres-

(1) N. B. Pilling and R. E. Bedworth, *J. Inst. Metals*, 29, 529 (1923).
(2) L. L. Bircumshaw and G. D. Preston, *Phil. Mag.*, 25, 769 (1938).

sure of about 10^{-7} mm., as indicated on an ionization gage, was achieved. Because of its pumping action and the likelihood of augmenting the rate of oxidation by the production of thermally activated oxygen, the ionization gage was not used to monitor oxygen pressure during a reaction, but this was done with a McLeod gage. Where necessary, a correction was made for thermal transpiration. When using carbon dioxide–oxygen or water vapor–oxygen mixtures, the oxygen pressure was measured after freezing out the second component in a side arm with liquid air. Although the vapor pressure of carbon dioxide at liquid-air temperature is about 10^{-5} mm., this introduces a negligible error by comparison with oxygen pressures in the range 10^{-2} to 10^{-3} mm. A Pirani gage was calibrated against the McLeod using oxygen and was used roughly to measure the pressure of water vapor when making up water vapor–oxygen mixtures. When working with oxygen, the refrigerated traps were cooled with liquid air, but with xenon and with carbon dioxide–oxygen mixtures Dry Ice was used. Water vapor–oxygen mixtures were introduced into the reaction vessel after warming the traps to 273°K. Dead-space measurements were made with helium using the McLeod as a standard volume.

Electrical Measurements on Orthorhombic Lead Monoxide. The use of compressed-powder pellets for conductance and thermal e.m.f. measurements was unsatisfactory because of the very high specific resistance (about 10^{10} ohm-cm.) and because of the slow rate of equilibration with gaseous oxygen. Measurements were therefore made in an apparatus (Fig. 1) in which the lead monoxide specimen was prepared as a thin layer by evaporation. This method has also been used by Heijne,[3] but the present apparatus has been designed to permit the attainment of better vacuum conditions by baking and to allow specimen preparation and subsequent measurements to be made without the necessity of breaking the vacuum. The evaporating coil F1, made from 0.5-mm. diameter platinum wire, was used to evaporate the lead monoxide (300 mg.) and measurements were made on that portion which condensed onto the glass surface B. The latter was made conducting by the method given by Gomer[4] and electrical connection to it was made *via* the imbedded platinum strip S. After preparation of the lead monoxide specimen, a thin silver layer was evaporated on top of it from F2, contact to the silver being finally made with the movable contact C. The movable aperture A was withdrawn into position 1 during the evaporation of the lead monoxide and was used in position 2 to confine the silver deposit to a spot of diameter about 1 cm. near the center of B. The temperature of the lead

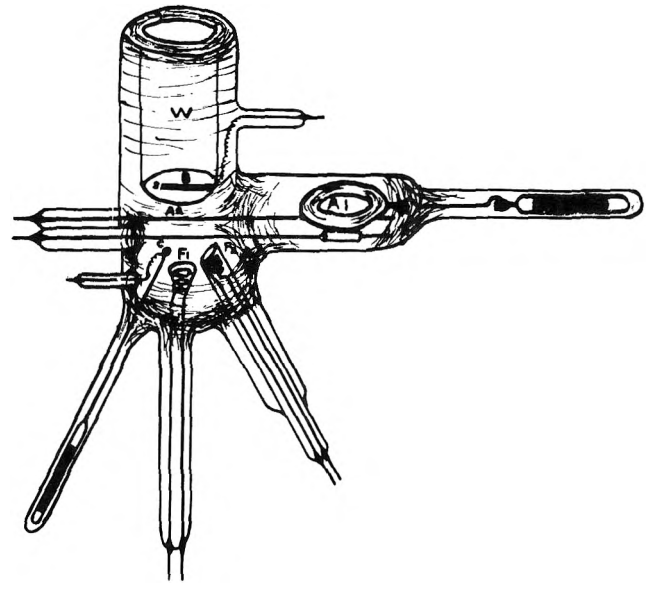

Figure 1. Apparatus used to study the electrical properties of thin layers of lead monoxide: F1, evaporator for lead monoxide; F2, evaporator for silver; B, surface upon which measurement specimen was condensed: S, platinum contact; C, movable contact; A, movable aperture; W, temperature control well.

monoxide specimen was adjusted using the well W. The current flowing through the specimen during resistance measurements was measured with a Keithley Model 610A electrometer. Only a measurement of the sign of the thermal e.m.f. was made and to do this, the temperature of the conducting glass surface was raised by about 70° by introducing hot water into W. Since thermal equilibration across the lead monoxide layer was complete in about 30 sec., the thermal e.m.f. was observed as a transient and was indicated on a Keithley Model 150A electrometer.

The evaporation of the lead monoxide was carried out in about 10^{-3} mm. of oxygen (*cf.* Heijne[3]). After evaporation, the specimen was heated to 620°K. for 2 hr. in 10^{-3} mm. of oxygen and was cooled to room temperature. The apparatus was then evacuated to about 10^{-6} mm. and the silver layer was deposited. From the weight of oxide evaporated and from the geometry of the apparatus, the thickness of the oxide layer on B was estimated to be about 10 μ.

Materials. Lead was of purity 99.999%, obtained from the Metallurgy Department, University of Melbourne. Lead monoxide was Johnson and Matthey Specpure grade, with the following impurities in p.p.m.: silicon 5, calcium 3, iron 2, magnesium 1, and aluminum bismuth, copper, and silver each <1. Oxygen was prepared

(3) L. Heijne, *Philips Res. Rept. Suppl.*, No. 4 (1961).
(4) R. Gomer, *Rev. Sci. Instr.*, 24, 993 (1953).

by heating A.R. grade potassium permanganate under vacuum and the gas was stored after passage over solid potassium hydroxide and through liquid-air traps. Water vapor was obtained from distilled water which had been thoroughly outgassed on the line. Carbon dioxide was obtained from a commercial cylinder and purified by three distillations on the line, retaining in each case the middle third. Xenon was used as supplied in glass bulbs by the British Oxygen Co.

Results

Properties of Evaporated Lead Films. To determine the conditions under which evaporated lead films would retain a known and constant surface area, a preliminary study of film sintering was made. Surface areas were measured by the B.E.T. method using xenon adsorption at 90°K. B.E.T. plots were accurately obeyed in the range studied ($0.001 < p/p_0 < 0.06$), and a monolayer was reached at $p/p_0 \simeq 0.01$. Surface areas were calculated on a lattice-packed monolayer model (Anderson and Baker[5]), using an effective area per xenon atom of 22.4 Å.^{2}. Films were deposited at 90°K. and subsequently maintained either at 90°K. or at 195, 253, or 293°K. and areas were measured as a function of time. Sintering occurred at all temperatures except 90°K. and plots of log $(A - A_\infty)$ against time (*cf.* Anderson, *et al.*[6]) are linear if A_∞, the ultimate sintered area, is taken as 200 cm.^{2} (equal to the geometric film area). The apparent activation energy for the sintering process is ~2 kcal. mole^{-1}.

A film deposited at 90°K. (with an initial area of 2130 cm.^{2}), on being maintained at 90°K. and treated with oxygen at 1 mm. for 30 min., suffered an area reduction of 745 cm.^{2} which is attributed to chemisorption sintering. On the other hand, films deposited at 293°K. were found to have a surface area of 200 cm.^{2}, independent of time. It was concluded that films of well-defined and constant surface area equal to the geometric area could be readily produced by evaporation with the substrate at 293°K. and subsequent experiments used films prepared in this manner. Unless otherwise specified, all results refer to films with nominal surface areas of 200 cm.^{2}.

Films deposited at 293°K. were removed from the glass substrate (Anderson, *et al.*[6]) and examined by transmission electron microscopy and electron diffraction. The former method showed the films to be polycrystalline with average crystal width about 1500 Å. Intercrystal gaps were not observed and extinction contours were infrequent, in confirmation of the measured roughness factor of about unity. Electron diffraction examination showed the films to be face-centered cubic and to have, within experimental error the same lattice parameter as bulk lead.

Oxidation Reactions. Oxidation kinetics were studied at 548, 503, 373, 293, 195, and 90°K. It is convenient to classify the results for a high temperature region (548 and 503°K.) and a low temperature region (373–90°K.). Doses of oxygen were added sequentially to the film. It was generally observed that for each dose there was an initial fast uptake (complete in less than about 1 min.), followed by a slow process, the rate of which could be measured. The extent of rapid uptake from each successive dose decreased with increasing uptake, as shown in Fig. 2; however, at 90°K. the extent of subsequent slow uptake was so small that kinetic data could not be obtained.

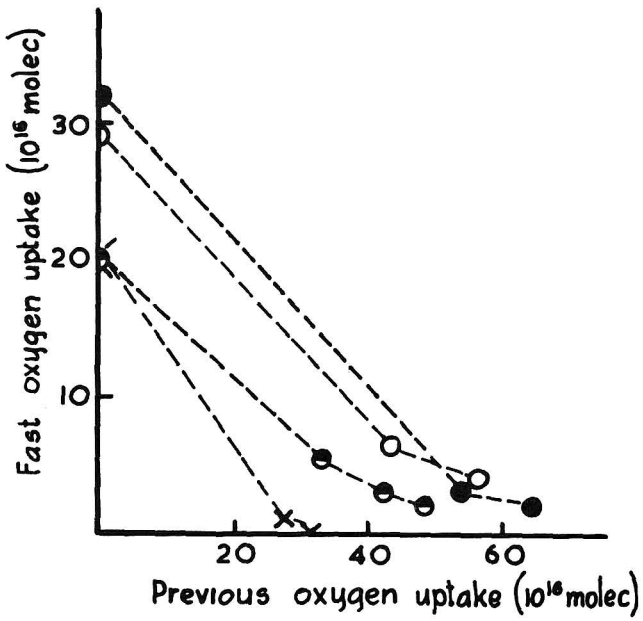

Figure 2. The variation of rapid oxygen uptake on evaporated lead films with total amount of oxygen previously reacted; rapid uptake measured at 10^{-3} mm.

High Temperature Region. The dependence of the oxidation rate on oxygen pressure was determined by adding a second dose of gas while the uptake rate from the previous dose was still sufficiently large to be measured accurately. The data are given in Table I, where x is the exponent in the expression $(dq/dt) \propto p^x$. The values of x clearly indicate that under these conditions the oxidation rate is first order in oxygen pressure.

(5) J. R. Anderson and B. G. Baker, *J. Phys. Chem.*, **66**, 482 (1962).

(6) J. R. Anderson, B. G. Baker, and J. V. Sanders, *J. Catalysis*, **1**, 443 (1962).

Table I: Dependence of Oxidation Rate on Pressure

Temp., °K.	Before addition: Oxygen pressure, 10^{-3} mm.	Before addition: Rate of oxygen uptake[a]	After addition: Oxygen pressure, 10^{-3} mm.	After addition: Rate of oxygen uptake[a]	x
503	2.10	3.6	6.9	10.2	0.88
503	1.22	1.2	13.0	13.0	0.98
548	3.15	4.4	6.9	9.4	0.95
548	0.96	1.8	4.22	8.8	1.02

[a] Arbitrary units.

At both 503 and 548°K. the data can be represented, except in the initial stages, by a linear rate law with first-power pressure dependence. For any given dose, we may write $p \propto (q_0 - q)$ where q_0 is the total number of molecules in the dose and q is the number taken up. With this substitution, the linear law

$$dq/dt = Ap \qquad (1)$$

becomes, after integration

$$\log \frac{q_0 - q_1}{q_0 - q} = Bt \qquad (2)$$

or

$$-\log p = Bt + \text{constant}$$

where q_1 is the oxygen uptake at $t = 0$ and A and B are constants.

Figure 3 shows data for both 503 and 548°K. plotted according to eq. 2. The data in Fig. 3 yield an apparent activation energy of 11 ± 1 kcal. mole^{-1}.

Low Temperature Region. At 195, 293, and 373°K. the uptake *vs.* time data could only be satisfactorily represented by a kinetic law in which dq/dt decreased exponentially with q, *i.e.*, a rate law of the form

$$dq/dt = Cp^x \exp(-Dq) \qquad (3)$$

where C, D, and x are constants. At these temperatures the rate of reaction decreased too rapidly to permit a direct estimation of the kinetic dependence on oxygen pressure as was done at higher temperatures. Furthermore, the fit of the data to eq. 3 is insensitive to the value of x; within experimental error the fit is equally good for $x = 0$ and $x = 1$. For the purpose of presenting the data, we shall thus assume that the pressure-dependence exponent of unity established at high temperatures is also valid at low temperatures; and Fig. 4 shows examples of data plotted as log $(1/p\ dq/dt)$ *vs.* q. At these temperatures, the oxygen uptake approached limiting values, beyond which no further uptake could be measured. These limiting uptakes are given in Table II and refer to oxygen pressures up to about 10^{-2} mm.

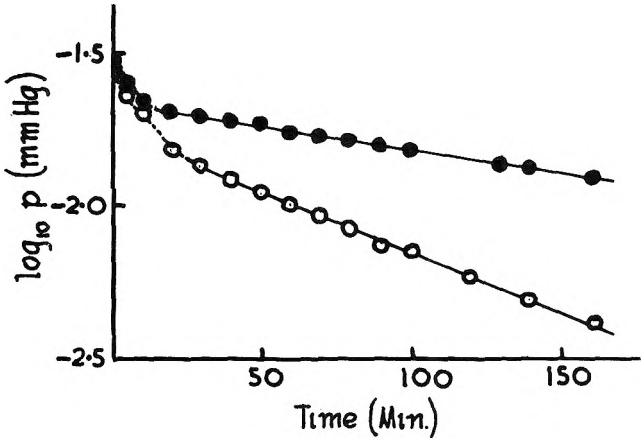

Figure 3. Oxygen uptake data on evaporated lead films at 503°K. (●) and at 548°K. (○), plotted according to a linear growth law with first power pressure dependence (eq. 2).

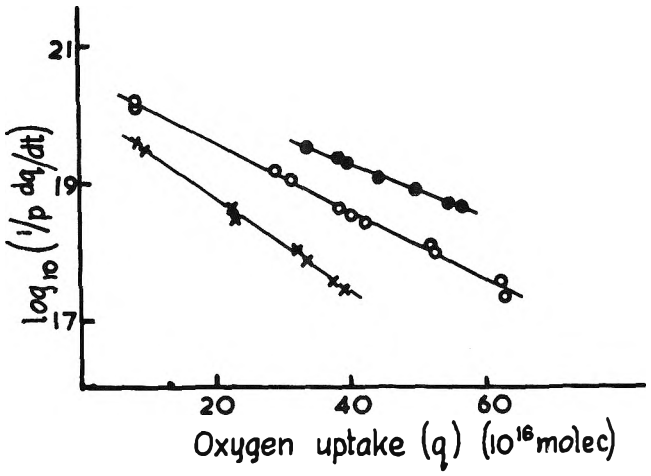

Figure 4. Oxygen uptake data on evaporated lead films at 195°K. (×), 293°K. (○), and 373°K. (●), plotted according to a logarithmic growth law (eq. 3 assuming $x = 1$); p in mm.

Reaction with Oxygen–Water Vapor and Oxygen–Carbon Dioxide Mixtures. The data for the rate of oxygen uptake at 293 and 373°K. in the presence of a pressure of about 10^{-2} mm. of vapor are shown in Fig. 5. The kinetic data deviate only to a quite small extent from the corresponding data in the absence of water vapor. The latter are also shown in Fig. 5 for comparison.

Reaction with oxygen in the presence of carbon dioxide at about 10^{-2} mm. resulted at 293 and 373°K. in limiting oxygen uptakes that were achieved in about the same time as in the absence of carbon dioxide, and

Table II: Limiting Oxygen Uptakes and Oxide Layer Thicknesses

Temp., °K.	Limiting oxygen uptake, 10^{14} O_2 molecule cm.$^{-2}$	Limiting oxide layer thickness, Å.[a]
90	15	11
195	27	20
293	41	31
373	114	87

[a] Calculated assuming the oxide layer to be orthorhombic lead monoxide.

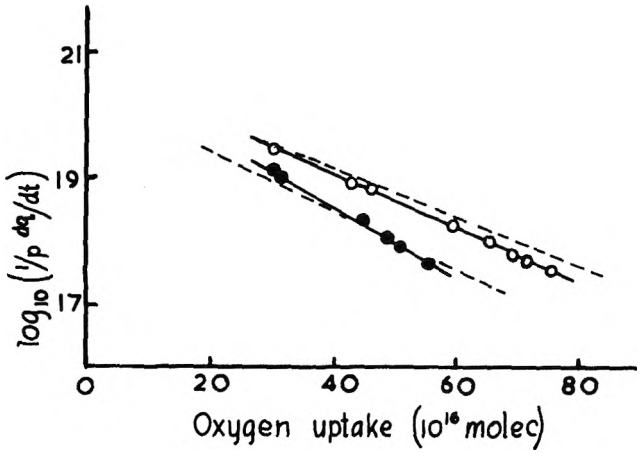

Figure 5. Oxygen uptake data on evaporated lead films at 373°K. (○) and 293°K. (●) in the presence of 10^{-2} mm. of water vapor, plotted according to a direct logarithmic growth law (eq. 3 assuming $x = 1$); p in mm. Dotted lines show, for comparison, corresponding kinetic data in the absence of water vapor.

although detailed kinetic data were not obtained, the influence of carbon dioxide under these conditions can be no more than slight.

Structure of the Oxide Layer. The electron diffraction pattern of the oxide product was measured with 50 kv. electrons at grazing incidence, using a Metropolitan Vickers camera. The specimen substrate was a heavy platinum strip which was recovered from the bottom of the reaction vessel. At 293°K. the oxide layer was too thin for measurement to be possible; oxidation at 373, 503, and 548°K. resulted in diffraction patterns which indexed as orthorhombic lead monoxide. Oxidation in the presence of water vapor or of carbon dioxide also gave only orthorhombic lead monoxide patterns, with no extra features.

Electrical Properties of Orthorhombic Lead Monoxide. Electron diffraction examination of thin layer specimens prepared by the method described above (*cf.* Experimental) showed them to be orthorhombic lead monoxide. Electrical measurements were made in an enclosure partly screened from light, and it was established that no photoconductive component was present. Measurements of the current–voltage relation in the range −200 to +200 v. showed nonohmic behavior in agreement with Heijne,[3] the curve being symmetrical about the origin. The deviation from linearity was, however, less than 10% in the range −45 to +45 v., and all subsequent measurements were made with 45 v. across the specimen.

The procedure was adopted of heating the oxide to 473°K. at a given oxygen pressure. The resistance slowly changed, and a steady value was reached in about 90 min. The temperature variation of resistance then was measured at a constant pressure. Maintaining an oxide specimen under vacuum (10^{-7} mm.) for a further period of 1 hr. at 473°K. resulted in no detectable resistance change and it is concluded that solution of silver into the oxide was inappreciable; however, temperatures above 473°K. were avoided because of this risk. Temperatures appreciably below 273°K. or oxygen pressures much above 10^{-1} mm. could not be used because of resultant current instability. Figure 6 shows the dependence of resistance on temperature and oxygen pressure.

Thermal e.m.f. measurements were made on specimens prepared by heating to 473°K. under conditions ranging from vacuum to 2×10^{-1} mm. until constant resistance was achieved. In *all* cases the polarity of the thermal e.m.f. was with the hot electrode positive, corresponding to an n-type semiconductor.

Discussion

The Electrical Properties and Defect Structure of Orthorhombic Lead Monoxide. The results of Thompson and Strong[7] for the rate of diffusion of oxygen in orthorhombic lead monoxide in the range 770–920°K., when compared with the known rate of oxidation of lead and the rate of diffusion of lead in lead monoxide (*cf.* Lindner and Terem[8]), show conclusively that at these temperatures oxidation occurs by oxygen diffusion. It seems reasonable to accept the conclusion, obtained by extrapolation to lower temperatures, that this is also true at the temperatures used in the present work. Since we have also shown that orthorhombic lead monoxide is an n-type semiconductor, we suggest

(7) B. A. Thompson and R. L. Strong, *J. Phys. Chem.*, **67**, 594 (1963).

(8) R. Lindner and H. N. Terem, *Arkiv Kemi*, **7**, 273 (1954).

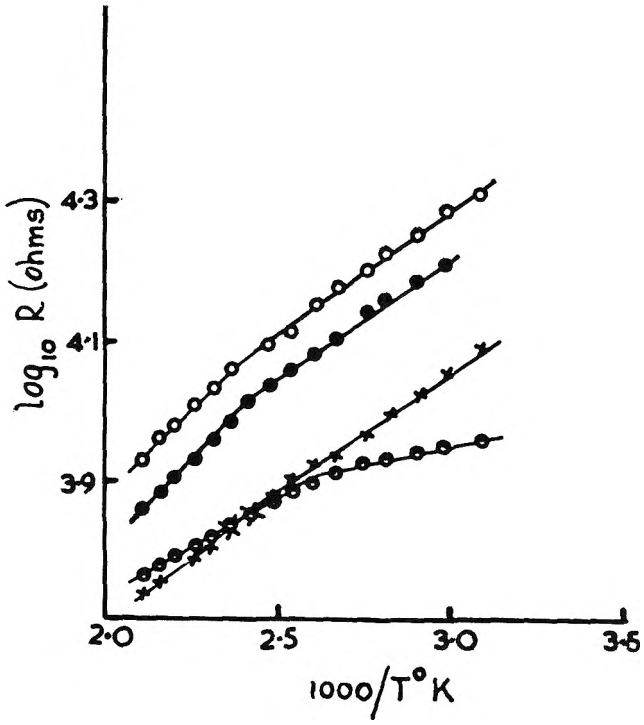

Figure 6. Variation of electrical resistance of thin layer specimens of orthorhomic lead monoxide with temperature and oxygen pressure: ×, $<10^{-6}$ mm.; ●, 4.1×10^{-3} mm.; ○, 4.3×10^{-2} mm.; ⊖, 2.3×10^{-1} mm.

that the dominant mode of nonstoichiometry is the presence of anion vacancies, with the equilibrium

$$PbO \rightleftharpoons 0.5O_2 + (O^{2-}\square) + 2e + Pb^{2+} \quad (4)$$

where $(O^{2-}\square)$ is an anion vacancy. Thus, in the initial increase of electrical resistance with increasing oxygen pressure, both conduction electrons and anion vacancies are destroyed. However, even with a thin layer specimen it is possible that reaction with oxygen did not reach true equilibrium throughout the specimen. With increasing oxygen pressure the resistance passed through a maximum at about 4×10^{-2} mm. in agreement with Heijne.[3] This maximum cannot be explained in terms of eq. 4 alone. The state Pb^{4+} is, of course, well known and it has been reported[9] that *tetragonal* lead monoxide, specially prepared in a state of exceptional reactivity (possibly an extreme state of subdivision), may be oxidized with gaseous oxygen up to about $PbO_{1.5}$. It is, thus, reasonable to ascribe the decrease in resistance with increasing pressure above about 4×10^{-2} mm. to the generation of positive holes Pb^{4+} (and/or Pb^{3+}) by the adsorption of oxygen. However, this must be confined to the surface of the specimen, since under no circumstance were we able to observe p-type thermoelectric behavior. This proposal is consistent with the theory of Parravano and Domenicali,[10] who showed that if in a polycrystalline specimen the width of the temperature gradient region is greater than the width of the space-charge layer, the measured thermal e.m.f. will be nearly independent of changes in positive hole concentration at the surface consequent upon chemisorption. The present thermal e.m.f. results disagree with Heijne,[3] who reported a p-type thermal e.m.f. in oxygen pressures above about 10^{-2} mm. This apparent disagreement could be reconciled if the crystals in Heijne's specimen were much smaller than ours.

Oxidation Reactions. The initial very rapid reaction of oxygen with a virgin lead surface probably occurred by a place-exchange mechanism[11] and in the subsequent slow reactions with which we are concerned, oxygen adsorption occurred at an oxide–oxygen interface. We shall assume that the conversion of O_2 to O^{2-} in the lattice occurred *via* the following sequence of adsorbed species: O_2 (physically adsorbed), O_2^-, and O^-. However, since oxygen adsorbed physically or as O_2^- would be weakly bound compared to O^-, we shall assume that adsorption equilibrium for both was established and that their surface concentrations were directly proportional to oxygen pressure so we may, for simplicity, formulate the kinetics as though O^- were being formed directly from O_2 without considering the intermediate stages explicitly.

Oxidation at 503 and 548°K. From the known densities of lead and lead monoxide, the volume ratio of oxide formed to metal consumed is 1.2, so it is unlikely that the linear oxidation law can be explained in terms of mechanical breakdown in the oxide layer (*cf.* Evans[12]). We shall, therefore, explore the model in which the slow step in the reaction involves dissociation of oxygen.

Adsorbed O^- may be present on the surface either as a simple adsorbed ion (O^-/ads) which will be responsible for the creation of an electric field across the oxide layer, or associated with a positive hole ($e\square$) as a neutral pair ($O^-e\square$). Some consequences of the formation of neutral pairs in tarnishing reactions have been discussed by Grimley and Trapnell,[13] and to facilitate comparison we shall retain their notation.

(9) J. S. Anderson and M. Sterns, *J. Inorg. Nucl. Chem.*, 11, 272 (1959).

(10) G. Parravano and C. A. Domenicali, *J. Chem. Phys.*, 26, 359 (1957).

(11) M. A. H. Lanyon and B. M. W. Trapnell, *Proc. Roy. Soc.* (London), **A227**, 387 (1955).

(12) U. R. Evans, *Trans. Electrochem. Soc.*, 91, 547 (1947).

(13) T. B. Grimley and B. M. W. Trapnell, *Proc. Roy. Soc.* (London), **A234**, 405 (1956).

In the following we shall assume for simplicity that each positive hole is singly charged; the basic argument remains unaltered if formulated in terms of a doubly charged positive hole. We may thus write

$$0.5O_2 + \square S \longrightarrow (O^-e\square) \quad (5)$$

and the associated equilibria

$$(O^-e\square) \rightleftharpoons (O^-/ads) + (e\square) \quad (6)$$

$$(O^-e\square) + e \rightleftharpoons O^-/ads \quad (7)$$

where $\square S$ is a free adsorption site, for instance, above a surface cation. Regeneration of adsorption sites then occurs by

$$O^-/ads + O^{2-}\square/X + e \longrightarrow O^{2-}/X + \square S \quad (8)$$

where $O^{2-}\square/X$ and O^{2-}/X are an anion vacancy and an anion at the oxide–oxygen interface, respectively. Anion vacancies are themselves generated at the metal–oxide interface by eq. 9 and migrate to the oxide–

$$Pb + O^{2-}/O \rightleftharpoons PbO + 2e + O^{2-}\square/O \ldots \quad (9)$$

oxygen interface; where O^{2-}/O and $O^{2-}\square/O$ are an anion and an anion vacancy, respectively, at the metal–oxide interface. We thus propose that reaction 5 is rate controlling, and the rate of oxidation will then be proportional to $p[n(\square S)]^2$ where $n(\square S)$ is the concentration of free adsorption sites. If at these temperatures the degree of surface coverage is small so that $n(\square S) \simeq N$, the total number of adsorption sites per unit area, a law of the form of eq. 1 results. Possible rate laws corresponding to alternative rate-controlling steps are considered in Appendix I.

Oxidation in the Range 195–373°K. A number of mechanisms have been proposed by Grimley and Trapnell[13] to account for a direct logarithmic growth law in tarnishing reactions, based on Mott's[14] proposal for migration in a very strong field. However, all these models require $\theta \simeq 1$, so that the adsorption sites are completely covered by field-creating ions; and if N is of a magnitude comparable with the number of crystallographic sites on the surface, the criterion $\theta \simeq 1$ would demand a potential across the oxide layers at least a factor of ten greater than values of the surface potential which have been measured for a large number of systems (*e.g.*, Hackerman and Lee[15]). Furthermore, it is expected that the mechanism at these temperatures should be simply related to that operating at higher temperatures. Therefore, we suggest that in this temperature region reaction 5 is again rate controlling, but $n(\square S) \ll N$. By using steady-state theory it is shown in the Appendix II that if $\theta \ll 1$ and $\ln \Gamma \gtrsim 1$, where Γ is the chemical part of the equilibrium constant of reaction 6, $n(\square S)$ decreases approximately exponentially with increasing oxide thickness, giving a direct logarithmic rate law of the form of eq. 3 with $x = 0$. The experimental value of x in this temperature region is too uncertain for comparison with that required by the theory.

Acknowledgments. This work was supported by a research contract from the I.L.Z.R.O. of New York. The authors are also grateful to Dr. J. Sanders of C.S.I.R.O. Division of Tribophysics for making available electron diffraction and electron microscope facilities.

Appendix I. Growth Laws Involving Anion Vacancies

Except for assuming the presence of anion vacancies rather than cation vacancies, our assumptions are the same as those of Grimley and Trapnell,[13] whose notation we also use. In particular, we assume that adsorbed oxygen is present either as field-creating ions (O^-/ads) of as neutral pairs ($O^-e\square$) and that adsorption is controlled through an adsorption isotherm. Following Grimley and Trapnell, the equilibria

$$0.5O_2 + \square S \rightleftharpoons (O^-e\square) \quad (A1)$$

$$(O^-e\square) + e \rightleftharpoons (O^-/ads) \quad (A2)$$

$$0.5O_2 + e + \square S \rightleftharpoons (O^-/ads) \quad (A3)$$

yield

$$\theta(1 + p^{1/2}\Gamma' + p^{1/2}\Gamma'' \exp(-\alpha)) = p^{1/2}\Gamma'' \exp(-\alpha) \quad (A4)$$

and

$$\Gamma'' = \Gamma\Gamma' \quad (A5)$$

where Γ', Γ, and Γ'' are the chemical parts of the equilibrium constants for reactions A1, A2, and A3. Further

$$\theta = n(O^-/ads)/N = \alpha\lambda/X$$

$$\alpha = \epsilon V/kT \ (\alpha = \text{positive number})$$

$$F = V/X = 4\pi\epsilon n(O^-/ads)K^{-1}$$

$$\lambda = KkT/4\pi\epsilon^2 N$$

where X is the thickness of the oxide layer of dielectric constant K, and F and V are the field and potential difference across the oxide, respectively.

We require a relation between α and X. Two limiting cases can be analyzed.

(14) N. Cabrera and N. F. Mott, *Rept. Progr. Phys.*, 12, 163 (1948).
(15) N. Hackerman and E. H. Lee, *J. Phys. Chem.*, 59, 900 (1955).

Case 1. $n(O^-e\square) \gg n(O^-/ads)$ and $\theta \ll 1$. This case was considered by Grimley and Trapnell, who showed that then eq. A4 and A5 lead to

$$\alpha \ (\exp \alpha) = \Gamma(X/\lambda) \qquad (A6)$$

and, provided Γ is sufficiently large, α will be approximately independent of X.

Case 2. $n(O^-e\square) \ll n(O^-/ads)$ and $\theta \ll 1$. These criteria require that $p^{1/2}\Gamma'' \exp(-\alpha)$ and $\Gamma' p^{1/2}$ are both $\ll 1$, so that eq. A4 becomes

$$\frac{\alpha\lambda}{X} = p^{1/2}\Gamma'' \exp(-\alpha) \qquad (A7)$$

provided Γ'' is sufficiently large, α will be approximately independent of X and p.

The growth laws may now be obtained in a manner quite analogous to that used by Grimley and Trapnell, except that here anion vacancies are produced by

$$Pb + O^{2-}/O = PbO + 2e + O^{2-}\square/O \qquad (A8)$$

In the following results, Ω is the volume of oxide per anion, γ is the vibration frequency of an anion in the oxide lattice, and $\Delta\mu^\circ$ is the nonelectrostatic part of the standard free energy change of reaction A8.

1. Surface Reaction Rate Controlling. (i) Generation of anion vacancies, reaction A8 rate controlling

$$dX/dt = \Omega\gamma n(O^{2-}/O) \exp(-Q/kT) \exp(a'\alpha/2X) \qquad (A9)$$

where Q is the activation energy for the motion of an anion through a distance a' in the creation of an anion vacancy.

(ii) Destruction of anion vacancies rate controlling

$$O^-/ads + O^{2-}\square/X + e \longrightarrow O^{2-}/X \qquad (A10)$$

$$dX/dt = (\alpha\lambda/X)\Omega\gamma N n(O^{2-}/O) \times \exp\left(-\frac{Q + \Delta\mu^\circ}{kT}\right) \exp\left(-\alpha\left[2 - \frac{a'}{2X}\right]\right) \qquad (A11)$$

where Q is the activation energy for the motion of an anion through a distance a' in the destruction of an anion vacancy.

2. Transport of Anion Vacancies Rate Controlling. (i) A very thin oxide layer is used so that the drift velocity is exponentially dependent on the field and

$$dX/dt = \gamma a\Omega n(O^{2-}/O) \exp(-U/kT) \times \exp(-\Delta\mu^\circ/kT) \exp(a\alpha/2X) \qquad (A12)$$

where a is the anion jump distance required for anion vacancy migration which occurs with an activation energy U.

(ii) The oxide layer is sufficiently thick so that the drift velocity of anion vacancies is directly proportional to F.

$$dX/dt = k'(\lambda/\Gamma)(\alpha^2/X^2) \text{ (case 1)} \qquad (A13)$$

$$dX/dt = k'(\lambda/\Gamma'')p^{-1/2}(\alpha^2/X^2) \text{ (case 2)} \qquad (A14)$$

with

$$k' = \gamma a^2\Omega n(O^{2-}/O) \exp(-\Delta\mu^\circ/kT) \exp(-U/kT)$$

where a and U have the same meaning as before.

In the limiting situation of cases 1 and 2, eq. A9 and A12 give an inverse logarithmic law and eq. A11 an approximately inverse logarithmic law, all pressure independent. Both eq. A13 and A14 correspond to cubic growth laws, pressure independent with case 1 and with an inverse half-order pressure dependence with case 2.

We emphasize that we consider the situation $\theta \simeq 1$ to be physically unrealizable (see comment in text), and this limiting condition thus is not considered.

Appendix II. Variation of Number of Free Sites with Layer Thickness

The rate of destruction of free sites by reaction 5 (main text) will be $kp[n(\square S)]^2$. The rate of generation of free sites by reaction 8 (main text) will be $k_2 n(O^-/ads)n(O^{2-}\square/X)\exp(-\alpha)$, where k_1 and k_2 are constants. For equilibrium 9

$$n(O^{2-}\square/X) = n(O^{2-}/O) \exp(-\Delta\mu^\circ/kT) \exp(-\alpha) \qquad (A15)$$

and thus, when the rates of site generation and destruction are equal

$$n(\square S) = (k_2/k_1)^{1/2}p^{-1/2}N^{1/2}\theta^{1/2}[n(O^{2-}/O)]^{1/2} \times \exp(-\Delta\mu^\circ/2kT) \exp(-\alpha) \qquad (A16)$$

However, provided $n(O^-e\square) \gg n(O^-/ads)$ and $\theta \ll 1$, from eq. A6

$$\theta = \Gamma \exp(-\alpha)$$

so that

$$n(\square S) = kp^{1/2} \exp\left(-\frac{3\alpha}{2}\right) \qquad (A17)$$

with

$$k = (k_2/k_1)^{1/2}N^{1/2}\Gamma^{1/2}[n(O^{2-}/O]^{1/2} \exp(-\Delta\mu^\circ/2kT)$$

Now the results of Grimley and Trapnell show that in the region $\ln \Gamma \lesssim 1$, α varies strongly with X. If this variation is approximated as a linear dependence, an approximately exponential dependence of $n(\square S)$ on X results.

Laser Emission from a Europium Benzoylacetonate Alcohol Solution[1]

by M. L. Bhaumik, P. C. Fletcher, L. J. Nugent, S. M. Lee, S. Higa, C. L. Telk, and M. Weinberg

Electro-Optical Systems, Inc., Pasadena, California *(Received January 9, 1964)*

Laser emission at 6130 Å. from a cooled alcohol solution of europium benzoylacetonate has been verified. The exact chemical constitution of the microcrystalline solute has been determined to be 1 mole of europium with 3 moles of benzoylacetonate, 1 mole of benzoylacetone, and 1 mole of piperidine. These units are combined to form a microcrystalline chemical adduct with unknown structure. Details of the chemical preparation, the melting point, and some of the characteristic emission spectra from the alcohol solution and the microcrystalline state are presented. Finally, a discussion is given of the laser threshold condition, and a reason why some europium chelates do not yield laser emission is proposed.

Introduction

Observation of stimulated emission of 6130 Å. from an alcohol solution of europium benzoylacetonate was reported by Lempicki and Samelson[2] and by Schimitschek.[3] The former authors designate the europium chelate as the three-ligand compound $Eu(B)_3$ but give no method of preparation or melting point; the latter author gives no indication of the chemical composition and no melting point but states that the compound was prepared by the piperidine method of Whan and Crosby.[4] However, Whan and Crosby did not report the use of the piperidine method for the preparation of europium benzoylacetonate; they report this method for the preparation of the rare earth dibenzoylmethides and give another method, in aqueous solution, for the preparation of the rare earth benzoylacetonates. This means that the reported europium benzoylacetonate laser emission has been obtained from a chelate which is essentially uncharacterized. The purpose of this paper is to report the preparation, the melting point, the chemical composition of the solute, and the wave lengths of some of the emission lines for the europium benzoylacetonate which yields laser emission.

The importance of the characterization of the europium benzoylacetonate laser material became apparent when samples of widely varying melting point, degree of hydration, coordination number, chemical composition, and emission wave lengths were obtained, depending upon the method of preparation and the technique of purification employed. For example, recrystallization from solution gave products varying in melting point from 90 to 180°, depending upon the solvent, the fraction taken, the solution temperature, and the time the solution stands before precipitation. Of more consequence is the fact that laser emission has been observed only from a particular europium benzoylacetonate product obtained by a modification of Whan and Crosby's piperidine method.[4]

Preparation and Characterization

Preparation of europium benzoylacetonate by the aqueous method described by Whan and Crosby[4] and by Sacconi and Ercoli[5] gives the dihydrate. This material showed no evidence for laser oscillation when repeatedly tested under various conditions of low temperature and concentration in alcohol solution.

In the same paper Whan and Crosby describe another nonaqueous method, which we call the piperidine method, for the preparation of rare earth trisdibenzoylmethides. In the piperidine method the product is vacuum-dried at 125 to 150° in order to remove a fourth mole of chelating agent. However, when this method was applied in the synthesis of europium benzoylacetonate, the products were of varying melting

(1) Work supported in part by the Rome Air Development Center under Contract AF 30(602)-2914.

(2) A. Lempicki and H. Samelson, *Phys. Letters*, **4**, 133 (1963).

(3) E. J. Schimitschek, *Appl. Phys. Letters*, **3**, 117 (1963).

(4) R. E. Whan and G. A. Crosby, *J. Mol. Spectry.*, **8**, 315 (1962).

(5) L. Sacconi and R. Ercoli, *Gazz. chim. ital.*, **79**, 731 (1949).

point and composition depending upon the time allowed for the high temperature drying; decomposition obviously occurs during the drying process.

By eliminating the vacuum drying step in the piperidine method, a stoichiometric crystalline compound was obtained that yielded laser emission from alcohol solution. The results of chemical analysis, as shown in Table I, indicate that the empirical formula of the crystalline compound is EuB_4HP, a new chemical adduct

Table I: Theoretical Percentages of Constituents for EuB_4HP and Measured Percentages of the Constituents of the Laser Chelate

	C	H	N	Eu_2O_3
EuB_4HP				
Theoretical	61.2	5.5	1.6	19.9
Measured	61.5	5.6	1.7	19.9

of europium trisbenzoylacetonate with one molecule of benzoylacetone and one molecule of piperidine. The data presently available are insufficient to give any indication of the molecular structure of the crystalline compound or of the chemical composition in alcohol solution. So a question not yet settled is whether the hydrogen ion is attached to the nitrogen of the piperidine base and the four benzoylacetonate ions are coordinated to the europium ion; or, on the other hand, whether the hydrogen ion is attached to a benzoylacetonate ion, forming benzoylacetone, and the other three benzoylacetonate ions are coordinated to the europium ion, either alone or possibly together with the piperidine base.

Whether this compound produces laser action depends upon its purity and that in turn depends upon small details of the preparation. The following technique consistently produced a chelate that lased: To a solution at about 90° containing 2.5 g. (0.0155 mole) of benzoylacetone and 1.5 ml. (0.0155 mole) of piperidine in 25 ml. of absolute ethanol was added a warm filtered solution of 1 g. (0.00387 mole) of $EuCl_3$ in a similar amount of absolute ethanol. The cooled reaction mixture was maintained at ambient temperature for 4 days and then filtered. The crystalline precipitate was washed with cold absolute alcohol and air-dried to give 1.81 g. of product (52% yield), m.p. 125.5–126.5°. The results of a test for chloride ion in the product were negative indicating that the piperidine hydrochloride formed in the preparation is not a contaminant.

Luminescence and Laser Emission Characteristics

Laser action was demonstrated using a test system slightly modified from that described by Schimitschek.[3] The EuB_4HP was dissolved in an ethanol–methanol (3:1) solution in order to maintain a liquid state with sufficient chelate solubility at temperatures as low as −150°. The solution was tested in a confocal laser cell 5 cm. in length and 0.1 cm. in i.d. Adjustable pistons with silver mirrors of 1% transmission are inserted into the ends of the test cavity forming a confocal optical system. The solution in the test cavity is optically pumped with a Kemlite high-energy helical flashtube. The flash energy passes through a filter with a 1500 Å. bandpass centered at 3700 Å., and is delivered to the system in a time of the order of 1 msec. Low temperatures are maintained by passing precooled nitrogen gas through the system. The entire unit is enclosed in a magnesium oxide coated reflector in order to lower the pump power requirements. The test cell output signal passes through a neutral density filter, then through a 100-Å. bandpass interference filter with maximum transmission at 6130 Å., then to a phototube, and finally it is displayed on an oscilloscope.

Following ultraviolet pumping, a characteristic intense Eu^{3+} red luminescence is observed at 6130 Å. and at 6142 Å. from a 10^{-2} *M* alcohol solution of EuB_4HP at −150°. The output of the laser test cell showing the emission intensity *vs.* time is displayed in Fig. 1. The test cell was pumped at 5000 joules to produce this display; threshold energy was 1800 joules; laser spiking patterns are clearly demonstrated.

In order to substantiate the interpretation of this phenomenon as laser oscillation and to determine which

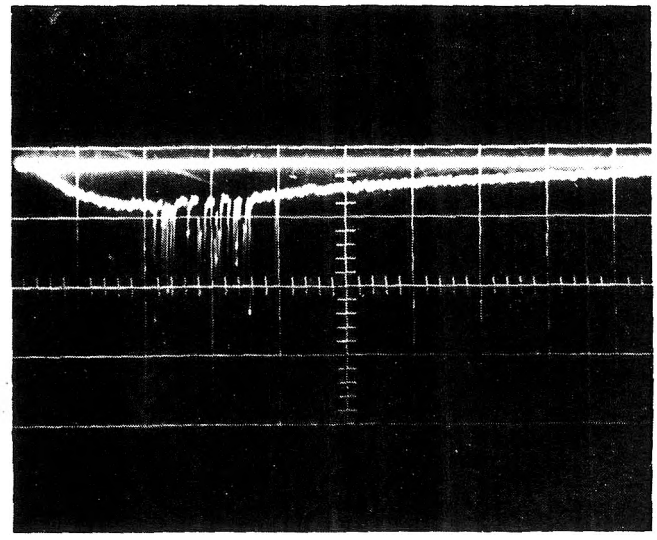

Figure 1. Spiking of europium benzoylacetonate laser, sweep 100 μsec./division.

of the red lines yield laser emission, the spectrum of the test cell output, under the same conditions as for Fig. 1, was measured on a medium resolution Bausch and Lomb quartz spectrograph. In Fig. 2 we show the 6130 and the 6142 Å. emission lines measured during normal emission and during laser emission. For purpose of line width comparison, the fluorescence emission from a low-pressure neon discharge is also shown. The neon lines are instrument broadened to about 1 Å. in the 6100-Å. region. During laser oscillation the

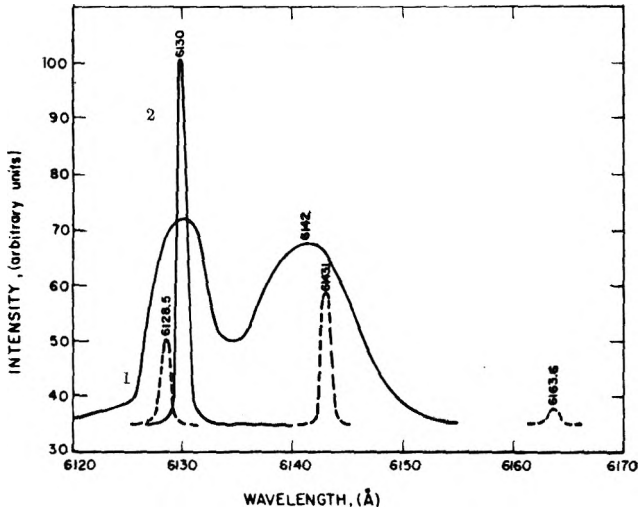

Figure 2. Spectral line narrowing due to simulated emission in the alcohol solution of the europium chelate. Curve 1 shows the normal emission, curve 2 shows the laser emission, and the dotted curve shows the emission from the neon standard. The width of the neon lines is a measure of the instrument line broadening.

6130-Å. line is about 1 Å. in width while the emission intensity of the 6142-Å. line is so low that it is not observed. Clearly from the narrowing in width and the relative increase in intensity of the 6130-Å. line, laser emission from the alcohol solution of europium chelate is established.

When the cell was near room temperature, the laser phenomenon was not observed, probably because of a higher threshold arising from decreased quantum efficiency, decreased emission decay time, increased line width, and increased thermal population of the $^7F_2$ terminal state ($\sim 10^3$ cm.$^{-1}$). This is reasonable in view of the temperature dependence of the spectroscopic properties: the quantum efficiency for emission from the 6130-Å. line is 10% at $-150°$ and less than 0.1% at 27°; the luminescence decay time is 440 μsec. at $-150°$ and 140 μsec. at 27°; the line width is 7 Å. at $-150°$ and 15–20 Å. at 27°.

In addition to the spectroscopic measurements made on the solution, the emission spectra of the microcrystalline solid were measured in order to further characterize the sample. As in the case of the ethanol–methanol solution, the luminescence spectrum of the EuB_4HP microcrystals consists of two strong lines in the 6100-Å region. These are well known[6] to arise from the transition $^5D_0 \rightarrow {}^7F_2$ of Eu^{3+}. Two lines are observed because the degeneracy of the $^7F_2$ state is removed by asymmetric ligand fihlds.[7] The measured wave lengths and line widths are presented in Table II.

Table II: Strong Emission Spectrum of Microcrystalline EuB_4HP in the 6130-Å. Region

λ_{air}, Å.	Line width, Å.[a]	Temp., °K.
6125.1	2.0	77
6132.6	1.0	77
6123.6	4.0	298
6130.6	3.5	298

[a] These values contain no contribution from instrument broadening.

Threshold Consideration and Discussion

Assuming a Gaussian line shape, the minimum inverted population per cc. required for the threshold condition is given by[8]

$$\Delta N = N_2 - N_1 = \frac{4\pi^2}{(\pi \ln 2)^{1/2}} \frac{\tau}{\lambda^2} \Delta\nu \frac{(1-R)}{l} \frac{1}{\phi} \frac{g_1}{g_2}$$

where N_2 and N_1 are the population per ml. of the upper and lower states, τ is the lifetime for spontaneous emission, λ is the wave length of the emission peak, $\Delta\nu$ is the emission line width, R is the reflection coefficient, l is the length of the cavity, g_2 and g_1 are the degeneracies of the initial and terminal states, and ϕ is the fraction of excited ions which decay by emitting the desired radiation. Only cavity losses due to transmission through the mirrors are included in this equation; cavity losses due to scattering, absorption, and diffraction at the mirrors can make the observed value of ΔN somewhat larger.

The total quantum efficiency for the 6130- and 6142-Å. lines in the laser solution was measured to be 0.3, and

(6) E. V. Sayre and S. Freed, *J. Chem. Phys.*, **24**, 1213 (1956).

(7) C. J. Ballhausen, "Introduction to Ligand Field Theory," McGraw-Hill Book Company, Inc., New York, N. Y., 1962.

(8) A. L. Schawlow, *Solid State J.*, 21 (1961).

about $^1/_3$ of the emission is in the 6130-Å. line so ϕ is 0.1 in this case. Because the quantum efficiency is 30% instead of close to 100%, the spontaneous emission lifetime can be longer than the measured fluorescence lifetime with an upper limit of 3.3 times this value. The degeneracy g_2 of the initial $^5D_0$ state is one, and from the observed fine structure of the transition the degeneracy g_1 of the terminal ligand field state is either two or one with the latter most probable. For the 6130-Å. transition in the Eu^{3+} ion, the terminating state is $\sim 10^3$ cm.$^{-1}$ above the ground state so N_1 can be considered to be zero at $-150°$. Substituting values into the above equation, we calculate ΔN to be 5×10^{16} to 17×10^{16} per ml. depending on whether the lower or the upper limit is taken for the radiative lifetime. The minimum concentration of chelate molecules for which laser emission was observed was 10^{-3} M or 60×10^{16} molecules/ml. Since the actual population inversion at threshold must be less than the molecular concentration, an upper limit for the measured ΔN is 60×10^{16} molecules/ml., a factor of 3 to 12 greater than the calculated value. The difference between the measured and calculated threshold is a measure of optical losses from sources other than transmission through the mirrors. Other important losses are mirror diffraction, refractive index gradients caused by thermal effects, or absorption from the initial laser level to higher energy levels.

A comprehensive program has been undertaken to learn why only certain samples of europium benzoylacetonate show stimulated emission and why others do not. This study is expected to point out specifically the molecular structure and composition of these chelates in alcohol and in other solvents, and to establish the factors determining the stimulated emission processes. Threshold analysis on the basis of the luminescence characteristics has given no clue. An explanation is offered as follows: it is possible that absorption to a higher level from the emitting state occurs; this can compete with stimulated emission and thus eliminate or reduce laser action. Such an absorption may occur in those europium benzoylacetonate chelates showing no laser emission. The higher absorbing state may be the ligand singlet, some higher triplet of the ligand, or an ion absorption band.

Acknowledgment. The authors wish to thank M. A. El-Sayed, E. Schimitschek, D. L. Fridge, E. Gonzalez, and S. George for their interest and helpful discussions.

The Thermal Decomposition of Nitryl Chloride in Solution[1]

by David Beggs, Catherine Block, and David J. Wilson

Department of Chemistry, University of Rochester, Rochester, New York *(Received January 13, 1964)*

The decomposition of nitryl chloride (NO_2Cl) dissolved in trifluorochloroethylene polymer oil was studied in the temperature range 127–141°. The rate constant is satisfactorily represented by $k = 10^{12.0} \exp(-28{,}500/RT)$ sec.$^{-1}$. The results are in disagreement with calculations made by Slater. This may be due to solvent cage effects.

Introduction

The gas phase pyrolysis of nitryl chloride, first studied by Schumacher and Sprenger,[2] was intensively reinvestigated by Johnston and his co-workers.[3] These investigators showed that the rate-controlling step in the reaction is unimolecular, and that the mechanism of the reaction is almost certainly that given in eq. 1.

$$NO_2Cl \longrightarrow NO_2 + Cl \quad k_1 \text{ (slow)} \qquad (1)$$

$$NO_2Cl + Cl \longrightarrow NO_2 + Cl_2 \quad k_2 \text{ (fast)}$$

Photochemical evidence for the second step has also been found.[4] The reaction has also been studied at high temperatures by shock tube techniques.[5] Cordes and Casaletto[3] agree that the high-pressure limiting value of the activation energy is about 29.0 kcal./mole; however, none of the gas phase measurements was at a pressure high enough for the rate constant to have approached its high-pressure limit. (This result is expected, since the pressures at which the high-pressure limit is approached increase rapidly with decreasing molecular complexity.)

Slater has published[6] a calculation of the rate of decomposition of nitryl chloride; he finds a frequency factor at the high-pressure limit of about $1.5\text{–}1.6 \times 10^{13}$ sec.$^{-1}$ and concludes that one should be within 25% of the high-pressure limit at pressures of the order of 50 atm. We desired to check his high-pressure factor and to check the extrapolated value of the activation energy. However, we were not enthusiastic about the experimental difficulties of studying this reaction at pressures of several hundred atmospheres of nitrogen. Since the relevant parameter in reaching the high-pressure limit is the frequency with which a reactant molecule suffers collisions, the possibility of studying the reaction at ordinary pressures in solution suggested itself. There follows a report of such an investigation.

Experimental

Nitryl chloride was prepared and purified by the method of Wise and Volpe, as described by Volpe and Johnston.[3] The solvent used was Fluorolube HO-125 trifluorochloroethylene polymer oil, obtained from the Hooker Chemical Corp. This material was pretreated with nitryl chloride for several hours at 127°; this was necessary to eliminate impurities which react with nitrogen dioxide.[7] All stopcocks were lubricated with Kel-F No. 90 grease (obtained from the 3 M Company).

The apparatus is diagrammed in Fig. 1. A tungsten lamp (GE1188) was used as a light source (1); the beam was collimated (2), filtered (3) through Corning filters 3389 and 5113 (nitrogen dioxide absorbs strongly in the region 400–475 mμ passed by the filters, while nitryl chloride does not), chopped (3) so as to pass alternately through the reaction cell (4) or an empty tube (5), and focused (2) onto an R.C.A. 1P21 photomultiplier tube (6), the output of which was monitored by a Varian G 11A recorder. The experimental set-up

(1) This work was supported by the National Science Foundation.

(2) H. J. Schumacher and G. Sprenger, *Z. Elektrochem.*, **35**, 653 (1929); *Naturwiss.*, **17**, 997 (1929); *Z. physik. Chem.*, **B12**, 115 (1931).

(3) H. F. Cordes and H. S. Johnston, *J. Am. Chem. Soc.*, **76**, 4264 (1954); M. Volpe and H. S. Johnston, *ibid.*, **78**, 3903 (1956); M. Volpe and H. S. Johnston, *ibid.*, **78**, 3910 (1956); G. Casaletto, Ph.D. Thesis, Stanford University, 1956; D. J. Wilson, Ph.D. Thesis, California Institute of Technology, 1957.

(4) A. S. Dohner and D. J. Wilson, *J. Chem. Phys.*, **35**, 1510 (1961)

(5) H. Hiraoka and R. Hardwick, *ibid.*, **36**, 2164 (1962).

(6) N. B. Slater, "Theory of Unimolecular Reactions," Cornell University Press, Ithaca, N. Y., 1959, pp. 175–180.

(7) We are indebted to Prof. Gilbert Mains for helpful words of caution and advice in connection with the preparation of the solvent.

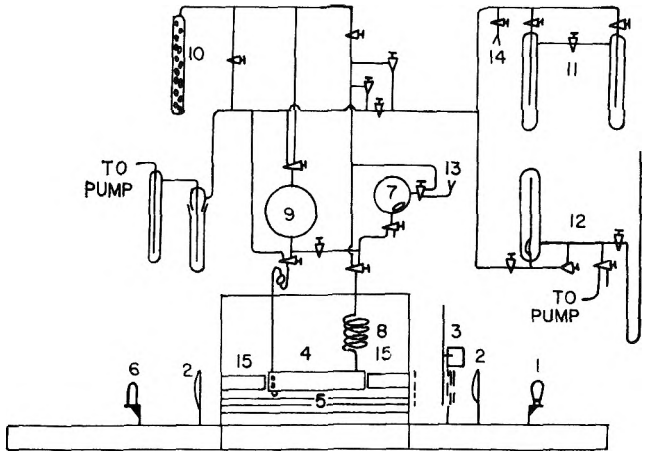

Figure 1. The apparatus: 1, light source; 2, collimating lens; 3, light chopper and filters; 4, sample cell; 5, empty tube; 6, photomultiplier tube; 7, 100-ml. bulb, magnetic stirrer; 8, heat transfer coil; 9, 250-ml. bulb; 10, $CaSO_4$ drying tube; 11, nitryl chloride storage and purification traps; 12, Bourdon gage assembly; 13, solvent port; 14, nitryl chloride port.

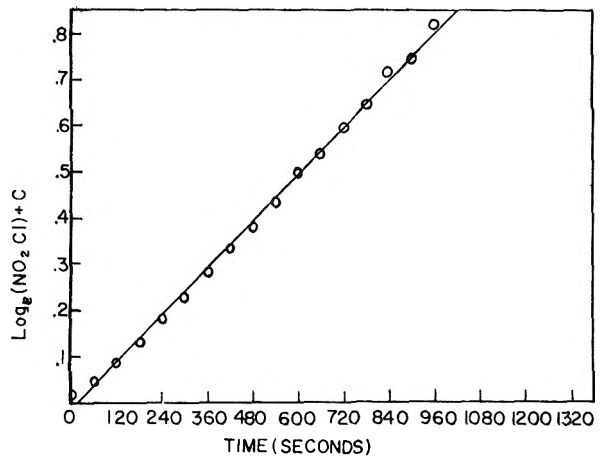

Figure 2. First-order rate plot.

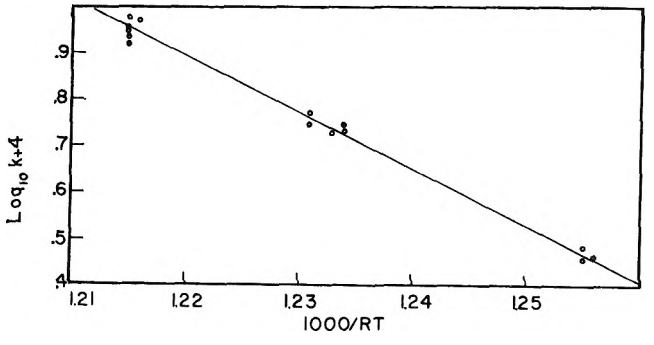

Figure 3. Activation energy plot.

was similar to those used by Johnston and his coworkers.[3] The thermostat was filled with inhibited mineral oil, stirred, and heated electrically. The temperature was controlled to ±0.1°. The presence of small thicknesses (about 1 mm.) of oil in the optical path at either end of the 10-cm. Pyrex cell caused no difficulties. Solvent was introduced into bulb 9 from port 13; it was then degassed by boiling under vacuum. Runs were made as follows. A suitable pressure (about 10–20 mm.) of nitryl chloride was introduced into bulb 7 from the purification and storage traps (11). Then dry air was used to drive solvent from bulb 9 to bulb 7, and the gaseous reactant readily dissolved (with magnetic stirring) in the solvent. Next, dry air was used to drive this solution through the heating coil 8 into the reaction cell 4. The stopcocks between bulb 7 and the cell were left open to prevent thermal expansion of the solution from bursting the cell or causing leaks; the nitryl chloride solution in the cell was under a pressure of slightly over 1 atm., and showed no signs of degassing nitryl chloride. After the reaction had gone to completion (as indicated by the phototube output), the solution was driven by dry air into bulb 9, where it was degassed by boiling under vacuum before the solvent was used again.

Table I

T	$K \times 10^4$, sec.$^{-1}$
134.8	5.608
134.8	5.366
135.0	5.442
135.6	5.928
135.8	5.607
140.8	9.375
140.9	9.520
141.2	8.957
141.2	8.943
141.2	8.691
141.2	8.305
127.4	2.909
127.7	2.850
127.8	3.048

Results

The reaction was first order, as indicated by the plot in Fig. 2; and the rate constants were independent of initial nitryl chloride concentration. The time required to heat the solution to the temperature of the thermostat is appreciable, which prevents one from making measurements at temperatures much above 140°; below 127° the reaction is too slow for convenient measurement. Table I lists the rate constants (calculated on an IBM 1620 by the method of least squares) and temperatures; the standard deviations of the rate

constants were about 1–2% as large as the rate constants themselves.

A plot of log k *vs.* $1000/RT$ is shown in Fig. 3; the Arrhenius parameters calculated from this graph are given by

$$k = 10^{12.0 \pm 0.3} \exp(-28{,}500 \pm 500/RT) \text{ sec.}^{-1}$$

This value for the activation energy is in satisfactory agreement with the extrapolations of Cordes and Casaletto,[3] especially in view of the narrow temperature range to which we were limited. Our value for the pre-exponential factor is lower than that calculated by Slater by a factor of 15–16; this could either be due to inadequacies in his theory or to the recombination of solvent-caged nitrogen dioxide and chlorine atoms, since this is a dissociation reaction.

Far-Infrared Spectra of Some Mono- and Polynuclear Aqua-Substituted Cobalt–Ammine Complexes

by George Blyholder and Nora Ford

Department of Chemistry, University of Arkansas, Fayetteville, Arkansas
(Received January 16, 1964)

The infrared spectra in the CsBr region of *cis*-$[Co(NH_3)_4(H_2O)_2]_2(SO_4)_3 \cdot 3H_2O$, *cis*-$[Co(NH_3)_4(H_2O)(OH)]SO_4 \cdot H_2O$, and *cis*-$[Co(NH_3)_4(H_2O)(Cl)]SO_4$ have been obtained. Frequencies for skeletal vibrations of the first complex ion are found at 521, 494, 461, 449, 428, and about 330 cm.$^{-1}$. The spectra of the latter two compounds are similar. These bands are assigned as skeletal vibrations by treating these molecules as perturbations of $[Co(NH_3)_6]^{+3}$. The correlation treatment lends further support to the assignment of a weak band at 502 cm.$^{-1}$ as a fundamental vibration of $[Co(NH_3)_6]^{+3}$. The infrared spectra in the CsBr region of several polynuclear complexes, of which $[Co\{<^{OH}_{OH}>Co(NH_3)_4\}_3](SO_4)_3 \cdot 4H_2O$ is a representative example, were obtained. The spectra of these polynuclear complexes are similar to the corresponding mononuclear complexes except for a strong absorption at 535 cm.$^{-1}$ which is presumed to be due to the presence of the four-membered cobalt–oxygen ring.

Introduction

There have been relatively few infrared spectral studies of aqua complexes. Fujita, Nakamoto, and Kobayashi[1] investigated the infrared spectra in the rock salt region of three complex ions with and without water in the primary coordination shell. For these Ni(II), Cu(II), and Cr(III) complexes they attributed some bands in the 800–1000 cm.$^{-1}$ region to some wagging, twisting, or rocking vibrations of coordinated water. Mathieu[2] and Lafont[3] have reported some work on the Raman spectra of Mg(II) and Zn(II) hydrates. Infrared spectra of aqua complexes of chromium have been reported by Blyholder and Vergez[4] for

(1) J. Fujita, K. Nakamoto, and M. Kobayashi, *J. Am. Chem. Soc.*, **78**, 3963 (1956).

(2) J. P. Mathieu, *Compt. rend.*, **231**, 896 (1950).

(3) R. Lafont, *ibid.*, **244**, 1481 (1957).

(4) G. Blyholder and S. Vergez, *J. Phys. Chem.*, **67**, 2149 (1963).

the CsBr region from 650 to 300 cm.$^{-1}$. This region is of interest because only vibrational frequencies within the ligand are found in the rock salt region whereas some of the skeletal modes are expected to absorb in the CsBr region.[5] Since many metal ions either in aqueous solution or in hydrated salts contain water in their primary coordination shell, the skeletal vibrations of aqua complexes are important.

There is a question in the assignment of the spectrum of $[Co(NH_3)_6]^{+3}$ as to whether a weak band at 502 cm.$^{-1}$ is or is not a fundamental. Nakamoto[6a] has recently reviewed both sides of the question. In view of the similarity of H_2O and NH_3 ligands it might be expected that a correlation of the spectra of mixed aqua–ammine complexes with that of the hexaammine complex would aid in deciding this question. This correlation is a further dividend of studying the spectra of aqua complexes.

While magnetic data indicate that the bonding of hydroxyl groups in most complexes is essentially ionic, cobalt(III) complexes are exceptions to this.[7] Even though polynuclear cobalt complexes with hydroxyl bridges have been known for many years,[8] the only report[6b] dealing with their infrared spectra covers only the 4000–650 cm.$^{-1}$ region. Although hydroxo complexes in general have received scant attention, Scargill[9] has reported the spectra of hydroxo complexes of ruthenium in the rock salt region.

The following compounds were prepared and their infrared spectra determined in the CsBr region: I, *cis*-$[Co(NH_3)_4(H_2O)_2]_2(SO_4)_3 \cdot 3H_2O$; II, *cis*-$[Co(NH_3)_4(H_2O)(OH)]SO_4 \cdot H_2O$; III, *cis*-$[Co(NH_3)_4(H_2O)(Cl)]SO_4$; IV, $[(NH_3)_4Co<^{OH}_{OH}>Co(NH_3)_4](SO_4)_2 \cdot 2H_2O$; V, $[Co\{<^{OH}_{OH}>Co(NH_3)_4\}_3](SO_4)_3 \cdot 4H_2O$; VI, $[Co\{<^{OH}_{OH}>Co(NH_3)_4\}_3](SO_4)_3 \cdot 6H_2O$; VII, $[Co\{<^{OH}_{OH}>Co(NH_3)_4\}_3](SO_4)_3 \cdot 9H_2O$. Hereafter these compounds will be referred to by number.

Experimental

The compounds were all prepared by standard procedures.[10–12] The samples in 1.0 and 0.2% by weight concentration in KBr were pressed into disks with a hydraulic press using an evacuated die. All spectra were recorded on a Perkin-Elmer Model 21 spectrophotometer equipped with a CsBr prism. KBr disks were placed in the reference beam.

Results

The observed frequencies are listed in Table I. The

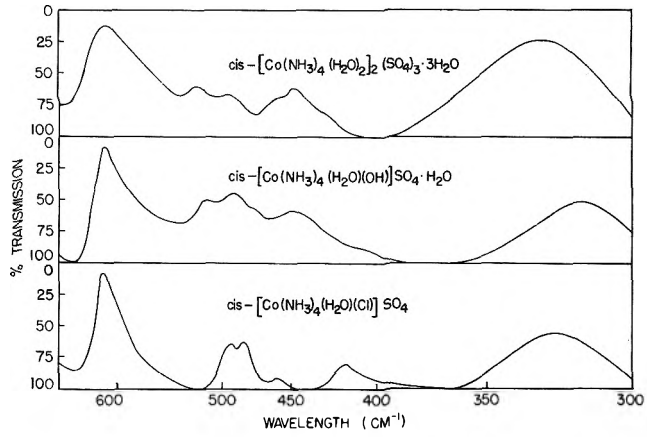

Figure 1. Infrared spectra of some cobalt–ammine–aqua complexes in the CsBr region. Samples are 1% complex salt in KBr disks.

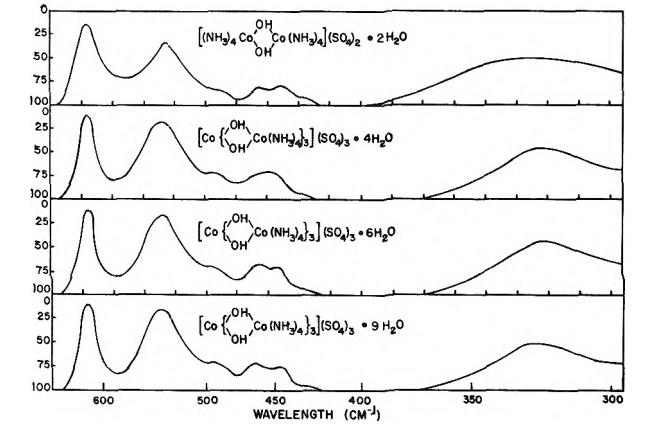

Figure 2. Infrared spectra of some polynuclear cobalt complexes. Samples are 1% complex salt in KBr disks.

appearances of the spectra obtained are shown in Fig. 1 and 2.

Discussion

The intense band at about 620 cm.$^{-1}$ appearing in all spectra may immediately be disposed of as being due to

(5) F. A. Cotton, "Modern Coordination Chemistry," Interscience Publishers, Inc., New York, N. Y., 1960, p. 383.

(6) K. Nakamoto, "Infrared Spectra of Inorganic and Coordination Compounds," John Wiley and Sons, Inc., New York, N. Y., 1963: (a) pp. 146–151; (b) p. 158.

(7) A. Martell and M. Calvin, "Chemistry of the Metal Chelate Compounds," Prentice-Hall, Inc., Englewood Cliffs, N. J., 1952, pp. 213–219.

(8) J. C. Bailar, Jr., and D. H. Busch, "The Chemistry of the Coordination Compounds," Reinhold Publishing Corp., New York, N. Y., 1956.

(9) D. Scargill, *J. Chem. Soc.*, 4440 (1961).

(10) G. Brauer, "Handbuch der Praparativen Anorganischen Chemie," Ferdinand Enke, Stuttgart, 1954, p. 1148.

(11) "Inorganic Synthesis," E. G. Rochow, Ed., McGraw-Hill Book Co., Inc., New York, N. Y., 1960, p. 176.

(12) J. W. Mellor, "Inorganic and Theoretical Chemistry," Vol. 14, Longmans, Green and Co., London, 1935: (a) p. 796; (b) p. 804.

Table I: Observed Far-Infrared Bands for Some Mono- and Polynuclear Aqua-Ammine Cobalt Complexes[a]

Compound	Observed frequencies, cm.$^{-1}$										
I	630 (sh)	620 (s)	580 (sh)		521	494	461	449	428		330 (s, b)
II		620 (s)	590 (sh)		505	483	465	442		395	320 (s, b)
III		620 (s)	590 (sh)		492	485	460		417	398	330 (s, b)
IV	635 (sh)	620 (s)		530 (s)	510	485	460	450	420		330 (s, b)
V	635 (sh)	620 (s)		540 (s)	520	490	460	445	420		330 (s, b)
VI	635 (sh)	620 (s)		540 (s)	520	490	460	445	420		330 (s, b)
VII	635 (sh)	620 (s)	580 (sh)	540 (s)	520	490	460	445	420		330 (s, b)

[a] (s), strong; (sh), shoulder; (b), broad.

the SO_4^{-2} ion.[13] The shoulder at 580 cm.$^{-1}$ which appears in all spectra and the shoulder at 630 cm.$^{-1}$ which appears quite distinctly in the spectrum of a 0.2% sample of compound I which is not shown are assigned to vibrations of the sulfate ion. All of these bands appear in the spectra[14] of salts containing sulfate ions.

The remaining bands of compounds I, II, and III are assigned by considering them as perturbations of the cobalt(III)–hexaammine complex ion. The mass of a H_2O or OH^- ligand is only slightly different from that of NH_3 so that if the Co–O stretching force constant is not too different from the Co–N stretching force constant this will be a reasonable treatment. Since we have no *a priori* knowledge of the Co–O force constants, the only justification for this approximation will be in terms of the results produced.

The $[Co(NH_3)_6]^{+3}$ ion has octahedral symmetry. The representation of the normal coordinates has the structure

$$\Gamma = A_{1g} + E_g + 2F_{1u} + F_{2g} + F_{2u}$$

A diagram of motions[13] of atoms which have the requisite symmetry is given in Fig. 3. It should be pointed out that these are not normal modes which can only be determined by calculation, but as motions with the proper symmetry it is hoped that they are similar to the normal modes. Vibrations ν_1, ν_2, and ν_5 of species A_{1g}, E_g, and F_{2g}, respectively, are Raman active while ν_3 and ν_4 of species F_{1u} are infrared active. Vibration ν_6 of species F_{2u} is inactive.

Bose and Datta[15] report Raman lines at 575 and 483 cm.$^{-1}$ for $[Co(NH_3)_6]Cl_3$. These lines are assigned to ν_1 and ν_2, respectively. Vibrations ν_5 and ν_6, whose symmetry coordinates involve only bond bending coordinates, are assumed to occur below 300 cm.$^{-1}$. The situation with respect to the infrared active bands ν_3 and ν_4 is a little less certain. Powell[16-18] has examined the spectra in the KBr region down to about 450 cm.$^{-1}$

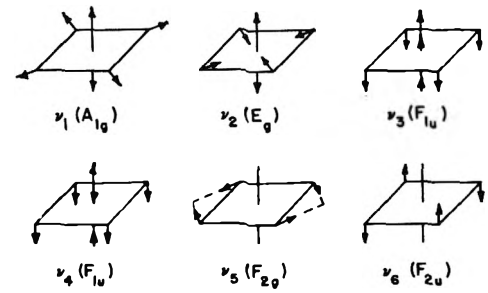

Figure 3. Symmetry motions of octahedral XY_6 molecule.

of a number of ammine complexes. He reports a very weak band for $[Co(NH_3)_6]Cl_3$ at 502 cm.$^{-1}$ which he assigns to a Co–N stretching vibration corresponding to our ν_4. Block,[19] also working in the KBr region, reports a weak band at 490 cm.$^{-1}$. Barrow, Krueger, and Basolo[20] have reported the spectra of a number of ammine complexes down to about 300 cm.$^{-1}$. For $[Co(NH_3)_6]Cl_3$ they found a strong band at 330 cm.$^{-1}$ and report no band near 502 cm.$^{-1}$. They attributed the 330 cm.$^{-1}$ band to a Co–N stretching frequency. For $[Co(NH_3)_6]Br_3$ and $[Co(NH_3)_6]I_3$ Shimanouchi and Nakagawa[21] observe a very weak band at 465 cm.$^{-1}$ and a strong band at 330 cm.$^{-1}$. In view of these discrepancies we decided to rerun the spectrum of $[Co(NH_3)_6]Cl_3$ and observed a weak band at 502 cm.$^{-1}$ and

(13) G. Herzberg, "Infrared and Raman Spectra," D. van Nostrand Co., Inc., New York, N. Y., 1945.

(14) F. A. Miller, G. L. Carlson, F. F. Bentley, and W. H. Jones, *Spectrochim. Acta*, **16**, 135 (1960).

(15) D. M. Bose and S. Datta, *Nature*, **128**, 725 (1931).

(16) D. B. Powell, *Chem. Ind.* (London), **34**, 314 (1956).

(17) D. B. Powell, *J. Chem. Soc.*, 4495 (1956).

(18) D. B. Powell and N. Sheppard, *ibid.*, 3108 (1956).

(19) H. Block, *Trans. Faraday Soc.*, **55**, 867 (1959).

(20) G. M. Barrow, R. H. Krueger, and F. Basolo, *J. Inorg. Nucl. Chem.*, **2**, 340 (1956).

(21) T. Shimanouchi and I. Nakagawa, *Spectrochim. Acta*, **18**, 89 (1962).

a strong band at 330 cm.$^{-1}$. The question arises as to whether or not the weak band at 502 cm.$^{-1}$ should be regarded as a fundamental. If the band at 502 cm.$^{-1}$ is not regarded as a fundamental, then the correlation treatment which we will subsequently apply predicts only three bands in a region where we observe at least five bands. Therefore, the spectra of the aqua complexes given here together with the correlation treatment support the assignment of the band at 502 cm.$^{-1}$ as a fundamental with all assignments given by ν_1 = 575, ν_2 = 483, ν_3 = 330, ν_4 = 502, ν_5 and ν_6 below 300 cm.$^{-1}$.

When two NH_3 groups are replaced by two *cis* H_2O groups, the symmetry is reduced to C_{2v}. A correlation diagram prepared from tables in Wilson, Decius, and Cross[22] is shown in Fig. 4. Vibrations of species A_1, B_1,

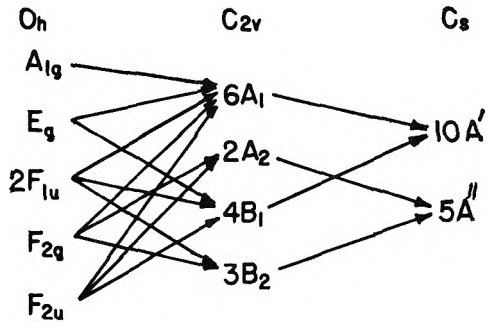

Figure 4. Correlation diagram.

and B_2 are infrared active. Using the assumption that the frequencies for compound I will be perturbed only moderately from those of $[Co(NH_3)_6]^{+3}$, the correlation diagram can be used to estimate frequencies for compound I. Vibrations of C_{2v} which correlate with ν_5 and ν_6 of O_h would therefore be expected to be below 300 cm.$^{-1}$. Vibrations of C_{2v} correlated with ν_3 of O_h would be expected to produce bands in the vicinity of 300 cm.$^{-1}$. It is also seen that there are six infrared active bands in A_1, B_1, and B_2 of C_{2v} which correlate with ν_1, ν_2, and ν_4 of O_h and therefore would be expected to be in the 400–600 cm.$^{-1}$ region.

Inspection of these frequencies indicates that for compound I we should find six frequencies between 400 and 600 cm.$^{-1}$ and the remainder around or below 350 cm.$^{-1}$. Table I reveals that this expectation is in reasonable agreement with observation. This fact supports the assignment of the weak band near 500 cm.$^{-1}$ in the spectra of $[Co(NH_3)_6]^{+3}$ as a fundamental. While only five bands are found in this region for each of the compounds I, II, and III, it is observed in Table I that the frequencies seem to fall into six groups. We suspect that the blanks should contain very weak bands. The overlapping of these bands observed in Fig. 1 could also result in a band being easily missed due to being buried in the other bands.

There is also an intense band or bands in the 300–350 cm.$^{-1}$ region. Our treatment predicts three bands in this region and a little lower which is beyond the range of our instrument.

The motions of the atoms which have the proper symmetry for the C_{2v} vibrations are shown in Fig. 5. Their derivation *via* the correlation diagram from Fig. 3 for some cases is fairly obvious.

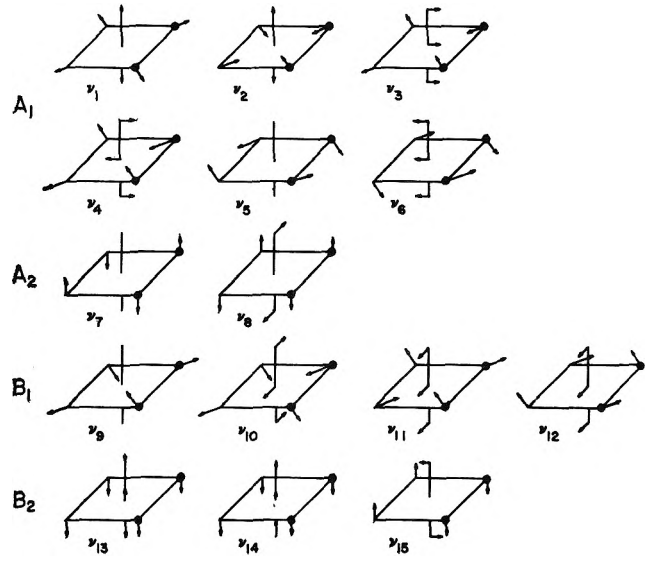

Figure 5. Symmetry motions of *cis*-XY_4Z_2 molecule of symmetry C_{2v}.

Compound II differs from compound I only in that a proton has been removed leaving an OH^- ion instead of a H_2O molecule as a ligand. The symmetry of compound II is reduced to C_s. The correlation between the C_{2v} and C_s symmetry groups is shown in Fig. 4. Application of the previously used procedure for correlating frequencies between structures is certainly legitimate here where the bonds are all the same and the only change is a small mass change in one ligand. On this basis the spectra of compounds I and II would be expected to be quite similar, which they are. In view of this similarity of spectra shown in Fig. 1, it is concluded that the OH^- ion is certainly covalently bonded to the central cobalt ion.

In compound III the OH^- ion is replaced by a Cl^- ion. The symmetry is C_s, the same as compound II.

(22) E. B. Wilson, Jr., J. C. Decius, and P. C. Cross, 'Molecular Vibrations," McGraw-Hill Book Co., Inc., New York, N. Y., 1955.

The spectrum has the same general appearance with the bands of interest being shifted to lower wave numbers. Here a considerable amount of the shift can be accounted for by the increased mass of the Cl^- ion over the OH^- ion. However, without detailed vibrational analysis the relative contribution of mass and force constant effects cannot be evaluated.

By analogy to $[Co(NH_3)_6]^{+3}$ the highest frequency among the skeletal vibrations of compounds I, II, and III is tentatively assigned as the symmetric stretching vibration like ν_1 of Fig. 5. While there is no basis for assigning the other frequencies within the general groups given by the correlation treatment, the assignment of ν_1 furnishes a good idea of the effect of substituting H_2O, OH^-, and Cl^- ligands in place of NH_3 ligands. This is a particularly good frequency to compare since all bonds are simultaneously stretched. The shift in ν_1 upon substituting two H_2O ligands is from 575 $cm.^{-1}$ in $[Co(NH_3)_6]^{+3}$ to 521 $cm.^{-1}$ in compound I. This shift is larger than the change in mass alone would produce, thus indicating a smaller force constant for the Co–O bond than for the Co–N bond and also perhaps a decrease in the Co–N force constant caused by the presence of the Co–O bonds.

In going from compound I to II the decrease in mass would tend to increase ν_1. However, this frequency is decreased from 521 to 505 $cm.^{-1}$. Thus, the effect of removing a proton from a water ligand is to decrease ν_1 and lower the Co–O force constant.

Compound IV is a binuclear complex with the two hydroxide groups bridging between the two cobalt ions to create a four-membered ring. This complex ion has symmetry D_{2h}. The representation of the normal coordinates has the structure, $\Gamma = 6A_g + 2B_{1g} + 3B_{2g} + 4B_{3g} + 2A_u + 5B_{1u} + 4B_{2u} + 4B_{3u}$. The 13 vibrations belonging to species B_{1u}, B_{2u}, and B_{3u} are infrared active. If one ignores the bridging of the OH^- groups, then about half of the complex ion is very similar to compounds I and II. The infrared spectrum of compound IV in Fig. 2 and Table I is like that of compounds I and II with the addition of a strong band at 530 $cm.^{-1}$. This band is presumed to arise from a motion of the cobalt–oxygen four-membered ring.

Compounds V, VI and VII are different hydrates of the same polynuclear complex ion with four cobalt atoms. The spectra of these ions are shown in Fig. 2. The spectra of the three different hydrates were observed to make sure that none of the bands observed was due to water of hydration. Since the three spectra are essentially identical, it is assumed that the bands observed are due to the complex and not to hydrated water. The fact that the spectra of compounds V, VI, and VII are the same as the spectrum of compound IV is consistent with the assignment of the band at 530 $cm.^{-1}$ to a cobalt–oxygen ring vibration.

Summary

The correlation treatment supports the assignment of the weak band near 500 $cm.^{-1}$ for $[Co(NH_3)_6]^{+3}$ as a fundamental. The effect of substituting H_2O, OH^-, and Cl^- ligands for NH_3 ligands in compounds I, II, and III is to lower the symmetric stretching frequency, ν_1, from 575 $cm.^{-1}$ for $[Co(NH_3)_6]^{+3}$ to 521, 505, and 492 $cm.^{-1}$ for compounds I, II, and III, respectively. This indicates the Co–O force constant is smaller than the Co–N force constant. The spectra of the polynuclear complexes indicate that the vibrations of the four NH_3 groups and two OH^- groups are remarkably similar to the vibrations of the same groups in mononuclear complexes. A strong band at 530 $cm.^{-1}$ is assigned to a motion of the cobalt–oxygen four-membered ring in the polynuclear complexes.

Acknowledgment. This work was supported in part by a grant from the National Science Foundation. Acknowledgment is made to the donors of the Petroleum Research Fund, administered by the American Chemical Society, for partial support of this research.

Color and Constitution: The x- and y-Bands of Pyrazolone Azomethine Dyes

by Wendell F. Smith, Jr.

Research Laboratories, Eastman Kodak Company, Rochester, New York 14650 *(Received January 20, 1964)*

Pyrazolone azomethine dyes characteristically have an intense absorption band (the x-band) in the green region of the spectrum and a less intense band (the y-band) in the blue region; the y-band usually appears as a shoulder on the short wave length side of the x-band. The nature of the electronic transitions responsible for these bands is investigated by applying molecular orbital theory, together with the quantitative theory of solvent effects on frequency shifts, as discussed elsewhere. The results permit an interpretation of the configuration of these dyes about the azomethine bridge, the changes in the dipole moment accompanying the N → V_1 and N → V_2 transitions, and the angle between the transition moment vectors responsible for the two bands. The electron densities in the N, V_1, and V_2 states, calculated by an ASMO–CI method, are presented.

Pyrazolone azomethine dyes (I) are well known as

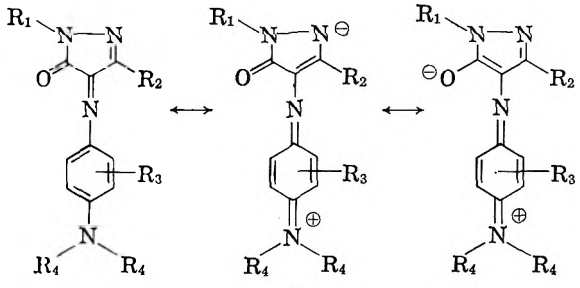

Ia Ib Ic

magenta image dyes in color photography. These dyes characteristically have an intense absorption band (the so-called "x-band")[1] in the green region and a less intense band (the "y-band")[1] in the blue region. The y-band usually appears as a shoulder on the short wave length side of the x-band, although there are examples in which the y-band is the more intense of the two. The visible absorption spectrum of three representative dyes in cyclohexane solution is reproduced in Fig. 1.

Since these dyes may exist in one of two configurations (II and III), the following nomenclature has been adopted. Those dyes in which the p-phenylenediamine moiety is closest to the pyrazolone carbonyl oxygen (structure II) will be referred to as *syn*-pyrazolone dyes. Dyes with configuration III are then *anti*-pyrazolone dyes.

The nature of the electronic transitions associated with the x- and y-bands has been discussed in two

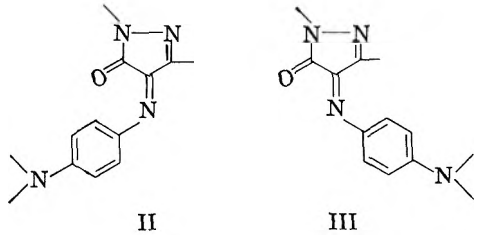

II *syn* III *anti*

papers.[1,2] Based upon solvent and substituent effects on the electronic absorption spectra, it was suggested[1] in 1951 that the x-band is associated with excitation involving a large contribution from structure Ib, whereas the shorter wave length y-band is associated with excitation involving a large contribution from structure Ic. It was also proposed that, for dyes in which R_2 = H (I), the *anti* configuration (III) obtained; other dyes ($R_2 \neq$ H) have the *syn* configuration (II).

In 1958, Ono, *et al.*,[2] studied the dichroism of a pyrazolone dye (I, R_1 = p-$KO_3SC_6H_4$, R_2 = CH_3, R_3 = H, R_4 = C_2H_5) in stretched polyvinyl alcohol (PVA) sheets. The angle between the transition moment vectors responsible for the x- and y-bands was measured and found to be 4 or 67.4°, the experiment not permitting a distinction between the two angles. On the as-

(1) G. H. Brown, B. Graham, P. W. Vittum, and A. Weissberger, *J. Am. Chem. Soc.*, 73, 919 (1951).

(2) H. Ono, Y. Tanizaki, and I. Tanaka, *J. Soc. Sci. Phot. Japan*, 21, 115 (1958).

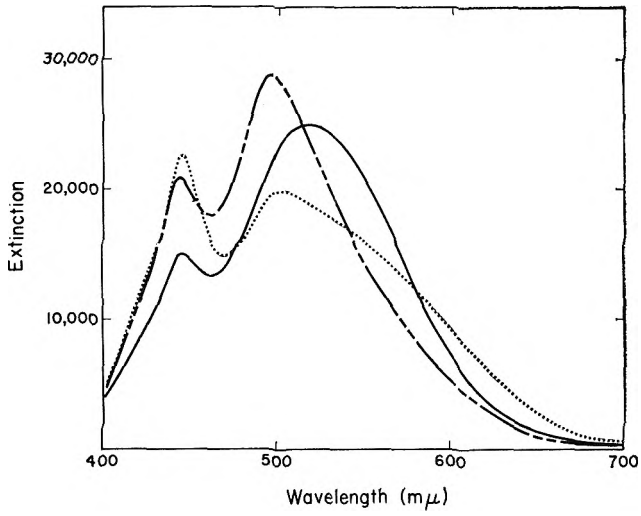

Figure 1. Visible absorption spectrum in cyclohexane solution of dyes IVa (———), IVb (—— – –), and IVc (- - - - -).

sumption that Ib and Ic were the important contributors to the excited state corresponding to the two bands, the smaller of the two angles was selected as the more plausible.[3] By considering the probable orientation of the dye in the stretched PVA sheet, it was concluded that the x-band is associated with excitation involving a large contribution from Ic, whereas the y-band is associated with excitation involving a large contribution from Ib.

The absorption spectra of pyrazolone azomethine dyes have previously been reported[1] in the solvents cyclohexane, n-butyl acetate, and methanol. The solvent effect on frequency shifts in electronic spectra has been discussed qualitatively by Bayliss and McRae[4] and from a quantum-mechanical standpoint by McRae[5] and Ooshika.[6] Since the quantitative treatments of solvent effects[5,6] afford an insight into the changes in dipole moment which a molecule undergoes upon light absorption, it was decided to measure the absorption spectra of some of these dyes in a series of nonhydrogen-bonding solvents. In addition, we have examined the nature of the x- and y-bands from the standpoint of molecular orbital theory.

Experimental and Calculations

The pyrazolone azomethine dyes used in this investigation were supplied by G. H. Brown, of these laboratories. The structures of the dyes used in the quantitative treatment of solvent effects are given in formulas IVa–IVc (configuration not specified).

All spectra were run on a G.E. recording spectrophotometer. The solvents used are given in Table I, with their refractive index (sodium d-line) and dielectric constant. All solvents were Eastman Grade.

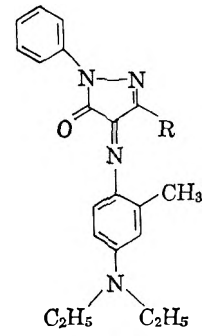

IVa, R = C_6H_5
IVb, R = CH_3
IVc, R = $C(CH_3)_3$

Table I

Solvent	n_D	D
Cyclohexane	1.419	2.05
Diethyl ether	1.350	4.34
n-Butyl acetate	1.395	5.14
Pyridine	1.502	12.5
Acetone	1.360	21.4
Acetonitrile	1.346	38.8

The absorption frequencies for the x- and y-band maxima were fitted to eq. 1[5] by a linear regression treatment.

$$\nu_{max} = \nu_0 + (AL_0 + B')\frac{n^2_D - 1}{2n^2_D + 1} + C\left[\frac{D - 1}{D + 2} - \frac{n^2_D - 1}{n^2_D + 2}\right] \quad (1)$$

In this equation ν_0, A, B', and C are characteristic of the dye, ν_0 being the absorption frequency in the gas phase; L_0 is a function of the solvent, and was given the value[5] 1000 Å. for cyclohexane and 1250 Å. for the other solvents in Table I. The B'/A ratio was not specified in the regression treatment.

The molecular orbital calculations were carried out on the pyrazolone dye framework, substituents such as 1-phenyl being neglected. The parameters used for the Hückel molecular orbital (HMO) calculations[7–9] are given in Table II.

(3) Based upon the geometry used later in this paper for the ASMO–CI calculation, Table III, the angle between the lines joining the terminal dialkylamino nitrogen with the carbonyl oxygen and 2-nitrogen of the pyrazolone ring (for numbering, see Table II) is, for a *syn*-dye, about 12.5°, and for the *anti*-dye, about 24°.

(4) N. S. Bayliss and E. G. McRae, *J. Phys. Chem.*, **58**, 1002 (1954).

(5) E. G. McRae, *ibid.*, **61**, 562 (1957).

(6) Y. Ooshika, *J. Phys. Soc. Japan*, **9**, 594 (1954).

Table II: Parameters for Hückel Molecular Orbital Calculations on Pyrazolone Azomethine Dyes

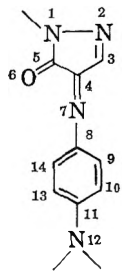

Parameter[a]	Calculation I[b]	II[c]	III[d]	IV[e]
$h_{\ddot{N}}$	1.50	2.00	1.00	1.34
$h_{\dot{N}}$	0.50	1.00	0.50	1.00
h_O	1.00	2.00	1.00	1.00
$k_{1,2}$	0.70	1.00	0.70[f]	0.70
$k_{1,5}$	0.80	1.00	1.00	0.80
$k_{5,6}$	1.00	1.80	1.41	1.00
$k_{7,8}$	0.80	1.00	1.00	0.80
$k_{11,12}$	0.80	1.00	1.00	0.80

[a] $\alpha_X = \alpha_C + h_X\beta_0$; $\beta_{CX} = k_{CX}\beta_0$; $\dot{N}$ = azomethine nitrogen; $\ddot{N}$ = amino nitrogen. [b] Parameters of ref. 7. [c] Parameters of ref. 8. [d] Parameters of ref. 9. [e] Parameters used for starting MO's in ASMO–CI calculation. [f] Not specified in ref. 9; assumed value.

Since there is some ambiguity regarding the choice of HMO parameters, it was decided to carry out a semi-empirical antisymmetrized molecular orbital (ASMO) calculation with limited configuration interaction (CI). For this purpose the method of Pariser and Parr[10-12] was used, with the exception that penetration integrals were neglected. Starting MO's were calculated assuming $h_{\dot{N}} = h_O$, *i.e.*, equal electronegativity for oxygen and azomethine nitrogen, since with *limited* configuration interaction the results are still partly determined by the choice of these parameters. The assumed geometry for the *syn*- and *anti*-dyes is given in Table III.

Resonance integrals are usually empirically evaluated from spectroscopic intervals in this type of treatment. However, the large number of different resonance integrals in these dyes required that they be estimated on the basis of previously reported calculations. For this purpose carbon–carbon resonance integrals were calculated from eq. 2 and all others, except β_{12}, from eq. 3.[13]

$$\beta_{CC} = -1779.5 \exp[-4.7862r] \text{ e.v.} \quad (2)$$

$$\beta_{pq} = A_{pq}/r^6 \text{ e.v.} \quad (3)$$

Equation 2 fits the ethylene and benzene resonance integrals calculated by the semi-empirical ASMO method with $(11/11)_{CC} = 11.08$ e.v.[14] Pariser and Parr[11] derived a similar equation based upon $(11/11)_{CC} = 10.53$ e.v. The A_{pq}-values (eq. 3) were determined by fitting data for *sym*-triazine,[11] pyrrole,[16] and formaldehyde[17] to the inverse sixth-power formula. The calculated values are: $A_{C\dot{N}} = -16.3000$, $A_{C\ddot{N}} = -16.0933$, and $A_{CO} = -9.3226$. For β_{12}, the value -1.649 e.v. was used. This is a theoretical value computed by formulas consistent with the ASMO π-electron theory.[18]

Since penetration integrals were neglected, the core Coulomb integrals were calculated from the formula

Table III: Nuclear Coordinates for Pyrazolone Azomethine Dyes

Atom[a]	*syn* x[b]	*syn* y[b]	*anti* x[b]	*anti* y[b]
1	−0.700	2.154	−0.700	2.154
2	0.700	2.154	0.700	2.154
3	1.132	0.824	1.132	0.824
4	0.000	0.000	0.000	0.000
5	−1.132	0.824	−1.132	0.824
6	−2.313	0.440	−2.313	0.440
7	0.000	−1.340	0.000	−1.340
8	−1.238	−2.055	1.238	−2.055
9	−1.238	−3.445	2.442	−1.360
10	−2.442	−4.140	3.646	−2.055
11	−3.646	−3.445	3.646	−3.445
12	−4.850	−4.140	4.850	−4.140
13	−3.646	−2.055	2.442	−4.140
14	−2.442	−1.360	1.238	−3.445

[a] For numbering system, see Table II. [b] Units are Ångströms.

(7) A. Streitwieser, Jr., "Molecular Orbital Theory for Organic Chemists," John Wiley and Sons, Inc., New York, N. Y., 1961, p. 135.

(8) A. J. Owen, *Tetrahedron*, **14**, 237 (1961).

(9) M. J. S. Dewar, *J. Chem. Soc.*, 2329 (1950).

(10) R. Pariser and R. G. Parr, *J. Chem. Phys.*, **21**, 466 (1953).

(11) R. Pariser and R. G. Parr, *ibid.*, **21**, 767 (1953).

(12) R. Pariser, *ibid.*, **24**, 250 (1956).

(13) H. Kon, *Bull. Chem. Soc. Japan*, **28**, 275 (1955).

(14) Formulas for the energies of the N and V_1 states of ethylene are given by R. G. Parr and B. L. Crawford, Jr., *J. Chem. Phys.*, 16, 526 (1948). With the zero differential overlap approximation, the N → V_1 transition energy is, in the notation of Pariser and Parr,[10] $K_{12} + (4\beta^2 + K_{12}^2)^{1/2}$. The experimental N → V_1 interval is 7.6 e.v. Assuming $(11/11)_{CC} = 11.08$ e.v.[15] and using the extrapolation formula given by Pariser and Parr (ref. 11, eq. 13) for determining $(11/22)_{CC}$, one calculates $\beta = -2.784$ e.v. ($r = 1.35$ Å.). The $^1A_{1g} \rightarrow {}^1B_{2u}$ transition energy in benzene is 4.71 e.v. (experimental) or $-2\beta + {}^1/_2[(11/22) - 3(11/33) + 2(11/44)]$ (theoretical[12]). Using the same method of calculating electron repulsion integrals, one calculates $\beta = -2.299$ e.v. ($r = 1.39$ Å.).

(15) R. G. Parr and R. Pariser, *J. Chem. Phys.*, **23**, 711 (1955).

(16) R. D. Brown and M. L. Heffernan, *Australian J. Chem.*, **12**, 319 (1959).

(17) R. D. Brown and M. L. Heffernan, *Trans. Faraday Soc.*, **54**, 757 (1958).

(18) H. E. Simmons, personal communication.

$$\alpha_p = -I_p - \sum_{q \neq p} X_q(qq/pp) \qquad (4)$$

In which I_p is an appropriate valence state ionization potential, X_q is the charge on core q, and (qq/pp) are bicentric Coulomb repulsion integrals. The last-named were calculated using the uniformly charged sphere approximation[10,11] for $r \geq 2.80$ Å. and the extrapolation formula of Pariser and Parr[11] for $r < 2.80$ Å. Monocentric Coulomb repulsion integrals (pp/pp) were calculated from the formula[11]

$$(pp/pp) = I_p - A_p \qquad (5)$$

where A_p is an appropriate valence state electron affinity. Values for I_p and A_p were obtained by interpolation from data in the literature.[19,20] The values used are given in Table IV.

Table IV: Valence State Ionization Potentials and Electron Affinities

Atom	I_p, e.v.	A_p, e.v.
—C<	11.54	0.46
—N=	14.16	1.34
—N<	28.86	12.26
=O	17.44	3.41

Interconfigurational matrix elements were calculated using the formulas given by Pariser.[12] In the configuration interaction treatment, all singly excited states within 7 e.v. of the ground state were included.

Results

The observed frequencies of maximum absorption for dyes IVa–IVc in the solvents listed in Table I are presented in Table V. The results of the regression analysis according to eq. 1 are given in Table VI. Recently, Balasubramanian and Rao[21] pointed out that, for two solvents of similar refractive index, eq. 1 simplifies to

$$\nu_{max(a)} - \nu_{max(b)} = C\left[\left(\frac{D-1}{D+2}\right)_a - \left(\frac{D-1}{D+2}\right)_b\right] \qquad (6)$$

Two such solvents are diethyl ether and acetonitrile (*cf.* Table I). The values of C calculated by this method are included in Table VI for comparison with the values calculated by the regression treatment. Although the values of C calculated by the two methods differ, the relationship between the C values is practically identical for both methods.

The last column in Table VI gives the multiple correlation coefficients, the squares of which give the fraction of the variability accounted for by eq. 1. Clearly the x-bands are much better correlated than the y-bands. In eq. 1 the quadratic Stark effect[5] (the interaction between solvent permanent dipoles and solute induced dipoles) has been neglected, and this might account in part for the lower multiple correlation coefficients in the case of the y-bands. We have not attempted to include this term in the regression analysis.

Table V: Frequencies of Maximum Absorption for Pyrazolone Azomethine Dyes IVa–IVc[a]

		ν_{max}, cm.$^{-1}$					
Dye	Band	C_6H_{12}	$(C_2H_5)_2O$	n-$C_4H_9O_2$-CCH$_3$	C_6H_5N	CH_3-COCH$_3$	CH_3CN
IVa	x	19268	18762	18315	17575	17953	17762
		19345	*18588*	*18354*	*17594*	*17900*	*17854*
	y	22371	22321	22272	22989	22472	23364
		22275	*22500*	*22223*	*22927*	*22907*	*22956*
IVb	x	20121	19608	19157	18657	18868	18832
		20175	*19481*	*19184*	*18664*	*18892*	*18848*
	y	22523	22371	22321	22321	22321	22472
		22500	*22417*	*22309*	*22310*	*22393*	*22400*
IVc	x	19881	19305	18939	18315	18553	18484
		19924	*19204*	*18961*	*18322*	*18558*	*18508*
	y	22472	22321	22321	22173	22197	22371
		22453	*22356*	*22312*	*22161*	*22283*	*22290*

[a] Numbers in roman type are experimental ν_{max}. Italicized numbers are ν_{max} calculated by eq. 1.

Table VI: Regression Analysis, Eq. 1

Dye	Band	ν_0, cm.$^{-1}$	$A \times 10^{-8}$, cm.$^{-2}$	B', cm.$^{-1}$	C,[a] cm.$^{-1}$	MCC[b]
IVa	x	21413	−9.848	−339.7	−1880 (*−2500*)	0.988
	y	21403	−0.441	4726	1151 (*2608*)	0.768
IVb	x	21778	−8.946	1053	−1618 (*−1940*)	0.993
	y	22773	−2.286	932.3	−50.05 (*252.5*)	0.814
IVc	x	21675	−8.815	192.9	−1780 (*−2053*)	0.996
	y	22975	−2.417	−161.2	−177.2 (*125.0*)	0.862

[a] Numbers in parentheses calculated from ether–acetonitrile data; see text. [b] Multiple correlation coefficient.

(19) H. A. Skinner and H. O. Pritchard, *Trans. Faraday Soc.*, **49**, 1254 (1953).

(20) H. O. Pritchard and F. H. Sumner, *Proc. Roy. Soc.* (London), **235**, 136 (1956).

(21) A. Balasubramanian and C. N. R. Rao, *Spectrochim. Acta*, **18**, 1337 (1962).

The term C in eq. 1 is related to the ground and excited state dipole moments by the formula[5]

$$C = \frac{2}{hca^3}\mathbf{M}_0(\mathbf{M}_0 - \mathbf{M}_i) \qquad (7)$$

in which h is Planck's constant, c is the velocity of light, a is the cavity radius, and $\mathbf{M}_0$ and $\mathbf{M}_i$ are the dipole moment vectors of the solute in the ground and excited states, respectively. In terms of the *lengths* of the dipole moment vectors, eq. 7 may be transformed to

$$C = \frac{2}{hca^3}M_0(M_0 - M_i \cos\theta) \qquad (8)$$

in which M_0 and M_i are the lengths of the vectors in the ground and excited states, respectively, and θ is the angle between $\mathbf{M}_0$ and $\mathbf{M}_i$.

The values of the C-terms (Table VI) indicate that, for absorption corresponding to the y-band, the sign of the change in the dipole moment is dependent upon the nature of the 3-substituent in the dye. For R = CH_3 or $C(CH_3)_3$ (dyes IVb and IVc), there is a slight increase in the dipole moment during the N → V_2 transition. For R = H (dye IVa), however, either there is a large decrease in the dipole moment during this transition or, if the moment increases, then the angle θ must be large.

By considering the term $(AL_0 + B')[n_D^2 - 1]/[2n_D^2 + 1]$ an indication of the sign of $(M_0 - M_i)$ may be obtained. This term represents the contribution to the solvent frequency shift of dispersive interactions (the so-called "polarization red-shift"[4,22]) and interactions between solute permanent dipoles and induced solvent dipoles. When the solute dipole moment decreases during a transition, then the dipole–polarization forces result in a blue-shift, superimposed on the polarization red-shift, in going from the gas phase to a nonpolar solvent (case IIIa of Bayliss and McRae[4]). The resulting shift may be either to the red or the blue, depending upon the relative magnitudes of these terms. On the other hand, if the solute dipole moment increases during the transition (C negative), then this requires the term $(AL_0 + B')[n_D^2 - 1]/[2n_D^2 + 1]$ to be negative, *i.e.*, the shift will always be to the red, since the above dipole–polarization forces will always result in a red-shift (case IIIb of Bayliss and McRae[4]). In nonpolar solvents, the term $C[(D - 1)/(D + 2) - (n_D^2 - 1)/(n_D^2 + 2)]$, which results from dipole–dipole forces, will make little, if any, contribution to the frequency shift.

Since for all solvents $(n_D^2 - 1)/(2n_D^2 + 1)$ will be positive, the effect of the polarization red-shift and the dipole–polarization forces is determined by the sign of $AL_0 + B'$. This term is negative for all dyes in Table VI, with the exception of the y-band for dye IVa, where $AL_0 + B' = 4285$ cm.$^{-1}$. For solvent n-heptane ($n_D = 1.390$), the calculated shift of the y-band for dye IVa due to these forces is 821 cm.$^{-1}$ to the blue, thus indicating that $M_0 > M_i$ for $i = V_2$.

This behavior of the y-band of dye IVa suggests that this dye differs in some way from dyes IVb and IVc. Courtauld molecular models indicate that when the 3-substituent in these dyes is hydrogen, the *anti* configuration is preferred on steric grounds, but when this substituent is methyl or t-butyl, the *syn* configuration is preferred. This conclusion substantiates that of Brown, Graham, Vittum, and Weissberger.[1]

These results are, at least in the case of dye IVa, incompatible with a description of the V_2 excited state as involving a large contribution from *only* Ib and/or Ic. It is possible that one or both of these structures contributes to the state, but there must be other compensating electron-density changes which result in a net decrease (or in the case of dyes IVb and IVc, a small increase) in the dipole moment during the N → V_2 transition.

The data in Table VI indicate that for dyes IVa–IVc the dipole moment increases during the N → V_1 transition. This result is compatible with either of the previous interpretations[1,2] of the x-band.

Examination of extinction coefficients of the x- and y-bands for several dyes affords further evidence that the electronic transitions associated with these bands are quite different. In Fig. 2–4 the relationship between ϵ_x and ϵ_y for several dyes as a function of substituents and solvents is shown. The graphs show that increasing ϵ_x is usually accompanied by decreasing ϵ_y. Increasing the polarizability of the dialkylamino group[23] or an increase in solvent dielectric constant results in higher ϵ_x/ϵ_y ratios. The data in Fig. 4, although plotted for dye IVb, are also characteristic of dyes IVa and IVc. These data are hard to reconcile with the basically similar descriptions of the two excited states, Ib and Ic. Since both involve charge migration from the developer moiety to the pyrazolone ring, one would expect an increase in the polarizability of the dialkylamino group or an increase in solvent polarity to enhance both ϵ_x and ϵ_y.

In Table VII are presented the theoretical transition moments for the x- and y-bands calculated using the HMO parameters of Table II and by the ASMO–CI method (calculation V). The moments calculated by

(22) N. S. Bayliss, *J. Chem. Phys.*, **18**, 292 (1950).

(23) The dipole moments of the gaseous halide are: HCl, 1.08 D.; CH_3Cl, 1.87 D.; C_2H_5Cl, 2.05 D.

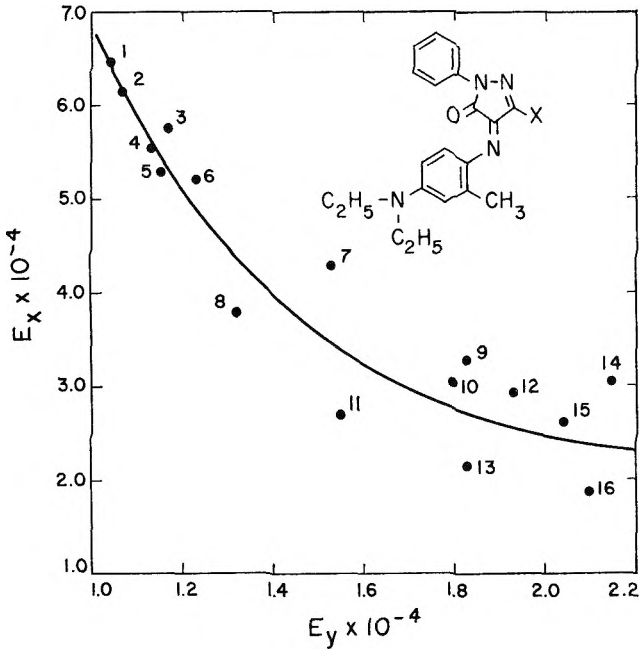

Figure 2. Variation of molar extinction coefficients with the nature of the 3-substituent. X = (1) -NHCONHPh; (2) $-NHCOC_3F_7$; (3) $-N{=}C(NH{-})OC_6H_4$; (4) $-NHCO(CH_2)_2Ph$; (5) $-NHCOCH_2Ph$; (6) $-NHCOCH(C_2H_5)Ph$; (7) -Cl; (8) $-NH_2$; (9) $-CH_2CO_2C_2H_5$; (10) $-C_6H_4NO_2$-*p*; (11) $-C{=}CH-CH{=}CHO$; (12) $-CO_2C_2H_5$; (13) -Ph; (14) $-C_8H_{17}$; (15) $-C_6H_4OCH_3$-*o*; and (16) $-C(CH_3)_3$.

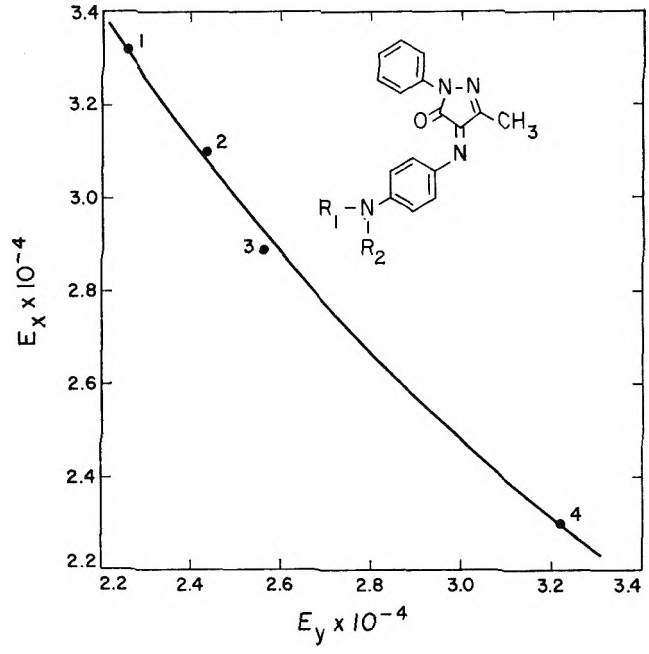

Figure 3. Molar extinction coefficients in cyclohexane solution of pyrazolone azomethine dyes in which (1) $R_1 = R_2 = C_2H_5$; (2) $R_1 = C_2H_5$, $R_2 = CH_3$; (3) $R_1 = R_2 = CH_3$; and (4) $R_1 = CH_3$, $R_2 = H$.

Table VII: *Theoretical Transition Moments* for *syn*-Pyrazolone Azomethine Dyes

Calculation[a]	$Q(N \rightarrow V_1)$	$Q(N \rightarrow V_2)$	θ_1[b]	θ_2[b]	$\theta_1 - \theta_2$
I	1.78	0.98	71° 49′	4° 1′	67° 48′
II	2.29	0.34	58° 44′	−60°	118° 44′[d]
III	2.23	1.13	61° 7′	4° 18′	56° 49′
IV	2.05	1.13	62° 13′	−25° 46′	87° 59′
V[c]	1.27	0.56	67° 24′	−22° 14′	89° 38′

[a] Roman numerals refer to calculations given in Table II. [b] Angle with respect to a horizontal x-axis (structure II), measured counterclockwise. θ_1 refers to the $N \rightarrow V_1$ transition; θ_2, to the $N \rightarrow V_2$ transition. [c] ASMO–CI calculation. [d] Equivalent to an experimentally observed angle of 61° 16′.

the ASMO–CI method were determined by formulas consistent with the theory.[12] The results are qualitatively in agreement with the experimental data, leading to the prediction that $f_x > f_y$, where f is the oscillator strength. In addition, the calculated angle between the transition moment vectors is ~56–89°, thus indicating that the value[2] 67.4° is the preferred angle of the two experimentally determined.

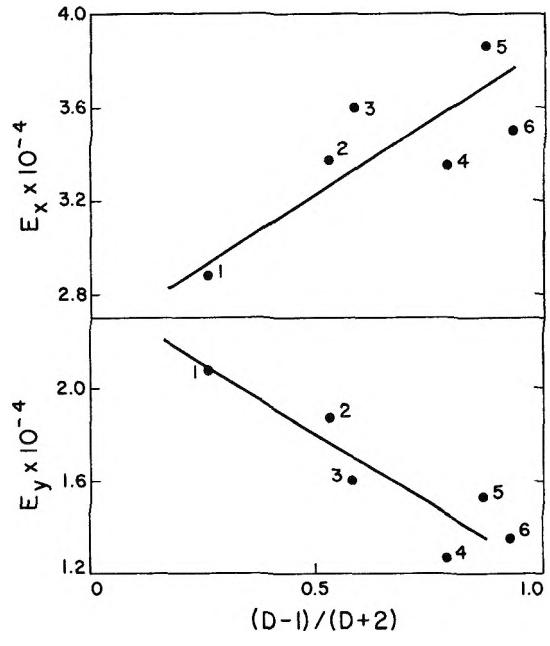

Figure 4. Dependence of molar extinction coefficients for dye *IVb* on solvent dielectric constant, *D*: (1) cyclohexane; (2) diethyl ether; (3) *n*-butyl acetate; (4) pyridine; (5) acetone; and (6) acetonitrile.

From the HMO calculations I–IV it can be predicted that the electron density on the pyrazolone oxygen (q_O)

should decrease during the N → V_1 transition. From calculations I and II it can be predicted that the electron density on N_2 (q_{N_2}) also will decrease during this transition, whereas from III and IV, a slight increase is probable. From the ASMO–CI calculation a very small increase in q_O during this transition, but a slightly larger increase in q_{N_2}, is predicted. However, *all* calculations (I–V) show that the largest increase in electron density during the N → V_1 transition will occur on the bridge azomethine nitrogen (position 7). The calculated increase ranges from +0.230 to +0.290. These results imply that, although Ib and Ic may contribute slightly to the V_1 excited state, they are not nearly so important as has been previously assumed. In Table VIII are presented the electron densities in the N, V_1, and V_2 states calculated by the ASMO–CI method for a *syn*-pyrazolone dye. The π-moments calculated with these data are: M_N^{π} = 4.1 D.; $M_{V_1}^{\pi}$ = 11.8 D.; $M_{V_2}^{\pi}$ = 7.9 D.

Table VIII: π-Electron Densities for *syn*-Pyrazolone Azomethine Dyes (ASMO–CI Calculation)

Position	N	V_1	V_2
1	1.746	1.698	1.590
2	1.367	1.400	1.417
3	0.800	0.860	0.797
4	0.854	0.915	0.946
5	0.719	0.786	0.791
6	1.562	1.570	1.590
7	1.249	1.479	1.433
8	0.973	0.891	0.968
9	0.958	0.946	0.921
10	1.033	0.950	0.951
11	0.894	0.872	0.933
12	1.854	1.738	1.791
13	1.033	0.950	0.951
14	0.958	0.946	0.921

For the *anti*-dye, the π-moments calculated by the ASMO–CI method are: M_N^{π} = 9.7 D.; $M_{V_1}^{\pi}$ = 11.9 D.; $M_{V_2}^{\pi}$ = 13.9 D. From the solution spectra data, however, it was shown that $M_N > M_{V_2}$. The inclusion of σ-moments, using the data of Orgel, *et al.*,[24] does not change the order of dipole moments. The electron densities calculated by the ASMO–CI method cannot, therefore, be considered quantitative. The inclusion of penetration integrals and/or the inclusion of higher energy (>7 e.v.) singly excited states in the configuration interaction treatment should bring the results into better agreement with the experimental data. In view of such uncertainties as the geometry of the dye and the values for the resonance integrals, it is questionable whether much is to be gained by the additional labor required for such a treatment.

In summary, the following conclusions are presented: (1) Dyes IVb and IVc have the *syn* configuration, whereas dye IVa has the *anti* configuration. (2) The dipole moment increases during the N → V_1 and N → V_2 transitions for dyes IVa–IVc, with the exception of the N → V_2 transition of dye IVa, in which the dipole moment decreases. (3) The angle between the transition moment vectors Q(N → V_1) and Q(N → V_2) is ~67.4° rather than 4°. (4) The first excited state (V_1) of *syn*-dyes probably involves little contribution from structures Ib and Ic, although Ib is probably more important than Ic. The N → V_1 transition is better described as involving a large increase in electron density on the bridge azomethine nitrogen with a decrease in electron density at the two amino nitrogens.

(24) L. E. Orgel, T. L. Cottrell, W. Dick, and L. E. Sutton, *Trans. Faraday Soc.*, **47**, 113 (1951).

Measurement of Short Radical Lifetimes by Electron Spin Resonance Methods[1]

by Richard W. Fessenden

Radiation Research Laboratories, Mellon Institute, Pittsburgh, Pennsylvania *(Received January 23, 1964)*

Experiments have been performed demonstrating two methods by which it is possible to measure short radical lifetimes in electron spin resonance (e.s.r.) experiments. These methods are an adaptation of the rotating sector or intermittent illumination technique, often used in photolysis studies, and a sampling technique. Both methods circumvent the limitations imposed by long output time constants and operate with only a moderate loss of signal-to-noise ratio over the steady-state experiment, even when direct observation of the radical formation and decay is not possible. These methods are used in a study of the reaction kinetics of ethyl radicals produced in liquid ethane by radiolysis with a 2.8-Mev. electron beam from a Van de Graaff accelerator. For these studies the accelerator was equipped with electronically controlled pulsing circuits. The two methods were compared and found to agree within 7% in experiments performed under the same conditions. At $-177°$ and an electron beam current of 0.100 μa. (6.9×10^{17} e.v. ml.$^{-1}$ sec.$^{-1}$) the ethyl radical lifetime in the sampling experiment was 7.3 msec. A plot of data showing the second-order radical decay in this experiment (reciprocal concentration *vs.* time) showed excellent linearity over the whole range studied (a factor of ten in concentration). The rate constant found for the second-order disappearance of ethyl radicals in liquid ethane is $1.7 \pm 0.4 \times 10^8\ M^{-1}$ sec.$^{-1}$. Over the temperature range -140 to $-177°$ this may be expressed as $1.3 \times 10^{10} e^{-830/RT}\ M^{-1}$ sec.$^{-1}$.

Introduction

A previous paper[2] described e.s.r. studies of the alkyl radicals present during radiolysis of liquid hydrocarbons. In these experiments radicals were produced directly in the e.s.r. cavity and studied at the steady-state concentration produced by a 2.8-Mev. electron beam from a Van de Graaff accelerator. The signal-to-noise ratio ($\sim$100 or less with a 3-sec. time constant) and radical lifetime ($\sim$5 msec.) were always such that it was not possible to observe directly the decay of the e.s.r. signal when the electron beam was interrupted.[3] The inability to observe fast decays is a result of the long time constant necessary to give acceptable signal-to-noise ratios when detecting small concentrations of radicals [$S/N \propto (RC)^{1/2}$].[4] Thus, the e.s.r. methods cannot be used in such experiments to study the kinetics of radical disappearance in a way completely comparable to the use of optical techniques in flash photolysis and pulse radiolysis. (With the optical methods it has not been necessary to use long time constants to achieve satisfactory signal-to-noise ratios.)

The present paper illustrates the use of two methods by which the limitations of a long time constant can be partly circumvented allowing the kinetics of disappearance of these reactive radicals to be studied in a direct fashion. The first method is an adaptation of the intermittent illumination or rotating sector technique used in photolysis and allows the lifetime of the radicals to be determined. The second method utilizes sampling

(1) Supported, in part, by the U. S. Atomic Energy Commission.

(2) R. W. Fessenden and R. H. Schuler, *J. Chem. Phys.*, 39, 2147 (1963).

(3) With a time constant of 1 msec. it is calculated that ethyl radical should give a signal-to-noise ratio of $\sim$3. Little information could be gotten by observing this decay.

(4) With disappearance rate constants somewhat smaller than those pertaining here and radical lifetimes of 0.1 sec. and above, L. H. Piette and W. C. Landgraff [*J. Chem. Phys.*, 32, 1107 (1960)] were able to observe radical decays directly.

techniques to determine the complete curve of the radical formation and decay. These methods require the use of a pulsed beam from the Van de Graaff accelerator. It should be emphasized that both methods involve an inherent reduction in signal-to-noise ratio over the d.c. (steady-state) experiment.

For an initial experiment it is desirable that, for comparison purposes, there be other data concerning the particular radical lifetime or disappearance rate constant. Also, proper use of the rotating sector technique requires that the dependence of radical concentration upon (in this case) electron beam current be known. For these reasons the liquid ethane system seems to be a good choice because the rate constant for ethyl radical disappearance has been determined from the radical production rate and concentration[2] and because the ethyl radical signal has been shown to be proportional to the square root of the electron current below about 0.1 μa.[2] In addition, it is known that essentially only ethyl radical is present giving a rate constant for this species alone and not an average for several species. Finally, the excellent signal-to-noise ratio for this system, even with the necessary reduction, permits taking good data.

Experimental

The irradiation arrangement consisting of the Van de Graaff electron accelerator, axial-hole magnet, and e.s.r. cavity was as described previously.[2] The TE_{103} cavity was used with the lower two electrical half wave lengths filled with ethane. The irradiation zone was in the center of this volume and all of the ~1 cm. diameter of the electron beam was effective in irradiating the liquid. The e.s.r. spectrometer was a Varian unit with 100 kc./sec. field modulation. For measuring the average radical concentration in the intermittent radical production experiment, double-field modulation at 100 kc./sec. and 200 c.p.s. was used since with this method there is no base-line drift and only the height of the line at its center need be measured. If drift of the cavity resonance frequency and magnetic field are sufficiently small it is even possible to sit on the top of the peak and record the height for different pulse repetition rates. In this way no scanning of the line is necessary and a very long time constant can be used. With the sampling method a relatively high frequency response is necessary in the circuits before the sampling unit so that only the 100-kc./sec. modulation is used. The output of the 100-kc./sec. unit ordinarily used for oscilloscope presentation was found to have sufficient response. Since a first-derivative presentation was used in this type of experiment, base-line drift did occur. It was necessary to operate under conditions, such as a stable temperature and a relatively low beam current, which minimized this drift. Since only one line need be recorded, conditions are not as severe as if a whole spectrum were desired. To average out the base-line drift the line of interest was recorded with field scans in both directions and the average peak-to-peak height used. With the excellent signals available for ethyl radical at the lower temperatures, drift was not a major consideration.

Pulsing of the Van de Graaff beam is accomplished electronically with direct external control of both the beginning and end of the electron pulse. The basic means of conveying the timing information to the high voltage terminal is by a light pulse from a neon bulb (NE-2H).[5] The light pulse travels through a Lucite light pipe to the terminal where it is detected by a photomultiplier. The signal from the photomultiplier is amplified in a video amplifier which is d.c.-connected through the use of Zener diodes. The output of this amplifier, after some clipping to square the pulse, controls the voltage on the electron-emitting filament. The d.c. coupling is necessary because of the very low frequencies, ~0.1 c.p.s., needed for some of the experiments. The observed rise and fall times of the electron pulse were about 1 μsec.

Because of the requirements of the rotating sector technique that the ratio of beam pulse period to the repetition period be constant for various repetition rates, individual control of these periods is not desirable. Consequently, a control circuit was designed which used digital techniques. The separation between consecutive pulses in a pulse train derived from the output of a square wave generator determines the length of the beam pulse while the spacing between every second, fourth, or eighth pulse in the train determines the repetition period of the beam pulses. The output of this control unit increases the current through the neon bulb for the beam pulse duration. For beam pulse lengths longer than 100 μsec. the duty cycle of the beam is within 0.5% of the expected value of $^1/_2$, $^1/_4$, or $^1/_8$ and becomes even closer for longer pulses.

The beam measuring equipment was of the usual electronic type with the output read on a chart recorder. It was verified that the correct *average* current was read with pulsed currents whenever the frequency was high enough that the recorder did not respond to the individual pulses.

The ethane used was Phillips research grade. Samples were transferred to a vacuum line and de-

(5) This method had been used previously in similar equipment developed by Mr. S. Wagner of Brookhaven National Laboratory. The author is indebted to Dr. H. A. Schwarz for pointing out that such a pulse has sufficiently fast rise and fall times.

gassed by pumping at liquid nitrogen temperature. Two bulb-to-bulb distillations were carried out at −78° to remove any high boiling impurities. From studies of the ethane–ethylene system[2,6] it is known that small amounts of ethylene, either as an initial impurity or that produced during irradiation, have no detectable effect on the ethyl radical concentration.

The sample temperature was measured and controlled during irradiation by a copper–constantan thermocouple with the sample junction soldered to the rear cavity wall. The temperature measured is more nearly that of the sample than of the rest of the cavity and heat sink because of the low conductivity of the cavity wall. The temperature at this position can be maintained to within ±0.5° although it is felt that during irradiation there may be temperature differences of several degrees within the sample. Differences of 1 or 2° will not significantly affect the results.

The Method of Intermittent Radical Production

Theory. The effects of intermittent illumination (or the rotating sector technique) have been used for years in photochemical studies to determine the lifetime of active species. The theory has been presented a number of times.[7] In the original method, radicals are produced photochemically by a mechanically chopped light beam. The chopping system, for instance a slotted disk rotating at an adjustable rate, is constructed to maintain a constant ratio of light to dark periods while the length (and therefore repetition rate) of the light periods can be varied. The average light input is, therefore, independent of chopping rate. For there to be any effect of chopping rate, the species of interest must disappear by other than a first-order reaction. The discussion to follow will be limited to a simple system containing one kind of radical which disappears by second-order reaction with itself.

At slow chopping rates the radical concentration will closely follow the light pulse and will remain at the steady-state concentration $[R]_s$ for essentially the whole time the light is on. The average concentration $[\bar{R}]$ over one cycle is then given by $[\bar{R}]/[R]_s = \beta$, where β is the fraction of the time the light is on. At very fast chopping rates the radical concentration changes very little over one cycle and the effect is the same as using a light intensity smaller by the factor β. Because of the dependence of the steady-state concentration upon the square root of the light intensity, the average concentration at this limit is $[\bar{R}]/[R]_s = \beta^{1/2}$. As the chopping rate is varied from slow to fast, $[\bar{R}]/[R]_s$ increases by $\beta^{-1/2}$. The detailed analysis[7] gives for a particular β an explicit equation for the sigmoid curve of $[\bar{R}]/[R]_s$ as a function of m, the ratio of the light period to the steady-state radical lifetime. The steady-state radical lifetime, τ_s, is defined by $\tau_s = [R]_s/P_R$, where P_R is the rate of radical production, and is the time it takes for the concentration to drop by half after interruption of the light.

In the chemical experiments the average radical concentration is measured by the rate of a pilot reaction which is first order in the radical concentration and hence is unaffected by the intermittent radical production. Conditions must be adjusted so that the presence of the pilot reaction does not significantly affect the radical concentration to be measured. In the variation of the method used here the electron beam for the radiolysis is pulsed electronically and the average radical concentration measured directly by the height of the recorded e.s.r. signal. The method is, therefore, simpler in concept in that nothing of the nature of a pilot reaction, with attendant complications, is needed. In Fig. 1 are shown typical results giving the height of a line in the e.s.r. spectrum of ethyl radical (in irradiated ethane) as a function of the length of the electron-beam pulse. The solid curves give the theoretical behavior expected for the two values of β ($^1/_4$ and $^1/_8$). These curves have been translated along the time axis to give

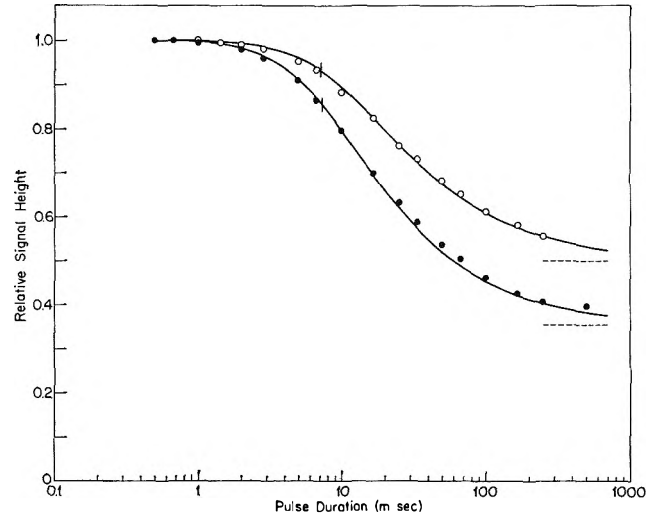

Figure 1. Ethyl radical signal heights as a function of electron beam pulse duration: O, $\beta = {}^1/_4$; and ●, $\beta = {}^1/_8$. The smooth curves are theoretical and have been translated along the time axis to give the best fit. The vertical bars show the position of $m = 1$.

(6) R. W. Fessenden and R. H. Schuler, *Discussions Faraday Soc.*, **36**, 147 (1963).

(7) See (a) H. W. Melville and G. M. Burnett in "Technique of Organic Chemistry," Vol. VIII, S. L. Friess and A. Weissberger, Ed., Interscience Publ., Inc., New York, N. Y., 1953, p. 138 ff.; (b) R. G. Dickinson, in "Photochemistry of Gases," W. A. Noyes, Jr., and P. A. Leighton, Ed., Reinhold Publ. Co., New York, N. Y., 1941, p. 202 ff.

the best fit. The lifetime at the steady state is given directly by the value of the pulse length which corresponds to $m = 1$ on the theoretical curve. In the e.s.r. experiment it proves easier to compare signal heights to the value at high pulse repetition rates than to the height for a steady d.c. beam; for this reason all points are normalized to the height at a fast pulse rate where no departure from the limiting value is expected.

Up to this point it has been assumed that the recorded output of the double modulation–double phase detection system does, in fact, represent the average radical concentration even though the radical concentration is varying. By writing the radical concentration as a Fourier series in the beam-pulse repetition frequency and considering the integrals which represent the output after the field modulation process, it is possible to show that the output (averaged by the output time constant) does represent the average concentration as long as no integral relation exists between the field modulation and pulse repetition frequencies. In practice no "beats" in the output have been observed which might be evidence for the approach to such a condition. The excellent agreement of the observed curves with the theoretical ones also suggests that no difficulty is encountered in practice.

Results and Discussion. The relative ideality of the ethane system referred to above suggests that the measured curve of ethyl radical signal height against electron beam pulse duration should follow the theoretical one very closely. The points shown in Fig. 1 for $\beta = {}^1/_4$ and ${}^1/_8$ do agree well with the theoretical curves and the lifetimes determined for the two experiments, 7.7 and 7.9 msec., also agree. These stated values have been corrected for slight differences in the beam current at which the experiments were performed and refer to a beam current of 0.100 μa. and a temperature of −177°.

Once the general agreement of the data with the theoretical behavior is accepted, further study shows a slight departure of the $\beta = {}^1/_8$ data from the curve. This departure is quite reproducible; the experimental curve tends to be a bit flatter than the theoretical. The reasons for this behavior are not apparent although possible causes are suggested later. Because of this deviation, determination of the proper way to overlap the two curves is a bit more difficult than the scatter of the points would suggest. With data such as those of Fig. 1 the lifetime can be determined to better than ±5%. Relative measurements can be made even more accurately if a smooth curve is drawn through the $\beta = {}^1/_8$ data of Fig. 1 and this curve used to overlap further data.

As was stated above, normalization is always to the signal height at a high pulse repetition rate. This method is used because the heating caused by a d.c. beam makes accurate comparison to these conditions difficult. Nevertheless, it is important to demonstrate that the expected behavior occurs. A comparison of the signal height was made for fast pulse repetition rates at the same pulse current with $\beta = 1, {}^1/_2, {}^1/_4$, and ${}^1/_8$. The good agreement between the expected and observed heights is shown in Table I. (A pulse duration of 0.1 msec. was used and is short enough to ensure being at the limiting signal height.) No attempt was made to compare directly signals at the low repetition rate limit because the output time constant is no longer sufficient to average the signal over an on and off cycle. An indirect comparison can be made through the data of Table I and of Fig. 1.

Table I: Ethyl Radical Signal Heights at the High Pulse Rate Limit for Various Values of β

β	Theory	Measurement[a]
1	1.000	1.000
${}^1/_2$	0.707	0.679
${}^1/_4$	.500	.527
${}^1/_8$	.354	.365

[a] Measured for a pulse duration of 0.1 msec. at 0.100 μa. and − 174°.

To check the dependence of lifetime on beam current, experiments were performed at three different pulse currents, 0.0235, 0.111, and 0.432 μa. The three sets of points (at −174°) with the theoretical curves fitted to them are given in Fig. 2. Taking the lowest current as the base value, the lifetimes can be calculated from the expected square root dependence. These values (A) are given with the measured values in Table II. Clearly there is a departure from the expected dependence. To help in determining the

Table II: Ethyl Radical Lifetimes for Several Electron Beam Currents

	Lifetime		
		Calculated	
Current, μa.	Measured	A[a]	B[b]
0.0235	14.4	14.4	14.4
0.111	7.4	6.62	7.16
0.432	4.4	3.36	4.01

[a] Calculated from the reciprocal of the current. The first value is defined. [b] Calculated from the curve of signal height *vs.* beam current in ref. 2. The first value is defined.

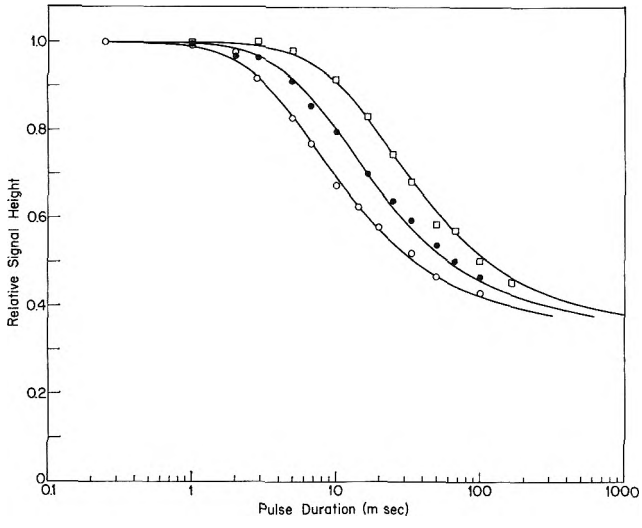

Figure 2. Ethyl radical signal heights as a function of electron beam pulse duration: □, 0.0235 μa.; ●, 0.111 μa.; ○, 0.432 μa. Curves are theoretical.

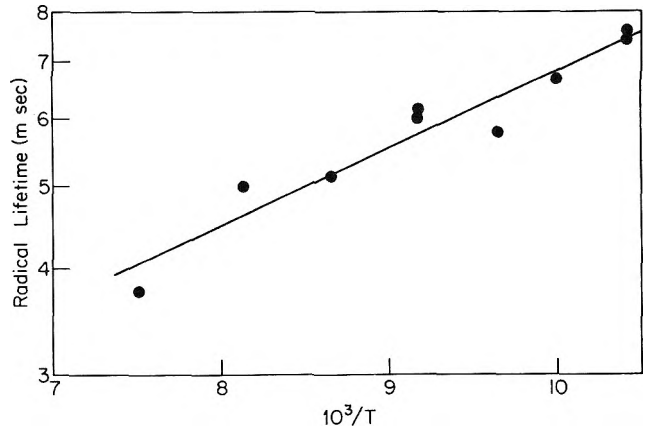

Figure 3. Ethyl radical lifetime as a function of $1/T$; 0.108-μa. beam current. The lifetimes have been adjusted by the square root of the density so they all refer to the absorbed dose rate at −177°. The straight line is determined by the least-squares procedure and corresponds to an activation energy for the disappearance reaction of 830 cal./mole ($k \propto r^{-2}$).

reasons for this, lifetimes are also shown (B) which represent the previously measured[2] curve of signal height as a function of beam current. The similar behavior of the two types of data suggests a common cause for the departures. The suggestion made earlier[2] that ionization in the vapor above the sample reduces cavity Q could not explain both sets of data. Possibly convection currents caused by the heating of the irradiated portion sample could distribute the radicals over a larger volume and increase the radical lifetime although it is not clear why the effects should be the same for similar d.c. and pulse currents rather than for the same average current. In any case the previous curve of signal height against beam current shows that the lifetime measured at 0.0235 μa. can safely be taken to represent the true second-order disappearance.

A very important study that can be made with this technique is the measurement of radical lifetime as a function of temperature in a determination of the activation energy for the disappearance reaction. This method is much superior to that of measuring signal height as a function of temperature because all other temperature-dependent factors affecting the signal height need not be known. It is only necessary that the spectrometer sensitivity not depend on the pulse repetition rate and that the absorbed dose rate as a function of temperature be known. These two requirements are easily met.

The measured lifetimes for temperatures from −140 to −177° are given in Fig. 3. Small corrections have been applied for changes in the absorbed dose rate because of density changes and to correct all values to a common current. The straight line was determined by the least-squares method and corresponds to a value of E_a in $k = Ae^{-E_a/RT}$ of 830 cal./mole with a probable error of 70 cal./mole. If the expression $k = A'T^{1/2} e^{-E_a'/RT}$ is used, E_a' is 720 cal./mole with a similar probable error. The value corresponding to E_a' determined previously[2] was 780 cal./mole in excellent agreement despite several possible sources of error in the earlier work. No change in the discussion given there is necessary.

The Sampling Method

Theory. The intermittent production method avoids the problem of long time constants by detecting only the time average radical concentration. To use this method the dependence of radical concentration upon electron beam current should also be known. Direct measurement of the growth and decay of the radical concentration such as can be done optically is superior in that, in principle at least, the decay curve shows the order of the reaction and any changes in it during the decay. It was shown in the introduction that the direct measurement cannot be carried out with the type of system under consideration. However, if a number of similar formation and decay curves can be added together the signal-to-noise ratio improves as the square root of the number added and measurements become practical. A number of methods of doing this exist. In the method used here the e.s.r. signal is observed or sampled for a short interval at a given time after the start or finish of the irradiation pulse. This point

on the formation–decay curve is then represented by a pulse the amplitude of which is just the signal level plus any noise. The series of such pulses which occur when the irradiation pulse is repeated and the signal sampled with the same intervening time delay can be added electrically. After a number of pulses, the noise components tend to cancel and the d.c. level represents the average signal during the sampling interval. This procedure is illustrated in Fig. 4. Two formation–decay curves which might occur are shown on the upper line with the sampling interval indicated. The series of pulses resulting after the sampling process are shown on the lower line. The dashed line shows the the average level. To get the whole formation–decay curve, the amplitude of the selected e.s.r. line must be determined at a number of delay times.

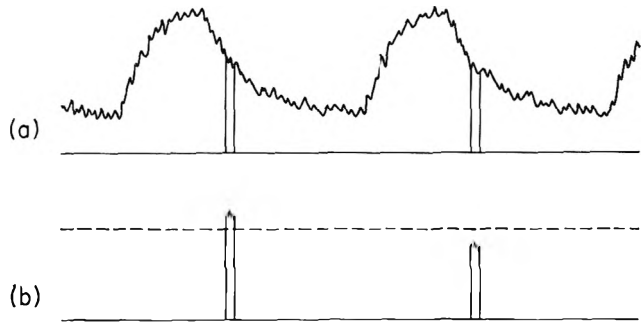

Figure 4. The basic sampling idea. The upper line shows two hypothetical formation–decay curves with the sampling interval marked. The lower line shows the pulses resulting from the sampling procedure with the average height of a number of such pulses indicated by the dashed line.

The sampling unit used is the "boxcar" integrator described by Blume.[8] With this circuit a capacitor is charged through a resistance during the sampling interval. A number of samples are necessary before the voltage across the capacitor reaches the final level so that the noise component on any one sample changes the voltage very little. The detailed theory[9] shows that the signal-to-noise ratio at the boxcar output is less than that of a steady-state experiment by the square root of the ratio of the sampling period to the repetition period.

A more elegant technique has been used by Piette[10] to determine simultaneously a number of points on the decay curve of a photolytically generated radical. In this method the voltage in successive time intervals is converted into a digital form and stored in a number of core memories. A number of decays are sampled and the results for the various time intervals added to the appropriate memories. The process continues until sufficient data are accumulated to provide a satisfactory signal-to-noise ratio. This method is more efficient than a point by point determination in that many less irradiations periods are needed for the same final result. Fortunately, in the radiolysis studies reported here the total irradiation time available is not a limiting factor.

To use the sampling method for determining formation–decay curves where the radical lifetimes are short, it is necessary that the output of the 100-kc./sec. phase detector used to feed the boxcar integrator be such that little distortion of the curve occurs by loss of high-frequency components. Measurements performed by gating an input to the 100-kc./sec. unit show that the output rises to 90% of the steady-state value in about 0.4 msec. Most of this delay occurs in the filtering circuits after the phase detector. Analysis shows that for a ramp function, which is a better description of portions of the formation–decay curves than a step, little distortion other than a 0.1-msec. delay is expected. With radical lifetimes of the order of 5–10 msec. these delays are of little consequence.

Results and Discussion. The formation and decay curve of ethyl radical in liquid ethane at −177° and 0.11 μa. beam current, as measured by the sampling technique, is shown in Fig. 5. Line 8 of the spectrum, which is one of the two most intense lines, was used to provide

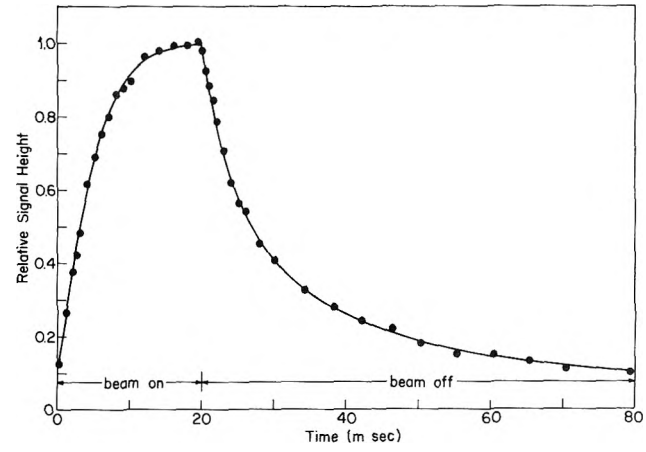

Figure 5. Growth and decay of the ethyl radical signal at −177° and 0.110 μa. as measured by the sampling technique. The beam-on and beam-off intervals are indicated. Solid curves are theoretical and are based on τ_s = 6.93 msec. derived from the decay (see Fig. 6).

(8) R. J. Blume, *Rev. Sci. Instr.*, 32, 1016 (1961).

(9) J. L. Lawson and G. E. Uhlenbeck, "Threshold Signals," McGraw-Hill Book Co., New York, N. Y., 1950, p. 273 ff. This theory applies to a slightly different type of boxcar but the form of the result should apply here.

(10) L. H. Piette, presented at the Sixth International Symposium on Free Radicals, Cambridge, England, July, 1963.

the best signal-to-noise ratio. As is indicated in the figure, the beam was on for 20 msec. and off for 60 msec. The sampling period was 0.5 msec. for the first 30 msec. and 1 msec. for the rest. Points are correctly plotted at the center of the sampling interval because there is little curvature over this interval. The solid curves are theoretical curves based on the steady-state lifetime, τ_s, of 6.93 msec. determined from the first 18 msec. of the decay (see below). These curves are for the formation, $[R]/[R]_s = \tanh(t/\tau_s)$, and for the decay, $[R]/[R]_s = (1 + t/\tau_s)^{-1}$. The curve is normalized to the expected value of 0.995 for $[R]/[R]_s$ at 19.75 msec. Agreement of the data with the theoretical curves is excellent.

A more severe test of the decay curve is to plot it in the form appropriate to give a straight line for a second-order decay. This plot ($[R]_s/[R]$ against time) is given in Fig. 6. The straight line here is a least-squares fit to the data of the first 18 msec. of the decay

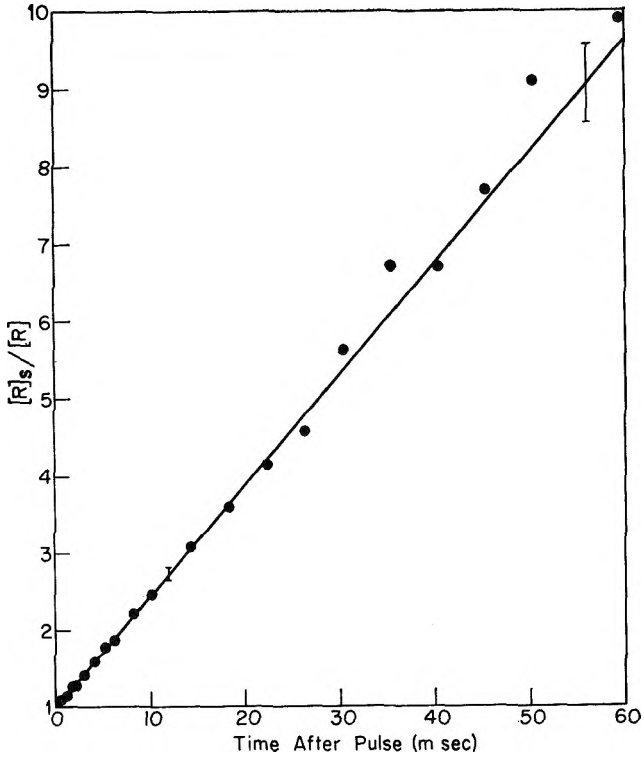

Figure 6. Plot of reciprocal concentration against time for the decay of the ethyl radical signal (data from Fig. 5). The straight line was determined from the first 18 msec. of the decay by the least-squares procedure. Its slope corresponds to $\tau_s = 6.93$ msec.

and gives the value mentioned above for τ_s. The straight line agrees well with the data over the whole range which extends over a factor of 10 in concentration. The vertical bars at 12 and 56 msec. are conservative estimates of the expected errors based on the recorded noise level. The reciprocal form of the plot causes the error to increase rapidly near the end of the decay. The value of 6.93 msec. corrects to 7.3 msec. at 0.100 μa. This value is to be compared to those of 7.9 and 7.7 msec. determined by the sector technique for the same current and temperature. The differences are a bit outside the sum of the expected errors and may be associated with some slight imperfections in one or the other method but nevertheless the agreement is quite gratifying.

In view of the various small departures of the data up to this point from the theoretical behavior, particularly the departure of the lifetime from the square root dependence, it is somewhat surprising to find such an excellent fit of the data to the expected second-order decay. It is quite possible that, in fact, two compensating effects are at work. Although it is not at all evident what these effects may be, the magnitude is very likely measured by the difference between the lifetime determined by the two methods. This difference, about 7% is hardly cause for great concern but does seem to place a limit on the accuracy possible for either method.

Absolute Rate Constant

In the earlier work[2] the rate constant for disappearance of ethyl radicals was determined from the relation, $2k = P_R/[R]_s^2$, in which P_R is the production rate of ethyl radicals and $[R]_s$ their concentration. Because of the difficulties associated with the measurement of $[R]_s$ by e.s.r. techniques the value of $3 \times 10^8\ M^{-1}$ sec.$^{-1}$ found for k was believed to be good to only a factor of two. In the present work the lifetime can be combined with P_R according to the equation, $2k = (P_R\tau_s^2)^{-1}$, to give a much more accurate value for k.

As in the earlier work, the absorbed dose rate was measured by the rate of disappearance of galvinoxyl from a solution in cyclohexane. Two separate determinations were made at different total doses and were found to agree to within 3%. Since the cavity contains about 6 ml. of solution the whole cross section of the beam is effective. At 0.100 μa. beam current the measured absorbed dose rate in cyclohexane is 9.0×10^{17} e.v./sec. (This value is in perfect agreement with the figure of 1.8 Mev. (g./cm.^{2})$^{-1}$ for the energy-loss parameter for electrons at these energies.) This dose is absorbed in a volume of 1.15 ml. defined by the 1-cm. cavity dimension and the diameter of the beam. The beam diameter in the sample was determined to be 1.2 cm. by the bleaching of colored cellophane in a phantom arrangement. This active sample volume is probably the least accurately known factor in the equa-

tion for k. With a value for the yield of ethyl radicals of 4.4 radicals/100 e.v.,[2] the production rate becomes $5.0 \times 10^{-5} M$ sec.$^{-1}$ at 0.100 μa. in our geometry. After making a correction for the presence of a small concentration of methyl and vinyl radicals[11] the effective values become 4.7 radicals/100 e.v. and $5.4 \times 10^{-5} M$ sec.$^{-1}$. Because of the slight departure from the square-root dependence at the higher currents the lifetime at 0.0235 μa. (see Table I) should be the best figure to use in determining the rate constant. The value so determined is $1.68 \times 10^{8} M^{-1}$ sec.$^{-1}$ at $-177°$. (This value has been corrected to $-177°$ by the curve of Fig. 3.) Values of 1.80×10^{8} and 1.56×10^{8} are found from the sampling experiment and from the curve of Fig. 3, respectively. A value of $1.7 \pm 0.4 \times 10^{8} M^{-1}$ sec.$^{-1}$ is chosen as the final value at $-177°$. The stated error (20%) comes from a consideration of the errors expected in both P_R and τ_s[2]. Combination of the final value for k with the activation energy determined from the temperature study gives $k = 1.3 \times 10^{10} e^{-830/RT} M^{-1}$ sec.$^{-1}$.

Implicit in the calculation of the rate constant and, in fact, in the use of both methods of measuring lifetime, is the assumption that the radical concentration is uniform over the irradiated volume. This assumption cannot be completely valid and the extent to which it affects the lifetime measurements and ultimately the calculated rate constant is not readily apparent. However, calculations show that for a system with two subgroups containing equal numbers of radicals which have respective lifetimes of 1 and 1.5, the form of the sector curve is essentially unchanged and gives the average lifetime. This method, then, is not sensitive to the concentration distribution. The decay curve would, however, be expected to show any large spread in the radical lifetimes. In fact, no curvature is observed in Fig. 6 which might be attributed to such a distribution. In the absence of any evidence to the contrary it will be assumed that this effect does not change the stated error of the rate constant.

The radical concentration calculated for this experiment is $1.7 \times 10^{-7} M$ at $-177°$ and 0.100 μa. This value cannot be compared directly to the previously measured value because of the differing geometries, but is of a similar magnitude. A more interesting comparison is possible if the previously measured radical concentration (through the calculated rate constant) and the value for the lifetime measured in this experiment are combined. In this way the production rate of ethyl radicals can be determined by purely physical methods. The value obtained, 3.8 radicals/100 e.v. gives better than expected (30%) agreement with the chemically measured value of 4.4. Although this calculation is not of practical importance because of the 30% error associated with the measurement of the concentration, it reaffirms confidence in the chemical methods (scavenger studies and product analysis) used to measure radical yields.

Acknowledgment. The author gratefully acknowledges the assistance of W. L. Siegmann in treating several of the mathematical problems encountered in this work.

(11) The presence of these radicals should not affect the form of the results in the two experiments. However, their contribution to the total effective radical production rate should be included. For this small correction the assumption can be made that these radicals react with the same rate as do ethyl radicals. The correction is then just an increase in the radical yield by the factor 1.07 to take into account the 7% concentration of vinyl and methyl radicals.

Vaporization of Thorium Dicarbide[1]

by Donald D. Jackson, George W. Barton, Jr., Oscar H. Krikorian, and Ray S. Newbury

Lawrence Radiation Laboratory, University of California, Livermore, California *(Received January 24, 1964)*

A mass spectrometric investigation was carried out on the vaporization processes and thermodynamics of vaporization of solid ThC_2. The carbide was heated in a graphite Knudsen cell and the vapors were analyzed. The partial pressures of Th(g) and ThC_2(g) in equilibrium with the carbon-saturated solid were found to be of comparable magnitude in the temperature range investigated, 2371–2642°K. The enthalpy of sublimation of ThC_2(s) to ThC_2(g) is 198.1 ± 3.5 kcal./g.f.w., and to Th(g) is 168.4 ± 3.5 kcal./g.f.w. The calculated $\Delta H_f^\circ{}_{298}$ of formation of ThC_2 is −30.7 ± 3.7 kcal./g.f.w.

Introduction

A mass spectrometric investigation has been made of the gaseous species present in the carbon-rich region of the Th–C system, as well as the thermodynamics of the vaporization processes and the enthalpy of formation of ThC_2. The gaseous species have not been studied previously, whereas several prior determinations have been made of the enthalpy of formation of ThC_2. Considerable uncertainties are present in the ΔH_f° values, resulting partly from a lack of heat capacity data and partly from experimental procedures.

Free energy data were given by Prescott and Hincke[2] for the equilibrium $ThO_2(s) + 4C(\text{graphite}) = ThC_2(s) + 2CO(g)$ at temperatures between 2057 and 2494°K. Krikorian[3] made a third-law treatment of the Prescott and Hincke data by using estimated free energy functions and obtained a $\Delta H_f^\circ{}_{298}$ of formation of −33.0 ± 8 kcal./g.f.w. for ThC_2. Kubaschewski and Evans[4] estimated the $\Delta H_f^\circ{}_{298}$ of ThC_2 as −44.8 kcal./g.f.w. and $S^\circ{}_{298}$ as 19.3 cal./deg.-g.f.w. Egan and Bracker[5] reported high-temperature galvanic cell measurements of $\Delta H_f^\circ{}_{1073} = -29.6$ kcal./g.f.w. and $\Delta H_f^\circ{}_{1073} = -37.35$ kcal./g.f.w. for formation of ThC_2.[5a] Lonsdale and Graves[6] calculated a ΔH_f° of ThC_2 of −46 ± 6 kcal./g.f.w. between 2300 and 2900°K. on the basis of target-effusion experiments by assuming that Th(g) was the only gaseous species. Lofgren and Krikorian[7] investigated the vapor pressure and enthalpy of vaporization of Th(g) from ThC_2(s) by emission spectroscopy and found −26.9 ± 5 kcal./g.f.w. by the second law and < -24.9 kcal./g.f.w. by the third law for $\Delta H_f^\circ{}_{298}$ of ThC_2.

Gaseous species in the vaporization of several carbide systems have been studied, and a considerable number of carbon-containing molecules have been found. Chupka, Berkowitz, Giese, and Inghram[8] discovered La(g) and LaC_2(g) to be the important species in the carbon-rich region of the La–C system. The ratio $P(LaC_2)/P(La)$ was found to increase from 0.2 to 0.8 in going from 2200 to 2600°K. Ga and Al also formed low carbide concentrations in the vapor phase. The evaporation behavior of SiC was studied by Drowart, De Maria, and Inghram,[9] who found no less than six species containing both silicon and carbon. Drowart, De Maria, Boerboom, and Inghram[10] observed six carbon-containing species in the Ge–C and Ge–Si–C sys-

(1) Work done under the auspices of the U. S. Atomic Energy Commission.

(2) C. H. Prescott and W. B. Hincke, *J. Am. Chem. Soc.*, **49**, 2744 (1927).

(3) O. H. Krikorian, Lawrence Radiation Laboratory, Livermore, Calif., Rept. UCRL-2888 (1955).

(4) O. Kubaschewski and E. Evans, "Metallurgical Thermochemistry," 3rd (revised) Ed., Pergamon Press, Ltd., New York, N. Y., 1958.

(5) J. Egan and J. Bracker, BNL-583, 595, 618, 659. Also see paper presented at the Second Conference on Nuclear Reactor Chemistry, Gatlinburg, Tenn., Oct. 10–12, 1961.

(5a) Note Added in Proof.—The galvanic cell measurements of Egan have been published without significant alteration: *J. Phys. Chem.*, **68**, 978 (1964).

(6) H. K. Lonsdale and J. N. Graves, GA-3015 (April 2, 1962). Also see "Thermodynamics of Nuclear Materials," International Atomic Energy Agency, Vienna, 1962, pp. 601–623.

(7) N. L. Lofgren and O. H. Krikorian, Lawrence Radiation Laboratory, Livermore, Calif., Rept. UCRL-7448 (1963).

(8) W. A. Chupka, J. Berkowitz, C. V. Giese, and M. G. Inghram, *J. Phys. Chem.*, **62**, 611 (1958).

(9) J. Drowart, G. De Maria, and M. G. Inghram, *J. Chem. Phys.*, **29**, 1015 (1958).

tems. In the B–C system, Verhaegen, Stafford, and Ackerman[11] discovered BC(g), BC_2(g), and B_2C(g). Also, BCSi(g) was produced upon addition of SiC. Eick, *et al.*,[12] determined that UC_2(g) is a minor species in equilibrium with the UC_{2-x}(s) phase.

In the present investigation, vapors were produced in a Knudsen cell in a furnace attached to a mass spectrometer. The vapors were allowed to effuse into the mass spectrometer, where they were ionized by electron bombardment and analyzed for mass. By following the ion intensities as a function of temperature, enthalpies of formation were determined for the various species by means of the second law of thermodynamics. In addition, a third-law determination was made using silver and molybdenum to determine the sensitivity of the mass spectrometer for the thorium-containing species.

Experimental

Equipment. The mass spectrometer furnace is illustrated in Fig. 1. A graphite Knudsen cell, 1.9 cm. in diameter and 1.6 cm. high, was placed in a tantalum holder mounted on a tantalum stand. The cell orifice was 3.238 mm. in diameter. Several tantalum shields were placed above the cell lid. A heater consisting of a self-supported tungsten helix surrounded the holder and stand. The heater had B5 turns and was made from 0.32-cm.-diameter tungsten rod, 85 cm. long. The windings were 3.2 cm. inside diameter and 5.7 cm. total height. The ends of the heater were clamped onto massive water-cooled copper electrodes. One of the electrodes operated at ground potential and was attached to the vacuum system, while the other was insulated from it by means of a Kovar-to-glass seal. Radiation shielding consisted of seven layers of 0.1-mm.-thick tantalum foil, dimpled to decrease contact area. The openings in the top shields were designed to minimize vaporization from the cooler shields into the mass spectrometer. A 2-mm.-thick shield was used at the bottom of the top shields to reduce the amount of sagging at high temperatures. The shell of the furnace had a thickness of 3 mm. of tantalum on top, 1 mm. on the sides, and 6 mm. at the base. The side shell and sample stand were fastened to the furnace base by means of tantalum screws. The lid was held in place by means of a tungsten pin fitted into a 0.75-mm. hole drilled into the side shell. Three adjustable stainless steel legs supported the furnace base. Using 250 amp. at 13 v. a.c., the furnace could be operated for several hours at 2100° under high vacuum without appreciable sagging. Maximum temperature of use was about 2300°.

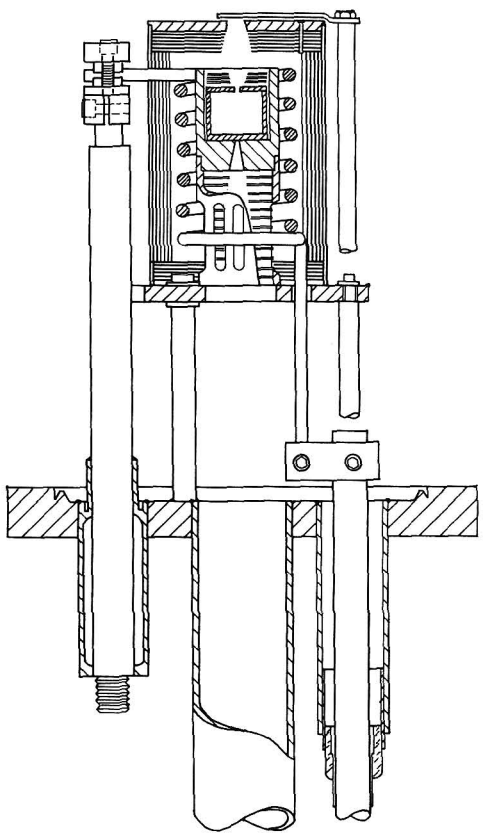

Figure 1. Schematic diagram of mass spectrometer furnace.

A 1.9-cm.-diameter hole in the furnace base served the dual purpose of a vacuum pump-out and sight hole for optical pyrometry. A sight tube with a quarts window and a magnetically actuated shutter was located on the vacuum base plate below the furnace An optical glass prism was attached to the window for convenience in taking pyrometer readings.

Temperatures were measured with a Leeds and Northrup disappearing-filament-type optical pyrome ter that had been standardized by comparison with an NBS-calibrated standard lamp. Appropriate correct tions were applied for transmission of the window and prism. Sightings were made into a blackbody cavity in the bottom of the graphite Knudsen cell.

A shutter was provided above the furnace opening to permit measurement of background intensities. The shutter could be used in partially open stages to study the intensity profile of the molecular beam. The vacuum seal for the shutter was a Teflon compression

(10) J. Drowart, G. De Maria, A. J. H. Boerboom, and M. G Inghram, *J. Chem. Phys.*, **30**, 308 (1959).

(11) G. Verhaegen, F. E. Stafford, and M. Ackerman, *Nature*, **193**, 1280 (1962).

(12) H. Eick, E. Rank, and R. Thorn, "Thermodynamics of Nuclear Materials," International Atomic Energy Agency, Vienna, 1962, p. 549.

fitting. A water-cooled copper shield surrounded the top and sides of the furnace to minimize heat flow into the mass spectrometer. An insulated copper ring was placed on the water-cooled shield in concentric alignment with the effusing beam. A bias voltage of -300 v. on the copper ring suppressed interference from negative ions effusing from the furnace.

The vacuum jacket for the furnace was made of stainless steel and was water-cooled on the outside. It sealed onto the mass spectrometer by means of an indium-coated soft copper gasket. Evacuation was by means of the mass spectrometer vacuum system. Construction of the vacuum enclosure was either by heliarc welding or by silver or indium soldering. Seals were made either with indium-coated soft copper gaskets or pure indium gaskets.

The major features of the mass spectrometer and its associated counting system have been described previously.[13] Certain modifications have been made in the instrument since that time. These include a fast magnetic field sweep,[14] getter-ion (VacIon) pumps, and a 30.5-cm.-radius, 60° sector cylindrical energy selector, which in these experiments was operated at low (<200) resolving power.

The ion source was a grid-controlled source suggested by the work of Winn and Nier.[15] We, however, used a real control grid and provided amplified feedback from the collector to the control grid to maintain the collector current constant. As will be seen from Fig. 2, the electrical structure resembled a tetrode, and indeed its control characteristics were similar to those of a 6L6 tube. No magnetic field was used to collimate the electron beam; hence a magnetic shield was used to prevent the stray magnetic field from the analyzer from modulating the electron beam. The cathode was a 0.03 × 0.75-mm. rhenium ribbon operated at about 3 v. and 6 amp. The control grid was taken from a 6SL7 tube. The acceleration slit was approximately 0.75 mm. wide and 12 mm. long. On the far side of the ionization box was a coarse grid at the box potential to prevent the 22.5-v. bias on the collector from distorting the field within the box. The ion exit slit was about 1.2 mm. wide and the only drawing-out potential was that furnished by leakage through the ion exit slit. The cathode-to-box potential was controlled to better than 100 mv. over a range of 5 to 175 v. ionization potential. The regulator amplifier was capable of controlling the control-grid potential in the region from -20 v. with respect to the cathode (beyond cut-off) to above the box potential. Above the box potential, however, defocussing effects take place, causing the ion current to be no longer proportional to the collector current. A change of cathode power by $\pm 20\%$ within

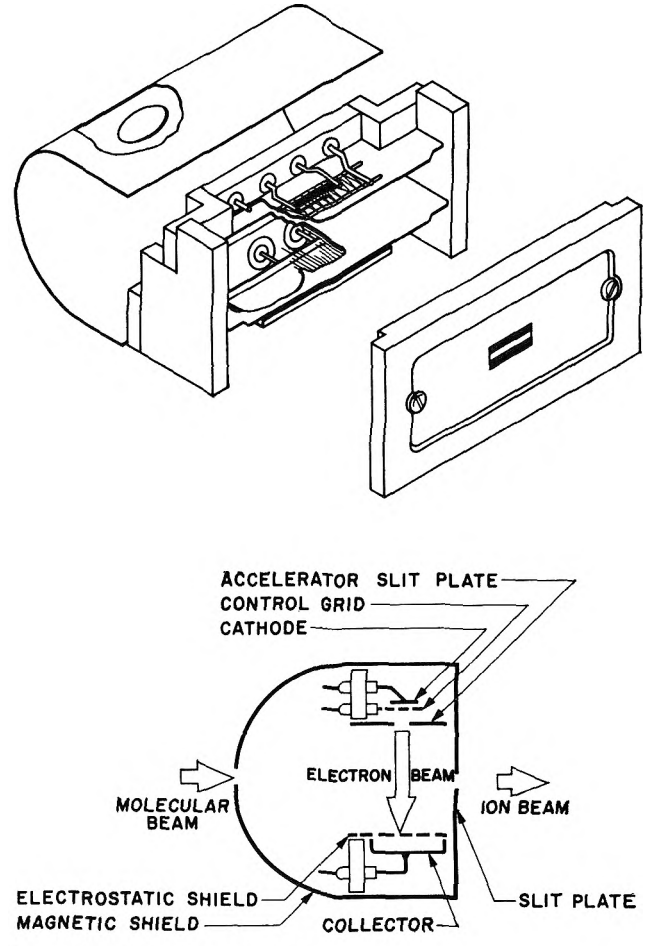

Figure 2. Schematic diagram of ion source.

the operating range caused less than 1% change in the ion beam current.

It was convenient on this instrument to mount the ion source on the regular quick-change carriage at the accelerating potential of 10,000 v. The Knudsen cell assembly was mounted at ground potential, so that only neutral molecules entered the ion source. Negative thermal ions were suppressed by the charged ring previously described.

Procedure. The ThC_2 was made by arc melting in a furnace employing a nonconsumable tungsten electrode and a water-cooled copper hearth. A mixture of thorium and carbon powders with carbon in 5% excess was pressed into a pellet, placed in the furnace, and melted under 0.5 atm. of argon. The ingot was inverted and remelted several times to ensure homo-

(13) G. W. Barton, Jr., L. E. Gibson, and L. F. Tolman, *Anal. Chem.*, 32, 1599 (1960).

(14) G. W. Barton, Jr., L. F. Tolman, and R. E. Roulette, *Rev. Sci. Instr.*, 31, 995 (1960).

(15) E. B. Winn and A. O. Nier, *ibid.*, 20, 11 (1949).

geneity. It was then stored under mineral oil until ready for use. The thorium metal was from the Fairmont Chemical Co. and contained about 1% ThO_2. Spectroanalysis showed the principal impurities to be Fe, 0.05%; Ca, 0.03%; and Al, 0.02%. The graphite powder was Acheson Grade 38 (National Carbon Co.) −400 mesh powder, outgassed under vacuum at 1675°K. before use. It had an ash content of 0.1% before outgassing, with Ca and Fe being the principal impurities. X-Ray diffraction patterns of the solid residues taken immediately after the vaporization experiments showed only the lines of ThC_2. The films were of good over-all quality and the lines were of strong intensity.

ThO was never observed effusing from arc-melted ThC_2 in the Knudsen cell, but was found to be present when ThC_2–C filaments were used as a source of vapor. These were fabricated by spreading thorium powder on graphite filaments and heating them resistively in the mass spectrometer. In these experiments, the small amounts of oxide in the thorium always produced high initial intensities of ThO, which decayed to negligible values in a few minutes.

For the determination of absolute vapor pressures, sensitivity calibrations on the mass spectrometer were made in the following manner. A disk of silver weighing 25.54 mg., of the same diameter as the inside of the graphite crucible, was supported on a graphite sleeve inside the crucible above the ThC_2 sample. The intensity of the ion beam produced from the effusing silver vapors was measured at six temperatures between 1134 and 1219°K. The temperature was then raised above the melting point of silver and the residual silver was completely removed by volatilization. Above the melting point, the Ag^+ intensity decreased with time. The enthalpy of sublimation of silver was calculated from the slope of log IT *vs.* $1/T$ to be 64.1 kcal./g.f.w. at a median temperature of 1176°K.

At higher temperatures, a similar calibration procedure was carried out with molybdenum. The molybdenum was a washer that externally surrounded the effusion orifice. Tantalum shields were used to define the vaporization area of the molybdenum as 19.013 mm.^{2}, and to prevent it from reacting with the graphite crucible cover. Fourteen intensity determinations between 2337 and 2539°K. gave a second-law enthalpy of sublimation of 167.9 kcal./g.f.w. for molybdenum at a median temperature of 2438°K.

The experimental procedure was to increase the furnace temperature in steps of approximately 20°, allow it to remain at each power setting until no further temperature change occurred, and measure ion intensities with the shutter open and closed. Not all possible species were looked for at all temperatures. However, the mass peaks corresponding to species considered most probable were measured. The species found were Th(g) and ThC_2(g). All others were essentially at background. In Fig. 3 are illustrated the calculated partial pressures of Table II, and in Fig. 4 are shown the ion intensity ratios of Table IV.

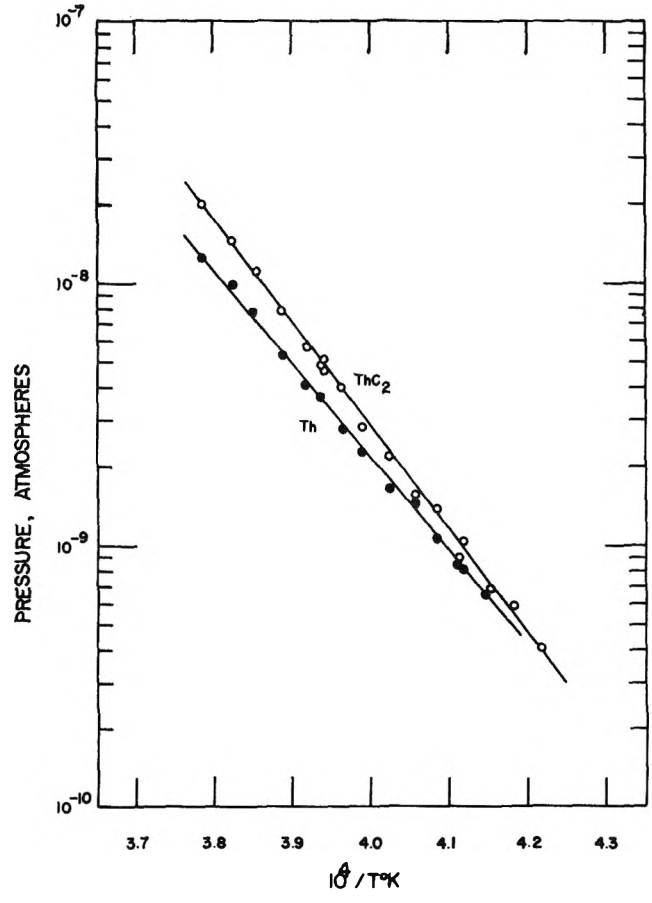

Figure 3. Equilibrium partial pressures of species above solid ThC_2.

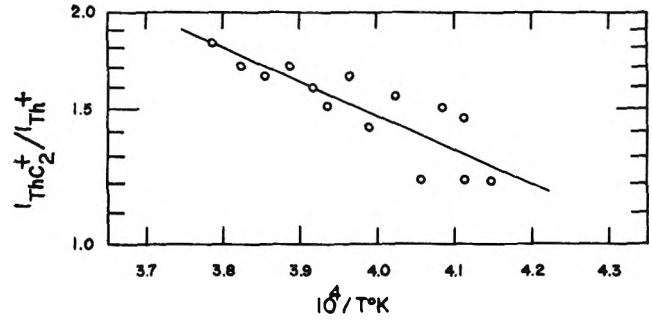

Figure 4. Observed ion-intensity ratio ThC_2^+/Th^+.

Calculations

Vapor pressures for molybdenum were calculated from the equation of Edwards, Johnston, and Black-

burn.[16] Data for the thermal expansion of molybdenum and tantalum are from Edwards, Speiser, and Johnston.[17] The thermal expansion of graphite was evaluated from data compiled by Goldsmith, Waterman, and Hirschhorn.[18] An evaporating area was calculated for each species only at the midpoint of its range of observation. Values for the vapor pressure of silver are those given by McCabe and Birchenall.[19] Isotopic abundances for silver and molybdenum are from Strominger, Hollander, and Seaborg,[20] and relative ionization cross sections were estimated by the method of Otvos and Stevenson.[21]

We took as a basis of comparison of the intensities of the various species accelerating voltages which were three times the respective first ionization potentials. This was a voltage at which each maximum intensity was nearly reached, yet where competing ionization processes had not become important. Ionization potentials are 7.574 and 7.131 v. for silver and molybdenum, respectively,[22] and 4 to 5 v. for both thorium and thorium dicarbide.

The sensitivity of the mass spectrometer for each species was evaluated by means of the following expression, similar in form to that used by Chupka and Inghram[23]

$$S = \frac{F_C R_C}{R_X} \frac{1}{B} \frac{\sigma(X)}{\sigma(C)} \frac{T_C}{T_X}$$

where S is the sensitivity of the mass spectrometer for the species to be determined (counts $\times$ atm.$^{-1}$); X refers to the species to be measured; C refers to the species used for calibration; F is the intensity of the isotope at its experimental voltage and temperature (counts $\times$ atm.$^{-1}$); R is the ratio of intensity produced at the reference voltage to that produced at the operating voltage; B is the isotopic abundance of the calibrating isotope; σ is the relative ionization cross section; and T is the temperature in °K. at which the intensity of the isotope was determined. The values of the factors used are listed in Table I.

Vapor pressures were calculated by means of the expression $P_{atm} = (I_{X^+}/S)(A_{X^+}/A_{C^+})$, where A is the evaporating area. The intensity I is given by the expression $[Q/(1 - Q\tau)] - B$, where Q is the gross counting rate, τ is the dead time of the counting equipment, and B is the background counting rate.

Table I

$R_{Ag} = 0.952$	$1/B(Ag^{107}) = 1.947$
$R_{Mo} = 1.48$	$1/B(Mo^{98}) = 4.211$
$R_{ThC_2} = 1.022$	$\sigma(Ag) = 34.8$
$R_{Th} = 1.075$	$\sigma(Mo) = 52.5$
	$\sigma(Th) = 89.5$
	$\sigma(ThC_2) = 97.8$

The following were found to be the principal reactions involved in the vaporization of ThC_2(s)

$$ThC_2(s) = ThC_2(g) \quad (1)$$

$$ThC_2(s) = Th(g) + 2C(\text{graphite}) \quad (2)$$

We should, of course, in speaking of ThC_2, more properly designate it as ThC_{2-x}, where x is, in the case of the carbon-saturated phase, some unknown function of temperature.[24] Lacking the proper information, we have assumed x to be equal to 0. Equilibrium pressures for the reactions are presented in Table II. Third-law values of ΔH°_{298} for the reactions were evaluated by means of the equation

$$\Delta H^\circ_{298} = -\Delta\left[T\left(\frac{F^\circ_T - H^\circ_{298}}{T}\right)\right] - RT \ln P$$

The necessary free energy functions for Th(g), ThC_2(g), ThC_2(s), and C(graphite) are listed in Table III. They were obtained in the following ways.

(*1*) *Th(g)*. The functions were taken from the tabulation of Gordon.[25]

(*2*) *ThC_2(g)*. (*a*) *Vibrational*. For estimating vibrational contributions, we employed a set of assumptions similar to those of Chupka[8] for the case of LaC_2. The Th–C internuclear distance was estimated to be 1.90 Å., and the C–C distance. 1.31 Å. By Badger's rule,[26] we obtained a Th–C stretching force constant of 5.5×10^5 dynes/cm. The C–C stretching force constant was taken to be 9.238×10^5 dynes/cm. and the bending force constant 0.20×10^5 dynes/cm. The vibrational frequencies were then calculated to be $\omega_1 = 592$ cm.$^{-1}$, $\omega_2 = 399$ cm.$^{-1}$, and $\omega_3 = 1756$ cm.$^{-1}$.

(*b*) *Electronic*. The approximation was made that

(16) J. W. Edwards, H. L. Johnston, and P. E. Blackburn, *J. Am. Chem. Soc.*, **74**, 1539 (1952).

(17) J. W. Edwards, R. Speiser, and H. L. Johnston, *J. Appl. Phys.*, **22**, 424 (1951).

(18) A. Goldsmith, T. E. Waterman, and H. J. Hirschhorn, WADC TR 58-476 (1960).

(19) C. L. McCabe and C. E. Birchenall, *J. Metals*, **5**, 707 (1953).

(20) D. Strominger, J. M. Hollander, and G. T. Seaborg, *Rev. Mod. Phys.*, **30**, 585 (1958).

(21) J. W. Otvos and D. P. Stevenson, *J. Am. Chem. Soc.*, **78**, 546 (1956).

(22) W. Finkelnburg and W. Humbach, *Naturwiss.*, **2**, 35 (1955).

(23) W. A. Chupka and M. G. Inghram, *J. Phys. Chem.*, **59**, 100 (1955).

(24) S. Langer, C. Hancock, and F. L. Kester, paper presented at the 141st National Meeting of the American Chemical Society, Washington, D. C., March 21–29, 1962, Abstracts of Papers, p. 51R.

(25) J. S. Gordon, *J. Chem. Phys.*, **35**, 2252 (1961).

(26) R. M. Badger, *ibid.*, **3**, 710 (1935).

Table II: Vapor Pressures and Third-Law ΔH°_{298} Values for the Vaporization Processes of $ThC_2(s)$

T, °K.	$P_{atm} \times 10^{10}$ from Ag	$P_{atm} \times 10^{10}$ from Mo	ΔH°_{298} from average P, kcal./g f.w.
	(1) $ThC_2(s) = ThC_2(g)$		
2371	4.78	3.29	198.2
2391	7.01	4.80	197.8
2408	8.13	5.57	198.5
2431	10.66	7.35	198.8
2428	12.35	8.46	197.9
2448	16.42	11.28	198.0
2464	18.31	12.58	198.5
2485	25.87	17.76	198.4
2506	33.43	22.95	198.5
2523	47.46	32.57	198.1
2530	60.42	41.47	197.6
2540	57.53	39.48	198.2
2537	54.67	37.55	198.3
2553	67.80	46.57	198.3
2572	92.82	63.77	197.9
2593	131.1	90.00	197.6
2616	173.5	119.2	197.7
2641	236.0	162.1	197.8
		Av.	198.1
	(2) $ThC_2(s) = Th(g) + 2C(graphite)$		
2411	7.73	5.32	168.5
2432	10.16	6.96	168.6
2428	9.75	6.70	168.5
2449	12.54	8.61	168.7
2464	17.33	11.88	168.0
2485	19.16	13.15	168.9
2506	27.01	18.54	168.6
2522	32.97	22.63	168.5
2540	43.74	30.01	168.3
2540	43.81	30.06	168.3
2553	48.69	33.44	168.6
2572	62.72	43.06	168.4
2597	91.32	62.69	168.0
2614	117.0	80.40	167.9
2642	148.6	102.1	168.2
		Av.	168.4

Table III: Free Energy Functions in cal./deg.-g.f.w.

T, °K.	$-\left(\frac{F^\circ_T - H^\circ_{298}}{T}\right)$ $ThC_2(g)$ total	Th(g)	$ThC_2(s)$	C(graphite)
2200	76.79	51.91	35.56	5.93
2300	77.27	52.18	36.40	6.13
2400	77.72	52.44	37.21	6.32
2500	78.17	52.70	37.99	6.50
2600	78.54	52.96	38.76	6.69
2700	78.94	53.20	39.51	6.87
2800	79.33	53.44	40.24	7.04
2900	79.72	53.68	40.95	7.21

the electronic contribution is the same as that for Th(III), whose spectrum has been analyzed.[27] A similar approximation has been used by Brewer[28] for gaseous oxides.

(*c*) *Rotational.* On the basis of a linear asymmetric model, we calculated a moment of inertia $I = 252.8 \times 10^{-40}$ g.-cm.^{2}.

(*d*) *Translational.* This contribution was calculated in the usual manner by means of the Sackur–Tetrode relation.

(*3*) *$ThC_2(s)$.* A value of 14.0 ± 1.0 cal./deg.-g.f.w. was estimated for S°_{298},[7] and the method of Krikorian[29] was employed to obtain the high temperature heat capacity relation: $C_p^\circ = 18.26 + 3.11 \times 10^{-3}\,T - 4.05 \times 10^5/T^2$ cal./deg.-g.f.w.

(*4*) *C(graphite).* Free-energy functions were taken from Stull and Sinke.[30]

Second-law values for the room temperature enthalpies of the reactions were obtained by use of the expression

$$\frac{\Delta H^\circ_{298}}{T} = -\Delta\left(\frac{F^\circ_T - H^\circ_{298}}{T}\right) - R \ln P$$

which for brevity we call Σ. The necessary values of the free energy functions were again taken from Table III and equilibrium pressures were obtained from Table II. Since Σ could be computed for each experimental temperature, we could now obtain ΔH°_{298} as the slope of Σ plotted *vs.* $1/T$.

Results

The calculation outlined above was performed by the method of least squares using an IBM-650 computer. The second-law results are

$$ThC_2(s) = ThC_2(g); \quad \Delta H^\circ_{298} = 202.6 \pm 2.4 \text{ kcal./g.f.w.} \quad \text{(I)}$$

$$ThC_2(s) = Th(g) + 2C(graphite); \quad \Delta H^\circ_{298} = 174.1 \pm 2.3 \text{ kcal./g.f.w.} \quad \text{(II)}$$

$$Th(g) + 2C(graphite) = ThC_2(g); \quad \Delta H^\circ_{298} = 30.7 \pm 3.5 \text{ kcal./g.f.w.} \quad \text{(III)}$$

where the limits of error quoted are standard deviations of the slopes, representing random experimental errors.

(27) T. L. DeBruin, P. F. A. Klinkenberg, and P. Schuurmans, *Z. Physik*, 118, 58 (1941).

(28) L. Brewer and M. S. Chandrasekharaiah, Lawrence Radiation Laboratory Rept. UCRL-8713 (1959).

(29) O. H. Krikorian, Lawrence Radiation Laboratory Rept. U CRL-6785 (1962).

(30) D. R. Stull and G. C. Sinke, "Thermodynamic Properties of the Elements," Advances in Chemistry Series, No. 18, American Chemical Society, Washington, D. C., 1956.

The third-law computations gave for reaction (I), $\Delta H°_{298}$ = 198.1 ± 0.3 kcal./g.f.w.; for (II), $\Delta H°_{298}$ = 168.4 ± 0.3 kcal./g.f.w; and for (III), $\Delta H°_{298}$ = 27.5 ± 0.4 kcal./g.f.w; again, the errors are standard deviations.

Using the reported value[31] for the enthalpy of sublimation of Th(s), $\Delta H°_{298}$ = 137.7 ± 1.0 kcal./g.f.w., we obtained for the second-law enthalpy of formation of ThC_2 from (II), $\Delta H_f°_{298}$ = −37.4 ± 2.5 kcal./g.f.w., and from (I) and (III), $\Delta H_f°_{298}$ = −34.2 ± 4.4 kcal./g.f.w. Similarly, using the third-law method, we found from (II), $\Delta H_f°_{298}$ = −30.7 ± 1.0 kcal./g.f.w.

The discrepancy between the second- and third-law treatments indicates the presence of systematic errors. However, this discrepancy is less than the systematic errors of about ±6% noted in the enthalpy of sublimation determinations for silver and molybdenum. Because of the systematic errors involved, however, the third-law value is believed to be the more reliable determination.

We consider now the most likely sources of systematic experimental errors, with the best estimates we are able to make as to their magnitude. Such sources are pyrometer calibration (±3°), window transmission calibration (±2°), temperature reading (±3°), thermal gradients in the cell (±5°), geometric changes in the furnace (±0.5%), revaporization processes (0–2%), evaporation area (±3.6%), and ionization cross section (±100%).

In assessing geometric errors, we consider that if the molecular beam were collimated only by the ion source entrance slit, there would have to be a differential thermal expansion in the furnace sufficient to cause an 8° tilt to change the intensity at the center of the slit by 1%. If the beam were collimated by the furnace, thermal expansion might be a source of error. In considering evaporating area, ±3.6% is arrived at from the standard deviations of the measurements of the three diameters which determine the ratio of molybdenum evaporating surface area to orifice area. Errors arising from the difference in evaporating area geometry between molybdenum and silver, thorium, or thorium dicarbide are negligible, unless there was additional collimation of the molybdenum beam. Effects resulting from changing equilibrium phase composition with temperature are unknown, but considered negligible. According to Wilhelm and Chiotti,[32] the solubility of carbon in ThC_2 is probably quite small. A 1° error in temperature caused an error of 1.29% in the observed pressure at 2546°K., the midpoint of the experimental range. Using this conversion and treating the above estimates according to the law of the propagation of errors[33] indicated a total standard deviation for systematic errors of ±3.5 kcal./g.f.w. in $\Delta H_f°_{298}$ of gaseous species and for the third-law $\Delta H_f°_{298}$ of ThC_2(s).

Table IV: Observed Ion Intensities of ThC_2^+ and Th^+

T, °K.	$I_{ThC_2^+}$	I_{Th^+}
2410	146	121
2431	190	157
2428	220	151
2448	290	193
2464	322	265
2485	451	290
2506	577	406
2523	814	492
2540	980	648
2553	1150	719
2572	1562	918
2595	2188	1324
2615	2871	1687
2641	3868	2119

The sources and magnitudes of random errors were estimated as temperature reading ±3°, fluctuations in heater current ±3°, statistical errors in counting pulses, variable, about ±1%. Analysis shows that these combine to produce a total standard deviation for random errors of ±0.3 kcal./g.f.w., which is the same as the observed statistical errors.

The over-all errors may be calculated by combining the observed statistical and estimated systematic errors. We therefore report as the best values that can be obtained from this experiment for reaction (I), $\Delta H°_{298}$ = 198.1 ± 3.5 kcal./g.f.w.; for (II), $\Delta H°_{298}$ = 168.4 ± 3.5 kcal./g.f.w.; for (III), $\Delta H°_{298}$ = 27.5 ± 3.5 kcal./g.f.w., and $\Delta H_f°_{298}$ = −30.7 ± 3.7 kcal./g.f.w.

Discussion

The results obtained in this experiment differ somewhat from other work and from previous estimates. The higher pressures reported by Lonsdale and Graves may be in part a result of collimation of light to their pyrometer by their target holder, which would cause a low temperature reading. If, as seems likely, oxygen were absorbed by their sample during target changing, a portion of it must have been vaporized as ThO, and hence, due to the lack of a protective shutter, contributed to the transport of Th to the target.

In order to compare directly the results of Lonsdale

(31) H. L. Schick, D. F. Anthrop, R. E. Dreikorn, R. C. Feber, P. L. Hanst, M. B. Panish, and C. H. Ward, RAD-SR-62-251 (1962).

(32) H. A. Wilhelm and P. Chiotti, *Trans. Am. Soc. Metals*, 42, 1295 (1950).

(33) R. T. Birge, *Am. J. Phys.*, 7, 351 (1939).

and Graves with our own, we apportioned their analytically determined weights of thorium between Th(g) and $ThC_2(g)$, using our pressure ratios. Then, using the free energy functions of Table III, we carried out the same calculations as with our own data. This produced the values listed in Table V.

Table V

Reaction	Results of Lonsdale and Graves, kcal./g.f.w. Second law	Third law
$ThC_2(s) = ThC_2(g)$	204.4 ± 4.6	188.9 ± 1.7
$ThC_2(s) = Th(g) + 2C(graphite)$	176.4 ± 4.8	160.1 ± 1.7
$Th(s) + 2C(graphite) = ThC_2(s)$	−38.7 ± 5.8	−22.4 ± 2.7
	−36.0 ± 9.1	

A recalculation of the data of Prescott and Hincke is presented in the Appendix. A value of $\Delta H_f°_{298}$ for $ThC_2(s)$ of −31.6 ± 2.4 kcal./g.f.w. was obtained, in good agreement with our third-law result.

Galvanic cell measurements such as those of Egan and Bracker[5] are potentially very useful in determining thermodynamics of refractory materials. Their free energy measurements on ThC_2 are of comparable accuracy to the results of many methods now in more common use. The principal problems encountered in such investigations are the well-known difficulty in attaining solid state equilibrium at low temperatures and, most of all, in identifying the reactions taking place. Insufficient information is available to evaluate the study properly, but their free energy measurements appear to be in reasonable agreement with this work. A third-law calculation gives $\Delta H_f°_{298} = -28.5$ kcal./g.f.w.

Some trends in the vaporization of carbides and oxides are beginning to emerge. It appears to us that there is indeed a correlation between the stabilities of gaseous monoxides and dicarbides, as has been proposed.[7] The parallel between ThO(g) and $ThC_2(g)$ is obvious. Moreover, work currently in progress at this laboratory has demonstrated the presence of gaseous dicarbide species in equilibrium with solid MC_2, where M = La, Ce, Pr, Gd, and Lu. It should be noted that the oxides of these rare earths produce MO(g) most abundantly in vaporization,[34,35] just as $ThO_2(s)$ produces ThO(g) as a major species.[36]

Moving across the actinide series, we observe somewhat similar relationships. As previously mentioned, $UC_2(g)$ is a vapor component over $UC_2(s)$, although not so important in the case of ThC_2. UO(g) has been found to be the most important species in equilibrium with a mixture of U(l) and $UO_2(s)$,[37] just as Th(s) containing dissolved O produces large amounts of ThO(g).[38]

No detailed theoretical explanation of such behavior has yet been made. However, it is likely that other gaseous carbide and oxide complexes will soon be identified and that species ratios as a function of stoichiometry will be better explored. For example, from the above observations, and from similarities between certain of the lanthanides and actinides, we may, by analogy, expect to detect vapor molecules such as $CmC_2(g)$.

Acknowledgment. A preliminary version of this study appeared in the Proceedings of the Symposium on the Thermodynamics of Nuclear Materials, held by the International Atomic Energy Agency, Vienna, 1962.

Appendix

We have recalculated the heat of formation of ThC_2 from the data of Prescott and Hincke[2] using the following information.

1. The temperature scale is converted to ITS-1948 by using $C_2 = 1.4380$ cm.-deg.

2. Free-energy functions are derived (a) for ThO_2, from high-temperature enthalpy and entropy data of Kelley,[39] the high-temperature enthalpies of Hoch and Johnston,[40] and the $S°_{298}$ given by Kelley[41]; (b) for graphite, as given by Stull and Sinke[30]; (c) for $ThC_2(s)$, as presented in Table III; (d) for CO, from data by Kelley.[39]

From a third-law treatment, we find

$$ThO_2(s) + 4C(graphite) = ThC_2(s) + 2CO(g)$$

$$\Delta H°_{298} = 208.79 \pm 2.0 \text{ kcal./g.f.w.}$$

Using the values $\Delta H_f°_{298} = -293.2 \pm 0.4$ kcal./g.f.w. of ThO_2[42] and $\Delta H_f°_{298} = -26.42 \pm 0.01$ kcal./g.f.w. of CO,[42] we calculate $\Delta H_f°_{298} = -31.6 \pm 2.4$ kcal./g.f.w. of ThC_2.

(34) M. B. Panish, *J. Chem. Phys.*, **34**, 1079 (1961).

(35) M. B. Panish, *ibid.*, **34**, 2197 (1961).

(36) R. J. Ackermann, E. G. Rauh, R. J. Thorn, and M. C. Cannon, *J. Phys. Chem.*, **67**, 762 (1963).

(37) G. De Maria, R. P. Burns, J. Drowart, and M. G. Inghram, *J. Chem. Phys.*, **32**, 1373 (1960).

(38) A. J. Darnell, W. A. McCollum, and T. A. Milne, *J. Phys. Chem.*, **64**, 341 (1960).

(39) K. K. Kelley, U. S. Bureau of Mines Bulletin 584, U. S. Govt. Printing Office, Washington, D. C., 1960.

(40) M. Hoch and J. L. Johnston, *J. Phys. Chem.*, **65**, 1184 (1961).

(41) K. K. Kelley and E. G. King, U. S. Bureau of Mines Bulletin 592, U. S. Govt. Printing Office, Washington, D. C., 1961.

(42) J. P. Coughlin, U. S. Bureau of Mines Bulletin 542, U. S. Govt. Printing Office, Washington, D. C., 1954.

The Rates of Reaction of the Hydrated Electron in Aqueous Inorganic Solutions[1]

by J. K. Thomas, Sheffield Gordon, and Edwin J. Hart

Chemistry Division, Argonne National Laboratory, Argonne, Illinois *(Received January 30, 1964)*

The pulsed radiolysis technique has been used to follow the rate of decay of the hydrated electron in the presence of inorganic compounds. The exact technique is described together with the absolute rate constants for these reactions. The activation energy for the reaction of the hydrated electron with H_3O^+ was measured as 3.2 kcal./mole and is close to that expected for a diffusion-controlled reaction, while the activation energy for the reaction, $e_{aq}^- + H_2O$, was 4.6 kcal./mole.

Introduction

In the past year the literature has contained information on the rates of reactions of hydrated electrons with solutes.[2-4] The basis of the experimental methods used has been the pulse radiolysis technique which enables one to observe the hydrated electrons, e_{aq}^-, decaying with time as they pursue any particular reaction. From the standpoint of radiation chemistry and also the theory of reaction rates these processes are at the present time of great interest. This paper presents and discusses the reaction rates of the hydrated electron with some inorganic ions in aqueous solution.

Experimental

All vessels used in the preparation of solutions were washed with distilled water prior to baking at 500° for 3 hr. The methanol used was distilled from the perchloric acid salt of 2,4-dinitrophenylhydrazine; the water was triply distilled and all chemicals used were *reagent grade.*

Solutions were prepared by a method based on the already described syringe technique.[5,6] The experimental arrangement which is similar in some aspects to that used by Dorfman and Matheson[7] is shown in Fig. 1. Pulses (0.2–5.4 μsec.) of 13-Mev. electrons were directed from the accelerator through the thin plane mirror, E, into the reaction cell, D. The species produced absorbed some of the light beam emitted from the lamp, A. This was an Osram HBO 100-watt mercury super pressure lamp. The light from this lamp was focused by the lens, B, through the cell, D, onto the mirror, E. This reflected it to the concave mirror C, which refocused the beam back through the cell to E and subsequently back again to the plane mirror, F. In this way the effective path of the light was four cell lengths. The light reflected from F was focused into the slits of a Bausch and Lomb monochromator by lens, G. The light of a selected wave length was then directed into a 1P28 photomultiplier tube, H, the signal from which was amplified and displayed on a Tektronic SSl scope and subsequently photographed with Polaroid Type 3000 film. The phototube was shielded from stray γ-radiation by placing it in a lead castle with 5-cm. thick walls and by a 20-cm. lead shield. The over-all rise time of the secondary circuits was less than 0.2 μsec.

In the present work second-order reactions such as $e_{aq}^- + OH$, $e_{aq}^- + e_{aq}^-$, and $e_{aq}^- + H^+$ were minimized by working at low intensities. Some solutions were made 1 m*M* in methanol to eliminate the OH radical by

(1) Based on work performed under the auspices of the U. S. Atomic Energy Commission.

(2) S. Gordon, M. S. Matheson, E. J. Hart, J. Rabani, and J. K. Thomas, *J. Am. Chem. Soc.*, 85, 1375 (1963).

(3) S. Gordon, M. S. Matheson, E. J. Hart, J. Rabani, and J. K. Thomas, *Discussions Faraday Soc.*, 36, 193 (1963).

(4) J. P. Keene, *Nature*, 197, 47 (1963).

(5) E. J. Hart, S. Gordon, and D. A. Hutchison, *J. Am. Chem. Soc.*, 75, 6165 (1953).

(6) C. B. Senvar and E. J. Hart, *Proc. 2nd Intern. Conf. Peaceful Uses At. Energy, Geneva*, 29, 19 (1958).

(7) L. M. Dorfman and M. S. Matheson, *J. Chem. Phys.*, 32, 1870 (1960).

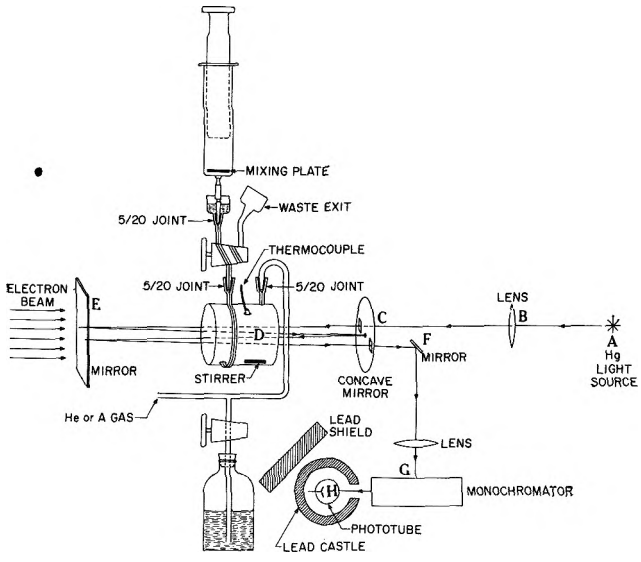

Figure 1. Diagram of the pulsed radiolysis experimental layout.

producing the inert CH_2OH radical, and in some cases the pH of the solution was 10 when the reaction, $OH^- + H^+$ ($k = 1.5 \times 10^{11}\ M^{-1}\ sec^{-1}$), removed the H^+. By taking the above precautions it was possible to follow the simple e_{aq}^- solute reaction without any complications. Normally electron beam currents up to 40 ma. were used, the pulse length was 0.4 μsec., and approximately 0.5 μM of e_{aq}^- was produced per liter per pulse.

A 4-cm. cell was used throughout the work. The assembly used to fill the cell is shown in Fig. 1. Pure helium or argon was used to flush out the cell and 3-way stopcock. Keeping the whole unit under a small increased pressure of He or Ar, the solution in the syringe was forced into the bottom of cell D. By increasing the inert gas pressure and by turning the 3-way stopcock, the solution could be forced out for analysis or disposal after irradiation.

Figure 1 shows a side view of the irradiation cell with a built-in thermocouple and magnetic stirrer. This type of cell was used for measuring rates at elevated temperature. This cell was heated by passing a suitable current through nichrome wire in silica sleeving which was wound around the cell. At a given current the cell reached an equilibrium temperature and from thermocouple readings, these measurements were made to an accuracy of $\pm 1°$.

Results

The reactions reported here may be conveniently divided into three groups: buffers, anions, and cations. Some preliminary work is also reported on iodine.

Buffers. In studying reactions of the hydrated electron it is desirable to buffer the system at the desired pH; hence, the necessity for this investigation. In a previous communication,[2] we reported that the un-ionized form of acetic and formic acids reacted with the hydrated electron with $k = 1.76 \pm 0.3 \times 10^8$ and $1.43 \pm 0.1 \times 10^8\ M^{-1}$ sec.$^{-1}$, respectively. Further studies revealed that succinic and oxalic acids also react with second-order rate constants of $\backsim 10^7$. However, 0.1 M citric acid appeared to be unreactive as did 0.1 M disodium monohydrogen phosphate. However, the potassium salt of the dihydrogen form of this phosphate reacted rapidly with $k = 1.5 \times 10^9$. Two other buffer materials were tried: (a) boric acid which reacted with e_{aq}^-; and (b) sodium tetraborate which did not react with e_{aq}^-, but gave some evidence of reaction with OH radicals. In this latter case, the methanol might eliminate the reaction of the tetraborate with OH and it may be a possible buffer. Thus, we conclude that, of the materials studied, only citric acid, disodium hydrogen phosphate, and possibly sodium tetraborate may be used to buffer an aqueous solution when reactions of e_{aq}^- are being studied.

Anions. The second group of compounds studied is listed in Table I and consists of certain inorganic anions. The first two listed are normally stable and unreactive in standard inorganic reactions and show the same behavior with respect to reactivity with the hydrated electron. The remainder of the ions listed are normally quite reactive in an oxidizing sense and show quite high reactivity also with the e_{aq}^-, the rates of the reactions being close to the diffusion-controlled value of 2×10^{10}.

Cations. The third group of compounds is the inorganic cations. The rapid reactions of the e_{aq}^- with H^+, Ag^+, Cu^{2+},[2] Zn^{2+}, and Pb^{2+} [8] have already been reported together with reference to the apparent inertness of Na^+, K^+, etc. Table II gives the rate constants for the reaction of e_{aq}^- with the rare earths. These were all prepared by dissolving the pure metal oxide in the calculated amount of H_2SO_4 and then adjusting to a pH of 6 or greater. Concentrations from 20–500 μM were used depending on the reactivity of the particular ion. Only three of the ions are very reactive: Sm^{3+}, Eu^{3+}, and Yb^{3+}, the others apart from Ho^{3+} being of the order of one hundred times less reactive. It has been known for some time that the aforementioned three elements show the divalent state whereas this has not been observed in the other rare earths. In fact the rates of reaction of the hydrated electron with Sm^{3+}, Eu^{3+}, and Yb^{3+} follow the same trend as the electrode

(8) J. H. Baxendale, E. M. Fielden, and J. P. Keene, *Proc. Chem. Soc.*, 242 (1963).

Table I: Rate Constants of Hydrated Electron Reactions with Inorganic Anions

Compound	Concn., mM	Conditions	pH	Slope[a] × 10^{-6}	k,[b] M^{-1} sec.$^{-1}$	
SO_4^{2-}	10	...	~7	...	Unreactive (<10^6)	
Cl^-	1	...	~7	...	Unreactive (<10^6)	
ClO_4^-	10	1 mM MeOH	~10		Unreactive (<10^6)	
CO_3^{2-}	1	...			Unreactive (<10^6)	
CNS^-	0.2	1 mM MeOH	~7	...	Unreactive (<10^6)	
HCO_3^-	1	...	...	...	Unreactive (<10^6)	
ClO_3^-	10	1 mM MeOH	~10	0.0185	4×10^6	
$S_2O_8^{2-}$	0.2	1 mM MeOH	~7	8.95	1.06×10^{10}	
$S_2O_3^{2-}$	0.2	1 mM MeOH	11.9	0.04	<10^8	
NO_3^-	0.2	...	7.0	1.02	1.17×10^{10}	1.1×10^{10}
	0.06	...	7.0	0.27	1.0×10^{10}	
NO_2^-	0.2	1 mM MeOH	~7.0	3.98	4.58×10^9	
$Cr_2O_7^{2-}$	0.20	...	~7.0	2.85	3.3×10^{10}	$4.4 \pm 1 \times 10^{10}$
$Cr_2O_7^{2-}$	0.033	1 mM MeOH	~13.0	0.785	5.4×10^{10}	
MnO_4^-	0.20	...	~7.0	1.75	2.2×10^{10}	$2.9 \pm 0.8 \times 10^{10}$
MnO_4^{--}	0.033	1 mM MeOH	~13.0	0.535	3.7×10^{10}	

[a] Slope, $\Delta \log D/\Delta t$, of the first-order plot of log optical density (D) *vs.* time. [b] $k = 2.3\ \Delta \log D/\Delta t \times 1/C_0$ where C_0 = concentration of solute.

potential E° (R^{2+}–R^{3+}) again indicating that the formation of the two valency state is a prime factor in these reactions.

Table II: Rate Constants of Hydrated Electron Reactions with Rare Earth Ions

Ion	pH	Concn., M	k, M^{-1} sec.$^{-1}$	E° (R^{2+}–R^{3+})
Eu^{3+}	5.55	2×10^{-6}	6.1×10^{10}	0.43
Yb^{3+}	6.03	3.3×10^{-6}	4.3×10^{10}	1.15
Sm^{3+}	5.96	2×10^{-5}	2.5×10^{10}	1.55
Nd^{3+}	4.66	1×10^{-3}	5.9×10^8	
Pr^{3+}	6.10	1×10^{-3}	2.9×10^8	
Gd^{3+}	6.05	5×10^{-4}	5.5×10^8	
Tb^{3+}	6.15	5×10^{-4}	3.7×10^8	
Dy^{3+}	5.90	5×10^{-4}	4.6×10^8	
Lu^{3+}	6.20	1×10^{-3}	2.5×10^8	
La^{3+}	6.98	1×10^{-3}	3.4×10^8	
Tm^{3+}	6.05	8×10^{-5}	3×10^9	
Ho^{3+}	5.88	8×10^{-5}	2.4×10^9	

Iodine. An interesting situation arises in the case of the reaction of the hydrated electron with iodine at pH 7. The reaction is rapid and second order with $k = 5.10 \pm 0.3 \times 10^{10}\ M^{-1}$ sec.$^{-1}$. The well-known transient I_2^- also forms.[9] The appearance of this transient may be followed and corresponds to a second-order $k = 5.17 \pm 0.3 \times 10^{10}\ M^{-1}$ sec.$^{-1}$. Since the decay of e_{aq}^- and the formation of I_2^- proceed at identical rates, proof of the reaction

$$e_{aq}^- + I_2 \longrightarrow I_2^-$$

is established.

Effect of Temperature on the Rate Constants. Figure 2 shows an Arrhenius plot of log K or log (slope) *vs.* T^{-1}

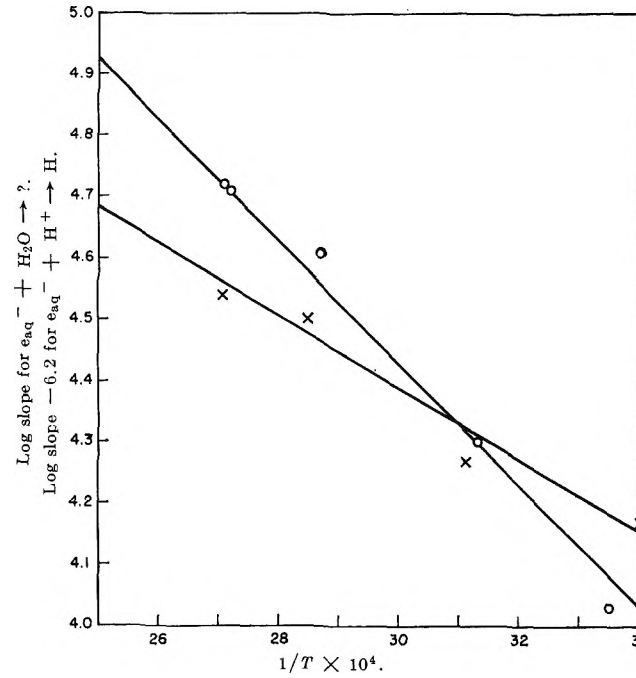

Figure 2. Arrhenius plots for the reactions: ○, $e_{aq}^- + H_2O$; ×, $e_{aq}^- + H^+$.

(9) L. I. Grossweiner and M. S. Matheson, *J. Chem. Phys.*, 61, 1098 (1957).

for the reaction $e_{aq}^- + H^+$ at a H^+ concentration of 4.4×10^{-5} N. The results agree with the simple Arrhenius equation, and it was found that the activation energy, ΔE, equals 3.2 kcal./mole. It is instructive to compare the activation energy of 3.2 kcal./mole with the values 2.6 ± 0.3 kcal./mole for the reaction $H_3O^+ + H_2O \rightleftharpoons H_2O + H_3O^+$,[10] and 2–3 kcal./mole for $H^+ + OH^- \rightarrow H_2O$.[11]

The rate constants for the above reactions are close to the diffusion-controlled limit; and the fact that the activation energies are in the range 2–3 kcal./mole would indicate that this is approximately the activation energy of diffusion for the above species in water.

Figure 2 also shows the plot of log k *vs.* $1/T$ for the reaction $e_{aq}^- + H_2O \rightarrow H + OH^-$. This was measured under two conditions: 1 mM MeOH, 10^{-1} N NaOH; and 1 mM MeOH, 10^{-4} N NaOH. The disappearance of the e_{aq}^- spectrum was first order. At 20° the rate constant of 2.3×10^4 M^{-1} sec^{-1} agreed with that found by Keene.[12] The measured activation energy of 4.6 kcal./mole was lower than one expected assuming that the diffusion-controlled rate constant would be $\backsim 2 \times 10^{10}$ and that the steric factor would be unity in this case. In our experiments, the e_{aq}^- decay at pH 13 was identical with that at pH 10. At the latter pH, the reaction $H + OH^- \rightarrow e_{aq}^- + H_2O$ (a), which has a rate constant of 2×10^7,[3] has a half-life which is much greater than the half-life (25 μsec.) for the reaction $e_{aq}^- + H_2O \rightarrow H + OH^-$ (b). However, at pH 13, the half-life of reaction (a) is much shorter that the half-life for (b) and yet the same kinetics were observed at the two pH values. In view of this result, we consider our second-order rate constant of 2.3×10^4 M^{-1} sec.$^{-1}$ for the $e_{aq}^- + H_2O$ reaction to be an upper limit. It is possible that impurities present in low concentration at these pH values contribute to e_{aq}^- disappearance.

Acknowledgments. It is a pleasure to thank Miss P. Walsh for helping with the work, and Messrs. B. A. Clifft and E. Backstrom who operated the linear accelerator.

(10) A. Loewenstein and A. Szoke, *J. Am. Chem. Soc.*, **84**, 1151 (1962).

(11) M. Eigen and L. de Maeyer, *Naturwiss.*, **42**, 413 (1955).

(12) J. P. Keene, in press.

The Vapor Pressure of Liquid Thallous Chloride and the Partial Pressures of Monomer and Dimer[1]

by Daniel Cubicciotti

Stanford Research Institute, Menlo Park, California *(Received February 10, 1964)*

The vapor pressure of liquid thallous chloride was measured by a quasi-static method from the melting point to the boiling point. The results can be represented by the equation: $\log p = -6923/T + 19.850 - 3.5 \log T$. The vapor pressure was also measured by a transpiration method. The partial pressures of monomer and dimer in the gas were calculated from these measurements. The dimer was the minor species and constituted about 5% of the vapor near the melting point and about 15% near the boiling point. The heats of evaporation at 1000°K. were 24.4 kcal. to monomer and 31.8 kcal. to dimer. The corresponding entropies were 22.0 and 25.7 e.u. The thermodynamic functions for the gaseous dissociation of the dimer were compared with those for alkali chlorides.

Introduction

The vapors of the alkali halides have been found to contain polymers (M_nX_n) of the simple diatomic molecules (MX). A summary of the thermodynamic properties of such species is given by Brewer and Brackett.[2] The thallous halides are in many ways similar to the alkali halides, and one would expect to find measurable proportions of polymers in their vapors. Furthermore, because of their lower boiling points, a higher pressure of vapor can be established at lower temperatures; and this would favor the formation of polymers. (However, the lower dipole moments of the gaseous thallous halides would give rise to smaller attractive forces leading to polymers.)

A qualitative examination of the vapors produced from liquid thallous chloride was made using a Bendix time-of-flight mass spectrometer. In this experiment the TlCl was contained in a graphite cell having a narrow slit orifice. With the sample somewhat above the melting point of TlCl the shutter-dependent peaks observed were: Tl^+ (relative intensity unknown because of interference by Hg^+ peaks), $TlCl^+$ (strong), Tl_2^+ (medium), Tl_2Cl^+ (strong), and $Tl_2Cl_2^+$ (medium). No higher-molecular-weight species were observed. These results were interpreted as indicating that dimers constituted an important fraction of the vapor and that higher polymers were of negligible importance.

A search of the literature revealed that the composition of the equilibrium vapor had been investigated by Bolshakov, Fedorov, and Shakhova.[3] They did indeed find evidence for polymerization since their transpiration pressures (calculated on the assumption of monomer) were greater than vapor pressures from boiling point measurements. It can be shown, however, that their data are internally inconsistent. They indicate that below 460°, the saturated vapor is essentially all Tl_2Cl_2 and above 620° essentially all TlCl. Also, according to their results, the heat of evaporation to these two species is approximately the same and equal to about 29 kcal. per mole of gaseous species. (The equality of the two heats of evaporation results from the equality of the slopes of their log p *vs.* $1/T$ curves for the two species.) Thus, from their results

$$TlCl(l) = TlCl(g) \qquad \Delta H = 29 \text{ kcal.}$$

$$2TlCl(l) = Tl_2Cl_2(g) \qquad \Delta H = 29 \text{ kcal.}$$

and therefore

$$Tl_2Cl_2(g) = 2TlCl(g) \qquad \Delta H = 29 \text{ kcal.}$$

(1) This work was made possible by the support of the Research Division of the U. S. Atomic Energy Commission under Contract No. AT(04-3)-106.

(2) L. Brewer and E. Brackett, *Chem. Rev.*, **61**, 425 (1961).

(3) K. A. Bolshakov, P. I. Fedorov, and M. N. Shakhova, *Nauchn. Dokl. Vysshei Shkoly, Khim. i Khim. Tekhnol.*, **No. 3**, 408 (1958) (translation available from OTS-61-19131).

In the region 460–620° their results indicate comparable pressure of the two species; and thus, equilibrium constants for the dissociation can be calculated from the pressures. The change of these equilibrium constants with temperature yields a heat of dissociation of 67 kcal. Thus, their data are internally inconsistent.

In view of this inconsistency it seemed desirable to redetermine the partial pressures of these species in the equilibrium vapor. The results obtained were quite different from those of ref. 3.

Experimental

The composition of the saturated vapor was determined from measurements of the vapor pressure and transpiration pressure. These data, together with the indication from the mass spectrometer results that higher polymers were unimportant, permitted a calculation of the partial pressure of monomer and dimer in the equilibrium vapor as a function of temperature.

The vapor pressure was measured by the "quasi-static" method of Rodebush, *et al.* The details of our apparatus for this measurement have been described elsewhere.[4] For the present work the cell was made of fused quartz and required about 150 g. of TlCl. The inert gas used was high purity, dry nitrogen. The transpiration apparatus has also been described in ref. 4. In the present work high purity, dry nitrogen was again used as a carrier gas.

Thallous chloride was made by dissolving pure thallium (99.95% from American Smelting and Refining Co.) in dilute HNO_3 and adding sufficient dilute HCl to precipitate TlCl. The precipitate was collected on a sintered glass filter, air-dried, and transferred to a fused-quartz bulb attached to the apparatus. It was then distilled under dry nitrogen into the system. Analysis of a sample taken after such treatment indicated a chloride content of 14.78% compared with 14.78% theoretical for TlCl. The freezing point of material prepared in this was found to be 430.8 ± 0.5°.

Temperatures in both sets of measurements were determined with a platinum–10% rhodium thermocouple that had been checked against a similar N.B.S. calibrated thermocouple.

Results

Vapor pressures were obtained over the range from a few mm. to slightly more than 1 atm. The results are shown in Fig. 1. The quasi-static results can be represented by the equation

$$\log p(\text{mm.}) = \left[-\frac{6923}{T} + 19.850 - 3.5 \log T\right] \pm 2\%$$

from 475 to 840°. These results should be comparable

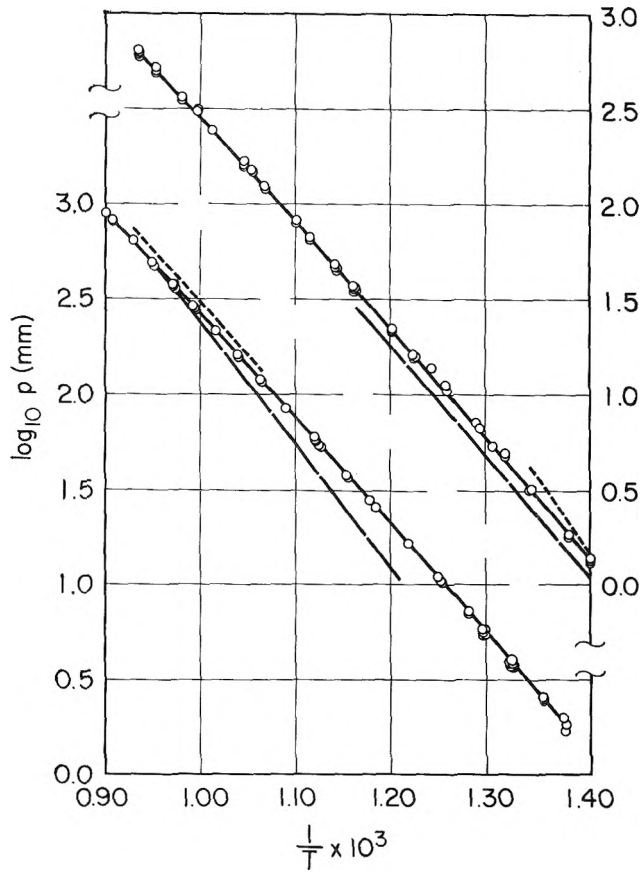

Figure 1. Vapor pressure of TlCl. Lower set of curves from quasi-static or boiling point method: full line and points, present data; dashed line, Bolshakov, *et al.*; dotted line, von Wartenberg and Bosse. Upper set of curves from transpiration: full line, present data; dashed line, Bolshakov, *et al.*; dotted line, Volmer.

with the boiling point data obtained by others. There is little agreement with the boiling point data of Bolshakov, *et al.*[3] The data of von Wartenberg and Bosse[5] have the same slope as the present data but their curve is displaced toward lower temperatures by about 11°. von Wartenberg, *et al.*, calibrated their thermocouples against the melting point of sodium chloride and so their temperature scale probably differed by no more than 2° from ours. However, von Wartenberg, *et al.*, do mention that with some salts they observed superheating by as much as 20° and in such cases they chose the lowest temperature. It may be that they overcorrected their readings for this effect.

The results of the transpiration measurements were reduced to the pressure of TlCl using 240 for the molecu-

(4) F. J. Keneshea and D. Cubicciotti, *J. Chem. Phys.* **40**, 191 (1964).

(5) H. von Wartenberg and O. Bosse, *Z. Elektrochem.*, **28**, 384 (1922). See also H. von Wartenberg and P. Albrecht, *ibid.*, **27**, 162 (1921), for technique.

lar weight of the gaseous species. When calculated in this way, the transpiration pressures are greater than the vapor pressure by approximately the partial pressure of the dimer. The accurate relation for calculating partial pressures of species is given below. The results of the transpiration study are also shown in Fig. 1. Multiple points at a given temperature were obtained at different flow rates of carrier gas usually over a five- or tenfold range. The results at different flow rates were within a 2% range indicating that for our experimental arrangement the gas stream was saturated with thallium chloride. These data are compared in Fig. 1 with the transpiration results of Bolshakov, *et al.*,[3] and those of Volmer.[6] Although the slope of the curve of ref. 3 is essentially the same as the present data, their pressures are about 20% smaller. The curve from ref. 6 is higher than the present results and has a greater slope.

The vapor pressures were combined with the transpiration results to calculate partial pressures of monomer and dimer in the following way. A smooth curve was drawn through each of the sets of data, fitting the points as well as possible. Then values for the vapor pressure and transpiration pressure (calculated as monomer) were taken from the smoothed curves at several temperatures over the range studied. Since there are only two important gaseous species—TlCl and Tl_2Cl_2, as shown by the mass spectrometer study—then their partial pressures can be calculated from the equations

$$P_D = \frac{P(\text{tr}) - P(\text{vap})}{P(\text{tot}) - P(\text{tr})} P(\text{tot})$$

$$P_M = P(\text{vap}) - P_D$$

In these equations, P_D is the partial pressure of the dimer (Tl_2Cl_2); P_M is that of the monomer (TlCl); P(tr) is the transpiration pressure calculated as monomer; P(tot) is the total pressure in the transpiration experiments, *i.e.*, 1 atm.; P(vap) is the vapor pressure of the liquid, determined by the quasi-static method.

The partial pressures of monomer and dimer calculated in this way are shown as the points in Fig. 2. The monomer data showed a small curvature, which was presumed to be due to the effect of the difference in heat capacities of the monomer and the liquid. Accordingly, a Σ-plot treatment[7] of the data was applied. Σ for the monomer was defined in the usual way as

$$\Sigma_M = -\log P_M + \frac{\Delta C_p}{R} \log T$$

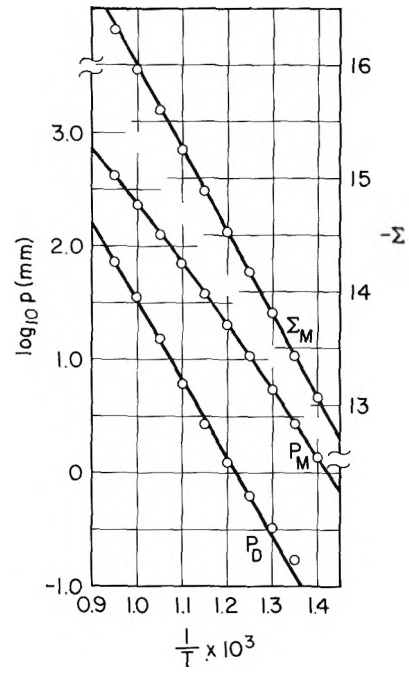

Figure 2. Partial pressures of monomer (P_M) and dimer (P_D) and Σ-plot for monomer (Σ_M).

The heat capacity of gaseous TlCl can be calculated from molecular constant data.[8] In the temperature range of interest for this work the heat capacity of TlCl was taken to be constant and equal to 8.9 cal./mole deg. The heat capacity of liquid thallium chloride has been found to be constant and equal to 17.9 cal./mole deg. at these temperatures.[9] The Σ-plot for the monomer is shown in Fig. 2. The points fall quite well on a straight line which indicates that the curvature of the vapor pressure curve did, indeed, arise from the heat capacity difference. The partial pressure of monomer can be represented by the equation

$$\log P_M(\text{mm.}) = \left[-\frac{7311}{T} - 4.53 \log T + 23.304 \right] \pm 5\%$$

The partial pressure of the dimer is also shown in Fig. 2. It increases from about 5% of the vapor pressure just above the melting point to about 15% near the boiling point. Because the dimer is the less im-

(6) F. Volmer, *Physik. Z.*, **30**, 590 (1929).

(7) See K. K. Kelley, U. S. Bur. Mines Bull. 383 (1935), reprinted in U. S. Bur. Mines Bull. 601 (1962), or G. N. Lewis and M. Randall, "Thermodynamics," revised by K. S. Pitzer and L. Brewer, McGraw-Hill Book Co., Inc., New York, N. Y., 1961, p. 175 ff.

(8) Internuclear distance from M. Mandel and A. H. Barrett, *Phys. Rev.*, **98**, 1159 (1955); vibration frequencies from G. Herzberg, "Molecular Spectra and Molecular Structure," Vol. I, 2nd Ed., D. Van Nostrand Co., Inc., New York, N. Y., 1950.

(9) H. Eding and D. Cubicciotti, *J. Chem. Eng. Data*, in press.

portant component of the vapor, the accuracy with which it is calculated from these data is less than that of the monomer. A straight line was drawn as well as possible through the points to represent them. The deviations from the line were presumed to reflect experimental error. The dimer pressure is given by the equation

$$\log P_D(\text{mm.}) = \left[8.500 - \frac{6970}{T}\right] \pm 10\%$$

Barrow, *et al.*,[10] have measured the vapor pressure over solid thallous chloride by a torsion-effusion method. Their data are shown in Fig. 3. A straight-line extrapolation of their data to the melting point joins remarkably well with the partial pressure of monomer extrapolated from the present data to the melting point. The heat of fusion calculated from the change in slope of the monomer curve at the melting point gives a value of 4.3 kcal. For a heat of fusion derived from a vapor pressure curve this is adequately good agreement with the calorimetric[9] value, 3.72.

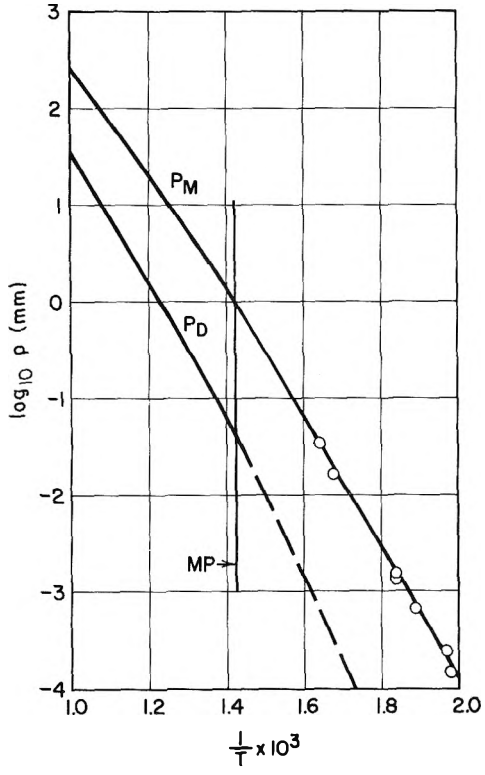

Figure 3. Pressures of species above and below melting point. P_M = partial pressure of monomer; above m.p. present data; below m.p. and points, data of Barrow, *et al.* P_D = partial pressure of dimer; above m.p., present data; below m.p., extrapolation of present data.

The partial pressure of dimer over solid thallous chloride was calculated from the values over the liquid. The heat of evaporation to dimer from the solid must be larger than that from the liquid by twice the heat of fusion; and, of course, the dimer pressure curves must join at the melting point. The curve so calculated is shown dashed in Fig. 3. The partial pressure of dimer is less than 2% of that of the monomer over the solid in the range of the measurements of Barrow, *et al.* Therefore their pressure measurements can be assumed to be monomer pressures, within experimental accuracy.

Discussion

The thermodynamic functions for the evaporation process were obtained as follows. The heat of evaporation for the monomer was derived from the slope of the Σ-plot curve for the monomer. The expression obtained was

$$\Delta H_T(\text{kcal./mole of monomer}) = [33.4 - 9.0 \times 10^{-3}\, T(°\text{K.})] \pm 0.2$$

The heat of evaporation at 800°K. is thus 26.2 kcal. The heat content of gaseous TlCl was calculated from molecular constant data[8] to be $(H_{800} - H_{298})_g = 4.4$ kcal. The heat content of the liquid above room temperature[9] is $(H_{800} - H_{298})_{liq} = 10.8$ kcal. Thus, the heat of sublimation of solid thallous chloride to gaseous TlCl at 298°K. is 32.6 ± 0.2 kcal. per mole as evaluated by this "second-law" method.

The free-energy functions for gaseous TlCl were calculated from molecular constant data. The free-energy function for the condensed phases were calculated from the room temperature entropy of Bartky and Giauque[11] and high temperature heat content measurements.[9] With these free-energy functions a "third-law" value of the heat of sublimation at 298°K. was calculated for each monomer pressure shown in Fig. 2. The values ranged from 32.6 to 32.9 with an average of 32.7 kcal. per mole. This "third-law" value is in reasonable agreement with the "second-law" value.

Barrow, *et al.*,[10] derived a third-law heat of sublimation from their data over the solid. Their average value was 32.64 kcal., in good agreement with the present data.

The standard thermodynamic functions for the evaporation processes at 1000°K. as evaluated from these

(10) R. F. Barrow, E. A. N. S. Jeffries, and J. M. Swinstead, *Trans. Faraday Soc.*, 51, 1650 (1955). Also R. F. Barrow, *Proc. Phys. Soc.* (London), 75, 933 (1960).

(11) I. R. Bartky and W. F. Giauque, *J. Am. Chem. Soc.*, 81, 4169 (1959).

data are as follows. The heats of evaporation to monomer and dimer were 24.4 ± 0.2 and 31.8 ± 0.4 kcal. per mole of gaseous species, respectively. The standard entropies of evaporation calculated from the heats and partial pressures were 22.0 ± 0.3 and 25.7 ± 0.6 cal. per degree per mole of gaseous species for the monomer and dimer. These entropies of evaporation are within a few units of the comparable quantities for the alkali halides.[12] The heats of evaporation, however, are substantially smaller than those for the alkali halides and result in the markedly greater vapor pressures of thallous chloride. The larger partial pressure of monomer than dimer is reflected in its smaller heat of evaporation since the entropies are approximately equal. The relative importance of the minor species (dimer) is seen to increase as the temperature increases in accord with "Brewer's rule."[13]

The standard thermodynamic functions for the dissociation of the dimer, *i.e.*

$$Tl_2Cl_2(g) = 2TlCl(g)$$

at 1000°K. are $\Delta H^\circ_{1000} = 17.0 \pm 0.8$ kcal. and ΔS°_{1000}, 18.3 ± 1.2 e.u., also $P_D/P_M = 0.15$. Brewer and Brackett have collected similar information for the alkali halides. For the heavier alkali chlorides the heat of dissociation lies in the range from 39 to 45 kcal., the entropies are all about 28 e.u., and the ratio of dimer to monomer ranges from 0.2 to 0.4. Although the heat of dissociation of Tl_2Cl_2 is more than 20 kcal. less favorable (for dimer) than those of the heavier alkali chlorides, the entropy is ten units more favorable; and since the vapor pressure is larger, the resultant P_D/P_M is about the same.

The absolute entropy of the dimer is equal to that of two monomers minus its dissociation entropy. At 1000°K. the absolute entropy of the gaseous monomer[9] is 71.85 e.u.; thus, the absolute entropy of the dimer is 125.2 e.u. The translational entropy of the dimer was calculated to be 49.9, and the rotational 32.2 e.u. (on the assumption of a square-planar molecule 2.5 Å. on a side—by analogy with the alkali halides). Thus, the vibrational entropy is 43 e.u. at 1000°K.

Berkowitz[14] has calculated the vibration frequencies expected for the alkali halide dimers on an ionic model. For the heavier alkali chlorides one can roughly summarize the frequencies he obtained: four frequencies with values about two-thirds that of monomer, and two about one-third that of monomer. Using this approximation, one calculates the vibrational part of the entropy of Tl_2Cl_2 at 1000°K. to be 30 e.u., about 13 e.u. smaller than the "experimental" value deduced above.

Since the "experimental" vibration entropy is so much larger than that expected by extrapolation from the alkali halide values, it may be that the structure of Tl_2Cl_2 differs substantially from those of the alkali halide dimers in the direction of having lower vibration frequencies, or being a "looser" molecule. The smaller heat of dimerization also tends to indicate a less tightly bound molecule.

Acknowledgment. The author is indebted to Mr. W. E. Robbins, who carried out much of the experimental work.

(12) See ref. 4, Table VII, for a comparison.

(13) For a discussion see L. Brewer in "Chemistry and Metallurgy of Miscellaneous Materials," Natl. Nucl. Energy Series, Vol. IV-19B, McGraw-Hill Book Co., Inc., New York, N. Y., 1950, p. 261.

(14) J. Berkowitz, *J. Chem. Phys.*, **32**, 1519 (1960).

Bond Dissociation Energies and Conjugation Effects in Bromopropadiene and 3-Bromopropyne

by J. J. Throssell

Department of Chemistry, Westfield College, Hamstead, London, N.W.3, England
(Received June 14, 1963)

Dissociation energies have been measured for the carbon–bromine bonds in the isomeric molecules 3-bromopropyne and bromopropadiene which yield identical radicals in the unimolecular fission process. The rate constants for the fission processes are $k = 10^{12.15} \exp[-(46{,}800 \pm 2000)/RT]$ and $k = 10^{13} \exp[-(50{,}000 \pm 2000)/RT]$, respectively. An attempt is made to correlate the difference in the dissociation energies with the difference in the degree of through-conjugation between the bromine atom and the π-electron system of the hydrocarbon radical.

Introduction

The strength of a chemical bond in a molecule $R–R_1$ must be interpreted in terms of the structures of the radicals R and R_1, into which the molecule dissociates when the bond is broken, and the structure of the parent molecule. Thus, it follows from the definition of the bond dissociations energy $D(R–R_1)$ that

$$D(R–R_1) = \Delta H_f(R) + \Delta H_f(R_1) - \Delta H_f(RR_1) \quad (1)$$

where $\Delta H_f(X)$ is the heat of formation of the species X.

Consider two pairs of isomeric molecules $R'R_1$, $R''R_1$ and $R'R_2$, $R''R_2$, in which the components of each pair yield the same radicals R* and R_1 or R_2, *i.e.*

$$R'–R_1 \longrightarrow R^* + R_1$$
$$R''–R_1 \longrightarrow R^* + R_1$$

(The structures of the radical R* and the fragments R′ and R″ in the molecule are related in such a way that the structure of R* is a resonance hybrid to which the canonical structures of R′ and R″ make the principal contributions.) Then

$$D(R'–R_1) - D(R''–R_1) = \Delta H_f(R''R_1) - \Delta H_f(R'R_1) \quad (2)$$

It has been shown by Szwarc and Taylor[1] how the difference in the nature of the two bonds may be understood by considering in a qualitative way the various contributions to the electronic energies of the molecules and of the dissociation products. Thus, if $E(R'R_1)$ represents the total electronic energy of the $R'–R_1$ molecule

$$E(R'R_1) = E_{nb}{}^1(R') + E_{nb}(R_1) + \sigma(R'R_1) + \pi(R'R_1) \quad (3)$$

where $E_{nb}{}^1(R')$ = energy of the electrons localized in the fragment R′ of the molecule $R'R_1$ and not involved in the $R'R_1$ bond, the superscript 1 denoting the fact that the fragment R′ is attached to R_1, $\sigma(R'R_1)$ = energy of the σ-electrons, and $\pi(R'R_1)$ = energy of the π-electron, in the $R'R_1$ bond. If $E(R^*)$ and $E(R_1)$ represent the corresponding total electronic energies of the dissociation products, then

$$D(R'–R_1) = E(R^*) + E(R_1) - E(R'R_1) \quad (4)$$

Similar equations to (3) and (4) may be written for the isomer $R''R_1$, and thus, (2) may be expressed in the form

$$D(R'–R_1) - D(R''–R_1) = E(R''R_1) - E(R'R_1) = [E_{nb}{}^1(R'') - E_{nb}{}^1(R')] - [\sigma(R'R_1) - \sigma(R''R_1)] - [\pi(R'R_1) - \pi(R''R_1)] \quad (5)$$

(1) M. Szwarc and J. W. Taylor, *Trans. Faraday Soc.*, **47**, 1293 (1951).

For the second pair of isomers $R'R_2$, $R''R_2$

$$D(R'\text{–}R_2) - D(R''\text{–}R_2) = [E_{nb}^2(R'') - E_{nb}^2(R')] - [\sigma(R'R_2) - \sigma(R''R_2)] - [\pi(R'R_2) - \pi(R''R_2)] \quad (6)$$

Now consider the difference

$$\Delta D = [D(R'\text{–}R_1) - D(R''\text{–}R_1)] - [D(R'\text{–}R_2) - D(R''\text{–}R_2)] \quad (7)$$

If it is assumed that $E_{nb}^1(R') = E_{nb}^2(R')$ and $E_{nb}^1(R'') = E_{nb}^2(R'')$, *i.e.*, that differences in the energies of the electrons isolated on the fragments R′, and on the fragments R″, in the two sets of molecules $R'R_1$, $R'R_2$ and $R''R_1$, $R''R_2$, may be neglected, together with differences in the corresponding σ-electron energies, then (7) becomes simply

$$\Delta D = \pi(R''R_1) - \pi(R'R_1) \quad (8)$$

Now if the structure of R′ is such that $\pi(R'R_1)$ may be neglected, for example, in the case of an R′–halogen bond when the carbon atom to which the halogen is attached is saturated, then $\Delta D = \pi(R''R_1)$, and thus comparison of the dissociation energies of the two pairs of isomers may be related directly to the π-contribution to the bond.

In the present investigation C–Br dissociation energies in 3-bromopropyne $CH{\equiv}C{-}CH_2{-}Br$ and bromopropadiene $CH_2{=}C{=}CH{-}Br$ were measured by a kinetic method. These molecules both give a Br atom and the C_3H_3 radical on dissociation; the structure of the radical formed may be regarded as a resonance hybrid to which the canonical structures $CH{\equiv}C{-}CH_2\cdot$ and $CH_2{=}C{=}\dot{C}H$ make the principal contributions. The results are compared with those obtained by the electron impact method for the corresponding hydrocarbon in an attempt to illustrate the contribution of through-conjugation between the π-electron system of the radical and the vacant $p\pi$–$d\pi$ hybrid orbitals[2] of the Br atom.

Experimental

The bond dissociation energies were determined by the kinetic method using the toluene carrier technique. The apparatus used was essentially the same as that used in previous investigations, and has been described fully elsewhere.[3]

For completeness sake, and to give a check on the reliability of the experimental procedure, the C–Br bond dissociation energy in allyl bromide was determined. The pyrolysis of this compound has been investigated previously,[3] and the results obtained in the present investigation agree well with the earlier ones.

The sample of allyl bromide used was a commercial sample obtained from Eastman Kodak Co. and purified by distillation on a small column. The sample of 3-bromopropyne was obtained from General Aniline and Film Corp. and was purified by distillation. The sample of bromopropadiene was prepared by the isomerization of 3-bromopropyne, by refluxing over cuprous bromide.[4]

Results

The pyrolysis of bromopropadiene was investigated between 513 and 586°. In a typical experiment at 537° a total pressure of 10.16 mm. was used with a bromide partial pressure of 0.023 mm. and a contact time of 0.3 sec. The reaction was established as kinetically first order since it was observed that alteration of the partial pressure of the compound had no effect on the rate constant. The rate constant was found to be given by the expression $k = 10^{13} \exp(-50{,}000 \pm 2000)/RT$.

The pyrolysis of 3-bromopropyne was investigated between 469.5 and 564°. Again the reaction was found to be first order and the rate constant to be given by $k = 10^{12.15} \exp(-46{,}800 \pm 2000)/RT$.

The pyrolysis of allyl bromide was studied between 525 and 578°. The rate constant is given by the expression $k = 10^{12.6} \exp(-47{,}000 \pm 2000)/RT$ which may be compared with the value obtained by Szwarc, Ghosh, and Sehon, $k = 10^{12.7} \exp(-47{,}500 \pm 2000)/RT$.

In all these pyrolyses the extent of the decomposition was determined by analysis of the HBr formed, assuming in the usual way that the only reaction producing HBr is

$$Br + C_6H_5CH_3 \longrightarrow HBr + C_6H_5CH_2$$

The fate of the C_3H_3 radical was not investigated but it appeared from the negligible quantities of noncondensible gases formed during the reaction that no "cracking" of this radical occurred. (Reactions of the C_3H_3 radical are currently under investigation in this laboratory.)

Discussion

The C–Br bond dissociation energy in 3-bromopropyne has previously been reported by Farmer

(2) J. R. Hoyland and L. Goodman, *J. Phys. Chem.*, **64**, 1816 (1960).

(3) M. Szwarc, B. N. Ghosh, and A. H. Sehon, *J. Chem. Phys.*, **18**, 1142 (1950).

(4) T. L. Jacobs and W. F. Brill, *J. Am. Chem. Soc.*, **75**, 1315 (1953).

and Lossing,[5] who found a value of 57.9k cal. mole^{-1} by the electron impact method, which may be compared with the present value of 46.8 kcal. Collin and Lossing[6] have also reported the appearance potentials of the $C_3H_3^+$ ion from $CH_2{=}C{=}CH_2$ and from $CH{\equiv}C{-}CH_3$ as 12.00 ± 0.05 and 12.02 ± 0.03 e.v., respectively, which correspond to values $D(CH_2{=}C{=}CH{-}H)$ = 81.2 ± 1.1 kcal. and $D(CH{\equiv}C{-}CH_2{-}H)$ = 82.8 ± 0.7 kcal. Taken together with the known heats of formation[7] of the hydrocarbons, these give a mean value of 75 kcal. mole^{-1} for the heat of formation of the the $C_3H_3\cdot$ radical.

Unfortunately, no value is available for the heat of formation of 3-bromopropyne from which an independent estimate of the C–Br dissociation energy may be obtained. In Table I values of bond dissociation energies in the propynes with groups substituted in the 3-position are compared with those in the corresponding propenes. In both series of compounds the bond which is broken links a group X with a saturated carbon atom. In two cases $D(C_3H_5{-}X)$ is less than $D(C_3H_3{-}X)$ by about 6 kcal., whereas the difference in the case where X = Br is about 10 kcal. if the electron impact value is accepted. On the other hand, the kinetic result appears to be too low since it shows that $D(C_3H_5{-}X) \sim D(C_3H_3{-}X)$. It is interesting here to compare these values with those predicted by the empirical equations of Errede.[8] Taking the quoted ϵ values the $C_3H_3{-}X$ dissociation energies are predicted to be 88, 72, 57.4, and 45.4 kcal. mole^{-1} for X = H, CH_3, Br, I, respectively. It appears probable that the ϵ value for the $CH{\equiv}C{-}CH_2$ group was calculated from the available data for 3-bromo- and 3-iodopropyne. If the electron-impact dissociation energies for $C_3H_3{-}H$ and $C_3H_3{-}CH_3$ are taken as correct then a new value ϵ = 0.88 may be calculated for the propynyl group which gives $D(C_3H_3{-}Br)$ = 53.5 kcal. and $D(C_3H_3{-}I)$ = 42.5 kcal., which are to be compared with the values for $D(C_3H_5{-}Br)$ = 47.5 kcal. obtained experimentally and 46.7 kcal. obtained from the bond additivity rules, and for $D(C_3H_5{-}I)$ = 35–37 kcal. obtained experimentally and 33.6 kcal. obtained from the bond additivity rules. In the case of the bromo compounds the difference is again about 6 kcal., while for the iodo compound the difference may be between 5 and 9 kcal. It is not possible at present to say which value for $D(C_3H_3{-}Br)$ is the more correct, and while these considerations are in no way conclusive about the actual magnitude of this quantity they do indicate that the electron impact value may be too high while the kinetic value is too low.

It does, however, appear reasonable that $D(CH_2{=}C{=}CH{-}Br)$ should be greater than $D(CH{=}C{-}CH_2{-}Br)$, (a) because of the use of the carbon sp^2 orbital as compared with sp^3, and (b) because of the degree of π-bonding between the π-electron system of the hydrocarbon fragment and the vacant p_π–d_π orbitals of the Br atom.

Using eq. 5 a mean value for the quantity $\pi(CH_2{=}C{=}CH{-}Br)$ may be calculated as −4.8 kcal. mole^{-1} using the value for $D(CH{=}C{-}CH_2{-}Br)$ obtained in the present investigation.

Because of the uncertainties in the experimental values for the C–Br dissociation energies, it cannot be said at this stage that this is due mainly to the through-conjugation effect, but it does illustrate how bond dissociation energy data may be used in the analysis of such an effect in certain cases.

Table I

3-Substd. propyne	$D(C_3H_3{-}X)$	Ref.	3-Substd. propene	$D(C_3H_5{-}X)$	Ref.
C_3H_3Br	(57.9)	5	$C_3H_5{-}Br$	(47.5)	3[a]
	(46.8)	[a]		(46.7)	[b]
$C_3H_3{-}H$	82.8	6	$C_3H_5{-}H$	77.0	6
$C_3H_3{-}CH_3$	67.5	6	$C_3H_5{-}CH_3$	61.5	[c]
$C_3H_3{-}I$	46.0	5	$C_3H_5{-}I$	(35–37)	[c]
				(33.6)	[b]

[a] Present investigation. [b] Calculated by means of the bond additivity rules of Benson, *et al.*, *J. Chem. Phys.*, **29**, 548 (1956); **36**, 3464 (1962). [c] A. H. Sehon and M. Szwarc, *Proc. Roy. Soc.* (London), **A202**, 263 (1950); M. Szwarc, *Chem. Rev.*, **47**, 75 (1950).

Acknowledgment. This work was carried out under the direction of Prof. M. Szwarc in the State University College of Forestry, Syracuse, N. Y.; the author wishes to acknowledge Prof. Szwarc's encouragement and to thank him for suggesting this problem. Thanks are also due to the National Science Foundation for a grant.

(5) J. B. Farmer and F. P. Lossing, *Can. J. Chem.*, **33**, 861 (1955).

(6) J. Collin and F. P. Lossing, *J. Am. Chem. Soc.*, **79**, 5848 (1957).

(7) F. D. Rossini, *et al.*, "Selected Values of Physical and Thermodynamic Properties of Hydrocarbons and Related Compounds," American Petroleum Institute, Project 44, 1953.

(8) L. A. Errede, *J. Phys. Chem.*, **64**, 1031 (1960).

A Carbon Dioxide Formation Cell[1]

by Lowell A. King and F. R. Duke

Contribution No. 1826 from the Institute for Atomic Research and Department of Chemistry, Iowa State University, Ames, Iowa *(Received July 29, 1963)*

An electrochemical cell of the type: C; Na_2WO_4, WO_3; O_2(Pt) was studied. Cell reactions were: $C + 2WO_4^{2-} \rightarrow CO_2 + 2WO_3 + 4e$; and $O_2 + 2WO_3 + 4e \rightarrow 2WO_4^{2-}$, unless secondary reactions occurred. Thermodynamic data of a fundamental nature were not obtained from the cell, because the carbon electrode behaved irreversibly. However, the cell appears to have interesting possibilities as a fuel cell.

An electrochemical cell in which the net reaction occurring represented only the consumption of oxygen and carbon and the production of carbon dioxide would have significance in two areas. First, such a device would have fundamental importance in fuel cell research. Secondly, such a cell would provide the possibility of direct determination of the thermodynamics of formation of carbon dioxide. In a molten, oxyanionic electrolyte, electrode reactions may be written generally as

$$O_2 + 4e^- \longrightarrow 2[O^{2-}] \qquad \text{cathode reaction}$$

$$C + 2[O^{2-}] \longrightarrow CO_2 + 4e^- \qquad \text{anode reaction}$$

$$C + O_2 \longrightarrow CO_2 \qquad \text{net cell reaction}$$

where $[O^{2-}]$ represents some form of solvated oxide ion.

In previous studies, it has been common to use an oxide in an appropriate melt to furnish the oxide ion for the cell reaction.[2] However, the oxide ion is potentially available from any oxyanion for which the corresponding oxide exists. For example, the sulfate–sulfur trioxide system, the borate–boric oxide system, or many others of similar nature might be used. Here, the known potentiometric inactivity of carbon caused us to choose a system which is quite basic; that is, a system in which the oxide ion is quite available. At the same time it was necessary to choose a system less basic than carbonate to prevent reaction of any carbon dioxide formed at the electrode with the melt. These considerations led to the choice of Na_2WO_4–WO_3 melts.[3]

Experimental

Baker Analyzed $Na_2WO_4 \cdot 2H_2O$ was oven-dried to the anhydrous salt. U.S.P. grade oxygen was passed through a $Mg(ClO_4)_2$-charged drying tower. These materials and North Metal and Chemical Co. WO_3 were used without further purification. A gas train was set up for purification of CO, CO_2, Ar, and mixtures of these gases. Each gas was passed over $Mg(ClO_4)_2$ and hot copper powder to remove water and oxygen. Tubes of hot CuO powder and of Ascarite and $Mg(ClO_4)_2$ were used to prepare CO-free CO_2 and CO_2-free CO. On occasion, exceptionally pure argon was desired. In such instances, the tube containing copper powder was replaced by a tube filled with tantalum chips and heated to 800°.

Tube furnaces were used to heat the electrochemical cells. Any given cell temperature could be held to a one-degree variation once thermal equilibrium was reached. Bristol and Honeywell proportional controllers were used for furnace regulation. In all experiments, fused salt containers were of relatively large cross section and contained shallow melts; convection was relied upon to provide uniform temperature throughout all regions of the melt.

Temperature within the electrochemical cell was measured by a Leeds and Northrup Model 8662 thermocouple potentiometer. Chromel–alumel thermocouples were used.

Cells were made of Vycor and fused silica. They

(1) Work was performed in the Ames Laboratory of the U. S. Atomic Energy Commission.

(2) G. J. Young and R. B. Rozelle, *J. Chem. Educ.*, **36**, 68 (1959).

(3) L. A. King and F. R. Duke, U.S.A.E.C. Rept. IS-667 (1963).

consisted merely of a large test tube (38–54 mm. i.d.) suspended in a furnace and containing the salt under study. Immersed in the melt were two electrodes. They were physically isolated from one another by placing one of them within a second, smaller, test tube which had a very small hole in the bottom through which electrical contact was made.

National Carbon Co. spectrographic grade 0.3-cm. diameter graphite rods and 0.14-cm. diameter platinum wires were used as electrodes. Each electrode was sealed in a small fused silica tube. Lateral holes, out through which bubbled the electrode sweep gases, were provided below the melt level.

For experiments in which current was passed through the cell, reference electrodes were employed. A graphite reference electrode was used when the graphite working electrode was under study; a platinum reference electrode was used when the platinum working electrode was under study. Each reference electrode was located immediately adjacent to its corresponding working electrode.

Use of platinized platinum foil instead of shiny platinum wire as the oxygen electrode did not appear to be advantageous. Neither did prior "soaking" of either the platinum or the graphite electrode in the melt under investigation affect experimental results.

Cell voltages were measured by connecting, in series, the cell, a potentiometer, and an electrometer. The potentiometer supplied a potential of equal magnitude and opposite polarity to the cell e.m.f. at the electrometer null point. (Keithley Instruments, Inc., Models 600A and 603 were used. For the purposes of this research, the two electrometers were identical in operation and characteristics and no distinction will be made between them.) According to the manufacturer's specifications, electrometer input impedance was greater than 10^{14} ohms. It was, therefore, assumed that any electrode polarization caused by current drain through the electrometer would be completely negligible.

For those experiments in which electrode overpotential was studied as it depended on cell current, the electrometer and potentiometer were placed in series with a reference electrode and the electrode under study. The potentiometer was set to the zero cell current null point. As cell current increased from zero, the voltage indicated by the electrometer was identical with the electrode overpotential.

A 6-v. storage battery supplied polarizing currents. The battery was connected in series with a multirange ammeter, a variable resistor, and the Pt, O_2 and C, CO_2 electrodes. A Moseley x–y recorder (with internal time base) was used to record the rates of growth and decay of overpotential. The x-axis signal was provided by the electrometer output terminals. A dual trace Tektronix oscilloscope and Beattie–Coleman oscilloscope camera were used to record overpotential changes which occurred immediately after cell current was switched on or off. As before, an internal time base and the electrometer output provided signals.

Results and Discussion

The calculated standard potential of the carbon dioxide formation cell is 1.03 v., practically invariant with temperature.[4] The experimental potential is very low, below 900°K., where the cell begins to operate and over a small temperature interval reaches a value about 20% below the calculated value. Therefore, the studies were confined to the range of temperature between 950 and 1300°K.

In order to determine the electrode reaction, dry argon was passed over the carbon anode. The effluent gases were analyzed for CO_2 and CO, and at the same time the number of equivalents of oxidation taking place were compared with the equivalents of charge passed. In each case the electrochemical equivalents agree within 5% with the chemical equivalents. The ratio of CO_2 to CO was always larger than that calculated from calorimetric thermodynamic data as indicated in Table I.

Table I: CO_2/CO Ratios from Operating Cell

T, °K.	CO_2/CO, calcd.[a]	CO_2/CO, found	Current density, ma. cm.$^{-2}$
1027	0.25	29.3	3
1139	0.05	11.9	4

[a] Standard thermodynamic values (ref. 4) were used to make the calculations assuming $P_{CO} + P_{CO_2} = 1$ atm. The calculated ratio decreases with decreasing pressure.

It is evident from Table I that equilibrium pressures of CO are not obtained and that the cell preferentially forms CO_2. This lack of equilibrium between CO and CO_2 points to the probable lack of electrochemical equilibrium at the carbon electrode.

The variation of the potential with temperature is much larger than one would expect if CO_2 were formed, but smaller than the expectation if the equilibrium amounts of CO and CO_2 were present. The data are well represented by the linear equation E (v.) = 0.44

(4) For thermodynamic functions required to calculate voltages, see G. N. Lewis and M. Randall, "Thermodynamics," 2nd Ed., McGraw-Hill Book Co., Inc., New York, N. Y., 1961, pp. 680, 682.

$+ 4.0 \times 10^{-4}T$ (°K.). Thus, the lack of equilibrium is further confirmed.

Variation in potential with composition of the melt follows the linear equation, E (v.) $= 0.89 - 0.004C$, where C is per cent WO_3 by weight in the mixture. Under reversible conditions, there should be no dependence of potential on composition. The direction of the change is what would be expected if the oxygen electrode responded to the oxide ion activity in the melt to a greater extent than did the carbon electrode.[5] It is also possible that the electrode process at the anode is secondary, the carbon reducing the tungstate melt[6,7] to deposit a thin layer of tungsten bronze on the surface of the electrode; the tungsten bronze could possess a free energy characteristic of the melt, not in equilibrium with the carbon. In order to determine more about the electrode processes, polarization studies were done.

Electrode Overpotential. If the electrochemically active ionic species is not carrying an appreciable fraction of the cell current, and if the active species is diffusing toward the electrode under study, concentration overpotential of an electrode obeys the equation[8]

$$\eta = \frac{RT}{nF} \ln\left(1 - \frac{I}{I_l}\right)$$

where η is concentration overpotential; I is cell current; I_l is a constant, the "limiting" cell current; and R, T, n, and F have their usual electrochemical significance. If the active species is diffusing away from the electrode, the logarithmic term becomes ln $(1 + I/I_l)$. Ohmic overpotential was measured by high speed photography of an oscilloscope screen. The trace was photographed while cell current was on, then again several microseconds to several milliseconds after current was switched off. Ohmic overpotentials were small and were neglected.

Both platinum and graphite electrodes, immersed in tungstate melts, were anodically and cathodically polarized at temperatures from 950 to 1225°K. In all instances, the equations of concentration overpotential were obeyed. The design of the electrodes precluded knowing current densities; however, the assumption was made that current density was directly proportional to cell current. (The platinum and graphite electrode diameters were 0.14 cm. and 0.3 cm., respectively. They were immersed in the salt to a depth of about 2.5 cm.)

Typical anodic and cathodic polarization curves for a Pt, O_2 electrode are shown in Fig. 1. The melt was 85 wt. % Na_2WO_4, 15 wt. % WO_3. Both curves, and

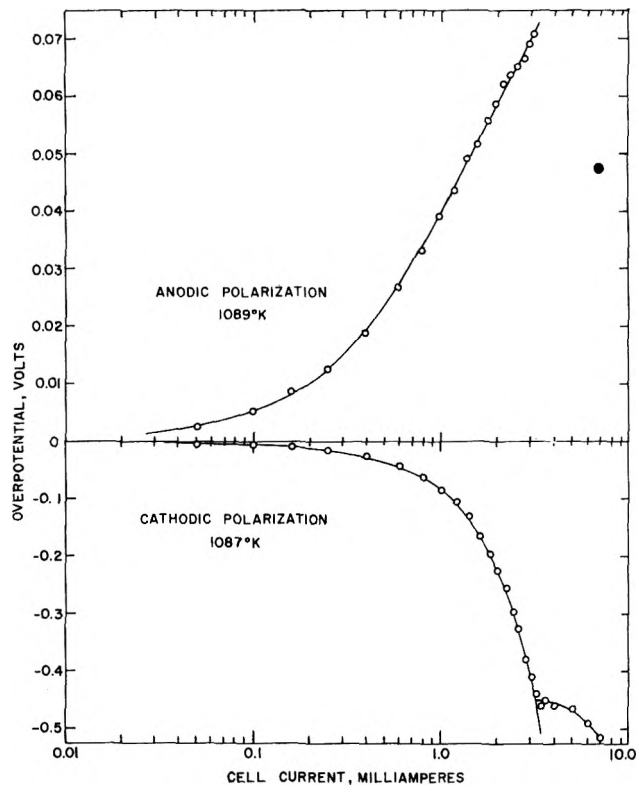

Figure 1. Polarization of platinum, oxygen electrode.

their relative magnitudes, are of the form predicted by the equations for concentration overpotential. They apparently correspond to an ionic species moving toward a platinum cathode and away from a platinum anode.

The data were analyzed by converting the overpotential equations to the form

$$\exp(nF\eta/RT) = 1 \pm I/I_l$$

and constructing graphs of the exponential function *vs.* cell current. Any given set of data was assigned the values $n = 1, 2, 3, 4$. That value of n for which a straight line was obtained was assumed to be the number of electrons transferred in the rate-determining process. The number of electrons transferred was clearly one for the cathodic process. The anodic polarization curves were less sensitive to the value of n, but unity was strongly indicated.

(5) F. R. Duke and J. L. Copeland, U.S.A.E.C. Rept. IS-665 (1963).

(6) Iu. K. Delimarskii and B. F. Markov, "Electrochemistry of Fused Salts," The Sigma Press Publishers, Washington, D. C., 1961, pp. 166, 167.

(7) For the thermodynamic functions necessary to show this, see ref. 5 and "Handbook of Chemistry and Physics," 42nd Ed., Chemical Rubber Publishing Co., Cleveland, Ohio, 1960–1961, p. 1848.

(8) See, for example, S. Glasstone, "An Introduction to Electrochemistry," D. Van Nostrand Co., Inc., New York, N. Y., 1942, pp. 438–458.

It is of interest to compare the present results for platinum overpotential with the work of others. The only cathodic study amenable to quantitative study is that of Agar and Bowden.[9] They attributed their overpotential data (in molten NaOH) to concentration polarization. Flood and Förland[10] and Janz and Colom,[11] studying sulfate and carbonate melts, respectively, explained their anodic polarization data in terms of activation overpotential, assuming n to be 2 and the symmetry coefficient to be 0.5. It should be noted that at sufficiently high currents, the equation for anodic concentration overpotential assumes the same form as the Tafel equation for activation overpotential.

Typical anodic and cathodic polarization curves for a C(gr), CO_2 electrode are shown in Fig. 2. The melt was 85 wt. % Na_2WO_4, 15 wt. % WO_3. The data were analyzed in the same manner as were the Pt, O_2 data. Again polarization appeared to be caused by concentration gradients; however, the rather peculiar observation was made that outward diffusing species seemed to be responsible for both anodic and cathodic polarization. Some of the cathodic curves displayed breaks at about 5 ma. cell current. Tungsten bronze crystals formed at higher currents. Anodic curves were smooth to at least 310 ma. and did not appear to follow the Tafel equation. One electron was transferred in the anodic and cathodic rate-determining steps.

The graphite electrode data were marred by several factors. Overpotentials were not highly reproducible, either from run to run, or from hour to hour in the same run. At any given cell current, graphite overpotentials were quite slow in reaching stable values. The rate of attainment of stability was not strongly temperature dependent; however, short term fluctuations became serious above about 1175°K. Voltages were recorded 3 min. after setting each new current value; the time interval after which the new current value had reached about 90% of its ultimate.

The anodic limiting current temperature coefficient, $d \ln I_l/dT$, was 0.010 deg.$^{-1}$.

The rate of decay of anodic overpotential of graphite was followed with an x–y recorder. Rates were measured at various temperatures and cell currents, and found to be neither linear nor logarithmic with respect to time.

Published information on graphite anodic polarization in oxyanionic melts is extremely limited. With the exception of one study with the melt KCl–NaCl–Na_2SO_4,[12] all investigations have been made with cryolite–alumina melts.[13-19] In such melts the overpotential–current relationship is complex and apparently consists of three distinct regions as current density is increased from zero to 0.3 amp. cm.$^{-2}$. At low currents (0.1 amp. cm.$^{-2}$) the results generally have been interpreted as arising from the formation of surface oxides of graphite. Once the surface oxides are formed, bond rearrangements occur and eventually CO_2 and CO are desorbed. The slowness of bond reformation and gas evolution are proposed to be the cause of anodic overpotential. A similar mechanism was involved for KCl–NaCl–Na_2SO_4 results.[12]

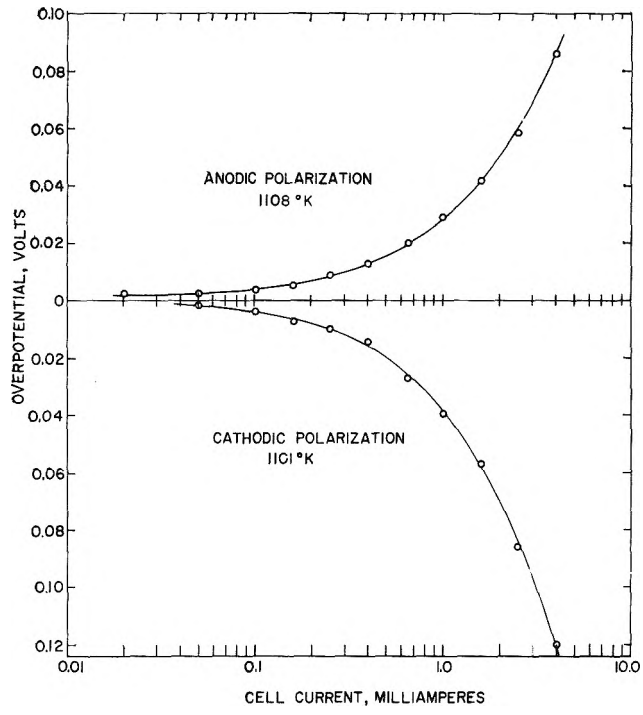

Figure 2. Polarization of graphite, carbon dioxide electrode.

(9) J. N. Agar and F. P. Bowden, *Proc. Roy. Soc.* (London), **A169**, 220 (1939).

(10) H. Flood and T. Förland, *Discussions Faraday Soc.*, **1**, 302 (1947).

(11) G. J. Janz and F. Colom, U. S. Dept. Comm., Office Tech. Serv., PB Rept. 148, 1959, p. 566.

(12) S. I. Rempel, *Dokl. Akad. Nauk SSSR*, **117**, 648 (1957).

(13) L. N. Antipin and A. N. Khudyakov, *ibid.*, **100**, 93 (1955).

(14) L. N. Antipin and A. N. Khudyakov, *Zh. Prikl. Khim.*, **29**, 908 (1956).

(15) L. N. Antipin and N. K. Dudyrev, *Zh. Fiz. Khim.*, **31**, 2032 (1957).

(16) V. P. Mashovets and A. A. Revazyan, *J. Appl. Chem. USSR*, (English Transl.), **30**, 1069 (1957).

(17) S. Karpachev, S. Rempel, and E. Iordan, *Zh. Fiz. Khim.*, **23**, 422 (1949).

(18) S. I. Rempel and L. P. Khodak, *Dokl. Akad. Nauk SSSR*, **75**, 833 (1950).

(19) S. I. Rempel and L. P. Khodak, *Zh. Prikl. Khim.*, **26**, 931 (1953).

It does not necessarily follow that graphite anodes would behave in tungstate melts in the same fashion as they do in alumina systems; however, activation overpotential cannot be ruled out as a possible explanation of the results of the present research. Further study of graphite anodic polarization in a variety of oxyanionic melts (including tungstate melts) is warranted.

Micellar Properties and Phase Separation in Dimethyldodecylamine Oxide–Sodium Halide–Water Systems

by K. W. Herrmann

Miami Valley Laboratories, The Procter & Gamble Company, Cincinnati, Ohio *(Received November 12, 1963)*

Micelles formed in 0.2 *M* NaBr at pH 3, where dimethyldodecylamine oxide is protonated and behaves as a cationic surfactant, were found to be large and rod-like in shape. Experimental data are consistent with a micelle molecular weight (MMW) of 680,000 and with rods one surfactant molecule in radius (22 Å.) and 730 Å. long. At pH ≥ 7, where almost all of the amine oxide is in the nonionic form, the micelles are small and probably spherical both in water and in 0.2 *M* sodium halide solution. Light scattering and sedimentation results also indicate that micelles increase in MMW and axial ratio as the pH of 0.2 *M* NaBr solutions approaches 4.9, where there are equimolar concentrations of the cationic and nonionic surfactant species. Separation into two isotropic phases occurs between pH 4.4 and 5.4 near room temperature, but only one isotropic phase exists above 32°. MMW and micellar axial ratio appear to decrease with increased temperature. Increased NaBr concentration increases the pH range over which phase separation occurs. Chloride ion is less effective than bromide in promoting micellar growth. Surfactant crystals are formed with iodide ion below pH 4.9 and possibly higher. The factors leading to phase separation and existing theories on this subject are discussed.

Introduction

Debye and Anacker[1,2] and Trap and Hermans[3] have shown that the MMW of some cationic surfactants are very high (of the order of 10^6) in the presence of certain electrolytes and that these micelles are rod-like in shape. These results indicate that although micelles may be spherical and of low MMW in water, the addition of certain electrolytes will promote further aggregation and greater asymmetry. Cohen, *et al.*,[4-6] have recently reported similar results for another long-chain cationic surfactant in various electrolyte solutions. The effectiveness of electrolyte anions in increasing micellar size was found to increase in the order: $Cl^- < NO_2^- << NO_3^-, ClO_3^-, Br^- < SCN^-$. The effect of varying the cation was small. Dervichian, Joly, and Titchen[7] obtained qualitative evidence for the existence of large surfactant aggregates and plotted viscosity

(1) P. Debye and E. W. Anacker, *J. Phys. Chem.*, **55**, 644 (1951).

(2) E. W. Anacker, *J. Colloid Sci.*, **8**, 402 (1953).

(3) H. J. L. Trap and J. J. Hermans, *Koninkl. Ned. Akad. Wetenschap.*, **583**, 97 (1955).

(4) I. Cohen and T. Vassiliades, *J. Phys. Chem.*, **65**, 1774 (1961).

(5) I. Cohen and T. Vassiliades, *ibid.*, **65**, 1781 (1961).

(6) I. Cohen, P. Economou, and A. Libacky, *ibid.*, **66**, 76 (1962).

contours in the isotropic solution region of the phase diagrams of potassium laurate–electrolyte–water systems. Corkill and Herrmann[8] have also obtained evidence for very high degrees of aggregation in concentrated surfactant solutions free of electrolytes. Balmbra, *et al.*,[9] have shown that the micellar size and asymmetry of a nonionic surfactant increase as the lower consolute temperature is approached. In summary, all of the above observations indicate that aggregation increases markedly as phase boundaries are approached in both binary (surfactant–water) and ternary (surfactant–electrolyte–water) systems.

Evidence relating increased aggregation with phase separation for a novel system wherein the ionic character of the surfactant varies with pH is presented herein. The surfactant studied is dimethyldodecylamine oxide: it is essentially nonionic (DDAO) at pH ≥ 7, cationic ($DDHA^+$) at pH ≤ 3, and a nonionic–cationic mixture between pH 3 and 7. These two species have been described earlier[10,11] and are related by the equilibrium

$$C_{12}H_{25}N(CH_3)_2OH^+ \rightleftharpoons C_{12}H_{25}N(CH_3)_2O + H^+$$

dimethyldodecyl-N-hydroxyammonium ion ($DDHA^+$) — dimethyldodecylamine oxide (DDAO)

$$K_A = \frac{[H][DDAO]}{[DDHA^+]} = 10^{-4.9}$$

Light scattering results, supplemented by ultracentrifuge data and phase diagrams, are reported. These data were obtained as a function of pH (change in the ionic character of surfactant), temperature, electrolyte identity, and concentration. The concepts of critical opalescence phenomena, coacervation, and phase separation in general have been used to interpret the data in terms of structural variations in solution.

Experimental

Materials. The dimethyldodecylamine oxide used in this investigation was that described previously.[10] Its purity is >99.5%. The electrolytes employed (NaCl, NaBr, and NaI) were of C.P. grade.

Preparation of Solutions. Stock solutions of surfactant were prepared on a weight/volume basis and diluted volumetrically to the desired concentrations. Doubly distilled water was used in preparing all solutions. Adjustment of pH was made using HBr when NaBr solutions were employed as solvent, and with HCl when NaCl solutions or water were used. The pH's given both in the text and in the figures were measured at 27°.

Light Scattering Measurements. Light scattering measurements were made with a commercial apparatus (Phoenix Precision Instrument Co.) similar to that described by Brice, *et al.*[12] The narrow slits provided with the instrument were employed with a cylindrical cell (catalog no. C101) which was painted black except for the window. Calibration of the instrument, temperature control, and the method of solution clarification were identical with those described previously.[10] The blue line of mercury (λ 4358 Å.) was used throughout.

Refractive Index Measurement. A Brice–Phoenix differential refractometer was used to determine the refractive index increments (dn/dc) required for MMW calculation. The instrument was calibrated with sucrose solutions using light of λ 4358 Å. Temperature was controlled by circulating water of a known temperature through the jacket surrounding the cell.

Ultracentrifuge Measurements. Sedimentation constants were determined by the sedimentation velocity method using a Spinco Model E analytical ultracentrifuge equipped with schlieren optics. Temperature was maintained at 29 ± 0.1° with a rotor temperature indicator control unit. Speeds of about 60,000 r.p.m. were employed.

Phase Diagrams. Phase boundaries were determined by sealing solutions of known composition in glass tubes, placing them in a controlled temperature water bath, and observing the temperature of phase separation on cooling. Either high turbidity, when two isotropic phases are formed, or surfactant crystals can be observed at characteristic temperatures. The reverse process of heating to determine the temperature of formation of a single phase was also used, but the results obtained on cooling were more reproducible and are believed to be more accurate. Phase boundaries at fixed pH and temperature were determined by adding concentrated NaBr solution (4 *M*) from a buret to the solution until turbidity (phase separation) first appeared and persisted indefinitely with stirring. Final concentrations were then calculated from the initial concentrations and the known volumes.

(7) D. G. Dervichian, M. Joly, and R. S. Titchen, Compt. rend. réunion ann. avec comm. thermodynam., Union intern. phys. Changements de phase, 1952, pp. 152–159; *Chem. Abstr.*, **47**, 10,315*i* (1953).

(8) J. M. Corkill and K. W. Herrmann, *J. Phys. Chem.*, **67**, 934 (1963).

(9) R. R. Balmbra, J. S. Clunie, J. M. Corkill, and J. F. Goodman, *Trans. Faraday Soc.*, **58**, 1661 (1962).

(10) K. W. Herrmann, *J. Phys. Chem.*, **66**, 295 (1962).

(11) D. G. Kolp, R. G. Laughlin, F. Krause, and R. E. Zimmerer, *ibid.*, **67**, 51 (1963).

(12) B. A. Brice, M. Halwer, and R. Speiser, *J. Opt. Soc. Am.*, **40**, 768 (1950).

Results

Phase Boundaries. Figures 1 and 2 show the effect of pH, temperature, and NaBr concentration on the phase boundaries of the DDAO–NaBr–H_2O system. Only one DDAO concentration (0.6 g./100 ml.) was examined, but this is in the concentration region of interest and is well above any of the observed critical micelle concentrations. The diagrams are primarily of interpretive value when relating the changes in light scattering properties of the solutions to phase separation.

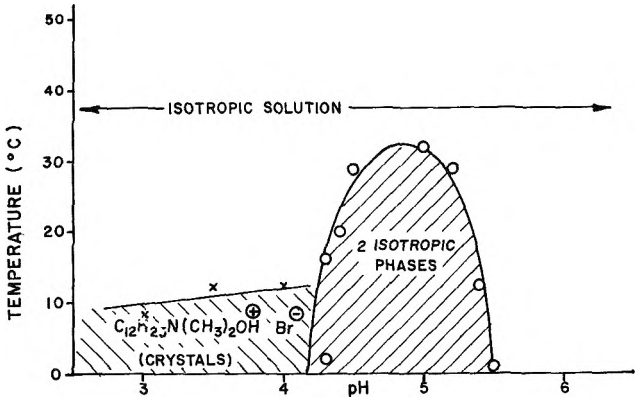

Figure 1. Phase behavior as a function of temperature and pH for 0.6 g. of DDAO in 100 ml. of 0.2 *M* NaBr.

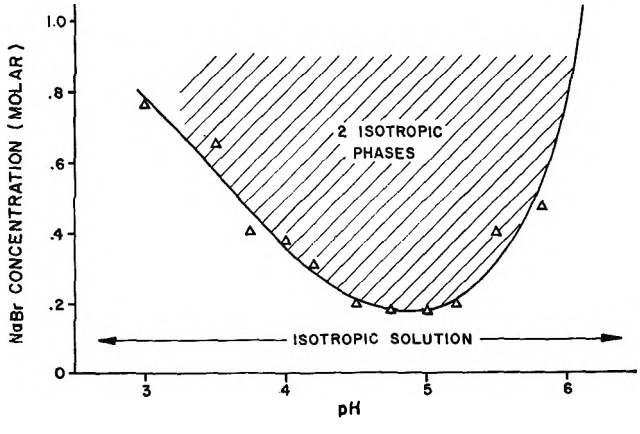

Figure 2. Phase behavior as a function of NaBr concentration and pH for 0.6 g. of DDAO/100 ml. at 27°.

The boundaries in Fig. 1 show that separation into two isotropic phases on cooling is favored at pH's where comparable concentrations of the nonionic and cationic forms are present, the maximum temperature of phase separation occurring about pH 4.9. Surfactant crystals are formed at pH ≤ 4 when the temperature is dropped below about 12°. Figure 2 shows that at room temperature (27°), increased NaBr concentration will induce phase separation over a wider range of pH, and that a minimum NaBr concentration is required for phase separation at about pH 4.9, *i.e.*, the single isotropic solution state is least stable at pH 4.9.

Chemical analyses of the upper and lower phases in a system consisting of 2 g. of DDAO in 100 ml. of 0.2 *M* NaBr at pH 5, 27°, show that the surfactant concentrates in the upper phase and that the NaBr concentration is about equal in both phases.

Micellar Properties in 0.2 *M* NaBr at pH 3

In the present study the critical micelle concentration (c.m.c.), micelle molecular weight (MMW), and micelle shape of the *cationic* form (pH 3) were determined in 0.2 *M* NaBr at 27° and at 50°. Figures 3 and 4 show the experimental data from which the c.m.c.'s and MMW's were determined, respectively. The c.m.c.'s were taken as the concentrations where the linear regions of Fig. 3 intersect. Micelle molecular

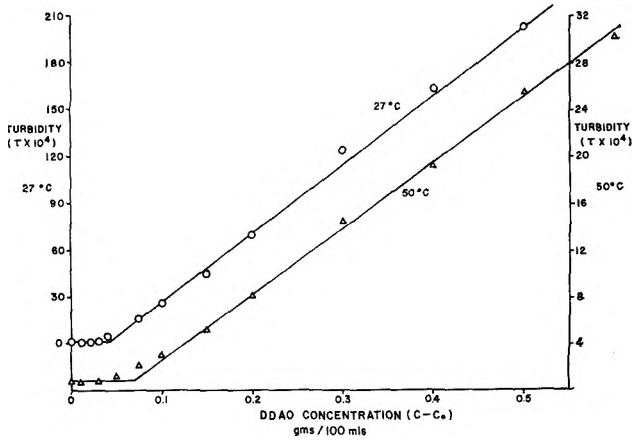

Figure 3. Turbidities for DDAO at pH 3 in 0.2 *M* NaBr solution.

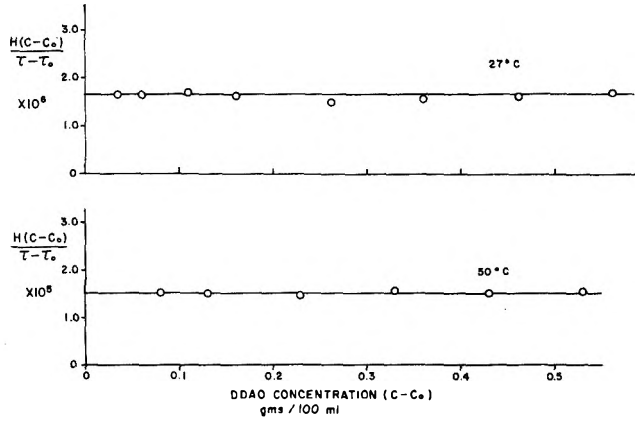

Figure 4. Light scattering results for DDAO at pH 3 in 0.2 *M* NaBr.

weights were calculated from the intercepts in Fig. 4 and the usual relationship

$$\frac{H(c - c_0)}{\tau - \tau_0} = \frac{1}{P_\theta}\left[\frac{1}{M} + 2B(c - c_0) + \cdots\right]$$

where these symbols have their usual meanings. The zero slopes in Fig. 4 indicate that any electrostatic interactions are swamped out in the presence of 0.2 *M* NaBr. No correction was made for the possible preferential concentration of NaBr around the micellar species.[13] Dissymmetry values over the concentration range examined at 50° were small (~1.03) and no corrections P_θ were applied. At 27°, however, an intrinsic dissymmetry of 1.12 was obtained and the MMW was corrected accordingly (P_θ = 0.91), based on a rod-like shape for the micelles. The micellar properties are summarized in Table I, along with data reported previously for the nonionic (pH ≥7) and cationic (pH ≤ 3) forms of the amine oxide in water and 0.2 *M* NaCl.[10]

Table I: Summary of Micellar Properties

Form of surfactant	Added electrolyte, moles/l.	C.m.c.,[a] g./100 ml.	MMW,[a] cor.	Z_{44}
DDHABr (27°)	0.20 *M* NaBr (pH 3)	0.04	680,000	1.12
(50°)	0.20 *M* NaBr (pH 3)	0.07	67,000	1.03
DDHACl (27°)	0.001 *M* HCl (pH 3)	0.19	20,400	1.02
(27°)	0.20 *M* NaCl (pH 3)	0.034	31,100	1.00
DDAO (27°)	None (pH >7)	0.048	17,300	1.00
(27°)	0.20 *M* NaCl (pH >7)	0.034	17,800	1.01

[a] All results expressed in terms of nonionic DDAO formula weight for easy comparison.

Micelle shape at 27° was determined from angular scattering measurements using the method of Debye and Anacker.[1] Experimental intensity data as a function of angle are superimposed on the theoretical plot for rod-shaped aggregates in Fig. 5. The separation of the origins for the horizontal axes is 0.15 and, according to the theory, is equal to $2\pi L/\lambda$ where L is the rod length and λ is the wave length of light employed. L is, thus, computed to be 730 Å. The molecular weight of a rod having this length, a diameter twice the estimated extended length of the cationic surfactant (DDHABr) molecule (diameter about 44 Å.), and using a density of unity, is calculated to be 670,000. The MMW determined from the Hc/τ *vs.* c plots is 680,000. Such good agreement is probably fortuitous but does indicate that a rod-like model for these micelles is the proper one. Similar molecular weight computations using sphere and disk shaped models show poor agreement with the MMW determined from the Hc/τ *vs.* c plots.

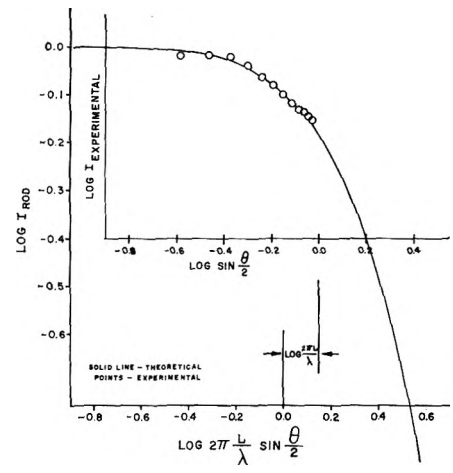

Figure 5. Superposition of experimental data and theoretical curve, assuming rod-like micelles for DDHABr at pH 3, 27°, in 0.2 *M* NaBr.

Although angular scattering data at 50° were not suitable for treatment as above (dissymmetry too small), it can be noted that a MMW of 67,000 is not consistent with a spherical micelle of radius equal to the length of a DDHABr molecule (~22 Å.). Adoption of the rod-like model would require a rod length of about 73 Å. to account for the experimental MMW at 50°. Micelles of these dimensions would not be expected to give significant dissymmetry values and this agrees with experiment.

Variations with pH. The system chosen for studying the effect of pH was 0.6 g. of DDAO in 100 ml. of 0.2 *M* NaBr solution. This surfactant concentration lies well above any expected c.m.c. but is in the concentration range where the light scattering properties were previously examined in detail. The intensity of light scattered from these fixed surfactant–NaBr compositions was determined as a function of pH at 29° and at 50°. Sedimentation constants were also determined as a function of pH at 29°.

Relative intensities scattered at a 90° angle (I_{90}/I_0) are plotted against pH in Fig. 6. Phase separation occurs between pH 4.4 and 5.4 at 29° but does not occur at any pH in the range studied at 50°. The maximum in relative intensity occurs near pH 4.9 at 50°, and it is at this pH where about equal molar concentrations of the nonionic and cationic species are present. At pH 7 and above, the relative intensities are similar to those previously obtained for a like concentration of DDAO in

(13) A. Vrij and J. Th. G. Overbeek, *J. Colloid Sci.*, **17**, 570 (1962).

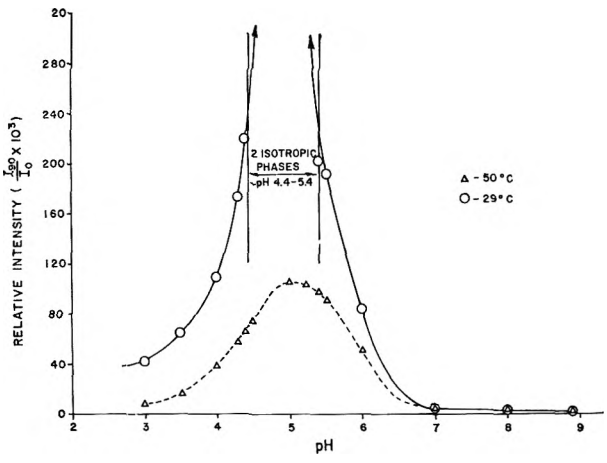

Figure 6. Variation of scattered light intensity with temperature and pH for 0.6 g. of DDAO in 100 ml. of 0.2 *M* NaBr.

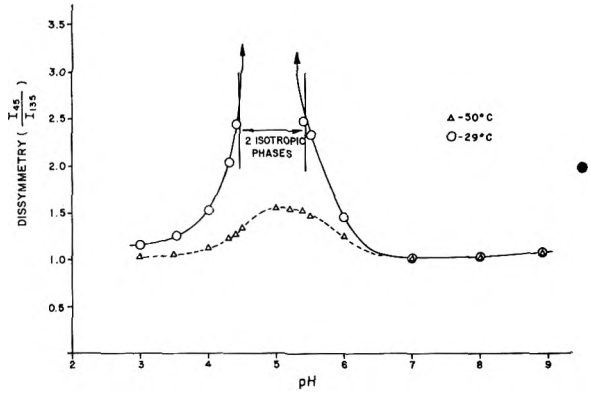

Figure 7. Variation of dissymmetry with temperature and pH for 0.6 g. of DDAO in 100 ml. of 0.2 *M* NaBr.

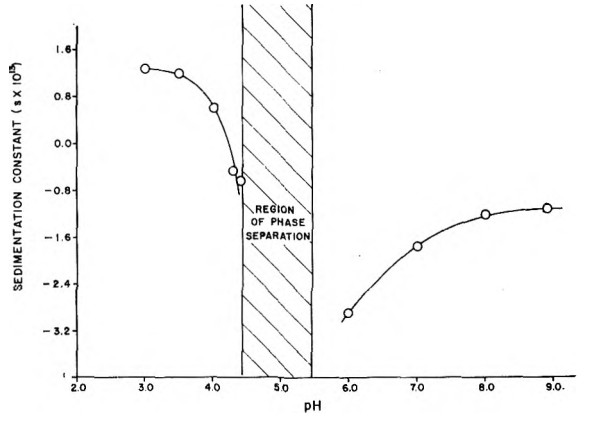

Figure 8. Variation of sedimentation constant (s) with pH for 0.6 g. of DDAO in 100 ml. of 0.2 *M* NaBr (29°).

0.2 *M* NaCl. It is, thus, indicated that the nonionic micellar properties of 0.2 *M* NaBr above pH 7 are comparable to those in 0.2 *M* NaCl (see Table I). Dissymmetries (I_{45}/I_{135}) are plotted against pH in Fig. 7, and it is evident that these also rise toward a maximum near pH 4.9 at both 29° and 50°.

Variation of sedimentation constant (s) with pH at 29° is shown in Fig. 8. Qualitative density (ρ) data show that the partial specific volume ($\bar{v}$) of the surfactant is less than unity at pH ≤ 3 (it concentrates at the bottom) and is greater than unity at pH ≥ 7 (it rises to top of cell). This explains why s goes through zero as the pH is increased from 3 to 9, *i.e.*, $(1 - \bar{v}\rho)$ becomes zero at about pH 4.2. A sharpening of the sedimentation boundary as phase separation conditions are approached was also observed.

Specificity of Electrolyte in Promoting Phase Separation. Data already presented show that phase separation occurs below 32°, in solutions containing 0.6 g. of DDAO per 100 ml., 0.2 *M* NaBr, and near pH 4.9. Phase separation is most sensitive at this pH; and thus the influence of other sodium halides on phase behavior was examined at pH 4.9 and at 0.2 *M* concentration. These results are summarized in Table II. It can be concluded from these data that the halide ions of greater ionic radius (more polarizable) are more effective in inducing phase separation. This agrees with earlier reported observations.

Table II

Electrolyte concentration	*Description of* system at 27°	Relative intensity of *scattered light*, I_{90}/I_0
None	1 isotropic phase	57×10^{-6}
0.2 *M* NaCl	1 isotropic phase	23×10^{-3}
0.2 *M* NaBr	2 isotropic phases	...
0.2 *M* NaI	1 isotropic phase and surfactant crystals	...

Discussion

In the following discussion, the mole ratio of nonionic to cationic surfactant species at a given composition is considered to remain constant over the temperature range examined. This assumption is reasonable, particularly at or below the pH of greatest interest, pH 4.9, since here the number of protons contributed by the water is small compared to that provided by the added acid. Existing data also indicate that dissociation constants of weak acids are not greatly affected by temperature[14] and this is likely to be true for the amine oxide surfactant as well.

(14) H. S. Harned and B. B. Owen, "The Physical Chemistry of Electrolytic Solutions," 3rd Ed., Reinhold Publishing Corp., New York, N. Y., 1958, pp. 661–669, 755.

Micellar Aggregation. Micellar results obtained at pH 3 show that the cationic micelles are large and rod-like in 0.2 *M* NaBr and most likely are small and spherical in water and 0.2 *M* NaCl. Furthermore, the MMW and rod length of these aggregates in 0.2 *M* NaBr decrease with increased temperature. Using the pH 3 results as a base, the increase in scattered intensity and dissymmetry with increasing pH (Fig. 6, 7) can quite reasonably be interpreted as being due to increased aggregation. Both MMW and rod length appear to increase markedly from pH 3 up to the pH of phase separation at 29° (pH ∽4.4), or pH 4.9 at 50°. Between pH 5.4 and 7 at 29° and pH 4.9 and 7 at 50°, the data are consistent with a decreasing MMW and rod length with increased pH. At pH ≥7 the results can be interpreted using the more common spherical model for micelles.

Even though it is tempting to interpret the intensity changes quantitatively in terms of micellar size, there is another phenomenon that must be considered. Critical opalescence theory as described by Debye, *et al.*, for binary systems[15-17] predicts high intensities of scattered light as phase separation conditions are approached. For very large molecules or aggregates such as are contemplated here for a ternary system, the local gradients of the concentration fluctuations might make a sizable contribution to the total intensity of scattered light even when conditions are fairly distant from those required for phase separation. Thus, quantitative interpretations cannot be made since the magnitude of the fluctuation gradient term is not known and no theory is available for these complex systems.

The sedimentation data cannot be interpreted by themselves since the sedimentation constant (s) is a function of molecular weight (M), diffusion coefficient (D), and $(1 - \bar{v}\rho)$ where ρ is the density of the solution and $\bar{v}$ is the partial specific volume of the sedimenting particle. The sign of s can be satisfactorily accounted for by the predictable variation in $(1 - \bar{v}\rho)$, since the change in $\bar{v}$ with pH is qualitatively known to decrease with decreasing pH. Furthermore, the variation of s with pH is consistent with the light scattering results *only* if increased aggregation occurs as phase separation conditions are approached. This can be seen if one considers what happens to s as the pH is decreased from 7 to 5.4. Remembering that

$$s = \frac{MD(1 - \bar{v}\rho)}{RT}$$

and that the absolute magnitude of $(1 - \bar{v}\rho)$ decreases from pH 7 to 5.4, the observed increase in the absolute value of s (Fig. 8) can only be due to an increase in M and/or D. It must be concluded that it is M that increases if these data are to be consistent with the light scattering results. The observation that the schlieren boundary sharpens as phase separation conditions are approached also supports the conclusion that M increases and that D probably decreases.

Factors Influencing Phase Separation. It is interesting to speculate on the factors responsible for separation of the one-phase system into two isotropic phases.

The theories of Verwey and Overbeek[18] and Hamaker[19] concerning the stability of colloidal particles indicate that coagulation or ordering of colloidal particles can occur in systems having large, asymmetric particles. In these systems the attractive London–van der Waals forces can overcome the electrostatic repulsive forces and cause coagulation. Phase separation of the coagulated particles can sometimes occur; an example of this is the separation of an anisotropic phase from solutions of tobacco mosaic virus. In our system, ordering of this type is most likely to occur at pH 4.9 where micellar size and asymmetry appear to be greatest. This is also the pH where phase separation is most readily induced. One can, therefore, correlate increased micellar size and asymmetry and the ordering of these aggregates with separation of the one-phase system into two isotropic liquids.

Onsager,[20] Isihara,[21] Oster,[22] Flory,[23] and Veis[24] have also interpreted phase separation phenomena occurring in solutions containing large asymmetric particles as being due chiefly to particle asymmetry and, where asymmetry is insufficient, to higher-order interactions between the electric double layers of charged colloidal particles. It seems likely that these theories are qualitatively applicable to the surfactant system described here. Nevertheless, it is not known what happens on a molecular scale to induce the small, spherical micelles to grow into large asymmetric aggregates, or why NaBr is so much more effective than NaCl in inducing these changes. Changes in surfactant solvation with temperature and changing ionic character of the surfactant should be important, and the concepts of Frank and Wen[25] and Némethy and

(15) P. Debye, *J. Chem. Phys.* **31**, 680 (1959).

(16) P. Debye, H. Coll, and D. Woermann, *ibid.*, **33**, 1756 (1960).

(17) P. Debye, B. Chu, and D. Woermann, *ibid.*, **36**, 1803 (1962).

(18) E. J. W. Verwey and J. Th. G. Overbeek, "Theory of Stability of Lyophobic Colloids," Elsevier Publishing Co., Inc., New York, N. Y., 1948, pp. 124–126.

(19) H. C. Hamaker, *Rec. Trav. Chim.*, **56**, 727 (1937).

(20) L. Onsager, *Ann. N. Y. Acad. Sci.*, **51**, 627 (1949).

(21) A. Isihara, *J. Chem. Phys.*, **19**, 1142 (1957).

(22) G. Oster, *J. Gen. Physiol.*, **33**, 445 (1950).

(23) P. J. Flory, *Proc. Roy. Soc.* (London), **A234**, 73 (1956).

(24) A. Veis, *J. Phys. Chem.*, **65**, 1798 (1961).

Scheraga[26] regarding the structure of water may be pertinent.

Conclusions

It is concluded that the size and axial ratio of micelles formed from the *cationic* species ($DDHA^+$) increase on the addition of electrolytes (NaX), and in the halide (X) order: $Cl^- << Br^-$. Surfactant crystals form with I^-.

In NaBr solutions at pH ≤ 3, micelles of the cationic species are large and asymmetric; MMW's of the order of 10^6 are obtained and the aggregates can be satisfactorily represented by rod-like particles. The data indicate that an increase in pH from 3 to 4.9 in these NaBr solutions results in increased MMW and axial ratio. Under certain conditions of NaBr concentration, pH, and temperature, sufficient ordering of these rod-like micelles may occur in solution so as to result in separation into two isotropic phases. This occurs most readily at pH 4.9 where equivalent concentrations of the cationic and nonionic amine oxide species are present. Further increase in pH of the surfactant–NaBr solution from 4.9 to 7 results in decreased MMW and axial ratio to the point where the presence of small, spherical micelles satisfies the data. Speculation on the factors influencing phase separation is made and theories on this subject are referred to. It must be concluded, however, that there are enough unknowns in the theories proposed that, for the moment at least, we will have to be satisfied with the qualitative knowledge of the factors affecting phase separation in surfactant systems.

Acknowledgments. The author is indebted to Mr. W. Gagen for making the sedimentation measurements and to Mr. P. Baumgardner, who assisted in obtaining the light scattering data.

(25) H. S. Frank and W. Y. Wen, *Discussions Faraday Soc.*, **24**, 133 (1958).

(26) G. Némethy and H. A. Scheraga, *J. Chem. Phys.*, **36**, 3382 (1962).

Determination of Interdiffusivities of Argon and Metal Vapor Mixtures at Elevated Temperatures

by P. Grieveson and E. T. Turkdogan

Edgar C. Bain Laboratory for Fundamental Research, United States Steel Corporation, Research Center, Monroeville, Pennsylvania *(Received February 10, 1964)*

Interdiffusivities for the metal vapors, iron, cobalt, nickel, and chromium, with argon at 1600° have been measured. The experimental technique is based on the absorption of metal vapor by a thin platinum foil positioned at a known distance from the surface of a metal reservoir of known surface area. The agreement of the results with the calculated values is satisfactory. In the case of manganese, interdiffusivity values were measured at three temperatures and the temperature dependence also agrees with the theory. At 1600°, the values of the interdiffusion coefficients of binary metal vapor–argon mixtures at 1 atm. are within the range 3–4 cm.²/sec. In the Appendix some considerations are given to the effect of convection currents in enclosed spaces on the rate of apparent diffusion of gaseous species.

Introduction

In the study of the kinetics of high temperature reactions, one of the possible rate-controlling reaction processes is the transport of gaseous reactants and products to or from the gas–condensed phase interface. In a study of the effect of reactive atmosphere on the diffusion-controlled rate of vaporization of metals by Turkdogan, Grieveson, and Darken,[1] it was pointed out that some accurate knowledge of diffusion coefficients in gas and gas–metal vapor mixtures was necessary for the interpretation of the experimental data. Although the diffusivities of most gases and gas mixtures can be computed readily from the formulas based on the rigorous kinetic theory of gases, difficulties are encountered in similar calculations for gas–metal vapor mixtures, because of the lack of knowledge of interatomic force constants of metal vapors. Recently, Turkdogan[2] derived empirically interatomic force constants for metal vapors and computed the coefficients of diffusion in gas–metal vapor systems. In order to test the validity of these calculated diffusion coefficients, an experimental method has been developed to measure diffusion coefficients of metal vapor–argon mixtures.

Experimental

The experimental technique is based on the absorption of metal vapor by a thin platinum foil positioned at a known distance from the surface of a metal reservoir of known surface area. The vaporization cell (Fig. 1) consisted of a recrystallized alumina crucible of 15 mm. i.d., wall thickness 2 mm., and 25 mm. high. About 8 g. of pure metal was melted in the crucible in a carefully purified argon atmosphere and the metal was quenched. The alumina crucible was then precision machined to an internal diameter of 17 mm. and to a known height, 2, 4, 6, 8 or 10 mm., above the surface of the metal. The crucible was then placed in a drybox filled with purified argon where the vaporization cell was assembled for an experiment. A close fitting platinum disk 0.05 cm. thick weighing about 2.1 g. was placed on the ledge which had been machined in the crucible. A recrystallized alumina ring, ground to a close fit, was used to keep the platinum sheet in place at the predetermined height above the sample. The vaporization cell was transferred quickly from the drybox to the vertical reaction tube of a molybdenum resistance furnace maintained at the required reaction temperature ±2°. A gas stream of argon, 80 cm.³/min., previously purified by passing over titanium

(1) E. T. Turkdogan, P. Grieveson, and L. S. Darken, *J. Phys. Chem.*, 67, 1647 (1963).

(2) E. T. Turkdogan, Proceedings of Physical Chemistry and Technology of Steelmaking Conference, to be published.

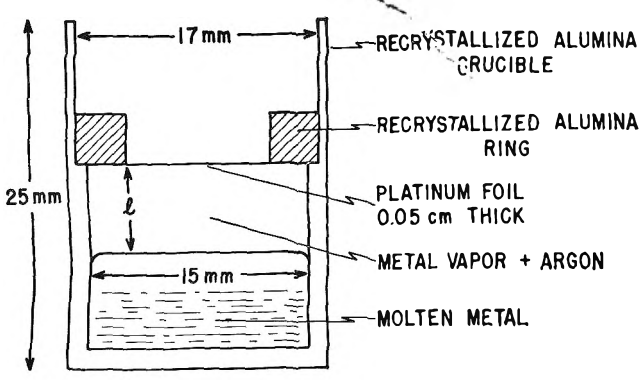

Figure 1. Vaporization cell.

heated to 900°, was continuously passed through the furnace during the experiments. After about 1 hr., the cell was lowered to the hot zone of the furnace. In most experiments the time of diffusion was 24 hr., but in the experiments with chromium and manganese the duration of an experiment varied from 6 min. to 4 hr. such that all the vapor absorbed by the platinum disk was less than 4%. The platinum disks were weighed before and after the experiment, and subsequently analyzed for the diffusing metal. In all cases, the amount of reacting metal absorbed by the platinum disk determined by weight change and chemical analysis agreed within 1.5%. The vapor pressure of platinum is lower than the other metals used in these experiments by a factor of about 10^4–10^5. Therefore, any loss of platinum due to vaporization is considered to be insignificant. The amount of material as determined by chemical analyses was used in all calculations. Special care was taken in the measurement of the distance, l, between the ledge on which the platinum disk rests and the surface of the metal, due allowance being made for the expansion of the crucible and the metal at the experimental temperature.

Results

In these experiments the metal vapor diffuses through the stagnant argon atmosphere only under a concentration gradient, and assuming that a steady-state flux is established soon after diffusion commences, by Fick's first law, the rate of vaporization of metal vapor is given by

$$J = D_{M,Ar} \frac{p^0 - p}{RTl} \qquad (1)$$

where J = the flux of metal vapor, moles of M/cm.^{2} sec.; $D_{M,Ar}$ = the metal vapor–argon interdiffusion coefficient; p^0 = the vapor pressure of metal at the surface of the melt; p = the vapor pressure of metal at the surface of the platinum disk; l = distance between the platinum disk and the surface of the melt; R and T = gas constant and temperature.

In all of these experiments, the amount of diffusing metal vapor absorbed by the platinum foil was below 3.5% by weight. Assuming that the coefficient of diffusion of the absorbed metal in platinum is about 10^{-4} cm.^{2}/sec. at 1600°, for a fixed partial pressure of metal vapor at the surface of the platinum, the concentration gradient of dissolved metal across the foil should diminish in about 40 sec. In order to test the validity of this deduction, back reflection X-ray diffraction patterns were taken from both sides of the platinum foil at the end of some experiments. As seen from the results in Table I, the lattice constant of platinum is the same on both sides, indicating uniform distribution of the metal in solution. All the lattice constants for the alloyed foils are slightly below that for pure platinum, *i.e.*, a_0 = 3.924 Å.

Table I: Lattice Constants of Alloyed Platinum Disks Derived from Back Reflection X-Ray Diffraction Patterns Taken from Both Sides of the Foil

Metal absorbed	Unit cell dimension, Å. Surface on which vapor condenses	Unit cell dimension, Å. Opposite side of foil
None	3.924	3.924
2.0% Ni	3.921	3.921
1.7% Co	3.922	3.921
2.9% Fe	3.920	3.920
2.1% Mn	3.923	3.922

In view of the above evidence, it is reasonable to state that at any instant during a vaporization experiment, the metal dissolved in platinum is evenly distributed across the foil; and hence, from the concentration of metal in the foil the value of p at the platinum surface can be estimated. In the case of iron vaporization, the amount of iron in the foil was below 3.5% after 1 day of vaporization. For this concentration, the activity of iron in platinum[3] is $a_{Fe} = 3 \times 10^{-4}$ (with respect to pure liquid iron) at 1600°. The iron vapor pressure corresponding to this activity is much lower than the vapor pressure of pure iron; and therefore, p_{Fe} at the gas–foil interface can be taken as zero. On similar reasoning, the partial pressures of other metal vapors are taken to be zero at the platinum surface.

The surface area of the melt was 1.78 cm.^{2}; using this value and converting the flux J to the total amount of

(3) H. R. Larson and J. Chipman, *Acta Met.*, 2, 1 (1954).

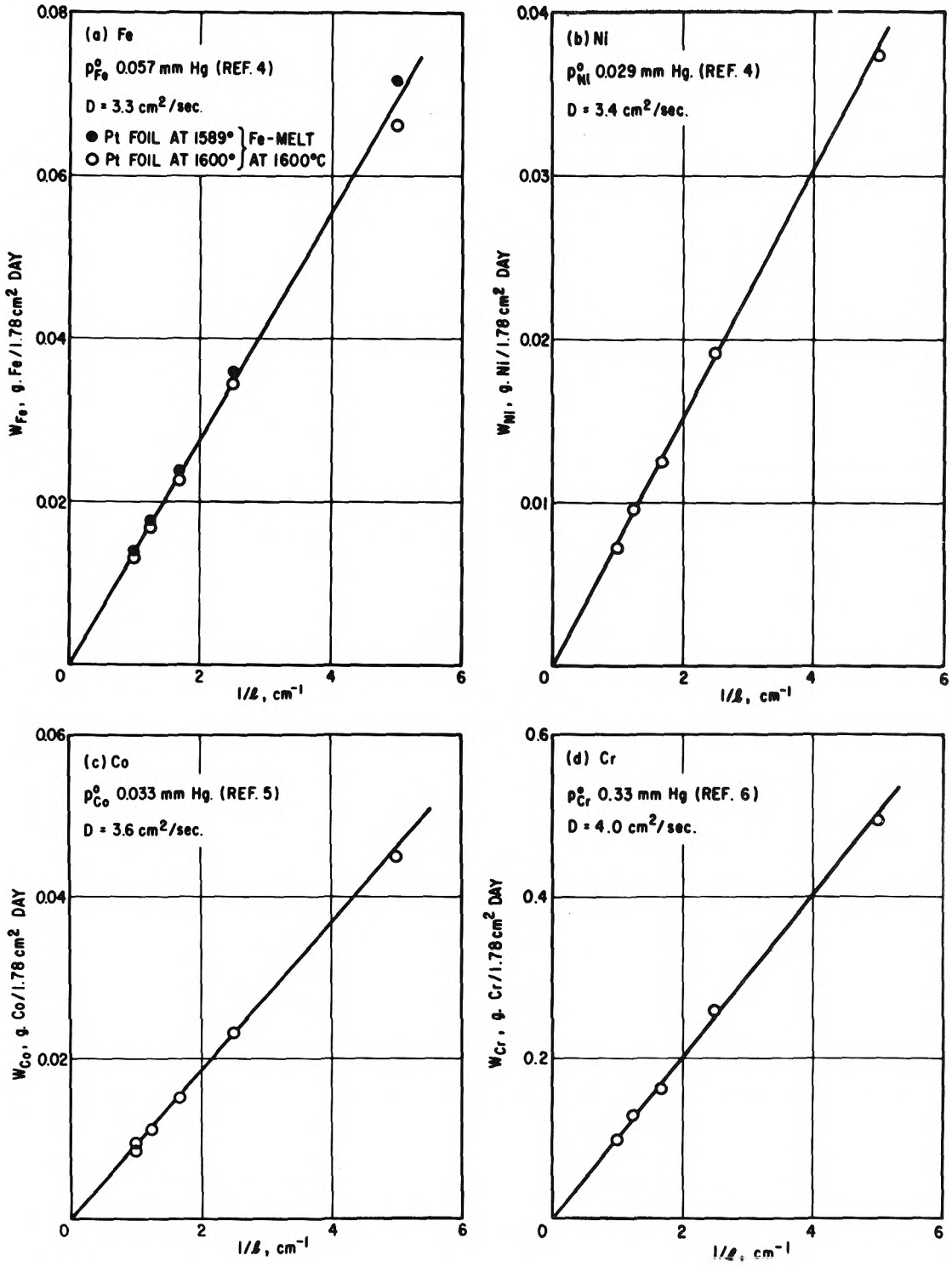

Figure 2. Experimental results on steady-state diffusion of metal vapors in stagnant atmospnere or argon at 1.0 atm. and 1600°: (a) Fe, (b) Ni, (c) Co, and (d) Cr.

metal in grams vaporized in 24 hr., W, eq. 1 takes the following form

$$W = 2.47 \frac{D_{M,Ar}}{l} \frac{p^0 M}{T}, \text{ g./1.78 cm.}^2 \text{ deg.} \quad (2)$$

where W is in g., l in cm., $D_{M,Ar}$ in cm.²/sec., p^0 in mm., and M is the atomic weight of the metal.

The experimental results for the rate of diffusion of cobalt, nickel, chromium, and iron vapor in argon at

1600° are given in Fig. 2, where W is plotted against the *reciprocal of the diffusion distance, l.* The results for the interdiffusion of manganese vapor and argon are given in Fig. 3 for the temperatures 1250, 1300, and 1400°. From the slopes of lines the interdiffusivities are calculated.

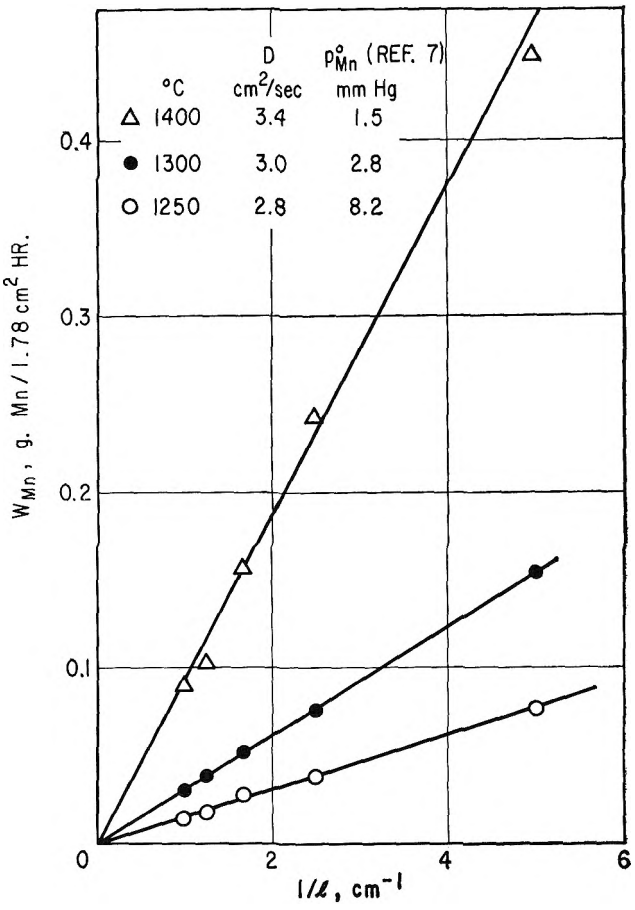

Figure 3. Data on the steady-state diffusion of manganese vapor in a stagnant atmosphere of argon at 1 atm.

When measuring diffusivities in fluid media, care should be taken to ensure that the unidirectional rate of migration in the diffusion cell is not enhanced by convection currents resulting from small lateral or longitudinal temperature gradients. As discussed in the Appendix, no convection currents could have interfered with the present diffusion experiments even if there were a noticeable temperature gradient along the diffusion distance. To verify this fact, a series of experiments was carried out in which the platinum disk was held at 1589° while the metal was held at 1600°. As seen from the results in Fig. 2a, the rates of vaporization in these experiments were almost the same as those obtained when the entire diffusion cell was maintained at 1600 ± 2°. (For further details on convection in enclosed spaces, see the Appendix.)

Discussion

Theoretical Metal Vapor–Gas Interdiffusivities. As discussed by Chapman and Cowling,[4] the following expression can be derived as a first approximation of the coefficient of diffusion in binary nonpolar gas mixtures from the kinetic theory of gases developed by Enskog and Chapman for monatomic gases.

$$D_{12} = 0.0018583 \frac{T^{3/2}}{P(\sigma_{12})^2(\Omega^{(1,1)*})_{T_{12}*}} \sqrt{\frac{1}{M_1} + \frac{1}{M_2}} \quad (3)$$

where D_{12} = interdiffusion coefficient in cm.²/sec.; T = temperature in °K.; P = pressure in atm.; M_1, M_2 = molecular weights of species 1 and 2; σ_{12} = collision diameter in Å., arithmetical mean of collision diameters of species 1 and 2; $(\Omega^{(1,1)*})_{T_{12}*}$ = dimensionless collision integral for mixtures of 1 and 2 at a given reduced temperature T_{12}^*; $T_{12}^* = (k/\epsilon)T$, where k is Boltzmann's constant, ϵ is the maximum energy of intermolecular attraction, and $(k/\epsilon)_{12}$ is that for the geometrical mean of force constants for species 1 and 2.

The values of the collision integral as functions of reduced temperature and the force constants (σ, ϵ/k) for simple gases, based on the Lennard-Jones (6–12) potential energy function, are tabulated by Hirschfelder, *et al.*[5]

The force constants for metal vapors are not known; however, as discussed elsewhere by Turkdogan,[2] the force constants may be estimated using the following empirical relations

$$\epsilon/k = 1.15T_b \quad (4a)$$

$$= 1.92T_m \quad (4b)$$

$$\sigma = 1.166(V_b)^{1/3} \quad (5a)$$

$$= 1.221(V_m)^{1/3} \quad (5b)$$

where T_b and T_m are boiling and melting temperatures in °K.; V_b is the molar volume, in Å., of liquid metal at its boiling temperature, and V_m the molar volume, in Å., of solid metal at its melting temperature. Although the value of ϵ/k estimated for a metal vapor from T_b and T_m may differ considerably, the interdiffusivities obtained[2] using these values of ϵ/k generally agree within about 5%. For the vapors Ni, Co, Fe, and Cr the estimated average value of ϵ/k is 3500°K. and for Mn

(4) S. Chapman and T. G. Cowling, "The Mathematical Theory of Non-Uniform Gases," Cambridge University Press, 1939.

(5) J. O. Hirschfelder, C. F. Curtiss, and R. B. Bird, "Molecular Theory of Gases and Liquids," John Wiley and Sons, Inc., New York, N. Y., 1954.

vapor, ϵ/k is 2300°K.; for all these vapors the estimated average value of σ = 2.44 Å.

Comparison of Experimentally Observed and Estimated Interdiffusivities. The variation of measured manganese vapor–argon interdiffusivity with temperature is shown in Fig. 4 in a log–log plot. As seen from eq. 3, if the collision integral were to remain constant over the temperature range studied, the slope of the line in Fig. 4 should have been 3:2. However, with increasing temperature the value of $\Omega^{(1,1)*}$ decreases, hence the slope of the line, as derived from the experimental results, in Fig. 4 has to be greater than 3:2. The experimental results on the interdiffusivities of gas–metal vapor binary mixtures are compared in Fig. 5 with the values calculated using eq. 3 and the estimated force constants.

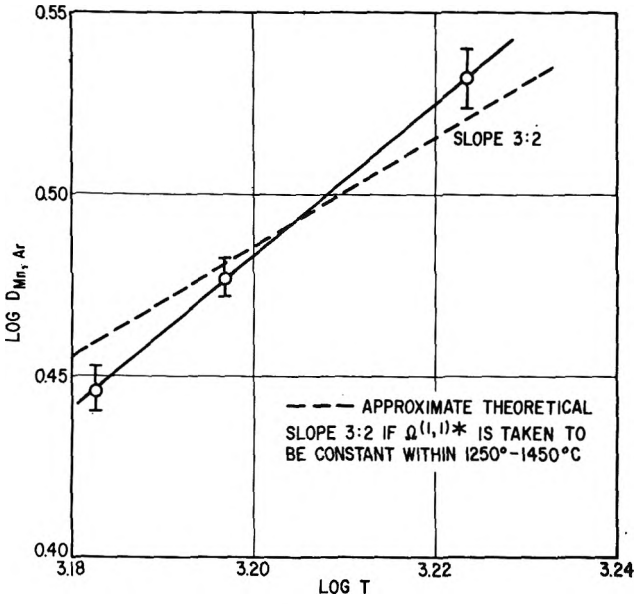

Figure 4. Variation of Mn vapor–argon interdiffusivity with temperature. If $\Omega^{(1,1)*}$ were constant within the temperature range stated, the theoretical slope should have been 3:2.

One of the major sources of error in the experimental determination of the interdiffusivity by the method described is that due to the uncertainty of vapor pressure data. For example, the limit of uncertainty on the vapor pressure of iron is estimated to be about ±0.007 mm. at 1600° (±12%); this reflects an uncertainty of about ±0.4 cm.²/sec. on the experimental value of D_{12}.

Considering the errors involved in the estimation of the force constants, and errors arising from the uncertainties of the vapor pressure data, the agreement between the estimated and the observed diffusivities is reasonable.

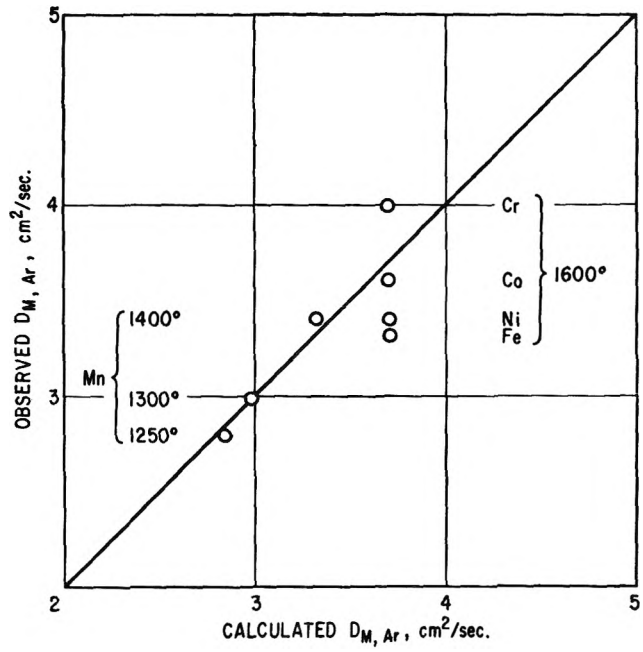

Figure 5. Comparison of estimated and experimental interdiffusivities of metal vapor–gas binary mixtures at 1 atm. pressure.

Conclusions

A method of measuring interdiffusivities of metal vapor and argon has been described and values were obtained for the interdiffusivity of several metal vapors and argon. In general, there is reasonably good agreement between the observed and calculated interdiffusivities.

Appendix

Detailed studies have been made, notably by Mull and Reiher,[6] on heat transfer by free convection in enclosed horizontal and vertical plane air layers, and some generalizations have been made by Jakob[7] and McAdams[8] concerning this phenomenon. In connection with the present studies some consideration should be given to these findings.

When heat is transferred between two horizontal planes in an enclosed space, there are two heat transfer equations to be considered

$$\text{convection, } q_c = h_c(T_1 - T_2) \qquad \text{(A1)}$$

$$\text{conduction, } q = \kappa/l(T_1 - T_2) \qquad \text{(A2)}$$

where q_c = heat transferred by convection per unit

(6) W. Mull and H. Reiher, *Gesundh-Ing.*, **28**, 1 (1930).

(7) M. Jakob, "Heat Transfer," Vol. I, John Wiley and Sons, Inc., New York, N. Y., 1949.

(8) W. H. McAdams, "Heat Transmission," McGraw-Hill Book Co., Inc., New York, N. Y., 1956.

area; q = heat transferred by conduction per unit area; h_c = heat transfer coefficient; T_1, T_2 = temperatures of lower and higher planes, $T_1 > T_2$; κ = thermal conductivity; l = distance between the horizontal planes.

In the previous studies mentioned above, it has been observed that the Nusselt number $h_c l/\kappa$ is a function of the product of the dimensionless parameters Grahof and Prandtl numbers.

$$\frac{h_c l}{\kappa} = C(\mathrm{Gr} \times \mathrm{Pr})^n \qquad \text{(A3)}$$

When the product Gr × Pr is below 10^3, the heat transfer (less that due to radiation) is controlled essentially by conduction, *i.e.*, $h_c l/\kappa \simeq 1.0$. For Gr × Pr within the range 10^4–3.2×10^5, $C = 0.21$ and $n = {}^1/_4$; for Gr × Pr within 3.2×10^5–10^7, $C = 0.075$ and $n = {}^1/_3$.

In view of the well-known analogies between heat and mass transfer equations, a correlation similar to eq. A3 may be written for mass transfer

$$\frac{m_c l}{D} = C\left[\frac{gl^3}{\nu^2}\left(\frac{\rho_2}{\rho_1} - 1\right)\frac{\nu}{D}\right]^n \qquad \text{(A4)}$$

where m_c = mass transfer coefficient due to convection; D = interdiffusivity; g = acceleration of gravity; ν = kinematic viscosity; ρ_1, ρ_2 = densities at temperatures T_1 and T_2, respectively. The product of the first two terms in the brackets is of course the Grashof number for mass transfer and ν/D is the Schmidt number. It should be emphasized that the above correlation is considered at best to be approximate, particularly for small enclosed spaces at elevated temperatures. It is used here to demonstrate only approximately the extent of convection current effect on diffusion in gases.

The Schmidt number for argon is 0.73 and is practically independent of temperature over a very wide range, and the kinematic viscosity is readily calculable from the kinetic theory of gases. Now, let us consider the transfer of a gaseous species at low concentrations from the lower (hotter) plane 1 to the higher (cooler) plane 2. Assuming that $T_1 = 1600°$, the ratio $m_c l/D$ is calculated for $T_2 = 1200$, 800, and 400° for different diffusion distances l and the results are given in Fig. 6. As customary, the value of ν is that for the mean temperature of $(T_1 + T_2)/2$. It should be noted that even at steep temperature differences, the ratio $m_c l/D$ is very close to unity when the planes are a few centimeters apart. Therefore, in the present gas-diffusion

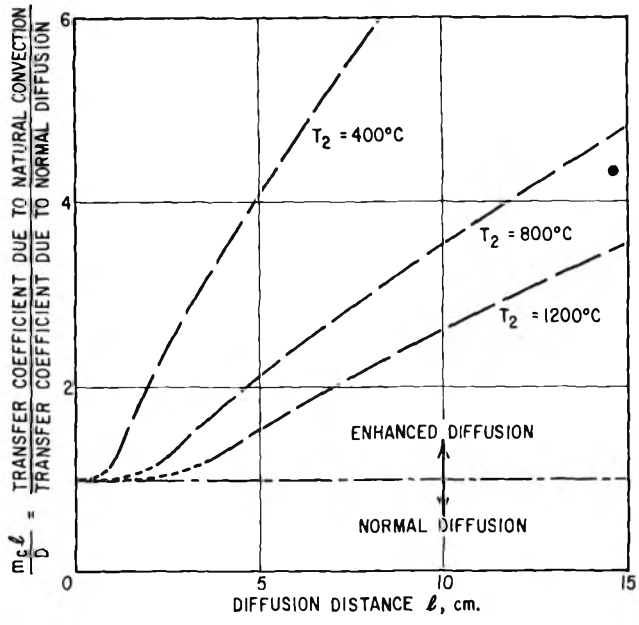

Figure 6. Effect of temperature gradient on mass transfer coefficient of gaseous species transferred between two parallel planes of distance l in an atmosphere of argon. Lower plane is taken to be at $T_1 = 1600°$ and higher plane, at a distance l, is taken to be $T_2 = 400$, 800, or 1200°. (Calculations giving these results are only approximate.)

experiments at high temperatures, using relatively small reaction cells, slight temperature fluctuations are not likely to affect the rate of diffusion under a concentration gradient.

However, in connection with vaporization of metals in inert gases, steep temperature gradients enhance the rate of vaporization as a result of condensation of the vapor near the surface of the metal. This is discussed elsewhere by one of the authors.[9]

As seen from eq. A4, the parameter which has a pronounced effect on the value of $m_c l/D$ is the product νD. For ordinary gases at, say, 1600° the value of νD is in the range 5–100; at room temperature, the product νD is in the range of 10^{-4}–10^{-5}. Therefore, for a given temperature gradient and diffusion distance, the effect of convection on rate of diffusion becomes more serious at lower temperatures. For liquid metals and liquid metal oxides the value of νD is very small; even at elevated temperatures, *e.g.*, at 1600°, νD is about 10^{-6}–10^{-7}. Therefore, much care has to be taken in measuring diffusivities in liquid systems to avoid convection currents.

(9) E. T. Turkdogan, *Trans. Met. Soc. AIME*, in press.

The Kinetics of Decomposition of Acetylene in the 1500°K. Region[1]

by Howard B. Palmer and Frank L. Dormish

Department of Fuel Technology, The Pennsylvania State University, University Park, Pennsylvania
(Received February 15, 1964)

Acetylene has been pyrolyzed in a flow system at three temperatures near the lower limit of shock tube work. The decomposition is of mixed first and second order, kinetically, the former being heterogeneous and the latter homogeneous. Rate constants for the second-order reaction, together with shock tube data, define the high-temperature kinetics reasonably well. Recent work at low temperatures is reviewed, and it is concluded that second-order rate constants at low temperatures cannot be compared directly with those at high temperatures. An heuristic mechanism is presented that exhibits rate behavior broadly consistent with both low- and high-temperature experiments reported in the literature.

Introduction

The thermal decomposition of acetylene is one of the most studied phenomena in the chemistry of gases. Despite the apparent simplicity of the C_2H_2 molecule, its thermal behavior is exceedingly complex. Within the past 10 years, it has been studied in static systems,[2,3] in flow systems,[4-8] in shock tubes,[9-12] and in flames.[13] The temperature range covered in these studies has spanned the region from about 625 to 2500° K. but with a gap in the 1000°K. region that has been studied only very recently.[6,14] Explorations have been made of the product distributions, of the effects of vessel surfaces, of changing surface-to-volume ratios, of adding free radical capturers such as NO, and of adding organic compounds that might participate in the mechanism. The rate of formation and the characteristics of the carbons and polymers formed in the decomposition have been studied extensively.

There is substantial agreement on some aspects of the decomposition. It appears to be settled that at low temperatures, a homogeneous reaction which is second order in $[C_2H_2]$ dominates the behavior. The reaction is a chain and leads to the formation of high molecular weight compounds, with some side products such as H_2, C_2H_4, CH_4, and C_4H_4. The activation energy is approximately 50 kcal. and the frequency factor of the uninhibited reaction is very large. Silcocks[3] gives

$$k = 3.72 \times 10^{16} \exp(-50.2 \text{ kcal.}/RT) \text{ ml./mole sec.}$$

A heterogeneous reaction is also observed at low temperatures. Silcocks reports that it is first order in $[C_2H_2]$, with an activation energy of 42.7 kcal. He gives values of the rate constant at five temperatures.

The situation at high temperatures contains more

(1) Work supported in part by the U. S. Atomic Energy Commission under Contract AT(30-1)-1710.

(2) (a) G. J. Minkoff, D. M. Newitt, and P. Rutledge, *J. Appl. Chem.*, 406 (1957); (b) G. J. Minkoff, *Can. J. Chem.*, **36**, 131 (1958).

(3) C. G. Silcocks, *Proc. Roy. Soc.* (London), **A242**, 411 (1957).

(4) F. C. Stehling, J. D. Frazee, and R. C. Anderson, Symposium (International) on Combustion, 6th, August 19–24, 1956, Yale University, New Haven, Conn., Reinhold Publishing Corp., New York, N. Y., 1957, p. 247.

(5) F. C. Stehling, J. D. Frazee, and R. C. Anderson, Symposium (International) on Combustion, 8th, August 28–September 3, 1960, Pasadena, Calif., Williams and Wilkins Co., Baltimore, Md., 1962, p. 775.

(6) M. S. B. Munson and R. C. Anderson, *Carbon*, **1**, 51 (1963).

(7) C. R. Kinney and R. S. Slysh, Proceedings of the Fourth Carbon Conference, Pergamon Press, Oxford, 1960, p. 301.

(8) G. D. Towell and J. J. Martin, *A.I.Ch.E. J.*, **7**, 693 (1961).

(9) C. F. Aten and E. F. Greene, *Combust. Flame*, **5**, 55 (1961).

(10) W. J. Hooker, Symposium (International) on Combustion, 7th, August 28–September 3, 1959, London and Oxford, Butterworth Co., Ltd., London, 1959, p. 949.

(11) G. B. Skinner and E. M. Sokoloski, *J. Phys. Chem.*, **64**, 1952 (1960).

(12) J. N. Bradley and G. B. Kistiakowsky, *J. Chem. Phys.*, **35**, 264 (1961).

(13) J. D. Chase and F. J. Weinberg, *Proc. Roy. Soc.* (London), **A275**, 411 (1963).

(14) C. F. Cullis, Dept. of Chemical Engineering and Chemical Technology, Imperial College, London; private communication of work in press.

conflict. It has been difficult to determine the order of the reaction and the activation energy, either with flow systems[8] or in shock tubes. However, if one presumes the reaction order to be integral, the best choice at high temperatures appears to be second order in acetylene. The rate constants at the highest temperatures[9,12] disagree by a factor of about 10, but agreement is considerably better at temperatures below 1900°K.

Both Aten and Greene[9] and Minkoff and Tipper[15] agree that the rate constants at high and low temperature can be used to define the rate over the whole range; *i.e.*, they agree that the mechanism remains the same, at least up to and including the rate-determining step. However, Aten and Greene prefer their own high-temperature data, while Minkoff and Tipper prefer those of Kistiakowsky and Bradley.[12] These choices yield markedly different results, respectively

$$k = 10^{12.89} \exp(-39 \text{ kcal.}/RT) \text{ ml./mole sec.}$$

(data of ref. 9)

$$k = 10^{15.15} \exp(-45.8 \text{ kcal.}/RT) \text{ ml./mole sec.}$$

(data of ref. 12)

Quite aside from questions raised by such a discrepancy, we think it unjustifiable to assume that one is measuring the rate of the same reaction sequence at 2000°K. and at 700°K. The low-temperature homogeneous reaction is a chain of length[3] on the order of 100 or more. There is no evidence that the reaction at high temperature is a chain. Indeed the only direct experimental evidence[12] of which we are aware indicates that it is essentially a simple sequence of consecutive reactions.

It is clearly important to discover what happens between the lower limit of the shock tube studies, *ca.* 1400°K., and the upper limit of the studies in vessels, *ca.* 800°K. This intermediate region is appropriate for studies using flow systems. Anderson and his colleagues[4,5] have done exactly this, but have concentrated most of their attention upon product distributions and the implications of these regarding the mechanism. Very recently, however, Munson and Anderson[6] have published work from which it is possible to extract rate constant data, and we shall discuss these later. Towell and Martin[8] used a flow reactor to study the decomposition over temperatures from about 1200°K. to 1450°K. They had difficulty in defining the order of reaction, but their data compare reasonably well with shock tube data if one assumes second-order behavior.

The present experiments represent an effort to study the decomposition very carefully at three temperatures, the highest of which overlaps the shock tube studies. Particular attention has been given to determining the order of reaction and the absolute magnitudes of rate constants at these three temperatures. The work is basically an extension of that performed by Kinney and Slysh.[7]

Experimental Procedure

The apparatus was only slightly modified from the arrangement used by Kinney and Slysh[7] and will therefore be described only briefly. It was a flow system operating at ambient pressure. The pyrolysis tube was 5 mm. i.d. refractory porcelain, sealed to Pyrex at the ends, and mounted in a furnace capable of attaining 1500°. C_2H_2 was metered with a capillary flow meter before being mixed with the helium carrier. Input rates were varied so as to produce mixture compositions ranging from 0.20 to 1.30 mole % C_2H_2.

Temperature profiles within the pyrolysis tube were measured with a Pt–Pt:Rh thermocouple for each of three temperature settings and at several flow rates. They were found to be essentially independent of flow velocity, from which it is inferred that the gas temperature was indeed being measured. This conclusion is supported by estimates of the radial temperature distribution in the tube based upon approximate values for the thermal diffusivity of the gas. The estimates show that the temperature at the center of the tube (2.5 mm. from the wall) should not differ from the wall temperature by more than a few degrees. Because the furnace was short, the temperature profiles did not possess a plateau region. A typical profile is shown in Fig. 1, together with what we call the "staircase" approximation to it, by means of which it was possible to correct the experimental data to the temperature of an imaginary 5-cm. long hot zone having a constant temperature near the actual temperature peak. It was also convenient to discuss the effect of flow velocity upon the % decomposition in terms of the fictitious residence time ("contact time") of the gas in the imaginary hot zone.

Calculations of the extent of decomposition in the hot zone were carried out for each run by an iterative procedure in which an equation for the rate constant was assumed in order to compute the relative contributions from decomposition at each of the temperature levels on the staircase. Most of the decomposition occurred on the top level, which meant that it was quite easy to correct for the other contributions, using rough values for the rate constants in the first

(15) G. J. Minkoff and C. F. H. Tipper, "Chemistry of Combustion Reactions," Butterworth Co., Ltd., London, 1962.

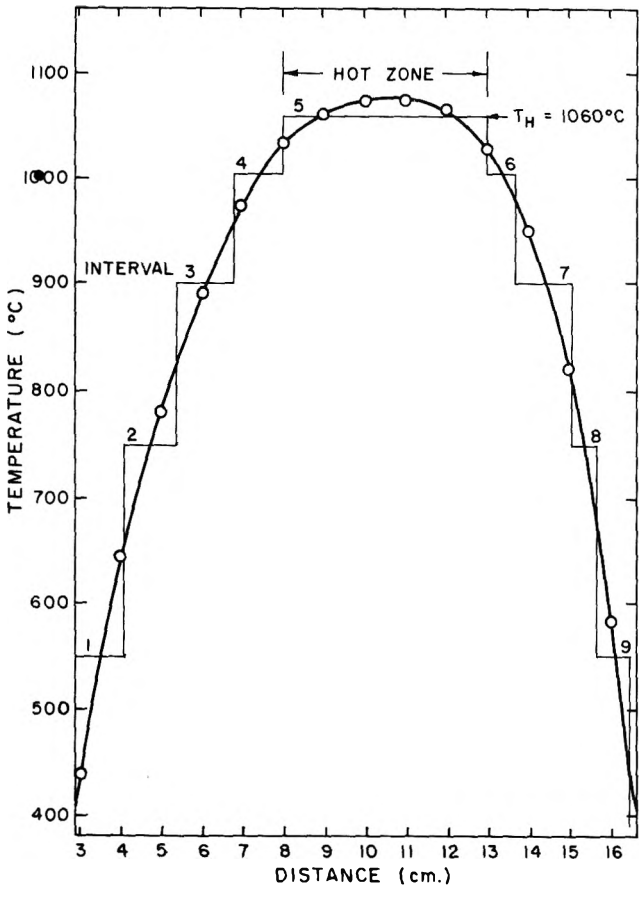

Figure 1. Temperature profile for the furnace having the hot zone at 1060° (1333°K.). The "staircase" approximation to the profile is illustrated.

trial. From the results of the runs at three different temperature settings, a better expression for the temperature-dependent rate constant was derived and used in the second calculation of corrections. This single iteration was found to yield satisfactory values for rate constants at each of the three hot-zone temperature levels (1333, 1433, and 1528°K.). Details of these calculations are presented by Dormish.[16]

The helium used was Matheson "research grade" gas, purity approximately 99.99%. It was passed through a bed of copper at 400° for oxygen removal and then through a tower containing Ascarite and Anhydrone to remove CO_2 and H_2O. The C_2H_2, a purified grade of 99.5% minimum purity, was bubbled through concentrated H_2SO_4 to remove acetone before introduction into the helium stream. The mixture of C_2H_2 and helium was routed through a Dry Ice-cooled glass wool-packed trap before entering a coil of tubing 1.2 m. in length that served to ensure homogeneity of the mixture that entered the pyrolysis tube.

Beyond the water-cooled exit of the furnace were three traps in series. The first was cooled by Dry Ice and served principally as a precooler to ensure good trapping efficiency in the subsequent liquid nitrogen-cooled traps. These traps captured acetylene, diacetylene, vinylacetylene, methylacetylene, and allene. Hydrogen and methane were not trapped, but were converted to H_2O and CO_2 over CuO filings at 700°. Vitreous carbon that formed on the tube wall during the run was determined by burning it off with oxygen at 1255°, running the effluent gas through a CuO trap, and capturing the CO_2 in Ascarite. A very small amount of reddish polymer, deposited just beyond the furnace exit, was the only product ignored. Analyses were performed using vapor chromatography and (for CO_2 and H_2O) by weighing Ascarite and Anhydrone absorption towers.

Results and Discussion

The decomposition has been studied at three temperatures: 1333, 1433, and 1528°K. These represent the effective hot-zone temperatures to which the decomposition data were corrected. Because the emphasis in the present paper is upon the kinetics of decomposition, details of product analyses are not presented here. They were in broad agreement with the results of other investigations.[6,7] A note of special interest is that the more prominent C_4 product at 1333°K. was vinylacetylene, but at 1528°K. it was diacetylene.

In Table I are summarized the experimental data on the extent of decomposition of C_2H_2 at various nominal contact times. These formed the basis for calculations of rate constants. The order of reaction has been determined at the three hot-zone temperatures by examining the extent of decomposition as a function of the initial concentration at fixed flow rate, *i.e.*, at fixed effective contact time in the hot zone. The results appear in Fig. 2, and represent mixed first- and second-order behavior. This may be seen as follows: consider a reaction with rate given by

$$-dC/dt = k_u C + k_b C^2 \qquad (1)$$

Integration yields

$$\ln (C_0/C) = k_u t + \int_0^t k_b C dt \qquad (2)$$

$$= (k_u + k_b \bar{C})t \qquad (3)$$

where $\bar{C}$ is a mean concentration over the time interval and will approximately equal $(C_0 + C)/2$ when the

(16) F. L. Dormish, M.S. Thesis, Dept. of Fuel Technology, The Pennsylvania State University, University Park, Pa., 1962.

Table I: Summary of Experimental Data on the Decomposition Rate

1333° K.[a]			1433° K.[a]			1528° K.[a]		
c.t.,[b] sec.	C_0, mole %	% Dec.	c.t.,[b] sec.	C_0, mole %	% Dec.	c.t.,[b] sec.	C_0, mole %	% Dec.
0.100	0.58	3.9	0.100	0.50	8.2	0.046	0.50	9.1
0.150	0.57	5.6	0.150	0.22	11.2	0.094	0.50	18.2
0.150	0.81	6.3	0.150	0.27	11.4	0.150	0.50	31.2
0.150	0.96	6.5	0.150	0.52	12.8	0.150	0.69	37.7
0.150	1.02	7.2	0.150	0.97	14.3	0.150	0.78	39.7
0.150	1.28	7.5	0.150	1.25	16.5	0.180	0.50	37.0
0.200	0.52	7.5	0.150	1.30	16.8	0.190	0.50	37.8
			0.200	0.53	18.1			

[a] Hot-zone temperature. [b] Nominal contact time = (hot-zone volume)/(vol. flow rate at hot-zone temperature).

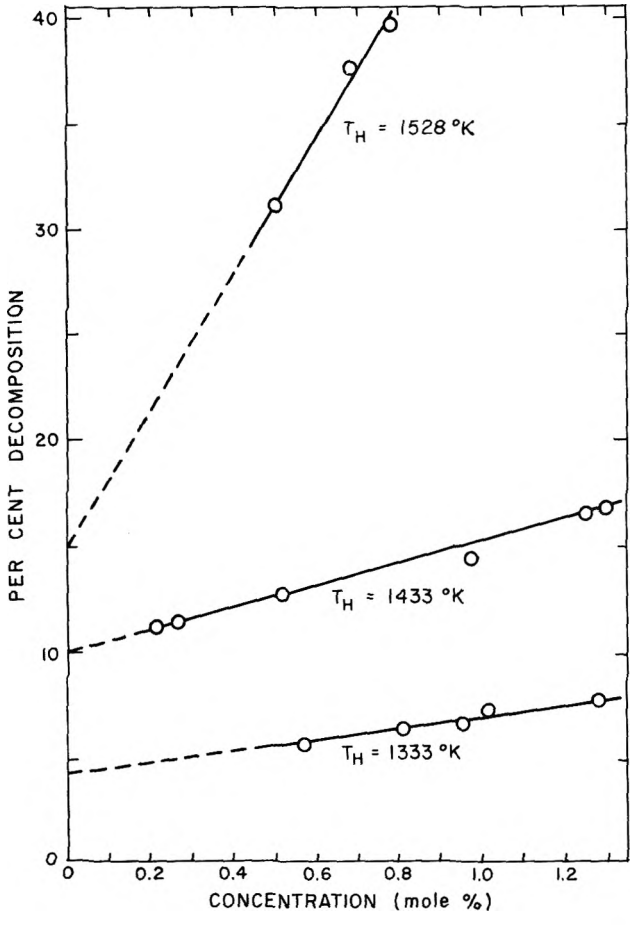

Figure 2. Effect of change in initial concentration upon extent of decomposition at fixed contact time (0.150 sec.).

extent of decomposition is small. When this is the case, eq. 3 yields

$$1 - (C/C_0) = (k_u + k_b\bar{C})t$$

Thus, for mixed first and second order, a study at fixed time (*i.e.*, fixed flow rate) and small extent of decomposition should show an approximately linear dependence of the extent of decomposition upon the input concentration, with a finite intercept at $C_0 = 0$ if there is in fact a first-order contribution. This is the case in Fig. 2.

One can calculate first-order rate constants from the intercepts in Fig. 2. The result for 1528°K. is not as reliable as the other two because of the smaller number of points, the long extrapolation to $C_0 = 0$, and the larger extent of decomposition. The calculations involve a correction to yield the extent of decomposition in the effective hot zone. This is in principle a multiply iterative procedure, but we found that the correction was sufficiently small that a rough treatment of the data could provide crude rate constants from which corrections could be formed to yield good rate constants in a single iteration, as discussed earlier.

The k_u values obtained are 0.221 sec.$^{-1}$ at 1333°K.; 0.482 sec.$^{-1}$ at 1433°K.; and 0.745 sec.$^{-1}$ at 1528°K. On an Arrhenius plot, these define a line given by

$$k_u = 4.2 \times 10^3 \exp(-26 \text{ kcal.}/RT) \text{ sec.}^{-1}$$

The uncertainties in the numerical values of this expression are surely considerable (but difficult to estimate). Nevertheless, it is clear that both the frequency factor and the activation energy rule out a homogeneous unimolecular reaction. If we assume that the reaction is heterogeneous, the rate constant k_{het} will be $k_{het} = k_v(V/S)$, where (V/S) is the volume-to-surface ratio. In our reactor, this ratio was 1.25×10^{-4} l./cm.^{2}, where the units have been chosen so as to permit easy comparison with the low-temperature results of Silcocks.[3] The comparison is shown in Fig. 3.

$$k_{het} = 5.25 \times 10^{-1} \exp(-26 \text{ kcal.}/RT) \text{ l. cm.}^2 \text{ sec.}^{-1}$$

An extension of this line goes through the middle of Silcocks' data. It is tempting to conclude that the heterogeneous reactions are the same, but caution is required because a modest alteration of the parameters

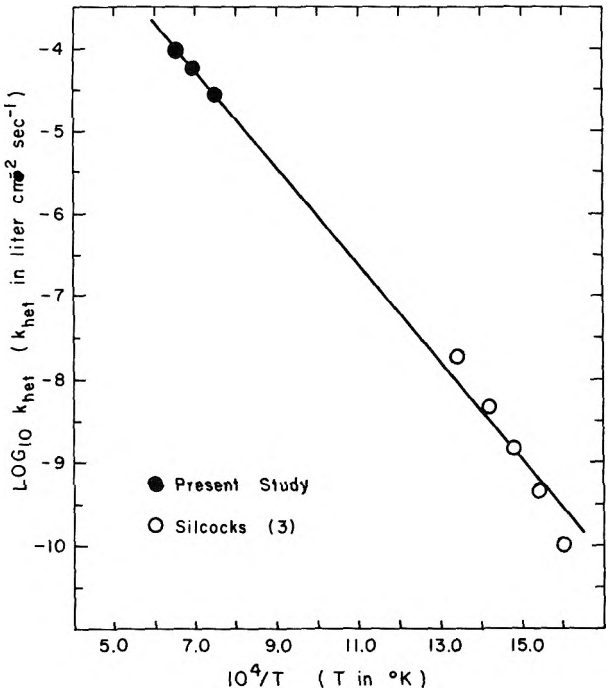

Figure 3. Arrhenius plot of heterogeneous rate constants for C_2H_2 decomposition from the present work and from Silcocks.[3]

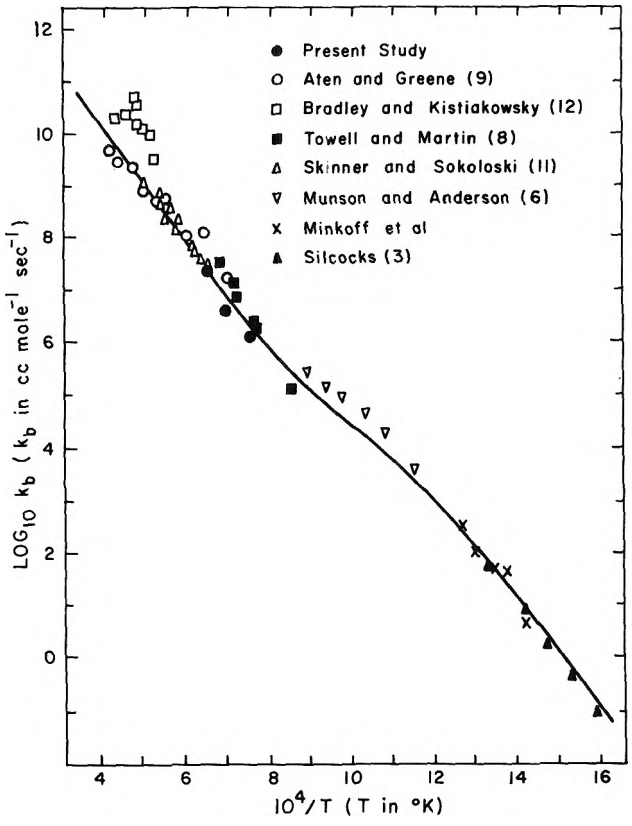

Figure 4. Arrhenius plot of second-order rate constants for acetylene decomposition from the present work and from the literature.

in the expression for k_{het} could cause the extension to miss Silcocks' points altogether. There is much more to be explored on the matter of a heterogeneous decomposition. We have noted with interest that the yields of H_2, C_4H_4, and C_4H_2 all move toward zero at $C_0 = 0$, and carbon plus CH_4 become virtually the only products. Clearly the mechanism of the surface decomposition must be grossly different from the gaseous process.

Figure 2 shows that the gaseous decomposition conforms nicely to second-order kinetics, and it is possible to obtain k_b from the slopes. We have preferred to use data on the % decomposition as a function of the effective contact time in the hot zone, averaging the rate constants obtained from a number of runs (6–8) at the same temperature but at various flow rates and input concentrations. The results have been corrected, in each case, for the first-order contribution. The procedure[16] is tedious and will not be outlined here.

The results for k_b, in units of ml./mole sec. are: $(1.40 \pm 0.10) \times 10^3$ at 1333°K.; $(3.42 \pm 0.23) \times 10^3$ at 1433°K.; and $(2.49 \pm 0.36) \times 10^4$ at 1528°K. The uncertainties attached to each result are the average absolute deviations of the experimental points.

Figure 4 is an Arrhenius plot of all available data for k_b, ranging from about 650 to 2500°K. The solid curve will be discussed later. Our data and those of Skinner and Sokoloski[11] agree very well, in the sense that their higher temperature points fall on the best line through our results. However, their values below about 1500°K. (not included in the figure) show a change in slope that requires comment at a later point in this discussion. The data of Towell and Martin,[8] obtained in reactors very similar to ours, parallel our data well. Agreement would be even better if their results could be readily corrected for the contribution from the heterogeneous decomposition. The results of Aten and Greene[9] are in reasonable agreement with ours and with Skinner's but show a smaller slope. The best high-temperature line, which we have selected by eye, defines k_b as

$$k_b = 3.2 \times 10^{14} \exp(-50 \text{ kcal.}/RT) \text{ ml./mole sec.}$$

The frequency factor seems close to normal, in contrast to that cited earlier for the low-temperature reaction. This does not prove that one is observing an elementary reaction at high temperatures, but suggests that the hot reaction is not a chain. An extrapolation of the best high-temperature line falls below the low-temperature k_b values by a factor of 10^2 or more.

Thus, the question remains: what happens between 800 and 1400°K.? The work of Munson and Anderson[6] contributes much toward an answer. They used a flow reactor of diameter 2.2 cm. and, at high concentrations of C_2H_2 (20–21 mole % at p_{tot} = 1 atm.), covered temperatures from 773 to 1123°K. They did not obtain rate constants, but they do report the time dependence of the C_2H_2 concentration at six temperatures. These results are of precision sufficient to permit examination of the reaction order by the usual methods of kinetics. Our analysis shows that the reaction is second order in $[C_2H_2]$ at 873, 923, and 973° K., but that the order is not well defined at the higher temperatures. The second-order rate constants at the three lower temperatures are in remarkably good agreement with an extrapolation of low-temperature data.

If one approximates the kinetics at the three higher temperatures (1023, 1073, and 1123°K.) by a first-order expression, the rate constants so obtained show a temperature coefficient corresponding to an activation energy in the vicinity of 30 kcal. Thus, it seems quite clear that the kinetics of the decomposition undergo a transition at about 1000°K. and that one cannot make a direct comparison of second-order rate constants at low and high temperatures.

In view of the known complexity of the decomposition, it is not really surprising to find complications in the kinetics; but the behavior does seem extraordinary. An acceptable mechanism must: (a) give second-order kinetics at low temperature, with a rate constant similar to that cited from the results of Silcocks; (b) there must be some sort of transition region at intermediate temperatures; and (c) at high temperatures the reaction must be second order but now with k_b similar to that cited previously from our data and the shock tube data.

Behavior of this sort can occur in the mechanism presented below. This is offered as a stimulus to further work. It makes no attempt to account in detail for all products, and there is no direct evidence for the steps involved in it. Our comments follow each reaction postulated.

$$C_2H_2 + C_2H_2 \longrightarrow C_2H_2^* + C_2H_2 \qquad (I)$$

This represents unimolecular excitation of acetylene to its lowest-lying triplet state. C_2H_2 is shown as the collision partner for the excitation on the presumption that in a mixture of C_2H_2 and a monatomic gas, *e.g.*, helium, C_2H_2 will be many times more effective than helium because it can possess vibrational energy. The actual change of multiplicity probably occurs most rapidly when the amount of energy to be transferred is not very large.[17] Thus, a detailed mechanism for reaction I would include vibrational excitation. However, because establishment of vibrational equilibrium is probably rapid relative to the rate of reaction I, one can think of at least one of the C_2H_2 molecules as being highly excited vibrationally without introducing a necessity for modifying the simple equation above.

Minkoff[2a] has suggested that the first step is double excitation, $2C_2H_2 \rightarrow 2C_2H_2^*$. This has the virtue of being spin-allowed, but the energy requirement will be very much greater (roughly double) that for step I above; this should weigh more heavily against the double excitation than does the forbiddenness factor (perhaps 10^{-4}) entering into the rate constant of reaction I.

Reaction I will probably have an energy barrier somewhat higher than the singlet–triplet excitation energy, which has been estimated[9] to lie between 42 and 67 kcal. above the ground state, using data discussed by Laidler.[17]

$$C_2H_2^* + C_2H_2 \longrightarrow 2C_2H_2 \qquad (II)$$

Reaction II is the deactivation of triplet acetylene. By microscopic reversibility, C_2H_2 must be much more effective than helium in the deactivation. There will presumably be a small activation energy in the rate constant, and a forbiddenness effect in the pre-exponential factor.

$$C_2H_2^* + C_2H_2 \longrightarrow C_4H_4^* \qquad (III)$$

This is an addition reaction to yield a triplet dimer. The reaction will be in competition with step II, and will be fast. The rate constant for a reaction that may be comparable, *viz.*, the addition of NO_2 to C_2H_2, has been reported[18] to equal $10^{12.1}\exp(-15\ \text{kcal.}/RT)$ ml./mole sec.

$$C_4H_4^* + C_2H_2 \longrightarrow C_2H_2^* + C_4H_4 \qquad (IV)$$

Reaction IV is a chain-transfer reaction that is not simply an exchange of multiplicities because formation of vinylacetylene from $C_4H_4^*$ requires hydrogen atom migration. There should be an appreciable but small activation energy. We suspect that in a reaction of this type the collision efficiency ("steric" factor) may be very low.

$$C_4H_4^* + C_2H_2 \longrightarrow \text{products} \qquad (V)$$

This alternative to reaction IV is thought of as a radical addition reaction leading to stable products such as benzene. It is oversimplified for the sake of

(17) K. J. Laidler, "The Chemical Kinetics of Excited States," Oxford University Press, Oxford, 1955.

(18) J. H. Thomas, *Trans. Faraday Soc.*, **48**, 1142 (1952).

allowing a tractable expression for the over-all kinetics. That is, it might also be thought of as a deactivation; or it might not end the chain at all, but rather continue it by a subsequent transfer reaction analogous to step IV; or the product might in turn add to C_2H_2. However, observations by Robertson, *et al.*,[19] of the yield of benzene in C_2H_2 pyrolysis do support the suggestion that a large fraction of the reaction events in step V do not lead to a continuation of the chain. It further appears from that work that reaction V has a large temperature coefficient. We shall assume that its activation energy is much larger than that for step IV, and that its collision factor is also much larger; in this way it becomes possible for its rate to be less than that of step IV at low temperature but to exceed it at higher temperatures.

The postulated reaction scheme is terminated at this point. It is of course recognized in doing so that other reactions must occur. The scheme is a simplified version of that discussed by Minkoff and Tipper,[15] but with the difference in the singlet–triplet excitation step noted previously. A steady-state treatment of the scheme yields

$$-\mathrm{d}[C_2H_2]/\mathrm{d}t = [C_2H_2]^2k_3(k_1/k_2)\{[3 - k_4/(k_4 + k_5)]/[1 + (k_3/k_2)k_5/(k_4 + k_5)]\} \quad (4)$$

At low temperatures, we expect $k_4 >>> k_5$. Then

$$-\mathrm{d}[C_2H_2]/\mathrm{d}t = 2[C_2H_2]^2k_3(k_1/k_2)[1/(1 + k_3k_5/k_2k_4)] \quad (5)$$

We expect k_3 to be considerably greater than k_2; but with $k_4 >>> k_5$, the result is

$$-\mathrm{d}[C_2H_2]/\mathrm{d}t = 2[C_2H_2]^2k_3(k_1/k_2) \quad (6)$$

At higher temperatures, k_5 will compete with k_4 and the chain length will be reduced. In the limit that $k_5 >> k_4$, continuing to assume $k_3 >> k_2$, the steady-state treatment yields

$$-\mathrm{d}[C_2H_2]/\mathrm{d}t = 3k_1[C_2H_2]^2 \quad (7)$$

This rate will be substantially less than that given by the previous results, if extended to high temperature. The consequence is that at the temperature where k_5 begins to compete effectively with k_4, an Arrhenius plot of the apparent second-order rate constant should begin to show a decreasing slope. Once the condition, $k_5 >> k_4$, is reached, the slope will rise again to that characteristic of k_1. This seems to conform rather well to the plot in Fig. 4. The transition region for k_4 *vs.* k_5 appears to begin at about 900°K. and extends to about 1400°K.

The high-temperature results cited earlier now yield

$$k_1 = 1.1 \times 10^{14} \exp(-50 \text{ kcal.}/RT) \text{ ml./mole sec.}$$

and, using this k_1, the low-temperature results of Silcocks yield

$$(k_3/k_2) = 1.60 \times 10^2$$

If we require that $(k_4/k_5) = 10(k_3/k_2)$ at 700°K. and $(k_4/k_5) = 0.2$ (*i.e.*, $<< 1$) at 1400°K., the temperature dependence of (k_5/k_4) is found to be

$$(k_5/k_4) = 4.2 \times 10^4 \exp(-25.1 \text{ kcal.}/RT)$$

Employing these three parameters, k_1, (k_3/k_2), and (k_5/k_4), eq. 4 may be used for a computation of the second-order rate constant over the whole temperature range. The result is shown by the solid curve in Fig. 4. The fit seems quite successful, particularly when it is realized that the C_2H_2 disappearance rates reported by Munson and Anderson may have been appreciably enhanced by heterogeneous decomposition on carbon particles formed in their reactant stream. It is not possible to make a correction for this effect; the point is that the k_5 values computed from their results are probably too large.

Some comment on the parameters is in order. k_1 has a surprisingly large pre-exponential factor, in view of the violation of spin conservation in reaction I. However, in a recent study of SO_2 decomposition, Gaydon, *et al.*,[20] have found that unimolecular excitation of SO_2 to its lowest triplet state appears to be aided by energy transfer from internal degrees of freedom. This has the effect of raising the pre-exponential factor so as largely to compensate for the forbiddenness of the reaction. The apparent energy of activation is lowered in such a case. In C_2H_2–C_2H_2 collisions, there are many possibilities for energy transfer from internal modes and it is possible to rationalize k_1 on this basis. If the interpretation is correct, then the true activation energy of step I probably lies between 55 and 60 kcal., and a simple Arrhenius expression for k_1 is not very realistic. However, refinement of k_1 does not yet seem justifiable.

The (approximate) temperature independence of (k_3/k_2) is about what one would expect on the basis of the earlier discussion of these reactions. The magnitude of the ratio, *i.e.* 160, is also reasonable.

As for (k_5/k_4), the large ratio of pre-exponential factors is not unexpected, but no particular signifi-

(19) W. W. Robertson, E. M. Magee, J. Fain, and F. A. Matson, Symposium (International) on Combustion, 5th, 1954, Pittsburgh, Pa., Reinhold Publishing Corp., New York, N. Y., 1955, p. 628.

(20) A. G. Gaydon, G. H. Kimbell, and H. B. Palmer, *Proc. Roy. Soc.* (London), **A276**, 461 (1963).

cance can be attached to the 25 kcal. difference in activation energies except to say that it seems consistent with the experimental results of Robertson, *et al.*[19] Beyond this, our ignorance of the details of the postulated steps IV and V is almost total.

A final remark should be made on the report by Skinner and Sokoloski[11] that the rate constant for formation of vinylacetylene below about 1500°K. lies *above* the low-temperature extension of their results for conversion to all products at temperatures above 1500° K. (points shown in Fig. 4). If the result is real, it presents a severe complication. We would suggest tentatively that their low yields of vinylacetylene may have led to analytical errors, as indicated to some extent by their difficulty in obtaining a mass balance on reactants plus products.

Conclusions

It is possible to reconcile most low- and high-temperature data in the literature on acetylene pyrolysis by a chain mechanism in which the main chain-ending reaction has a stronger temperature dependence than does one of the chain-carrying reactions. This leads to long chains at low temperatures and essentially nonchain behavior at high temperatures. It seems very probable that the first step in the mechanism is excitation of C_2H_2 to its lowest-lying triplet state, and that one of the chain steps is a spin–exchange reaction.

In systems possessing high surface-to-volume ratios, *e.g.*, in heavily sooting systems, a first-order heterogeneous decomposition reaction, the products of which appear to be principally carbon and CH_4, is expected to dominate the kinetics.

NOTES

Deuterium Isotope Effect in the Ionization of Substituted Succinic Acids in Water and in Deuterium Oxide

by Paul K. Glasoe

Wittenberg University, Springfield, Ohio

and Lennart Eberson

University of Lund, Lund, Sweden

(*Received May 27, 1963*)

The fact that certain dicarboxylic acids have unusually high ratios of the first to the second ionization constant has been attributed to intramolecular hydrogen bonding in the monoanion.[1,2] This explanation for the very high value of the ratio for maleic acid to that for fumaric acid (20,000 to 23) is substantiated by evidence that the monopotassium salt exists in a hydrogen-bonded condition in aqueous solutions.[3]

Eberson[4] has shown that the K_1/K_2 ratio for highly substituted succinic acids is very high if the acid is in the racemic form and that the monopotassium salt of the racemic acid shows evidence of intramolecular hydrogen bonding both by infrared[5] and by proton magnetic resonance.[6]

It is well-established that the ionization of a deuterio acid is less than that of the corresponding hydrogen acid and that the difference is dependent to some extent on the strength of the hydrogen acid, becoming slightly larger as the acid gets weaker. For many acids, the values of $pK_D - pK_H$ are around 0.5 and fall in the vicinity of a straight line having a slope of 0.02 in the plot of ΔpK *vs.* pK_H.[7] Long and Dahlgren[8] measured pK_H and pK_D for maleic and fumaric acids and found that ΔpK_1 for maleic acid was abnormally high, 0.62, and that ΔpK_2 was abnormally low, 0.38. Fumaric acid, as well as the monoesters of both acids, had what can be considered as "normal" values of ΔpK. They suggested that this high value of ΔpK_1 for

(1) L. Hunter, *Chem. Ind.* (London), 155 (1953).

(2) D. H. McDaniel and H. C. Brown, *Science*, **118**, 370 (1953).

(3) R. E. Dodd, R. E. Miller, and W. F. K. Wynne-Jones, *J. Chem. Soc.*, 2790 (1961).

(4) L. Eberson, *Acta Chem. Scand.*, **13**, 211 (1959).

(5) L. Eberson, *ibid.*, **13**, 224 (1959).

(6) L. Eberson and S. Forsen, *J. Phys. Chem.*, **64**, 767 (1960).

(7) R. P. Bell, "The Proton in Chemistry," Cornell University Press, Ithaca, N. Y., 1959, p. 189.

(8) G. Dahlgren, Jr., and F. A. Long, *J. Am. Chem. Soc.*, **82**, 1303 (1960).

Table I: Ionization Constants for Substituted Succinic Acids and Their Monoesters in Water and in Deuterium Oxide

Acid	pK_1^H	pK_1^D	$pK_2^H - pK_1^H$	ΔpK_1
Succinic acids				
Tetramethyl	3.56 ± 0.02	4.20 ± 0.02	3.85	0.64
Tetraethyl	3.39 ± 0.02	4.29 ± 0.02	4.67	0.90
rac-α,α'-Di-*t*-butyl	2.20 ± 0.01	2.77 ± 0.01	7.95	0.57
Monomethyl esters				
Tetramethyl	4.98 ± 0.01	5.48 ± 0.01		0.50
Tetraethyl	5.34 ± 0.02	5.83 ± 0.02		0.49
rac-α,α'-Di-*t*-butyl	5.57 ± 0.05	6.08 ± 0.03		0.51
	pK_2^H	pK_2^D		ΔpK_2
Succinic acids				
Tetramethyl	7.41 ± 0.02	7.75 ± 0.02		0.34
Tetraethyl	8.06 ± 0.06	8.50 ± 0.05		0.44
rac-α,α'-Di-*t*-butyl	10.25 ± 0.05	10.92 ± 0.05		0.67

maleic acid might be due to the difference in the strength of deuterium bonds compared to hydrogen bonds in the monoanion, the deuterium bonds being weaker.

In view of the fact that the succinic acids investigated by Eberson show high K_1/K_2 ratios and show evidence for hydrogen bonding in the acid salt, it was of interest to see whether these acids would show an abnormal deuterium isotope effect similar to maleic acid. To examine this point, the ionization constants of some substituted succinic acids and their monoesters were measured in water and in deuterium oxide.

Experimental

Materials. The succinic acids and the monomethyl esters were prepared by Eberson as described previously.[9] Deuterium oxide was obtained from Liquid Carbonic Corp. as greater than 99.5% D_2O. Solutions of the deuterio acids were made by dissolving the solid hydrogen acid in deuterium oxide. Solutions of alkali deuterium oxide were made by diluting concentrated carbonate-free alkali hydroxide with deuterium oxide. Since the concentration of the diluted solutions was around 0.02 *M*, the deuterium concentration was not changed by more than 0.1%.

Titrations. pH titrations were carried out on small volumes, usually around 10 ml., of the acid solution by adding standard alkali from a platinum tip microburet. The pH was measured with a Beckman Model GS pH meter equipped with a Beckman No. 39167 glass electrode and a No. 39168 silver–silver chloride reference electrode. The titrations were conducted at 25 ± 0.05° in an atmosphere of nitrogen. The glass electrode system was standardized against water buffers; usually 0.0500 *M* potassium acid phthalate (pH 4.00) was used. In titrations with deuterium oxide solutions values of pD were obtained from the reading of the pH meter, which had been standardized in water buffers, by adding 0.40 to the pH meter reading according to the method given by Glasoe and Long.[10] Values for pK_1 and for pK_2 were calculated at several points on the titration curve above and below the points of half-neutralization. The following formulas were used

$$pK_1 = pH - \log \frac{C_{HA^-} + C_{H^+}}{C_{H_2A} - C_{H^+}} - \log y_{\pm}$$

$$pK_2 = pH - \log \frac{C_{A^{-2}}}{C_{HA^-}} - 3 \log y_{\pm}$$

where pH is defined as $-\log(C_{H^+}y_{\pm})$, $C_{A^{-2}}$, C_{HA^-}, and C_{H_2A} are the added molar concentrations of anions and free acid, respectively, and $y_{\pm}$ was calculated from $-\log y_{\pm} = 0.509\sqrt{\mu}/(1 + \sqrt{\mu})$ where μ is the ionic strength of the solution. A program was set up on an IBM 1401 computer which made it possible to make a large number of calculations all along the titration curve.

No additional electrolyte was added to increase the ionic strength. In no case was the ionic strength greater than 0.01 in solutions for which pK_1 was calculated or greater than 0.02 in pK_2 calculations.

The second pK for α,α'-di-*t*-butylsuccinic acid is so large that only one break is obtained in the titration curve. To determine pK_2 a definite amount of the acid was dissolved in twice the molar quantity of standard alkali and this solution was titrated with standard acid.

A summary of the results is given in Table I.

(9) L. Eberson, *Acta Chem. Scand.*, **13**, 40 (1959).

(10) P. K. Glasoe and F. A. Long, *J. Phys. Chem.*, **64**, 188 (1960).

Discussion

Tetramethylsuccinic and tetraethylsuccinic acids show an abnormal $pK_D - pK_H$ difference and in this respect are like maleic acid. The value of ΔpK for tetraethylsuccinic acid is the highest reported for any acid. However, the di-*t*-butylsuccinic acid, which has a very high K_1/K_2 ratio, does not show a significant abnormal deuterium effect.

The monomethyl esters show what can be considered as normal acid strengths and the deuterium–hydrogen difference is the normal value of around 0.50 pK unit. The weakening of the acid with increasing size of the alkyl substituents is the normal inductive effect.

The very low value for pK_1 for the di-*t*-butylsuccinic acid, compared to the high value for the monoester, suggests that there may be strong hydrogen bonding in the monoanion of this acid. However, the deuterium effect is relatively small. In this respect, this acid resembles γ-resorcylic acid which, according to Long and MacDougall,[11] also has a low pK_1, probably due to strong hydrogen bonding, but has a ΔpK of 0.56, near to the "normal" value for carboxylic acids. On the other hand, salicylic acid, which is probably less strongly internally hydrogen bonded, shows an abnormal ΔpK of 0.75. If these results are compared to those for the succinic acids, it appears that the abnormal deuterium effect shows up in moderately strong internal hydrogen-bonded acids but not in acids in which this bonding is very strong. There is no readily apparent explanation for these results.

Acknowledgment. The work on the measurement of the ionization constants was carried out under a grant from the Research Corporation.

(11) A. C. MacDougall and F. A. Long, *J. Phys. Chem.*, 66, 429 (1962).

Deuterium Isotope Effect in the Ionization of Substituted Malonic Acids in Water and in Deuterium Oxide

by Paul K. Glasoe and James R. Hutchison

Wittenberg University, Springfield, Ohio
(Received May 27, 1963)

In view of the abnormal deuterium isotope effect obtained in the ionization of maleic acid[1] and in the ionization of certain substituted succinic acids[2] having high K_1/K_2 ratios, it was considered of interest to study a series of alkyl-substituted malonic acids. These acids show a marked increase in the ratio of K_1 to K_2 when both malonic hydrogens are replaced by alkyl groups. The ratio for malonic acid is about 700 and that for diethylmalonic acid is 121,000. If the K_1/K_2 ratio and the abnormal deuterium isotope effect in ionization are related, the highly alkylated malonic acids, especially from diethylmalonic up, should show pronounced deuterium effects.

To examine this point, the ionization constants for a series of malonic acids were measured in water and in deuterium oxide. To get a measure of the effect of the alkyl substituents on the strength of the acid without the complication of electrostatic effects or hydrogen bonding between the oxygen of the monoanion and the second acid hydrogen, the ionization constants of some monoesters were also measured in the two solvents.

The malonic acids and the monoesters were prepared from the diethyl esters. The monoesters were obtained as sirupy liquids which were analyzed by titration and showed no detectable amount of the diacid.

Appropriate amounts of a standard solution of a particular malonic acid were mixed with standard base and the pH was measured with a glass electrode on a Beckman Model GS pH meter at 25°. To this solution was added a measured amount of the solvent to decrease the ionic strength and the pH was measured again. Usually five different concentrations were used. The same procedure was followed with water and with deuterium oxide, using solutions of comparable concentrations to produce nearly the same change in the ionic strength of the five solutions. The values for pD were obtained from the readings of the pH meter which had been standardized with water buffers by the addition of 0.40.

The pK values for the monoesters were obtained from pH titration curves of the monoesters with potassium hydroxide or potassium deuterium oxide in water or in deuterium oxide. In these titrations the solutions had ionic strengths less than 0.01.

The values for pK_1' and pK_2' were calculated in the same manner as described for the succinic acids. The calculated values of pK' were then plotted against $\sqrt{\mu}$. The value of pK obtained by extrapolation of the straight line to zero concentration is the value given in Table I.

The results are summarized in Table I. A value of $pK_D - pK_H$, listed as ΔpK, was computed from the zero ionic strength pK for the malonic acids and from

(1) G. Dahlgren, Jr., and F. A. Long, *J. Am. Chem. Soc.*, 82, 303 (1960).

(2) P. K. Glasoe and L. Eberson, *J. Phys. Chem.*, 68, 1560 (1964).

Table I

pK_1^H and pK_1^D for malonic acids

Alkyl group substituents	pK_1^H	pK_1^D	ΔpK	pK_1^H (lit.)
None	2.87	3.37	0.50	2.855[a]
Ethyl	2.96	3.46	0.50	2.961[b]
Isopropyl	2.92	3.43	0.51	2.93[c]
Phenyl	2.52	3.02	0.50	
Diethyl	2.21	2.70	0.49	2.150[b]
Ethylisopropyl	2.02	2.52	0.50	
Dibutyl	2.16	2.64	0.48	

pK_2^H and pK_2^D for malonic acids

	pK_2^H	pK_2^D	ΔpK	pK_2^H (lit.)	K_1/K_2
None	5.69	6.12	0.43	5.696[d]	660
Ethyl	5.81	6.28	0.47	5.83[c]	710
Isopropyl	5.88	6.36	0.48		910
Phenyl	5.59	5.96	0.47		1200
Diethyl	7.33	7.74	0.41	7.29[c]	132000
Ethylisopropyl	8.29	8.73	0.44		1900000
Dibutyl	7.70	8.23	0.53		350000

pK^H and pK^D for monoesters of malonic acids

	pK_E^H	pK_E^D	ΔpK_E	K_1/K_E
None	3.45	3.90	0.45	3.6
Ethyl	(3.35)[e]			
	3.43	3.90	0.47	3.0
Diethyl	3.70	4.13	0.43	32
Ethylisopropyl	3.87	4.34	0.47	71

[a] G. H. Jeffrey and A. I. Vogel, *J. Chem. Soc.*, 2156 (1936). [b] G. H. Jeffrey and A. I. Vogel, *ibid.*, 1756 (1936). [c] R. Gane and C. K. Ingold, *ibid.*, 1691 (1929). [d] W. J. Hamer, J. O. Burton, and S. F. Acree, *J. Res. Natl. Bur. Std.*, **24**, 269 (1940). [e] J. Walker, *J. Chem. Soc.*, **61**, 696 (1892).

pK' at comparable ionic strengths for the monoesters. It was found that there was no significant difference in the value for ΔpK computed from the zero ionic strength pK and that computed from pK' at essentially the same ionic strength.

There is no simple explanation for the fact that the "normal" deuterium effect is obtained with diethylmalonic and ethylisopropylmalonic acids, both of which have high K_1/K_2 and K_1/K_{ester} ratios. The steric effect of these large groups on the malonic carbon could promote H bonding in the monoanion by restricting rotation of the carboxyl groups and this could account for these high ratios. This is made more plausible by the fact that there is a large difference in the K_1/K_2 ratio of diethylmalonic acid compared to methylethylmalonic acid. Some preliminary measurements in this laboratory of infrared absorption by the monoanions of some substituted malonic acids in deuterium oxide solution show a considerable difference in H bonding in the diethyl acid anion compared to the monosubstituted acid anion. The situation with these acids may be similar to that with di-*t*-butylsuccinic acid and γ-resorcylic acid. The former gives a ΔpK_1 of 0.57 whereas that of tetraethylsuccinic acid is 0.90 and the latter gives ΔpK_1 of 0.56 whereas that of salicylic acid is 0.75.[3] It would be expected that the H bonding in di-*t*-butylsuccinic acid would be stronger than in tetraethylsuccinic acid and the H bonding in γ-resorcylic acid would be stronger than that in salicylic acid. These results strongly suggest that some effect other than H bonding must play an important role in the deuterium isotope effect. The situation is far from simple and such factors as electrostatic effects, solvation of the ions, and H bonding between molecules of solvent and between solvent molecules and the anion are probably all involved to some degree.

Acknowledgment. This work was supported by a grant from the Research Corporation.

(3) A. C. MacDougall and F. A. Long, *J. Phys. Chem.*, **66**, 429 (1962).

Hydrogen Ion Equilibria in Cross-Linked Polymethacrylic Acid–Sodium Chloride Systems

by Richard L. Gustafson

Rohm & Haas Company, Research Division, Philadelphia 37, Pennsylvania *(Received April 22, 1963)*

Although several workers have calculated apparent dissociation constants for polycarboxylic acids, relatively few attempts have been made to determine the thermodynamic dissociation constants of such materials. Michaeli and Katchalsky[1] have shown that the intrinsic dissociation constant of the monomer unit of a polymeric weak acid may be calculated by the relationship

$$K_a = \frac{\alpha}{1-\alpha} a_{H^+}{}^r e^{(\partial F/\partial \alpha)_x/kT} \qquad (1)$$

where α represents the degree of ionization of the functional groups, $a_{H^+}{}^r$ refers to the hydrogen ion activity in the resin phase, and the last term represents the con-

(1) I. Michaeli and A. Katchalsky, *J. Polymer Sci.*, **23**, 683 (1957).

tribution to the total free energy produced by the mutual interactions of charged functional groups on the polymer chains. Reasonably good agreement between calculated and experimental pH values was obtained by these authors in cases of polymethacrylic acid (PMA) gels of low cross linking in 0.008–0.5 *m* 1:1 salt solutions. Recently, Chatterjee and Marinsky[2] determined the intrinsic dissociation constants of PMA resins which were cross-linked with 1% and 5% divinylbenzene (DVB) in 0.1 and 0.3 *m* NaCl solutions. A value of $pK_a = 5.16 \pm 0.35$ was calculated, in fair agreement with a value of 4.85 which is obtained for isobutyric acid,[3] which may be considered to be the monomer unit of polymethacrylic acid.

In the present study values of K_a have been calculated by a different modification of eq. 1 from that employed in either of the aforementioned studies. Substitution of the Donnan equation

$$a_{H^+}{}^s a_{Cl^-}{}^s = a_{H^+}{}^r a_{Cl^-}{}^r e^{\pi \bar{V}_{HCl}/RT} \qquad (2)$$

into eq. 1 leads to the expression

$$K_a^* = K_a/\gamma_{Na^+}{}^r e^{\pi(\bar{V}_{NaCl} - \bar{V}_{HCl})/RT} \qquad (3)$$

$$= \frac{\alpha}{1-\alpha} \frac{m_{H^+}{}^s m_{Cl^-}{}^s \gamma_{H^+}{}^s \gamma_{Cl^-}{}^s}{m_{Cl^-}{}^r \gamma_{\pm}{}^{*2}} e^{(\partial F/\partial \alpha)_\kappa/RT}$$

Here π is the osmotic pressure, $\bar{V}$ is the partial molal volume, m is the ionic molality, γ is the molal activity coefficient, and

$$\gamma_{\pm}^* = (\gamma_{Na^+}{}^r \gamma_{Cl^-}{}^r e^{\pi \bar{V}_{NaCl}/RT})^{1/2} = (m_{Na^+}{}^s m_{Cl^-}{}^s \gamma_{Na^+}{}^s \gamma_{Cl^-}{}^s / m_{Na^+}{}^r m_{Cl^-}{}^r)^{1/2}$$

is the mean molal activity coefficient of NaCl in the resin phase. Superscripts r and s refer to resin and solution phases, respectively. Values of the electrostatic term were calculated by the relationship derived by Katchalsky and Michaeli.[4] Values of K_a^* have been determined at various degrees of neutralization in 1.0, 0.4, 0.1, and 0.02 *m* NaCl solutions at 25° for a PMA resin which contained 5% DVB as cross linker.

Experimental

The properties of the methacrylic acid polymer and the calculations of $\gamma_{\pm}^*$ were described in a previous publication.[5] Samples of H^+-form resin were equilibrated at 15.0, 25.0, and 35.0° with NaCl solutions which contained varying amounts of carbonate-free NaOH. Measurements of the hydrogen ion concentrations of the solution phases were made with a Beckman Model G pH meter equipped with extension glass and calomel electrodes. Calibration of the electrode system was made with standard hydrochloric acid, sodium hydroxide, and acetic acid–sodium acetate solutions which contained appropriate amounts of sodium chloride.

Results

Plots of $-\log [H^+]$ *vs.* $\log \alpha/(1-\alpha)$ in accordance with the empirical equation

$$-\log [H^+] = pK + n \log \frac{\alpha}{1-\alpha} \qquad (4)$$

were linear within ±0.01 pH unit over the α-range 0.2–0.75. The values of n and pK obtained at various ionic strengths and temperatures are summarized in Table I. The constancy of the pK values obtained at various temperatures at constant NaCl concentrations shows that no change in the degree of ionization is produced by a change in temperature at the two highest ionic strengths studied, although a small trend toward a decreasing degree of dissociation with increasing temperature is apparent at $\mu = 0.10$ and 0.02.

Table I: Values of pK and n for PMA–5% DVB Gel at Various Ionic Strengths at 15, 25, and 35°

Temp., °C.	μ, NaCl	pK	n
15	0.02	7.28	1.61
15	0.10	6.64	1.65
15	0.40	6.13	1.62
15	1.00	5.90	1.59
25	0.02	7.32	1.65
25	0.10	6.67	1.65
25	0.40	6.15	1.65
25	1.00	5.92	1.60
35	0.02	7.34	1.65
35	0.10	6.68	1.67
35	0.40	6.16	1.62
35	1.00	5.91	1.60

Determination of pK_a^*. The calculated values of pK_a^* and associated quantities are shown in Table II. Included for comparison are values of pK_a calculated on the basis of eq. 16a and 16b of Michaeli and Katchalsky.[1] Average values of pK_a^* in the range $\alpha = 0.1$–0.75 at various ionic strengths were found as follows: $\mu = 1.00$, $pK_a^* = 4.84 \pm 0.02$; $\mu = 0.40$, $pK_a^* = 4.81 \pm 0.02$; $\mu = 0.10$, $pK_a^* = 4.81 \pm 0.05$; $\mu = 0.02$, $pK_a^* = 4.79 \pm 0.06$. The results are in remarkably good agreement with the value of $pK_a = 4.85$ for isobutyric

(2) A. Chatterjee and J. A. Marinsky, *J. Phys. Chem.*, **67**, 41 (1963).
(3) D. H. Everett, D. A. Landsman, and B. R. W. Pinsent, *Proc. Roy. Soc.* (London), **A215**, 403 (1952).
(4) A. Katchalsky and I. Michaeli, *J. Polymer Sci.*, **15**, 69 (1955).
(5) R. L. Gustafson, *J. Phys. Chem.*, **67**, 2549 (1963).

Table II: Values of pK_a^* Calculated by Eq. 3 for Polymethacrylic Acid–5% DVB Resins in NaCl Solution at 25.0°

α	$\frac{(\partial F/\partial\alpha)_\kappa}{2.303kT}$	$-\log m_{H^+}{}^s$	$-\log m_{Cl^-}{}^r$	$-2\log\gamma_\pm{}^*$	$pK_a(16a)^a$	$pK_a(16b)^a$	$pK_a(3)^b$
		$\mu = 1.00$, $-\log m_{Cl^-}{}^s = 0.004$–$0.008$, $-\log \gamma_{H^+}{}^s\gamma_{Cl^-}{}^s = 0.248$					
0.107	0.145	4.35	0.321	0.257	4.86	4.80	4.79
0.214	0.249	4.99	0.327	0.380	4.97	4.97	4.84
0.320	0.342	5.40	0.345	0.428	5.00	5.04	4.86
0.427	0.431	5.73	0.368	0.445	5.01	5.05	4.86
0.534	0.514	6.00	0.385	0.456	4.99	5.03	4.83
0.641	0.593	6.30	0.409	0.467	4.99	5.04	4.82
0.748	0.668	6.67	0.432	0.476	5.04	5.09	4.86
0.854	0.738	7.23	0.452	0.491	5.20	5.26	5.02
		$\mu = 0.40$, $-\log m_{Cl^-}{}^s = 0.390$–$0.385$, $-\log \gamma_{H^+}{}^s\gamma_{Cl^-}{}^s = 0.274$					
0.107	0.167	4.58	0.758	0.399	4.93	4.97	4.84
0.214	0.282	5.21	0.792	0.526	4.99	5.09	4.84
0.320	0.384	5.62	0.832	0.567	5.00	5.12	4.83
0.427	0.476	5.95	0.869	0.588	4.99	5.12	4.81
0.534	0.561	6.24	0.899	0.609	4.97	5.11	4.77
0.641	0.640	6.59	0.917	0.636	5.01	5.17	4.81
0.748	0.713	6.92	0.938	0.658	5.02	5.18	4.80
0.854	0.811	7.49	0.951	0.684	5.16	5.34	4.93
		$\mu = 0.10$, $-\log m_{Cl^-}{}^s = 0.991$–$0.988$, $-\log \gamma_{H^+}{}^s\gamma_{Cl^-}{}^s = 0.206$					
0.107	0.187	5.10	1.476	0.652	5.13	5.35	4.90
0.214	0.308	5.74	1.562	0.745	5.16	5.42	4.89
0.320	0.412	6.14	1.622	0.797	5.13	5.42	4.83
0.427	0.504	6.47	1.655	0.842	5.12	5.43	4.79
0.534	0.589	6.77	1.679	0.883	5.10	5.43	4.76
0.641	0.667	7.08	1.694	0.919	5.11	5.46	4.74
0.748	0.741	7.46	1.705	0.957	5.16	5.53	4.78
0.854	0.806	8.01	1.712	0.993	5.32	5.71	4.92
		$\mu = 0.02$, $-\log m_{Cl^-}{}^s = 1.685$, $-\log \gamma_{H^+}{}^s\gamma_{Cl^-}{}^s = 0.118$					
0.107	0.194	5.75	2.483	0.887	5.36	5.68	4.91
0.214	0.317	6.39	2.592	0.979	5.31	5.73	4.83
0.320	0.421	6.79	2.652	1.033	5.27	5.73	4.82
0.427	0.513	7.12	2.703	1.064	5.24	5.72	4.77
0.534	0.597	7.42	2.733	1.105	5.22	5.72	4.73
0.641	0.675	7.73	2.712	1.184	5.25	5.78	4.71
0.748	0.747	8.11	2.731	1.218	5.30	5.85	4.75
0.854	0.814	8.68	2.706	1.287	5.49	6.08	4.91

[a] Calculated according to eq. 16a and 16b of ref. 1. [b] Calculated according to eq. 3.

acid. Although Michaeli and Katchalsky obtained good agreement between theory and experiment in cases of lightly cross-linked resins, poor agreement was obtained in the present study in cases in which either eq. 16a or 16b was employed. It is apparent that the assumptions concerning the calculations of the activity coefficients in the resin phase are not valid in the case of a moderately cross-linked polymer.

The good agreement between the calculated values of pK_a^* and the theoretical value of 4.85 is perhaps somewhat fortuitous since the value of the activity coefficient of the sodium ion in the resin phase is not a constant, but instead decreases with an increasing degree of neutralization. The transference and diffusion experiments of Huizenga, *et al.*,[6] have shown that the fraction of sodium ion bound to linear polyacrylic acid is approximately 0.23, 0.40, 0.52, and 0.60 at degrees of neutralization equal to 0.2, 0.4, 0.6, and 0.8, respectively. Inclusion of these values in eq. 3 would give

(6) J. R. Huizenga, P. G. Grieger, and G. T. Wall, *J. Am. Chem. Soc.*, 72, 4228 (1950).

values of $pK_a = pK_a^* - \log \gamma_{Na^+}{}^r$ which would be 0.06–0.40 unit greater than the values of pK_a^* listed in Table II in the range $\alpha = 0$–0.85. The calculation of the electrostatic term by the theory of Katchalsky and Michaeli[4] is based on the assumption that no interactions occur between neighboring chain segments. It is probable that such interactions do occur in the present case and that the actual values of $(\partial F/\partial \alpha)_\kappa$ are somewhat higher than the calculated values. The increases of pK_a^* observed at $\alpha = 0.75$ and 0.85 are perhaps produced by the increasing importance of neighboring chain interactions as the degree of neutralization increases. In general, the effects produced by neglect of the $\gamma_{Na^+}{}^r$ term and the lack of conformity to Katchalsky's assumptions seem to offset one another such that values of pK_a^* which are quite close to the theoretical value of 4.85 are obtained.

Discussion

Salt Sorption by Ion-Exchange Resins. The data of Table II show that the variation of NaCl sorption with a change in ionic strength at a constant degree of neutralization is such that the calculated values of the mean molal activity coefficient of NaCl in the resin phase decrease with decreasing μ and actually approach zero as the external electrolyte concentration approaches zero. Such behavior is contrary to that observed in aqueous solutions of simple electrolytes and has been the subject of a good deal of controversy in recent years.

The careful experimental work of Glueckauf and Watts[7] and others[5,8] has demonstrated that these "anomalous" variations in activity coefficients are not produced by occlusion of electrolyte on the bead surfaces or in internal cavities of the resin. However, disagreement still exists regarding the nature of the phenomenon which produces the abnormally high degree of electrolyte sorption at low ionic strengths. It has been suggested in a previous publication[5] that the degree of sodium ions in a polymethacrylate gel–sodium chloride system is essentially independent of ionic strength at salt concentrations below 0.4 *m* at a given value of α, whereas the degree of association of chloride ions increases with decreasing ionic strength. The good agreement which is obtained in the present study by the use of these "anomalous" activity coefficients, particularly at a constant value of α where the effects *of omission of the* $\gamma_{Na^+}{}^r$ *term and neglect of inter*-chain interactions are essentially constant at various ionic strengths, lends support to the above concept.

(7) E. Glueckauf and R. E. Watts, *Proc. Roy. Soc.* (London), **A268**, 339 (1962).

(8) J. S. Mackie and P. Meares, *ibid.*, **A232**, 485 (1955).

Interatomic Potential Energy Functions for Mercury, Cadmium, and Zinc from Vapor Viscosities

by K. Douglas Carlson and K. R. Kuschnir

Department of Chemistry, Case Institute of Technology, Cleveland, Ohio 44106 *(Received October 10, 1963)*

In connection with previous experiments,[1] we were led to consider the viscosity data of Hg, Cd, and Zn vapors. These have not been correlated successfully within the framework of molecular theory[2] for reasons suggested to involve the possibility that electronic excitations are important[2] and that the data are inaccurate.[3] The purpose of this note is to show that one of two sets of measurements of Hg appear to be reliable, that these data are in agreement with conclusions reached by Epstein and Powers,[3] and to show that the measurements for Hg, Cd, and Zn comprise a consistent set of data of limited precision which can be correlated approximately with an exp-6 function.

It is necessary first to consider the experiments. In 1883 Koch[4] reported 18 values of the viscosity of Hg measured by the transpiration method. These have a temperature dependence of $T^{1.6}$ from 543 to 650°K. In 1928, Braune, Basch, and Wentzel[5] reported 13 values for Hg in the range 491 to 883°K., values for Cd and Zn in smaller ranges, and measurements of bromine and air as a test of their oscillating disk method. The mercury viscosities have a temperature dependence of $T^{1.09}$. Thus, the two sets of Hg data are in serious disagreement. The measurements of Koch are unreliable owing to his crude apparatus and the lack of temperature control. Braune and associates paid close attention to the temperature problem, which is less severe in their method, and their results for air are in agreement with others. Therefore, their measurements appear to be reliable. These are represented graphically in Fig. 1.

Epstein and Powers[3] derived parameters for the Lennard-Jones 12–6 function for Hg: $\epsilon/k = 851 \pm 32$°K., $r_0 = 3.25 \pm 0.04$ Å. With the exclusion of

(1) K. D. Carlson, P. W. Gilles, and R. J. Thorn, *J. Chem. Phys.*, **38**, *2725 (1963)*.

(2) J. O. Hirschfelder, C. F. Curtiss, and R. B. Bird, "Molecular Theory of Gases and Liquids," John Wiley & Sons, Inc., New York, N. Y., 1954.

(3) L. F. Epstein and M. D. Powers, *J. Phys. Chem.*, **57**, 336 (1953).

(4) S. Koch, *Wied. Ann. Phys.*, **19**, 857 (1883).

(5) H. Braune, R. Basch, and W. Wentzel, *Z. Physik. Chem.*, **A137**, 176, 447 (1928).

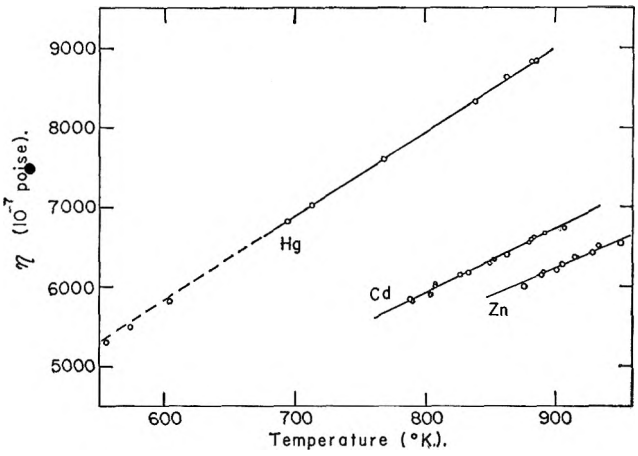

Figure 1. Vapor viscosity coefficients from measurements of Braune, Basch, and Wentzel. Three values for Hg at lower temperatures are not included. Solid lines represent viscosities calculated from the exp-6 function.

Koch's data, these yield viscosities having a root-mean-square deviation from experiment of ±1.8%. Their comparison shows a systematic discrepancy, amounting to theoretical values exceeding the experimental by 1.5% at low temperatures to values smaller by 1.5% at high temperatures. However, they conclude that these parameters are reasonable and that a potential function having a weaker repulsion term might give better agreement. To test this, we employed the modified Buckingham exp-6 function[2] with $\alpha = 12$ and the above parameters and obtained agreement within ±0.94%. Nevertheless, a similar systematic discrepancy is found. One expects further improvement with $\alpha < 12$, but calculations necessary to test this are unavailable.

It is necessary to consider the experimental precision. Viscosities measured at comparable temperatures differ by 0.5%. This is the precision of a single measurement. Furthermore, least-squares adjustments to several empirical equations fit the data within no better than ±0.4%. This is the precision to which the temperature dependence is defined. Therefore, the least-squares adjustment of the data to the Sutherland formula

$$\eta(10^{-7}\ \text{poise}) = kT^{1/2}/(1 + S/T) \qquad (1)$$

is satisfactory. Braune, *et al.*, report values of S to be 942.2, 1053, and 876°K. for Hg, Cd, and Zn, respectively, and except for the Zn data, which do not converge, these may be reproduced within 2% by a nonlinear analysis. The average temperatures $\langle T \rangle$ of the measurements are 680.7, 843.8, and 910.5°K. for Hg, Cd, and Zn. The seven high temperature data for Hg with $S = 970$°K. and $\langle T \rangle = 805.5$°K. fall in a range more comparable with the others. We consider these values for Hg and those for Cd and Zn to comprise a consistent set of data.

Then in view of the limited precision, we select $S/\langle T \rangle$ as the most probable values for comparison with published[6] theoretical ratios tabulated as a function of kT/ϵ for the exp-6 function with $\alpha = 12$. Because there is a maximum in these ratios, one obtains two values of ϵ/k appropriate to $\langle T \rangle$. The smaller of 850 and 1265°K. is selected for Hg, the average of 990 and 1212°K. is selected for Cd, and the larger of 695 and 1946°K. is selected for Zn. The equilibrium separation r_0 is obtained by scaling. The parameters and errors estimated from the spread in S are

$$\begin{aligned}
&\text{(Zn)}\ \epsilon/k = 1950 \pm 300\text{°K.};\ r_0 = 2.35 \pm 0.08\ \text{Å}.\\
&\text{(Cd)}\ \epsilon/k = 1100 \pm 100\text{°K.};\ r_0 = 3.02 \pm 0.08\ \text{Å}. \qquad (2)\\
&\text{(Hg)}\ \epsilon/k = 850 \pm 40\text{°K.};\ r_0 = 3.24 \pm 0.04\ \text{Å}.
\end{aligned}$$

Viscosities derived from these are represented by the solid lines in Fig. 1. It is easily demonstrated that this method is satisfactory for imprecise data by applying it to viscosities derived from the parameters (2). Note that the values for Hg are nearly identical with those selected by Epstein and Powers but are adjusted to the high temperatures. The low temperature data then are in disagreement, which may represent a systematic error in the experiments.

Spectroscopic dissociation energies[7,8] are reported to be 0.07, 0.09, and 0.25 e.v. for Hg, Cd, and Zn dimers. These are uncertain owing to difficulties in the interpretation of the diffuse bands, and they are in qualitative agreement with the viscosity values. However, Winans and Heitz[8] concluded that 0.07 e.v. ($\epsilon/k = 812$°K.) for Hg represents dissociation from states of comparable rotational energy. They give 0.146 ± 0.01 e.v. ($\epsilon/k = 1694 \pm 116$°K.) for D_0 at zero rotational energy. We find this value to be incompatible with the viscosity data and second virial coefficient of Hg vapor.[9] The situation for Zn and Cd may be comparable. Therefore, considerable uncertainty remains in the interpretation of the experimental data, if they are reliable.

(6) E. A. Mason, *J. Chem. Phys.*, 22, 169 (1954).

(7) A. G. Gaydon, "Dissociation Energies," Chapman and Hall, Ltd., London, 1953.

(8) J. G. Winans and M. P. Heitz, *Z. Physik*, **133**, 291 (1952); **135**, 406 (1953).

(9) W. T. Hick, *J. Chem. Phys.*, **38**, 1873 (1963).

The Entropy of Micellization: The Effect of Temperature and the Concentration of Gegenions on the Critical Micelle Concentration of Potassium Perfluorooctanoate

by Kōzō Shinoda and K. Katsura

Department of Chemistry, Faculty of Engineering, Yokohama National University, Minamiku, Yokohama, Japan
(Received October 18, 1963)

In the preceding paper, it was proposed to treat the micelle as a separate pseudo-phase whose dimensions are very small compared with those normally characteristic of macroscopic phases.[1] If the formation of micelle is akin to phase separation, it is possible to calculate the heat and entropy of micellization from the temperature dependence of the activity of micelle forming species.[1-5] Thermodynamic equations which relate the entropy of micellization and the temperature dependence of the critical micelle concentration (c.m.c.) under various conditions have been derived.[1] In the case when no salts are added, the entropy of micellization is given as follows: $\Delta S_m = \Delta H_m/T = -(1 + K_g)RT(\partial \ln \text{c.m.c.}/\partial T)$, where K_g is an experimental constant. Potassium perfluorooctanoate and potassium nitrate were the same materials used in the preceding surface tension study.[6] The c.m.c. was determined by the electrical conductivity method.

Results

The c.m.c. values as functions of temperature and the concentration of gegenions were determined. As the Krafft point of potassium perfluorooctanoate was 26°, the change of solubility with the concentration of gegenions was observed at 25°. Solid agent also appeared at the higher gegenion concentration at 30°. The results are plotted in Fig. 1. Filled circles express the solubility, not the c.m.c. The logarithm of the c.m.c. *vs.* the logarithm of the concentration of gegenions, C_3, was linear. The relation can be expressed as follows

$$\ln C_2 = K_g \ln C_3 + \text{constant} \qquad (1)$$

In the absence of added salts, $C_3 = C_2 = \text{c.m.c.}^0$, so that

$$(1 + K_g) \ln \text{c.m.c.}^0 = \ln C_2 + K_g \ln C_3 \qquad (2)$$

where K_g is the experimental constant and gradually changed with temperature. The c.m.c. (or solubility) of agent and K_g values are summarized in Table I.

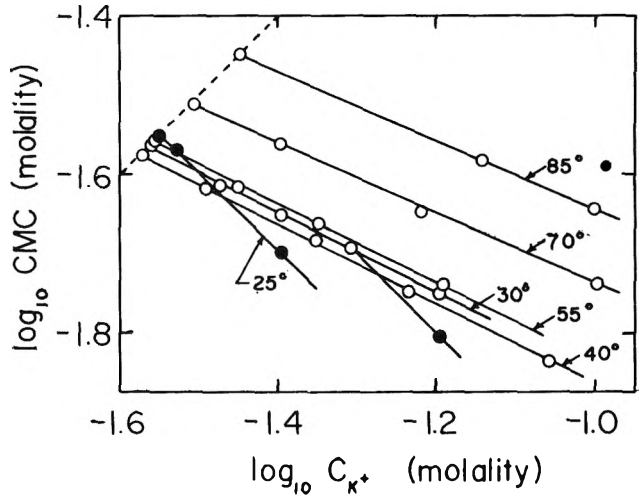

Figure 1. The effect of temperature and the concentration of gegenions on the c.m.c. in aqueous solutions of potassium perfluorooctanoate.

At the temperature where the solid agent appeared above the saturation concentration of single dispersion, K_g was, of course, close to 1.

Table I: The C.m.c. (or Solubility) and the Slope of log C_2 *vs.* log C_3 in Aqueous Solutions of Potassium Perfluorooctanoate and Potassium Nitrate

Temp., °C.	C.m.c., *m*	$K_g = -\frac{d \ln C_2}{d \ln C_3}$
25	0.0281 (solid)	0.98
25	0.0288 (supercooled micelle)	...
30	0.0274	0.52
40	0.0265	0.51
55	0.0276	0.49
70	0.0307	0.45
85	0.0354	0.43

Theory and Discussion

In solutions of ionic agents, the activity of the micelle forming species is a function of the concentrations of both surface active ions (component 2) and

(1) K. Shinoda and E. Hutchinson, *J. Phys. Chem.*, **66**, 577 (1962).
(2) G. Stainsby and A. E. Alexander, *Trans. Faraday Soc.*, **46**, 587 (1950).
(3) E. Hutchinson, A. Inaba, and L. G. Bailey, *Z. physik. Chem.* (Frankfurt), **5**, 344 (1955).
(4) E. Matijević and B. A. Pethica, *Trans. Faraday Soc.*, **54**, 589 (1958).
(5) B. D. Flockhart, *J. Colloid Sci.*, **16**, 484 (1961).
(6) K. Shinoda and H. Nakayama, *J. Colloid Sci.*, **18**, 705 (1963).

gegenions (component 3). Experimentally we know that eq. 2 holds, *i.e.*, the (electro)chemical potential of micelle forming species is expressed as

$$\bar{\mu}_{23} - \bar{\mu}_{23}^0 = RT(1 + K_g) \ln \text{c.m.c.}^0 + \text{constant} = RT \ln X_2 + RTK_g \ln X_3 + \text{constant} = -\Delta\bar{G}_m \quad (3)$$

where X_2 and X_3 are the concentration of surface active ions and gegenions expressed in mole fraction unit at the c.m.c. If we regard the micelle as a phase, the entropy and enthalpy of micellization is given as follows[1,7]

$$\Delta S_m = \frac{\Delta H_m}{T} = -RT\left[\left(\frac{\partial \ln X_2}{\partial T}\right)_{\Delta\bar{G}_m} + K_g\left(\frac{\partial \ln X_3}{\partial T}\right)_{\Delta\bar{G}_m}\right] \quad (4)$$

In the case where no salts are added, $X_2 = X_3$

$$\Delta S_m = \frac{\Delta H_m}{T} = -(1 + K_g)RT\left(\frac{\partial \ln X_2}{\partial T}\right)_{\Delta\bar{G}_m} \quad (5)$$

If X_3 is kept constant the second term in eq. 4 is zero

$$\Delta S_m = -RT\left(\frac{\partial \ln X_2}{\partial T}\right)_{\Delta\bar{G}_m X_3} \quad (6)$$

If the ratio of X_2 to X_3 is kept constant in the presence of salt, relation 5 also holds.

The entropy of micellization was calculated from the temperature dependence of the c.m.c. under the condition of a definite concentration of gegenions. The values are summarized in Table II.

Table II: The Entropy of Micellization in Aqueous Solution of Potassium Perfluorooctanoate

Temp., °C.	ΔS_m, e.u.	C_2, *m*	ΔS_m, e.u.	C_2, *m*
27.5	9.9	(0.028)	. . . . .	
35	3.1	(0.027)	2.6	(0.063)
47.5	−2.5	(0.027)	−2.9	(0.063)
62.5	−7.0	(0.029)	−8.1	(0.063)
77.5	−9.6	(0.033)	−10.5	(0.063)

As the concentration of gegenions is kept constant, the activity of gegenions is constant and the activity of micelle forming species is dependent only on the concentration of surface active ions. The above values are, as can be seen in eq. 5 and 6 or in Fig. 1, equal to the temperature dependence of the c.m.c. multiplied by $1 + K_g$ in the absence of added salts.

Hence, it is shown that the entropy of micellization can be calculated from the temperature dependence of the c.m.c. under a definite concentration of gegenions. In order to obtain the entropy of micellization from the temperature dependence of the c.m.c. in the absence of added salts, it is necessary to determine the K_g value as shown in eq. 5.

(7) K. Shinoda in "Colloidal Surfactants," Academic Press, Inc., New York, N. Y., 1963, Chapter 1, p. 35.

Cobaltous Ion in Alumina

by M. G. Townsend

Mullard Research Laboratories, Redhill, Surrey, England
(Received October 25, 1963)

The spin-orbit and trigonal-field splitting of the octahedral field ground state $^4{}_aT_1$ of Co^{2+} may be described by the Hamiltonian[1]

$$W = \Delta(l_z^2 - {}^2/_3) - \alpha\lambda l_z S_z - \alpha'\lambda(l_x S_x + l_y S_y) \quad (1)$$

where λ (the spin-orbit coupling parameter) $= -180$ cm.$^{-1}$, $l = 1$, $\alpha = \alpha' = 1.5$ in the weak field limit and 1 in the strong field limit, and Δ is the trigonal-field splitting.

Electron spin resonance (e.s.r.) measurements by Zverev and Prokhorov[2] on Co^{2+} in Al_2O_3 showed evidence for Co^{2+} ions in two different sites, those normally occupied by Al^{3+} ions and vacant octahedral sites, present in the Al_2O_3 lattice. For the substitutional site they found, on the assumption that α, α' were the same for both sites, $\Delta = +760$ cm.$^{-1}$, $\alpha = 1.32$, and $\alpha' = 1.38$. Geusic's[3] measurements indicated only the presence of a substitutional site. The point-group site symmetry of the Al^{3+} ions in Al_2O_3 is strictly C_3 but approximates very closely to C_{3v}.[4]

In the present work an attempt is made to evaluate α, α', and v, the one-electron trigonal-field parameter, for the excited $^4{}_bT_1$ state, from the recorded optical absorption spectrum. Certain inferences are drawn from this spectrum, and the mechanism of charge compensation occurring in the crystals is investigated.

(1) A. Abragam and M. H. L. Pryce, *Proc. Roy. Soc.* (London), **A206**, 173 (1951).

(2) G. M. Zverev and A. M. Prokhorov, *Soviet Phys. JETP*, **12**, 41 (1961).

(3) J. E. Geusic, *Bull. Am. Phys. Soc.*, **11**, 4, 261 (1959).

(4) D. S. McClure, *J. Chem. Phys.*, **36**, 2757 (1962).

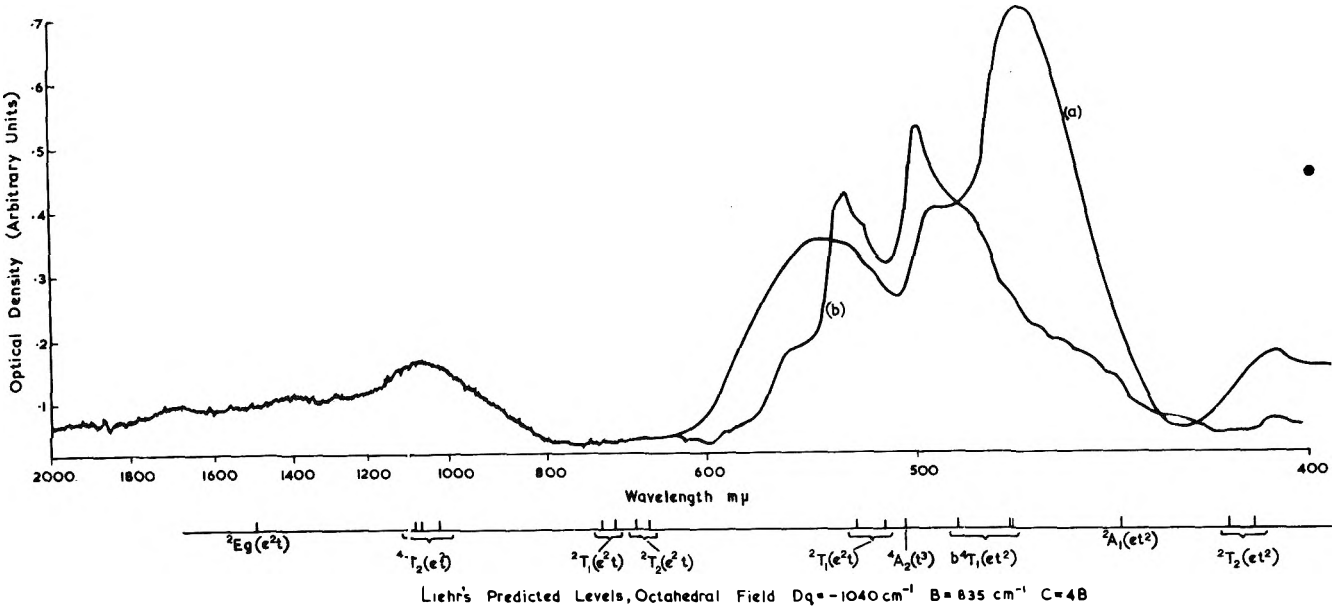

Figure 1. Co^{2+}–Al_2O_3, absorption spectrum, 110°K.: (a) E $\|$ c-axis; (b), E $\perp$ c. The infrared and visible spectra were recorded using different detectors.

Sturge[5] predicted the trend but not the absolute magnitudes of v for the series V^{2+}, Cr^{3+}, and Mn^{4+} ($3d^3$) in Al_2O_3, using McClure's point charge model.[4] Displacement of oxygen ions due to substitution of ions of different valence from those they replace, and covalence effects were accounted for by multiplying the averages $\langle r^n \rangle$ obtained from the free ion wave functions by a scale factor ρ^n where $\rho^4 = \langle r^4 \rangle_{crystal} / \langle r^4 \rangle_{free\ ion}$, and $\langle r^4 \rangle_{crystal}$ is estimated from the experimental magnitude of Dq.

Using this model and evaluating $\langle r^2 \rangle$ and $\langle r^4 \rangle$ from Watson's Hartree–Fock wave functions,[6] we calculate a value $v = +150$ cm.$^{-1}$ for Co^{2+}. No significance can be attached to this absolute value but the model suggests, in variance with experiment,[2] that v is less than that found for V^{2+}, Cr^{3+}, and Mn^{4+}, *i.e.*, $< +450$ cm.$^{-1}$.[5] Recently, Macfarlane[7] has shown the importance of the second trigonal-field parameter v'.

Pink single crystals of Al_2O_3 doped with approximately 0.02% by weight of cobalt were grown by slow cooling from a lead oxide–lead fluoride melt. E.s.r. measurements at 4.2°K. with a spectrometer operating at 1 cm. wave length using phase-sensitive detection with 100 kc./sec. modulation showed one set of eight hyperfine lines centered at $g_{\|} \simeq 2.32$, $g_{\perp} \simeq 4.95$. These measurements are in agreement with Geusic's[3] and indicate the presence of Co^{2+} in a substitutional site. No other resonance apart from a very weak absorption due to Fe^{3+} was detected.

The absorption spectrum of these crystals, polarized in the visible region, using HN22 polaroid filters, and recorded at 110°K. in a Perkin–Elmer 4000A double beam spectrophotometer, is shown in Fig. 1.

Liehr[8] has diagonalized the spin-orbit matrices of the complete Co^{2+} configuration in an octahedral field. The extension of this calculation to include the trigonal field has not been attempted here. Instead, the intense broad absorption bands have been approximately fitted to the excited quartet spin states predicted by Liehr's energy diagram with $Dq = -1040$ cm.$^{-1}$, $B = 835$ cm.$^{-1}$, and $C = 4B$, Fig. 1.

These values of Dq and B have been used to calculate the intermediate coupling of the $^4{}_bT_1(^4P)$ and $^4{}_aT_1(^4F)$ weak field states. The divergence of α, α' for $^4{}_aT_1$ from the weak field limiting value 1.5 depends mainly on the cubic-field admixture of $^4{}_bT_1$ into $^4{}_aT_1$. Mixing of excited states into the $^4{}_aT_1$ state by the trigonal field should have a relatively less important effect.[1] Neglecting this last interaction we have calculated isotropic values $\alpha = \alpha' = 1.34$, in good agreement with the values obtained from e.s.r.[2]

The matrices of the Coulombic, cubic, and trigonal field operators between the $^4{}_aT_1$, $^4{}_bT_1$, $^4A_2$ (^4F), and $^4T_2$ (^4F) states[7] have been used to calculate, to first order in trigonal field, the trigonal-field splittings of $^4{}_aT_1$

(5) M. D. Sturge, *Phys. Rev.*, **130**, 639 (1963).

(6) R. E. Watson, "Tech. Rept. No. 12," Solid State and Molecular Theory Group, Massachusetts Institute of Technology, Cambridge, Mass., June, 1959.

(7) R. M. Macfarlane, *J. Chem. Phys.*, **39**, 3118 (1963).

(8) A. D. Liehr, *J. Phys. Chem.*, **67**, 1314 (1963).

and $^4{}_bT_1$. These are $v - v'$ and $v/2 + 0.7v'$, respectively.

Expressing α and α'[1] in terms of v and v', by using first-order perturbation theory, and varying v' from 0 to 1000 cm.$^{-1}$ with $\Delta = 760$ cm.$^{-1} = v - v'$, suggests that $\alpha' - \alpha = 0.06$[2] for $v' \simeq 100$ cm.$^{-1}$ and $v \simeq 860$ cm.$^{-1}$.

The $^4{}_aT_1$ and $^4{}_bT_1$ states both split in trigonal field with spin-orbit coupling to give six Kramers doublets. Spin-lattice relaxation measurements suggest that, for $^4{}_aT_1$, the ground state Kramers doublet $E_{1/2}$[4] lies 110 cm.$^{-1}$ below the next doublet, $E_{3/2}$.[9] Consequently, at 110°K. 80% of the ions should be in the $E_{1/2}$ state, and at 293°K., 67%. In addition electric-dipole transitions to upper levels from the $E_{3/2}$ first excited state should increase by over 50% on warming from 110 to 293°K.

The room-temperature absorption spectrum is broader and much less well resolved, but the intensity ratios of the absorption bands appear to be approximately the same, as at 110°K. As a result we assume that the observed bands arise mainly from transitions from the $E_{1/2}$ ground state.

In C_{3v} symmetry the following selection rules are predicted: $E_{1/2} \rightarrow E_{1/2}$ ($E \parallel + E \perp c$-axis), $E_{1/2} \rightarrow E_{3/2}$ ($E \perp c$-axis).[4]

Using (1) with $\Delta = v/2 + 0.7\,v'$ and $\alpha = \alpha' = -0.89$ the spin-orbit and trigonal field splitting of $^4{}_bT_1$ has been calculated for a wide range of the parameters v and v'. Using the energy matrices of the quartet spin states,[7] the position of $^4A_2$ relative to the $^4{}_bT_1$ state, for the appropriate values of the parameters chosen, has also been calculated.

Attempts to correlate the fine structure of the intense, broad, visible absorption band, Fig. 1, with the calculated levels were unsatisfactory. Discrepancies between the theoretical and experimental spin-orbit splitting of the $^4{}_bT_1$ state in octahedral field for Co^{2+} in MgO were found previously.[8,10]

In this connection Liehr[8] has summarized the incompleteness of simple ligand field theory in crystalline media.

Alternatively the fine structure of the visible band could arise from weaker superimposed, sharp absorption bands due to doublet spin states of the same configuration (te^2) as the ground state. [The states here, and in the following, are described, in the strong-field limit, by their subshell configurations in the "hole" scheme.] However, the sharp band at 18,900 cm.$^{-1}$ occurs with $E \perp c$-axis, and it can be shown that all doublet spin states would give a transition with $E \parallel c$.

In the C_{3v} spinor group $^2E[C_{3v}]$ becomes $E_{1/2} + E_{3/2}$. These two states can mix, by second-order spin-orbit coupling and the trigonal field, with $E_{1/2}$ and $E_{3/2}$ [$^4E(^4{}_bT_1)$], respectively, to give transitions with $E \parallel + E \perp c$-axis. Splitting of the resultant absorption lines arising from this second-order splitting of ^2E would be small. Similarly, $^2A_1$ and $^2A_2[C_{3v}]$ should both give transitions with an $E \parallel c$-axis component.

Using McClure's[4] point charge model with p-d mixing, and his values of the potential field constants for Al_2O_3, the relative intensities of the electric-dipole transitions from the ground state doublet to the six doublets of the $^4{}_bT_1$ state have been calculated. From these results, by comparison with Fig. 1, tentative assignments of the main observed transitions have been made, as shown in Table I. The doublets in the first column of Table I are in increasing order of energy as calculated with $v = 860$ and $v' = 100$ cm.$^{-1}$. The intensity ratios have been calculated using separately the dipolar and octupolar parts of the anion field. Their interference, which cannot be estimated because of the uncertainty in the ratio of $\langle r \rangle / \langle r^3 \rangle$, will produce a resultant value in between the two extreme calculated values.

Table I: Calculated Relative Intensity

Excited state	Dipolar terms only		Octupolar terms only		Energy of observed transition, cm.$^{-1}$	
	$\parallel$	$\perp$	$\parallel$	$\perp$	$\parallel$	$\perp$
$E_{1/2}$	4.5	0	0.05	0	18650	
$E_{3/2}$	0	0.1	0	0.2		18900
$E_{1/2}$	0	0	0	0		
$E_{3/2}$	0	0.3	0	0.5		20000
$E_{1/2}$	0.75	0	0.1	0	21500	
$E_{1/2}$	3.5	0	1.5	0		

Transitions to the $^4A_2(t^3)$ state may be relatively weak, since they involve a two-electron jump, and their intensity depends upon the trigonal field mixing of the $^4A_2(t^3)$ with the $^4A_2[^4{}_bT_1(t^2e)]$ states. We have neglected this mixing as the value of v'/v,[4] and the exact position of $^4A_2(t^3)$ is uncertain. However, the broad band at 18,650 cm.$^{-1}$ is probably due in part to the $^4A_2$ state.

The $^4T_2(t^2e)$ absorption band does not split in polarized light, using HR polaroid filters. Similar effects were noted for the $^3T_2(et)$ band of Cu^{3+}[11] and the $^3T_2(et)$ band of V^{3+}[4] in Al_2O_3. For Cu^{3+} Blumberg, *et al.*,[11] suggested a spin-orbit splitting of comparable magnitude masked the trigonal-field splitting. Mc-

(9) G. M. Zverev and N. G. Petelina, *Soviet Phys. JETP*, **15**, 820 (1962).

(10) R. Pappalardo, D. L. Wood, and R. C. Linares, *J. Chem. Phys.*, **35**, 2041 (1961).

Clure[4] proposed for V^{3+} that the $^3T_2$ state was distorted into a configuration of lower symmetry. Evidence was found for this distortion for $^4T_2(et^2)$ of Cr^{3+} in Al_2O_3.[4]

The measured oscillator strength[4] of the infrared band $f \simeq 1.7 \times 10^{-4}$; for the visible band, E $\perp$ c, $f \simeq 10.8 \times 10^{-4}$, and E $\|$ c, $f \simeq 22.5 \times 10^{-4}$. These values are of the same order as those of Co^{3+} in Al_2O_3[4] and 100-fold greater than those of Co^{2+} in MgO.[10] This is reasonable since Al_2O_3 in contrast to MgO is non-centrosymmetric.[4]

Pink crystals with extensive localized green areas were grown from a lead oxide–lead fluoride melt using as solute Al_2O_3 doped with 0.02% Co + 0.02% Mg. Their optical spectrum is characteristic of Co^{3+}[4] together with that of Co^{2+}, Fig. 2. Apparently, in these crystals, Mg^{2+} is required to charge compensate for Co^{3+}. The mechanism of charge compensation operating on substitution of Al^{3+} by Co^{2+} in Al_2O_3 crystals is complex and most probably depends upon the technique of sample preparation.

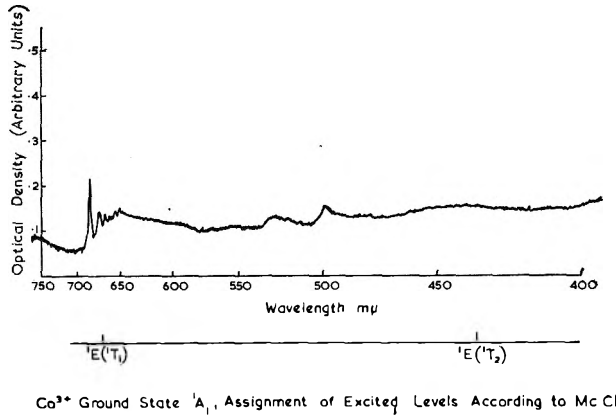

Figure 2. Visible absorption spectrum of Co^{2+} + Co^{3+} in Al_2O_3 at 110°K., E $\perp$ c.

Zverev and Prokhorov[2] did not describe their method of crystal growth. They observed two resonance signals of relative intensity 2:1 and deduced that for every two Co^{2+} ions substituting for Al^{3+} ions, a third Co^{2+} ion was in an interstitial site.

Alternatively one Al^{3+} ion in an interstitial site could compensate for $3Co^{2+}$ ions in substitutional sites. A glance at the crystal structure[12] shows that, providing two Co^{2+} ions are not substituted in adjacent Al^{3+} sites, this normally gives only one Co^{2+} site. A second site occurs when an Al^{3+} ion is in an interstitial site adjacent to a Co^{2+} ion, if the degree of association $\leq 100\%$, the statistical ratio of the two sites is $\geq 2:1$.

In the present work e.s.r. measurements detected only one, a substitutional, Co^{2+} site. Chemical analysis showed that the concentrations of impurities (F, Pb) were insufficient to account for compensation by mechanisms such as F^- replacing O^{2-} or Pb^{4+} replacing Al^{3+}.

To clarify this problem further e.s.r. measurements with more sensitive equipment are planned.

Acknowledgment. The author thanks Mr. O. F. Hill, who prepared the crystals, and Dr. J. W. Orton, who made the e.s.r. measurements.

(11) W. E. Blumberg, J. Eisinger, and S. Geschwind, *Phys. Rev.*, **130**, 900 (1963).

(12) S. Geschwind and J. P. Remeika, *J. Appl. Phys.*, **33**, 1, 370 (1962).

Calculated Effect of Bond Magnetic Anisotropy on the Methyl Group in Some Cyclohexanes[1a]

by I. Yamaguchi[1b] and S. Brownstein

Division of Applied Chemistry, National Research Council, Ottawa, Canada *(Received October 30, 1963)*

Proton resonance studies of some methylcyclohexanes have revealed unusual chemical shifts for both ring and methyl protons.[2] Previous calculations have only considered the effect of the carbon–carbon bond anisotropy upon shielding and could not explain the observed chemical shifts.[2-4] In this investigation carbon–hydrogen as well as carbon–carbon bond anisotropies were considered. Calculations of the shielding effect of bond anisotropy upon the methyl protons of a molecule in the chair form were made using the formula of McConnell.[5] All pairs of carbon–carbon and carbon–hydrogen bonds were included in the calculations except for the carbon–hydrogen bonds in the methyl group. The positions of the point magnetic dipoles on the bonds were assumed as in the study of Narasimhan and Rogers,[6] and the anisotropy was assumed to be cylindrically symmetrical about the bonds. The ratio of the carbon–hydrogen to carbon–carbon bond

(1) Issued as N. R. C. No. 7961; (b) National Research Council Postdoctorate Fellow, 1962–1963.

(2) N. Muller and W. C. Tosch, *J. Chem. Phys.*, **37**, 1167 (1962).

(3) A. A. Bothner-By and C. Naar-Colin, *Ann. N. Y. Acad. Sci.*, **70**, 833 (1958).

(4) J. I. Musher, *J. Chem. Phys.*, **35**, 1159 (1961).

(5) H. M. McConnell, *ibid.*, **27**, 226 (1957).

(6) P. T. Narasimhan and M. T. Rogers, *ibid.*, **31**, 1302 (1959).

anisotropies has not been experimentally determined, but theoretical calculations suggest a ratio of about 0.75. The present calculations were made for anisotropy ratios of 1.00, 0.75, 0.50, 0.25, and 0. Numerical integration was performed for free rotation of the methyl protons around the carbon–methyl bond.

The geometry of the substituted cyclohexanes in this study is such that both chair conformations are identical. Therefore, it is reasonable to compare the chemical shift observed at room temperature with the averaged value of the calculated results for axial and equatorial substituents. Only with *trans*-1,3-dimethylcyclohexane, which shows separate peaks for axial and equatorial methyl groups at low temperature, can calculated and experimental results be compared for the individual conformations. In Fig. 1 the observed

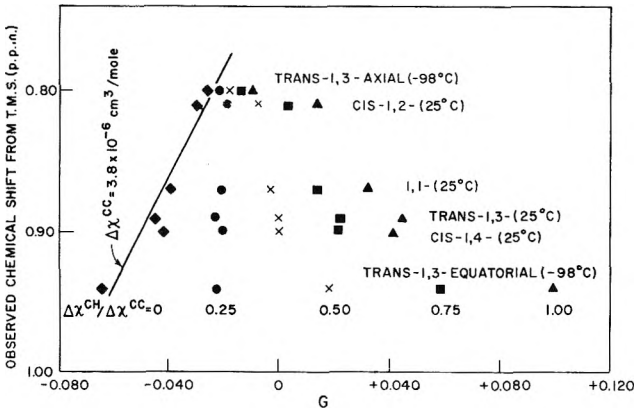

Figure 1. Observed and calculated methyl chemical shifts.

chemical shifts of the methyl protons are plotted against the calculated geometrical factor of the anisotropy effect, G, as a function of $\Delta\chi^{CH}/\Delta\chi^{CC}$. $G = \Sigma\,(g_{CC} + \alpha g_{CH})$, where $g = (1 - 3\cos^2\theta)/3r^3$ and $\alpha = \Delta\chi^{CH}/\Delta\chi^{CC}$. From the slope of the line for each value of α, $\Delta\chi^{CC}$ may be obtained. It is 3.8×10^{-6} cm.^{3}/mole for $\alpha = 0$ and even larger for $\alpha > 0$. When α is greater than about 0.25 the calculated values of $\Delta\chi^{CC}$ become negative. This possibility seems unlikely from the results of theoretical[7,8] and experimental studies.[3,6,9,10] Therefore, other effects at least comparable in magnitude to the effect of bond anisotropy must be influencing the chemical shift of the methyl groups.

In addition to spectra of the compounds listed in Fig. 1, the spectra of 1,1,3,3,5,5-hexamethylcyclohexane and 1,3-*trans*-di-*t*-butylcyclohexane in carbon disulfide solution were observed between −120 and 25°. Throughout this temperature range only a single peak was observed for the methyl groups in each compound. *trans*-1,3-Dimethylcyclohexane appears unique as the only methylcyclohexane with an observable chemical shift between axial and equatorial methyl groups. The reason for this is not obvious. Greater resolution at low temperature than previously reported[2] has allowed calculation of chair–chair inversion rates from peak coalescence.[11] For the *trans*-1,3 isomer $\Delta H^* = 4.8 \pm 0.1$ kcal./mole and log $A = 6.7$. The chemical shift of the methine protons as a function of temperature was obtained by proton double resonance techniques.[12] Little change with temperature was noted except for *cis*-1,4-dimethylcyclohexane where τ decreased from 8.32 at 25° to 8.14 at −110°.

Acknowledgment. The authors thank Prof. N. Allinger and Prof. R. Y. Levina for kindly supplying samples of 1,3-di-*t*-butylcyclohexane and 1,1,3,3,5,5-hexamethylcyclohexane. Mr. M. Bednas purified, by gas chromatography, most of the compounds used in this investigation.

(7) J. Guy and J. Tillieu, *J. Chim. Phys.*, **24**, 1117 (1956).
(8) J. Tillieu, *Ann. phys.* (Paris), **2**, 471 (1957).
(9) R. F. Zürchen, *Helv. Chim. Acta*, **44**, 1755 (1961).
(10) A. G. Monitz and N. Sheppard, *Mol. Phys.*, **5**, 361 (1962).
(11) H. S. Gutowsky and C. H. Holm, *J. Chem. Phys.*, **25**, 1228 (1956).
(12) R. Kaiser, *Rev. Sci. Instr.*, **31**, 963 (1960).

Measurement of Formal Oxidation–Reduction Potentials of Cerium(IV)–Cerium(III) System in Acetonitrile

by G. Prabhakar Rao and A. R. Vasudeva Murthy

Department of Inorganic and Physical Chemistry, Indian Institute of Science, Bangalore 12, India
(Received November 4, 1963)

It has been observed by the present authors that a solution of ammonium hexanitratocerate in acetonitrile functions as a versatile oxidant. Analytical procedures have been standardized in the case of hydroquinone,[1,2] potassium iodide,[2] ascorbic acid,[3] oxalic acid,[4] xanthate,[5] and ferrous salts[6] dissolved in acetonitrile or a mixture

(1) G. P. Rao and A. R. V. Murthy, *Z. anal. Chem.*, **180**, 169 (1961).
(2) G. P. Rao and A. R. V. Murthy, *ibid.*, **182**, 358 (1961).
(3) G. P. Rao and A. R. V. Murthy, *ibid.*, **187**, 96 (1962).
(4) G. P. Rao and A. R. V. Murthy, *ibid.*, **195**, 406 (1963).
(5) G. P. Rao and A. R. V. Murthy, *ibid.*, **177**, 86 (1960).
(6) G. P. Rao and A. R. V. Murthy, unpublished observations in these laboratories.

of acetonitrile and glacial acetic acid. Oxidation–reduction indicators such as ferroin, diphenylamine, methyl red, and janus green function as useful indicators to register the end point in the titrations. Potentiometric titrations can easily be carried out in all these cases making use of bright platinum as the indicating electrode while glass or antimony electrodes could serve as reference electrodes. The interesting feature of this nonaqueous cerimetry is that there is no need for the presence of a strong mineral acid in such systems, and the cerate solutions in acetonitrile can be stored without deterioration for a considerably long period. It was, therefore, of interest to measure the oxidation–reduction potential of ceric–cerous system in nonaqueous medium employing the usual potentiometric method.

In the present investigation, oxidation–reduction potentials have been measured employing silver–silver nitrate (0.01 *M* in acetonitrile) (Pleskov's reference electrode) and aqueous–saturated calomel electrodes as reference half-cells. The other half-cell consisted of ceric–cerous mixtures in acetonitrile. The formal oxidation–reduction potentials of these systems have been measured and are reported in this communication.

Experimental

Reagents and Apparatus. A standard solution of ammonium hexanitratocerate (0.025 *M*) was prepared in acetonitrile and its exact strength was determined against a standard solution of hydroquinone taken in acetonitrile as described earlier.[1,2]

Solutions of cerous salt of known concentrations were obtained by reducing the ceric reagent with oxalic acid in acetonitrile,[4] to prepare suitable ceric–cerous mixtures.

Cerous perchlorate was prepared[7] and solutions of appropriate molarities were prepared in acetonitrile to study the formation of cerous complex.

Silver–Silver Nitrate Cell in Acetonitrile. An all-glass cell fitted with appropriate ground-glass joints similar in design to that described by Britton[8] was found to be convenient to serve the present purpose. The capacity of the cell was limited to about 20 ml.; the cell was filled with 0.01 *M* silver nitrate solution in acetonitrile. A pure silver wire on which a thin coating of fresh crystals of silver was electroplated was introduced into the cell.[9]

Potentials were measured with a Leeds and Northrup potentiometer at 25 ± 0.2° in an air thermostat. A Hilger Uvispeck H700 spectrophotometer was used for spectral measurements of cerous complexes.

Procedure. Mixtures containing both ceric and cerous salt in various proportions were put in the titration cell fitted with an appropriate lid having inlets for the insertion of electrodes. The contents were stirred well for 10–15 min. with the help of a magnetic stirrer. A bright platinum electrode was inserted into the solution and potential measurements were made of the following two cells.

$$\mathrm{Ag/AgNO_3(0.01\ \textit{M}\ in\ acetonitrile)} \;\Big|\; \mathrm{Ce(IV)}(C_2) + \mathrm{Ce(III)}(C_1) \;\Big|\; \mathrm{Pt} \quad (1)$$
(in acetonitrile)

$$\mathrm{Hg,\ Hg_2Cl_2(s),\ saturated\ KCl} \;\Big|\; \mathrm{KCl\ agar\text{–}agar\ bridge} \;\Big|\; \mathrm{Ce(IV)}(C_2) + \mathrm{Ce(III)}(C_1) \;\Big|\; \mathrm{Pt} \quad (2)$$
(in acetonitrile)

Oxidation–Reduction Potential against Silver–Silver Nitrate Reference Electrode. The measured potentials (*E*) *vs.* $Ag/AgNO_3$ electrode using cell 1 were plotted against log Ce(IV)/Ce(III) (Fig. 1). It can be seen that a straight line is obtained in agreement with the

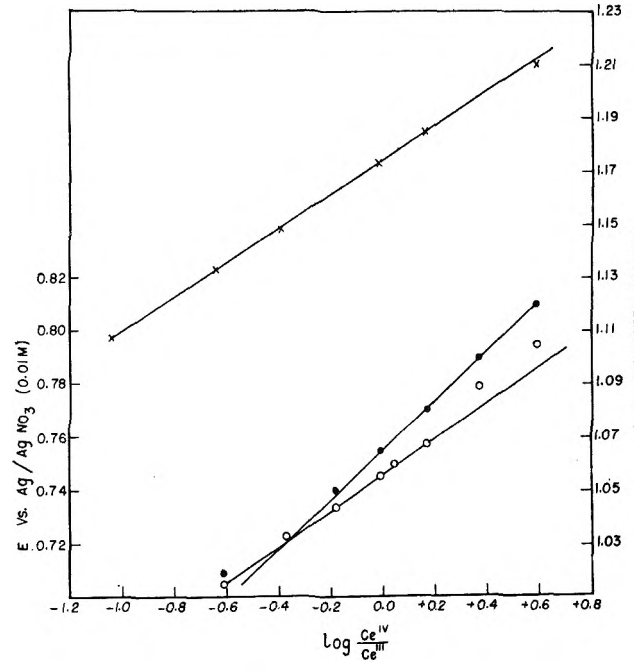

Figure 1. Variation of oxidation–reduction potential with log Ce(IV)/Ce(III): cell 1, ●–●–●; cell 2, O–O–O; cell 4, ×–×–×. The scale of the left-hand ordinate refers to cell 1 and that at the right-hand ordinate refers to the cells 2 and 4.

(7) L. J. Heidt and J. Berestecki, *J. Am. Chem. Soc.*, **77**, 2049 (1955).

(8) H. T. S. Britton, "Hydrogen Ions," Chapmann and Hall, London, 1955, p. 35.

(9) A. Findlay, "Experimental Physical Chemistry," Longmans, Green, and Co., 1955, p. 254.

Nernst equation: $E = E_0 + RT/nF \log$ Ce(IV)/Ce(III). The formal oxidation–reduction potential of the system Ce(IV)–Ce(III) was observed to be 0.755 ± 0.002 v. *vs.* $Ag/AgNO_3$ half-cell given by the point on the graph corresponding to the ratio of oxidant to reductant equal to unity, *i.e.*, log Ce(IV)/Ce(III) = 0.

Oxidation–Reduction Potential against Aqueous Saturated Calomel Electrode. When a similar graph was drawn with measured potentials (E) *vs.* aqueous saturated calomel electrode against log Ce(IV)/Ce(III) using cell 2, a straight line was obtained. The formal oxidation–reduction potential in this case was found to be 1.056 ± 0.002 v. This value corresponds to 1.300 ± 0.002 v. on the standard hydrogen scale (1.056 + 0.244).

For purposes of comparison of the potential measurements made in nonaqueous medium with the measurements involving aqueous medium, it became necessary to measure the potential of the system silver–silver nitrate in acetonitrile with reference to a saturated calomel electrode.

Hg, Hg_2Cl_2(s) saturated KCl	KCl agar–agar bridge	
	$AgNO_3$(0.01 M in acetonitrile)	Ag (3)

The potential of this system was found to be 0.300 v. at 25°. This value was found to be quite stable and reproducible, and compared favorably with the value reported by Adams, *et al.*[10]

It is possible to compute the formal oxidation–reduction potential of the following system from the experimental values obtained using cells 1 and 3.

Hg, Hg_2Cl_2(s) saturated KCl	KCl agar–agar bridge	
	Ce(IV)(C_2) + Ce(III)(C_1) in acetonitrile	Pt

This can easily be seen to be the algebraic sum of the potentials obtained in the two systems *viz.*, 0.755 + 0.300 = 1.055 v. The same potential has been observed with cell 2. Thus, the computed formal potential is in very good agreement with the experimentally observed value, although the liquid-junction potential in these systems may not be the same. This value corresponds to 1.299 v. on the standard hydrogen scale.

Oxidation–Reduction Potential in Acetonitrile and Acetic Acid Mixed Solvents. While studying several oxidation–reduction reactions with cerate in acetonitrile with various types of reducing agents in the same solvent, it was found advantageous to add glacial acetic acid to the system. Such an addition helped in detecting sharp color changes with different oxidation–reduction indicators. Steep jumps and reproducible stable potential readings could be registered when the titrations were conducted potentiometrically. It was, therefore, of interest to find the effect of glacial acetic acid on the oxidation–reduction potential of the

Hg, Hg_2Cl_2(s) saturated KCl	KCl agar–agar bridge	
	Ce(IV)(C_2) + Ce(III)(C_1) in acetonitrile + varying amounts of glacial acetic acid	Pt (4)

system. Cell 4 was used for this purpose. The formal potential of the above system was measured first in pure acetonitrile and subsequently in the presence of glacial acetic acid at different concentrations. The measurements of the formal potential were made in the first instance by keeping the ratio of ceric–cerous concentrations the same. It was observed that the potential value in the presence of acetic acid was slightly higher than the corresponding value observed in the pure solvent. The potential increased with increasing concentration of acetic acid in the mixture. When the concentration of acetic acid was more than 1000 times the concentration of cerium, it was noted that a steady value was attained. Similar observations were made with systems having different ratios of ceric–cerous reagents.

The plot of the measured potentials (E) *vs.* log Ce(IV)/Ce(III) is also included in Fig. 1. The formal oxidation–reduction potential of this system was found to be 1.174 v. corresponding to 1.418 v. on the standard hydrogen scale.

The observed increase in the formal oxidation–reduction potential of Ce(IV)–Ce(III) system from 1.300 v. in acetonitrile to 1.418 v. in the presence of glacial acetic acid was found to be due to the complex formation of cerous ion with glacial acetic acid. Owing to this complex formation, it is possible that the value of the ratio log Ce(IV)/Ce(III) increases, which consequently results in an increase in the formal oxidation–reduction potential of the system. The complex formation of cerous salt with glacial acetic acid was confirmed by examining the ultraviolet absorption spectra of cerous ion in pure acetonitrile and in the presence of varying amounts of glacial acetic acid.

Cerous perchlorate in acetonitrile (10^{-4} M solution) exhibits three absorption peaks around 220, 234, and 264 mμ and a shoulder around 252 mμ. It has been

(10) R. C. Larson, R. T. Iwamoto, and R. N. Adams, *Anal. Chim. Acta*, 25, 371 (1961).

observed that the peak around 264 mμ is sensitive to acetic acid concentration. With the increase in the concentration of acetic acid, the intensity of this peak increases considerably, suggesting possible complex formation. It may be mentioned that these results are in general agreement with those reported by Benson and Sutcliffe,[11] who have also observed complex formation between cerous ion and acetate in acetic acid media. It is, therefore, reasonable to expect a reduction in the concentration of cerous species and consequent increase in the oxidation–reduction potential of ceric–cerous system in the presence of acetic acid.

Acknowledgment. G. P. R. is indebted to the University Grants Commission of India for the award of a research fellowship.

(11) D. Benson and L. H. Sutcliffe, *Trans. Faraday Soc.*, **56**, 246 (1960).

Radiolysis of Methane-C^{14} [1]

by William P. Hauser

Radiation Research Laboratories, Mellon Institute, Pittsburgh, Pennsylvania (*Received November 6, 1963*)

Within recent years the radiation chemistry of methane has received considerable attention.[2-12] Although some insight into the mechanism has been obtained, the role of the products as intermediates in the radiolysis of methane still remains a question. In this respect the yield of ethylene in pure methane radiolysis and in the radiolysis of methane with added scavengers is of interest. Values for the yields of ethylene produced when pure methane is irradiated generally range from 0.004 to 0.3 molecule/100 e.v.[4-7,11] although recently yields have been reported which linearly increase from 0.3 to 3 molecules/100 e.v. as the pressure is reduced from 800 to ~3 mm.[10] In addition, a significant dose rate dependence of ethylene production has been observed at 5 mm. pressure.[10] When methane is irradiated in the presence of added nitric oxide,[5,11] oxygen,[10] or unsaturated hydrocarbons,[10] the ethylene yield is enhanced (G = 0.6–1.5 at initial pressures near 1 atm.). This suggests that when pure methane is irradiated, the ethylene produced participates in secondary reactions.

The present study was undertaken to determine the initial yield of ethylene and the role of products in methane radiolysis. The radiolysis of pure methane labeled with carbon-14 was first examined at low conversion. Methane-C^{14} was then irradiated in the presence of small amounts of added unlabeled ethylene in order to determine the initial yield of ethylene-C^{14}. (The unlabeled ethylene was added to protect from further reaction any ethylene-C^{14} produced during the radiolysis.) Unlabeled methane was also irradiated in the presence of added ethylene-C^{14} to determine the fate of ethylene in methane radiolysis.

Experimental

Research grade methane and ethylene were obtained from Phillips Petroleum Co. Methane was further purified by repeated sublimation from −182 to −196° and irradiation in the liquid phase with 2.8-Mev. electrons. After subsequent sublimation during which sizeable end fractions were discarded the sample was degassed on activated charcoal held at −196°. Analysis by mass spectrometry and gas chromatography, using a molecular sieve column, indicated that impurities were less than 0.001% except for nitrogen which was less than 0.03%. Ethylene was passed through a trap at −78° and was thoroughly degassed at −196°. Ethylene-C^{14} (≅0.1 mc./mmole) previously purified at this laboratory[13] was used without further purification. Methane-C^{14} was obtained from Volk Radiochemical Co. (specific activity, 1 mc./mmole) and from New England Nuclear Corporation (specific activity, 2 mc./mmole). The 1 mc./mmole sample was purified by irradiation with Co^{60} γ-rays to remove traces of oxygen. Similarly the 2 mc./mmole sample was purified by irradiation with 2.8-Mev. electrons; however, even after extensive irradiation carbon monoxide produced from oxygen impurity could not be eliminated in this sample. Samples were prepared for each experiment by expanding methane-C^{14} from the storage bulb held at −196° into a known

(1) Supported, in part, by the U. S. Atomic Energy Commission.

(2) L. H. Gevantman and R. R. Williams, Jr., *J. Phys. Chem.*, **56**, 569 (1952).

(3) G. G. Meisels, W. H. Hamill, and R. R. Williams, Jr., *ibid.*, **61**, 1456 (1957).

(4) F. W. Lampe, *J. Am. Chem. Soc.*, **79**, 1055 (1957).

(5) K. Yang and P. J. Manno, *ibid.*, **81**, 3507 (1959).

(6) G. J. Mains and A. S. Newton, *J. Phys. Chem.*, **65**, 212 (1961).

(7) J. Maurin, *J. Chim. Phys.*, **59**, 15 (1962).

(8) R. R. Williams, Jr., *J. Phys. Chem.*, **66**, 372 (1962).

(9) P. J. Ausloos and S. G. Lias, *J. Chem. Phys.*, **38**, 2207 (1963).

(10) R. W. Hummel, *Discussions Faraday Soc.*, to be published.

(11) L. W. Sieck and R. H. Johnsen, *J. Phys. Chem.*, **67**, 2281 (1963).

(12) P. J. Ausloos, S. G. Lias, and R. Gorden, Jr., *J. Chem. Phys.*, **39**, 3341 (1963).

(13) R. A. Holroyd and G. W. Klein, *J. Am. Chem. Soc.*, **84**, 4000 (1962).

volume followed by dilution with sufficient unlabeled methane to provide a pressure of about 100 mm. in the irradiation cells. When the irradiated 1 mc./mmole sample was used, the diluted sample contained less than 0.03% nitrogen. No oxygen or carbon monoxide was detected by gas chromatography. When the 2 mc./mmole sample was used, resulting mixtures contained between 0.1 and 0.03% nitrogen and less than 0.01% carbon monoxide.

Samples were irradiated at 25° with the electron beam (energy, 2.8 Mev.) of a Van de Graaff accelerator at a dose rate of approximately 2.6×10^{20} e.v.-min./g. of CH_4. The dose rate was determined from ethylene dosimetry. Pure ethylene at 300 mm. was irradiated in the cells used for methane radiolysis and the yields of hydrogen and acetylene were measured. The dose rate was then calculated from these measured yields and the values $G(H_2) = 1.2$ and $G(C_2H_2) = 2.4$ reported by Sauer and Dorfman.[14] Each of two spherical irradiation cells used (304 ml. and 317 ml.) were made of Pyrex glass and were each fitted with a brass Hoke valve (Type R1247) by means of a glass–Kovar seal. In the case of experiments involving pure methane, the sample was expanded directly into the cell. For experiments involving added ethylene, the ethylene was first condensed in the cell followed by methane. The cell was closed and then brought to room temperature. The sample was allowed to mix for 30 min. before the cell was opened and the pressure measurement made.

Analysis of radiolysis products was carried out by gas chromatography using a proportional counter to measure the activity of the effluent from the thermal conductivity detector. Details of the counting and recording techniques are similar to those described elsewhere.[15] All but a small amount of methane (> 0.01 mm.) was transferred by means of a Toepler pump from the reaction cell, kept at −196°, through a spiral trap also kept at −196°, and into a trap connected directly to the gas chromatographic unit. A portion of the methane was analyzed with a 2.5-m. molecular sieve column to determine concentrations of oxygen, nitrogen, and carbon monoxide in the sample. The reaction products were then transferred into the same trap and were subsequently separated using a 5-m. column of tetraisobutylene on a firebrick base along with a 2.5-m. temperature programed column of silica gel. To aid in identification of activity peaks, unlabeled hydrocarbons were added to the reaction mixture before separation. A blank analysis was carried out on the unirradiated portion of the methane sample to determine the extent of residual activity due to trace quantities (<0.001%) of high activity ethane and ethylene and when necessary, corrections were made accordingly on the results of the product analysis.

Results and Discussion

Products of pure methane-C^{14} radiolysis which were generally measured were ethane, ethylene, acetylene, propane, and propylene. Other products which were detected included hydrogen, butanes, butenes, and pentanes. Values of $G(C_2H_6)$ in methane radiolysis were determined using ethylene dosimetry; however, the ethane yield was not reproducible (due probably to error introduced in the irradiation procedure). To circumvent this problem, yields of other products were determined relative to the amount of ethane produced in a given experiment. Table I presents values of product yields in pure methane-C^{14} radiolysis at 100 mm. pressure where the absorbed dose varies by a factor of 130. The average yield of ethane is 1.5 ± 0.3[16] molecules/100 e.v. and the average relative yield of propane is 0.17 ± 0.02. The average values for the yield of ethane is in good agreement with values (G = 1–2.2) reported previously[4-7,10-12] although

Table I: Product Yields in Pure Methane-C^{14} Radiolysis at 100 mm. Pressure

Absorbed dose, (e.v./g. of CH_4) × 10^{-19}	$G(C_2H_6)$ molecules/ 100 e.v.	C_2H_4/C_2H_6[c]	C_2H_2/C_2H_6[c]	C_3H_8/C_2H_6[c]	C_3H_6/C_2H_6[c]
2[a]	1.2	0.38	0.032	0.20	0.074
2	1.4	0.49	...	0.16	0.091
4	1.9	0.18	...	0.17	0.063
9	1.4	0.12	...	0.15	0.038
26	1.0	0.071	...	0.19	0.019
43[b]	2.4	0.048	0.014	0.14	0.012
43	1.2	0.061	...	0.16	0.017
86	1.5	0.029	...	0.19	0.009
260	1.8	0.017	...	0.15	...

[a] The 2 mc./mmole sample of methane-C^{14} was used in this experiment. Other experiments listed here employed the 1 mc./mmole sample. [b] Relative yields of other products measured in this experiment are: $(i\text{-}C_4H_{10}/C_2H_6) = 0.021$; $(n\text{-}C_4H_{10}/C_2H_6) = 0.029$; $(i\text{-}C_4H_8/C_2H_6) = 0.005$; $(1\text{-}C_4H_8 + 2\text{-}C_4H_8)/C_2H_6 \cong 0.005$; $(i\text{-}C_5H_{12}/C_2H_6) = 0.015$, and $(\text{neo-}C_5H_{12}/C_2H_6) \cong 0.006$. [c] It should be recognized that anything which influences the experimental ethane yield will have a proportionate influence on the relative yields of other products.

(14) M. C. Sauer, Jr., and L. M. Dorfman, *J. Phys. Chem.*, **66**, 322 (1962).

(15) R. A. Holroyd and G. W. Klein, *J. Appl. Radiation Isotopes*, **13**, 493 (1962).

(16) Deviations of values presented in this study are mean deviations.

it is somewhat lower than values (G = 1.9–2.2) reported most recently.[10-12] In this respect it is of interest to note that Sieck and Johnsen[11] observed a slight increase in $G(C_2H_6)$ as pressure is decreased to 100 mm. and also a decrease as the amount of conversion of methane is reduced below 0.2%. The present study was carried out at 100 mm. and ordinarily below 0.2% conversion; however, no decrease in $G(C_2H_6)$ could be observed. The relative yield of propane (C_3H_8/C_2H_6 = 0.17) is in excellent agreement with the relative yields 0.18 and 0.16 which were calculated from the results of methane radiolysis reported, respectively, by Hummel[10] and Sieck and Johnsen.[11] The yield of ethylene increases by a factor of more than 20 with decreasing dose. The calculated absolute yield (calculated from the relative yield and $G(C_2H_6)$ = 1.5) increases from 0.03 to 0.7 molecule/100 e.v. in good agreement with previous values reported by Hummel.[10] The observed increase indicates that ethylene is undergoing rapid secondary reactions in methane radiolysis and that an initial yield greater than 1 is not unreasonable. Previously, propylene has been reported only in studies where methane was irradiated in the presence of added gases[3,5,10,11] or at elevated temperatures.[7] In the present study of pure methane-C^{14} radiolysis propylene was measured. The calculated absolute yield of propylene rises from 0.01 to 0.1 molecule/100 e.v. as the dose decreases. It appears that propylene like ethylene is an important intermediate in methane radiolysis and possibly a primary molecular product. The yield of acetylene also appears to increase with decreasing dose (from G = 0.02 to G = 0.05); however, there is insufficient evidence in this study to substantiate the increase.

Unlabeled methane at 500 mm. pressure was irradiated in the presence of a trace ($\cong$0.006%) of ethylene-C^{14}. Labeled ethane, propane and n-butane were produced along with the usual unlabeled products. (Other labeled products appeared including isobutane, but they were not measured.) For a dose of 1.1×10^{20} e.v./$g._{CH_4}$, the yield of unlabeled ethane is 0.8 molecule/100 e.v. and the yield of ethane-C^{14} is 0.4 molecule/100 e.v. The yield of labeled propane is 0.3 molecule/100 e.v., whereas the yield of unlabeled propane is approximately zero. The yield of labeled n-butane is between 0.1 and 0.2 molecule/100 e.v. (depending on whether two ethylenes or one ethylene participate in the formation of n-butane). No labeled propylene was observed. Since in the course of this experiment a large fraction of the labeled ethylene was consumed, values of product yields presented here are somewhat qualitative; nevertheless these results have some significance. Ethane was produced from ethylene to an extent which is difficult to explain by a free radical mechanism which involves the scavenging of hydrogen atoms followed by the disproportionation combination of the resulting ethyl radicals. Not enough n-butane was observed to justify this process. A possible explanation for the formation of ethane from ethylene is the termolecular combination reaction of hydrogen atoms with ethyl radicals in the presence of a third body as suggested by Sieck and Johnsen.[11] A large portion of propane also appears to have resulted from ethylene. It is possible that propane formed from ethylene-C^{14} could have masked any propane ordinarily formed by other mechanisms. However, since a significant amount of propane-C^{14} was produced by the addition of only 0.006% of ethylene-C^{14}, it is plausible that ethylene is important in the formation of propane in methane radiolysis. These results as well as results of the radiolysis of CD_4–C_2H_4 mixtures carried out by Ausloos and Lias[9] are consistent with a mechanism involving the scavenging of hydrogen atoms with ethylene to form ethyl radicals followed by the combination reaction of ethyl and methyl radicals. The fact that no labeled propylene was observed precludes the possibility of ethylene as an intermediate in its formation. Acetylene could be an intermediate in the formation of propylene as suggested by Hummel[10]; however, there is no direct evidence in the present study to substantiate the suggestion.

The irradiation of methane-C^{14} at 100 mm. in the presence of unlabeled ethylene was studied at a low degree of conversion to prevent the labeled ethylene produced from being consumed; as a result only labeled products could be measured. Calculations could be made only for products where labeling was unambiguous, namely for ethylene, ethane, acetylene, and to some extent for propane. The yields of labeled ethane and the relative yields of labeled ethylene are presented in Table II. During the course of the experiment usually some of the labeled ethylene was consumed along with the unlabeled ethylene. A correction equivalent to the per cent of unlabeled ethylene consumed was applied to the labeled ethylene produced (final column, Table II). This is a maximum correction; however, the fraction of ethylene consumed was ordinarily small and the error resulting from the correction is not expected to be significant. The average yield of labeled ethane is 1.2 $\pm$ 0.3 molecules/100 e.v., and the average corrected relative yield of labeled ethylene is 0.94 $\pm$ 0.08. (The fifth experiment in the table was neglected since an excessive amount of added ethylene was consumed.) The average value for the yield of ethane-C^{14} observed here is lower than the average value observed for pure meth-

Table II: Yields of Ethane-C^{14} and Ethylene-C^{14} from the Radiolysis of Methane-C^{14} at 100 mm. Pressure in the Presence of Added Ethylene

% C_2H_4 added	Absorbed dose (e.v./g. of CH_4) $\times 10^{-19}$	$G(C^{14}{}_2H_6)$, molecules/100 e.v.	$C^{14}{}_2H_4/C^{14}{}_2H_6$	$C^{14}{}_2H_4$ (cor.)/$C^{14}{}_2H_6$
0.17	2	0.66	0.98	0.98
0.06	4	1.7	0.57	0.84
0.05	2	0.83	0.85	0.85
0.04	9	1.2	0.71	0.99
0.04[a]	43	1.9	0.07	1.16
0.03	2	1.1	0.91	0.91
0.03	2	1.7	0.76	0.93
0.02	2	1.5	0.66	0.86
0.02	2	0.85	0.73	1.14

[a] The 1 mc./mmole sample of methane-C^{14} was used in this experiment. Other experiments listed here employed the 2 mc./mmole sample.

ane-C^{14} radiolysis (G = 1.5). However, it is not unreasonable since, as demonstrated by the results of the methane–ethylene-C^{14} radiolysis, some ethane is produced from ethylene. (The yield of unlabeled ethane produced from unlabeled ethylene was not measured in the ethylene–methane-C^{14} radiolysis.) Using the value of 1.2 for the yield of ethane-C^{14}, the initial yield of ethylene is then 1.1 molecules/100 e.v.[17] Other labeled products obtained in the radiolysis of methane-C^{14} in the presence of unlabeled ethylene included acetylene, propane, propylene, and isobutene. If propane is considered to be singly labeled as suggested by the results of the methane–ethylene-C^{14} experiment, then an enhanced relative yield, ($CH_3CH_2C^{14}H_3/C^{14}{}_2H_6$) = 1.6, is obtained. Assuming complete labeling, the yields of unsaturates also appear to be enhanced: *i.e.*, ($C^{14}{}_2H_2/C^{14}{}_2H_6$) = 0.1; ($C^{14}{}_3H_6/C^{14}{}_2H_6$) = 0.2; and ($i$-$C^{14}{}_4H_8/C^{14}{}_2H_6$) = 0.08. (These yields are approximate and could be in error by more than 50%.) The yields of propane and unsaturates are expected to be high, however, due to the relatively large quantities of added ethylene present during the radiolysis.

The present study clearly demonstrates that both ethylene and propylene are important products in methane radiolysis. Ethylene appears to be a primary molecular product with an initial yield of approximately 1.1 molecules/100 e.v.; however, a significant fraction of the ethylene produced is converted during the radiolysis to ethane and propane. Propylene was produced in the radiolysis of pure methane and in radiolysis of methane in the presence of added ethylene. It appears that propylene is not formed from ethylene during the radiolysis.

Acknowledgment. The author wishes to express his appreciation to Dr. Richard Holroyd for helpful discussions on this study.

(17) If a value of 2 is assumed for the yield of ethane in methane radiolysis and if, as is suggested by the methane–ethylene-C^{14} results, one third of the ethane observed is produced from ethylene then the initial yield of ethylene calculated from its relative yield is 1.3 molecules/100 e.v. which is in agreement with values (G = 1.4 and 1.5) suggested previously[10] in studies of the irradiation of methane in the presence of added propylene and acetylene, respectively.

Dissociation of the Bisulfate Ion[1]

by H. S. Dunsmore

Chemistry Department, The University, Glasgow W. 2, Scotland

and G. H. Nancollas

Chemistry Department, Brookhaven National Laboratory, Upton, New York *(Received November 8, 1963)*

The second dissociation constant of sulfuric acid, K_2, has been the subject of extensive study and discussion. The bisulfate ion is relatively highly dissociated and in calculating the thermodynamic equilibrium constant, which may be approximated by

$$\log K_2 = \log \frac{[H^+][SO_4^{-2}]}{[HSO_4^-]} - 4A\left\{\frac{I^{1/2}}{1 + B\mathring{a}I^{1/2}} - CI\right\} \quad (1)$$

much depends upon the choice of parameters, $\mathring{a}$ and C, in the activity coefficient expression.[2,3] In eq. 1, I is the ionic strength, and A and B are the usual Debye–Hückel constants.

Some of the earliest work on sulfuric acid was that of Sherrill and Noyes,[4] who combined transference number and conductance data and obtained a value K_2 = 0.0115 mole $l.^{-1}$ at 25°. Assuming the first hydrogen to be completely ionized, they expressed the degree of dissociation, α, by the equation

(1) Research performed in part under the auspices of the U. S. Atomic Energy Commission.

(2) V. S. K. Nair and G. H. Nancollas, *J. Chem. Soc.*, 4144 (1958).

(3) W. J. Hamer in "The Structure of Electrolyte Solutions," W. J. Hamer, Ed., John Wiley and Sons, Inc., New York, N. Y., 1959, p. 236.

(4) M. S. Sherrill and A. A. Noyes, *J. Am. Chem. Soc.*, **48**, 1861 (1926).

$$\alpha = (\Lambda + \Lambda T - \Lambda_H)/(\Lambda_H + \Lambda_{SO_4})$$

$$\Lambda_{HSO_4} = (\Lambda - \Lambda T - \alpha\Lambda_{SO_4})/(1 - \alpha)$$

where T is the stoichiometric transference number, and for the sulfuric acid solution, Λ is the observed conductance and Λ_H, Λ_{SO_4}, and Λ_{HSO_4} are the equivalent conductances of H^+, SO_4^{2-}, and HSO_4^- ions, respectively. The dissociation quotient K_2' ($= [H^+]\cdot[SO_4^{2-}]/[HSO_4^-]$) was calculated at each ionic strength, and K_2 was obtained by extrapolation on a plot of log K_2' against $I^{1/2}$. Kerker[5] has extended the calculations to other temperatures and to ionic strengths as high as 4.43 M. The method, however, is open to serious objection since it is impossible to correct for ion pairing in such concentrated sulfate solutions with any certainty. In addition it was assumed that the equivalent conductances of H^+ and SO_4^{-2} ions could be obtained from HCl and K_2SO_4 data at the same ionic strength as that prevailing in the sulfuric acid solution under consideration. Using a high-speed DEUCE electronic computer we have recalculated the conductance and transference number data for concentrations below 0.05 m. The K_2' values are in close agreement with those obtained by Kerker,[5] although the calculated Λ_{HSO_4}, given in Table I, show marked differences. Λ_H and Λ_{SO_4} at each concentration were interpolated from ionic strength plots of HCl and K_2SO_4 conductance data. The steepness of these curves made estimation difficult at $I < 0.01$ M and, taking this into consideration, the best extrapolated $K_2 = 0.0104$ mole kg.$^{-1}$; Kerker[5] obtained 0.0102 mole kg.$^{-1}$.

Table I: The Dissociation Constant and Equivalent Conductance of HSO_4^- at 25°

$M_{H_2SO_4} \times 10^3$	5.00	6.25	12.50	25.00	50.00
$10^2K_2'$ (this work)	1.67	1.75	2.06	2.55	3.36
Λ_{HSO_4} (this work)	41.7	41.6	40.2	39.0	38.0
$10^2K_2'$ (Kerker)	1.69	...	2.09	2.53	3.38
Λ_{HSO_4} (Kerker)	46.8	...	45.3	39.8	38.7

A number of electromotive force studies have been made in cells without liquid junction of the type H_2, Pt|HCl, X|AgCl, Ag. Hamer,[6] using X = Na_2SO_4, obtained $K_2 = 0.0120$ mole kg.$^{-1}$ which was in poor agreement with 0.0104 from spectrophotometry.[7] Moreover, the temperature coefficient led to a heat of ionization, $\Delta H^\circ = -2.2$ kcal. mole^{-1}, very different from the calorimetric value, -5.2 kcal. mole^{-1}, of Pitzer.[8] Davies, Jones, and Monk[9] have recalculated Hamer's e.m.f. data with allowance for the formation of $NaSO_4^-$ ion pairs and obtained $K_2 = 0.0102$ mole kg.$^{-1}$. Mixed acid cells in which X = H_2SO_4 do not suffer from the disadvantage of secondary-ion association and two such studies have been made.[2,10] The derived K_2 value is markedly dependent upon the choice of parameters in eq. 1; assuming $B\mathring{a} = 1$, all the data have been recalculated using the computer programmed to yield the C value for zero slope of K_2 *vs.* I plots, a least-squares procedure being used. The results are summarized in Table II. Although Monk[10] had suggested that, using $C = 0.2$, there was a definite change with ionic strength in the K_2 values obtained by Nair and Nancollas, it is quite clear that a common $C = 0.36$ yields self-consistent K_2 values for all the available e.m.f. data. The use of $C = 0.3$ in the Davies equation

Table II: The Dissociation Constant of HSO_4^- at 25°

	Davies, Jones, and Monk[a]	Nair and Nancollas[b]
Best C value	0.36	0.36
Mean $K_2 \times 10^2$	1.020 ± 0.013	1.046 ± 0.009

[a] See ref. 10. [b] See ref. 2.

for activity coefficients has already been proposed by Davies[11] in the light of recent activity data. When X = H_2SO_4, plots of K_2 against I for different C values give a series of converging curves with the best C showing zero slope. For the sake of comparison, the computer program was then altered to set $C = 0$ and vary $B\mathring{a}$. Another series of convergent curves of K_2 *vs.* I was obtained, with $B\mathring{a} = 1.59$ giving zero slope and $K_2 = 0.0102$, again by a least-squares procedure. This leads to a value of 4.8 for $\mathring{a}$ and extrapolated K_2 values ranging from 0.0109 for $B\mathring{a} = 1$ to 0.0092 for $B\mathring{a} = 2.5$. This is shown in Fig. 1. Hamer observed nonconvergency of log K_2 *vs.* I plots of his data (X = Na_2SO_4) when various $\mathring{a}$ values were inserted in the activity coefficient expression, but he omitted using the same parameter in the calculation of H^+ activity as he used in the calculation of SO_4^{-2} activity. Recalculation of Hamer's data

(5) M. Kerker, *J. Am. Chem. Soc.*, **79**, 3664 (1957).

(6) W. J. Hamer, *ibid.*, **56**, 860 (1934).

(7) I. M. Klotz and C. R. Singleterry, Theses, University of Chicago, 1940; quoted by R. A. Robinson and R. H. Stokes, "Electrolyte Solutions," Butterworth and Co., Ltd., London, 1959.

(8) K. S. Pitzer, *J. Am. Chem. Soc.*, **59**, 2365 (1937).

(9) C. W. Davies, H. W. H. Jones, and C. B. Monk, *Trans. Faraday Soc.*, **48**, 921 (1952).

(10) C. B. Monk, "Electrolytic Dissociation," Academic Press, London, 1961.

(11) C. W. Davies, "Ion Association," Butterworth and Co., Ltd., London, 1962.

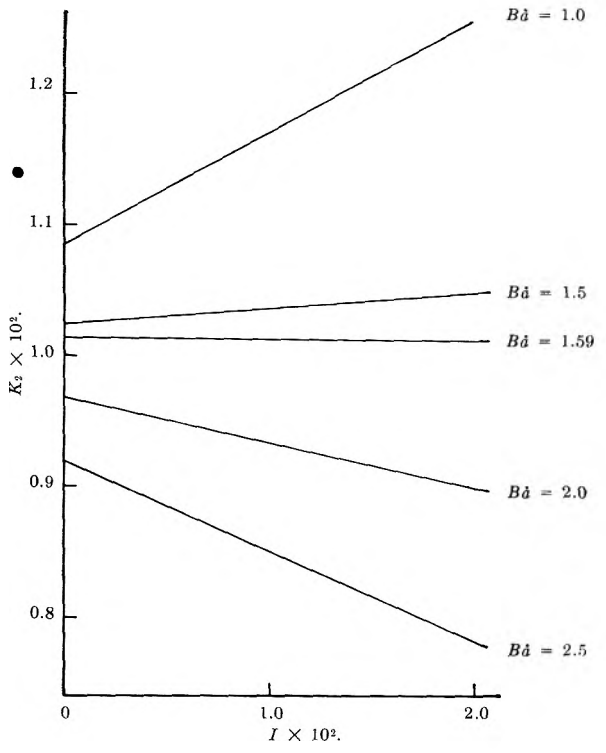

Figure 1. Variation of K_2 with I when various $B\mathring{a}$ values are used in the activity coefficient expression.

using consistent parameters and also allowing for $NaSO_4^-$ still shows that for this cell there is no convergency. The data of Nair and Nancollas[2] at 0° were also recalculated varying $B\mathring{a}$, and zero slope was obtained with $B\mathring{a} = 1.6$. This value was used to obtain K_2 at all the other temperatures. A least-squares method then gave $\Delta H = -5.3$ kcal. mole^{-1} and $\Delta S = -27.0$ cal. deg.$^{-1}$ mole^{-1}, which may be compared with the uncorrected values, -5.6 kcal. mole^{-1} and -27.7 cal. deg.$^{-1}$ mole^{-1}, respectively. The agreement with Pitzer's values,[8] $\Delta H = -5.2$ kcal. mole^{-1} and $\Delta S = -26.3$ cal. deg.$^{-1}$ mole^{-1}, is very good, but is not so satisfactory with those of Austin and Mair.[12]

Recently, Reynolds and Fukushima[13] have redetermined K_2 at various ionic strengths using a spectrophotometric method. Their data, when plotted according to eq. 1, show an appreciable curvature with an extrapolated $K_2 = 9.4 \times 10^{-3}$ mole l.$^{-1}$. These authors, however, assumed $K_2 = 0.0102$ and expressed its variation with ionic strength by the equation

$$\log K_2' = -1.991 + 2.04I^{1/2}/(1 + 1.70I^{1/2}) + 0.0314I \quad (2)$$

Experimental and calculated values are compared in Table III, and it is seen that deviations are appreciable at the lower ionic strengths.

Table III: The Dissociation of HSO_4^- at Higher Ionic Strengths

I	0.100	0.250	0.750	1.53
$10^2K_2'$ (ref. 12)	2.57	3.62	5.64	7.36
$10^2K_2'$ (eq. 2)	2.70	3.70	5.60	7.41

It is clear from the above calculations that the best value of K_2 is 0.0103 ± 0.0001 mole kg.$^{-1}$. Conductometric, spectrophotometric, and potentiometric values all fall within this range showing very good agreement for such a highly dissociated ion.

Lietzke, Stoughton, and Young[14] have calculated the dissociation constant of the bisulfate ion from solubility determinations of silver sulfate in sulfuric acid at temperatures between 25 and 225°. Although the method is least precise near room temperature when the dissociation is greatest, they give the same value, $K_2 = 0.0103$ mole kg.$^{-1}$ as the best average at 25°.

Acknowledgment. We wish to thank Dr. R. W. Dodson for valuable discussions.

(12) J. M. Austin and A. D. Mair, *J. Phys. Chem.*, **66**, 519 (1962).
(13) W. L. Reynolds and S. Fukushima, *Inorg. Chem.*, **2**, 176 (1963).
(14) M. H. Lietzke, R. W. Stoughton, and T. F. Young, *J. Phys. Chem.*, **65**, 2247 (1961).

The Conductance of Tetra-*n*-butylammonium Picrate in Chlorobenzene at 25°

by J. B. Ezell and W. R. Gilkerson

Department of Chemistry, University of South Carolina, Columbia, South Carolina *(Received November 18, 1963)*

The limiting equivalent conductance, Λ_0, of a salt may be much smaller due to the "Fuoss" effect[1] in solvents of low dielectric constant (less than 7, generally) than one would estimate assuming the Walden product for the salt, $\Lambda_0\eta_0$, where η_0 is the solvent viscosity, to be independent of solvent. If so, this would greatly affect values of the ion pair dissociation constant of the salt, K, reported in the literature. A report[2] from this laboratory indicated low values of Λ_0 (as much as 50% below the estimate based on the Walden product) for tetra-*n*-butylammonium picrate

(1) R. M. Fuoss, *Proc. Natl. Acad. Sci. U. S.*, **45**, 807 (1959).
(2) W. R. Gilkerson and R. E. Stamm, *J. Am. Chem. Soc.*, **82**, 5295 (1960).

in 75 and 50 mole % *o*-dichlorobenzene in benzene solvent mixtures at 25°. Because of the importance of Λ_0 in obtaining K from conductance data in such solvents, we were led to reinvestigate the conductance of the above salt in a pure solvent, chlorobenzene, of about the same dielectric constant as the 50 mole % *o*-dichlorobenzene–benzene solvent mixture.

Experimental

Chlorobenzene (Dow Chemical Co.) was passed through alumina (Alcoa grade F-20) on a 30 × 2 cm. column, distilled at 53–55° (60 mm.), and stored over alumina. Just prior to use it was passed through a 30 × 2 cm. column, the bottom half of which was packed with alumina and the top half with Molecular Sieve (Linde Air Products, Type 5A). In all cases, the alumina was heated to approximately 1000° for 0.5 hr. and stored in a desiccator prior to use. The specific conductance of the solvent varied from 0.6 to 1.2×10^{-11} mho/cm.

The tetra-*n*-butylammonium picrate was prepared as described elsewhere.[3] The solutions were made up in a nitrogen-filled drybox. For a particular set of data a stock solution (10^{-3} M) of salt was prepared. Weighed portions of this stock solution were then added from a weight buret equipped with a Teflon stopcock to a previously weighed portion of solvent in the conductance cell. The cell was then equilibrated with stirring (magnet) in an oil-filled thermostat set at 25.00°.

The cell was a Kraus type with bright platinum electrodes and a cell constant of 0.03043 cm.$^{-1}$ as determined by comparison with a similar cell (platinized, cell constant 0.6357 cm.$^{-1}$ using 0.01 demal KCl[4]). The conductance bridge used was constructed around a Leeds and Northrup Type 1554-A2 impedance bridge. The detector was a battery-operated General Radio Type 1232-A tuned amplifier and null detector. This detector has a very low noise level and a sensitivity of 0.1 μv. The oscillator was a General Radio Type 1302-A. The oscillator lead was a shielded twisted pair lead supplied by Leeds and Northrup. All other leads were coaxial cable with polyethylene inner insulation. This bridge was checked against a secondary standard resistor (Leeds and Northrup Type 4642) having a nominal resistance of 20,000 ohms ± 0.1%. The parallel resistance as determined on the bridge was 20,000.44 ± 0.04 ohms at 1 kc. and 19,999.49 ± 0.09 ohms at 100 kc.

Results

The equivalent conductances of tetra-*n*-butylammonium picrate in chlorobenzene at 25° appear in Table I. In each case, the solvent conductance was subtracted from that of the solution to obtain the specific conductance of the salt.

Table I: Equivalent Conductance of Tetra-*n*-butylammonium Picrate in Chlorobenzene at 25°

$10^5 \times M$ concentration	Λ, mho cm.²/equiv.
1.113	2.526
1.978	1.917
2.879	1.602
3.821	1.399
4.679	1.270
5.606	1.165
6.494	1.086
7.487	1.016
1.078	2.573
1.980	1.921
2.828	1.619
3.707	1.422
4.557	1.289
5.425	1.186
6.294	1.105
7.176	1.038

Measurements were also carried out in the 10^{-6} M range of concentration using a capacitance cell[5] having an air capacity of 24.75 pf. with the guard electrode grounded and thus a cell constant of 3.576 × 10^{-3} cm.$^{-1}$. This cell gave much increased precision in the conductance measurements at these low concentrations but a Shedlovsky plot[6] showed considerable curvature and had a large intercept corresponding to a Λ_0-value of 16. This we think is due to adsorption of solute on the walls. The cell has a large surface-to-volume ratio. Accordingly, these data are not reported in Table I.

The data were treated by the method of Shedlovsky[6] using an IBM 1620 computer. We are grateful to Dr. S. M. Katz of this University for the preparation and coding of the Fortran II program for this purpose. The physical constants (all at 25°) used in these calculations were: dielectric constant, 5.621[7]; density, 1.101 g./ml.[8]; and viscosity, 0.758 centipoise.[8] For

(3) H. L. Curry and W. R. Gilkerson, *J. Am. Chem. Soc.*, **79**, 4021 (1957).

(4) G. Jones and B. C. Bradshaw, *ibid.*, **55**, 1780 (1933).

(5) H. Sadek and R. M. Fuoss, *ibid.*, **76**, 5905 (1954).

(6) T. Shedlovsky, *J. Franklin Inst.*, **225**, 739 (1938).

(7) A. Maryott, National Bureau of Standards, Circular No. 514, U. S. Govt. Printing Office, Washington, D. C.

(8) J. Timmermans, "Physico-chemical Constants of Pure Organic Compounds," Elsevier Publishing Co., New York, N. Y., 1950.

the first set in Table I, the limiting equivalent conductance was found to be 40.9 with a probable error of ±0.5 unit and a dissociation constant of 4.20×10^{-8}. For the second set, values of 42.2 ± 0.5 and 3.96×10^{-8} were found. A similar treatment on a hand calculator of the four lowest concentration data (all in the 10^{-5} M concentration range) of McIntosh, Mead, and Fuoss[9] gave a value of Λ_0 of 36 and a K of 5.4×10^{-8}. The latter authors gave their data to only three significant figures in this concentration range. We feel that the agreement between the results reported here and those of Fuoss is quite satisfactory. The results of Flaherty and Stern[10] have not been included since they did not extend below 10^{-4} M and were in the range where triple ion formation becomes significant.

Discussion

We consider the average of the two values of Λ_0, as determined above, to be the best value to date for the limiting equivalent conductance of tetra-*n*-butylammonium picrate in chlorobenzene at 25°. This result, 41.5, is to be compared with the estimate of 62 obtained from the Walden product (using $\Lambda_0 = 36.8$ in *o*-dichlorobenzene[3,10] as reference). The 30% difference between the estimated and the observed values is an indication of the increased importance of the "Fuoss" effect in lower dielectric solvents. Hirsch and Fuoss[11] found the following expressions for the variation of the apparent radii of the tetra-*n*-butylammonium ion (R_+) and the picrate ion (R_-) in nitrobenzene–carbon tetrachloride mixtures

$$R_+ = 3.55 + 15/D$$

and

$$R_- = 2.36 + 13/D$$

where D is the dielectric constant of the solvent mixture. If one assumes that these apply in the present solvent, and calculates Λ_0 using

$$\Lambda_0 = \lambda_+ + \lambda_- = eF(1/R_+ + 1/R_-)/1800\pi$$

then one obtains $\Lambda_0 = 41$. The agreement between the calculated and experimental values is striking, but probably fortuitous. Boyd's derivation[12] shows that the slope of R_i *vs.* $1/D$ should be proportional to τ/η_0, where τ is the dipole relaxation time of the polar solvent molecules.

We conclude that estimates, based on constancy of the Walden product, of limiting equivalent conductances of salts in solvents of low dielectric constants are liable to a large error, and should be used with caution if used at all.

Acknowledgment. This work has been supported in part by a grant from the U. S. Army Research Office Durham.

(9) R. L. McIntosh, D. J. Mead, and R. M. Fuoss, *J. Am. Chem. Soc.*, **62**, 506 (1940).

(10) P. H. Flaherty and K. H. Stern, *ibid.*, **80**, 1034 (1958).

(11) E. Hirsch and R. M. Fuoss, *ibid.*, **82**, 1018 (1960).

(12) R. H. Boyd, *J. Chem. Phys.*, **35**, 1282 (1961).

Long-Range Proton Spin–Spin Coupling in Dimethyl Sulfone[1a]

by George M. Whitesides and John D. Roberts

Gates and Crellin Laboratories of Chemistry,[1b]
California Institute of Technology, Pasadena, California
(*Received November 26, 1963*)

A wide variety of chemical and spectral data suggest that a sulfone group is capable of interaction with an adjacent unsaturated center; however, it seems possible that the mode of this interaction may be significantly different from that of conjugation between first-row elements.[2] Moffit's molecular orbital treatment of sulfone groups indicates that two distinct types of conjugation are possible: "direct" conjugation utilizing the filled sulfur–oxygen molecular orbitals for overlap with an adjacent center, and "charge-transfer" conjugation, involving donation of electrons from the adjacent center into unfilled sulfone molecular orbitals having predominantly d-orbital character.[3] It is difficult to distinguish experimentally between these alternatives, but analysis of the e.p.r. spectrum of thioxanthone S,S-dioxide mononegative ion led Vincow to conclude that a charge-transfer mechanism was responsible for the observed conjugation through the sulfone group.[4]

To provide further evidence pertinent to the problem of conjugation in sulfones, we have compared the ability of several oxygen- and sulfur-containing groups to transmit proton spin–spin couplings (Table I).[5]

(1) (a) Supported in part by the Office of Naval Research and the National Science Foundation. (b) Contribution No. 3040.

(2) For reviews of this subject, see G. Cilento, *Chem. Rev.*, **60**, 147 (1960); C. C. Price and S. Oae, "Sulfur Bonding," The Ronald Press Co., New York, N. Y., 1962.

(3) W. Moffit, *Proc. Roy. Soc.* (London), **A200**, 409 (1950); H. P. Koch and W. E. Moffit, *Trans. Faraday Soc.*, **47**, 7 (1951).

(4) G. Vincow, *J. Chem. Phys.*, **37**, 2484 (1962).

(5) Somewhat similar results which are in agreement with those reported here have been published by N. van Meurs, *Spectrochim. Acta*, **19**, 1695 (1963).

Table I: Magnitudes of ^1H–^1H and ^{13}C–^1H Coupling Constants for CH_3XCH_3

Compound	Sample	$J_{^{13}CH}$,[a] c.p.s.	J_{HH},[a] c.p.s.	∠C–X–C, deg.
CH_3SSCH_3	Pure liquid	...	0.0	...
CH_3OCH_3	Pure liquid	139	0.25	111 ± 4[c]
CH_3SCH_3	Pure liquid	138	0.3	98.6 ± 10[d]
CH_3SOCH_3	Pure liquid	138	0.4	100 ± 5[e]
CH_3COCH_3	Pure liquid	127[h]	0.54[h]	119.6 ± 3[f]
CH_3SCH_3 (O)	50% in water	138	0.9	115 ± 15[g]
$(CH_3)_3S^+I^-$	50% in water	145	(0.4)[b]	...

[a] Measurements were made using ^{13}C of natural abundance, as described by A. D. Cohen, N. Sheppard, and J. J. Turner, *Proc. Chem. Soc.*, 118 (1958), and for J_{HH} are ±0.05 c.p.s. The signs of the coupling are unknown. [b] The accuracy of this value is low due to viscous broadening of the spectrum. [c] Private communication from V. Schomaker quoted by P. W. Allen and L. E. Sutton in *Acta Cryst.*, **3**, 46 (1950). [d] L. Pierce and M. Hayashi, *J. Chem. Phys.*, **35**, 479 (1961). [e] O. Bastiansen and H. Viervoll, *Acta Chem. Scand.*, **2**, 702 (1948). [f] P. W. Allen, H. J. M. Bowen, L. E. Sutton, and O. Bastiansen, *Trans. Faraday Soc.*, **48**, 991 (1952). [g] Private communication from R. E. Rundle, quoted by Allen and Sutton.[c] [h] J. R. Holmes and D. Kivelson, *J. Am. Chem. Soc.*, **83**, 2959 (1961).

The relative magnitudes of the four-bond coupling constant J_{HH} in dimethyl sulfone, dimethyl sulfoxide, and dimethyl sulfide suggest that coupling through the sulfone group involves important contributions from some mechanism other than the usual σ-bond interactions.[6] However, the unexceptional value observed for J_{HH} in trimethylsulfonium iodide makes it seem unlikely that charge transfer resulting from movement of the electrons of the methyl group orbitals to the empty sulfur d-orbitals is important in transmitting the coupling. Delocalization of the methyl group electrons into the d-orbitals is likely to be more important in the positively charged sulfonium salt than in the sulfone[7]; however, the observed coupling constant in the sulfonium compound is significantly the smaller of the two.

Alternately, coupling through the sulfone group might well involve contributions of structures such as

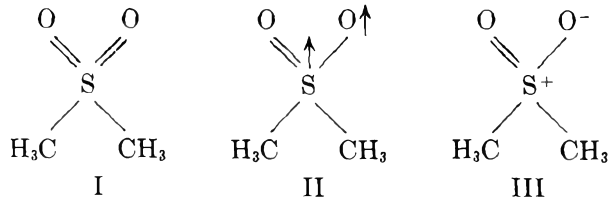

I II III

II, similar to the type invoked by Kivelson to account for the long-range proton coupling in acetone.[8]

It is interesting that $J_{^{13}CH}$ is the same for dimethyl sulfide, sulfoxide, and sulfone, but significantly larger for trimethylsulfonium iodide. If the dipolar structures of type III make an important contribution to the resonance hybrid of dimethyl sulfone, the resultant partial positive charge on sulfur would be expected to increase the orbital electronegativity of the sulfur bonding orbital directed toward the methyl group, relative to the corresponding orbital in dimethyl sulfide, and hence to increase $J_{^{13}CH}$.[9] The similarity of the ^{13}C–H coupling constants for dimethyl sulfide and dimethyl sulfone thus provides evidence that the sulfone is probably well represented by a structure of type I with predominantly covalent sulfur–oxygen bonds.

(6) The observed order is opposite to that which would be expected on the basis of variation in coupling through σ-bonds with changes in the C–X–C bond angle. See H. S. Gutowsky, M. Karplus, and D. M. Grant, *J. Chem. Phys.*, **31**, 1278 (1958), and the C–X–C bond angles listed in Table I.

(7) For discussions of the effect of charge on d-orbital contraction, see H. H. Jaffe, *J. Phys. Chem.*, **58**, 185 (1954); D. P. Craig, A. Maccoll, R. S. Nyholm, L. E. Orgel, and L. E. Sullivan, *J. Chem. Soc.*, 332 (1954); D. P. Craig and E. A. Magnusson, *ibid.*, 4895 (1956).

(8) J. R. Holmes and D. Kivelson, *J. Am. Chem. Soc.*, **83**, 2959 (1961); see also M. Barfield and D. M. Grant, *ibid.*, **85**, 1899 (1963).

(9) See, for example, N. A. Matwiyoff and R. S. Drago, *J. Chem. Phys.*, **38**, 2582 (1963); C. Juan and H. S. Gutowsky, *ibid.*, **37**, 2198 (1962), and references therein.

An X-Ray Survey of the Lead Chloride–Thallium Chloride System

by D. J. Kelsey and Lewis Katz

Department of Chemistry, University of Connecticut, Storrs, Connecticut *(Received December 4, 1963)*

Previous investigations of the $PbCl_2$–TlCl system, none involving the use of X-rays, have led to conclusions which were not entirely consistent. Korreng,[1] on the basis of cooling curves and crystallographic observations of thin sections, reported two compounds, both melting congruently: $2PbCl_2 \cdot TlCl$ and $PbCl_2 \cdot 3TlCl$.

Barlot,[2] basing his conclusions on the conductivity of mixtures of 0.01 N aqueous solutions of $PbCl_2$ and

(1) E. Korreng, *Neues Jahrb. Mineral.*, **37**, 50 (1914).

(2) M. Barlot, *Compt. rend.*, **171**, 794 (1920).

TlCl, reported clear indications for a compound $PbCl_2 \cdot TlCl$ and with less certainty $PbCl_2 \cdot 2TlCl$. The 1:1 compound was obtained on cooling a boiling equimolar solution of the two chlorides. The 1:2 compound was not obtained by crystallization.

Favorskii,[3] using thermal determinations of the liquidus primarily, but also physical measurements including electrical conductivity, agreed with Korreng concerning the congruently melting compounds, $2PbCl_2 \cdot TlCl$ and $PbCl_2 \cdot 3TlCl$. However, he reported in addition an incongruently melting compound $PbCl_2 \cdot TlCl$. This compound was indicated by the observation that the liquidus temperatures showed no change in the immediate vicinity of the 1:1 composition. The liquidus temperatures measured by Favorskii were about 10° lower than the corresponding measurements of Korreng.

Bergman and Tapchanyan,[4] in determining a melting diagram of the system $PbCl_2$–TlCl, reported identifying the compound $PbCl_2 \cdot TlCl$. Il'yasov and Bergman[6] agreed with Korreng and Favorskii that $2PbCl_2 \cdot TlCl$ and $PbCl_2 \cdot 3TlCl$ are formed and melt without decomposition.

In our work, a General Electric XRD-5 diffractometer was used to record patterns of samples prepared in two ways. One procedure was to use a bunsen flame to melt $PbCl_2$ and TlCl together in a crucible open to the atmosphere. These samples were stirred while molten and then allowed to cool. This technique will be referred to as fusion. A second procedure, carried out at room temperature, was to mix aqueous solutions of $TlNO_3$ and $Pb(NO_3)_2$ and then add HCl to precipitate the mixed chloride. This technique will be referred to as precipitation. The precipitation runs were easier to interpret and these results will be described first.

The patterns of TlCl and $PbCl_2$ obtained by precipitation matched those given in the ASTM index and by the National Bureau of Standards. As the percentage of TlCl was increased from zero, the lines of a new phase (A) appeared in addition to the unchanged pattern of $PbCl_2$. With increasing TlCl, the pattern of phase A grew stronger, and that of $PbCl_2$ grew weaker, until, at about mole fraction $PbCl_2 = 0.75$, $PbCl_2$ lines were no longer evident on the pattern. The best (most intense) pattern of phase A was obtained at the composition $2PbCl_2 \cdot TlCl$, which is compatible with earlier investigations. Although this phase was the only one observed on patterns of systems ranging in composition from mole fraction $PbCl_2 = 0.75$ almost down to mole fraction $PbCl_2 = 0.60$, the positions and relative intensities of the X-ray lines did not change. Thus, there is no evidence for solid solution. The absence of other lines on the pattern must be ascribable to the insensitivity of the X-ray method to small percentages of the additional components precipitated.

At mole fraction $PbCl_2 = 0.60$ the beginnings of a new pattern, in addition to that of A, were observed. The pattern of this new phase (B) was best, and most nearly pure, at compositions in the vicinity of $PbCl_2 \cdot 2TlCl$. At the 1:1 composition, where an intermediate phase had been reported,[2-4] the diffractometer tracing showed good patterns of both A and B and nothing else. A third intermediate phase (C) was also observed. Phase C appeared to be between $PbCl_2 \cdot 3TlCl$ and $PbCl_2 \cdot 4TlCl$. A composition for phase C very close to $PbCl_2 \cdot 3TlCl$ is possible, and in view of the weight of the earlier results should probably be accepted. Table I lists results of the precipitation runs. *Three* intermediate phases were needed to account for the observations.

Table I: Precipitation Runs

Mole fraction $PbCl_2$	Phases observed on diffraction pattern
0.85	$PbCl_2$; A
.80	$PbCl_2$; A
.75	A
.71	A
.67	A
.60	A; weak B
.50	A; B
.33	B; weak A
.31	B
.29	B; weak C
.27	B; C
.26	B; C
.25	C; B
.20	C; weak TlCl
.14	TlCl; C

Results of the fusion runs are listed in Table II. The mole fractions are starting compositions. There is always the possibility of some fractional volatilization and incomplete attainment of equilibrium; in addition, of course, there is the already mentioned insensitivity of the X-ray method to components present in small amount, a variable which depends on crystallinity. These factors make us cautious about claiming exact knowledge of the composition of intermediate phases. However, in the fusion runs *four* intermediate phases were observed. Both the pure

(3) L. I. Favorskii, *Ann. secteur anal. physico-chim., Inst. chim. gén.* (USSR), **13**, 281 (1940).

(4) A. G. Bergman and T. M. Tapchanyan, *ibid.*, **14**, 339 (1941).

(5) I. I. Il'yasov and A. G. Bergman, *Zh. Neorgan. Khim.*, **2**, 2771 (1957).

Table II: Fusion Runs

Mole fraction $PbCl_2$	Phases observed on diffraction patterns
0.75	A; $PbCl_2$
.67	A
.60	A; very weak B′
.50	A; B′
.40	B′
.33	B′
.29	B′; very weak C
.286	B′; C
.276	C; B′
.266	C; weak B′
.258	C; D
.25	D; weak C
.20	D; TlCl
.17	TlCl; D

TlCl and pure $PbCl_2$ patterns matched the precipitation patterns. Phase A was the same as in the precipitation runs and was best at about the same composition. $2PbCl_2 \cdot TlCl$. Phase B′, though it appeared in the same composition range as B, had a different pattern. Phase C was again the same as precipitation phase C, but it was observed only up through $PbCl_2 \cdot 3TlCl$ where phase D appeared to take over. From the TlCl side, phase D was the first new phase and was observed to about $PbCl_2 \cdot 3TlCl$.

Additional experiments were then performed to correlate the results of the precipitation runs and the fusion runs. The possibility of water present in the precipitation samples was checked by infrared absorption of the solid samples in Nujol mulls. Although the absorption background was increased by the solid samples, no peak was observed at 3500 $cm.^{-1}$. (Actually, since phases A and C were the same in both the precipitation and fusion experiments, water could only have been a factor in precipitation phase B; its absence here also was indicated by the infrared experiments.) In addition, samples dried in air at room temperature and in a drying oven at 100° gave the same patterns.

A sample of phase B (mole fraction $PbCl_2$ about 0.33) was heated to melting and cooled. The pattern then corresponded to B′. A precipitation sample containing mainly phase C (mole fraction $PbCl_2$ about 0.20) was heated to melting and cooled. It then showed the pattern of D. The conclusions were: phase B′ was a high-temperature modification of B; phase D was a high-temperature modification, or a phase obtainable by decomposition, of phase C. As is often the case, these high-temperature phases freeze in on free cooling, so that they are observable on room temperature X-ray patterns. Whether a reversion to the room temperature products could be brought about by annealing below their respective, and unknown, transition temperatures was not determined.

In summary, then, compounds are formed at three intermediate compositions in the $PbCl_2$–TlCl system. These compositions are about $2PbCl_2 \cdot TlCl$, $PbCl_2 \cdot 2TlCl$, and $PbCl_2 \cdot 3TlCl$. The second of these has a high-temperature modification, and the third has a high-temperature modification or a high-temperature decomposition product on the TlCl-rich side. We have found no evidence for a 1 : 1 compound.

Acknowledgment. We are grateful to the National Science Foundation for support for this work.

Wetting by Organic Liquids of Polymers Immersed in Water

by Henry Peper and Julian Berch

Harris Research Laboratories, Inc., Washington, D. C.
(Received December 14, 1963)

The object of this report is to describe the results of contact angle measurements of drops of organic liquids deposited on polymer films immersed in water, and particularly variation of the contact angle with the interfacial tension between the organic liquid and water. The aim was to characterize various polymers with respect to their tendencies to become contaminated by organic liquids suspended in water.

A useful technique for characterizing the surface energy of a solid was developed by Zisman, *et al.*,[1] who measured the contact angles of a series of liquids of varying surface tension. They plotted the cosine of the contact angle *vs.* the surface tension to obtain a straight line which can be extrapolated to zero contact angle. This gives the critical surface tension for spreading of liquids on that particular solid. Bascom and Singleterry[2] examined the wettability by water of solid surfaces submerged in oil as affected by the oil–water interfacial tension. They used soaps to vary the interfacial tension. The present study used a modified approach involving the deposition of drops of organic liquids having different interfacial tensions against water. Large contact angles were obtained at low interfacial tensions and these large angles are the principal subject matter of this report.

(1) E. G. Shafrin and W. A. Zisman, *J. Phys. Chem.*, **64**, 519 (1960).
(2) W. D. Bascom and C. R. Singleterry, *ibid.*, **66**, 236 (1962).

Experimental

Strips of high density polyethylene and polytetrafluoroethylene were made smooth by pressing them between heated platens as described by Bascom and Singleterry.[3] Mutually saturated water–organic liquid systems were prepared by shaking the two liquids in separatory funnels.

The organic liquids used and their interfacial tensions against water are listed in Table I. The liquid materials were all Fisher Certified Reagents.

Table I: Interfacial Tensions of Liquids against Water

Liquid	Water interfacial tension, dynes/cm.	Temperature, °C.
Paraffin oil	49.0	25
Oleic acid	15.6[a]	20
Methyl isobutyl ketone	9.7[a]	20
Benzyl alcohol	4.8[b]	22.5
Isobutyl alcohol	2.1[c]	18

[a] Experimental value taken from W. D. Harkins, G. L. Clark, and L. E. Roberts, *J. Am. Chem. Soc.*, **42**, 700 (1920). [b] Experimental value taken from W. D. Harkins, F. E. Brown, and E. C. H. Davies, *ibid.*, **39**, 354 (1917). [c] Experimental value taken from G. Antonow, *J. chim. phys.*, **5**, 364 (1907).

The contact angles were measured in the organic liquid phase using a telescope goniometer[4] and a special glass cell for mounting polymer film specimens in water. In most cases the organic liquids were less dense than water. Consequently, it was necessary to hang the films from the cell cover so that the liquid drops could be deposited on the underside of the film. The interfacial tensions were measured with a DuNouy tensiometer and the corrections of Zuidema and Waters applied to the data.[5] All of the measurements were carried out in a laboratory having filtered air and temperature controlled at 25 ± 0.5°.

Results

The contact angles in water of the organic liquids listed in Table I against Teflon (polytetrafluoroethylene) and polyethylene are plotted against the interfacial tensions of these liquids against water in Fig. 1. Each of the curves has a deep minimum. The contact angles do not approach zero at low interfacial tensions; instead they increase to about 50°. The physical significance of this contact angle minimum is that as the interfacial tension of organic liquids against water decreases, there is first an increasing tendency for the organic liquid to displace water from the solid followed by a decrease at lower interfacial tensions. An analogous effect in the petroleum–water–quartz system has been reported by Kusakov.[6]

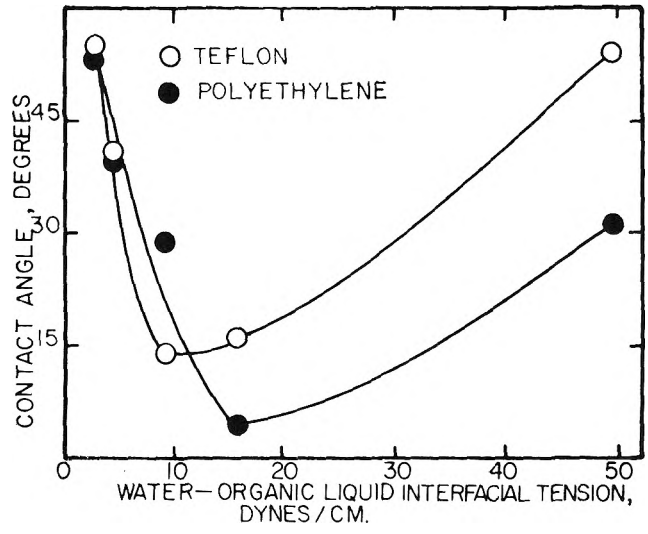

Figure 1. Contact angles of organic liquids against polymer surfaces immersed in water.

Reasons for the minima and the large contact angles at low interfacial tensions in Fig. 1 can be deduced by examining the Young–Dupré equation which relates the contact angle to the interfacial tensions of the system

$$\cos\theta = \frac{\gamma_{ws} - \gamma_{os}}{\gamma_{ow}}$$

in which θ is the contact angle; γ_{ws}, the water–solid interfacial tension; γ_{os}, the organic liquid–solid interfacial tension; and γ_{ow}, the organic liquid–water interfacial tension. The value of cos θ should increase (θ decrease) as γ_{ow} decreases, provided γ_{ws} and γ_{os} remain constant. Since large contact angles were obtained experimentally at low interfacial tensions, they could be due to changes in γ_{ws} or γ_{os}. A decrease in γ_{ws} or an increase in γ_{os} would tend to make the cos θ smaller (contact angles larger). Both of these changes in solid–liquid interfacial tensions could have occurred in mutually saturated systems of polar organic liquids and water, since organic liquid dissolved in water might lower γ_{ws} and water dissolved in organic liquid might raise γ_{os}. Unfortunately, it is not possible to measure directly the interfacial tension between a solid and a liquid. There is, however, the pos-

(3) W. D. Bascom and C. R. Singleterry, *J. Phys. Chem.*, **65**, 1683 (1961).

(4) H. W. Fox and W. A. Zisman, *J. Colloid Sci.*, **5**, 514 (1950).

(5) M. K. Zuidema and G. S. Waters, *Ind. Eng. Chem., Anal. Ed.*, **13**, 312 (1941).

(6) M. M. Kusakov and L. I. Mekenitskaya, "Research in Surface Forces," B. V. Deryagin, Ed., Consultants Bureau, New York, N. Y., 1963, p. 15.

sibility of estimating this effect by substituting a liquid analog for the solid polymer and then measuring the interfacial tension between the liquid analog and the mutually saturated liquids.

Paraffin oil was taken as a liquid analog of polyethylene. The interfacial tensions against paraffin oil of benzyl alcohol-saturated water and water-saturated benzyl alcohol were measured by the ring method and the results are listed in Table II. Water

Table II: Interfacial Tensions of Water and Benzyl Alcohol against Paraffin Oil

Liquid	Paraffin oil interfacial tension, dynes/cm. (25 ± 0.5°)
Benzyl alcohol (pure)	3.9
Benzyl alcohol (saturated with water)	4.0
Water (pure)	49
Water (saturated with benzyl alcohol)	7.6

dissolves in benzyl alcohol to the extent of 9.6 g./100 g. of benzyl alcohol, while the solubility of benzyl alcohol in water is 4.4 g./100 g. of water at 25°. The data in Table II show that the effect on the interfacial tension against paraffin oil of water dissolved in benzyl alcohol is small. On the other hand, benzyl alcohol dissolved in water effects a large lowering of the interfacial tension of paraffin oil.

The large contact angle that was obtained in the benzyl alcohol–water system against polyethylene is, therefore, quite likely due to a substantial lowering of the water–solid interfacial tension (γ_{ws}) brought about by the organic liquid dissolved in the water. The large contact angles obtained with the other polar organic liquids (methyl isobutyl ketone and isobutyl alcohol) are probably due to similar large decreases in the water–solid interfacial tensions. The low organic liquid–water interfacial tensions are the result of adsorption and orientation at this interface. The same adsorption and orientation probably occur at the polymer–water interface; consequently, it can be expected that the situation of high contact angles at low organic liquid–water interfacial tensions will be general for relatively hydrophobic polymers.

Substitution of the three measured interfacial tensions obtained for the paraffin oil–water–benzyl alcohol system into the Young equation gives a contact angle of 41°. The measured contact angle for the polyethylene–water–benzyl alcohol system is 40°, which is close agreement and justifies the assumption that paraffin oil can be substituted for polyethylene to obtain an approximation of the solid–liquid interfacial tension.

A Mass Spectrometric Study of Trimethyl Borate[1]

by Yasuo Wada and Robert W. Kiser

Department of Chemistry, Kansas State University, Manhattan, Kansas *(Received December 9, 1963)*

In connection with some recent studies of phosphite esters, we have had occasion to investigate mass spectrometrically a sample of trimethyl borate. Several years ago, Law and Margrave[2] included trimethyl borate in a mass spectrometric study of several boron-containing compounds. We have observed several differences between their earlier work and our present studies of the appearance potentials for many of the principal positive ions produced by electron impact. Therefore, we wish to present here our findings and interpretations of the ionization and dissociation processes which occur upon electron impact with gaseous trimethyl borate.

Experimental

The research sample of trimethyl borate was a gift of Callery Chemical Co., and was used as received. The 70-e.v. mass spectrum of the sample agreed very closely with that presented by Law and Margrave,[2] as may be seen from the results presented in Table I. A time-of-flight mass spectrometer, described previously,[3] was used for all measurements. Appearance potentials were evaluated using the methods of Warren[4] and of Lossing, Tickner, and Bryce[5] to interpret the ionization efficiency curves. Additionally, the energy compensation method[6] provided us with checks on our results. Xenon (I = 12.13 e.v.[7]), intimately mixed with the trimethyl borate sample, was used for calibration.

Results

Table I presents the results of our study. As was already noted, the relative abundances of the positive ions determined by us and by Law and Margrave[2] are in excellent agreement. Only at m/e values below 31 do

(1) This work was supported by the U. S. Atomic Energy Commission under Contract No. AT(11-1)-751 with Kansas State University.

(2) R. W. Law and J. L. Margrave, *J. Chem. Phys.*, **25**, 1086 (1956).

(3) E. J. Gallegos and R. W. Kiser, *J. Am. Chem. Soc.*, **83**, 773 (1961).

(4) J. W. Warren, *Nature*, **165**, 811 (1950).

(5) F. P. Lossing, A. W. Tickner, and W. A. Bryce, *J. Chem. Phys.*, **19**, 1254 (1951).

(6) R. W. Kiser and E. J. Gallegos, *J. Phys. Chem.*, **66**, 947 (1962).

(7) C. E. Moore, "Atomic Energy Levels," Natl. Bur. Std. Circ. 467, Vol. 3, U. S. Govt. Printing Office, Washington, D. C., May 1, 1958.

we find some small disagreement, in which the relative abundances we determined are somewhat higher than those reported by Law and Margrave.

Table I: Appearance Potentials and Heats of Formation of the Principal Positive Ions from Trimethyl Borate

m/e	70 e.v. rel. abund.	Appearance potential, e.v.	Probable process	ΔH_f (ion), kcal./mole
10	0.11			
11	0.47			
15	47.5	21.4 ± 0.5	$B(OCH_3)_3 \rightarrow CH_3^+ + ?$	
29	25.7	19.1 ± 0.3	$\rightarrow CHO^+ + ?$	
30	2.6			
31	10.9	12.7 ± 0.2	$\rightarrow CH_3O^+ + B(OCH_3)_2$	178
41	1.9			
42	8.4	17.1 ± 0.4	$\rightarrow BO_2^+ + CH_3O + 2CH_3$	121
43	25.1	17.5 ± 0.3		
45	3.1			
56	2.4	16.6 ± 0.3	$\rightarrow B(OCH_3)(CH_3)^+ +$	
57	9.8	17.0 ± 0.6	$CH_2O + OH$	189
58	3.6	13.2 ± 0.3	$\rightarrow BO_3^+ + 3CH_3$	−7
59	11.4	13.2 ± 0.3		
71	4.4	13.2 ± 0.2	$\rightarrow B(OCH_3)(OCH_2)^+ +$ $CH_2O + H_2$	116
72	43.2	13.1 ± 0.2	→ (see text)	
73	100.0	13.0 ± 0.2	$\rightarrow B(OCH_3)_2^+ + CH_3O$	85
88	1.3			
89	5.3	12.1 ± 0.2	$\rightarrow OB(OCH_3)_2^+ + CH_3$	31
102	0.8			
103	12.1	10.8 ± 0.3	$\rightarrow B(OCH_3)_3^+$	33
104	36.0	10.8 ± 0.3		
105	1.2			

The appearance potentials determined are presented in column 3 of Table I. Appearance potential measurements on isotopic peaks provided additional aid in determining the nature of the ions contributing in the threshold region to the various peaks.[8] The heats of formation for the various ions, given in the last column, were determined from the appearance potentials by assuming the "probable processes" listed in Table I. In these calculations, we have used the heat of formation of gaseous trimethyl borate ($\Delta H_f = -215.7$ kcal./mole) determined by Charnley, Skinner, and Smith.[9]

Discussion

The parent-molecule ion, $B(OCH_3)_3^+$, occurs at $m/e = 103$, 104, and 105, although $m/e = 103$ also is due partially to $B^{11}(OCH_3)_2(OCH_2)^+$. However, $A(103^+) = A(104^+)$, indicating that $A[B(OCH_3)_2(OCH_2)^+] \geq A[B(OCH_3)_3^+]$. The ionization potential determined for trimethyl borate is 10.8 e.v. This value is nearly 2 e.v. greater than that reported by Law and Margrave.[2] In fact, of the five ions for which both Law and Margrave and we have determined appearance potentials, there is agreement only for $A(BO_3^+)$. In the other four instances, our results are always higher, sometimes by as much as 6 to 8 e.v. We are at a complete loss to explain why such serious disagreement should exist. In the following few paragraphs we explain our process assignments, based on our appearance potential measurements.

Let us compare $I(HR)$ with $I(BR_3)$, where R is an atom or a group of atoms. Only scanty data are available for such a comparison: HF and BF_3; HCl and BCl_3; and H_2 and BH_3. It is anticipated that the electron withdrawn upon ionization would come from the F atom in both HF and BF_3 and from the Cl atom in both HCl and BCl_3 (*i.e.*, localization). Thus, one would not expect much difference in the ionization potentials of each member of a pair. In fact, $I(HF) = 15.77$ e.v.[10] and $I(BF_3) = 15.7$ e.v.[2,11,12] Similarly, $I(HCl) = 12.7$ e.v.[13,14] and $I(BCl_3) = 12.0$ e.v.[12,15] But for H_2 and BH_3, the electron withdrawn upon ionization cannot be considered as having been localized on the hydrogen atom, and so we would not expect $I(H_2)$ and $I(BH_3)$ to be similar. In fact, $I(H_2) = 15.43$ e.v.[16] and $I(BH_3) = 11$–12 e.v.[17]

Now, in the case of interest to us here, $I(HOCH_3)$ should be compared to $I[B(OCH_3)_3]$. We would anticipate that in both cases the electron which is withdrawn upon ionization would be one which could be considered as having been localized on an oxygen atom, and therefore that $I(CH_3OH) \simeq I[B(OCH_3)_3]$. $I(CH_3OH) = 10.85$ e.v.,[14,18] and we note that this is not greatly different from the value of $I[B(OCH_3)_3] = 10.8$ e.v. which we determined experimentally.

The ions of $m/e = 88$ and 89 are in the expected ratio of 1:4 for identical species differing only in the boron iso-

(8) The range of isotopic abundances for B^{10} and B^{11} which we used were those reported by A. E. Cameron and E. Wichers, *J. Am. Chem. Soc.*, **84**, 4175 (1962).

(9) T. Charnley, H. A. Skinner, and N. B. Smith, *J. Chem. Soc.*, 2288 (1952).

(10) J. A. R. Coope, D. C. Frost, and C. A. McDowell, *Nature*, **179**, 1186 (1957); D. C. Frost and C. A. McDowell, *Can. J. Chem.*, **36**, 39 (1958).

(11) H. Kreuzer, *Z. Naturforsch.*, **12a**, 519 (1957).

(12) J. Marriott and J. D. Craggs, *J. Electron. Control*, **3**, 194 (1957).

(13) J. D. Morrison, *J. Chem. Phys.*, **19**, 1305 (1951); J. D. Morrison and A. J. C. Nicholson, *ibid.*, **20**, 1021 (1952); R. E. Fox, *ibid.*, **32**, 385 (1960).

(14) K. Watanabe, *ibid.*, **26**, 542 (1957).

(15) O. Osberghaus, *Z. Physik*, **128**, 366 (1950).

(16) J. D. Morrison, *J. Chem. Phys.*, **22**, 1219 (1954); D. P. Stevenson, *J. Am. Chem. Soc.*, **82**, 5961 (1960).

(17) J. L. Margrave, *J. Phys. Chem.*, **61**, 38 (1957); W. S. Koski, J. J. Kaufman, C. F. Pachucki, and F. J. Shipko, *J. Am. Chem. Soc.*, **80**, 3202 (1958); **81**, 1326 (1959).

(18) T. M. Sugden, A. D. Walsh, and W. C. Price, *Nature*, **148**, 373 (1941); L. Friedman, F. A. Long, and M. Wolfsberg, *J. Chem. Phys.*, **27**, 613 (1957).

topes. Since the masses occur at (p − 15), it is apparent that ionization and cleavage of one of the O–CH_3 bonds has occurred. From the determined appearance potential, $\Delta H_f[OB(OCH_3)_2^+] = 31$ kcal./mole.

By similar argument, the ions of $m/e = 42$ and 43 are essentially identical, and are the BO_2^+ ions (although apparently another ion, such as $B^{11}OCH_3^+$, also contributes somewhat to $m/e = 42$). Here we see additional information provided by the observation that the appearance potentials for the two m/e values are the same, within experimental error. It is to be noted that Law and Margrave[2] obtained appearance potentials for these two ions which differed by two electron volts. Using our average value of $A(42^+)$ and $A(43^+)$, equal to 17.3 e.v., the heat of formation of the BO_2^+ ion is calculated to be 121 kcal./mole.

One might also note that the ions of $m/e = 30$ and 31 have relative intensities near the expected ratio of 1:4. However, neither of these ions can contain a boron atom. Because of the low appearance potential for $m/e = 31$, a relatively simple dissociation is anticipated. This would give the CH_3O^+ ion and probably the $B(OCH_3)_2$ fragment. Using the value of $\bar{D}$(B–OCH_3) = 114 kcal./mole[9] and $\Delta H_f(CH_3O) = -1.3$ kcal./mole,[19] $\Delta H_f[B(OCH_3)_2] = -100$ kcal./mole is calculated. Then from the appearance potential data, $\Delta H_f(CH_3O^+) = 178$ kcal./mole, in good agreement with the value of 173 kcal./mole listed by Field and Franklin.[20]

The ion of $m/e = 15$ is most probably CH_3^+, but the process for its formation is not decided by the appearance potential information. Similarly, the ion of $m/e = 29$ is likely CHO^+, but the appearance potential data do not enable one to specify a unique set of neutral fragments.

The relative abundances at 70 e.v. indicate that the majority of the ions of $m/e = 57$ are the $B(OCH_3)(CH_3)^+$ ions containing a boron-11 atom, and that the majority of the ions of $m/e = 58$ are the BO_3^+ ions containing a boron-10 atom. But the relative abundances also suggest a small, but apparently real, contribution to these two m/e peaks due to $OB(OCH_3)^+$ ions. The appearance potential measurements do not aid us, however, in attempting to obtain the heat of formation of the $OB(OCH_3)^+$ ion. It is rather obvious that the appearance potentials for $m/e = 56$ and 57 are the same within experimental error. Taking the average value for these two ions, $\Delta H_f[B(OCH_3)(CH_3)^+] = 189$ kcal./mole, using the process chosen in Table I. Similarly, $A(58^+) = A(59^+)$, and $\Delta H_f(BO_3^+)$ is found to be −7 kcal./mole.

This latter result is a rather intriguing one; it indicates that the species BO_3^+ is rather stable in the gaseous phase. Quite possibly then one may expect to find the solid, neutral species, BO_3(s), to be a stable molecule.

The ions at $m/e = 71$ and 73 may be readily attributed to $B^{10}(OCH_3)(OCH_2)^+$ and $B^{11}(OCH_3)_2^+$, respectively. $m/e = 72$ is then expected to be a mixture of $B^{11}(OCH_3)(OCH_2)^+$ and $B^{10}(OCH_3)_2^+$, and the relative abundances bear this out. The appearance potentials are quite close for both types of ions, but lead to heats of formation different for the two different ions. For the $m/e = 73$ ion, the very large relative abundance and the low appearance potential suggest a simple type of bond cleavage in the ionization and dissociation process. The formation of CH_3O as the neutral fragment would fulfill this expectation, and leads to a reasonable value of $\Delta H_f[B(OCH_3)_2^+] = 85$ kcal./mole. On the other hand, the low value for $A(71^+)$ requires that the neutral fragments have low heats of formation, since $\Delta H_f[B(OCH_3)(OCH_2)^+]$ is almost surely greater than $\Delta H_f[B(OCH_3)_2^+]$. Also, since $\Delta H_f(BO_2^+)$ should be greater than $\Delta H_f[B(OCH_3)(OCH_2)^+]$, we begin to bracket the possible processes, for then we expect $121 \geq \Delta H_f[B(OCH_3)(OCH_2)^+] \geq 85$ kcal./mole. A process which meets this requirement and which leads to $\Delta H_f[B(OCH_3)(OCH_2)^+] = 116$ kcal./mole is given in Table I.

It is noted that the probable processes assigned in Table I for the formation of ions of $m/e = 31$ and $m/e = 73$ constitute complementary reactions. Application of Stevenson's rule[21] would indicate that since $I(CH_3O) \simeq 7.6$ e.v. is slightly lower than $I[B(OCH_3)_2] \simeq 8.0$ e.v., the value of $\Delta H_f[B(OCH_3)_2^+]$ is probably somewhat less than 85 kcal./mole.

A mass spectrometric study of triethyl borate, currently underway in our laboratories, may aid in resolving the differences which we have discussed. Certainly these conflicting results also require additional studies by other investigators using high resolution techniques as well as appearance potential measurements.

Acknowledgment. We wish to thank Callery Chemical Co. for their generous gift of the trimethyl borate sample.

(19) T. C. Charnley, C. T. Mortimer, and H. A. Skinner, *J. Chem. Soc.*, 1181 (1953).

(20) F. H. Field and J. L. Franklin, "Electron Impact Phenomena and the Properties of Gaseous Ions," Academic Press, Inc., New York, N. Y., 1957.

(21) D. P. Stevenson, *Discussions Faraday Soc.*, **10**, 35 (1951).

A Relationship for Rotational Averaging

by J. M. Peterson and R. L. McCullough

Contribution No. 221 from Chemstrand Research Center, Durham, North Carolina *(Received December 17, 1963)*

There are occasions when an average is required of the quantity $|r_1 + r_2 + R|^{-q}$ (q not necessarily an integer) over all directions of r_1 and r_2, *e.g.*, in the calculation of the average London dispersion force between two diatomic molecules (see Fig. 1). This work reports a useful technique for evaluating this average which is simpler than the usual techniques (*e.g.*, expansion in terms of Gegenbauer polynomials,[1] or a straightforward Taylor series expansion in which the angular averaging is quite tedious). This technique leads to a general expression for $(|r_1 + r_2 + R|^{-q})_{av}$ which may be evaluated readily for any value of q greater than zero.

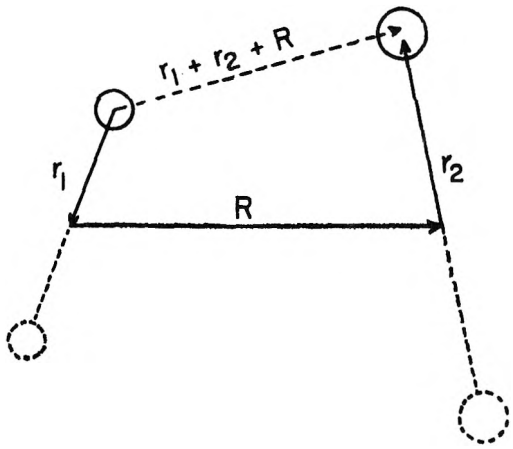

Figure 1. Schematic definition of vector distances.

The approach taken here also involves a Taylor series expansion (and hence, is limited to those relative values of $|r_1|$, $|r_2|$, and $|R|$ which lead to convergence); however, the angular averaging is greatly simplified. The key idea of this simplification is the recognition that for given $|r_1|$, $|r_2|$, and $|R|$, the vector length $|r_1 + r_2 + R|$ can be written in terms of only two angles. These angles are conveniently taken to be the angle θ between the two vectors r_1 and r_2 and the angle φ between $(r_1 + r_2)$ and R. Hence

$$|r_1 + r_2 + R| = [r_1^2 + r_2^2 + 2r_1r_2\cos\theta + 2(r_1^2 + r_2^2 + 2r_1r_2\cos\theta)^{1/2}R\cos\varphi + R^2]^{1/2} \quad (1)$$

The cases of interest are those for which $r_1 < R$, and $r_2 < R$; thus, it will be convenient to rewrite eq. 1 as

$$\begin{aligned}|r_1 + r_2 + R| &= R[d_1^2 + d_2^2 + 2d_1d_2\cos\theta + (2d_1^2 + d_2^2 + 2d_1d_2\cos\theta)^{1/2}\cos\varphi + 1]^{1/2} \\ &= R[1 + 2\mu\cos\varphi + \mu^2]^{1/2} \\ &= R(1 + \mu e^{i\varphi})^{1/2}(1 + \mu e^{-i\varphi})^{1/2} \end{aligned} \quad (2)$$

where, $d_1 = r_1/R$; $d_2 = r_2/R$; and $\mu = (d_1^2 + d_2^2 + 2d_1d_2\cos\theta)^{1/2}$. Therefore

$$|r_1 + r_2 + R|^{-q} = R^{-q}(1 + \mu e^{i\varphi})^{-q/2}(1 + \mu e^{-i\varphi})^{-q/2} \quad (3)$$

Equation 3 may be easily expanded in powers of μ by the use of Leibnitz rule,[2] *i.e.*

$$\frac{d^n}{dx^n}[f(x)g(x)] = \sum_{p=0}^{n}\binom{n}{p}\left(\frac{d^p f(x)}{dx^p}\right)\left(\frac{d^{n-p}g(x)}{dx^{n-p}}\right) \quad (4)$$

where $f(x)$ and $g(x)$ are arbitrary functions of x. Thus from the Maclaurin's series expansion

$$|r_1 + r_2 + R|^{-q} = R^{-q}\sum_{n=0}^{\infty}\frac{(-1)^n\mu^n}{n!} \times \sum_{p=0}^{n}\binom{n}{p}\frac{\Gamma(1/2q + p)\Gamma(1/2q + n - p)}{[\Gamma(1/2q)]^2} \times \exp[-(n - 2p)i\varphi] \quad (5)$$

An average over φ (limits, 0 to π; weighting factor, $\sin\varphi$) shows that only even powers of μ have non-vanishing coefficients and yields

$$|r_1 + r_2 + R|^{-q} = R^{-q}\sum_{k=0}^{\infty}\frac{\mu^{2k}}{(2k)!} \times \sum_{p=0}^{2k}\binom{2k}{p}\frac{\Gamma(1/2q + p)\Gamma(1/2q + 2k - p)}{(1 - 4(k - p)^2)[\Gamma(1/2q)]^2} \quad (6)$$

The remaining average over θ (limits, 0 to π; weighting factor, $\sin\theta$) yields the required relationship

$$(|r_1 + r_2 + R|^{-q})_{av} = R^{-q}\sum_{k=0}^{\infty}\frac{1}{(2k)!\,(k + 1)} \times \left[\frac{(r_1 + r_2)^{2k+2} - (r_1 - r_2)^{2k+2}}{4r_1r_2R^{2k}}\right] \times \sum_{p=0}^{2k}\binom{2k}{p}\frac{\Gamma(1/2q + p)\Gamma(1/2q + 2k - p)}{(1 - 4(k - p)^2)[\Gamma(1/2q)]^2} \quad (7)$$

Clearly, the relationship takes on a simpler form for $r_1 = r_2$ and/or for $1/2q$ = an integer.

(1) P. M. Morse and H. Feshbach, "Methods of Theoretical Physics," 1st Ed., McGraw-Hill Book Co., Inc., New York, N. Y., 1953, p. 782.

(2) R. Courant and D. Hilbert, "Methods of Mathematical Physics," Vol. II, Interscience Publishers, New York, N. Y., 1962, p. 577.

Even though the evaluation of the coefficients requires some effort, their determination is straightforward. Furthermore, such a general relationship permits the convenient inclusion of as many terms as may be desired without the necessity of laborious integrations.

The technique and the relationship reported in this work can be quite usefully employed in the consideration of many problems concerned with rotational averaging.

Certain Aspects of the Interpretation of Immersional Heats of Gels

by N. Hackerman and W. H. Wade

Department of Chemistry, The University of Texas, Austin, Texas *(Received December 19, 1963)*

In a recent publication from this laboratory[1] it was demonstrated that disagreements between Harkins–Jura and B.E.T. surface areas could be reconciled by measuring the B.E.T. areas of powdered samples pre-equilibrated with water vapor at $p/p^0 = 1.0$. This study showed initial differences between the two techniques of approximately 15% for particulate, dispersed samples, whereas more marked disagreement was noted for both a condensed alumina gel and an artificially compressed sample which had been used in infrared studies.

In the present study, the effect of a surface area varying during the process of pre-equilibration with various amounts of water vapor on the subsequent heats of immersion is discussed. The sample used was the gel reported earlier.[2,3] The heats of immersion in water were measured in a twin differential adiabatic calorimeter.[4]

Approximately 0.1-g. samples were pretreated at various values of p/p^0 of water vapor on an outgassing apparatus. The volumes adsorbed per gram corresponding to the dosing pressures were picked from a previously measured isotherm.[2] The heats of immersion, ΔH_i, for various values of V_{ads} are illustrated by the data points of Fig. 1. For these data points all ΔH_i values were normalized in the conventional manner to unit surface area (1 cm.^{2}) on the basis of the surface area of the outgassed gel (221 m.^{2}/g.).

Heats of immersion were measured in duplicate with a usual agreement of ±2%. Surface areas were obtained from N_2 isotherms measured over a relative pressure range of 0.04 to 0.25 and consisted of six or

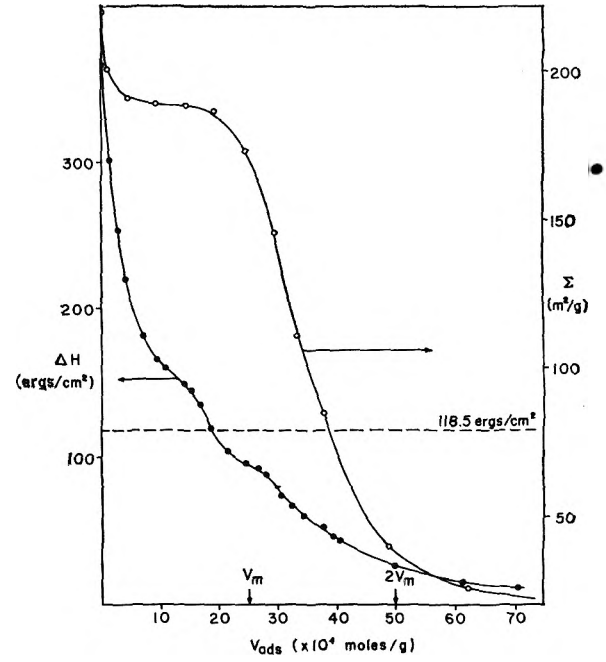

Figure 1. Open circle data points are heats of immersion based on a constant surface area of 221 m.^{2}/g. Closed circle data points are the surface areas for various amounts of water preadsorbed.

seven data points. All B.E.T. plots showed some slight curvature over this range and the surface areas of Fig. 1 represent the average values. The maximum and minimum values were always within ±5% of the average. Duplicate isotherms were obtained for several points with an agreement of better than 1%.

It is obvious that ΔH_i does not approach the surface enthalpy of water (118.5 ergs/cm.^{2}) asymptotically but actually drops below this value prior to nominal monolayer completion. (The B.E.T. analysis of the water adsorption isotherm yields 25.7×10^{-4} mole/g. for V_m.) It continues to drop to less than 10 ergs/cm.^{2} at the highest relative pressures. However, if the measured surface area of the gel sample with various values of V_{ads} (Fig. 1) is applied point by point to the raw data, the resulting smoothed curve shown in Fig. 2 is obtained. These corrected data are certainly more understandable in that the heats of adsorption do approach the 118 ergs/cm.^{2} expected of a hydrophilic surface.

The resulting two sets of data represent different thermal phenomena. The uncorrected data, though

(1) W. H. Wade, *J. Phys. Chem.*, **68**, 1029 (1964).

(2) R. L. Every, W. H. Wade, and N. Hackerman, *ibid.*, **65**, 937 (1961).

(3) W. H. Wade and N. Hackerman, *ibid.*, **64**, 1196 (1960).

(4) A. C. Makrides and N. Hackerman, *ibid.*, **63**, 594 (1959).

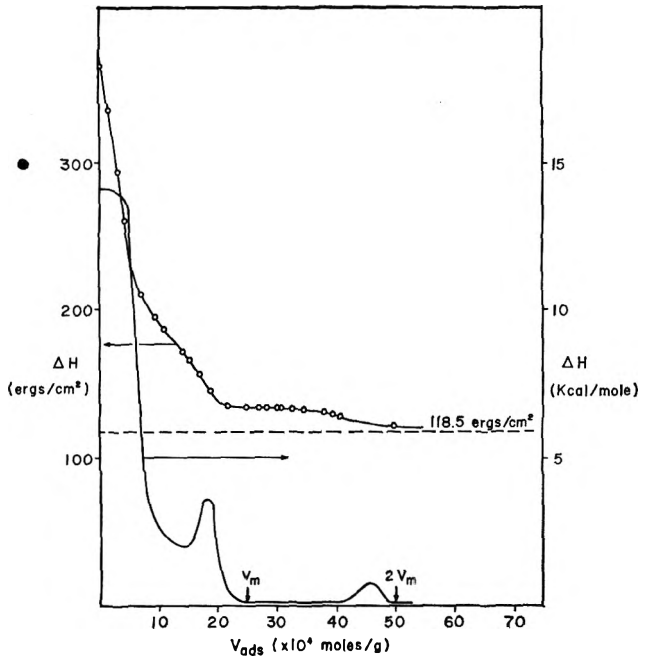

Figure 2. Open circle data points are the corrected immersional heats. The solid line is the differential heat of adsorption derived from the former.

normalized in the standard manner to unit area outgassed solid, might just as well, or even less ambiguously, have been normalized to unit weight of solid adsorbate (in units of ergs/g. or kcal./g.). These data are most closely related to the characteristics of the substrate. On the other hand, the corrected data are related to the surface of the adsorbate film and its modification by the substrate. It is this latter quantity which is pertinent to surface area determinations by the Harkins–Jura absolute method.[5]

Harkins and Jura,[5] in discussing the immersion process, picture two contributions to the ΔH_i: a heat corresponding to the heat of vapor phase adsorption referred to liquid water as reference, followed by subsequent exothermic destruction of a liquid water interface equal in area to that of the sample's surface area. The latter term is the surface enthalpy of the liquid (water in the present case). Harkins and Jura[5] point out that the calculations of Razouk[6] for methyl alcohol adsorption on charcoal are in error because he did not subtract the surface enthalpy per cm.^{2} of surface area from his heats of immersion per cm.^{2}. Unfortunately, Harkins and Jura themselves may also have been in error. The correct value to subtract is not the surface enthalpy of methyl alcohol per cm.^{2} times the area of the outgassed sample, but rather the experimentally measured heat of immersion for the surface preequilibrated with methyl alcohol. This surface may have a different area. For one sample of TiO_2 Harkins and Jura found the surface areas to be identical. The present authors have never found this to be the case, at least, for any samples with surface areas greater than 3 m.^{2}/g. Of course, the alumina gel discussed in this paper is an extreme example of surface area diminution during the adsorption process but nevertheless such diminution is an intimate part of the adsorption process. The heat contributions associated with such adsorption processes would be obtained from isosteric heat calculations from adsorption isotherms, by adsorption calorimetry, or by immersion calorimetry. If gels are considered to be an assemblage of spherical particles, the variation of surface area in gel samples can generally be traced to three sources: (a) formation of a uniform adsorbate film with either a resulting increase or decrease in surface area depending on the coordination number (average number of spheres in contact with any given sphere)[1]; (b) reversible capillary condensation in the contact zones of the spheres which always cause a diminution in surface area; and (c) irreversible filling of "pores" formed by gel particles which do not touch but are in close proximity—this further reducing the surface area. The interpretation of isosteric heats where process (c) is operative is thermodynamically questionable, severely limiting interpretations at high relative pressures.

Experimental surface area measurements for this gel sample show large (up to 40%) decreases at submonolayer coverages where no hysteresis was noted in the adsorption isotherms,[2] indicating that primarily mechanisms (a) and (b) are operative. Previous calculations[1] showed that a small fraction of water held in contact zones is the major factor in decreasing the surface area. This is especially true for hydrophilic gels with coordination numbers of 6–8 and indicates that there are sizeable contributions to the heat of adsorption from water molecules finding themselves in "force" fields of two gel particles surfaces, compounding the difficulties of interpretation of heats adsorption *vs.* coverage. Moreover, the quantitative concept of "coverage" is meaningless. Large variations of surface area below monolayer coverage invalidates B.E.T. V_m values and, of course, makes one wonder about the validity of the N_2 areas themselves.

Figure 2 illustrates that the differential heat of adsorption on the film, *i.e.*, the slope of the corrected data, exhibits two small maxima. The positions of the maxima are close to the closure points in the hysteresis loop of the adsorption–desorption isotherms for these

(5) W. D. Harkins and G. Jura, *J. Am. Chem. Soc.*, 66, 919 (1944).
(6) R. I. Razouk, *J. Phys. Chem.*, 45, 190 (1941).

samples.[2] Kiselev[7] has noted such maxima for narrow pore distribution samples.

In conclusion, the simple immersion process as envisioned by Harkins and Jura must be re-examined, especially when applied to gel samples. The present authors,[2] as well as others,[6,8-10] may have been wrong in arbitrarily subtracting the surface enthalpy of the immersion liquid from the experimental immersion heats of the outgassed surface in order to obtain the heat of adsorption.

Acknowledgment. The authors wish to express their appreciation to the American Petroleum Institute and the Robert A. Welch Foundation for their support of this work.

(7) A. V. Kiselev, "Proceedings, Second Congress on Surface Activity," Vol. 2, Butterworth, London, 1957, p. 189.

(8) B. Millard, E. G. Caswell, E. E. Leger, and D. R. Mills, *J. Phys. Chem.*, 59, 976 (1955).

(9) G. J. Young and F. H. Healey, *ibid.*, 58, 881 (1954).

(10) J. W. Whalen, *ibid.*, 65, 1676 (1961).

Proton Magnetic Resonance Spectrum of 4-Chloro-1,2-butadiene

by Raymond C. Ferguson

Contribution No. 142 from Elastomer Chemicals Department, Experimental Station, E. I. du Pont de Nemours and Company, Wilmington, Delaware *(Received December 19, 1963)*

The coupling constants of allenic systems are of interest because of measurable long range couplings[1] and evidence that the relative sign of the J_{13}(H,H) coupling through the allenic bonds in 1-chloro-1,2-butadiene[2] is negative. The spectrum of an isomer of the latter compound, 4-chloro-1,2-butadiene (I), is reported in this note.

$$\underset{(B_2)}{H_2\overset{1}{C}}=\underset{(C)}{\overset{2}{C}}=\underset{(A_2)}{\overset{3}{CH}}-\overset{4}{CH_2Cl} \qquad \text{I}$$

Results

The 60-Mc. proton resonance spectrum of I is a perturbed first-order pattern. Because of the geometry of the molecule and rapid rotation of the CH_2Cl group, the $=CH_2$ protons were magnetically equivalent, as were the CH_2Cl protons. Thus, the spectrum was analyzed as an A_2B_2C case.

The iterative computer method of Swalen and Reilly[3] was employed to fit the spectrum. Each of the four possible combinations of relative signs of the coupling constants (J_{AB} +, J_{BC} ±, and J_{CA} ±) was processed through the complete iterative procedure to a "best" fit. Two of these were rejected because of significantly poorer frequency and intensity matches to the observed spectrum. However, an unequivocal choice between case 1 (all signs +) and case 2 (J_{BC} −) could not be made on the same basis.

The relative signs of the coupling constants were established by the field-sweep double resonance method.[4] The definitive experiments involved observing the group A multiplet pattern while irradiating the group B multiplets.

In the first-order approximation, the group A multiplet pattern is a doublet due to the coupling J_{CA} = 7.7 c.p.s., each component of which is a triplet due to the coupling J_{AB} = 2.2 c.p.s. Similarly, the group B multiplet pattern is a doublet due to J_{BC} = 6.6 c.p.s., with each split into triplets with J_{AB} = 2.2 c.p.s. Most of the lines in the observed spectrum are also split by second-order effects.

For case 1, the high field "triplet" lines of group A (lines 1–8) have energy levels in common with the high field "triplet" lines (lines 17–24) of group B; similarly, the low field "triplet" lines of group A (lines 9–16) and group B (lines 25–32) have energy levels in common. The reverse situation holds for case 2: the high field "triplet" lines of group A and low field "triplet" lines of group B have energy levels in common, as do the low field "triplet" lines of group A and high field "triplet" lines of group B.

The conditions for spin decoupling groups A and B are that the second (irradiating) radiofrequency field should have an amplitude $\gamma H_2/2\pi \approx J_{AB}$ = 2.2 c.p.s. at a frequency $|\nu_2 - \nu_1|$ approximately equal to the frequency separation between the group A and group B "triplets" having energy levels in common.[4] Thus, the audio side-band (decoupling) frequencies differ for cases 1 and 2.

For case 1, the decoupling frequency would have been approximately 52 c.p.s. Instead, the high field "triplet" of group A collapsed at a decoupling frequency of 58 c.p.s., and the low field "triplet" of group A collapsed at 44 c.p.s. This was, in fact, the predicted behavior for case 2 and showed that the relative sign of J_{BC} is negative.

The n.m.r. parameters for I are summarized in the

(1) E. I. Snyder and J. D. Roberts, *J. Am. Chem. Soc.*, 84, 1582 (1962).

(2) S. L. Manatt and D. D. Elleman, *ibid.*, 84, 1579 (1962).

(3) J. D. Swalen and C. A. Reilly, *J. Chem. Phys.*, 37, 21 (1962).

(4) W. A. Anderson and R. Freeman, *ibid.*, 37, 85 (1962).

table. The assignment of proton C was unambiguous because the multiplet group intensities were A:B:C:: 2:2:1. The assignments of A_2 to the CH_2Cl group and B_2 to the $=CH_2$ group were based on chemical shift data from related allenic[5] and haloolefinic[6]

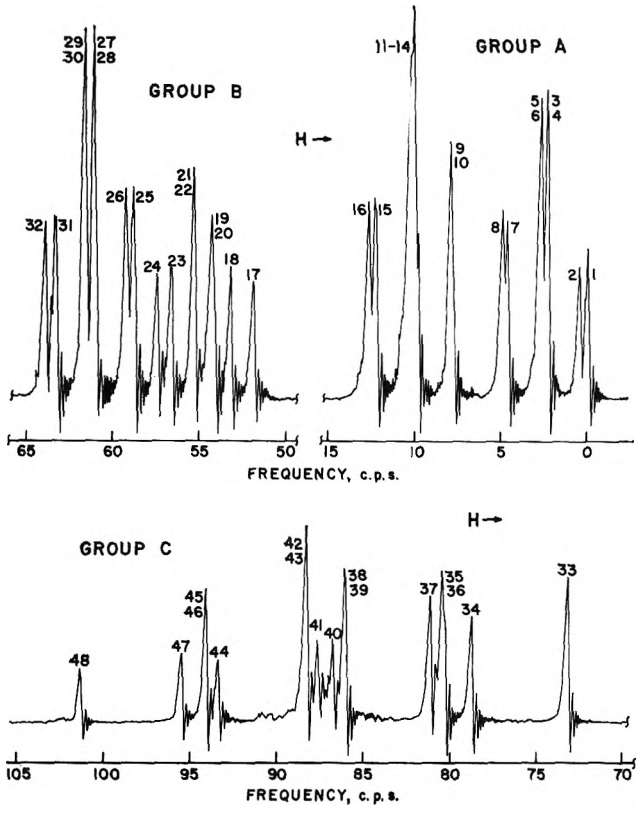

Figure 1. A 60-Mc. proton resonance spectrum of 4-chloro-1,2-butadiene (neat liquid). The high field line at 0 c.p.s. is 240.0 c.p.s. downfield from tetramethylsilane, internal.

compounds. The magnitudes and signs of the coupling constants based on this assignment are consistent with values found by Snyder and Roberts[1] for 1-chloro-1,2-butadiene: $J_{34} = +7.2$, $J_{13} = -5.8$, and $J_{14} = +2.4$ c.p.s.

The J_{34} coupling in these two isomers is a *vicinal* coupling, the absolute sign of which is believed to be *positive*.[7] It appears that allenic compounds may normally display a +, −, + sign alternation for the 3, 4, and 5 bond couplings, with magnitudes of about +7, −6, and +2 c.p.s.

Experimental

Compound I was prepared by 1,4-addition of HCl to monovinyl acetylene[8] and purified by distillation (b.p. 86–88°). Approximately 1% of the major expected impurity, 2-chloro-1,3-butadiene, was indicated by gas chromatography, but none of the known lines of this isomer were detected.

A Varian Associates A-60 n.m.r. spectrometer was employed to obtain spectra of the pure liquid and solutions. Tetramethylsilane was the internal standard. No marked solvent shifts were observed, so the analysis was performed on the spectrum of the pure liquid.

The line frequencies were determined by averaging two recordings (sweep rate, $r = 0.1$ c.p.s./sec., radio-frequency field strength, $H_1 = 0.08$ mgauss). The line intensities were obtained by averaging recorded electronic integrals ($r = 0.1$ c.p.s./sec., $H_1 = 0.05$ mgauss).

The double resonance experiments were performed on a Varian Associates HR-60 n.m.r. spectrometer equipped with an NMR Specialties PD60 homonuclear spin decoupler. The audio side-band signals were generated by a Hewlett-Packard 200CD audio oscillator, and the frequencies were measured with a Hewlett-Packard Model 522B frequency counter.

Table I: N.m.r. Parameters for 4-Chloro-1,2-butadiene

Group	Chemical shift, p.p.m.[a]	Coupling constant, c.p.s.
$H_2C=$	$\delta_1 = 4.972 \pm 0.001$	$J_{13} = -6.59 \pm 0.02$
$=CH-$	$\delta_3 = 5.434 \pm 0.001$	$J_{14} = +2.24 \pm 0.01$
$-CH_2Cl$	$\delta_4 = 4.110 \pm 0.001$	$J_{34} = +7.73 \pm 0.02$

[a] Downfield from tetramethylsilane, internal.

Acknowledgments. The author expresses his appreciation to the following persons for their assistance in this work. Dr. C. A. Aufdermarsh prepared and purified the samples. Drs. C. A. Reilly and J. D. Swalen provided a copy of their IBM 7090 computer program, which was employed by Mr. D. W. Marquardt and Mrs. Ruby Stanley in fitting the spectra. The spin decoupling experiments were performed by Prof. R. J. Kurland in Dr. E. G. Brame's laboratory.

(5) J. D. Roberts, private communication.

(6) N. S. Bhacca, L. F. Johnson, and J. N. Shoolery, "N.m.r. Spectra Catalog," Varian Associates, Palo Alto, Calif., 1962.

(7) P. C. Lauterbur and R. J. Kurland, *J. Am. Chem. Soc.*, **84**, 3405 (1962).

(8) W. H. Carothers, C. J. Berchet, and A. M. Collins, *ibid.*, **54**, 4066 (1932).

Ionic Mobilities and Tracer Diffusion Coefficients of *Alkali* Ions in Fused Alkali Nitrates

by J. A. A. Ketelaar and E. P. Honig

Laboratory for Electrochemistry, University of Amsterdam, Amsterdam, The Netherlands *(Received December 20, 1963)*

We wish to call attention to a remarkable observation concerning ionic mobilities and tracer diffusion coefficients (self-diffusion coefficients) of Na^+, K^+, Rb^+, and Cs^+ in each of the fused salts $NaNO_3$, KNO_3, $RbNO_3$, and $CsNO_3$ at 450°. Tracer diffusion coefficients of the alkali ions have been measured by the following method: a small amount of radioactive material which contains one of the isotopes ^{22}Na, ^{42}K, ^{86}Rb, or ^{137}Cs is brought on a certain spot of a glassfibre paper strip which is impregnated with alkali nitrate. The Gaussian distribution curve of radioactivity, which is the result of diffusion during a certain time, is determined after the experiment by a scanning technique. From this curve the tracer diffusion coefficient is calculated. The results are plotted in Fig. 1.

The ionic mobilities have been measured in an analogous way by applying a potential gradient along the impregnated paper strip and determining the radioactivity distribution curve after the experiment. The ionic mobility is then calculated from the displacement of the distribution curve, the potential gradient, and the time of the experiment.[1] The results are given in Fig. 2.

The proper cation in any of these four salts has the greatest ionic mobility and the greatest diffusion coefficient; all foreign cations, whether smaller or larger than the proper cation, have a lower mobility. There is only one slight exception to this rule, the diffusion coefficient of Rb^+ in $RbNO_3$ being slightly smaller than that of Cs^+ in $RbNO_3$, but this might very well be due to experimental errors. The ionic mobility of the nitrate

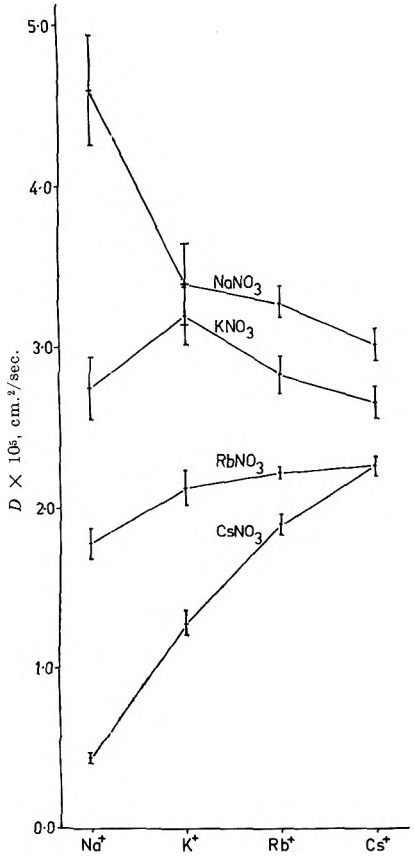

Figure 1. Tracer diffusion coefficients, D, of four alkali ions in $NaNO_3$, KNO_3, $RbNO_3$, and $CsNO_3$ at 450°.

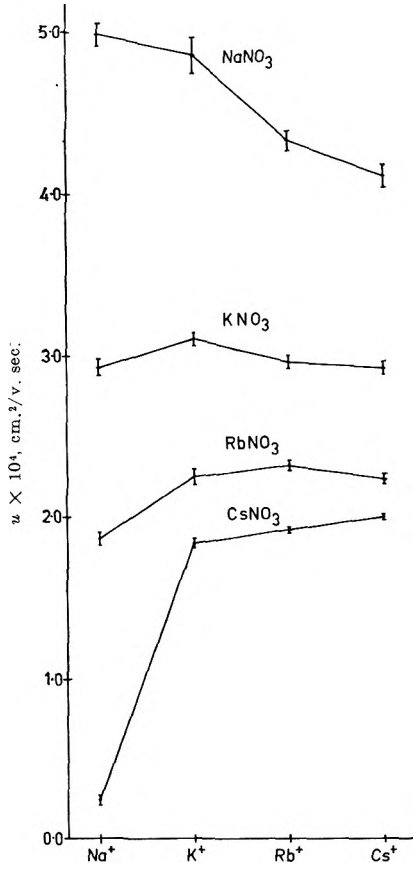

Figure 2. Ionic mobilities, u, of four alkali ions in $NaNO_3$, KNO_3, $RbNO_3$, and $CsNO_3$ at 450°.

(1) This method is similar to that of H. J. Arnikar, *Compt. rend.*, **244**, 2241 (1957).

ion is about the same in the four nitrates, *e.g.*, 2.55 ± 0.14 in $NaNO_3$, 2.45 ± 0.10 in KNO_3, 2.38 ± 0.08 in $RbNO_3$, and 2.38 ± 0.06 in $CsNO_3$ (units 10^{-4} cm.^{2}/v. sec.).

The ratio of the ionic mobility u and the diffusion coefficient D, $(RT/F)(u/D)$, has also been calculated in these sixteen different cases.[2] It has been found that this ratio is always less than unity (usually about $^2/_3$), contrary to the Nernst–Einstein equation which predicts $(RT/F)(u/D) = 1$.

Acknowledgment. The present investigations have been carried out under the auspices of the Netherlands Foundation for Chemical Research (S.O.N.) and with financial aid from the Netherlands Organization for the Advancement of Pure Research (Z.W.O.)

(2) The Nernst–Einstein equation has been discussed by several authors; for example: L. Yang, *J. Chem. Phys.*, **27**, 601 (1957); R. W. Laity, *ibid.*, **30**, 682 (1959).

The Activation Energy to Hindered Internal Rotation in Some Thionamides

by A. Loewenstein, A. Melera, P. Rigny, and W. Walter

Varian AG Research Laboratory, Zurich 8, Switzerland
(Received December 22, 1963)

The energy barrier, E, to hindered rotation of the C–N bond in several amides has been measured by the nuclear magnetic resonance (n.m.r.) technique. The temperature dependence of the internal rotation is conveniently described by the Arrhenius equation, $k = k_0 \exp(-E/RT)$, and the measured E values range from 6 to 18 kcal./mole.[1] It is of interest to compare these values to the corresponding ones in the thionamides[2] and this communication reports some results obtained for the latter with the n.m.r. technique. The compounds measured were: N,N′-dimethylthionformamide (DMTF) and N,N′-diisopropylthionformamide (DITF). In another compound, N-methyl-N′-phenylmethylthionformamide (MPTF), the enthalpy difference, ΔH, between the *cis* and *trans* forms, was obtained from the temperature dependence of the equilibrium constant. The n.m.r. spectra of DMTF and MPTF have previously been given by Walter and Maerten.[3]

A schematic description of the methyl, methylene, and methine proton resonances at low temperatures is given in Fig. 1. The resonances of the phenyl and H—C=S protons are shifted to lower fields and are omitted from the figure. Line positions are referred to tetramethysilane and are given in c.p.s. at 60 Mc. With increasing temperature, the following changes in the spectra are observed.

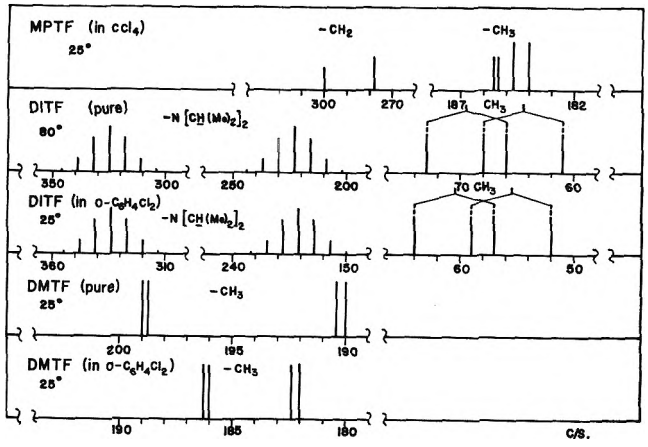

Figure 1. Schematic representation of the spectra of N-methyl-N′-phenylmethylthionformamide (MPTF), N,N′-diisopropylthionformamide (DITF), and N,N′-dimethylthionformamide (DMTF). The abscissa indicates the separation to lower magnetic field, in c.p.s., from tetramethylsilane. The relative intensities of the resonances in different groups are not drawn to scale.

(1) The intensities of the two CH_3 and two CH_2 resonances in MPTF change and tend to equalize. The logarithm of the intensity ratio of the CH_2 resonances was plotted as a function of the reciprocal absolute temperature and from the slope ΔH between the *cis* and *trans* forms was found to be 2.4 ± 0.5 kcal./mole (temperature range 25–90°).

(2) In DITF the two doublets and two septets broaden and eventually collapse to give a single doublet and a single septet folowing the well-established pattern of exchange modified n.m.r. multiplets.[1] The coalescence temperature of the doublet is approximately 173°. The mean lifetimes, $\tau = 1/k$, of the rotamers were obtained from the changes in the line shapes of the two doublets using the calculated curves for an exchange broadened doublet.[1] From the slope of a plot of ln $1/\tau$ *vs.* $1/T$, E was obtained. It should be noted that a complication arises from the fact that the chemical shift between the two spin–spin doublets

(1) A. Loewenstein and T. M. Connor, *Ber. Bunsenges. Physik. Chem.*, **67**, 280 (1963).

(2) Nomenclature follows R. N. Hurd and G. DeLaMater, *Chem. Rev.*, **61**, 45 (1961).

(3) W. Walter and G. Maerten, *Ann.*, **669**, 66 (1963).

Table I

Compound	Solvent	E, kcal./mole	k_0, sec.$^{-1}$	Number of measurements	Temp. range, °C.
DMTF	Pure	27.9 ± 1.1	(4.4 ± 0.5) × 10^{13}	4	176–193
DMTF	40% V in o-$C_6H_4Cl_2$	36.2 ± 1.7	(1.2 ± 0.3) × 10^{19}	7	141–179
DITF	Pure	31.8 ± 2.8	(8.9 ± 2.8) × 10^{14}	8	162–186
DITF	40% V in o-$C_6H_4Cl_2$	24.2 ± 5.6	(5.8 ± 4.2) × 10^{12}	6	147–175

is small; and thus, they partially overlap. Since only the chemical shift is averaged by fast rotation and the J splitting remains unaffected, the collapse occurs between neighboring pairs of lines.

(3) In DMTF the two closely spaced doublets of the methyl resonances collapse at high temperature to a single doublet. The rates of rotation were obtained by the approximate procedure used[4] in the similar case of dimethylformamide. A Lorentzian "envelope" was drawn on each of the closely separated doublets and the resulting, slightly broadened "doublet" was treated in the usual manner.[1] In pure DMTF, only "ratios" were used since the collapse temperature could not be attained, whereas in solution three measurements were obtained from the collapsed "doublet," using the fast exchange approximation.[1]

The results are summarized in Table I. All errors are probable errors calculated by least-squares fits of the lines. The number of measurements and the temperature ranges are also given.

The results show that the activation energies to hindered rotation in thionamides are much higher than the corresponding values in amides. Whereas in DITF some steric hindrance due to the bulky isopropyl groups might be effective, this can be ruled out for DMTF, the corresponding E value in N,N'-dimethylformamide being 10 kcal./mole.[4] The contribution of the polar form $^-X—C=N^+$, where X is oxygen or sulfur, probably determines the value of E. It must thus be concluded that this contribution is higher in thionamides than in amides. This is so in spite of the higher electronegativity of oxygen relative to sulfur. The same conclusion was reached in other studies of the carbon–sulfur double bond by means of infrared, ultraviolet, and dipole moment measurements.[5]

It should be noted that there is a marked solvent effect for E (Table I) and for the chemical shifts (Fig. 1). The solvent effect has opposite direction for DITF and DMTF. This suggests that the solvent molecules are strongly associated with the thionamides and are also involved in the transition state. Similar effects were noticed for E measurements in amides and for ring inversions.[1] The nature of the association seems to be different in the two thionamides studied and thus far is not understood.

All measurements were performed on a Varian A-60 n.m.r. spectrometer equipped with a V-6040 variable temperature attachment. Compounds were prepared by a method given by Walter and Maerten.[3]

Acknowledgment. A. L. and P. R. wish to thank Varian AG Research Laboratory for the kind hospitality during their summer visit.

(4) G. Fraenkel and C. Franconi, *J. Am. Chem. Soc.*, **82**, 4478 (1960).

(5) (a) L. J. Bellamy, "Organic Sulfur Compounds," N. Kharasch, Ed., *Pergamon Press, London*, 1961, p. 52; (b) C. M. Lee and W. D. Kumler, *J. Org. Chem.*, **27**, 2052 (1962); (c) S. C. Abrahams, *Quart. Rev.* (London), **10**, 407 (1956); (d) M. J. Janssen, *Rec. trav. chim.*, **82**, 931 (1963).

Relation between Steady-Flow and Dynamic Viscosity for Polyethylene Melts[1]

by Shigeharu Onogi, Tsuguo Fujii, Hideo Kato, and Sadahide Ogihara

Department of Polymer Chemistry, Kyoto University, Kyoto, Japan
(Received December 23, 1963)

The relation between steady-flow and dynamic viscosities is an important problem which has been studied theoretically and experimentally by many investigators cited below. Unfortunately, however, the conclusions of these investigations are diverse, and we cannot know the nature of apparent viscosity at present.

In the previous paper,[2] rheological properties of polyethylene melts at various temperatures were meas-

(1) Paper presented at the 12th Annual Symposium on Rheology, Tokyo, Japan, September, 1963.

(2) M. Horio, T. Fujii, and S. Onogi, paper presented at the 145th National Meeting of the American Chemical Society, New York, N. Y., September, 1963 (to be published).

ured with a rotating cylinder type rheometer, and the effects of temperature and blending were mainly studied. The rheometer used in this study enables us to measure not only the steady-flow viscosity in a wide range of rate of shear, but also the dynamic viscosity and rigidity in a wide range of frequency by a minor change in its driving system.[3] Therefore, the steady-flow and dynamic properties measured with this instrument can be very favorably compared with each other in their rate of shear and frequency dependences, because they are not affected by any factor due to the difference in measuring methods. This note is concerned with the comparison of our experimental results of flow properties for polyethylene melts with the current theories and existing data on the relation between the steady-flow and dynamic viscosities.

Experimental

The polyethylene samples used in this study are Dow polyethylene 544 (polymer A) and 910M (polymer B) and quite the same as those reported in the previous paper.[2] The method of measurement is also the same as the previous one, and accurate flow curves were determined by the single-bob method proposed by Krieger and Maron.[4] The apparent viscosity, η_a, and the consistency, η_c, or differential viscosity, η_d, were evaluated, respectively, as S/D and dS/dD, where S and D represent the shearing stress and rate of shear or velocity gradient.

Results and Discussion

As mentioned in the previous paper,[2] the rate of shear dependence curves of η_a at various temperatures can be superposed very well to give a master curve according to the usual method of time–temperature superposition without any correction for temperatures. Figure 1 gives master curves of η_a measured for polymers A and B at 140, 160, 180, and 200°. For the purpose of comparison, similar master curves of the dynamic viscosity, η', and the dynamic rigidity, G', for the same polymers and at the same temperatures are reproduced in Fig. 2.

In Fig. 3 the rate of shear, D, dependence of apparent viscosity, η_a, and apparent fluidity, $1/\eta_a$, are compared with the angular frequency, ω, dependence of dynamic viscosity, η', dynamic fluidity, $J''\omega$ (J'' is the loss compliance), and the absolute value of complex viscosity, $|\eta^*| = [\eta'^2 + (G'/\omega)^2]^{1/2}$, for polymer A at 160°, assuming $D = \omega$. Similar results for polymer B are shown in Fig. 4.

According to the theory of DeWitt,[5] the two curves at the top of these figures should coincide with each other, but the η'-curve decreases earlier. The same

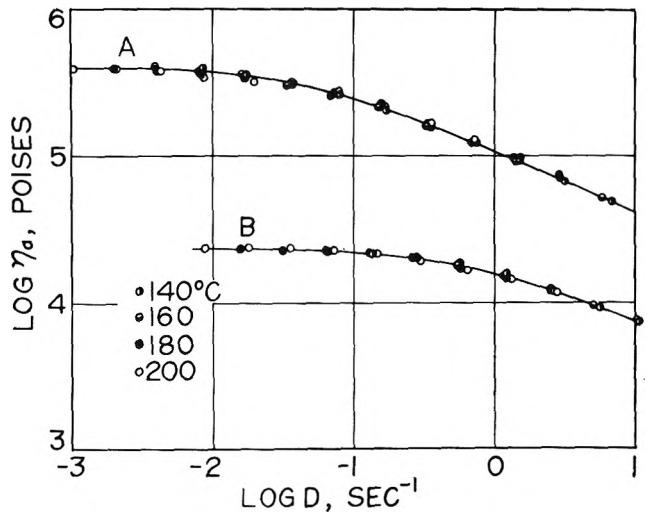

Figure 1. Master curves of η_a for polymers A (Dow polyethylene 544) and B (Dow polyethylene 910M). The reference temperature is 160°.

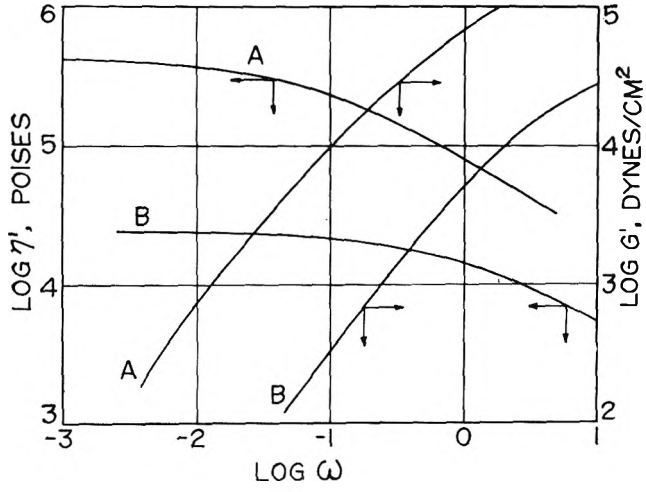

Figure 2. Master curves of η' and G' for polymers A and B (log ω in sec.$^{-1}$). The reference temperature is 160°.

tendency of η' has been reported by several authors,[6-10] and some of them stated that $\eta_a(D)$ is the same as $\eta'(c\omega)$, when $c = 1.4$–1.5,[6,7] or $c = 2.2$–2.3.[8,10] On the

(3) M. Horio, S. Onogi, and S. Ogihara, *J. Japan. Soc. Testing Mater.*, **10**, 350 (1961).

(4) I. M. Krieger and S. H. Maron, *J. Appl. Phys.*, **23**, 147 (1952); **25**, 72 (1954).

(5) T. W. DeWitt, *ibid.*, **26**, 889 (1955).

(6) T. W. DeWitt, H. Markovitz, F. J. Padden, and J. Zapas, *J. Colloid Sci.*, **10**, 174 (1955).

(7) H. Markovitz and B. Williamson, *Trans. Soc. Rheology*, **1**, 25 (1957).

(8) W. Philippoff, *J. Appl. Phys.*, **25**, 1102 (1954).

(9) S. Onogi, I. Hamana, and H. Hirai, *ibid.*, **29**, 1503 (1958).

(10) T. Arai, *Chem. High Polymers*, **18**, 292 (1961).

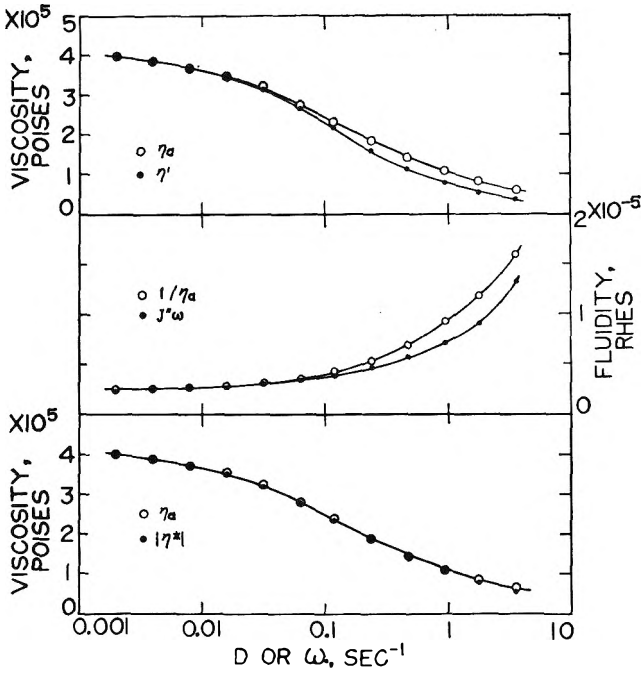

Figure 3. A comparison of steady-flow properties with dynamic ones for polymer A at 160°.

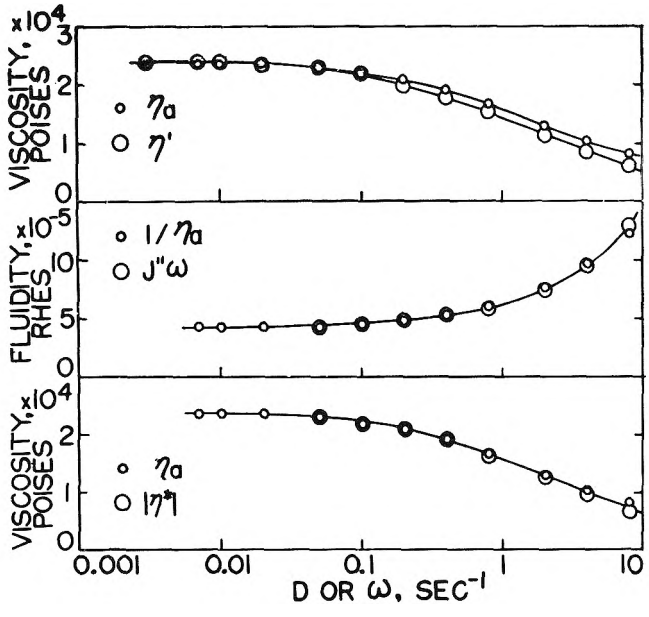

Figure 4. A comparison of steady-flow properties with dynamic ones for polymer B at 160°.

other hand, Williams and Bird[11] have recently derived $c = 1.24$ theoretically on the basis of the three-constant Oldroyd model.[12] According to our results shown in Fig. 3 and 4, however, c is not a constant and increases from 1 to about 3.1 for polymer A and to about 2.7 for polymer B with increasing D or ω. This means that η_a or η' curves cannot be superposed by a simple shift along the abscissa to coincide with each other. However, in the case of polymer B, in which the change in viscosity is rather small, the viscosity curves appear to be superposed fairly well by shifting either of the two by a factor of about 1.5.

Pao's theory[13] requires $1/\eta_a(D)$ to be the same as $J''\omega(\omega)$. Our result in Fig. 3 (middle) does not satisfy this requirement, especially at higher rates of shear or frequencies, while that in Fig. 4 (middle) does very well. The reason why such a difference arises between two polymers is not clear.

Next, Cox and Merz[14-16] have found empirically that $\eta_a(D)$ is equal to $|\eta^*|(\omega)$ for melts of polystyrene and polyethylene, and Williams and Bird[11] have showed that $\eta_a(D)$ should be the same as $|\eta^*|(k\omega)$, where k is a constant varying from 0.91 to 1.12. The above experimental studies by Cox, *et al.*, suggest that $k = 1$. As seen from Fig. 3 and 4 (bottom), $\eta_a(D)$ for polymers A and B coincides very well with $|\eta^*|(\omega)$, indicating that $k = 1$ here also.

Recently, Strella[17] has discussed the same problem of the relation between the steady-flow and dynamic viscosities, and derived the empirical law originated by Cox and Merz on the basis of a Voigt element. According to him, the consistency $\eta_c(D)$ or differential viscosity $\eta_d(D)$ should be the same as $\eta'(\omega)$, and hence $\eta_a = \eta_c + (G'/\omega)$, when $k = 1$. In Fig. 5, η_c is compared with η' and η_a with $[\eta_c + (G'/\omega)]$ for polymer A at 160°. It is clear from this figure that η_c is much lower than η' at intermediate rates of shear or frequencies. It coincides with η' very well only at very low and high rates of shear or frequencies. On the other hand, $[\eta_c + (G'/\omega)]$ is several per cent higher than η_a or $|\eta^*|$ at most frequencies except for the middle region. When one allows for the experimental errors in the measurements and in the time–temperature superposition, one may have to conclude that $[\eta_c + (G'/\omega)]$ is the same as η_a within experimental errors. However, the former shows a much different tendency from the latter, as is seen by comparing the curves in the figure.

In conclusion, the relation between the steady-flow and dynamic viscosities for polyethylene melts can be

(11) M. C. Williams and R. B. Bird, *Phys. Fluids*, **5**, No. 9 (1962).

(12) J. G. Oldroyd, *Proc. Roy. Soc.* (London), **A245**, 278 (1958).

(13) Y. H. Pao, *J. Appl. Phys.*, **28**, 591 (1957).

(14) W. P. Cox and E. H. Merz, *J. Polymer Sci.*, **28**, 619 (1958).

(15) W. P. Cox and E. H. Merz, *Am. Soc. Testing Mater.*, **247**, 178 (1958).

(16) W. P. Cox, *Offic. Dig., Federation Soc. Paint Technol.*, **32**, 2 (1960).

(17) S. Strella, *J. Polymer Sci.*, **60**, S9 (1962).

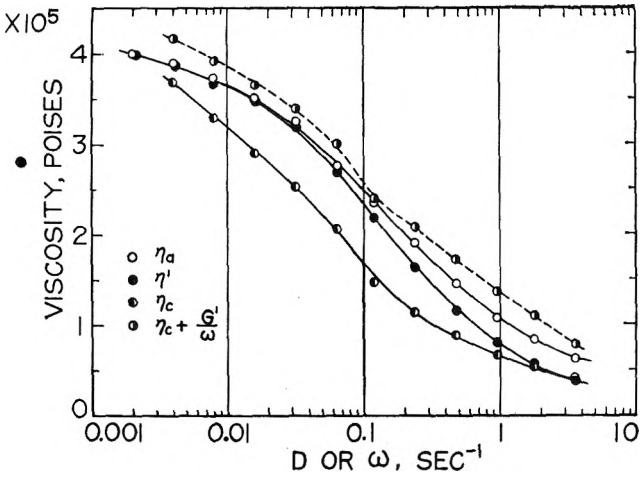

Figure 5. A comparison of η_c with η' as well as of $[\eta_c + (G'/\omega)]$ with η_a or $|\eta^*|$ for polymer A at 160°.

explained by none of the current linear theories cited above: the constant c appearing in the theory of Williams, *et al.*, varies with D or ω, and $\eta'(\omega)$ is not the same as $\eta_c(D)$ in contrast to the prediction of the theory by Strella. Very recently, Yamamoto[18] has presented a new phenomenological theory for non-Newtonian flow on the basis of the three-dimensional nonlinear model and compared theoretical curves for $\eta_a(D)$ with that for $\eta'(\omega)$. His result also shows that the constant c increases with increasing D or ω, in general. Therefore, we are inclined to ascribe the above lack of agreement of our observations with the linear theories to an essential difference between the steady-flow and dynamic behavior: the latter is linear while the former is nonlinear.

(18) M. Yamamoto, paper presented at the 12th Annual Symposium on Rheology, Tokyo, Japan, September, 1963 (to be published).

Pyridine Interactions with Phenol and Substituted Phenols

by Jerome Rubin, Bernard Z. Senkowski, Gilbert S. Panson

Chemistry Department, Rutgers University, Newark, New Jersey
(Received January 7, 1964)

Several investigations have appeared in the literature describing hydrogen bonding of phenol in the presence of pyridine. Values reported for the equilibrium constant at 20° obtained under different experimental conditions were 42,[1] 55 ± 10,[2] 64,[3] and 88.[4] The equilibrium constant at 21° was determined in this laboratory from near-infrared measurements and found to be 59 ± 5.

The effect of ring substitution in phenol on the equilibrium constant was also investigated. Only limited data, primarily dealing with substituted pyridines,[1] have appeared in the literature concerning this reaction. A correlation of the hydrogen-bonding equilibrium constants with the Hammett substituent parameters was obtained. Apparently this effect has not been studied or has not appeared in the literature prior to this investigation.

Experimental

The phenols and pyridine were purified by recrystallization and/or distillation *in vacuo* prior to use. The carbon tetrachloride was Matheson Coleman and Bell Spectroquality grade and used with no further treatment. All measurements were performed with a Beckman DK II ratio recording spectrophotometer at 21 ± 1°. Matched silica cells 5 cm. in length were used. All solutions were measured with an equivalent concentration of pyridine in the reference cell.

Absorbance measurements at 1.4 μ were utilized in the evaluation of the equilibrium constants. This overtone of the fundamental hydroxyl group vibration was selected since no interfering absorption was encountered at this wave length. The molar absorptivities of the pure phenols were determined under conditions where

Table I: Equilibrium Constant Values at 21°, l./mole[a]

Phenol[b]	*p*-Methyl[b]	*m*-Methyl[b]	*p*-Methoxy[b]	*p*-*t*-Butyl[b]	*p*-Iodo[c]	*m*-Chloro[c]	*p*-Chloro[b]
65.6	48.1	47.8	48.5	34.8	148	192	145
59.2	46.0	46.2	45.1	38.7	151	182	142
61.7	42.7	44.2	43.4	41.8	152	166	124
54.6	40.6	40.2	42.6	39.4	146	183	123
56.0	41.2	41.8	39.5	40.0	140	176	128
54.1	40.1	40.0	41.6	38.7	140	167	116
52.8	40.3	40.5	39.4	38.2	129	160	116
	42.5	41.1	40.4	38.9	128		112
	40.0	41.3	39.5	39.2			
	38.8	47.0		42.0			
59 ± 5	42 ± 2	43 ± 3	42 ± 2	39 ± 2	142 ± 8	175 ± 9	126 ± 10

[a] The phenol concentrations in all solutions was 0.025 *M*. [b] All solutions studied, except *p*-iodo- and *m*-chlorophenol, contained pyridine at concentrations from 0.01 to 0.10 *M*. [c] In the case of *p*-iodo- and *m*-chlorophenol, the pyridine concentration varied from 0.020 to 0.040 *M*.

(1) A. Halleux, *Bull. soc. chim. Belges*, **68**, 381 (1959).
(2) N. Fuson, *et al.*, *J. Chem. Phys.*, **55**, 454 (1958).
(3) G. Aksnes and T. Gramstad, *Acta Chem. Scand.*, **14**, 1485 (1960).
(4) A. K. Chandra and S. Banerjee, *J. Phys. Chem.*, **66**, 952 (1962).

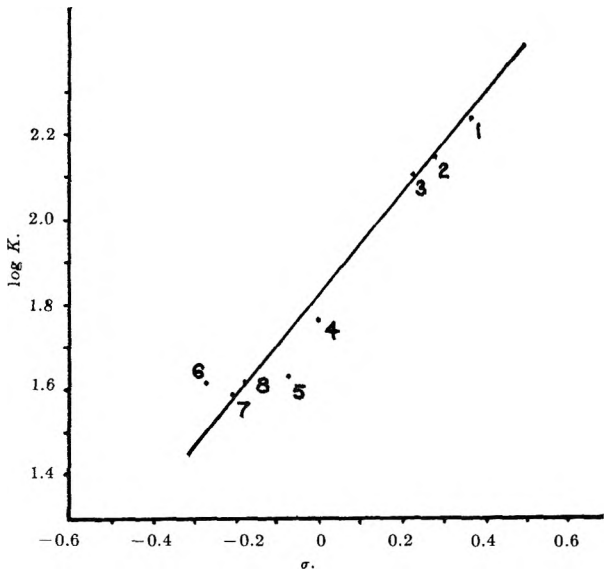

Figure 1. Log K *vs.* Hammett's σ-values. Points are: (1) *m*-chloro, (2) *p*-iodo, (3) *p*-chloro, (4) phenol, (5) *m*-methyl, (6) *p*-methoxy, (7) *p*-*t*-butyl, (8) *p*-methyl.

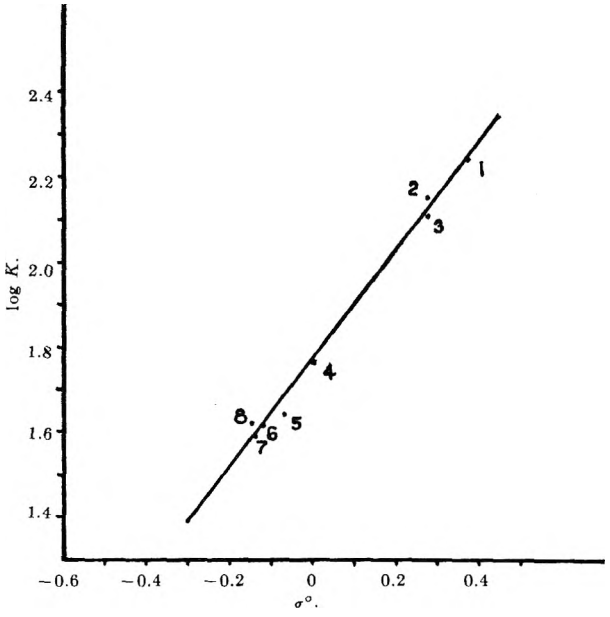

Figure 2. Log K *vs.* Tafts' σ°-values. Points are: (1) *m*-chloro, (2) *p*-iodo, (3) *p*-chloro, (4) phenol, (5) *m*-methyl, (6) *p*-methoxy, (7) *p*-*t*-butyl, (8) *p*-methyl.

self-bonding did not occur. The decrease in absorbance at 1.4 μ was used to calculate the concentration of the free phenol; the bonded-phenol concentration was obtained by difference. These data were utilized in evaluating the equilibrium constants. The results are given in Table I. The average values obtained were plotted against the Hammett σ-[5] and Taft σ°[6]-parameters in the usual manner and are presented in Fig. 1 and 2, respectively.

Discussion and Results

Although a good correlation was obtained using Hammett's σ-parameters, as is evident from Fig. 1, slightly better agreement results when Taft's σ°-values were used in the plot. The calculations of the slope [ρ] were obtained by least-squares treatment of the data. The equation of the line calculated using Hammett's σ-values was $y = 1.14x + 1.26$. Taft's σ°-values were plotted and the equation of the line calculated was $y = 1.29x + 1.13$.

Denyer, *et al.*,[7] had made a limited study of the equilibrium constants of phenol, *p*-chlorophenol, and *m*- and *p*-methylphenol with trimethylamine by partition between vapor phase and solution. These authors were primarily interested in the determination of hydrogen bonding and heats of formation. Their data were evaluated in this laboratory and the equation of the line using σ°-values was found to be $y = 1.20x + 1.34$. The ρ-value obtained from these data is 1.20 which is in good agreement with the value of 1.29 found in our study of pyridine and substituted phenols.

An extensive investigation is currently in progress to evaluate the interaction of substituted pyridines with additional substituted phenols.

(5) L. P. Hammett, "Physical Organic Chemistry," McGraw-Hill Book Co., Inc., New York, N. Y.

(6) R. W. Taft, Jr., *J. Phys. Chem.*, **64**, 1805 (1960).

(7) R. L. Denyer, *et al.*, *J. Chem. Soc.*, 3889 (1955).

Nuclear Magnetic Resonance Coupling Constants in Maleic and Itaconic Acids and Their Anhydrides

by H. M. Hutton[1] and T. Schaefer

Department of Chemistry, University of Manitoba, Winnipeg, Manitoba, Canada *(Received January 16, 1964)*

We wish to report some nuclear magnetic spin–spin coupling constants for maleic and itaconic acids and their anhydrides. They are given in Table I. In Table I the protons of itaconic acid and anhydride are labeled to indicate the type of proton magnetic resonance spectra they give rise to, *i.e.*, ARX_2 or ABX_2 spectra.[2] The proton coupling constants for maleic

(1) Canadian Industries Limited Fellow, 1962–1963.

(2) J. A. Pople, W. G. Schneider, and H. J. Bernstein, "High Resolution Nuclear Magnetic Resonance," McGraw-Hill Book Co., New York, N. Y., 1959, Chapter 6.

acid and anhydride were obtained from the analysis of the multiplets arising from those molecules containing C^{13} nuclei.[3] Muller[4] has reported $J(^{13}C-H) = 167.6 \pm 0.3$ c.p.s. and $J(H-H) = 11.9$ c.p.s. for diethyl maleate.

Table I: Coupling Constants in c.p.s. for Maleic and Itaconic Acids and Their Anhydrides

Compound	Coupling constants[a,b]
Maleic acid	$J(H-H) = 12.2 \pm 0.1$ $J(^{13}C-H) = 169.3 \pm 0.3$
Maleic anhydride	$J(H-H) = 5.72 \pm 0.18$ $J(^{13}C-H) = 189.5 \pm 0.7$
$HOCO(CH_2)_xC(:CH_AH_R)COOH$	$J_{AR} = J_{AX} = 1.28 \pm 0.05$ $J_{XR} \sim 0$
$OCO(CH_2)_xC(:CH_AH_B)CO$	$J_{AX} = 2.80 \pm 0.05$ $J_{BX} = 2.36 \pm 0.05$ $J_{AB} \sim 0$

[a] Error limits are r.m.s. deviations. [b] Relative signs could not be determined from the spectra.

There is a substantial change in the magnitude of the coupling constants on ring formation. The *gem*-proton coupling in the itaconic molecules increases on ring formation while the 1,3 couplings decrease. In the maleic molecules the carbon–hydrogen coupling increases markedly on ring formation, indicating an increase in s-character of the trigonal carbon bonding orbital to hydrogen.[5,6] The *cis*-proton coupling decreases by over 50% on ring formation, to a value typical of five-membered *cis*-cyclic olefins.[7] According to Karplus,[8] this represents an increase in the H—C=C angle on ring formation. This increase in angle might be expected from an increase in s-character of the carbon bonding orbitals to hydrogen, in agreement with the change found in the carbon–hydrogen coupling. As noted by Karplus,[8] the *cis* couplings depend on many other factors as well, and a quantitative discussion would hardly be justified in the present instance.

The coupling constant changes may find practical use in the determination of relative amounts of rings and chains in tautomeric equilibria. For instance, the extensive examination of ring–chain tautomerism of *cis*-β-aroylacrylic acids by ultraviolet spectroscopy[9] could perhaps be supplemented by proton resonance measurements. A recent review of ring–chain tautomerism[10] states that as yet nuclear magnetic resonance spectroscopy has not been employed in this connection.

Experimental

The proton resonance spectra were taken at 60 Mc.p.s. on a Varian DP-60 spectrometer. Spectra were calibrated using the side-band technique and a Hewlett–Packard 521-C frequency counter. Maleic acid was measured as a saturated solution in heavy water while its anhydride and itaconic acid were used as saturated solutions in acetone. Itaconic anhydride was measured as 10 mole % solutions in acetone and in benzene. The coupling constants were the same within experimental error in both solutions.

Acknowledgments. This research was supported by the National Research Council, Ottawa, and by Canadian Industries, Limited.

(3) A. D. Cohen, N. Sheppard, and J. J. Turner, *J. Chem. Soc.*, 118 (1958).
(4) N. Muller, *J. Chem. Phys.*, **37**, 2729 (1962).
(5) N. Muller and D. E. Pritchard, *ibid.*, **31**, 768, 1471 (1959).
(6) C. Juan and H. S. Gutowsky, *ibid.*, **37**, 2198 (1962).
(7) O. L. Chapman, *J. Am. Chem. Soc.*, **85**, 2870 (1963).
(8) M. Karplus, *ibid.*, **85**, 2870 (1963).
(9) R. E. Lutz and H. Moncure, Jr., *J. Org. Chem.*, **26**, 746 (1961).
(10) P. R. Jones, *Chem. Rev.*, **63**, 461 (1963).

Transference Numbers in Aqueous Sodium Chloride at Elevated Temperatures

by Josiah E. Smith, Jr., and Edward B. Dismukes

Southern Research Institute, Birmingham, Alabama
(Received January 30, 1964)

Cation transference numbers in aqueous 0.1 *N* potassium chloride at temperatures up to 115° were recently reported.[1] These data were obtained in moving-boundary experiments in which an electrometric method rather than a conventional optical procedure was used to determine the location of a moving boundary in a system at an elevated temperature and an elevated pressure. Cation transference numbers in aqueous 0.1 *N* sodium chloride at temperatures up to 125°, which were obtained by the same electrometric procedure, are now presented.

Calculations have been made of the conductance of chloride ion at 100°, based on transference numbers in sodium chloride and potassium chloride solutions. The values obtained are in agreement, as expected, within the limits of uncertainty imposed by the available conductance data.

(1) J. E. Smith, Jr., and E. B. Dismukes, *J. Phys. Chem.*, **67**, 1160 (1963).

Experimental

The apparatus and procedures used in moving-boundary experiments were essentially the same as described previously.[1] In brief, an electrolysis cell of the autogenic type, which permitted the formation and displacement of a boundary between sodium chloride and cadmium chloride solutions, was located in a heated oil bath inside a steel cylinder under nitrogen at a pressure of 30 p.s.i.g. The cell contained a capillary section with platinum probe electrodes sealed into its wall at different heights. Connections from these probe electrodes to an electrometer circuit permitted the determination of the times when the moving boundary reached each probe location.

The only significant change from the previous description was a simplification of the probe electrodes. Two electrodes about 10 cm. apart rather than four electrodes were found to be adequate. The electrometer was used to monitor the potential between the cathode of the electrolysis cell and one of the probe electrodes: first the lower probe until the boundary had passed that position, and then the upper probe until the boundary had passed that position. The potential was affected very little by changes in the electrolyte concentration near the cathode. It remained virtually constant until it began increasing at a constant rate when the boundary had passed the probe.

Approximately 0.1 N solutions of sodium chloride, which were used to fill the electrolysis cell initially in experiments for the determination of cation transference numbers, were prepared from weighed amounts of sodium chloride and conductivity water. The sodium chloride was reagent grade salt that had been precipitated from concentrated hydrochloric acid, recrystallized from conductivity water, and fused in platinum under dry helium. The conductivity water had a specific conductance of 0.8×10^{-6} ohm^{-1} cm.$^{-1}$, which was low enough to avoid a significant solvent effect in transference-number determinations. The concentration of sodium chloride in equivalents per liter at the temperature of a moving-boundary experiment was calculated from weights *in vacuo* and from density data in the "International Critical Tables."

Results and Discussion

The transference number of sodium ion, t_{Na}, was calculated from the equation

$$t_{Na} = (v + \Delta v)CF/i\Delta t$$

In this equation, v is the volume (ml.) between probe electrodes in the electrolysis cell, Δv is a "volume-correction" term,[2] C is the sodium chloride concentration (equiv./l.), F is the Faraday constant, i is the current (ma.), and Δt is the time (sec.) required for movement of the boundary from the lower probe to the upper probe.

The value of v was calculated from the results of calibration experiments with 0.09733 N sodium chloride at 35°, where the value of 0.3893 was used for t_{Na}. Allgood and Gordon[3] have reported t_{Na} to be 0.3892 in a 0.1 N sodium chloride solution at 35°, and the data of these authors for lower concentrations indicate that t_{Na} is 0.3893 ± 0.0001 in the slightly more dilute solution used in the calibration experiments. In six calibration experiments, a mean value of v of 0.2701 ml., with an average deviation from the mean of 0.0003 ml., was obtained. Because of the apparent scatter of about 0.1% in the experimental results, variations in the cell volume and in the correction term Δv were ignored in the determination of t_{Na} at elevated temperatures.

Experimental data for temperatures above 35° are listed in the second and third columns of Table I. As shown by this table, the solutions used varied between 0.09021 and 0.09595 in normality. For a comparison of values of t_{Na} at different temperatures but at a fixed concentration, the experimental values were recalculated for the concentration of 0.1 N. This was done by use of the value −0.05 for the coefficient $\Delta t_{Na}/\Delta C$, which is consistent with the data of Allgood and Gordon[3] at four temperatures, from 15 to 45°, and at concentrations throughout the relatively wide range from 0.05 to 0.10 N. The correction made to obtain t_{Na} at 0.1 N was in every case small, not exceeding 0.0005.

Table I: Cation Transference Numbers in Aqueous Sodium Chloride

Temperature, °C.	Normality	t_{Na}, obsd.	Normality	t_{Na}, calcd.
54	0.09360	0.3953	0.1000	0.3950
55	0.09360	0.3960	0.1000	0.3957
65	0.09312	0.3981	0.1000	0.3978
65	0.09595	0.3985	0.1000	0.3983
65	0.09595	0.3980	0.1000	0.3978
85	0.09478	0.4037	0.1000	0.4034
105	0.09342	0.4084	0.1000	0.4081
125	0.09191	0.4143	0.1000	0.4139
125	0.09021	0.4136	0.1000	0.4131

(2) D. A. MacInnes and L. G. Longsworth, *Chem. Rev.*, 11, 171 (1932).

(3) R. W. Allgood and A. R. Gordon, *J. Chem. Phys.*, 10, 124 (1942).

Values for t_{Na} in 0.1 N sodium chloride from the present investigation (open symbols) and from an earlier investigation[3] (closed symbols) are shown graphically in Fig. 1. In the preparation of this figure, the function log $(1 - t_{Na})/t_{Na}$ was calculated and plotted *vs.* the reciprocal of the absolute temperature, $1/T$, as in previous work.[1,3,4] The error limits indicated for 35° correspond to the range in values of Δv observed in calibration experiments. At each higher temperature where two or more values of t_{Na} were obtained, the range appears to be about the same.

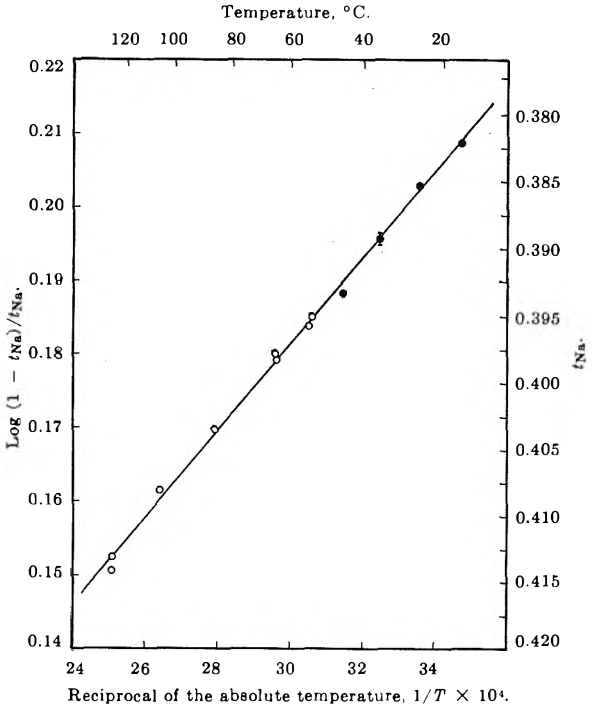

Figure 1. Temperature dependence of transference numbers in 0.1 N NaCl. (Values of log $(1 - t_{Na})/t_{Na}$ and $1/T \times 10^4$ are plotted on linear scales; values of the other properties are, consequently, not on linear scales, although those of t_{Na} are very nearly so.) O, this study; ●, ref. 3.

The apparent linearity between log $(1 - t_{Na})/t_{Na}$ and $1/T$ can be construed to mean that the activation energies for the electrical mobilities of sodium ion and chloride ion differ by an amount that is independent of the temperature. The difference is about 270 cal./g.-ion, the activation energy for chloride ion being less than that for sodium ion. The linearity of corresponding data for aqueous potassium chloride has indicated that the activation energy for chloride ion is about 120 cal./g.-ion, greater than that for potassium ion.[1]

Interpolations of the transference number data given in this article and in a previous article[1] lead to the following values for the transference number of chloride ion in 0.1 N solutions at 100°: NaCl, $t_{Cl} = 0.592$; KCl, $t_{Cl} = 0.520$. The following estimates have been made of the transference number of chloride ion in infinitely dilute solutions at 100°: NaCl, $t_{Cl}^0 = 0.581$; KCl, $t_{Cl}^0 = 0.522$. The estimate for t_{Cl}^0 in sodium chloride solution was obtained by use of the value 0.9822 at 100° for t_{Cl}^0/t_{Cl} (the ratio of the transference numbers at infinite dilution and at 0.1 N) in sodium chloride solutions. Allgood and Gordon's data[3] show that this ratio is equal to 0.9822 ± 0.0002 between 15 and 45° with no apparent dependence on the temperature. The estimate for t_{Cl}^0 in potassium chloride solution was obtained by use of the value 1.004 at 100° for the t_{Cl}^0/t_{Cl} ratio in potassium chloride solutions; values of this ratio from Allgood, LeRoy, and Gordon's data between 15 and 45°, showing an increase of about 0.006% per degree, were extrapolated to 100° by a least-squares treatment to obtain the value 1.004.

The estimated value of t_{Cl}^0 for potassium chloride at 100°, 0.522, agrees well with the value used by Robinson and Stokes,[5] 0.520, in their estimates of the Walden product $\lambda^0\eta^0$ at 100° for various ions. Robinson and Stokes' value was based upon an extrapolation of experimental data at much lower temperatures, 15° to 45°.

Values from the literature for the equivalent conductances of sodium chloride and potassium chloride

Table II: Conductances at 100°

Reference for Λ values	—NaCl solution— N	Λ	λ_{Cl}	—KCl solution— N	Λ	λ_{Cl}
International Critical Tables[a]	0	355	206	0	400	209
Landolt–Börnstein[b]	0	361	210	0	406	212
International Critical Tables[a]	0.1	296	175	0.1	336	175
Landolt–Börnstein[b]	0.1	298	176	0.1	327	170
Gorbachev and Kondrat'ev[c]	...	...	...	0.1	333	173

[a] "International Critical Tables," Vol. VI, McGraw-Hill Book Co., New York, N. Y., 1929, pp. 233–234. [b] "Landolt-Börnstein Zahlenwerte und Funktionen," Vol. II, 6th Ed., Springer-Verlag, Berlin, 1960, Part 7, p. 126. [c] S. V. Gorbachev and V. P. Kondrat'ev, *Zh. Fiz. Khim.*, **35**, 1235 (1961).

(4) R. W. Allgood, D. J. LeRoy, and A. R. Gordon, *J. Chem. Phys.*, **8**, 418 (1940).

(5) R. A. Robinson and R. H. Stokes, "Electrolyte Solutions," Butterworths Scientific Publications, London, 1955, pp. 121–124.

at 100° were multiplied by the values given above for the transference number of chloride ion in order to obtain values for the conductance of chloride ion at 100°. The results are listed in Table II. Within the apparent limits of uncertainty in the salt conductances, the values obtained for the chloride ion conductance in both salts are the same, as expected. In 0.1 N solution, the chloride ion conductance is 174 ± 4 cm.^{2} ohm^{-1} equiv.$^{-1}$; at infinite dilution, it is 209 ± 3 cm.^{2} ohm^{-1} equiv.$^{-1}$.

Acknowledgment. The authors express their appreciation to the Division of Research of the Office of Saline Water, U. S. Department of the Interior, for the financial support (Contract No. 14-01-0001-254) that made this research possible.

The Thermal Decomposition of Ethyl Cyclobutyl Ketone[1]

by B. C. Roquitte and W. D. Walters

Department of Chemistry of the University of Rochester, Rochester, New York *(Received February 1, 1964)*

Various studies in this laboratory have been concerned with the kinetics of the thermal decompositions of derivatives of cyclobutane and the influence of the change of molecular structure upon the rate of pyrolysis. Compounds[2,3] with CH_3CO or HCO attached to the cyclobutane ring have been found to decompose faster and have activation energies 7–9 kcal./mole lower than alkyl-substituted cyclobutanes.[4] The change from HCO to CH_3CO on the cyclobutane ring seems to result in a slight increase in activation energy (from 53.3 to 54.5 kcal./mole) and a somewhat slower rate. In the present work the decomposition of ethyl cyclobutyl ketone has been studied in order to ascertain the effect of the replacement of a methyl group by an ethyl group in the series of carbonyl derivatives.

Experimental

Materials and Apparatus. The ethyl cyclobutyl ketone used in this study had been prepared by Kellner at an earlier time.[4b] The sample was dried and then distilled under vacuum. A middle fraction, with a purity greater than 99%, was used in the early kinetic experiments. Due to the smallness of the sample only an approximate boiling point (153.5–155.5° at 749 mm.) was obtained for comparison with the literature value of 154–155° at 750 mm.[5] The refractive index was found to be n^{25}D 1.4340 (lit. n^{25}D 1.4339).[6] For later experiments the sample was purified on a Perkin-Elmer Model 154B vapor fractometer by the use of a 1-m. A column (diisodecyl phthalate on a Celite base). The purified sample was found to be 99.9% pure by gas chromatography. In the vapor phase the compound showed medium to strong absorptions at 3.40–3.45, 5.80–5.85, 7.35–7.40, and 8.9 μ. No difference in the kinetics was observed for the two samples. Ethyl vinyl ketone obtained from the K and K Laboratories was distilled under vacuum from −5 to −78° and the middle fraction was purified gas chromatographically with column A. The purified sample (99.9%) was dried over Linde Molecular Sieve 4A. Other substances used in this work were the same as those in the earlier study.[3] Likewise the apparatus was the same as that used previously.[3]

Analysis of Products. Ordinarily after about 30% decomposition the reaction mixture was removed and then separated into the following fractions: (a) substances volatile at −196°; (b) substances condensable at −196°, but volatile at −112°; (c) substances not volatile at −112°. Fraction a was not analyzed since it was only about 0.01% of fraction b. The infrared absorption spectrum of fraction b was in agreement with the spectrum of pure ethylene obtained with the same Perkin-Elmer Model 21 instrument. Since ethylene appeared to be essentially the only compound in fraction b, the quantity of fraction b measured in a gas buret was designated as ethylene. The infrared spectrum of the more volatile portion of fraction c showed medium to strong absorptions at 3.4, 5.8–5.9, 6.2, 7.1–7.2, 8.3–8.4, 8.9–9.0, 9.7, 10.2, and 10.6 μ. The spectrum agreed with that for pure ethyl vinyl ketone except that some minor details of the former spectrum were slightly different, perhaps as a result of trace amounts of other products or the reactant.

A solution of fraction c in 99.5% methanol showed a strong absorption in the region 210–216 mμ with a maximum at 213 mμ in agreement with the absorption of pure ethyl vinyl ketone under similar conditions. Optical density measurements with a Beckman DU spectrophotometer showed that ethyl vinyl ketone

(1) This work was supported by a grant from the National Science Foundation to the University of Rochester.

(2) L. G. Daignault and W. D. Walters, *J. Am. Chem. Soc.*, **80**, 541 (1958).

(3) B. C. Roquitte and W. D. Walters, *ibid.*, **84**, 4049 (1962).

(4) (a) M. D. Zupan and W. D. Walters, *J. Phys. Chem.*, **67**, 1845 (1963); (b) references to earlier studies are given in S. M. E. Kellner and W. D. Walters, *ibid.*, **65**, 466 (1961).

(5) N. D. Zelinskii and B. A. Kazanskii, *Ber.*, **60B**, 1101 (1927).

solutions followed Beer's law, and a spectrophotometric method was used for quantitative determinations of the ethyl vinyl ketone in the products.

The identification of ethylene and ethyl vinyl ketone in the reaction mixture and the fact that the decomposition in a constant volume system involves an increase in pressure indicated that the important over-all reaction is

$$\begin{array}{l} CH_2{-}CH{-}COC_2H_5 \\ \quad\;|\quad\;| \\ CH_2{-}CH_2 \end{array} \longrightarrow \begin{array}{l} CH_2{=}CH{-}COC_2H_5 \\ \\ CH_2{=}CH_2 \end{array} \qquad (1)$$

In several experiments at about 400°, gas chromatographic analysis of the entire reaction mixture revealed a minor component with a retention time lying between those for ethyl vinyl ketone and ethyl cyclobutyl ketone on column A. The substance was not identified, but if the molecular weight is near 112 and the chromatographic areas are approximately proportional to weight percentages, the amount of the substance after about one-quarter reaction probably did not exceed 0.015–0.02 times the moles of undecomposed reactant. When compared with ethyl vinyl ketone the amount present appeared to be not more than 0.04 ± 0.01 times as much. By analogy with the decomposition of cyclobutanecarboxaldehyde the substance might be a substituted dihydropyran which subsequently might also yield ethylene and ethyl vinyl ketone. As in the case of cyclobutanecarboxaldehyde such a process might be of only minor importance, but further work will be needed to determine this. Therefore, for the present study the results have been calculated in terms of the over-all formation of ethylene and ethyl vinyl ketone as shown in eq. 1.

To study the stoichiometry of the decomposition experiments were performed so that the pressure increases and analyses of the products could be compared after 30–35% reaction. Typical results from experiments under various conditions are shown in Table I. It is seen that in accordance with eq. 1 the pressure increase (ΔP) is essentially equal to the pressure of ethyl vinyl ketone (P_{EVK}) or the pressure of ethylene (P_E) in both the unpacked and packed vessels and in the absence or presence of propylene or nitric oxide. The average value of $P_{EVK}/\Delta P$ from thirteen experiments in which analyses were performed was 1.01 ± 0.01 and $P_E/\Delta P$ from fourteen experiments averaged 0.99 ± 0.01. Therefore, it was concluded that the over-all reaction indicated by eq. 1 can be followed by pressure measurements at least up to 35% decomposition. That ethyl vinyl ketone does not undergo a significant pressure change under the conditions used for the rate measurements was confirmed by observing the behavior of 3.5 mm. of pure ethyl vinyl ketone at 410°.

Table I: Analysis of the Products from the Decomposition of Ethyl Cyclobutyl Ketone

P_0, mm.	ΔP, mm.	P_{EVK}, mm.	P_E, mm.	Special conditions[a]
		Temp. 370°		
6.75	1.97		1.86	
		Temp. 380°		
9.92	2.65	2.70	2.62	
		Temp. 390°		
8.83	2.94	2.90	..	0.3 mm. of NO
18.27	5.65	5.78	..	3.9 mm. of C_3H_6
8.35	2.60	2.66	2.57	
9.52	2.94	3.01	2.91	p
		Temp. 400°		
5.38	1.73	..	1.76	
		Temp. 410°		
8.13	2.96	3.02	2.95	

[a] C_3H_6 means propylene and p denotes packed bulb with 28-fold greater surface to volume ratio.

Kinetics

The results from some of the experiments performed for the purpose of studying the kinetics and mechanism of the ethyl cyclobutyl ketone pyrolysis are shown in Table II. It appears that the quarter-time ($t_{1/4}$)

Table II: Decomposition of Ethyl Cyclobutyl Ketone under Various Conditions at 390°

—Unpacked vessel—		—Packed vessel—		
P_0, mm.	$t_{1/4}$, min.	P_0, mm.	$t_{1/4}$, min.	Special conditions[a]
5.48	11.5	9.52	11.0	p
5.78	10.9	9.36	11.4	p
8.35	11.0	9.19	10.8	0.5 mm. of NO
9.07	11.1	8.83	11.2	0.3 mm. of NO
17.47	10.7	18.27	10.6	3.9 mm. of C_3H_6
		10.03	10.6	4.9 mm. of C_3H_6

[a] The letter p denotes the packed bulb; C_3H_6 means added propylene.

for the formation of ethylene and ethyl vinyl ketone is not influenced by (1) a 3-fold change in pressure, (2) a 28-fold increase in surface to volume ratio, or (3) addition of propylene or nitric oxide. Thus, the decomposition seems to be a first-order, homogeneous reaction not involving free-radical chain processes. The essentially first-order character over the initial 30%

of the decomposition was indicated also by the fact that the ratio ($t_{1/4}/t_{1/8}$) was found to be 2.13 (compared to 2.15 for a first-order reaction) and a plot of log $[P_0/(2P_0 - P_t)]$ *vs.* time was linear as far as the experiment was carried (31%).

Experiments with pressures of 4–17 mm. were performed at temperatures from 370 to 410° and the rate constants from the experiments are shown in Fig. 1. From experiments in which the initial pressure was within a narrow range (5.4–7.4 mm.) the temperature

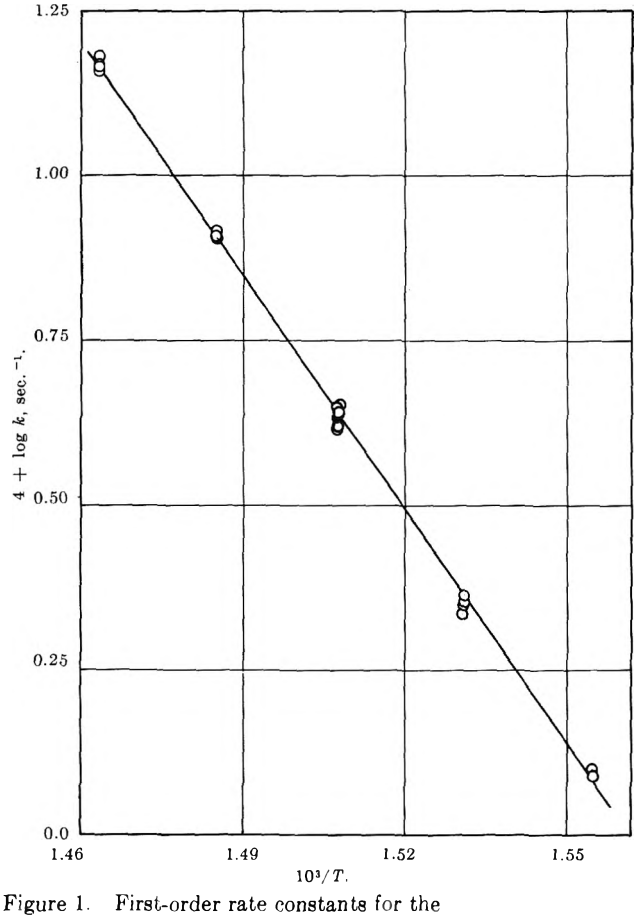

Figure 1. First-order rate constants for the pyrolysis of ethyl cyclobutyl ketone at different temperatures; initial pressure, 4–17 mm.

dependence was determined by a least-squares method with an IBM 650 computer. The activation energy was found to be 54.2 ± 0.5 kcal./mole which was in agreement with the value obtained from the slope of a log k *vs.* $1/T$ plot for the same experiments. From each rate constant a value of A was calculated from the expression $k = A \exp(-E/RT)$ with $E = 54.2$ kcal./mole. By the use of the mean value of A and its standard deviation the rate constant[6] for the 5–7 mm. experiments (and also for the entire series, 4–17 mm.) at 370–410° follows the relationship $k = 3.2 \pm 0.1 \times 10^{14} \exp(-54{,}200/RT)$sec.$^{-1}$.

Discussion

The results which have been obtained with respect to products and kinetics indicate that the decomposition of ethyl cyclobutyl ketone occurs chiefly by a first-order ring cleavage similar to that observed for other cyclobutane derivatives. Under the present experimental conditions the decomposition of ethyl cyclobutyl ketone appears to be free from the radical-chain processes existing in the pyrolyses of higher aliphatic ketones, such as methyl *n*-butyl ketone[7a] or diethyl ketone,[7b] the rates of which can be retarded by the addition of propylene and to some extent by packing.

In the series of cyclobutane derivatives[2,3] where R is HCO, CH_3CO, and C_2H_5CO the activation energies have been found to be 53.3, 54.5, and 54.2 kcal./mole. The latter two values, obviously, do not differ by more than the possible experimental error, but it does appear that the activation energy for the ketone decomposition may be slightly higher than that for the aldehyde and this causes the rate for each ketone at 390° to be approximately half that of the aldehyde. The frequency factors observed for the three pyrolyses were 2.7×10^{14}, 3.4×10^{14}, and 3.2×10^{14} sec.$^{-1}$. Apparent entropies of activation calculated for 390° from $A = (\kappa e k_B T/h) \exp(\Delta S^*/R)$ with $\kappa = 1$ are 3.9, 4.4, and 4.3 e.u., respectively.

The closeness of the activation energies and frequency factors for the methyl and ethyl cyclobutyl ketones shows that the rate constants should not be far apart. In order to compare the rates of the ketones under similar conditions, three experiments also were performed with methyl cyclobutyl ketone during the present study. The rate constant at 390° from the ethyl cyclobutyl ketone experiments was about 8% larger than that for the methyl cyclobutyl ketone. That a cyclobutane derivative with a C_2H_5CO substituent has a slightly faster rate than one with a CH_3CO group was found also by comparison of the rate constant observed here for the ethyl ketone with the value calculated from the rate expression obtained in the earlier study of the methyl ketone.[8]

If the results of a recent investigation of the decom-

(6) This is an over-all value which would include any formation of ethylene and ethyl vinyl ketone *via* an unstable intermediate compound.

(7) (a) W. T. Barry, Jr., and W. D. Walters, *J. Am. Chem. Soc.*, 79, 2102 (1957); (b) C. E. Waring and C. S. Barlow, *ibid.*, 78, 2048 (1956).

(8) The rate constant for the methyl ketone calculated from ref. 2 is about 9% smaller than that observed for the methyl ketone in the three experiments in this work.

position of methyl cyclobutanecarboxylate[9] are considered also, it is possible to compare the relative influence of four substituents containing a >C=O adjacent to the cyclobutane ring. The cyclobutane derivatives (C_4H_7R) may be arranged in the following order of decreasing rate constant at 390° according to the nature of R: HCO > C_2H_5CO > CH_3CO > CH_3OCO. The pyrolyses of the two ketones do not differ greatly in rate; but the rate constant for the ester at 390° is only about one-fifth that of the ethyl cyclobutyl ketone. The same order (aldehyde > ketone > ester) represents the effectiveness of the substituent in decreasing the activation energy below that for cyclobutane itself. As has been discussed previously,[9] the rate relationship [(aldehyde or ketone) > ester] would seem to be in accord with the mesomeric effect[10] of the whole substituent group upon the activated complex. The decrease in the resonance effect of the carbonyl group by replacement of an adjoining alkyl group with an alkoxyl group was attributed to cross conjugation by Branch and Calvin.[11] The lowering of the C=C infrared frequency is less for a conjugated ester than for a conjugated aldehyde or ketone,[12] but the frequency shifts observed for acrolein, methyl vinyl ketone, and ethyl vinyl ketone probably do not differ enough from one another to be useful for predictions about differences in the effects of the substituents HCO, CH_3CO, and C_2H_5CO upon the cyclobutane pyrolysis.

The mesomeric effects of aldehyde, ketone, and ester groups seem to be in accord with the sequence of optical exaltations (HC=O > RC=O > ROC=O) observed for olefins with these substituents.[13] As a measure of a composite inductive and mesomeric effect of a substituent a relationship involving n.m.r. data has been proposed,[14] but a subsequent analysis[15] of the n.m.r. data for substituents of interest here has not confirmed the numerical values of the n.m.r. parameters used in the proposed relationship.

The question of whether the transformation of an activated complex from cyclobutane (or a derivative) can lead to a biradical and/or directly to two molecular products has not been resolved experimentally.[16] Resonance stabilization by a carbonyl group would be expected for either the biradical[2,3,9,17] or molecular products and might cause a decrease in the energy of the activated complex. Likewise the lower entropies of activation for the cyclobutane derivatives with >C=O in the side chain in comparison with alkyl derivatives could be accounted for by the effect of resonance upon the stereochemistry of the activated complex. With respect to the lowering of the activation energy and frequency factor of the pyrolysis there is a similarity between the carbonyl derivatives and isopropenylcyclobutane.[18]

Acknowledgment. The authors wish to thank Mr. Carl Whiteman for his assistance and the General Railway Signal Co. for the use of an IBM computer.

(9) M. Zupan and W. D. Walters, *J. Am. Chem. Soc.*, 86, 173 (1964).

(10) C. K. Ingold, "Structure and Mechanism in Organic Chemistry," Cornell University Press, Ithaca, N. Y., 1953, pp. 76–78.

(11) G. E. K. Branch and M. Calvin, "The Theory of Organic Chemistry," Prentice-Hall, New York, N. Y., 1941, p. 238.

(12) W. H. T. Davison and G. R. Bates, *J. Chem. Soc.*, 2607 (1953); R. Mecke and K. Noack, *Chem. Ber.*, 93, 210 (1960).

(13) See ref. 10, p. 128.

(14) W. Brügel, T. Ankel, and F. Krückeberg, *Z. Elektrochem.*, 64, 1121 (1960).

(15) S. Castellano and J. S. Waugh, *J. Chem. Phys.*, 37, 1951 (1962).

(16) This question has been considered recently by R. W. Vreeland and D. F. Swinehart, *J. Am. Chem. Soc.*, 85, 3349 (1963), who discuss a suggestion of B. S. Rabinovitch.

(17) P. Nangia and S. W. Benson, *ibid.*, 84, 3411 (1962). Moreover, the importance of recyclization *vs.* decomposition of the biradical will influence the observed rate of formation of the final products.

(18) R. J. Ellis and H. M. Frey, *Trans. Faraday Soc.*, 59, 2076 (1963).

The Contraction of Polyvinyl Alcohol Films in Aqueous Media[1a]

by Hajime Noguchi[1b] and Jen Tsi Yang

Cardiovascular Research Institute and Department of Biochemistry, University of California Medical Center, San Francisco, California
(Received February 3, 1964)

Recently, we studied the contraction of poly-L-glutamic acid film as a result of conformational change (coil to helix).[2] By chance, we found that added salt affected the coiled form of a film previously cross-linked with polyvinyl alcohol (PVA) more than one that had been cross-linked with glycerol. This led us to believe that the conformation of PVA, an uncharged polymer, depends on the added electrolyte or nonelectrolyte in the solvent. Thus, in this note we present the results of experiments using PVA film under various conditions. The contraction of the films in the presence of certain monovalent ions or sucrose might be termed "osmotic" and can probably be attributed to

(1) (a) This work was supported by grants from the U. S. Public Health Service (GM-10880, GM-K3-3441, and HE-06285); (b) San Francisco Heart Association Research Fellow; on leave from Aichi-Gakugei University, Okazaki, Japan, 1962–1963.

(2) H. Noguchi and J. T. Yang, *Biopolymers*, in press.

the dehydration from hydroxyl groups inside the film. On the other hand, LiBr, divalent cations, and the "denaturing" agents (urea and guanidine hydrochloride) dissolved the films; the mechanism is probably related to the solubility of these compounds in alcohol.

Experimental

PVA was a gift of the DuPont Company. Two fractions having the molecular weights of 84,000 and 47,000 (as determined from their intrinsic viscosities in aqueous solutions; $[\eta]$ dl./g. $= 14 \times 10^{-4}M^{0.60}$)[3] were used; their contractile properties, however, were the same. The PVA films were prepared by spreading a 2% solution on a chromium-plated metal plate and heating to dryness for about 2 hr. at about 80°. The film strips peeled off the plate were further heated under a small load (2–3 g.) at 110° for 90 to 120 min. The dried films (about 0.03 × 4 × 40 mm.[3]) swelled isotropically when suspended in water and reached the equilibrium state within a few minutes, the length increasing by about 30%.

Kuhn and his co-workers[4,5] suggest the possible existence of cross linking in the film through etherification of the hydroxyl groups in the PVA during heating. The film prepared for this study was insoluble in water at room temperature. However, the dried film would dissolve in hot water at about 65° within 10 to 20 min. Thus, there is no evidence of such cross linking inside the film, and its insolubility in water might be attributed to the entanglement of the polymer chains and the formation of some crystalline regions during drying.

Results and Discussion

Reversible Contraction of PVA Film in NaCl Solution. Figure 1 shows the relative length, L/L_0, of the PVA films when they are suspended alternately in 50 ml. of double-distilled water (L_0) and 5 *M* NaCl. The 5-min. periods represented about 98% of the maximum contraction and elongation at the equilibrium state, which could be reached in about 30 min. This process is completely reversible, as is that observed for the polypeptide film.[2] As expected for an un-ionized polymer, the pH of the solvent media did not affect the length of the films; for example, length was constant between pH 2 and 11.5.

Effect of Solvent Composition. Figure 2 shows the L/L_0 of the PVA film in various solvent media.

(*a*) *Monovalent Salts.* Both NaCl and KF caused the film to contract. The L/L_0 changed linearly with increasing salt concentration up to 5 *M* and it leveled off at higher concentrations of KF. On the other hand, LiBr expanded the film at concentrations up to 3 *M*; in 4 *M* LiBr the film broke up after about 15 min.

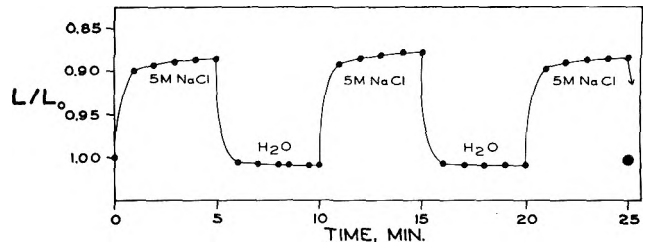

Figure 1. Reversible contraction of polyvinyl alcohol film in alternating water and 5 *M* NaCl.

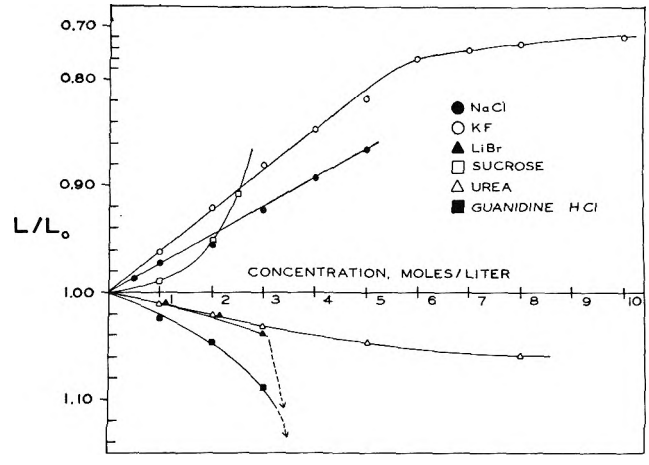

Figure 2. Relative lengths of polyvinyl alcohol films in various solvent media. Each point (but not the broken arrows) represents the equilibrium state.

and finally dissolved in about 9 hr. (see section c on divalent ions).

(*b*) *Sucrose.* The film shrank in sucrose, but the contraction was nonlinear (Fig. 2). The fact that salts and small organic compounds have the same effect on the PVA film leads us to believe that "osmotic contraction" is a plausible explanation for these results. Raising the osmotic pressure in the solvent causes the water of hydration to diffuse out of the film. This does not imply that the added salt or sucrose molecules cannot penetrate the film. Indeed, we observed that when sucrose was added to the solvent, the film contracted in the first few minutes and later elongated slightly to reach the equilibrium state. This seems to indicate that the rapid dehydration of the film was followed by a slow diffusion of sucrose molecules into the film. The extent of dehydration, however, outweighs the diffusion of the sucrose or salt molecules.

To substantiate this explanation further, we also

(3) H. Dieu, *J. Polymer Sci.*, 12, 417 (1954).

(4) W. Kuhn, *Experientia*, 5, 318 (1949).

(5) W. Kuhn, B. Hargitay, A. Katchalsky, and E. Eisenberg, *Nature*, 165, 515 (1950).

measured the intrinsic viscosities, $[\eta]$, of the PVA (fraction I) solution in various NaCl and sucrose concentrations. From pure water to 0.5 *M* NaCl or sucrose, $[\eta]$ remained virtually constant at 1.3 dl./g. At higher salt or sucrose concentrations, it dropped to 0.97 at 1 *M*, clearly indicating a coiling up of PVA. Beyond 1 *M* NaCl or sucrose, $[\eta]$ began to increase, probably because of aggregation; at 1.5 *M* it was 1.5 in sucrose and 1.15 in NaCl; at concentrations higher than 1.5 *M*, PVA began to precipitate. We also found that KCl, KF, and CsCl, but not LiBr (see section c), are all poor solvents for PVA, as is NaCl.

(c) *Divalent Cations.* In contrast to the monovalent salts (except LiBr), the divalent cations, Ca^{2+}, Mg^{2+}, and Cu^{2+} swelled the PVA film. The film elongated about 1 and 5% in 2 *M* $CaCl_2$ and $MgCl_2$, but dissolved in 4 *M* $CaCl_2$ or 3 *M* $MgCl_2$. The film length increased about 3% in 1 *M* $CuCl_2$, about 50% after 20 hr. in 2 *M* $CuCl_2$, and about 400% in 3 *M* $CuCl_2$. Furthermore, with Cu^{2+} the elongation was irreversible. For comparison, we found that the intrinsic viscosity of the PVA (fraction II) solution increased from 0.89 dl./g. in water (pH 6.4) to 1.18 in 3 *M* $MgCl_2$ (pH 5.7) and 1.08 in 4 *M* LiBr (pH 8.1). Thus, the chlorides of the three divalent cations and LiBr studied have a strong affinity for the PVA molecules. They penetrate into the film, probably break up the crystalline regions, and expand the polymer coils. This in turn prevents the "osmotic contraction" observed previously for some monovalent salts and small organic compounds. In this respect we note that LiBr, $CaCl_2$, $MgCl_2$, and $CuCl_2$ are all soluble in ethanol, whereas NaCl and KCl are only slightly soluble, and KF is insoluble in ethanol. Perhaps the different behavior of PVA with different salts is closely related to the affinity between the hydroxyl groups of PVA and these salts.

(d) *Urea and Guanidine Hydrochloride.* The PVA film elongated by about 7% in 8 *M* urea (Fig. 2). Guanidine hydrochloride is a more effective dispersing agent than urea; in 5 *M* salt the film dissolved after several hours of exposure. These two compounds are well known as denaturing agents for globular proteins, although the mechanism of denaturation is still unsettled. The effect of urea on a neutral polymer, polyvinylpyrrolidone, was studied by Klotz and Russell.[6] They found a slight decrease in the intrinsic viscosity when the polymer was dissolved in 8 *M* urea instead of pure water; this they attributed to a possible decrease in the degree of hydration of the macromolecule. We found, however, that the intrinsic viscosity of a PVA solution (fraction II) increased from 0.89 dl./g in water to 1.02 in 8 *M* urea. Thus, the PVA molecules can be swamped with urea or guanidine hydrochloride molecules, although the mechanism of such interaction is still unknown.

Acknowledgment. We thank Professor M. F. Morales for his stimulating discussions. Technical assistance by Miss K. Graham is gratefully acknowledged.

(6) I. M. Klotz and J. W. Russell, *J. Phys. Chem.*, **65**, 1274 (1961).

Common Ion Effects on the Solubility of Silver Chloride and Thallous Bromide in Fused Nitrate Solvents

by Ralph P. Seward and Paul E. Field[1]

Department of Chemistry, Pennsylvania State University, University Park, Pennsylvania *(Received February 10, 1964)*

The authors[2] have recently calculated solubilities for salts of type AC in fused salt solvents BD from the thermodynamic properties of the two components and those of the reciprocal salt pair AD and BC. In the systems investigated, where the solubilities were small, reasonable agreement of calculated and experimental values was found. It was thought to be of interest to extend the measurements to include the changes in solubility produced by the addition of salts having an ion in common with the solute to see to what extent similar thermodynamic calculations would serve to predict the observed effects. For this purpose the solubilities in potassium nitrate of thallous bromide in the presence of added thallous nitrate and potassium bromide and the solubility of silver chloride in sodium nitrate in the presence of added silver nitrate and sodium chloride have been measured.

In an earlier note one of the authors[3] showed how the solubility of silver chloride at 300° expressed as mole fraction of AgCl increased from a value of 7×10^{-4} in pure potassium nitrate on addition of silver nitrate to a mole fraction of 0.55 in pure silver nitrate. This behavior is qualitatively reasonable. When silver chloride dissolves in silver nitrate the number and kind of nearest neighbor, anion–cation interactions must be essentially equal to those existing in the separate com-

(1) From the Ph.D. Thesis of Paul E. Field, Pennsylvania State University, August, 1963; supported by the U. S. Atomic Energy Commission under contract AT(30-)-1881.

(2) R. P. Seward and P. E. Field, *J. Phys. Chem.*, **68**, 210 (1964).

(3) R. P. Seward, *ibid.*, **63**, 760 (1959).

ponents. Hence, the energy increase accompanying solution is very near to the heat of fusion of silver chloride. In contrast, when silver chloride dissolves in potassium nitrate, both silver and chloride ions acquire new nearest neighbors, to a large extent at least. These new contacts introduce interaction energies which are different from those existing in the pure components. In consequence the energy change accompanying the solution process approaches that of the metathetic reaction

$$AgCl(s) + KNO_3(l) = AgNO_3(l) + KCl(l)$$

the magnitude of this energy change being approximately five times that of the heat of fusion of silver chloride.

In the first mentioned report[2] the relation

$$-RT \ln N_1^2 = \Delta G_F^\circ + (\Delta G_R^\circ + \Delta H_{mix})(1 - N_1)^2 \quad (1)$$

was derived for the solubility (N_1) of a salt AC in the molten salt solvent BD, ΔG_F° and ΔG_R° being standard state changes in free energy for fusion of AC and for the liquid phase reaction

$$AC(l) - BD(l) = AD(l) + BC(l)$$

respectively. ΔH_{mix} is the enthalpy increase accompanying solution of AD(l) and BC(l) in excess BD(l). When the same procedure is applied to a solution constructed from n_1 moles of AC, n_2 moles of BD, and n_3 moles AD (or BC), the resulting equation is

$$-RT \ln N_1(N_1 + N_3) = \Delta G_F^\circ + (\Delta G_R^\circ + \Delta H_{mix})(N_2 + N_3)N_2 \quad (2)$$

N_1 as before is the desired solubility and N_2 and N_3 the mole fractions of the solvent salts. Equation 2 can be seen to become identical with (1) as N_3 approaches zero. Equation 2 at the other extreme, where N_2 approaches zero and $N_1 + N_3$ approaches unity, becomes

$$-RT \ln N_1 = \Delta G_F^\circ = \Delta H_F(T_0 - T)/T_0$$

the simple ideal solubility equation when ΔC_p is assumed to be zero.

The above relations in any case involve the assumption that the A cations are randomly dispersed among the B cations and that the C anions are randomly dispersed among the D anions. If there is preferential association or incomplete dissociation these relations will fail to describe the facts. It is shown below that although the calculated solubility of silver chloride in sodium nitrate is substantially correct, calculated solubilities where sodium chloride or silver nitrate have been added are far from the experimental values. In the case of thallous bromide, however, the calculations come much closer to accounting for the observed solubilities.

Experimental

Except for preparation of the mixed solvents and some necessary modification of the analyses, the experimental technique is that which has been previously described.[2]

Experimental and Calculated Solubilities. Experimentally determined solubilities of silver chloride at 600°K. in sodium nitrate in the presence of added silver nitrate and sodium chloride are given in Table I together with solubilities calculated by means of eq. 2 for the same solvent mixtures. ΔG_F° and ΔG_R° were evaluated from the thermodynamic data employed in the earlier report.[2] Because of uncertainty in its application to the mixed solvents, the ΔH_{mix} term was omitted in the calculations. Its inclusion would produce a small and essentially constant shift in the calculated solubilities.

Table I: Effect of Added $AgNO_3$ and NaCl on the Solubility of AgCl in $NaNO_3$ at 600°K.

Added salt	Mole % added salt	$10^2 \times$ mole % AgCl in solution: Experimental	Eq. 2
....	0.00	7.76	6.20
$AgNO_3$	0.22	3.19	1.63
	0.50	2.73	0.78
	1.00	2.81	0.43
	2.00	3.70	0.26
	5.00	8.93	0.15
NaCl	0.25	3.54	1.48
	0.50	2.84	0.78
	1.00	3.32	0.43
	2.00	4.68	0.26
	4.00	7.65	0.20

Examination of Table I reveals that eq. 2, although it predicts a solubility minimum, is far from adequate to account for the observed solubilities. The assumption of random distribution of the ions must be in error and the solubility changes may better be interpreted in terms of the formation of complexes such as AgCl, $AgCl_2^-$, and Ag_2Cl^+. The empirical equations

$$N_1 = 1.30 \times 10^{-4} + 46 \times 10^{-8}/N_{Cl^-} + 1.57 \times 10^{-2} N_{Cl^-} \quad (3)$$

$$N_1 = 1.30 \times 10^{-4} + 46 \times 10^{-8}/N_{Ag^+} + 1.10 \times 10^{-2} N_{Ag^+} \quad (4)$$

account reasonably well for the observed solubilities of AgCl in $NaNO_3$ in the presence of added NaCl and $AgNO_3$ respectively, N_{Cl^-} being moles of Cl^- divided by total moles of anion and N_{Ag^+} being moles of Ag^+ divided by total moles of cation. In eq. 3 and 4 the numerical value of 1.30×10^{-4} may be interpreted as a constant concentration of AgCl, 46×10^{-8} as a solubility product constant $N_{Ag^+} \times N_{Cl^-}$, and the third constant as the product of the first and an equilibrium constant for $AgCl + Cl^- = AgCl_2^-$ in eq. 3 and for $AgCl + Ag^+ = Ag_2Cl^+$ in eq. 4. In contrast to its behavior in aqueous solution AgCl appears to form cation complexes in excess Ag^+ to nearly the same extent that it forms anion complexes in excess Cl^- ion solutions.

Table II shows experimental and calculated solubilities for thallous bromide in potassium nitrate in the presence of added thallous nitrate and of added potassium bromide.

Table II: Effect of $TlNO_3$ and KBr on the Solubility of TlBr in KNO_3 at 660°K.

Added salt	Mole % added salt in solvent	Mole % TlBr in solution Experimental	Eq. 3
...	0.0	6.23	7.18
$TlNO_3$	5.0	5.11	5.45
$TlNO_3$	10.0	4.97	4.67
$TlNO_3$	20.0	6.54	4.74
KBr	2.0	5.59	6.35
KBr	5.0	4.88	5.45
KBr	10.0	4.62	4.67

The maximum deviation of the calculated from the experimental solubilities of TlBr in Table II is for the 20% thallous nitrate solvent where the calculated value is 73% of the experimental in contrast to the AgCl solubilities shown in Table I where the calculated values are as low as 2% of the experimental ones. Although the product of the ion fractions of Tl^+ and Br^- increases by as much as a factor of four on the addition of a salt with a common ion and hence there is no constant solubility product, there seems to be no need to attribute the increase to the formation of complex ions since eq. 3 gives solubilities in reasonable agreement with the experimental figures.

Diamagnetic Studies on Some Alkoxy Silanes and Silanols

by R. L. Mital

Maharaja's College of Science, Jaipur, India
(Received January 6, 1964)

A survey of the literature reveals that very few papers have appeared on the magnetic studies of organosilicon compounds. Much controversy exists over the atomic susceptibility value of silicon; values ranging from 20.7 to −3.01 have been reported.[1-3] To justify the validity of Pascal's law in silicon chemistry, different values for χ_{Si} in two different homologous series have been reported recently. Naturally we wish to determine how many different values are to be assigned to χ_{Si} or to conclude that there is something more fundamental which is involved in such studies. Keeping this point in view, the present note deals with the diamagnetic susceptibilities of five silicon compounds having Si–O bonds, and the results are discussed from the structural point of view.

Experimental

The substances used were of A.R. quality. Before the magnetic measurements were taken, the purity was checked by standard methods. The magnetic susceptibility of the compounds was measured with a very sensitive microbalance devised by Neogy and Lal.[4] This microbalance was capable of measuring the total susceptibility with an accuracy of the order of 0.5×10^{-12} c.g.s. e.m.u.

A capsule was filled with the compound whose susceptibility was to be measured. This capsule was then suspended from one end of the beam. When the field was switched on, the whole capsule experienced a force which was measured by sending a current through the copper coil and measuring the potential drop across the standard 1-ohm resistance with the help of a high-precision portable PYE potentiometer capable of measuring 0.05 mv. The push on the capsule filled with the sample was compared with that on the same capsule filled with pure benzene, mass susceptibility[5] =

(1) E. W. Abel and R. P. Bush, *Trans. Faraday Soc.*, **59**, 630 (1963).
(2) A. Kazuo, *Sci. Rept. Res. Inst. Tohoku Univ.*, **A2**, 205 (1950).
(3) R. M. Mathur, *Trans. Faraday Soc.*, **54**, 1477 (1958).
(4) D. Neogy and R. B. Lal, *J. Council Sci. Indust. Res. India*, **21B**, 103 (1962).
(5) B. C. Eggleston, D. F. Evans, and R. E. Richards, *J. Chem. Soc.*, 941 (1954).

-0.7081×10^{-6} c.g.s. unit, in order to determine the susceptibility of silicon compounds. The results are shown in Table I.

Table I: Diamagnetic Susceptibility of Silicon Compounds, -10^6 c.g.s. units

Compounds	χ_M, obsd.	χ_M, prev. recorded values[a]	χ_M, theor. obtd. from wave-mech. val.	χ_{Si}	χ_{Si}, mean value
Dimethyldiethoxysilane	104.7	104.6[b]	104.4	17.0	
Di-*n*-propyldiethoxysilane	150.8		149.8	16.4	
Trimethylsilanol	66.3		66.4	18.6	17.0
Dimethylsilanediol	58.4		58.3	16.9	
Diethylsilanediol	81.0		81.1	16.1	

[a] Ref. 6. [b] Ref. 3.

Results and Discussion

In Table I we find that the mean values for χ_{Si} is 17.0 while χ_{Si} for individual compounds varies from 16.1 to 18.6 units. χ_{Si} has been calculated from the molecular susceptibilities of the compounds by subtracting from these values the atomic susceptibilities of hydrogen (2.0)[6,7] and oxygen (5.3)[6] and the group susceptibilities χ_{CH_3} (13.45)[8] and χ_{CH_2} (11.68).[8] The value of χ_{Si} in trimethylsilanol is higher as compared to the values of χ_{Si} in other compounds. Trimethylsilanol contains only one Si–O bond, while the remaining four compounds contain two Si–O bonds. In Si–O bonds, the lone pairs of electrons on oxygen interact with vacant d orbitals of silicon. Such interactions bring about a decrease in Pauli's diamagnetic term, thus lowering the value of χ_{Si} in the compounds having such bonds. We know that

$$\chi_M = -\frac{Ne^2}{6mc^2}\Sigma r^2 + \frac{2}{3}N\sum_{n'\neq n}\frac{|m_0(n;n')|^2}{h\nu(n';n)}$$

In the above Van Vleck quantum mechanical equation,[9] the symbols have their usual meaning. The first term in the expression is the usual Pauli diamagnetism and the second is Van Vleck's high frequency paramagnetism. In tetraalkyl silanes p_π–d_π bonding to the silicon atom is not specious so the value of χ_{Si} in tetraalkyl-substituted silanes will be conclusively higher than in the compounds in which the above mentioned type liaisons are present. There is very good agreement between the experimental and the theoretical values derived from the wave mechanical considerations.

Acknowledgment. The author wishes to express his sincere thanks to Dr. S. Dayal for the gift of organosilicon compounds, to Prof. A. Mookherji for allowing laboratory facilities and giving valuable suggestions, and to Prof. R. C. Mehrotra for encouragement.

(6) A. Pacault, J. Hoarau, and A. Marchand, *Advan. Chem. Phys.*, **3**, 171 (1961).

(7) W. Haberditzl, *Z. Chem.*, **1**, 225 (1961).

(8) W. R. Angus, G. I. W. Llewelyn, and G. Stott, *Trans. Faraday Soc.*, **55**, 887 (1959).

(9) J. H. Van Vleck, "The Theory of Electric and Magnetic Susceptibilities," Oxford University Press, 1932; *J. Chem. Phys.*, **3**, 807 (1935).

Oxidation of Carbon Monoxide on Thin Films of Nickel, Palladium, and an Alloy

by Earl G. Alexander and W. Walker Russell

Department of Chemistry, Brown University, Providence, Rhode Island *(Received January 13, 1964)*

An effective method of studying the catalytic activity of metals has been to measure the reactivity of a gas preadsorbed on a metal film.[1-3] Such a method should also be valuable in studying the catalytic activity of alloys. Because hydride formation may be a complication in studying hydrogenations on palladium, the oxidation of CO to CO_2 was employed here. This reaction has already been studied by Stephens[3] on palladium films. As preliminary experiments indicated that simultaneous or successive evaporation of two different metal filaments appeared incapable of producing an alloy film uniform throughout in chemical composition,[4] evaporation from a homogeneous alloy pellet was used. Since nickel and palladium form a complete series of unordered-solid solutions, it was not unexpected that the behavior of their alloy was found to be intermediate to that of the pure component metals.

Experimental

Unless otherwise stated, all temperatures are in degrees centigrade, all pressures are in mm., and all gas volumes are in ml. (STP).

Materials and Apparatus. Wire form Ni (99.99%)

(1) O. Beeck, *Discussions Faraday Soc.*, **8**, 118 (1950).

(2) G. I. Jenkins and E. Rideal, *J. Chem. Soc.*, 2490, 2496 (1955).

(3) S. J. Stephens, *J. Phys. Chem.*, **63**, 188 (1959).

(4) M. K. Gharpurey and P. H. Emmett, *J. Phys. Chem.*, **65**, 1182 (1961).

and Pd (99.9%) were used for film preparation. Research grade O_2, CO, and helium, in sealed glass bulbs, were used as received. The all-glass apparatus comprised (1) a two-stage mercury diffusion pump and cold traps; (2) a dosage system containing mercury manometers and traps; and (3) an adsorption system which included the reaction vessel, two cold traps, and a Pfund gage[5] with which pressures could be read down to 1×10^{-7}. The adsorption system, which contained no stopcocks, could be isolated from the other parts of the apparatus by means of mercury manometers. Two types of reaction vessel were employed. Type I was constructed from a 200-ml. spherical, long-necked flask. Long molybdenum leads, introduced through a press seal at the end of the flask neck, extended to the center of the flask bulb. A loop of coiled palladium wire (0.2 mm. diameter) or nickel wire (0.3 mm. diameter) was spot-welded between two molybdenum lead ends. The Type II vessel was an inverted 500-ml., wide-necked, spherical flask. The spherical portion was joined to the neck through a 45-mm. diameter shoulder around which a four-turn induction coil could be placed. Inside the shoulder portion a metal or alloy pellet was supported in a shallow quartz cup atop a vertical axial glass spindle. The induction coil was energized by a 4-kw. spark gap converter.

Preparation of Catalyst Films

1. Filament Evaporation. Reaction vessel I and the two adjacent traps were evacuated and baked at 360° for 10–14 hr. Other parts of the system were flamed. The filament was flashed several times during bakeout. Then the trap next to the reaction vessel was cooled with Dry Ice–2-propanol and the adjacent trap with liquid nitrogen. After an ice bath was positioned around the reaction vessel the film was evaporated with a filament current of 2.9 amp. for nickel and 1.6 amp. for palladium. The pressure during film evaporation was about 1×10^{-6} to 4×10^{-7}. The evaporated film was stabilized by three times alternating between room temperature and that of liquid nitrogen. The weight of a film was determined by weighing the filament before and after evaporation. Even though the filament loop was placed close to the center of the spherical reaction bulb, the metal film was not uniform in thickness and showed a very thin streak in the plane of the filament loop. As simultaneous or successive evaporations from two different metal filaments could not be expected to produce a uniform alloy film under such conditions, evaporation from a preformed homogeneous alloy pellet was tried.

2. Induction Evaporation. The preparation of suitable metal or alloy pellets is described elsewhere.[6] After sealing to the system a Type II reaction vessel containing a prepared pellet, the evacuation, bakeout, flaming and cooling of the traps was as in part 1. To remove dissolved gases, once during bakeout the pellet was induction heated almost to melting. The reaction vessel was packed in Dry Ice during film evaporation. The pellet was further outgassed three short periods of induction heating at low power, then at maximum power the film was evaporated during about 5 min. The film was evaporated in one continuous heating operation, since the presence of the metal film on the reaction vessel interior walls appeared to decrease the ability of the metal pellet to couple with the field of the induction coil. The pressure during film evaporation was about 1×10^{-6}. The nickel films were stabilized as in part 1, but the Pd–Ni alloy film between −78° and 100°. Film weight was determined by weighing the pellet before and after evaporation. The films prepared by induction heating appeared brilliant and mirror-like as were the filament evaporated films. Although the thickness of the induction evaporated films appeared uniform with respect to cylindrical symmetry, film thickness decreased with distance from the pellet. That the composition of the alloy film was little affected by film thickness, however, was demonstrated by polarographically analyzing, for both nickel and palladium, five different portions of the alloy film, each portion representing a different distance from the pellet. The film portion on the edge of the pellet cup was slightly richer in palladium, *i.e.*, 7.4 atom %, but was so highly sintered that it probably contributed little to catalytic activity. The other film areas showed 6.0, 6.2, 6.1, and 6.2, respectively, yielding an average of 6.1 atom % palladium. Thus, it appeared that an alloy film having good uniformity in chemical composition throughout its extent could be prepared by the pellet evaporation technique.

Procedure for Adsorption and Reaction. With the reaction vessel cooled in ice, or Dry Ice–2-propanol, a known amount of oxygen was adsorbed on the metal film. Then after the gas phase was evacuated, the reaction vessel was thermostated at 0 or 100°, and doses of CO were admitted. For one nickel film CO was adsorbed first and oxygen added subsequently. In order to determine the amount of CO_2 desorbed from a film,[3] pressure measurements were made both with the second trap cooled in liquid nitrogen and at room temperature. At the conclusion of the reactions on a film, helium expansions were made to determine necessary apparent volumes.

(5) A. H. Pfund, *Phys. Rev.*, 18, 78 (1921).

(6) E. G. Alexander and W. W. Russell, to be published.

Table I: Summary of Adsorptions and Reactions on Films

Reaction of CO with Adsorbed Oxygen

Film	Wt., mg.	Temperature: O_2 ads	Temperature: Reaction	O_2[a] ads.	CO[a] ads.	CO_2[a] desorb.	% O_2 reacted	$\frac{CO_{total\ ads}}{CO_2\ desorb}$[b]
(Pd)1[c]	5	0°	0°	1.49	2.83	2.24	75	2.3
(Pd)2[c]	55	0°	0°	0.31	0.56	0.59	95	2.0
(Pd)3[c]	51	0°	0°	0.16	0.28	0.21	65	2.3
(Ni)4[c]	49	0°	...	7.08	...	...	...	...
(Ni)5[c]	28	0°	0°	9.34	0.39	0.07	0.4	6.6
(Ni)7[d]	12	−78°	0°	4.10	0.47	0.02	0.2	25
			100°	...	0.33	0.68	8.3	1.5
(Pd–Ni)10[d]	21	−78°	100°	8.05	1.12	0.82	5[e]	2.4

Reaction of O_2 with Adsorbed CO

Film	Wt., mg.	Temperature: CO_{ads}	Temperature: Reaction	CO[a] ads.	O_2[a] ads.	CO_2[a] desorb.	% CO reacted	$\frac{O_{2\ total\ ads}}{CO_2\ desorb}$[f]
(Ni)6[d]	30	0°	0°	0.48	1.38	0.47	98	3.4

[a] Ml. per g. of film. [b] $CO_{total\ ads}$ is sum of CO_{ads} plus $CO_{2\ desorb}$. [c] Evaporated from filament. [d] Evaporated from pellet. [e] Value would have been significantly larger had run been continued longer. [f] $O_{2\ total\ ads}$ is sum of $O_{2\ ads}$ plus $0.5CO_{2\ desorb}$.

Results and Discussion

Typical results are summarized in Table I in which it is to be noted that the sixth column refers to the amount of CO or oxygen remaining adsorbed at the end of reaction on a film, while the eighth column lists the % of oxygen or CO reacted in forming the CO_2 desorbed. About $^3/_4$ of the oxygen preadsorbed on a film was taken up rapidly to a low residual pressure ($<10^{-5}$). The remainder was adsorbed at measurable rates, which diminished rapidly with time. The adsorbed oxygen was not removed by pumping at 0°. While the amount of oxygen adsorbed at 0° per unit weight of palladium film varied by nearly tenfold, the variation was only about twofold per palladium film. The nickel films at 0° adsorbed from 15 to 45 times more oxygen than did the palladium films. At −78° oxygen adsorption per unit weight of nickel film was about half that at 0°. About 90% of the CO preadsorbed on (Ni)6 at 0° was taken up rapidly, but to a residual pressure higher than in the case of oxygen. Part of this CO could be removed by pumping at 0°.

Reaction of CO with Adsorbed Oxygen. Figures 1 and 2 show the amounts of CO and CO_2 appearing in the gas phase as doses of CO were added at 30-min. intervals, except the last dose which reacted several hours. It is evident from Fig. 1 that for reaction with CO at 0°, the activity of oxygen preadsorbed on palladium was much greater than on nickel. While the first six doses of CO added to (Pd)2 disappeared from the gas phase within a minute, and 99% of the first dose of CO on (Ni)5 disappeared in 2 min., subsequent

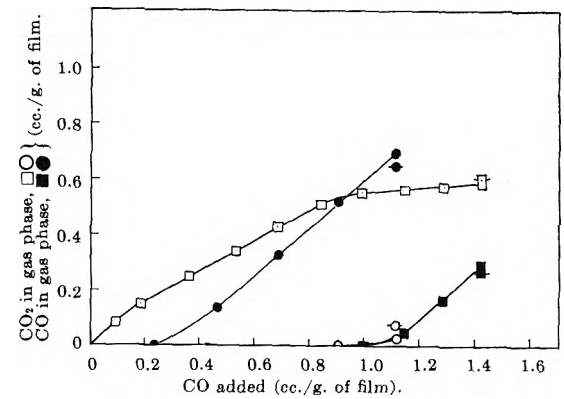

Figure 1. Reaction at 0° of CO with oxygen preadsorbed on: (Pd)2, □■; and (Ni)5, ○●.

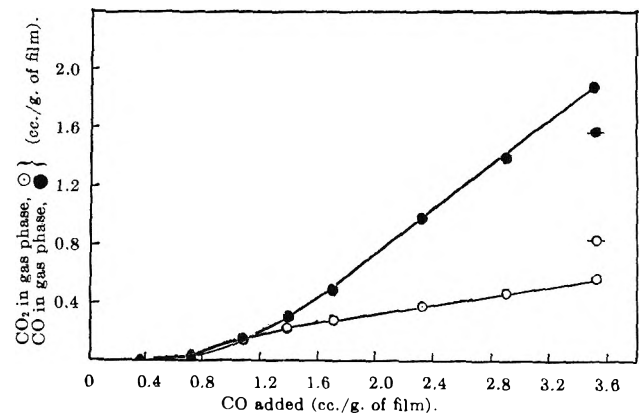

Figure 2. Reaction at 100° of CO with oxygen preadsorbed on (Pd–Ni)10.

CO doses were very incompletely adsorbed on the nickel film. While gaseous CO_2 appeared immediately over the palladium film, none appeared until after the fourth dose of CO was added to the nickel. Six hours after adding the final dose of CO to (Pd)2, 95% of the preadsorbed oxygen had reacted, but only 0.4% on (Ni)5 even though the last CO dose reacted for 11 hr. Although oxygen was preadsorbed on (Ni)7 at −78°, the extent of reaction with CO at 0° was similar to that of (Ni)5. However, standing 20 hr. at 25° caused 3.3% of the oxygen preadsorbed on (Ni)7 to react, and 2 additional hours at 100° raised reaction to 8.3%. From Fig. 2 it appears that the behavior of (Pd–Ni)10 was roughly intermediate to that of palladium and nickel. Like nickel at 0° gaseous CO appeared after adding the second CO dose, but like palladium at 0° gaseous CO_2 was increasing linearly after adding two or three CO doses. The last dose of CO reacted but 2 hr. on (Pd–Ni)10, and although still proceeding, this reaction was not followed further.

The ratio in the last column of Table I allows the catalysts to be compared on the basis of the number of molecules of CO or O_2 which were adsorbed to desorb a molecule of CO_2. This ratio may be considered as a rough measure of the difficulty of desorbing CO_2. In agreement with Stephens,[3] on the palladium film at 0° about one molecule of CO remains permanently adsorbed for every molecule of CO_2 desorbed. For nickel this value rises to over five at 0° and is much higher for oxygen preadsorbed at −78°. At 100° the ratio value of 2.4 for the Pd–Ni film is intermediate between 1.5 found for (Ni)7 and 3.5 found under comparable conditions for (Pd)9, not shown in Table I. Although at 100° the fraction of adsorbed oxygen reacted remained smaller on nickel and the Pd–Ni alloy, ratio values and absolute amounts of adsorbed oxygen reacted were comparable to palladium at 0°.

The much greater activity for oxidizing CO at 0° showed by oxygen preadsorbed on palladium is believed due in part to the more ready desorption of CO_2 from palladium[7] than from nickel, and also to the stronger interaction of oxygen with nickel than with palladium. While oxygen adsorption on palladium films is probably primarily chemisorption,[8] heats of oxygen adsorption on nickel films from 107[8] to 150 kcal./mole[9] have been reported. These heats are high enough to permit considerable oxide formation and consequent reduced reactivity at least of the oxygen so held. Although at least five times as much oxygen was adsorbed per unit weight of nickel film, at least three times as much adsorbed oxygen reacted on unit weight of palladium.

Reaction of Oxygen with Adsorbed CO. As is clear from Fig. 3 when doses of oxygen were added at 0°

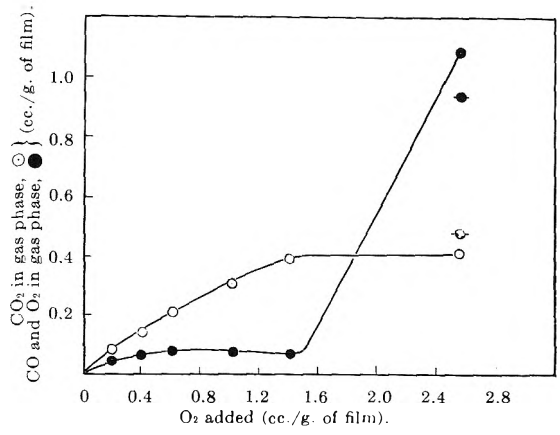

Figure 3. Reaction at 0° of oxygen with CO preadsorbed on (Ni)6.

to (Ni)6 containing preadsorbed CO, CO_2 was immediately desorbed and there was no long induction period as was found for this reaction on palladium films.[3] But a gas, noncondensable at liquid nitrogen temperature, immediately appeared in the gas phase and remained essentially constant in amount between the second and fifth oxygen doses. This gas is believed to have been a loosely-held portion of the preadsorbed CO. Oxygen might be expected to displace some of the adsorbed CO since the heat of oxygen adsorption on nickel is over three times that of CO which is about 35 kcal./mole.[10] Thus, enough suitable sites on the nickel surface could be pre-empted by the first oxygen dose to permit surface dissociation and reaction with still adsorbed CO without an induction period. After the fifth oxygen dose reaction became slow and the rapid increase in noncondensable gas is believed due to gaseous oxygen. The last dose of oxygen stood 14 hr. so that most of the initially desorbed CO eventually reacted. While the extent of reaction of oxygen with CO preadsorbed on either nickel or palladium[3] appears very similar, palladium films adsorbed about four times more CO, and the adsorption of about three times as many molecules of oxygen was required to liberate a molecule of CO_2 from nickel as from palladium.[3] Thus, the greater affinity of the nickel surface for oxygen, as compared to palladium, appears to be consistent with the lower activity of oxygen adsorbed on Ni, and with the comparable extent of re-

(7) A. C. Collins and B. M. W. Trapnell, *Trans. Faraday Soc.*, 53, 1476 (1957).

(8) D. Brennan, D. O. Hayward, and B. M. W. Trapnell, *Proc. Roy. Soc.* (London), A256, 81 (1960).

(9) D. F. Klemperer and F. S. Stone, *ibid.*, A151, 308 (1957).

(10) M. McD. Baker and E. K. Rideal, *Trans. Faraday Soc.*, 51, 1597 (1955).

action of CO adsorbed on palladium or nickel, inasmuch as gaseous oxygen aids the desorption of CO_2 from the nickel surface.

Acknowledgment. The support for this research by the Advanced Research Projects Agency and by University Fellowships is gratefully acknowledged.

Production of Methyl Radicals in the Recoil Chemistry of Carbon-11[1]

by Robert H. Schuler

Radiation Research Laboratories, Mellon Institute, Pittsburgh, Pennsylvania, and Department of Chemistry, Brookhaven National Laboratories, Upton, New York
(Received February 24, 1964)

During recent years considerable attention has been given to studies of the reactions of energetic carbon atoms with organic compounds.[2] In this work it is of interest to know at what stage of chemical combination these carbon atoms become thermalized.[3] The present contribution reports some brief observations which indicate that in aliphatic hydrocarbons ~3% of the carbon atoms are thermalized as methyl radicals. In benzene, reaction of the recoil atoms appears to be complete before this stage is reached.

In the studies reported here recoil carbon atoms are produced in liquid hydrocarbons *via* the nuclear reaction $C^{12}(n,2n)C^{11}$.[4] The carbon-11 atoms which reach the methyl stage as thermal radicals are scavenged by iodine present in solution. It is known from radiation chemical studies[5] on related systems that iodine is an efficient scavenger for methyl radicals at the concentrations employed in these experiments and that the radiomethyl iodide formed can be readily separated by means of gas chromatography even when present at very low concentrations. Because of the short irradiations employed and because of the removal of radical intermediates by the presence of scavenger iodine in the solutions, extraneous effects due to radiation chemical decomposition are expected to be minimized.

Experimental

Materials. The hydrocarbons used were Phillips research grade.

Irradiations. Irradiations were carried out at the Brookhaven 60-in. cyclotron with neutrons produced by bombarding a lithium hydride target with a ~50 μa. beam of 20-Mev. deuterons. The irradiation methods were similar to those previously employed[6] except that the substitution of the lithium hydride target for the beryllium target normally used for neutron production increased the yield of C^{11} relative to that of I^{128} by about a factor of 10. With this target the activity level of I^{128} produced in a solution of 5×10^{-2} *M* iodine in cyclohexane was only 30% of the C^{11} level. At the lower (10^{-2} *M* and less) iodine concentrations employed in the experiments described here complications due to the simultaneous production of CH_3I^{128} were therefore minimized. For normal activation periods of ~30 min. the total activities available under the counting conditions used were ~100,000 c.p.m./ml. of sample. This level corresponds to a saturation activation of $\sim 4 \times 10^6$ d.p.m./ml. This is sufficient to carry out useful measurements on C^{11} (half-life of 20.5 min.) for from 1 to 2 hr. after the irradiation.

Activity Measurements. Because of simultaneous production of I^{128} with a half-life of 25 min. some care must be used in the activity determinations. The samples were counted in a well-type scintillation counter with a single channel pulse-height analyzer in a manner similar to that previously described.[6] Measurements were made in the two channels corresponding to the photoelectric absorption maxima of the I^{128} and C^{11} radiations. Solution of the simultaneous equations involving the observed counting rates and the relative counting efficiencies in both channels showed that the contribution due to iodine activity in the C^{11} channel would be of the order of 1% for solutions 10^{-2} *M* in I_2. In the cases of cyclohexane and benzene methyl radicals are not formed in significant yield as a result of radiolysis[5] so that the production of CH_3I^{128} should not present a problem. In the case of 2,2,4-trimethylpentane a maximum correction of the order of 0.1% in the methyl iodide yield is indicated from the relative activity levels and the available radiation chemical information.[5] That CH_3I^{128}

(1) Supported in part by the U. S. Atomic Energy Commission.

(2) For a recent summary of this work see A. P. Wolf, "The Reactions of Energetic Tritium Atoms and Energetic Carbon Atoms with Organic Compounds," in "Advances in Physical Organic Chemistry," Vol. II, V. Gold, Ed., Academic Press, London, in press.

(3) When carbon atoms are born of a nuclear event such as the $C^{12}(n,2n)C^{11}$ reaction under discussion here they have a sufficiently high kinetic energy that they recoil initially as stripped carbon atoms. As they are slowed down they will react with the solvent in epithermal and thermal reactions and appear directly as reaction products or as radical intermediates.

(4) The first related studies of carbon-11 recoil chemistry in organic systems were reported by B. Suryanarayana and A. P. Wolf, *J. Phys. Chem.*, *62*, 1369 (1958).

(5) R. H. Schuler and R. R. Kuntz, *ibid.*, *67*, 1004 (1963).

(6) C. E. McCauley and R. H. Schuler, *ibid.*, *62*, 1364 (1958).

• does not contribute to the measurements is in fact born out by observations in the C^{11} and I^{128} channels. Normally counting periods were for 2 min. with activities for the organic fractions being up to ~1000 counts against backgrounds of ~10 counts. The total activity was obtained from an aliquot of the original sample counted under conditions identical with those used for the separated fractions.

Gas Chromatography. After irradiation 0.5 ml. of the sample to be analyzed was chromatographed at room temperature on a 250-cm. column of 25% silicone grease on firebrick. The activity in the effluent was trapped in tubes containing 2 ml. of 2,2,4-trimethylpentane chilled to Dry Ice temperature in a manner similar to that described earlier.[5] In this previous work it was shown that trapping of the methyl iodide is quantitative. Samples were collected for 5-min. intervals and subsequently counted. Under the column conditions used methyl iodide (elution time ~17 min.) will appear in the 15–25 min. fraction with division into the 15–20 and 20–25 min. fractions being somewhat dependent on the detailed operating conditions of the column.

Chemical Treatment of Irradiated Samples. Preliminary experiments on pure cyclohexane showed a very considerable fraction of the activity in the chromatographic region of interest (*cf.* upper histogram of Fig. 1). This activity was increased by only several per cent (in the 15–25 min. fraction) upon addition of iodine before irradiation. The background activity is presumably due predominantly to the production of unsaturated products.[7,8] It was found possible to remove most of the interfering activity by treatment of the irradiated sample (5 ml.) with 0.5 ml. of a solution of 0.2 *M* Br_2 in cyclohexane (*cf.* lower histogram in Fig. 1). Since IBr itself was found to be only partially effective it was necessary to keep the amount of Br_2 added in excess of the iodine present. Under the contact conditions used here this treatment does not affect the methyl iodide determination. Treatment with more concentrated bromine does, however, convert the $C^{11}H_3I$ to $C^{11}H_3Br$ (the latter being eluted in the 5–10 min. fraction). Except where noted the activity measurements are on samples treated with Br_2.

Results and Discussion

The elution curves given in Fig. 2 for cyclohexane which contained iodine during the irradiation show a significant activity in the fractions where methyl iodide is expected to accumulate. In the two runs illustrated here the methyl iodide fraction (corrected for the small blank) represents 3.0% of the activity produced in an air-saturated solution containing 10^{-2} *M* I_2 and 3.3% in an evacuated solution at the same concentration. When a similar air-saturated solution was treated with very concentrated bromine, 2.9% of the activity appeared in the methyl bromide fraction and only 0.05% in the methyl iodide fraction. The combined chromatography chemistry therefore indicates very strongly that the ~3% fraction being examined is indeed methyl iodide.

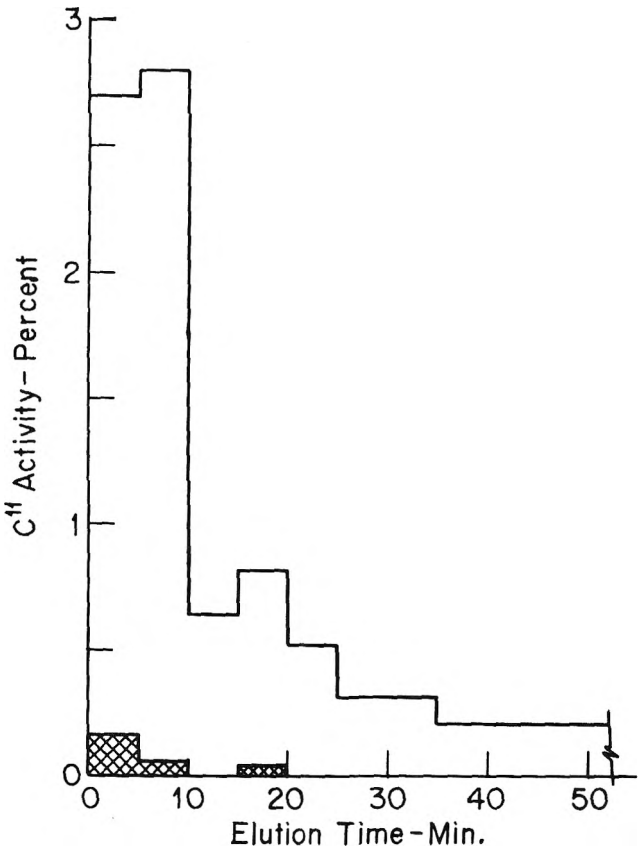

Figure 1. Distribution of activity produced in pure cyclohexane. Open histogram, untreated sample; hatched histogram, sample treated with Br_2. Activities are given in per cent accumulation in 5 min. fraction.

At lower iodine concentrations air-saturated solutions give a somewhat lower yield of activity in the methyl iodide fraction. This is expected since oxygen will competitively scavenge the radicals.[9] In two experiments at 10^{-3} *M* I_2, fractions of 1.3 and 1.4% of the activity were observed as methyl iodide.[10] If we assume that the 45% scavenging efficiency observed for 10^{-3} *M* I_2 in air-saturated cyclohexane[9] applies here

(7) C. MacKay and R. Wolfgang, *J. Am. Chem. Soc.*, **83**, 2399 (1961).

(8) C. E. Lang and A. F. Voight, *J. Phys. Chem.*, **65**, 1542 (1961).

(9) R. W. Fessenden and R. H. Schuler, *J. Am. Chem. Soc.*, **79**, 273 (1957).

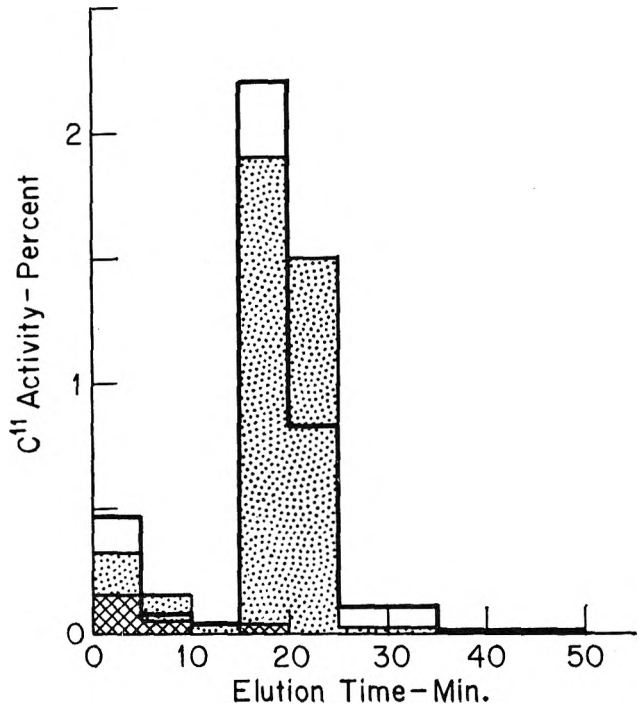

Figure 2. Distribution of activity produced in cyclohexane containing 10^{-2} M I_2 Open histogram, air-saturated sample; dotted histogram, evacuated sample; hatched histogram, blank (as per Fig. 1).

then the average of the above values corrects to a fraction of 3.0% for pure cyclohexane. This would seem to indicate that the value observed at 10^{-2} M I_2 in the presence of air should be only about 10% lower than for the pure compound (as observed). In one experiment on an evacuated sample containing 10^{-4} M I_2 a fractional methyl iodide activity of 2.2% was observed in spite of the fact that the iodine had, as a result of radiolysis, completely disappeared from the sample during the irradiation.[11] This result at least qualitatively indicates a high scavenging efficiency at the low iodine concentration.

Experiments on 2,2,4-trimethylpentane show a net activity of 3.2% in the methyl iodide fraction (blank of 0.2%) for an evacuated sample containing 10^{-2} M I_2 and 3.1% for a sample containing 10^{-3} M I_2. Two experiments on benzene, however, gave only 0.15% and 0.17% (10^{-2} and 10^{-3} M I_2, respectively; evacuated samples) of the activity as methyl iodide.[12] The addition of 10% benzene to 2,2,4-trimethylpentane reduces the methyl iodide fraction only moderately (to 2.2%).

The present numerical results are very much in line with those of Stocklin and Wolf, who find, for example, a methane yield of 2.9% in gaseous propane which is reduced to 0.5% upon the addition of oxygen scavenger.[13] They are however at variance with the work on cyclohexane by Rack and Voight,[14] who extrapolate the dose dependences of the methane yields in the absence and in the presence of iodine to a common value and who therefore conclude that the methane yield at zero dose is not affected by the presence of scavengers. Such a conclusion of course leaves no room for the production of thermal methyl radicals as observed here.

In these studies the formation of methyl radicals is examined in the presence of iodine. Since thermal methylene radicals will presumably react with either the solvent or with the iodine present rather than abstract hydrogen from the solvent it would seem that they cannot be precursors to the formation of the observed methyl radicals. The present results serve to demonstrate that in saturated hydrocarbons the fate of approximately 3% of the energetic carbon atoms produced by a (n,2n) process is to become thermalized after having picked up three hydrogen atoms in still ill-defined epithermal processes. The major fraction of the carbon atoms, of course, either undergo other epithermal reactions or are thermalized at other stages of reduction. From the results of Rack and Voight,[14] where a yield of methane from cyclohexane of 4% is found in the presence of iodine, it would seem that a substantial fraction of the carbon atoms go all the way to form CH_4 in epithermal processes. The work of Stocklin and Wolf[13] and MacKay and Wolfgang,[7] however, places a somewhat lower limit on this in gaseous systems. In benzene the epithermal chemistry would seem to be considerably different since reaction apparently occurs before the methyl stage is reached.

(10) In a similar experiment (10^{-3} M I_2; air-saturated sample) carried out without the bromine treatment 2.8% of the activity was observed in the methyl iodide fraction. This compares with 1.3% observed in the absence of iodine (*cf.* Fig. 1). Except for this observed difference of 1.5%, which agrees with the experiments quoted in the text, the elution curve is identical with the upper curve given in Fig. 1.

(11) *Cf.* Table I in ref. 6.

(12) From radiation chemical experiments on mixtures of benzene and 2,2,4-trimethylpentane, iodine, at the concentration employed here, is known to be a good scavenger for methyl radicals even in the presence of benzene (R. H. Schuler, unpublished results).

(13) G. Stocklin and A. P. Wolf, *J. Am. Chem. Soc.*, **85**, 229 (1963).

(14) E. P. Rack and A. F. Voight, *J. Phys. Chem.*, **67**, 198 (1963).